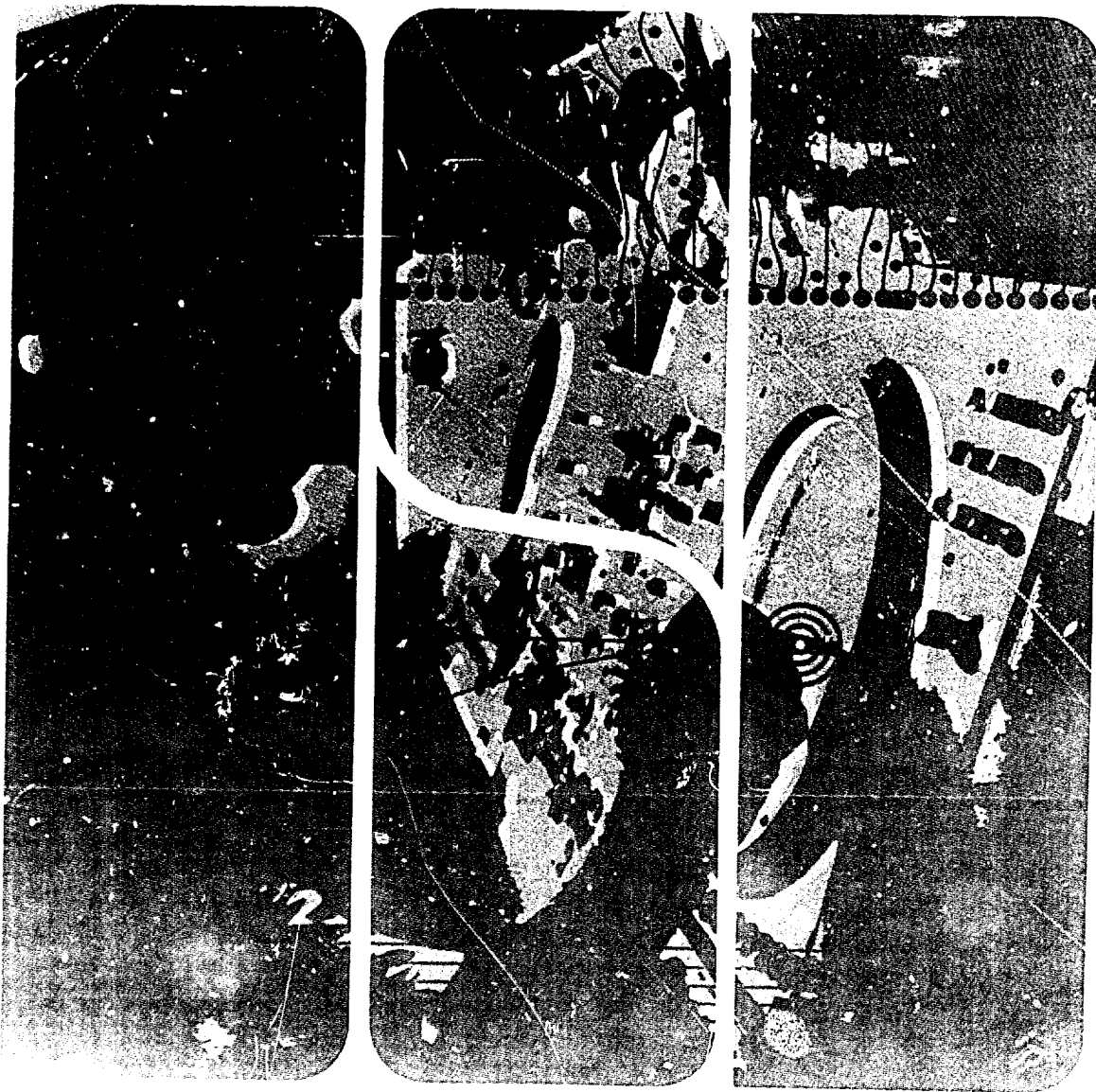AD NUMBER

AD903969

NEW LIMITATION CHANGE

TO

Approved for public release, distribution unlimited

FROM

Distribution authorized to U.S. Gov't. agencies only; test and evaluation; 13 Oct 1972. Other requests shall be referred to U.S. Army, Attn: SMUP-L3300 Frankford Arsenal, Philadelphia PA 19137.

AUTHORITY

FA, DLA D/A ltr, 9 Oct 1974

Litton DATA SYSTEMS

FINAL REPORT
SUPPLEMENT TO PARAMETRIC STUDY OF
ADVANCED FORWARD AREA AIR DEFENSE
WEAPON SYSTEM
(AFAADS)
VOLUME I, ANALYSIS

/ D D C

OCT 13 1972

A

15 September 1972

Submitted to:

U. S. Army, Frankford Arsenal
Bridge and Tacony Streets
Philadelphia, Pennsylvania 19137

Attn: SMUFA-L3300

Prepared Under Contract: DAAG05-70-C-0328

Prepared by:

Data Systems Division
Litton Systems, Inc.
8000 Woodley Avenue
Van Nuys, California 91409

TD 20871

ACKNOWLEDGEMENTS

FOREWORD

This report describes the research effort of the Data Systems Division of Litton Industries, Inc. under Supplemental Agreement 2 to Contract DAAG05-70-C-0328, with the U.S. Army, Frankford Arsenal. The objective was to provide additional analytic and simulation effort in support of the parametric analysis of predicted fire air defense weapon systems.

The report is presented in three volumes. Volume I, Analysis, by Herbert K. Weiss, reports the analysis effort and the simulation results. Volume II, Simulation Model, by Martin P. Ginsberg, describes the Litton Air Defense Simulation, designed by Mr. Ginsberg. The results of the simulation are included in Volume I. Volume III, Effectiveness, by Herbert K. Weiss, reports on methods of evaluating overall system effectiveness.

In the present report, frequent reference is made to the Final Report on the original contract. The previous report, titled Final Report, A Parametric Study of Advanced Forward Area Air Defense Weapon System (AFAADS) (two volumes), dated 2 October 1970, Revised Edition 1971, is referred to throughout this report as the "AFAADS-I Report."

TABLE OF CONTENTS

TABLE OF CONTENTS (Continued)

TABLE OF CONTENTS (Continued)

LIST OF ILLUSTRATIONS

LIST OF ILLUSTRATIONS (Continued)

LIST OF ILLUSTRATIONS (Continued)

LIST OF ILLUSTRATIONS (Continued)

LIST OF TABLES

LIST OF TABLES (Continued)

LIST OF TABLES (Continued)

SECTION 1
INTRODUCTION

During the period of performance, of the work reported in this contractual effort, antiaircraft guns and auomatic weapons continued to demonstrate their effectiveness against modern aircraft and helicopters in Vietnam. The continued capability of predicted fire weapons is difficult to maintain in proper perspective against the 'wizard war' of missiles and for this reason a brief summary, from unclassified sources, of air losses to guns in Vietnam is provided in Appendix I.

On the side of the attacker, a new capability achieved operational maturity. This capability is provided by air to surface guided missiles which home on laser designated targets. If press releases are even partially accurate, it appears at the present time that these, and other types of homing missiles, exhibit delivery accuracies so high, that even considering the increased cost of the munitions over iron bombs, they constitute a least cost solution for tactical aircraft attacks on small hard targets, even though the targets may be undefended.

Even this new capability of tactical air does not cause predicted fire weapons to become obsolescent. It does, however, introduce a new configuration of the tactical situation which must be evaluated. The analytical methodologies, parametric base, and simulation described in the present report can be applied to the new tactical situations, as well as those evaluated in detail in the report.

SECTION 2
SUMMARY

The purpose of the reported supplemental effort, is to extend and further detail the analyses and simulation modeling performed under the original contract. Major emphasis has been placed on providing an augmented data base and battery of methodologies for overall system evaluation. This has included more detailed attention to the initial processes of target acquisition, to the system implications of multiple attackers versus multiple defense units and to the consideration of weapons of all calibers, in addition to the 37-mm weapon on which the original effort was centered.

The Litton simulation has been expanded to allow the evaluation of many additional tactical parameters and modes of defense system operation.

The conclusions of the AFAADS-1 report are unchanged by the present effort. The following brief summary of additional, or augmented conclusions derives from the currently reported effort.

2.1 CONCLUSIONS

A summary of the principal conclusions is presented in the following paragraphs.

2.1.1 General

a. The principal determinants of potential effectiveness, of predicted fire systems, are the prediction and data smoothing algorithms.

b. The principal determinants of operational effectiveness, are tracking accuracy, and the ability to eliminate system errors of boresighting and calibration.

2.1.2 Target Acquisition

a. Visual detection and identification of high speed aircraft targets are inadequate for all defensive weapons, with the possible exception of light machine guns.

b. Even in clear weather, cloud cover represents a frequent difficulty for the attacking aircraft. With radar sensors the defense unit gains a tactical advantage in opening the engagement additional to that associated with the more rapid acquisition possible with radar.

c. Experimental data indicates that aural detection of low flying targets, especially helicopters, can often be accomplished at greater ranges than visual detection. For light weapons with elementary fire control systems, it is possible that aural sensings may be used to aid initial acquisition.

2.1.3 Target Tracking

a. The variance and power spectral densities of tracking sensors must be determined in advance of final choice of data filter and prediction algorithms, in order to obtain a preferred match. Since these quantifiers depend on the engagement geometry, theory must be validated by experiment. The current data base appears to be good for radar sensors, marginal for human tracking with advanced aids (regeneration) and still in process of development for infra-red and laser sensors.

b. A current, continuously updated, library of attack aircraft paths is a necessity for best choice of filter and prediction algorithms. This effort could not be initiated in the present period because the basic data was not available.

c. Although essential, a simple library of paths would be incomplete without a statistical analysis and summary of the probability density functions of predictable path segments.

2.1.4 Data Filtering and Prediction Algorithms

a. To realize the maximum capability of predicted fire systems of efficient exterior ballistic design, the data smoothing time should be an increasing function of range.

b. There is a strong indication that tangential prediction (i.e., an intermediate position between linear and full quadratic prediction) provides a 'robust solution' against moderate, intentional target 'jinking' without suffering unacceptable degradation against unaccelerated targets.

c. Prediction systems, incorporating corrections based on observation of projectile miss distance, appear to have an interesting potential. The stability of the correction algorithms can apparently be enhanced, and the solution improved by the use of a computer generated 'synthetic trajectory', against which to reference the observed miss distances.

d. The time span over which a system can continue to deliver effective fire on regenerated data, after loss of a sensor, is a sensitive function of data smoothing time. For this reason and reasons of accuracy with continuous inputs, the smoothing time should be as large as possible, consistent with target path irregularities. This places a major emphasis on a realistic assessment of probable target paths.

e. A current, continuously updated, library of air-

craft paths on attack paths is a necessity for sound development of filter and prediction algorithms.

2.1.5 Weapon Characteristics

a. Increasing weapon muzzle velocity has a high payoff in all situations. Shortening time of flight to a given range reduces the amplification of tracking noise, and has an even greater effect in reducing the aim errors associated with target maneuvers.

b. Major emphasis should be placed on designing the projectile envelope for low drag, to retain the advantage of high muzzle velocity.

c. Increased high explosive content of the projectile, in a given caliber, improves the effectiveness of contact fuzed projectiles, and increases the probability of obtaining an immediately observable kill. Rapid kill recognition conserves ammunition, and frees the weapon to engage a new target. However, HE capacity is limited by the stresses of firing and interacts with the desire for high muzzle velocity.

d. Even with, contact fuzed, HE projectiles, it is believed that most of the target damage is inflicted by the transfer of the HE energy to the shell fragments, and then to the target. This energy transfer suggests that design for maximum fragmentation effect should be a consideration, even for PD HE ammunition, for use against aircraft.

e. The above considerations suggest that ammunition development for predicted fire weapons is, at least, as important as gun development and may have received relatively inadequate funding in the past.

f. Reload times for many current antiaircraft guns appear to be excessively long, in proportion to the rate of fire. The system effectiveness, under heavy sustained attack, tends to be limited by reload time rather than by rate of fire. The reload time includes the time to replenish the, on-mount, ammunition load, and to change gun barrels.

g. The predicted fire system will normally operate as a part of an integrated defense, under a cover provided by surface to air missiles. If the cover is relatively low, the 'optimum caliber' of the defense weapon tends to lie at that caliber which is the best compromise between terminal effectiveness, and rounds per second which can be fired with a defense installation of a given cost. The result is then quite sensitive to the rise of terminal effectivenss with caliber in the 15-25 mm region, and is uncertain to the degree of uncertainty of the estimates of threat vulnerability. Prudence suggests biasing the solution to larger than the computationally determined 'optimum caliber'.

2.1.6 Cost Considerations

a. The escalation for procurement costs for Army ordnance items has been remarkably moderate over past years, when compared with the cost escalation of Air Force aircraft, for example.

b. Predicted fire air defense systems have a place in the air defense complex and can be justified on a cost, and effectiveness basis. The current deficiencies of U.S. systems have more to do with effectiveness than with cost and can probably be eliminated in a new system, without cost penalty, by provision of a p⋯⋯rly designed fire control data processing comp⋯ ent.

c. Developmer t cost economies might be achieved in the long run by identifying components with multiple system applications and insuring that development programs contain the proper structure, to allow the end products to be applied to multiple uses, this must be done with care. However, the U.S. Army and foreign governments have been successful in developing basic vehicles with a variety of applications. In the fire control field a similar policy might be extended for the following items:

(1) Sensors: Radar, infrared, and laser.

(2) Stabilized sights.

(3) Digital computers for fire control.

Since one application will usually dominate a development program, depending upon priorities of the moment, a burden is imposed on other potential users to continually fight for significant consideration of their application in the program. The pay-off for this effort however, if successful, is greater overall effectiveness of Army weapons within tight development budgets.

The smaller the number of diverse applications considered, the greater the likelihood of success in a program of this type. All Army guns have a predicted fire problem with varying degrees of difficulty. The ability of weapons to fire on the move is desired for a widening spectrum of armament; therefore, a development program integrating the requirements of sensors, sights, and computers for ground based weapons may be more feasible than one including helicopter armament as well.

2.1.7 Development Considerations

A development program for a new predicted fire weapon system should preferably follow the following guide lines:

a. Develop a preferred system concept including a preliminary design, without regard for component availability.

b. Modify the original design to employ as many off-the-shelf components as possible. In each case, log the influence on system effectiveness and determine that no unacceptable degradation is incurred.

c. Identify those required components which involve new development, because of high payoff in terms of cost, and allocate the major portion of the available development budget to those components.

This method approach is preferable to the alternate 'quick fix' method, of assembling data on available components and determining the best system than can be fabricated, by selecting from this limited set of data and components.

2.2 OVERVIEW OF THE REPORT

2.2.1 Detection, Acquisition and Tracking

To engage an aircraft target, the defending predicted fire system must have an unobstructed geometric line of sight to the target, the sensor must be able to acquire the target regardless of light level or weather, and the tracking system must provide accurate target data from which gun orders can be generated. These topics are developed and quantified in Sections 3 and 4.

Methods are provided for determining the probability density function describing the probability that a clear geometric line of sight exists, as a function of terrain type, target altitude, and defense site altitude. Conditional probabilities of detection, given exposure are then developed in parametric form for visual observation as a function of meteorological visibility. Weather as it affects both visual and infrared sensings is reviewed, from the viewpoint of the attacker and the defense.

An improved radar tracking model is presented, based upon limited experimental data on the characteristics of radar 'glint'. Desirable characteristics of tracking devices controlled by a human operator are reviewed, reinforcing the conclusions of the prior report on this contractual effort.

Improved simulation modules are developed for evaluating regenerative tracking, for radar glint noise, and a method of incorporating target 'flight roughness' in the simulation is described.

The possible utility of acoustic detection for simple defense fire units is discussed.

2.2.2 Data Processing and Prediction

Given valid tracking data, the effectiveness of the defense system is critically dependent on the characteristics of the data processing for tracking noise reduction, and the prediction algorithms. These topics are developed in Sections 5 and 6. Fixed memory filters designed as a compromise between settling time and variance reduction are analysed, and recursive filters are discussed. The ability of recursive filters to vary the amount of smoothing with engagement parameters such as time of flight or range is emphasized. Later analyses, including simulation runs, indicate the necessity of varying smoothing time with range to maximize the overall effectiveness of all predicted fire weapons, with the gain over that achievable with a fixed memory filter increasing with caliber.

A number of prediction algorithms are analysed. The advantage of prediction modes using a 'synthetic trajectory' in combination with a sensor capable of observing projectile miss distance is pointed up. Several of these modes are recommended for future evaluation analytically and by means of the simulation. A basic model for evaluating 'barrage fire' is developed, to indicate the very large comparative advantage of aimed fire.

2.2.3 Parametric Description of Threat and Defense Systems

The threat and defense weapon systems characteristics are developed in Sections 7 and 8 with the object of providing parametric relationships that will be of assistance in developing trade-offs in system evaluation.

The threat assessment of the prior report is updated from unclassified sources. Some effectiveness characteristics of the threat versus ground targets are summarized

A simple functional form is developed for aircraft vulnerability to impacting high explosive ammunition, as a function of caliber and HE content. This development is based on declassified antiaircraft gun action reports and aircraft damage and loss reports of mature vintage but the functional form has been programmed into the simulation with a sufficient number of defining coefficients so that it can be adjusted by choice of parameter to fit modern classified vulnerability data.

An improved terminal effectiveness module which has been programmed into the simulation is described in detail. The module incorporates ellipsoidal target wing and fuselage representations, orients them properly on the flight path, and automatically programs bank angle for zero-sideslip turns. The module includes the correct direction of approach of projectile relative to the target, and the effect of trajectory curvature. It allows the specification of round to round ammunition dispersion, separately designated in lateral

2-3

and vertical angle, and in muzzle velocity. In addition, constant azimuth, elevation, and muzzle velocity biases can be specified.

Finally, the interrelationships among rate of fire, caliber, muzzle velocity, projectile weight, and all-up fire unit weight are summarized for zero-order trade-off estimates of defense system options, to be used as a preliminary to detailed system design studies.

2.2.4 Interaction of Attack and Defense Options

The objective of a predicted fire defense system is to raise the cost of destroying its defended vital area to a level that is unacceptable to an enemy. At the lowest level of defense, this means denying the enemy the option of using his simplest, most reliable, lowest cost attack weapons and modes. Section 9 develops methods for analyzing some of these interactions.

It is shown that the interaction between defensive fire doctrine and attacker's release ranges in dive bombing can be expressed in game theoretic terms. A number of cases are worked to display the methods, and the results are then extended to demonstrate how the defense parametric trade-offs may be introduced to the analysis. As is the case in most evaluations of the present study effort, the accuracy of the defense system turns out to be the most sensitive parameter. Comparing a full caliber ammunition type with a sub-caliber type fired at very high muzzle velocity, the gain in hit probability from the increased muzzle velocity slightly outweighs the loss in terminal effect from the smaller projectile weight, for the conditions considered.

The concept of 'effective stand-off range' is introduced as a measure of defense effectiveness, all tactical options considered. This is a range such that if the attacker released his munitions in dive bombing with iron bombs, he would have the same probability of destroying the defended vital area that he would have using 'game optimal' tactics against the active defense, where the game optimal tactics depend on the relative value of the aircraft and the target it is attacking.

For the simple cases used as examples, the effective standoff range and the optimum caliber of the defense fire units increase with the aggregate weight of the defending fire units, and inversely with the aim error of defensive fire.

A model is developed for multiple attackers versus multiple defense units (M versus N). The vital elements of the assessment are the judgemental estimates of the pattern and duration of the attack, and their interaction with the reload time of the defense weapons. In heavy, sustained attacks, almost all of the current designs of high rate of fire defense weapons suffer severe degradation from the fact that it takes much longer to reload the mount than it does to fire a complete load of ammunition. This problem is somewhat mitigated if the weapon caliber is large enough

so that a hit produces an immediately observable kill. This allows fire to be immediately terminated with ammunition savings, and postponement of the reload event.

Some analysis is provided for the possibility of using automatic firing cues or control. It is determined that the effect of tracking error on aim error can be reduced, at the probable expense of number of rounds fired, if the operator fires only when the tracking reticle is on target. On the other hand, if the operator is only required to track without deciding when to fire, his tracking may be more accurate. Automatic fire algorithms are described, but experimental data on operator performance as a function of the number of tasks he must perform and the decisions he is responsible for, are critical to the final selection.

Optimum dispersion is reviewed, both analytically, and in the light of simulation results. It is concluded that some round to round dispersion is better than none, but the optimum value never exceeds about 5 mils except in those cases where bias errors are so large that burst kill probability, is very low, even with optimum dispersion. In general it is more profitable to attempt to reduce prediction error directly than to attempt to cover large prediction errors with a large shot pattern.

2.2.5 Simulation Results

The capability and flexibility of the simulation has been greatly improved over that used in AFAADS-I. The price paid is additional complexity, the difficulty in locating programming errors, and a higher probability of making errors in introducing parameters for new runs. A check-out package of programs is therefore recommended to counter these possibilities, but it was not implemented during the present effort.

The many parametric variations which can be explored with the simulation are listed in the Simulation report and examples are given in Section 10 of this report.

It seems clear that all of the systems simulated suffer at long range from the use of finite memory data smoothing filters with constant smoothing time. To maintain effectiveness at longer ranges, without suffering settling time penalties when targets are acquired at short ranges, filters should be employed with smoothing time increasing with range. Such filters are described analytically, but time did not allow their simulation.

The smoothing time also determines the length of time after loss of a sensor input that the system can fire effectively on regenerated data, and the rate of degradation with the 1.8 second filters used in these simulation runs is demonstrated.

2-4

Increasing muzzle velocity yields a substantial improvement in effectiveness in all cases in which this parameter was studied. As expected, the gain is most when the target is 'jinking'.

Some rather remarkable possibilities have been discovered for the concise representation and summarization of large numbers of simulation runs in terms of combinations of parameters. In addition to providing a simple means for presenting a great deal of simulation data in concise form, these results lead to parallel simple analytic models which can replace the need for simulation in the simpler tactical situations.

The unique advantage of the simulation is its ability to verify proposed system algorithms and to obtain effectiveness results against arbitrary and irregular target paths which would be difficult to handle analytically in a reasonable length of time. The unique disadvantage of this, or any other good simulation, is its ability to dissimulate. The proposed check-out program package is intended to constrain the Litton simulation's propensity for creative fabrication. Considering the much greater complexity of other simulations used by the military services for weapons evaluation and selection, there is cause for concern on this behalf in the case of all simulations.

2.2.6 Supporting Analyses

Some of the simpler analytic models to support the simulation work are described in Section 11. Also discussed is the problem of representing specified noise sequences digitally, when the system represented is a continuous system. A brief introduction to a general formulation of the predicted fire problem along lines which might allow a deterministic computation rather than a Monte Carlo solution is provided, but this effort has not been carried to the point of obtaining results suitable for computation.

2.2.7 Cost Considerations

In view of the fact that there does not seem to be a convenient unclassified reference handbook of the costs of Army equipment, Section 12 assembles cost data from a wide range of unclassified sources. The limited information of predicted fire systems is supplemented by data on other items of Army material which are related, to various degrees, including the common use of some components such as vehicles. On the whole, this panoramic view of Army ordnance costs indicates

that unlike airborne equipment, the cost escalation of Army ordnance has been moderate, and in the case of some equipment types has been less than that attributable to the shrinking ability of the dollar to purchase manufacturing effort.

The rapid rise in the cost directly associated with the average man in service (i.e., pay and allowances rather than equipment) is noted, and it suggested that this places increased emphasis on reduction of maintenance and logistic manpower support in the design of new systems.

The data summary of Section 12 cannot be considered definitive, in view of its unofficial sources. However, it may be helpful to a systems analyst in laying out the cost tasks which he desires to have performed by one of the many competent and professional cost analysis groups within the Army.

2.2.8 Additional Data, Test and Evaluation Requirements

It is pointed out in Section 13 that in the absence of a sufficient quantity of data on actual target paths on aircraft performing real or simulated attack missions, additional analytical and simulation effort is of marginal value. The problem centers on the predictability of the aircraft flight path. It is easily shown that a freely maneuvering aircraft is extremely difficult to hit with a predicted fire weapon. On the other hand it is known that an aircraft on an attack pass has limited freedom to maneuver. It is believed that even with 'free maneuver' bomb sights the permissible maneuvers fall within the ability of predicted fire systems to engage, but this can be determined only by the use of actual data.

The problem of acquiring data both for assessing prototype systems and to build a data base to establish requirements for new systems, and means for performing real time data processing are addressed in Section 14.

2.2.9 Recommended Programs

The final section of the report observes that a major deficiency in the Army's low altitude defense effort is the absence of a prototype predicted fire system development program. A number of recommended analytical and simulation tasks in support of, or in parallel to, but not as a substitute for such an effort, are described. In addition two component programs are suggested for brassboard implementation.

SECTION 3
DETECTION AND ACQUISITION

In order to detect a target, an unobstructed line of sight must exist from the sensor to the target, in the case of almost all sensors. Exceptions include acoustic detection, which may be important in the case of relative slow aircraft, such as helicopters and light spotting aircraft, or when the sensors can be placed remotely.

Given a line of sight, the ability of the sensor to detect the target depends on the transmission of the intervening atmosphere, hence illumination and weather affect sensor performance.

Identification of the target as friend or foe depends on the mode of IFF used. In the case of non-cooperative identification the resolution required of the sensor is, in general, much higher than for simple detection.

These considerations are developed in the following paragraphs.

3.1 EFFECT OF TERRAIN CHARACTERISTICS AND THEIR QUANTIFICATION

Terrain affects and interacts with the performance of ground based air defense systems in many ways. Some of these are displayed in Figure 3-1, and all, as well as others not yet defined, must be considered to varying degrees in the evaluation of air defense system potential.

For any particular tactical situation, terrain can be quantified to a level of detail limited only by time. However an analysis based on a particular sample of terrain is not necessarily definitive of system performance when associated with a different terrain sample. Since it is difficult to say precisely what one means by 'different', the problem of how to include terrain effects and their variability across situations is an important element in the evaluation of defense systems.

Although the detailed simulation of a specific terrain sample tends to lend plausibility to the analysis, the uncertainty as to how far the results can be extrapolated to other situations tends to reduce the value of such detailed analysis of only a few situations.

Since one must ultimately generalize in making overall conclusions regarding system effectiveness, it is probably at least as effective to try to represent terrain statistically with a few parameters, and then to determine the range of variation of those parameters worldwide.

3.1.1 The Line of Sight Problem

In order to track a target for antiaircraft fire direction there must be a clear line of sight from the tracking station to the aircraft. With the exception of sound, all other sensors (there may be a few unex-

ploited exotics still however) likewise require a line of sight for initial detection and acquisition. Given the unobstructed line to the target the sensor may still not acquire because of darkness, weather, ECM,...; the line of 'sight' is nevertheless necessary, if not sufficient.

Two of the basic problems to be solved are shown in Figures 3-2 and 3-3. In Figure 3-2, the target approaches at constant altitude. Once a clear line of sight exists, it continues to exist, until the target passes over the observer. As the target recedes, once it is obscured it is gone for good (or until its next pass).

The aircraft of Figure 3-3 on the other hand, is terrain following (or 'contour chasing'). Its path is a smoothed (low pass filter) version of the terrain contour. The aircraft as viewed from the observing station may be exposed and then obscured several times during a pass.

In general, 'elegant' solutions can be expected to be difficult to come by, since the first case described above can be interpreted as motion of a particle described as a stochastic process with a moving, absorbing boundary, and only simple cases have been solved in the literature. The second case appears to be somewhat more complex. In later sections, known, simple solutions for certain parameter sets will be summarized.

Since, in general, an aircraft may approach a sensor from any direction, the cases described above generalize to the problem of area 'coverage' about a sensor location, and the way in which the probability of having a clear line of sight to a target varies with azimuth angle as well as with range.

An additional consideration associated with the line of sight problem is that of multiple path returns in radar tracking when the tracking beam is low and illuminates terrain which is not quite high enough to interrupt the geometric line to the target, or is behind, but relatively close to the target. The latter problem can be mitigated by range gate width and doppler radar, but the multiple path problem can be an important source of tracking error. The methods of analysis to follow can be applied to the problem of determining the multiple path error, but it will not be dealt with explicitly in this section.

Two of the simplifying concepts which have been used in analytical studies are those of 'mask angle' and 'visibility angle'. These are discussed below.

3.1.2 Mask Angles

The simplest concept of a mask angle is that it defines a conical surface about a sensor, apex of the cone down, and axis vertical. A target is assumed to be visible to the sensor (i.e., unobstructed line of sight)

3-1
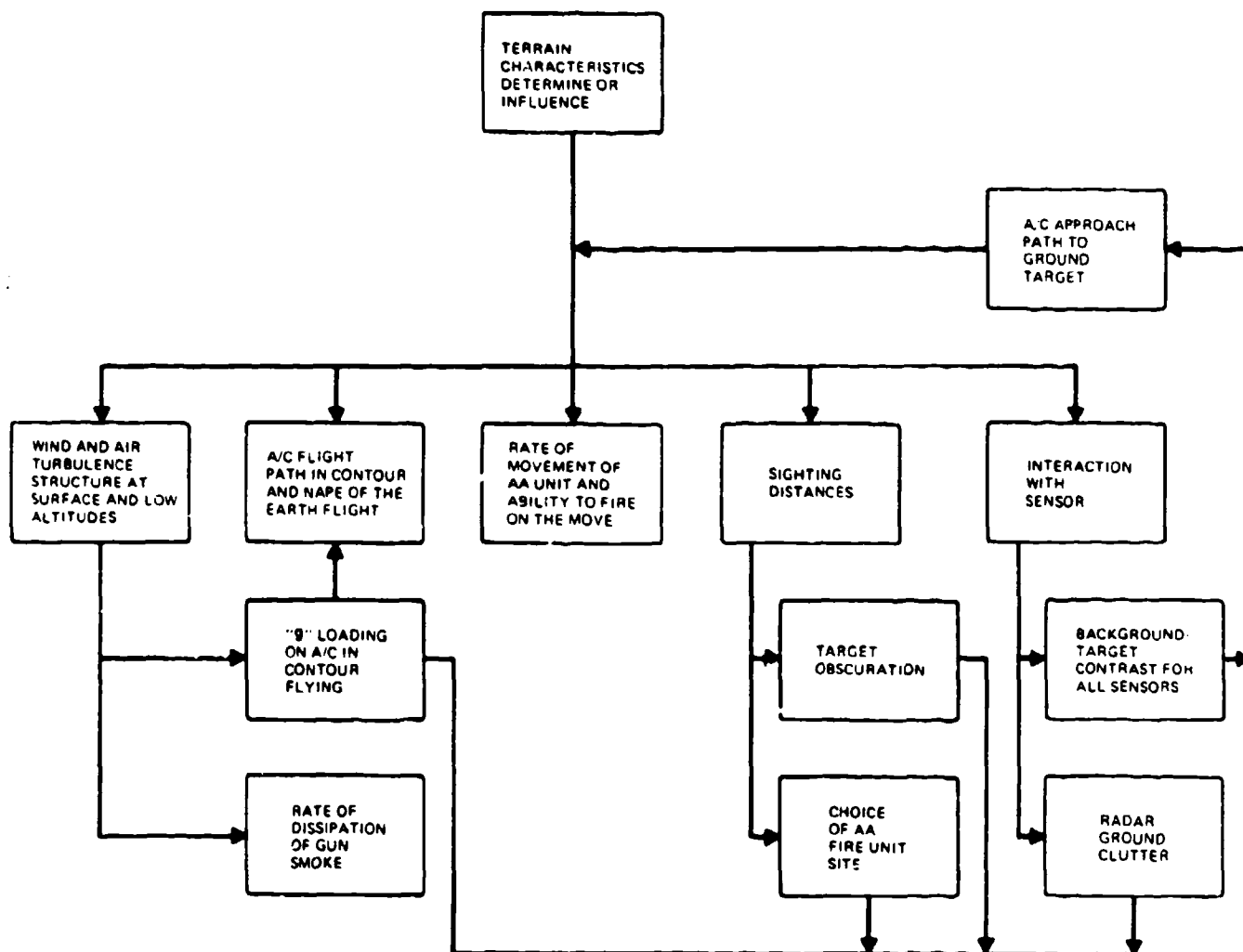
Figure 3-1. System Characteristics Affected by Terrain Characteristics
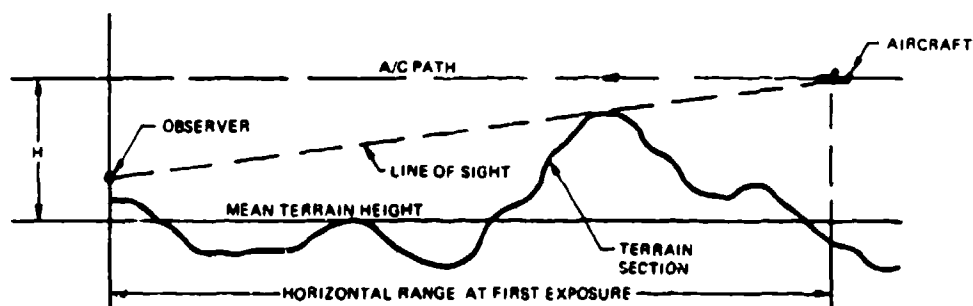
Figure 3-2. First Exposure Range: Level Flight
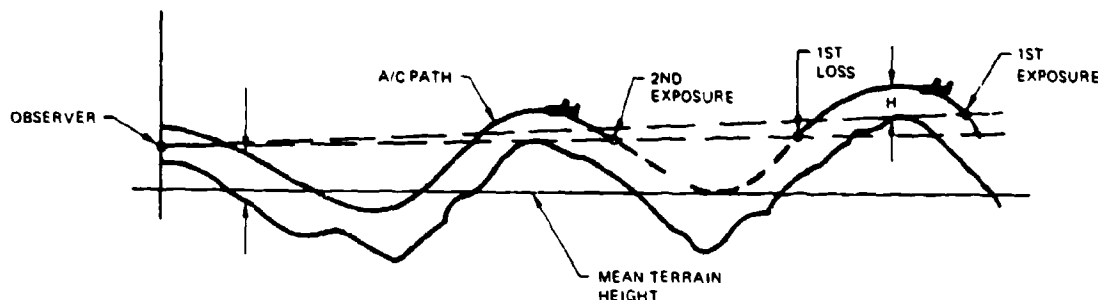
Figure 3-3. Exposure Sequence: Nap of Earth Flight

only within the cone. If m = mask angle and H_t = aircraft height, then the aircraft is visible at a ground range from the sensor

$$R = H_t/\tan m. \qquad (3.1)$$

A somewhat more sophisticated use can be made of mask angle when its distribution function is given, as a function of horizontal range. Stein has published a number of these distributions and referenced sources for others. Stein shows the 'probability' that mask angle is less than m for range R, as a function of m, for specified values of R, and typical curves from his report were reproduced in the AFAADS-I report, (Vol. I, p 4-40).

Designating

$F(m|R)$ = probability that mask angle is less than m at range R computed for a sensor height H above the ground.

$S(R|m)$ = probability of having an unobstructed line of sight at least to range R at an angle m

$$S(R/m) = F(m \mid R) \qquad (3.2)$$

and $P(R,H_t)$ the probability of having an unobstructed line of sight to an airplane flying at an altitude difference H_t above the sensor altitude

$$P(R,H_t) = F(m_a \mid R); \tan m_a = H_t/R \qquad (3.3)$$

An estimate of the distribution function of line of sight ranges to a target at given altitude can thus be obtained.

Note that the use of a constant mask angle cut-off m_s for a site is equivalent to writing

$$S(R \mid m) = 1.0, m > m_s; \text{ for all R}$$

$$S(R \mid m) = 0 \quad ; m < m_s; \text{ for all R} \qquad (3.4)$$

In obtaining F(m|R) the computation must be done each time the height of the sensor above the ground is changed. Implicit in the computation is the method for locating sensor sites in the sample. They might, for example be located at random, or chosen as the best within each equal subdivision of the area studied, etc.

Nevertheless mask angle has the advantage of extreme simplicity and is certainly adequate for preliminary computations.

3.1.3 Visibility Angle

Caywood, Schiller & Co. found the simple mask angle concept inadequate in some studies of air defense systems. In their analyses,[1] they used computer stored terrain data as a basis for comparison, and found in general that use of a constant mask angle underestimated target exposure distance for low altitude targets, and thus led to an underestimate of probability of target kill.

In their report (author not designated), an improved mask concept was developed by a combination of theoretical and empirical techniques. The technique leads to a measure designated as 'visibility angle'. In use it can be employed to define a surface of inverted bell shape to replace the cone of the simplest 'mask angle' concept. The shapes of the mask cone and the visibility surface are compared in Figure 3-4.

Visibility angle is an explicit function of target altitude above the ground level directly under it (AGL), sensor height above mean terrain level, standard deviation of terrain variation about the mean level, and the terrain correlation coefficient.

These are exactly the parameters one would use in attempting to obtain a solution of the problem from a model defining variations of ground level as a stochastic process. As noted later, elegant solutions of the stochastic formulation are hard to come by, and so the Caywood-Schiller solution is something of a tour de force.

The method of deriving visibility angle is based on first determining the area about a sensor sight in which a target is visible (such areas are usually very irregular
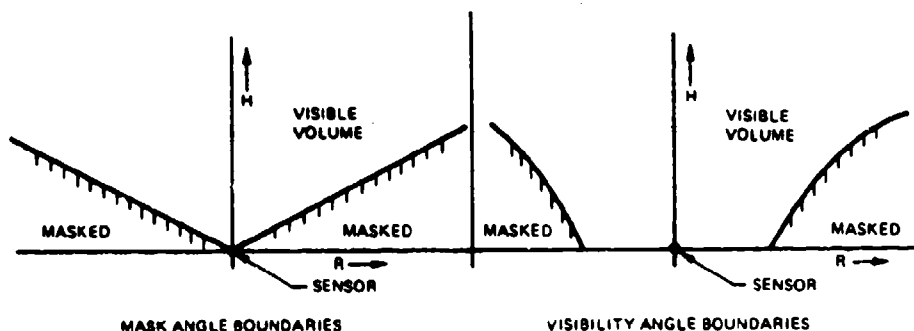
3-3

Figure 3-4. Boundaries Around Sensor Defined by Mask and Visibility Angle Concepts

and resemble the Torrance, California city boundaries) then expressing the area as a circle of equal area. This accounts for the form of the expression, which follows giving the effective radius (R_{ea}) of the equivalent circle.

In the CS&Co report, visibility angle is defined as

$$\tan a = H_t/R_{eff}$$

$$R_{eff} = 1000 \left[\frac{287\, e^{0.42(n+1.3m)}}{(\beta\sigma)^{0.85}} \right]^{1/2} \text{(meters)}$$

(3.5)

where

$$m = \frac{H_s \cdot \mu}{\sigma}; \quad n = \frac{H_t}{\sigma}$$

H_t = target altitude above ground level vertically below it (terrain following flight) (meters)

H_s = height of site above mean terrain altitude (meters)

μ = mean terrain altitude (meters)

σ = standard deviation of terrain altitude (meters)

β = terrain correlation coefficient (km⁻¹)

The report describes a simple manual method of obtaining the statistical parameters quickly from sample maps, with empirical conversion curves. Since the interest in the present report is to indicate representative terrain sighting parameters for evaluations, the set of parameters obtained by CS&Co is extracted (Table III-1), and Figures 3-5, 3-6 and 3-7 are replots of data from the referenced report for specific sites.

CS&Co suggest the following classification system for terrain.

$\beta\sigma < 20$ smooth terrain

$20 \leqslant \beta\sigma < 35$ rolling terrain

$\beta\sigma \geqslant 35$ rough terrain.

20871-600

The reader is referred to the report for further details on how to obtain the statistical descriptive parameters from maps, Equation (3.5) can be written as

$$R_{eff} = R_0\, e^{0.21(n + 1.3\, m)}$$

(3.6.1)

where R_o is a constant for each terrain selection. R_o is given in Table III-1. It depends only on $\beta\sigma$.

Note also that there is a maximum value of visibility angle associated with each terrain selection. This is obtained by differentiating Equation (3.6) with respect to H_t, and it is found that the maximum angle occurs when target height $H_t = \sigma/0.21$, i.e., about 5σ.

In addition to the expressions above for R_{ea}, Caywood-Schiller[21] (R. Rose) have given an expression for the probability of having a line of sight to R, P(R), as

$$P(R) = \min[1, (R-C)^{-k}]$$

where

$$C = 0.25(m+n) - 0.75$$

$$k = 1 - \exp - \left[\frac{\beta\sigma}{10(n+4m)} \right]$$

(3.6.2)

3.1.4 Stochastic Models of Terrain

It is a natural impulse to attempt to take advantage of modern developments in modelling and analysis of stochastic processes to construct mathematical models of terrain from which one can develop solutions to the many interesting siting and sighting problems described earlier. As will be shown, this is a promising line of approach. The analysis becomes quite intricate, and solutions in closed form are difficult to achieve.

3-4

Table III-1. Terrain Parameters

Terrain	$\beta\sigma$	μ	σ	β	R_O (meters)
Wetzlar, Germany	13	260	32	0.40	2800
Tongjin, Korea	16	44	30	0.52	2700
Majon-ni, Korea	19	115	37	0.52	2550
Wonju, Korea	20	227	61	0.32	2500
Ipo-ri, Korea	25	198	82	0.30	2300
Sanyang-ni, Korea	45	53	116	0.39	1850
Bad Tolz, Germany	98	1259	165	0.59	1450

20871-500

The intrinsic interest of the topic, however, and the activity of the field promise new findings in the future. Like many of the problem areas associated with fire control problems stochastic modelling of terrain can serve as the subject of numerous PhD theses.

The problem can be discussed in two steps, 1) the stochastic description of terrain along a line transect, a two dimensional problem, and 2) the more general problem of describing terrain stochastically in three dimensions.

In the first case, a difference between terrain variations along a line transect and noise amplitude fluctuations with time in a classical 'noise' problem is at once apparent. In the case of an electrical signal varying with time, the signal is not affected by its future. In the case of terrain variations, the height at a point along a line is certainly affected by heights to either side of the point. Fortunately, Whittle[6] has shown that the two problems can be reduced to identical form, and so results obtained in the analysis of signals varying stochastically with time can be applied to the line transect terrain problem.

3.1.5 Terrain Variations Along a Line Transect

The methodology to be used derives from the classic works of Markov, and Kolmogorov, and the modern applications by Stratonovich and others. Theory and conditions under which it applies are given in the cited references.[4,5,8,9,10,11,16]

Relationships required for the present discussion are abstracted in the following paragraphs.

The field is long on theory and short on solutions. Relevant solutions from the literature are given, as well as a few previously unpublished by Weiss.

For this class of problems it is, in principle, possible to obtain exact solutions, even though nonlinear functions are involved. Following Pervozvanskii[5] we assume that the equations of the process can be written in the form

$$dx_i/dt = f_i(x_i, \ldots, x_n, v_1, \ldots v_n); i = 1, 2, \ldots n$$

(3.7)

where the v_i are random function of time described by the means and correlation functions

$$\langle v_j \rangle = 0$$

$$R_{jk}(T) = \langle v_j(t)v_k(t+T) \rangle = D_{ij}\,\delta(T) \qquad (3.8)$$

In attempting to develop solutions to the terrain problems discussed earlier in this section, we will rarely have enough data to go beyond the examination of distributions of terrain height from a mean, and terrain slope. In addition, there is no advantage in first investigations to allowing non-linear relationships of the x to the v. Hence we use the simpler, and more limited form

$$dx_i/dt = f_i(x_1, \ldots x_n) + v_i \qquad (3.9)$$

If all of the x_i are continuous functions of t, we can write Kolmogorov's equation (also known as the Fokker-Planck equation) for the evolution of the probability density function, $w(x_1, \ldots, x_n, t)$

$$\frac{\partial w}{\partial t} = -\sum \frac{\partial}{\partial x_i}(f_i w) + (1/2)\sum_i \sum_j D_{ij}\frac{\partial^2 w}{\partial x_i \partial x_j}$$

(3.10)

For the cases we shall examine, the x_i can, in fact, be shown to be continuous functions of t. For these cases also there is no advantage in writing, for example

$$dx_i = f_i\, dt + v_i\, dt \qquad (3.11)$$

which is necessary in the case of some processes.

In the problem of a line transect of terrain, the $x_1, x_2, \ldots$ represent the terrain height measured from its mean, the terrain slope, rate of change of slope, etc., and t corresponds to horizontal distance from the observation point. Then a line of sight to a specified range at specified elevation angle exists if the realization of the process originating from the sensor position does not cross the line at any intervening point. One therefore wishes to solve the partial differential equations for w, given the x_i at $t = 0$, with the line of sight defining an absorbing boundary $b + \theta t$, where $\theta = \tan \alpha$; $\alpha =$ the elevation angle, $b =$ sensor height above terrain mean.
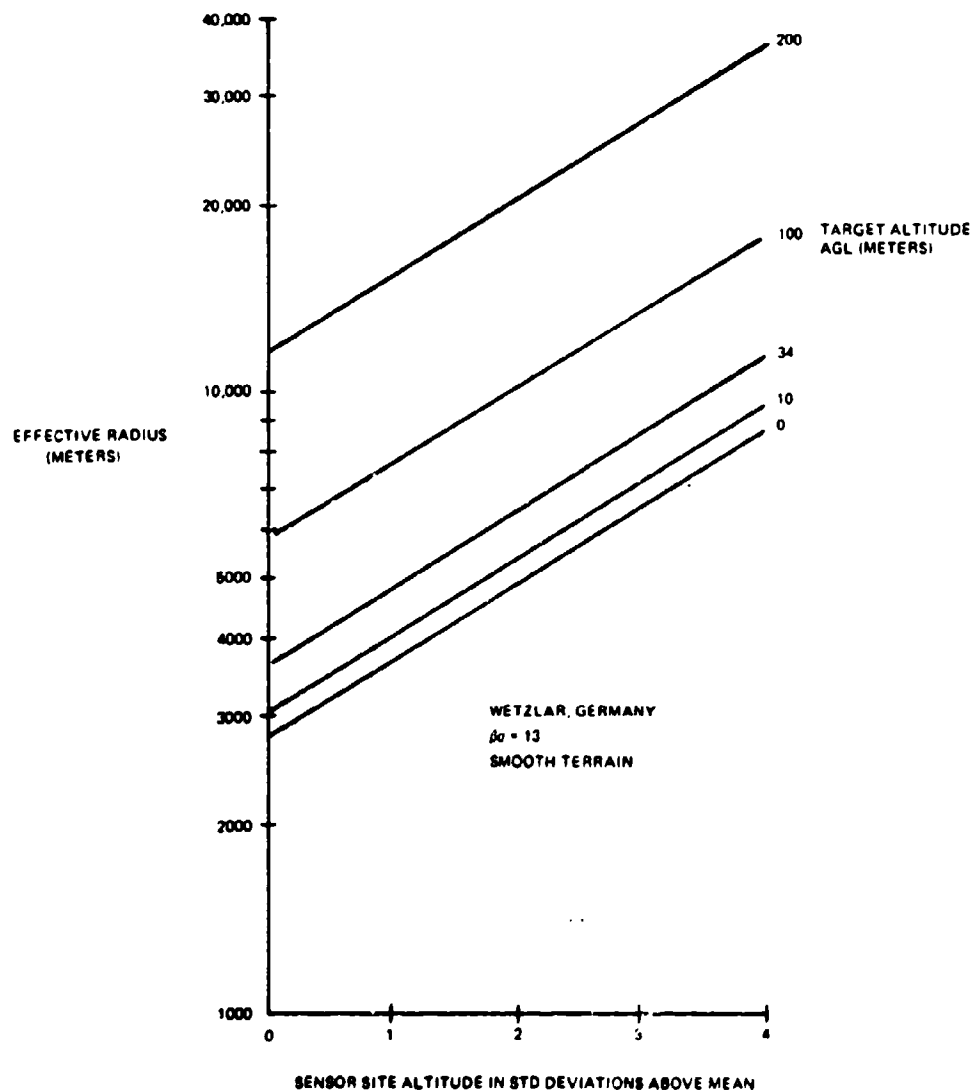
Figure 3-5. Effective Site Radius for Smooth Terrain

For $\theta = 0$ the problem is relatively, but not absolutely simple.

Uhlenbeck-Ornstein Process

Consider the relatively simple process defined by

$$dx/dt = -\beta x + v$$

$$\langle v^2 \rangle = D; \langle v \rangle = 0 \qquad (3.12)$$

The Kolmogorov forward equation is

$$\frac{\partial w}{\partial t} = \beta \frac{\partial (wx)}{\partial x} + (D/2) \frac{\partial^2 w}{\partial x^2} \qquad (3.13)$$

The boundary conditions are

$$w(x_b, t) = 0, x_b = b + \theta t$$

$$x(-\infty, t) = 0$$

The initial condition is

$$w(x_o, 0) = \delta(x - x_o)$$

3-6
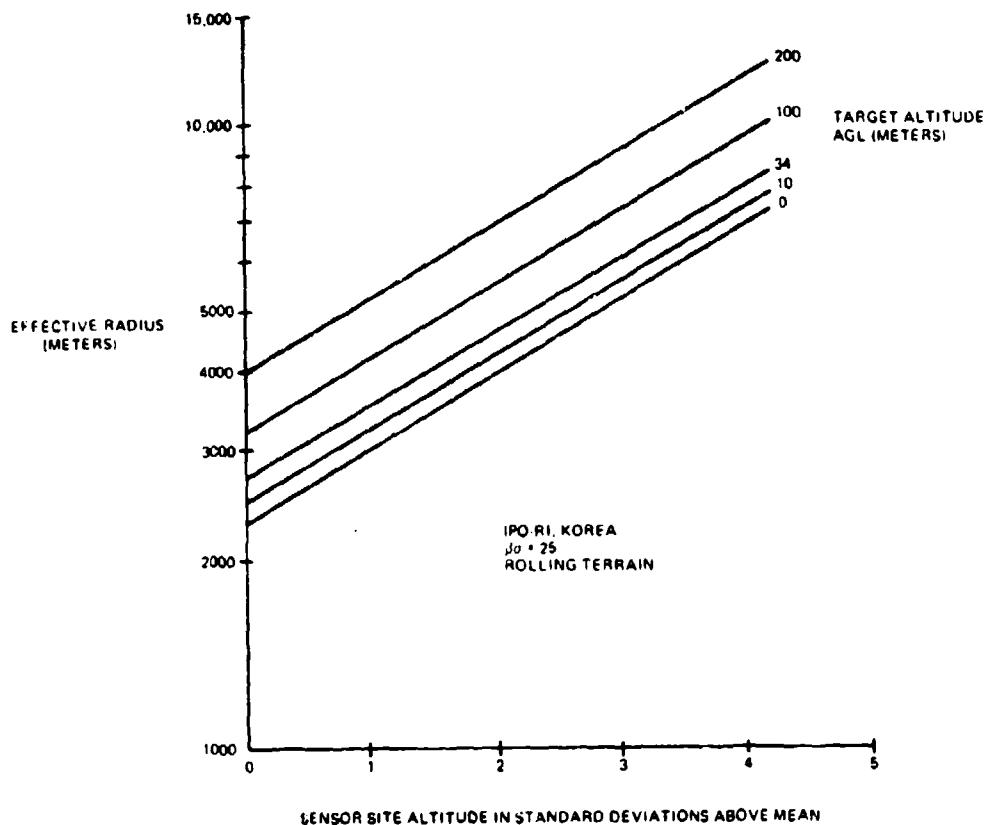
Figure 3-6. Effective Site Radius for Rolling Terrain

In the absence of the absorbing boundary, the solution for $w(x, t/x_0)$ is easy to obtain and is well known to be [8,9]

$$w(x,t \mid x_0) = \frac{1}{(2\pi)^{1/2} \sigma(1-\rho^2)^{1/2}} \; e^{-\frac{(x - \rho_0 x_0)^2}{2\sigma^2(1-\rho^2)}}$$

(3.14)

where

$$\rho = e^{-\beta\sigma}$$

$$2\sigma^2 = (D/\beta)$$

Solutions for $\beta = 0$

When β is very small, the initial evolution of the process is determined by D. This suggests first solving for the case of $\beta = \Gamma$ corresponding to a Wiener-Levy process (for which the variance is unbounded).

Defining

$I(t\beta) =$ the probability that the process continues to t without reaching the absorbing boundary b + θt,

and solving the partial differential equation with $\beta = 0$, the results are obtained that, setting a $= b - x_0 =$ height of the sensor above ground level,

3-7

$$I(t,\theta) = 1 - (1/2)\, e^{-A/2} \left\{ e^{|A|/2}\, \text{Erfc}\left[(1/z) + (Az/4)\right] \right.$$

$$\left. + e^{-|A|/2}\, \text{Erfc}\left[(1/z) - (Az/4)\right] \right\} \qquad (3.15)$$

where

$$A = 2a\theta/D;\ z = (2Dt)^{1/2}/a$$

$$\text{Erfc}(y) = 2/(\pi)^{1/2} \int_y^\infty e^{-x^2} dx$$

$$I(t,0) = \text{Erf}(1/z);\ \text{Erf}(y) = 1 - \text{Erfc}(y)$$

$$I(\infty,\theta) = 1 - e^{-2a\theta/D};\ \theta > 0 \qquad \text{(This is the probability}$$
$$= 0 \qquad\qquad ;\theta < 0 \qquad \text{of being able to "see}$$
$$\text{forev..r")}$$
$$(3.16)$$

and the mean time to first attainment of the boundary is determined to be

$$\underline{T}(\theta) = \left(\frac{2a}{D|\theta|}\right);\theta < 0$$

$$= \infty \qquad ;\theta > 0 \qquad (3.17)$$

Although relatively easy to obtain, these results have apparently not been previously published.

Since solutions for $\beta \neq 0$ will be more complex, we digress to see how well the above expressions represent real terrain statistics. For this purpose we use Stein's curves of the probability distribution of mask angle.[2]

Stein's curves, previously cited, were developed by computer processing of about 1200 points read from a map of a 144 x 72 mile area of Pennsylvania. From Stein's Figure 6, $I(\infty, \alpha)$ was read and has been replotted as $1 - I(\infty, \alpha)$. For the small values of α involved, $\alpha = \theta$. As shown in Figure 3-8, the exponential relationship of Equation (3.16) fits the map-generated points incredibly well. The inferred value of $D/2a$ from the fitted line is 0.044, i.e., tan 2.5°.

Next solving Equation (3.15) for $\alpha = -2.5, 0$ and 2.5 degrees, it is determined by trial and error that $I(t,0)$ fits the corresponding map derived data fairly well, if 'a' is chosen to be 11 meters. Figure 3-9 shows the agreement between the $I(t,\alpha)$ curve computed from Equation (3.16) with $D/2a = 0.044$ and $a = 11$ meters, and the points derived from the map data.

For zero and positive α, the agreement is much better than the accuracy to which the published map curves can be read. For negative α the agreement is poor. This is not surprising, since for the Wiener process, there is no regression to the mean by the process.

Whether the observed agreement between the data points and the two-parameter fit of the model is fortuitous or will hold up over other terrain samples remains to be investigated. Figure 3-9 provides substantially encouragement for this method of approach.

Although the corresponding computations have not been done, brief examination of the variation of the mask angle distribution functions with sampling interval as given in Stein's report indicates some dependancy. This suggests the interesting possibility of determining this effect theoretically from the stochastic model.

Solutions for $\beta \neq 0$

For small β, solutions of the partial differential equation have been obtained by Weiss in some unpublished work, as a Taylor's series in β. To indicate the interesting functions which appear in attempting to find a closed form solution of the general case, we note that for $\theta = 0$, one obtains for $I(t,\theta)$

$$I(t,0) = e^{(X^2 - B^2)/4} \sum_{j=1}^{\infty} \frac{D_{-sj}(-X)}{\beta s_j[\partial D_{-sj}(-B)/\partial s]}$$

$$\times \left(e^{\beta s_j t} - 1 \right);\ X = x_0/\sigma$$

$$B = b/\sigma \qquad (3.18)$$

where the terms of the sum are evaluated for values of s_j determined by the zeroes of

$$D_{-sj}(-B) = 0 \qquad (3.19)$$

and

$D_s(y)$ is the parabolic cylinder function.

Tables of the zeroes and the partial derivatives with respect to the index have been computed by Weiss, in some unpublished papers.[11] The above expression was first obtained by Siegert in 1951 in connection with a different problem.[16]

The mean value $T(\theta)$ for a horizontal boundary has been obtained by Weiss as[11]

3-8

$$\underline{T}(0) = (1/\beta) \left\{ \frac{\partial \text{Log}_e \ D_0 \left[-x_0/(\sigma)\right]}{\partial s} - \frac{\partial \text{Log}_e \ D_0 \left[-b/(\sigma)\right]}{\partial s} \right\}$$

(3.20)

and for small b, x_0

$$\underline{T}(0) = (\pi/2)^{1/2} \frac{a}{\beta\sigma} - \frac{a\left(a + 2x_{0_2}\right)}{\beta\sigma^2} + \ldots ; a = b - x_0$$

(3.21)

3.1.6 Non-Gaussian Probability Density Functions

An intriguing characteristic of Equation (3.7) is that the formulation is not limited to linear relationships. It is thus possible to describe processes for which the steady state probability density function is not Gaussian.

Peterson[3] has pointed out that in studies of terrain statistics it has been found that the distribution of slopes, for example, is not Gaussian, but exponential, i.e.,

$$f(x) = \frac{1}{(2)^{1/2} \sigma} e^{-|x| (2)^{1/2}/\sigma}$$

(3.22)

A number of studies do indicate that the probability density function of terrain elevation deviations about the mean is often Gaussian.[17,20]

A minor modification of Equation (3.12) allows the generation of exponential probability density functions.

For a simplified example, consider the following form of Equation (3.12)

$$dx/dt = -\beta \ \text{sgn} \ (x) + v \ ; \ \text{sgn} \equiv \text{sign of}$$

(3.23)

then

$$\partial w/\partial t = \beta \ \text{sgn} \ (x) \ (\partial w/\partial x) + (D/2) \ (\partial^2 w/\partial x^2)$$

(3.24)

The steady state probability density function is found to be (on setting $\partial w/\partial t = 0$ in Equation (3.24) and solving),

$$w (x, \infty) = (\beta/D) \ e^{-(2\beta/D) |x|}$$

(3.25)

This simplified case has been given by Stratonovich.[16]

A comparison of some characteristics of the Gaussian and Laplace distribution functions (also known to the French as Laplace distributions Types I and II) is given in Table III-2.

For a terrain model one step more sophisticated than Equation (3.25) we may write

$$dx_1/dt = x_2$$

$$dx_2/dt = f_1 (x_1) + f_2 (x_2) + v$$

(3.26)

where

$x_1 =$ deviation of terrain height about its mean

$x_2 =$ terrain slope

If the stochastic process is assumed to be stationary, then the probability density functions of height and slope are independent of each other.

If $\quad f_1 (x_1) = -k \ x_1 \ ; \ f_2 (x_2) = -cx_2$ (3.27)

the problem is linear, and the probability density functions are Gaussian. If either (or both) of the f is of the form

$$f(x_j) = -k_j \ \frac{x_j}{|x_j|} = -k_j \ \text{sgn} \ (x_j) \ ; \ \text{sgn} \equiv \text{sign of}$$

(3.28)

then the corresponding steady state probability density function is Laplacian.

In this case the Kolmogorov partial differential equations are still linear in each quadrant of the (x_1, x_2) plane, with continuity of x_1, x_2 across the axes. dx_2/dt_1 is discontinuous. Hence a solution can be obtained in each quadrant, and coefficients matched at the axes by the continuity conditions.

The simple type of non-linearity described above is of particular interest because of the frequency with which Laplacian probability density functions turn up in analysis of physical problems. It has been observed in measurements of the deviations in altitude of an aircraft attempting to fly a constant altitude path as shown in Figure 3-10. In the terrain problem, Peterson has determined by computation on terrain samples, that the probability density function of slopes is Laplacian.

Weiss has obtained the Laplace-Markov expression corresponding to the Gauss-Markov expression given
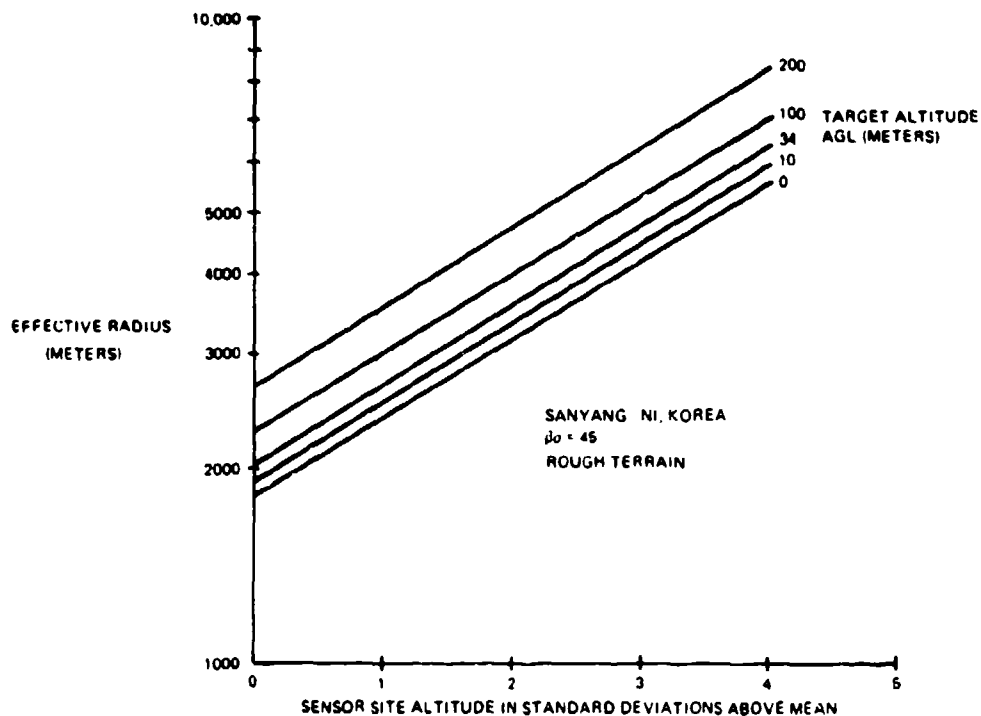
Figure 3-7. Effective Site Radius for Rough Terrain
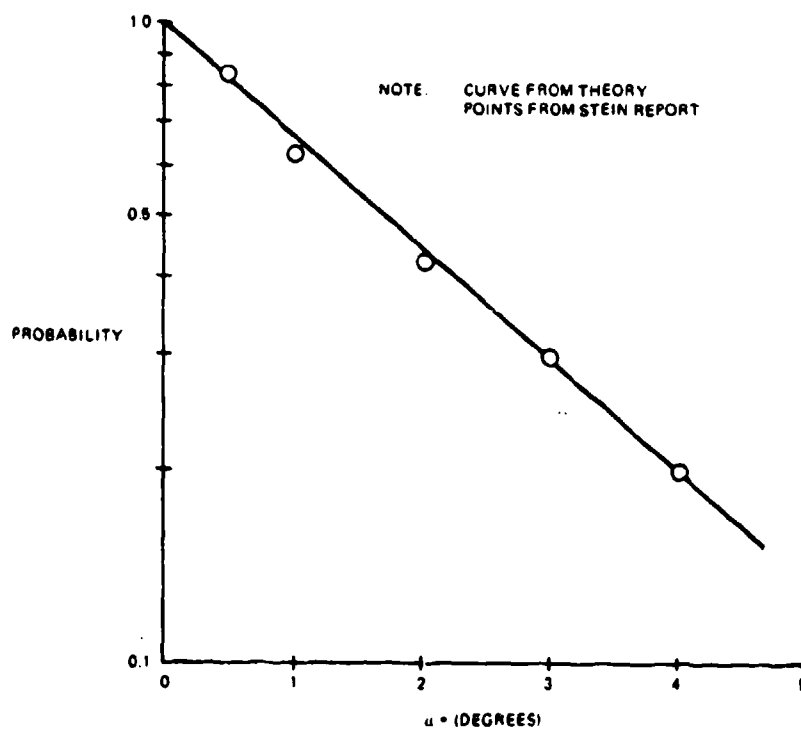
Figure 3-8. Probability of Not Having an Uninterrupted Line of Sight to all Ranges versus Elevation Angle
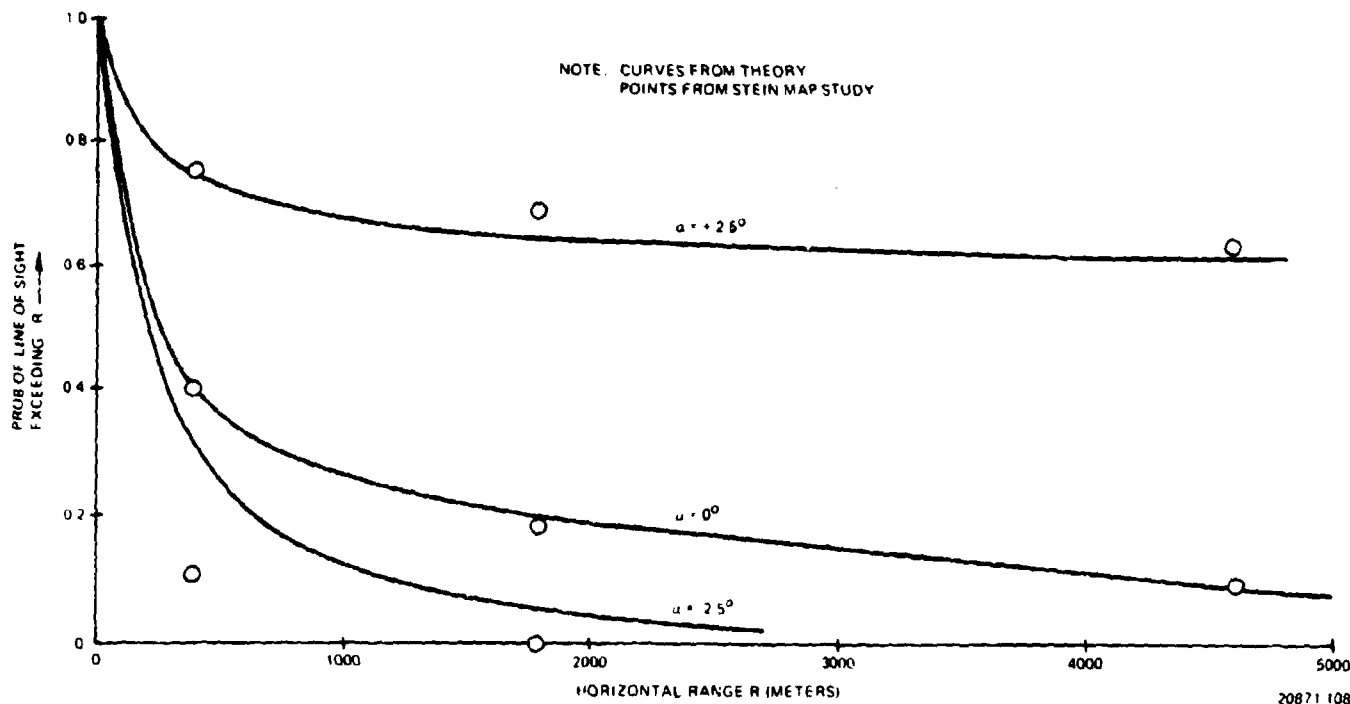
Figure 3-9. Probability of Unobstructed Line of Sight Exceeding Range R versus Elevation Angle of Sight Line

in Equation (3.14) in an unpublished paper. It is moderately but not excessively more complex.

3.1.7 Stationary Processes in a Plane

The line transect model discussed to this point has one obvious deviation from correspondence with the physical process and that is that terrain points along the transect are certainly correlated with those on adjacent and parallel lines, as well as those on the line. The consequences have been pointed out by Whittle, Peterson, and others.

One of the difficulties is that it is difficult and perhaps impossible, to describe a stationary stochastic process in a plane which will yield a simple exponential correlation along a transect.

Whittle suggests as the simplest second order scheme

$$[(\partial/\partial x)^2 + (\partial/\partial y)^2 - k^2]\, z(x,y) = v(x,y) \quad (3.29)$$

where w(x,y) is the two-dimensional equivalent of a Wiener process. Then the autocorrelation between two points spaced r apart in the plane is

$$\rho(r) = kr\, K_1(kr) \quad (3.30)$$

This Bessel function is very close to the simple exponential in shape, and perhaps explains why one can get useful approximations along a line transect with processes having a simple exponential correlation.

Heine[7] has generalized Whittle's formulation to a number of non-isotropic cases.

Since siting problems in air defense are really problems in the variation of a function over a plane, this general line of investigation has some practical interest. However, only one reference has been located which makes this application.[22] It is clearly an important area for applied mathematical research.

3.1.8 Approximations by the Concept of Bandwidth

In considering a stationary stochastic process, the concept of bandwidth is related to the minimum interval of time across which samples may be considered to be independent. Bandwidth is usually defined in terms of power spectral density, but it is directly related to the zero crossing rate of the process. The relationships are developed below and summarized in Table III-3.

The assumption of a stationary process allows the level crossing rate to be expressed very simply as

3-11

Table III-2. Comparison of Probability Density Functions

Single Variable: x		
Function Type	Gaussian	Laplacian
Range	$-\infty \leqslant x \leqslant \infty$	$-\infty \leqslant x \leqslant \infty$
Mean	μ	μ
Standard deviation	σ	σ
Probability density function	$\dfrac{1}{(2\pi)^{1/2}\sigma}\, e^{-\frac{(x-\mu)^2}{2\sigma}}$	$\dfrac{1}{(2)^{1/2}\sigma}\, e^{-(2)^{1/2}|x-\mu|/\sigma}$
Characteristic function	$e^{is\mu - (s^2\sigma^2/2)}$	$e^{is\mu}/[1+(\sigma^2 s^2/2)]$
Mean modulus $< |x| >$	$(2/\pi)^{1/2}\sigma$	$\sigma/(2)^{1/2}$
Probability of exceeding $(x-\mu)/\sigma = 5$	3.3×10^{-5}	1.7×10^{-3}

Difference of Two Independent Variables: $y = x_1 - x_2$

Individual Function Types	Gaussian	Laplacian
Mean: μ_y	$\mu_1 - \mu_2$	$\mu_1 - \mu_2$
Standard deviation: σ_y	$\left(\sigma_1^2 + \sigma_2^2\right)^{1/2}$	$\left(\sigma_1^2 + \sigma_2^2\right)^{1/2}$
Characteristic function	$e^{is\mu_y - (s^2\sigma_y^2/2)}$	$e^{is\mu_y}[1+(\sigma_1^2 s^2/2)]^{-1}[1+(\sigma_2^2 s^2/2)]^{-1}$
Probability density function	$\dfrac{1}{(2\pi)^{1/2}\sigma_y}\, e^{-\frac{(y-\mu_x)^2}{2\sigma_y^2}}$	$(2\sigma_y)^{-1}\left[1+\dfrac{2^{1/2}|y-\mu_y|}{\sigma_y}\right]e^{-2^{1/2}|y-\mu_y|/\sigma_y}$ For $\sigma_1 = \sigma_2$ only
Mean modulus $< |y| >$	$(2/\pi)^{1/2}\sigma_y$	$(3/4)\sigma_y$

20871-700

3-12

$$N(b) = p(b) \langle |\dot{x}| \rangle \qquad (3.31)$$

where

$N(b)$ = the average crossing rate of level $x = b$

$\langle |\dot{x}| \rangle$ = the expected value of the absolute rate of change of deviation x

$p(x)$ = the probability density function of x

The term $\langle |\dot{x}| \rangle$ is related to the standard deviation of dx/dt by the probability density function of dx/dt and since we consider the possibility that x may be a non-Gaussian variable, we should allow the same possibility for dx/dt.

If the autocorrelation of position deviations $\rho(s)$ is known, the variance of dx/dt, i.e., σ_v^2 is related to the variance of position, σ_x^2 by

$$\sigma_v^2 = \sigma_x^2 \left[-d^2 \rho(0)/ds^2 \right] \qquad (3.32)$$

The 'effective bandwidth' of a stationary process is often defined as

$$\omega_{eff}^2 = \int_{-\infty}^{\infty} \omega^2 \phi(\omega^2) \, d\omega \qquad (3.33)$$

where $\phi(\omega^2)$ is the Fourier transform of the autocorrelation and vice versa. The time, T_s, between independent samples is the inverse of the effective bandwidth. As a result of the above relationships

$$\omega_{eff} = \sigma_v/\sigma_x \qquad (3.34)$$

$$T_e = \sigma_x/\sigma_v \qquad (3.35)$$

We now apply some of these ideas to the terrain problem.

First consider those problems which are associated with the use of a line transect. The 'bandwidth' concept, which is very useful in servomechanism analysis, is that one can define a distance along the line, L, such that two samples of elevation taken a distance L apart, may be considered to be independent. Defining x as distance along the transect from the sensor and y as altitude, consider the probability that an unobstructed line of sight exists to horizontal range x, at an angle $\tan^{-1} \theta$.

There are n samples to x,

$$x_T = nL \qquad (3.36)$$

At the j'th sample, the sight line has a height at step midpoint

$$y(j) = y(0) + j L \phi \qquad (3.37)$$

If terrain height about its mean is described by the probability density function $f(y)$, the probability that the sight line is not obstructed in the j'th interval is

$$q(j) = \int_{-\infty}^{y(0) + j L \phi} f(y) \, dy \qquad (3.38)$$

and so the probability of a clear line of sight at least to x_T is

$$q(x_T) = \prod_{j=1}^{h} q(j) \qquad (3.39)$$

A bandwidth analog to the area problem can be devised by assuming that the terrain is divided into a number of hexagons of equal size, with dimensions such that the terrain elevation across hexagons can be assumed to be uncorrelated.

The problem then reduces to one of either computing $S(j)$ in the linear problem or finding good approximations to the product, with simpler operations to find the probability of specified arcs of clear sight about the sensor at specified range in the area problem.

To obtain the mean sighting distance at an angle $\tan^{-1} \theta$, $\underline{x}$ set $p(j) = 1 - q(j)$.

Then for the line transect case,

$$\underline{x}/L = p(1) + 2 q(1) p(2) + \ldots$$

$$= 1 + q(1) + q(1) q(2) + \ldots \qquad (3.40)$$

and for the area problem, the mean clear area about the site is

$$\underline{A}/A_{hex} = p(1) + 6\, q(1)\, p(2) + 12\, q(1)\, q(2)\, p(3) + \ldots$$

$$= 1 - q(1) + 6\, [\, q(1) + q(1)\, q(2) + \ldots\,]$$

(3.41)

For a level line of sight, $\theta = 0$ and

$$\underline{x}/L = 1/p$$

$$\underline{A}/A_{hex} = p + q\, (q/p) \qquad (3.42)$$

One method of approximating the sums indicated above is the following,

Let $\quad l\,(j) = (\underline{x}/L)$ summed to the j'th term only

Then $\quad l\,(j+1) - l\,(j) = [l\,(j) - l\,(j-1)]\, q\,(j+1) \qquad (3.43)$

Expand in a Taylor's series in j and retain only the first three terms

$$\partial^2 l / \partial j^2 + 2\,(\partial l / \partial j)\,\left[\frac{1 - q\,(j+1)}{1 + q\,(j+1)} \right] = 0 \qquad (3.44)$$

Depending on the form of q, this expression may be integrable.

3.1.9 Level Crossing Methods

The problem of determining the average crossing rate of a specified level by a stochastic process is simpler by an order of magnitude than the problem of determining the probability of a first crossing at a specified distance given an initial position for the process realization.

In addition, thanks to work by Cramer and Leadbetter,[12,13,14] only a slight increase in difficulty is incurred in determining the average number of crossings of an arbitrarily specified curve (with continuous first derivative) over a given interval.

When the expected number of crossings is small, this number is a good approximation to the probability of at least one crossing. When the expected number of crossings is not small, we have the familiar problem of correlation of successive bullets in kill probability computations, namely that one cannot get the probability of at least one crossing on a specified sample precisely from the expected number of crossings.

Because the crossing rate approach is computationally simple, however, it is worth investigating to use as a guide for obtaining possible empirical functions to fit real terrain data.

At this point we note simply the expression developed by Cramer-Leadbetter for the expected number of crossings of the line a + bt (the sighting problem) of a stochastic process with normal probability density function (the method is applicable to other pdf's as well, and to other curves). The expected number of crossings in the interval (0,T) is

$$C = [2\,(\sigma_2/b)\, \phi\,(b/\sigma_2) + 2\, \Phi\,(b/\sigma_2) - 1]$$

$$\times \left[\Phi\left(\frac{a+bT}{\sigma} \right) - \Phi\left(\frac{a}{\sigma} \right) \right]$$

$$\phi = \sqrt{\frac{1}{2\pi}}\, e^{-x^2/2} \; ; \; \Phi\,(x) = \frac{1}{\sqrt{2\pi}} \int_{-\infty}^{X} e^{-t2/2}\, dt$$

(3.45)

where

σ is the standard deviation of position.

σ_2 is the standard deviation of velocity and can be obtained from the autocorrelation function by twice differentiating.

Note: The method does not apply to the case of simple exponential correlation.

The expression for C can also be rewritten in terms of bandwidth which allows a comparison for this computation with the bandwidth approximation given earlier.

Note the three dimensionless ratios which define C

$$(b/\sigma_2); (a/\sigma); (bT/\sigma)$$

20871-601

These can be related to similar dimensionless ratios in the other approximation schemes.

If we ask for the expected number of crossings of a positively inclined line of sight extending to infinity, we observe that C is finite, and is the product of two terms, one of which compares the slope of the sight line with the rms velocity of the process, and the other of which compares the initial height of the sight line with the position standard deviation of the process.

3-14
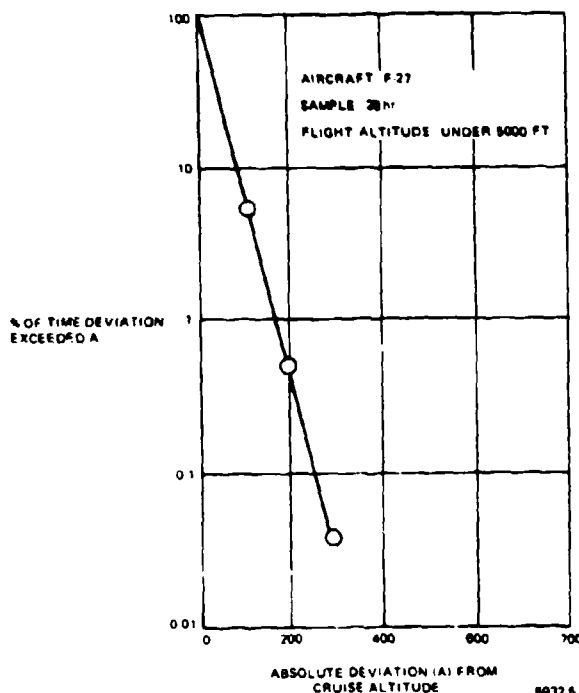
Figure 3-10. Distribution Function of Altitude
Deviations in Low-Level Flight

3.2 WEATHER AND ILLUMINATION

Given a geometric line of sight to a target, the actual detection of the target depends on the sensor characteristics and the characteristics of the intervening atmosphere.

Weather has such an important effect on military operations that its interaction with military systems capabilities and requirements deserves far more effort than is usually devoted to it in systems evaluations. The following sections are far from definitive, but attempt to outline the effect of weather on system operation, and the kinds of information and its usage required for a comprehensive analysis.

Both attacker and defender have the simplest problem in day, clear weather operations. In the absence of a defense, the attacking aircraft can use relatively inexpensive fire control, iron bombs, and close to a release range that insures a high probability of target destruction. Provision of an effective day, clear weather defense forces the attacker to more costly options, such as standoff missiles, or night operations. Both attacker and defender suffer equipment performance degradation in inclement weather.

3.2.1 Night Operations

A rough indication of the cost of providing a night attack capability for tactical aircraft is provided by an Aviation Week estimate of $285,000 initial cost for a package to be installed in the A-7D including FLIR, a laser designated target tracker, a modified head up display and the interface with the IBM computer.[44] The provision of flexibility of attack mode (level, glide, toss, loft and over the shoulder) and some freedom of maneuver during an attack pass in the A-7 fire control system is reflected in open source estimates of the increase in A-7 flyaway costs through successive models, given in Table III-4.[43]

There are various options for providing a nighttime capability for the defense, including radar, infra-red and light amplification sensors. Historically, the first response of the attacker to an effective day defense has been to develop a capability for night operations. It seems conservative to establish and maintain a requirement for night capability for defense against air attack.

3.2.2 Effect of Weather on the Attacker

Tactical air has developed and is improving its capability for effective night operation. The limitations of unfavorable weather, however, are still severe in spite of modern technology. These limitations are clearly indicated by the following reports on air operations in Vietnam.

'Shielded from the counterattacks of the U.S. fighter-bombers by low-lying monsoon clouds, the Communists advanced with virtual immunity.[23]

'Last week, whenever the cloud cover lifted, the flyers could sight the enemy on the ground ... Last week's bad weather compelled the flyers to take even more risks than usual. Fighter-bombers had to slice below the overcast to 'unload their ordnance' at heights of only 500 ft. or so. At that low altitude even a rifle bullet can bring down a jet if it strikes a vulnerable point.'

'A lot of 23 mm and 37 mm antiaircraft artillery have been moved south since the offensive began,' said Pekkola, (a forward air controller flying a Cessna). 'Usually they aim at any break in the clouds because they know that's where we'll be.[24]

'In the first days of the North Vietnamese drive, poor weather kept most allied strike aircraft grounded, and Saigon's forces reeled in retreat. But once the skies cleared, U.S. and South Vietnamese attack planes went to work catching enemy troops, supply trains and armor out in the open in conventional formations.[25]

'As low clouds and drizzle kept U.S. Phantoms on the ground, South Vietnam's own 700-plane Air Force took on an important role in the fighting; its ancient but effective Skyraiders, flown with daring by South

Table III-3. Comparison of Autocorrelation Functions

Autocorrelation of Position	$\epsilon^{-a|s|}$	$\epsilon^{-a|s|}[\cos bs + (a/b)\sin b|s|]$	$(be^{-a|s|} - ae^{-b|s|})/(b-a)$
Effective Bandwidth	∞	$a^2 + b^2$	ab
Ratio of Velocity Variance to Position Variance	∞	$a^2 + b^2$	ab
Autocorrelation of Velocity	—	$\epsilon^{-a|s|}[\cos bs - (a/b)\sin b|s|]$	$(be^{-b|s|} - ae^{-a|s|})/(a-b)$
Zero Crossing Rate Gaussian	∞	$(a^2 + b^2)^{1/2}/\pi$	$(ab)^{1/2}/\pi$
Laplacian	∞	$(a^2 + b^2)^{1/2}/2$	$(ab)^{1/2}/2$

20871-701

Table III-4. Comparison of A-7 Aircraft Costs

Model	Aircraft Flyaway Cost	Electronics Costs	Electronics % of Total Cost
A-7A	$1,400,000	$210,000	15%
A-7B	$1,440,000	$260,000	18%
A-7E	$2,500,000	$620,000	24%

20871-501

Vietnamese pilots at treetop level, have accounted for a large portion of the more than 100 Communist tanks knocked out in the fighting so far.[96]

'North Vietnamese troops ... tightened the grip on nearby Quang Tri and bombarded the provincial capital during a rainstorm that all but precluded air strikes in support of the city's defenders.[97]

Even in the case of lesser (and more frequent) weather problems of ceiling and visibility, it has been reported that, 'Experience has fairly well established that the weather-caused degradation of accuracy is virtually zero if the cloud ceiling is above 12,000 ft.

and visibility is about 7 miles or more, and that the degradation is close to 100 percent with a ceiling below 3,000 ft. or visibility is less than 2 miles.[34]

Figure 3-11, reproduced from the report by Huschke[34] shows these bounds by season and time of day for Sinuiju, North Korea. The probability contours indicate that only in January through April will there be a better than 80% chance of no degradation in dive bombing by day. It will be noted that the probabilities tend to be higher by night.

A similar study by Greenfield[38] describes a diurnal variation year round at Luang Prabang, Laos, where
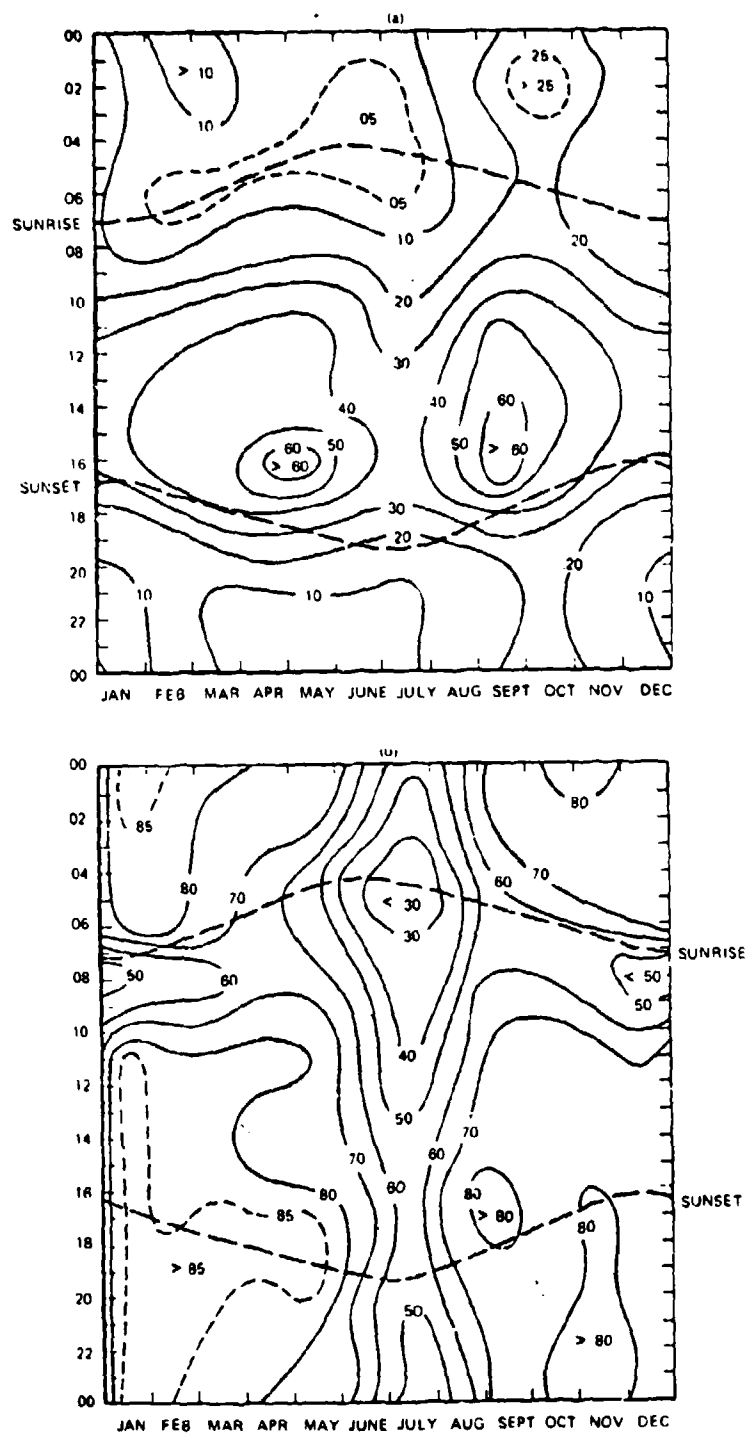
Figure 3-11. Joint ceiling and visibility probabilities for Sinuiju, North Korea, calculated as a function of month and hour (smooth dashed curves show times of sunrise and sunset). (a) Ceiling ≥ 10,000 ft and visibility ≥ 7 mi. (b) Ceiling ≥ 3,500 ft and visibility ≥ 5 mi.

3-17

the ground in the Mekong river valley region is obscured by ground fog in the morning with 50-75% probability the year round, but the afternoons are relatively clear over 90% of the time.

With fairly complete low level cloud cover, but good low level visibility, the attacker would be less likely to undertake dive bombing attacks as opposed to low level shallow dive or level attacks, if he depends on visual or IR sensors. On the other hand, if the attacker has a bombing radar system and the defense has no radar, the attacker is at a considerable advantage in a dive bombing attack through the cloud layer.

In addition to sensor problems created for the attacker by weather, high wind velocities and associated low level turbulence will limit his ability to fly nap of the earth.

3.2.3 Effect of Weather on the Defense

The relative effect of weather on attacker and defender depends on the sensors with which each is equipped. How much all-weather capability to provide for the defense depends on intelligence estimates of probable all weather capabilities of potential enemies. Specific effects on the defender's sensors are discussed in later paragraphs.

However, unfavorable weather can also degrade the defender's ability to move, to operate and maintain equipment, and large deviations in meteorological conditions may degrade performance if the system is not designed to compensate for meteorological changes.

3.2.4 Degradation of Sensor Performance by Weather

Table III-5, from Huschke,[33] lists a number of descriptors of weather and sensors subject to degradation by each. With increasing usage of optical and infra-red sensors by the defense, it is clear that supporting studies are required to determine, as a function of the probable theaters of operations, with what frequency they will be degraded or made inoperative.

Two descriptors associated with optical sighting range are the degree and height of cloud cover, and the horizontal (meteorological) visibility. One can often have low cloud cover, but good low angle visibility. Figure 3-12 shows these characteristics for a Finnish[32] airfield. Substantially lower horizontal visibility ranges are experienced, for example, in West Germany, as indicated in Figure 3-13.

Some worldwide averages on cloud cover[31] shown in Figure 3-14 indicate that less than half the time can one see blue sky straight up, and also that on the average the densest cloud layers center at about 5000 ft altitude.

Minimum requirements for an evaluation of defense system effectiveness for a specified operational theater would include joint probability density functions of ceiling and meteorological visibility, and of duration and amount of precipitation.

3.3 SENSORS

The principal current sensors for surveillance and initial target detection are the human observer and radar. The man can detect both visually and aurally. Under conditions of limited visibility the man will hear fast targets before he can see them, and even in day, clear weather, he may be able to hear nap of the earth flying helicopters long before he sights them.

Radar surveillance sets may have the future disadvantage of attracting radar-homing missiles. Increasing usage of distributed acoustic sensors on the battlefield may provide an alternate, or supplemental low cost means of providing surveillance information for local air defense.

Other possible sensors for surveillance which are not examined in this section are infra-red and various light intensification devices in the visual range. Although these are used for tracking, no current system is known which employs them for surveillance and initial detection.

3.3.1 Visual Detection

Among the factors that determine whether a human observer can detect a target visually are the target brightness, size, shape, color, range, background brightness and color and the angle of incidence of the sun's rays on the target and the observer's eye.[45,46]

Intensive experimental studies carried on during World War II indicated that in visual search for aircraft color and shape had minor effects on probability of seeing, compared with the other parameters, and could be neglected for most practical purposes.

For detection at low light levels, target and background brightness must be considered separately, but for daylight sighting these combine in a single parameter describing the target contrast against its background.

There is sufficient information on the complete process of target detection by the human eye to develop rather detailed models, however, considering the variety of tactical and environmental parameters which affect probability of sighting, some relatively simple approximations are considered in this section.

Early and classical experiments by Craik indicate that the threshold contrast above which a target can be detected can be represented as

$$C_t = 1.75\,\theta^{1/2} + \frac{19\,\theta}{a^2} \qquad (3.46)$$

where C_t is contrast in percent, the numerical coefficients are given for foveal vision, θ is the angle of the target off the center of the fovea (central part of the retina) in degrees, and α is the angle subtended by the target (represented as an equivalent circle) at the eye in minutes. A similar expression with different coefficients applies for other retinal regions.

This expression gives the minimum contrast as a function of angle-off of a target; to obtain the absolute minimum contrast for an on-axis target, set $\theta = 0.8°$.

For a target with contrast C_t, detection is not certain and C_t is computed as the point at which probability of detection is 57%. For other ratios C/C_t the 'glimpse' probability of detection can be approximated as a cumulative normal curve, so that the glimpse probability g is

$$g = f(C/C_t) \qquad (3.47)$$

The "intrinsic" contrast of a target against its background is defined as

$$C_o = (B_o - B_b)/B_s \qquad (3.48)$$

B_o = intrinsic brightness of the target

B_b = intrinsic brightness of the background

B_s = brightness of the sky

There is sufficient information on target reflectance, background reflectance and sky brightness of develop expressions for C_o explicitly in terms of sun angle, target and observer position. However, for present purposes, we use the following values for daylight viewing,

C_o = 30% if the target background is sky

C_o = 20% if the target background is terrain

The presence of haze in the atmosphere between the observer and the target reduces the apparent contrast as seen by an observer and is customarily approximated as

$$C = C_o\,e^{-\beta R/V_m} \; ; \text{ where } \beta = 3.44 - 3.912 \qquad (3.49)$$

where

R = range to the target

V_m = meteorological range (loosely defined as the maximum range at which large objects such as mountains can be seen against the sky. The lack of precision in the definition accounts for the range in the coefficient)

The effect of increasing contrast and/or target subtended angle is to increase the angle off the foveal axis at which a target can be detected. This angle increases very rapidly as target range decreases, once the target has come within the maximum range of detectability.

The effect of rain can be expressed by using

$$V_m = k_r\,a^3/z \qquad (3.50)$$

where a is the mean radius of the droplets and z is the rate of rainfall in cm/sec. However, this expression is pessimistic for very large drops as in a heavy thunderstorm, which for the same rainfall rate may be less opaque than a drizzle. Appropriate values for the coefficient and range of applicability will be found in Middleton.[45]

The maximum range of sighting at the 50% probability level for the complete spectrum of target size, contrast, meteorological range and background luminance, from clear high noon to overcast starlight by night can be obtained when desired, from a set of nomographs in Middleton.[45]

Cumulative Detection Probability

The function of the principal interest in system evaluation is the cumulative probability of target detection over a number of glimpses, each of which may be directed at a different part of the sky as the observer searches for a target.

A common method of estimating cumulative detection probability versus search time is to assume that the search process can be described as a sequence of 'scans' during each of which the probability of detecting a target is independent of the probability of detection in any other scan. The method can be extended to processes in which successive glimpse probabilities are correlated, but the simplest formulation is appropriate here.[46]

Define

p(r) = single scan probability of detecting a target at range r

3-19

Table III-5. A Sample of Sensors and Weather Parameters That Degrade Performance

Factor Causing Degradation	Sensor					
	LLLTV	IR	TV-Guidance	Laser	Eye	Radar
1. Precipitation	•	•	•	•	•	•
2. Visibility { haze	•	•	•	•	•	
{ fog	•	•	•	•	•	
{ smoke	•	•	•	•	•	
3. Clouds	•	•	•	•	•	•
4. Humidity		•				
5. Temperature		•				
6. Wind		•				
7. Ice	•	•	•	•		
8. Turbulence				•		
9. Sun angle	•	•	•	•	•	

20871-502

$P(R)$ = probability that the target has been detected by range R

Assuming that successive scans are independent

$$P(R) = 1 - \prod_j [1 - p(r_j)]$$

$$= 1 - e^{\sum_j \text{Log}_e [1 - p(r_j)]} \qquad (3.51)$$

Approximate the sum by an integral. If the scan rate is v,

$$P(R) = 1 - e^{v \int_r \text{Log}_e [1 - p(r_j)] (dt/dr) dr} \qquad (3.52)$$

$p(r_j)$ may vary with target aspect on a passing course, and with other parameters. For the simplest case of a directly incoming target $P(r_j)$ depends only on r_j and $dr/dt = V$ = target velocity. If $p(r) << 1.0$ the simplification $\text{Log}_e(1-p) = -p$ can be used, and this is often acceptable in computing cumulative detection probability even to very close ranges.

A man searching for a target 'scans' by intermittant eye movements, or jumps. Vision is not effective during eye motion, and detection can take place only during each 'fixation' which may have a duration of from 0.2 to 0.6 seconds. The search process is irregular, as compared with the search of a radar, for example. There is experimental information on the probability densities of fix duration and angular motion between fixes, but for present purposes we assume that there is some mean fixation rate which can be inferred from sighting data.

For a given target size and contrast, there is some threshold value of θ, which can be obtained from Equation (3.46), and which defines the solid angle within which a target may be detected with 57% probability in a single fixation. This solid angle multiplied by the fixation rate and divided by the solid angle scanned is closely proportional to the rate of target detection ρ. For area scan, the probability of detecting a target at constant range would then be, as a function of time

$$\rho_d = 1 - e^{-\rho t} \qquad (3.53)$$

Because of the inefficiency of the human scanning process, this expression is good only for small t, for large t the increase with time is less rapid than indicated by the expression.

3-20

PROB OF MET VIS
EXCEEDING RANGE V

PROB OF VISIBILITY EXCEEDING V METERS

MET VISIBILITY (THOUSANDS OF METERS)) V

PROB OF CEILING
EXCEEDING H METERS

PROB OF CEILING EXCEEDING H METERS

CEILING H (METERS)
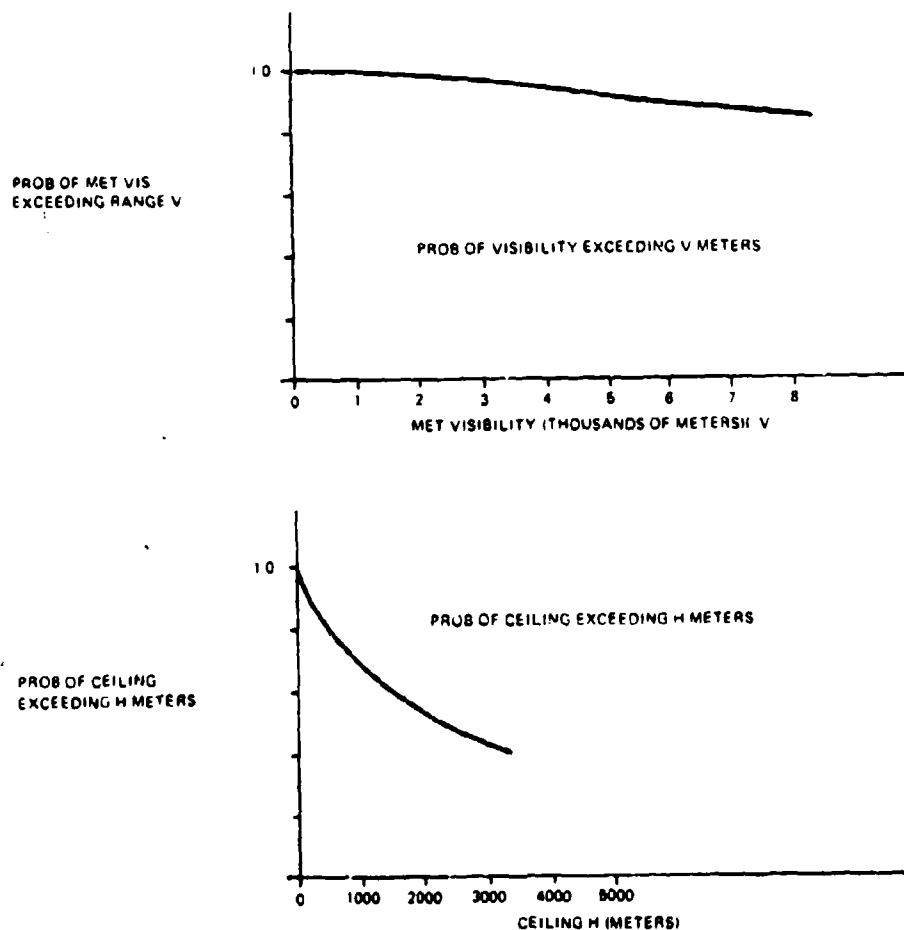
20871-111

Figure 3-12. Ceiling and Visibility at Kr·iununkyla Airport (Autumn)

By a process equivalent to the well known 'lethal area' computation, the probability density function for glimpse probability for an off axis target can be replaced by a step function, such that within a·. angle θ_o a target will always be detected, and outside θ_o it will not. If θ_o is the threshold angle from Equation (3.46) for specified contrast and target size, then

for line scan, $\theta_o = k_1 \theta_0$; $2.16 \leqslant k_1 \leqslant 2.56$

for area scan, $\theta_e = k_2 \theta_0$; $4.07 \leqslant k_2 \leqslant 5.05$

20871-602

where the smaller k values are the asymptotes for very small target subtended angles, and the large values are for very large targets.

3-21
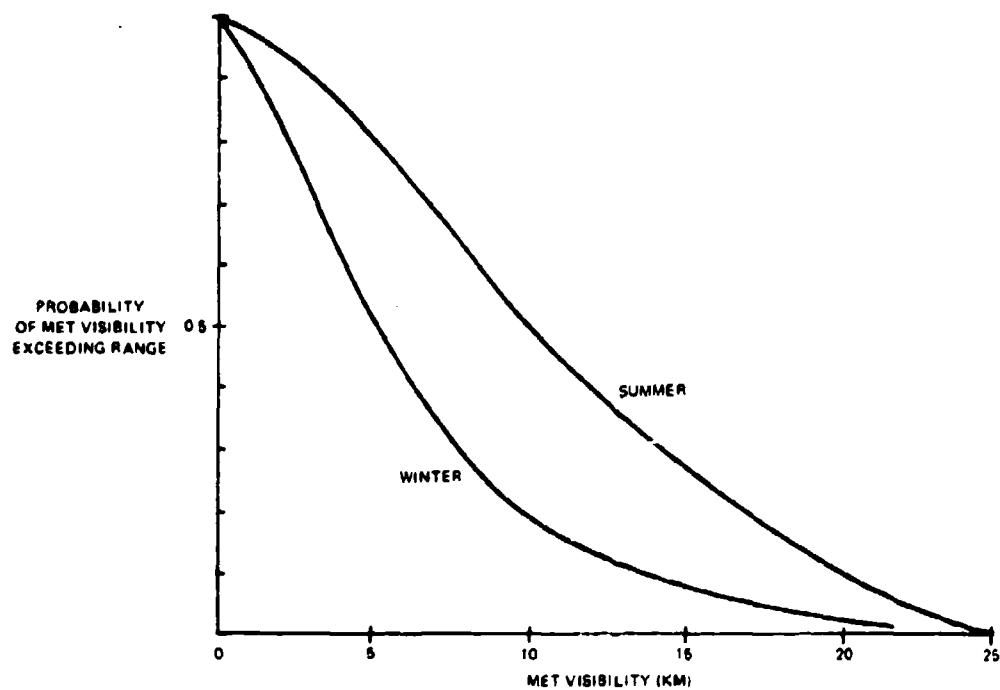
Figure 3-13. Average Meteorological Visibility in West Germany from Ground Meteorological Stations

PROBABILITY OF HAVING A CLEAR LINE OF SIGHT

(1) TO GROUND FOR NEGATIVE ANGLES
(2) TO HORIZON FOR ZERO ANGLE
(3) TO BLUE SKY FOR POSITIVE ANGLES
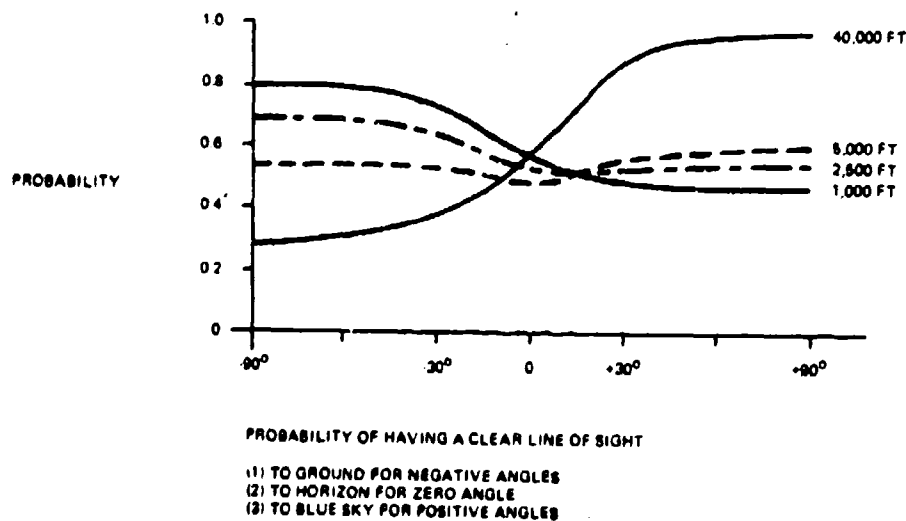
Figure 3-14. Worldwide Averages, Northern Hemisphere, 72,000 Observations, All Seasons

Then for line scan

$$\rho = k_4 \theta_o / \theta_s \; ; \; \theta_s = \text{angular sector scanned} \qquad (3.54)$$

and for area scan

$$\rho = k_5 \theta_o{}^2 / \Omega \; ; \; \Omega = \text{solid angle scanned} \qquad (3.55)$$

Consider the expression

$$C = a\theta_o{}^{1/2} + b\theta_o$$

where C is target contrast as seen by the observer at some specified range. For small target size the expression is dominated by $b\theta_o$. Hence, we can write

$$\theta_o = (C/b)$$

$$= (C a^2 / 19)$$

$$= K/R^2 \; e^{-K_2 R/V} \qquad (3.56)$$

The target detection rate then might be expected to vary with range about as

$$\rho = K_3 / R^a \; e^{-K_4 R/V} \qquad (3.57)$$

where the exponent a depends on the amount to which the observer scans vertically as well as horizontally (in searching for low altitude targets he may approximate line scan).

Even with unlimited meteorological visibility one might expect a value in the e^{-aR} term accounting for the threshold detection probability density function.

The expression Equation (3.57) was proposed by Glanzmann[49] with a = 2.0 and was developed from theoretical considerations not available at the time of writing the present report. He determined the coefficients experimentally and found that he could make an excellent fit to cumulative probability of detection data, also obtained experimentally.

The foregoing expressions are intended to give some plausibility to Equation (3.57), which will be compared against experimental sighting data. With some additional expenditure of effort a more rigorous development of an approximate form for r, including sighting at low light levels is possible. Currently there appears to be no intermediate set of expressions in the literature between the simplest expressions for sighting rate, and the rather complex computer simulation modules.

Using Equation (3.57), the cumulative probability of detecting a directly incoming target by range R is

$$P(R; \infty) = 1 - e^{-K_3/V} \int_R^\infty R^{-a} \; e^{-K_4 R/V_m} dR$$

$$= 1 - e^{-E(R; \infty)} \qquad (3.58)$$

Experimental Data

From sighting data[50,53,54,55] taken under conditions of essentially unlimited visibility, the cumulative probability of target detection is available for four values of search angle. These are also shown in AFAADS-I, (page 4-68). Figure 3-15 shows $-\text{Log}_e(1-P)$ plotted versus range on log-log paper. Approximate computations of the derivative with respect to R, which we identify with the function

$$dE/dR = K_3/V \; R^{-a} e^{-K_4 R/V_m} \qquad (3.59)$$

are shown in Figure 3-16.

Finally, plotting $R^2 \; dE/dR$ versus R on semi-log paper, we find that for the wide scan data this function is proportional to e^{-aR}, and for the limited scan data the exponential relations holds above about 3000 yards, as shown in Figure 3-17.

The peak in the limited scan curve requires further study. It is possible that it results from the plan of the experiment, in which a 360° coverage was always achieved by assigning sectors to multiple observers. For example, there were four observers for 90° sector assignments. It is possible that targets crossing a scan boundary 'fell between the chairs' in academic terms, and this would be most likely to happen at short ranges.

In this experimental data meteorological visibility was essentially unlimited, and so we identify the residual exponential with the variation of glimpse probability with apparent target size, for constant target contrast. We then obtain the expressions

$$45, 90° \text{ scan}, f(R_1) = 9.0 \; R_1{}^2 \; e^{-R_1/4}; R_1 = R/1000$$

$$180-360° \text{ scan}, f(R_1) = 3.5 \; R_1{}^2 \; e^{-R_1/4} \qquad (3.60)$$

For limited visibility, multiply f(R) by $e^{-3.44 \; R/V_m}$

Generalized Approximation for Cumulative Detection Probability

Using the form

$$f(R) = KR^{-2} e^{-\lambda R} \qquad (3.61)$$

$$P(R; \infty) = 1 - e^{-E(R)}$$

$$E(R) = K \int_R^\infty R^{-2} e^{-\lambda R} dR = KR^{-1}\Big[e^{-\lambda R}$$

$$+ \lambda R \, E_i(-\lambda R)\Big] \qquad (3.62)$$

where $E_i(-\lambda R)$ is the exponential integral function.

For large λR,

$$E(R) = e^{-\lambda R}/(\lambda R^2) \Big[1 - 2(\lambda R)^{-1}$$

$$+ 6(\lambda R)^{-2} \cdots \Big]$$

For small λR,

$$E(R) = R^{-1}\{1 + (\lambda R)(C-1 + \log_e \lambda R)$$

$$- (\lambda R)^2/2 + \cdots\} \quad C = 0.577$$

$$(3.63)$$

The function $\Big[e^{-X} + X\,E_i(-X)\Big]$ is plotted in Figure 3-18 as $g(\lambda R)$.

Using the above relations, the original cumulative sighting data under desert conditions of unlimited visibility has been adjusted to lesser conditions of meteorological visibility[67] and is shown in Figure 3-19.

The curves are based on the 45-90° scan data, ignoring the maximum of Figure 3-17. Hence, they slightly over-estimate the cumulative detection probability as this probability approaches unity. However, they do show a marked reduction in detection probability versus range under atmospheric conditions less ideal than those of the desert experiments.

Using hindsight, we note that the very simple approximation to $g(R)$

$$g(R) = 0.5 \, e^{-c\lambda R} \qquad (3.64)$$

would be equally valid at long ranges, and would reduce the amount of overestimation at short ranges.

Modification of Cumulative Detection Function for Other Exposure Ranges and Target Speeds

In the experimental data represented by Figure 3-15, the targets were initially exposed to an unobstructed geometric line of sight at very long, essentially infinite range. We now indicate how this data can be adjusted to represent initial target exposure at shorter ranges, as may be obtained from the terrain models of Section 3.1. This is a simple computation as a result of the

form of Equation (3.52). For the same reason the adjustment for other target velocities is simple.

For a direct incoming course, where the target is first exposed at range R_e, define

$P(R; R_e)$ = the cumulative probability of detection by range R.

From Equation (3.52)

$$P(R;R_e) = 1 - e^{-E(R;R_e)} \qquad (3.65)$$

where

$$E(R;R_e) = (v/V)\int_R^{R_c} p(r)\, dr = \int_R^{R_c} f(r)\, dr$$

$$(3.66)$$

Define: $Q(R;R_e) = 1 - P(R;R_e) \qquad (3.67)$

Now assume that we have data on cumulative detection probability on paths on which the target was initially exposed at very long ranges, - essentially infinite. It follows from the above expressions that

$$Q(R;R_1) = \frac{Q(R; \infty)}{Q(R_1; \infty)} \qquad (3.68)$$

and so, from the single $Q(R; \infty)$ curve we can obtain the cumulative detection probability subsequent to any initial exposure range.

We should also expect that changes in target speed will affect the cumulative detection probability as

$$Q_2(R; \infty) = [Q_1(R; \infty)]^{(V_1/V_2)} \qquad (3.69)$$

where the data was taken at V_1 and it is desired to convert it to a target speed V_2.

The averaging over the probability density function of exposure range is also simple, although it may have to be done numerically. It is accomplished as follows.

Combination with Line of Sight Data

If $f(R_1)\, dR_1$ is the probability that a target is first exposed at a range R_1, we may obtain the probability that it will be detected by the time it reaches a range R as

$$\underline{P}(R) = 1 - \underline{Q}(R)$$

$$= 1 - Q(R, \infty)\int_R^\infty \frac{f(R_e)dR_e}{Q(R_e, \infty)}$$

$$(3.70)$$

3.3.2 Radar Detection

A table of a few characteristics of current surveillance radars for antiaircraft gun fire control is contained in the Effectiveness Model volume of this report. X, S, C and L band radars are all available. The
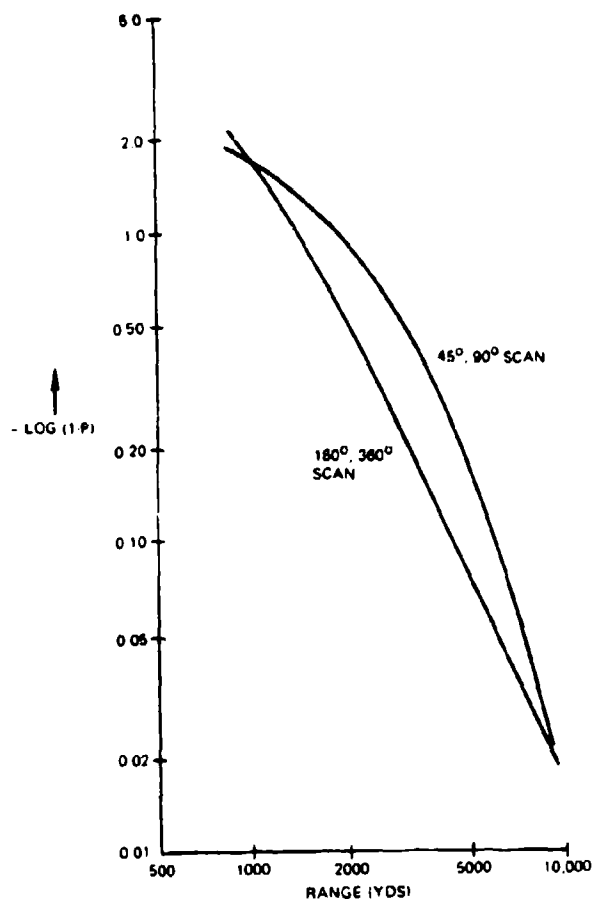
20871-114

Figure 3-15. Cumulative Glimpse Rate versus Range

2C871-115

Figure 3-16. Glimpse Rate versus Range

elevation beam pattern is typically cosecant^2 from 20-35° maximum, the scan rate is 45-60 rpm, the higher value typifying the latest models and detection ranges with 80% probability on a 1 m^2 target are 15-20 km. All of the radars listed in the table are of the coherent pulse doppler type, with radial velocity bands of about 10:1 above about 30-50 km/sec.

For present purposes the important characteristic is the maximum detection range, which, for an aircraft target greatly exceeds the effective range of the gun. Hence it seems reasonable to assume that, except in an effective ECM environment, or very heavy rain, high flying targets will be detected with ample time to acquire them for tracking and firing, and very low

flying targets, first exposed at short ranges, will be detected on the first scan, i.e., within one second.

The Mirador radar offers an automatic target alarm, track while scan on multiple targets, and automatic threat assessment. The surveillance-tracking radar set on the Skyguard fire control system provides automatic tracking radar put-on from surveillance radar detection. An estimate for the Swedish Ecstra system indi cates 4 seconds from detection to development of smooth tracking radar data.

Assuming proper functioning of the equipment, therefore, one might estimate no more than 4 seconds

3-25

$$\left(\frac{D}{1000}\right)^2 \frac{dE}{dD}$$

RANGE (YDS)

45°, 90° SCAN

180°, 360° SCAN
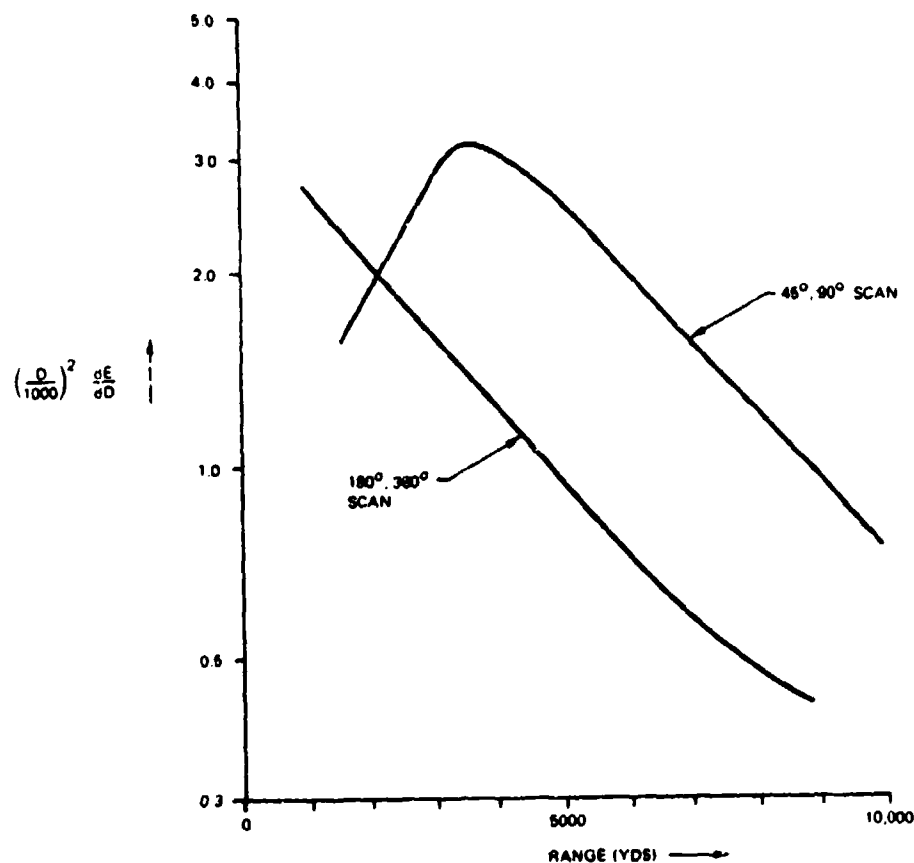
20871-116

Figure 3-17. Residual Function in Glimpse Rate versus Range

from target exposure to tracker lock-on against the more difficult short range targets.

For less sophisticated systems, the corresponding delay times might be expected to depend almost entirely on the human actions required to detect a blip, and transfer the data to the tracking sensor. These would depend on the system configuration and could be considerably in excess of 4 seconds.

Doppler Blind Zones

The minimum radial velocity of current coherent pulse doppler surveillance radars ranges from 30 m/s (Domino) to 50 m/s (Oeil Noir). The rate of change of target slant range is

$$dD/dt = -V \cos \Omega \qquad (3.71)$$

and these radars have a blind zone about path midpoint which is narrow for fast targets and wide for slow targets. The blind zones for a 30 m/s minimum window are sketched in Figure 3-20 for a 100 knot target and a 400 knot target. The lower velocity target might correspond to a helicopter, however a separate analysis would be required to estimate whether useful doppler signals might be extracted from the return from the rotating blades regardless of target velocity.

In addition to surveillance information the Oeil Noir provides range information for fire control between

3-26
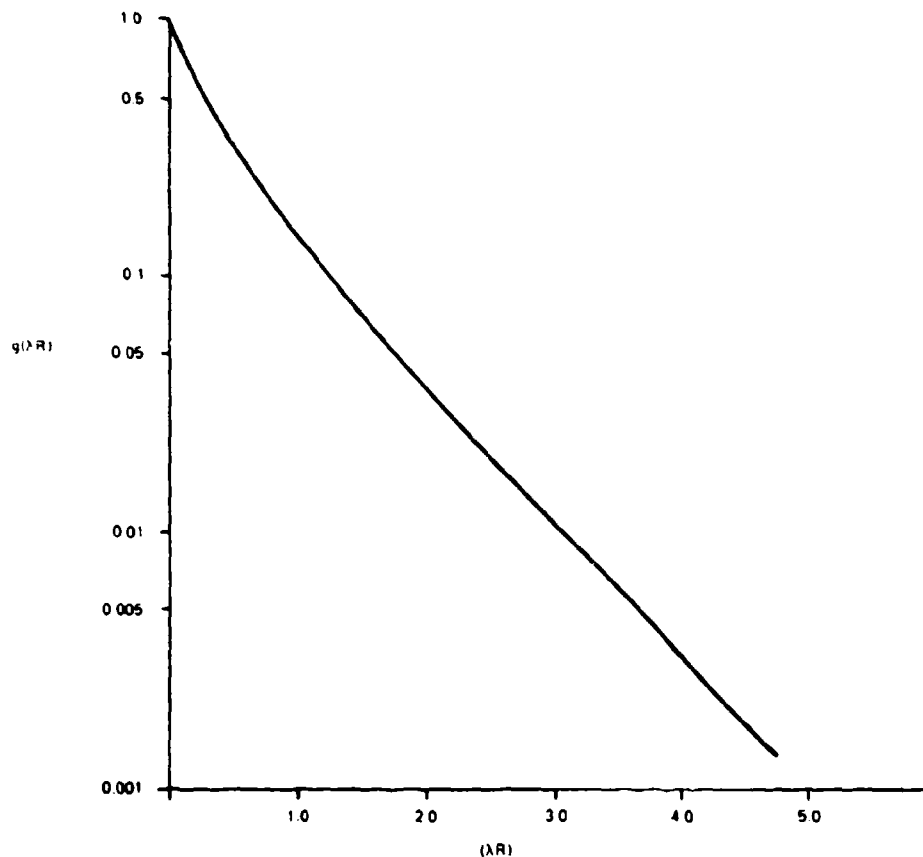
Figure 3-18. Visibility Function g(λ R)

1500 and 3800 meters, but between 500 and 1500 meters range is generated from 'memory'.

3.3.3 Acoustic Detection

Experiments versus high speed bombers and fighters in a desert environment indicate that the range of acoustic detection is not greatly different from that of visual detection under conditions of maximum visibility.[54] Against slow flying aircraft such as helicopters the range at which the aircraft can be heard may greatly exceed that at which it can be seen. Figure 3-21 shows the comparative distances along the flight path of helicopters over a variety of terrain types at Fort Ord, and Figure 3-22 shows the corresponding times.

A comprehensive set of experiments and analyses based on operations in Southeast Asia confirm the importance of aural detection of helicopters.[57,58,60]

Plans to use distributed acoustic sensors in large numbers for general battlefield surveillance suggest the possibility of using these sensors as part of an early warning net against low flying aircraft of all types.

The results of the field experiments on acoustic determination of direction of sound arrival by an unaided human listener suggest the following possible method of acoustic target acquisition.

It has been determined experimentally[55] that over the range 2000 – 4500 meters, an observer can track the

3-27

CUMULATIVE PROBABILITY OF DETECTION

EXCEPTIONALLY CLEAR

CLEAR

LIGHT HAZE

HAZE

LIGHT FOG

METEOROLOGICAL VISIBILITY (YARDS)

87,500

10,900

4400

2200

650
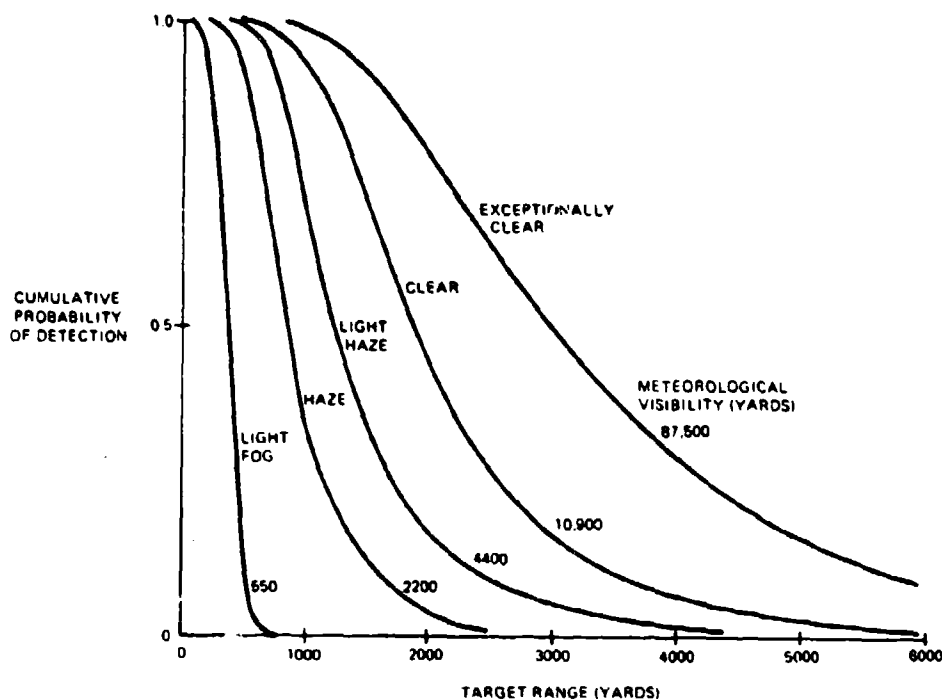
TARGET RANGE (YARDS)

20871 118

Figure 3-19. Cumulative Visual Detection Probability versus Target Range and Meteorological Visibility

400 KNOT TARGET

100 KNOT TARGET

TARGET FLIGHT DIRECTION

L

RADAR

20871 119

Figure 3-20. Doppler Radar Blind Zones for 30 m/s Velocity Minimum

sound of an aircraft (in these experiments a B-52) with a standard deviation of about $1/2$ of the acoustic lag angle. This suggests that in attempting to acquire a target at night, or in limited visibility by a defense system without a surveillance and acquisition sensor, it may be possible to use the operator's sensing of the sound direction. It has also been determined that auditory detection of low flying helicopters can be accomplished at substantially greater ranges than visual detection even by day.

The acoustic lag angle is the largest part of the error in determining target position. It is suggested that it may be possible to use the fire control system to correct for acoustic lag. A method is as follows.

The acoustic lag angle is approximately

$$\Delta_s = (V/V_s) \sin \Omega; \quad V = \text{target velocity}$$

$$V_s = \text{velocity of sound}$$

$$= \text{target angle of approach}$$

$$(3.72)$$

The fire control system computes approximately

$$\Delta_f \cong \omega D_o / V_p; \quad \omega = \text{target angular velocity}$$

$$D_o = \text{target slant range}$$

$$V_p = \text{average projectile velocity}$$

$$(3.73)$$

3-28

If a constant slant range D_s is set in the fire control system, the lead computed is

$$\Delta_{fs} \cong (V/V_p) \sin \Omega (D_s/D_o) \quad (3.74)$$

Suppose that it is desired to acquire the target at a range D_s. Then if

$$D_s = D_r(V_p/V_s) \cong 2.5 D_r \quad (3.75)$$

and the sound source is tracked, when the target closes to D_r it should appear over the gun barrel. The measured standard deviation of error in tracking a sound source was about 10^c at 2800 meters whereas the acoustic lag angle was about 40°.

A simple experiment with the Vulcan system would quickly determine whether the above method of acoustic acquisition has any validity.

3.4 TARGET IDENTIFICATION

The AFAADS-1 report contained a discussion of target identification by 'doctrine', i.e., non-conformity to friendly air corridors, overt hostile act, etc. The severe limitations of the human observer in identifying an aircraft target as determined by experiment were also noted.

The most useful method of identification with respect to maximizing defense effectiveness is electromagnetic IFF, which has some limitations associated with inter-Service confidence in mutual reliable usage of the equipment and the sensings from it.

Passive methods of target identification, other than the human eye appear to have some potential. Modern data processing allows much more information to be extracted from the radar return than is utilized in detection and tracking. It is possible that advanced data processing of infra-red signals and laser returns can also provide identification clues. The same may be true of acoustic signals.

Whether any of these non-cooperative identification techniques can be made to yield identification at a high enough confidence level to allow shooting is unknown. However the importance of identification to both the defense and to friendly air suggests non-cooperative identification as a useful area for research.
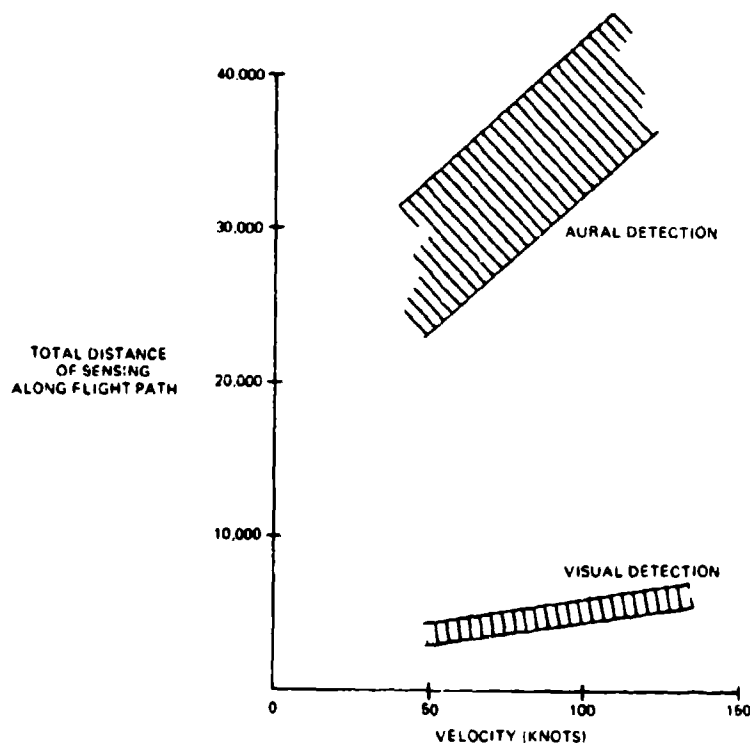
Figure 3-21. Comparison of Aural and Visual Sensing of Helicopters
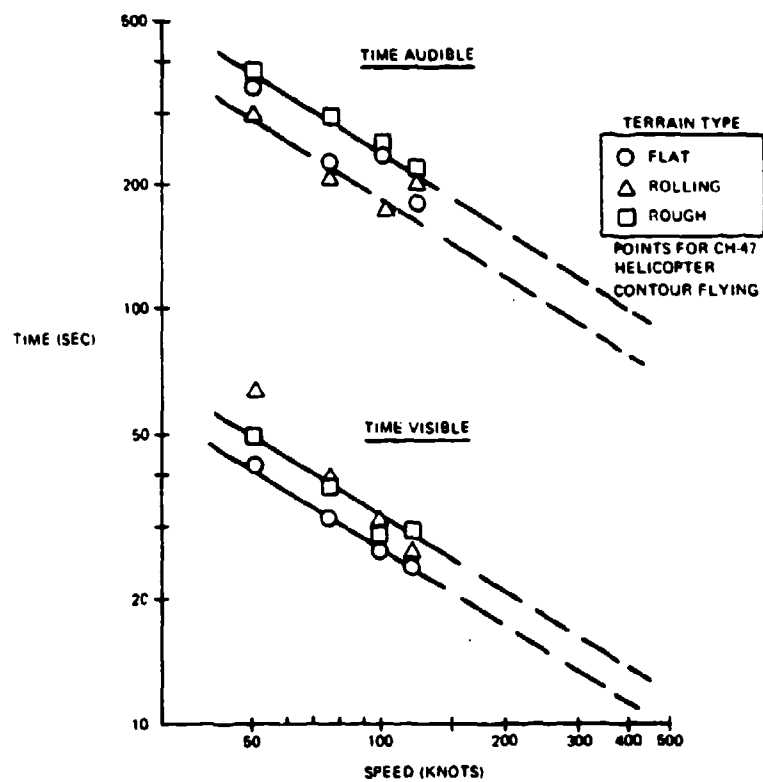
Figure 3-22. Comparison of Visual and Aural Sensing Times versus Helicopters

20871 121

3-30

This section extends the analysis of the tracking function. A detailed model of radar glint is developed and used as the basis for a simulation module. Only limited analysis of the human operator is presented here because it has not been possible to perform extensive analysis of actual tracking data.

An extended analysis of the regeneration function has been made and an improved simulation module developed which allows the determination of the effects of interruption of tracking data from one or more of the tracking sensors to be evaluated.

A simulation module to introduce the effects of flight roughness has been developed, but has not been programmed under the present task effort.

Although time has not permitted the modeling of infra-red or TV imaging tracking sensors, the radar tracking module has been designed so that it is believed that with minor changes, it can be used to represent these sensors when performance data on them becomes available.

4.1 RADAR

Errors of a tracking radar may be categorized and estimated in a number of categories. The principal error sources of a monopulse tracking radar at short ranges are probably 1) those associated with 'glint', 2) those resulting from servo lags at higher angular tracking derivatives, and 3) errors resulting from multipath returns at low elevations. In this section we consider a simple model of errors resulting from 'glint', i.e., phase interactions among returns from separate parts of the target, so that the apparent target direction, measured from the phase front of the return signal, may often lie off the target.

4.1.1 Radar Glint Analysis

The basis for this analysis is some recently published data taken by Mensa[1] on two aircraft models in a microwave anechoic chamber. The models were illuminated with a CW signal, and the amplitude and phase of returned signals were measured as the models were slowly rotated. From the records the glint error angle was computed and converted to linear displacement at the target.

The report indicates that:

a. The probability density function of the glint error could be adequately represented by a normal distribution.

b. The mean of the distribution varied with aspect, but only to about 0.10 of the target dimension.

c. The standard deviation varied slightly with as-

pect but was very close to 1/2 the target dimension in each aspect.

Additional computations given in the reference, show the result of processing the computed glint error through a simulated sensor servo system (second order with 0.707 damping ratio) in terms of the servo output. Standard deviation of glint error after processing by the servo was determined as averaged over 360° target rotation, for a range of values of servo bandwidth and constant angular velocity of target rotation. Only rotation in azimuth at zero elevation angle was studied.

For additional details, one may refer to the referenced report.

For the present analysis, the data cited above was examined along the following lines:

a. The curves of servo error were cross-plotted to show standard deviation against servo bandwidth for constant ratio of servo bandwidth to target angular velocity. Within the accuracy of curve reading, the error resulting from glint measured at the servo output depended only on the ratio of bandwidth to target angular velocity. This is the usual assumption, and is thus confirmed by the experiment.

b. The functional relationship thus indicated, and plotted in Figure 4-1, was used as a basis for developing a simple glint model. The model is described below.

It was assumed that the autocovariance of glint error as a function of target azimuth angle could be written as the sum of two exponentials

$$R(\theta) = \sigma_g^2 \left[\lambda_1 \, e^{-\theta/\theta_{01}} + (1 - \lambda_1) \, e^{-\theta/\theta_{02}} \right]$$

$$(4.1)$$

where

σ_g^2 = variance of glint error before servo processing.

θ_{01}, θ_{02} = 'characteristic angle' of each glint component; these are roughly the angular intervals across which two samples may be considered independent.
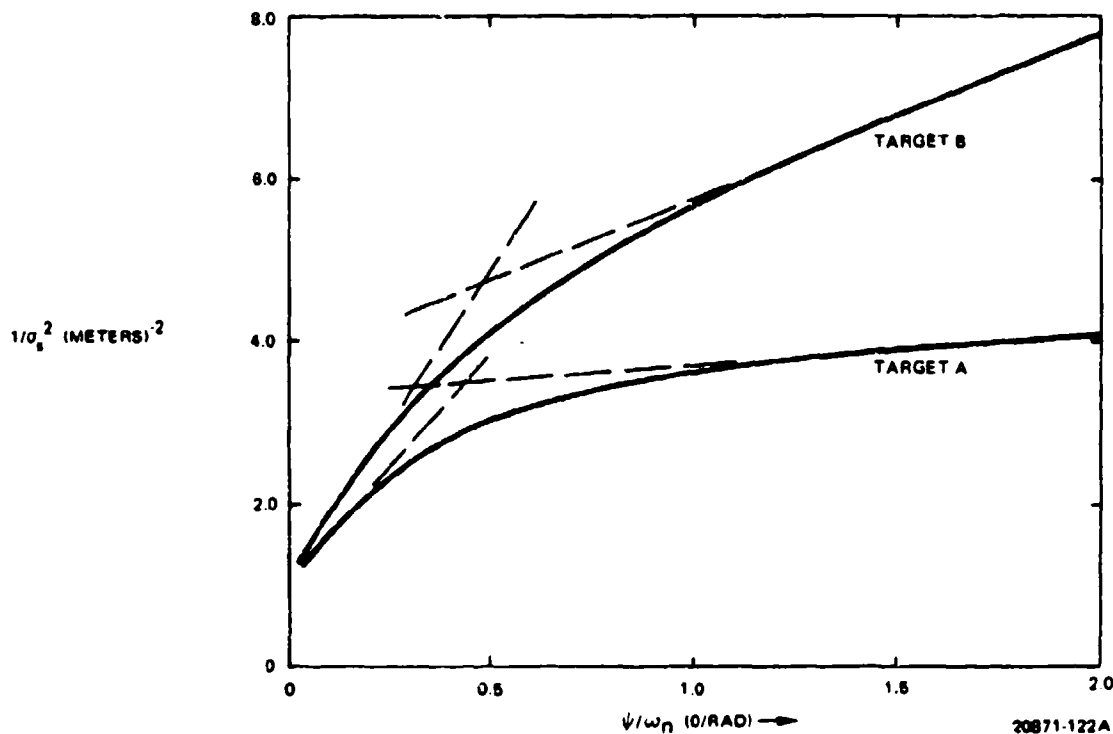
Figure 4-1. Reciprocal of Variance at Servo Output for Experimental Data versus Ratio Target Angular Velocity (°/sec) / Servo Bandwidth (rad/sec)

Two components were chosen because initial computations indicated that a satisfactory representation could not be obtained with a single component.

Note that for each component, the autocorrelation

$$e^{-\theta/\theta_{oj}} \tag{4.2}$$

has the Fourier transform, on the interval $-\infty < \Omega < \infty$

$$\phi(\Omega)\,d\Omega = \frac{(\pi)^{-1}\,\theta_o\,d\Omega}{[1 + (\Omega\theta_o)^2]} \tag{4.3}$$

If the airplane is rotating at a rate ω_a, the power spectral density of the glint error in terms of angular frequency is obtained by substituting the rate at which the 'static' spectrum is being sampled, i.e.,

$$\omega = \omega_a \Omega \tag{4.4}$$

The resulting power spectral density of the glint error before servo processing is

$$\phi(\omega)\,d\omega = (\sigma_g^2/\pi)\left[\frac{d\omega/\omega_o}{1 + (\omega/\omega_o)^2}\right]; \quad \omega_o = \omega_a/\theta_o \tag{4.5}$$

and the corresponding autocovariance is

$$R(s) = \sigma_g^2\left[\lambda_1\,e^{-\omega_a s/\theta_{01}} + (1 - \lambda_1)\,e^{-\omega_a s\theta_{02}}\right] \tag{4.6}$$

The λ, θ_{oj} could have been computed from the basic data if it were available; since it was not, it was necessary to infer these values from the servo output data which was given.

The servo transfer function used was

$$\frac{1}{[1 + 2\xi\,\omega\,T_b + (j\,\omega T_b)^2]};$$

$T_b = 1/\omega_n; \omega_n =$ "half power band width"

$$\xi^2 = 0.50 \tag{4.7}$$

Combining Equations (4.5) and (4.7) and performing the integration over ω, the result is obtained that

4-2

$$(\sigma_s/\sigma_g)^2 = \lambda_1 \left[\frac{2\xi + (\omega_{01}/\omega_n)}{2 [1 + 2\xi (\omega_{01}/\omega_n) + (\omega_{01}/\omega_n)^2]} \right]$$

$$+ (1 - \lambda_1) \left[\frac{2\xi + (\omega_{02}/\omega_n)}{2\xi [1 + 2\xi (\omega_{02}/\omega_n) + (\omega_{02}/\omega_n)^2]} \right]$$

(4.8)

A few trial computations indicate that the two glint components are widely separated in frequency, hence Equation (4.8) can be fitted to the asymptotic slopes of Figure 4-1 by fitting one component at low frequency and the other at high frequency. After a bit of trial and error, the following values for the glint parameters were obtained, as shown in Table IV-1.

Since the parameters were determined by fitting the two terms of Equation (4.8) separately at the two asymptotes, the comparison of the data and computed value at a mid range point above indicates a satisfactory fit over the whole range.

Note the large difference between the two θ_o values. For any given target angular velocity, the larger component has a wide bandwidth (θ_{01}'). Hence it can be more readily reduced by filtering. The smaller compo-

nent (about 25% of the total variance) has a very narrow bandwidth (θ_{02}') and will be difficult to reduce in a filter except at very high angular velocities of the target.

4.1.1.1 Scaling

The parameters of Table IV-1 are for the model and microwave frequency used in the referenced experiment. To convert to other frequencies and target sizes, the scaling relationship is

$$\theta_{oA} = 0.67 \, \theta_{oM} (\lambda_A/L_A)$$

(4.9)

where

θ_{oA} = 'characteristic angle' of glint for full scale aircraft.

θ_{oM} = 'characteristic angle' of glint for model (Table IV-1).

λ_A = wavelength in centimeters of radar.

L_p = full scale aircraft dimension perpendicular to sight line (for example, fuselage length side on) in meters.

Using the above relations, Figure 4-1 is replotted for Target 'B' in Figure 4-2 for an S band and a K_u band tracking radar.

4.1.1.2 Angular Velocities of Aircraft

The airplane changes aspect, as seen by the tracking radar for two reasons,

a. Angular velocity caused by the changing position of the aircraft relative to the tracking point.

b. Angular velocity of the aircraft about axes fixed in the aircraft caused by maneuvers and air turbulence.

A brief survey has been made of the angular velocities caused by air turbulence and normal flight wander about a mean path.[24]

Dunn and Howard[4] show some graphs of aircraft yaw data for a fighter and a bomber attempting to fly a straight course in clear medium-turbulence atmosphere, with the following rough indications.

Bomber: Maximum excursion (spread) 6° in 17 sec

rms angular velocity 1.3°/sec

Fighter: Maximum excursion, (spread), 5° in three 20 sec traces

rms angular velocity 1.5 - 3.1°/sec

NOTE: For the three traces, rms angular velocity increased roughly as the maximum spread in angle.

Table IV-1. Glint Parameters

Target Parameter	A	B	
λ_1	0.71	0.80	
$(1-\lambda_1)$	0.29	0.20	
θ_{01}	0.093°	0.074°	
θ_{02}	10.3	4.7°	
$(\sigma_s/\sigma_g)^2$	0.33	0 25	data at $\psi/\omega_n = 0.5$
$(\sigma_s/\sigma_g)^2$	0.38	0.25	Computed from above parameters

20871-503A

4-3
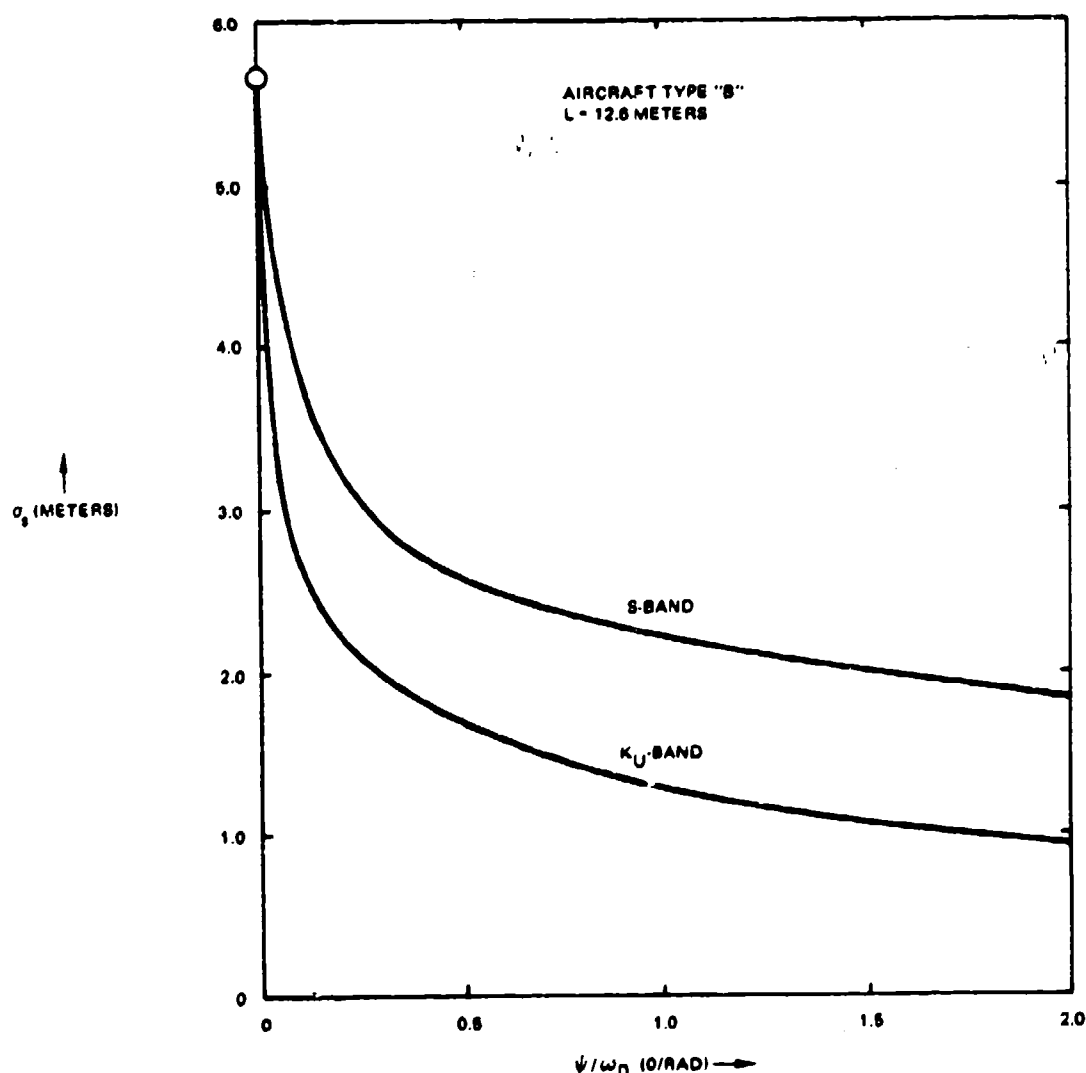
Figure 4-2. Effect of Radar Frequency on Glint Error at Servo Output as Function of Ratio of Target Angular Velocity ($^\circ$/sec) to Servo Bandwidth (rad/sec)

An NACA[3] report gives the power spectral density of several hypothetical aircraft in yaw and roll, when subjected to air turbulence, as a function of variance of gust velocity, and for a mean length of turbulence of 1000 feet. From this data some rough computations were made assuming pilot intervention to reduce deviations below about 0.2 Hz. In addition a 3 f/s rms gust velocity was assumed. The results are given in Table IV-2.

These values would be reduced somewhat if the pilot (human or robot) operated with a wider bandwidth. For example, for Aircraft B, even the human pilot might be expected to work harder to minimize the noted deviations, and he could widen his bandwidth

from the 0.2 Hz assumed to perhaps 0.8 for short periods of time.

Comparing the angular velocities noted above against Figure 4-2, it will be observed that they are high enough to produce a bandwidth of the larger glint component which can be reduced somewhat by the filtering of the tracking servo. The smaller glint component would be relatively unattenuated under the same conditions.

Note that the above angular motions, having a sinusoidal type of variation (generally a spectrum centered on the 'dutch roll' mode of the aircraft), require a more complex model for exact representation

4-4

Table IV-2. Estimated Angular Response of Aircraft to Turbulence

| NACA Aircraft | Weight (lbs) | Wing Loading lb/ft^2 | Velocity (f/s) | Altitude (ft) | Standard Deviations | | | |
| | | | | | Yaw | | Roll | |
					Angle	Angular Velocity	Angle	Angular Velocity
A	12,600	50	696	30,000	1.3°	1.6°/s	3.1°	5.5°/s
B	28,000	52	318	4,000	4.8°	5.7°/s	6.2°	11.1°/s
C	125.000	87	700	35.000	1.1°	1.3°/s	2.6°	4.6°/s

20871-504

of the interaction with the radar and servos than we have assumed. Only if the excursions are large compared with θ_o is the model a fair approximation. However, in view of the limited glint data on hand, an increase in model complexity does not seem appropriate at this time.

A radar glint module for the simulation based on the above analysis is given in the section of this report devoted to simulation.

4.1.2 Effect of Glint on Prediction Errors

As the radar frequency is increased, the glint bandwidth increases, and so, although the glint variance is assumed to remain constant, the variance of tracking error after processing by a low-pass servo decreases as shown in Figure 4-2. However, the increased high frequency content of the noise can result in increased prediction error because of the differentiating process in prediction. The increase, if any, depends on the bandwidth of the velocity filter and the acceleration filter, if acceleration prediction is employed.

Since the bandwidth of the differentiating filters will normally be much smaller than that of the tracking servos, the effect can be demonstrated without including the servo transfer function.

To show the effect assume a simple prediction algorithm including a velocity term, but not an acceleration term. The transfer function is

$$W(s) = \frac{1 + s(t_p + nT_s)}{(1 + sT_s)^n} \qquad (4.10)$$

where

t_p = time of flight,

T_s = filter time constant.

When $n = 1$, the filter does not attenuate high frequency errors. For $n = 2$, the high frequency attenuation is proportional to ω^2.

Consider a single glint component with characteristic time T_g. Then the variance of prediction error is obtained from

4-5

$$(\sigma_p/\sigma_g)^2 = (1/\pi) \int_{-\infty}^{\infty} \left[\frac{1 + \omega^2(t_p + nT_s)^2}{(1 + \omega^2 T_s^2)^n} \right] \left[\frac{T_g \, d\omega}{1 + \omega^2 T_g^2} \right]$$

(4.11)

Evaluation of the integral yields

$$n = 1; (\sigma_p/\sigma_g)^2 = \frac{\mu + (1 + a)^2}{1 + \mu}; \mu = T_g/T_n; a = t_p/T_s$$

(4.12)

$$n = 2; (\sigma_p/\sigma_g)^2 = \frac{\mu(A + \mu)}{(1 + \mu)^2}; A = (5 + 4a + a^2)/2$$

(4.13)

These functions are plotted in Figure 4-3 for $t_p/T_s = 1.0$. For a given target angular velocity, decreasing the radar wavelength widens the glint spectrum, but the input variance which is determined by target dimension, is unchanged. Differentiation for prediction amplifies the high frequency region, and the $n = 1$ filter is unable to do more than limit the growth of the prediction error variance. The $n = 2$ filter, on the other hand works effectively against the wide noise band, so that prediction variance for very wide band noise of constant input variance approaches zero.

Both curves are asymptotic to 1.0 for narrow-band noise. In this case the glint error varies so slowly that there is essentially no velocity error, and what remains is the position error, which because of its narrow band is essentially unsmoothed.

The $n = 2$ filter demonstrates a characteristic which is typical even of 'optimum' filters with constant memory time, as can be determined by using the expressions from Blackman[7] for optimum filters, instead of the $n = 2$ algorithm. The characteristic is that for a given target angular velocity, and smoothing time, there is a 'worst' radar frequency which develops a maximum prediction variance for constant input variance.

To take advantage of high frequency radar in the simple model for glint developed here, one should attempt to maintain T_g/T_s small, which is equivalent to setting

$$(T_s/\lambda)(\Omega L) > 0.1 \text{ for example} \qquad (4.14)$$

It then appears that the shorter the wavelength, the shorter the smoothing time can be for the same prediction variance, and this is of course desirable for many other reasons.

The analysis of the above section was prompted by initial runs on the simulation, reported later, which indicated that the large apparent gains in tracking
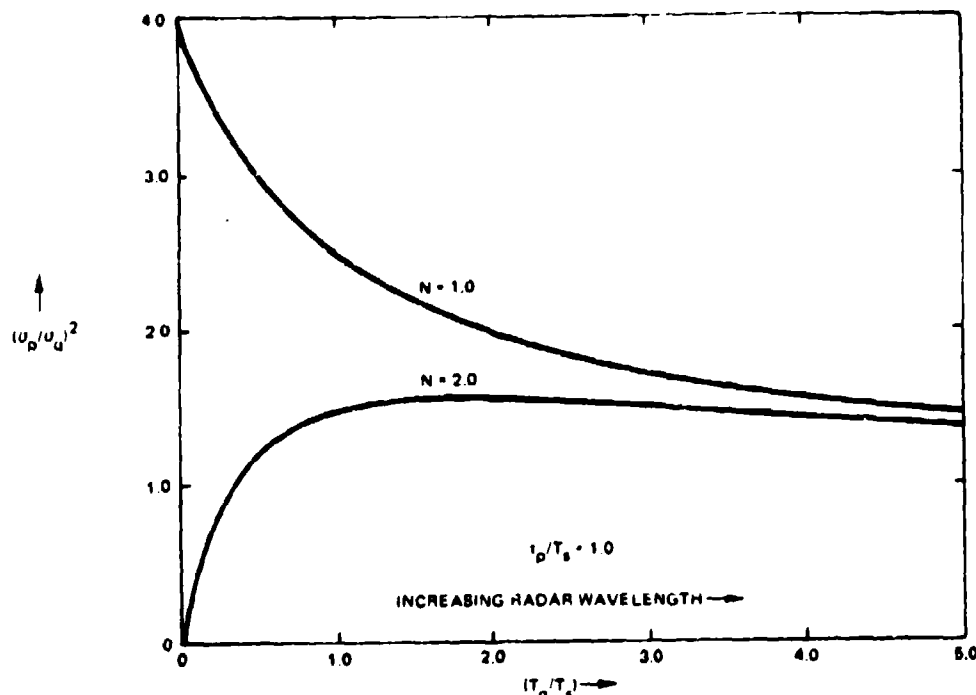
Figure 4-3. Effect of Glint Bandwidth on Prediction Variance for Two Simple Prediction-Filter Algorithms

precision suggested by Figure 4-2 were not realized in target kill probability, and the effect was not understood until the interaction of the noise bandwidth with the differentiation process was recalled.

4.1.3 Simulation Module for Radar Glint

Following the previous analysis, a glint module for the radar tracking mode of the simulation has been developed. The rationale, which recapitulates the conclusions of the previous paragraphs, and the algorithms are given below. Only angular glint has been simulated in this version, since range error has a smaller effect on prediction error (via average projectile velocity).

Based on the extremely limited glint data it is assumed that glint error can be considered independently in elevation and azimuth. More accurately, the 'azimuth' computation of error is developed as 'lateral' error across the line of sight.

In each coordinate there are two components of glint. The larger may be thought of as associated with phase interference of the signal, and it has a small correlation angle. The smaller component may be considered as associated with the center of gravity of the signal as it would appear in purely specular reflection. It has a large correlation angle. For a given angular velocity of the target relative to the line of sight, the larger component has a wide bandwidth and the smaller component has a small bandwidth.

Thus the angular velocity of the aircraft caused by the combination of gust-induced angular velocity and tracking angular velocity causes a rapid attenuation of variance of tracking error associated with the larger glint component, but only a slow attenuation of the smaller component.

The total glint variance as angular velocity approaches zero is asymptotic to $(L/2)^2$ where L = total target extent in meters in the relevant coordinate. Since L in azimuth and elevation depends on target aspect it must be computed for each point and this is done by a module described in Section 7 of this report.

The bandwidth of each glint component is proportional to

$$\Omega L/\lambda \qquad (4.15)$$

where Ω is the absolute value of angular velocity, and R is the radar wavelength.

The expressions used for glint are the following

	Larger component(1)	Smaller component(2)
Fraction of Variance	0.70	0.30
$\theta_{o1,2}$ Angular bandwidth (radians)	0.001 (λ/L)rad	0.10 (λ/L)rad

where L is in meters, and λ is in centimeters

20871-603

To get glint bandwidth in radians/second compute

$$\omega_{1,2} = \Omega/\theta \text{ (rad/sec)} \qquad (4.16)$$

where Ω is the absolute angular velocity of the airplane in radians per second and is the sum of the absolute value of the angular velocity of tracking in each coordinate and the absolute value of the angular velocity caused by air turbulence

$$\Omega = |\Omega_T| + |\Omega_W| \qquad (4.17)$$

Ω_W is taken as 0.03 rad/sec = 1.72°/sec for all computations. To convert azimuth rate to traverse rate

$$\Omega_{TA} = |(dA_o/dt)\cos e_o| \text{ radians/second} \qquad (4.18)$$

Elevation rate is already at the sight line so

$$\Omega_{Te} = |de_o/dt| \text{ radians/second} \qquad (4.19)$$

and so the bandwidths of the two glint components are

$$\omega_{1,2} = (1000) \Omega (L/\lambda) ; (10) \Omega (L/\lambda) \text{ rad/sec} \qquad (4.20)$$

4.1.3.1 Servo Approximation

The transfer function of the servo is approximated as

$$H(s) \cong \frac{1}{(1 + sT)^2} \qquad (4.21)$$

for simplicity; this approximation is considered adequate in view of the uncertainty in the glint characteristics. In addition, T is taken as 1/B where B is the servo bandwidth and is approximated as

$$B \sim 2\pi (K_a/2.5)^{1/2} \text{ rad/sec where } K_a = \text{rad/sec}^2 \qquad (4.22)$$

4-7

where K_a is the acceleration lag constant, rad/sec^2.

The result of processing one component of glint error through the servo is the variance

$$\sigma^2 / \sigma_{gl}^2 = \frac{1 + (M_1/2)}{(1 + M_1)^2} \qquad (4.23)$$

where

$$M_1 = \omega_1 / B$$

The two glint components are considered independent and since the servo is linear, the variances add, to result in

$$\sigma^2 = (L/2)^2 \left[0.7 \, \frac{1 + (M_1/2)}{(1 + M_1)^2} + 0.3 \, \frac{1 + (M_2/2)}{(1 + M_2)^2} \right]$$

$$(4.24)$$

This variance is computed at each sampling interval and is used to construct the tracking noise sequences.

4.1.3.2 Autocorrelation of Tracking Error

A separate section of this report shows how to compute a noise sequence that will have the same autocorrelation as sampling the continuous process described above. The complexity of the computations is considerably in excess of that justified by the knowledge of the basic glint characteristics.

There are three time constants involved, corresponding to the bandwidths of the two glint components and the servo. Each of these appears in exponential form in the complete expression and the simplifying approximation is adopted (which is asymptotically correct) that the correlation across two adjacent sampling points is dominated by the time constant which is largest at that point (i.e., the smallest bandwidth). This excludes ω_1, which is always 100 ω_2. The bandwidth $S(j)$ at j is therefore selected for each point as

$$S(j) = \min \, [B, \omega_2 \,] \qquad (4.25)$$

No attempt is made to correct for changes in the parameters between sampling points and the tracking error series is generated as a one-stage Markov process.

A further justification for this simplification is that tracking noise goes into the smoothing filters, which induce their own correlations, of about 1/2 the smoothing time. The effect of the above process is therefore to provide tracking noise which is not white (as in the real life case), has about the right correlation across sample points, and is operated on by filters which reduce the imperfections in representation of

noise correlation to a subordinate role. At the same time, for short smoothing times, the process prevents the simulation from erroneously overemphasizing the gain obtained from close sampling intervals: a gain which is limited by serial correlation of noise.

The computation of the correlated sequences is then performed according to

$$x(j+1) = a(j+1) \, x(j) + b(j+1) \, u(j+1)$$

$$a(j+1) = e^{-S(j+1)\Delta}$$

$$b(j+1) = \sigma(j+1) \left[1 - e^{-2S(j+1)\Delta} \right]^{1/2}$$

$$(4.26)$$

where the $S(j)$ and $\sigma(j)$ are computed for each point. If they were independent of j, and constant the variance of the generated sequence would, of couse be σ^2.

These sequences must be converted to mils since they are in meters. For azimuth, the mil tracking error is

$$EA(j) = 1020 \, x_A(j) / [D(j) \cos \epsilon_0(j)] \, \text{mils}$$

$$(4.27)$$

For elevation

$$Ee(j) = 1020 \, x_e(j) / D(j) \, \text{mils} \qquad (4.28)$$

For errors in radians omit the multiplying factor of $6200/2\pi = 1020$

If the simulation were to operate to very long ranges, an additional noise term for 'instrumental error' representing gear backlash, and similar mechanical imperfections. This has been omitted since it should be possible to hold this factor to less than 0.25 mils for a well designed radar and servo system, and so its effect at short ranges would be submerged in the other errors developed by the algorithms given. To include it, it might be added to the correlated noise sequence, possibly as white noise of constant angular standard deviation.

4.1.4 Simulation Studies of the Effect of Glint

A series of simulation runs was executed, using the glint module described in Section 4.1.3. The following engagement parameters were used:

Weapon:	25-mm
Radar wavelength:	0.50 to 10.0 cm

Target velocity: 300 meters/second

Target path: straight fly-by at 300 meters altitude and 600 meters crossing range

Probability of killing the target with a one-second burst was computed at points on the flight path 300, 600 and 900 meters before path midpoint. Three rates of fire were used, resulting in 16, 32, and 64 rounds per burst, respectively.

Target vulnerability and dimensions were 'standard' and are given elsewhere in this report.

Two prediction algorithms were used. One employed position and velocity smoothing. The other employed position and velocity smoothing, but each was updated by an acceleration component so that on a curved path the prediction vector would be tangential to present position. This is 'partial acceleration correction.'

The probability of kill curves as a function of radar wavelength were identical in shape for the three firing rates, but of different probability levels, and are shown in Figure 4-4.

Figure 4-5 shows burst kill probability versus radar wavelength for three points on the flight path for the position and velocity smoothing algorithm. There is a uniform improvement in kill probability as wavelength is decreased, but it is small. Figure 4-6 shows the same information for the filter with partial acceleration correction. The probabilities are lower, because of the increased noise amplification, and at the longer ranges where the velocity and acceleration components are multiplied by larger times of flight, the curves show a 'worst' wavelength.

4.1.5 Conclusions

The number of parametric variations in the simulation runs are too few to draw detailed conclusions. In particular, as shown in Figure 4-4, with 3 mils angular round to round dispersion, there is not much room for additional improvement by reducing tracking error. The 'zero tracking error' asymptotes shown in Figure 4-4 were hand computed for the assumed target, and 3 mils dispersion.

The analysis indicates the importance of smoothing time, and the interactions among smoothing time, prediction mode, and the tracking noise autocovariance. These interrelationships and their effect on burst kill probability can, of course, be examined by means of the simulation, at the expense of additional runs.

4.2 HUMAN OPERATOR

In the AFAADS-I Report, an extensive survey of the literature on human performance in the tracking function was made. It was hoped in the present contract to analyze sets of tracking data taken with human operators in the process of tracking real aircraft. However, the data was not available in the extent anticipated, hence this analysis is more limited in scope.

4.2.1 Desirable Control Dynamics

Additional experimental data was located on laboratory experiments of human trackings with a variety of control dynamics. These experiments are summarized below. The findings support the conclusions and recommendations of the AFAADS-I report.

Two tracking experiments are reported. In one set it was shown that for two-axis tracking, tracking error was reduced by about 40% for aided tracking over simple rate tracking without a position element.

The second set showed that given the position element of tracking, the addition of as many as four integrators in series was helpful when the input has principally low frequency rather than high frequency content, and that the integration 'aid' became inferior only when most of the input had frequency component so high, that both position and assisted tracking performed poorly.

The general conclusion is that operator tracking for AA must have a position element in the tracking loop. Given this element, the low frequency integration involved in the regenerative process will not degrade the operator's high frequency response, and will improve overall performance by unburdening him of the high and mid range frequency contents of the tracking input spectrum.

Experiments by Frost[9] compared 'rate' tracking with an 'optimum' control.

For rate tracking the control function is

$$\theta_o/\theta_c = K/s \qquad (4.29)$$

The "Optimum" function used was

$$\theta_o/\theta_c = (K/s) \; \frac{(T_1 s+1)^2}{T_2 s+1} \qquad (4.30)$$

and the Bode plots are shown in Figures 4-7 and 4-8.

For a single axis control against a mix of sine waves, the two control laws yielded the same tracking error averages.

It was suggested that this may have been too simple a task for the operator; he was then given two axis tracking of a CRT spot displaced by sine wave mixes in both coordinates.
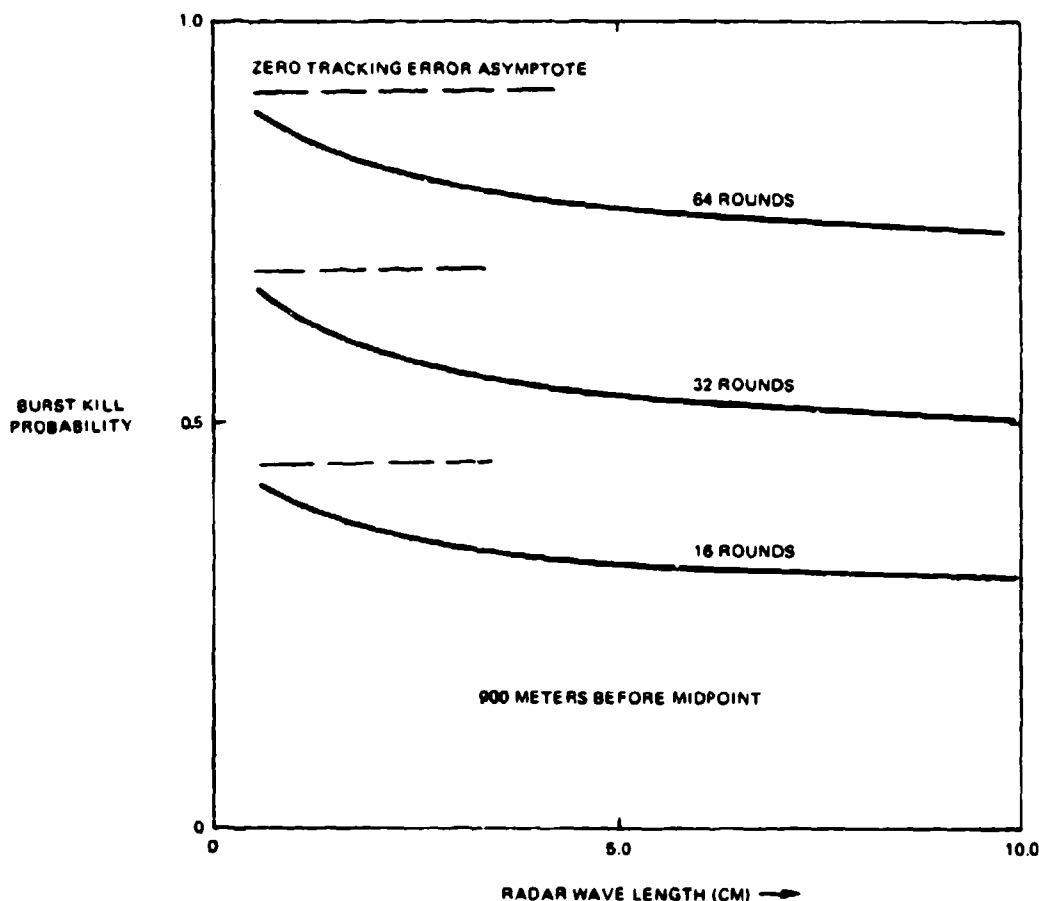
Figure 4-4. Effect of Radar Wavelength and Number of Rounds Fired on One-Second Burst Kill Probability from Simulation Position and Velocity Smoothing Only

The 'optimum' control function then yielded about 0.60 the mean absolute errors in each coordinate compared with that obtained with the rate laws.

Observing the Bode plots it can be seen that the principal characteristic of the 'optimum function' is that it eliminates the 90° phase lag of the integrator at frequencies above 2 Hz, and the phase lag improvement begins at about 0.20 Hz. In fact, the Bode plots are about the same as those of simple aided (rate + position) tracking with a time constant of about 0.15 sec.

The function designated as 'optimum' was developed on a theoretical basis from a survey of earlier tracking data with a variety of transfer functions; it was not determined to be optimum in the reported experiments (by possibly varying K, T_1 and T_2, for example), but it was significantly superior to rate tracking.

The conclusion is that the important element of this experiment was that the addition of the position component to rate tracking in a difficult two-axis tracking task provided significant reduction of tracking error in both coordinates.

Experiments by Chernikoff et al[6] compared with the control function

$$\theta_o/\theta_c = (1''/40^o)\,[.05\,s^{-4} + 0.4\,s^{-3} + 2.0\,s^{-2}$$

$$+ 4.0\,s^{-1} + 1.0]\qquad(4.31)$$

with

$$\theta_o/\theta_c = (1''/40^o)$$

and showed that the former law was superior against mixes of sine waves until the average input frequency approached about 1/2 Hz. For lower frequencies the more complex law was preferable, for higher frequencies both were bad, but the simple position law was slightly better.

The complex control law has two real and two complex roots. The shortest time constant present is about $(3.45)^1$ sec, the other real root corresponds to about 0.34^1 sec, and the complex roots have frequencies which are low compared with the man's bandwidth.

It thus appears that the system should appear to the man as simple aided tracking with a 0.3 second time constant, the increasing gain at the low frequencies tending to unburden him beneficially when the input has most of its content at low frequencies.

System gain versus frequency and error performance for the two modes are shown in Figures 4-9 and 4-10.

The general conclusion is that the low frequency characteristics of the control affect the operator's workload, but not his accuracy, as long as the position component is present at the high frequencies: above 1/2 Hz.

In summary:

a. In two-axis tracking the position component in the tracking control is necessary for high accuracy.

b. Given the position component and a stable set of control dynamics, phase lags at low frequencies do not degrade the operator's performance and if the lags are associated with elimination of some of the operator's loading, the overall effect will be beneficial.

The conclusions for regenerative tracking design are as follows:

a. Provide a position component.

b. Above about 1.0 rad/second the control should behave like rate plus position aided tracking.

c. Below 1.0 rad/sec there is considerable freedom in system design in introducing the regenerated aid.

The subject experiments were not run against inputs simulating antiaircraft tracking. However, once the medium and high frequencies of the AA problem have been subtracted out by regeneration, the residue to be handled by the operator may not be unrealistically different from the inputs in the referenced experiments.

4.2.2 Approximate Estimation of Human Bandwidth from Limited Tracking Data

A proper analysis of human error in tracking aircraft targets would require a large batch of tracking data showing error versus time, with concomitant records of relevant parameters such as target speed, heading, range, and the trackings angles and derivatives all as a function of time. From these one might hope to develop a useful 'model' of the human operator which could be used in simulations and analysis.

Unless taken with the above objective in mind, most tracking error summaries tend to list only mean tracking error (bias) on each path and the standard deviation about the mean.

An interesting question is whether from such abstracted summaries estimates can be made of the operator bandwidth, or equivalently the approximate correlation time of the error. The following paragraphs indicate that inferences of this type can sometimes be made.

For very short records the standard deviation about the mean will probably be small, and the mean itself will vary widely across records. For very long records it is conceivable that the mean will tend to be small, with most of the error falling into the standard deviation.

Using Tapper's method, as described in AFAADS-I we can make estimates about the noise bandwidth.

Two very limited sets of early Vulcan tracking data are at hand. For one set the method does not work. For the other it does, and gives reasonable results. The latter set is described below.

Readers with accurate computations of the same parameters may find it interesting to compare them with these very sketchy estimates.

Some limited tracking data taken early in the Vulcan program on the XM-167 mount gives measurements of mean error and standard deviation about the mean for a small number of courses. Dividing these into even smaller sets according to length of tracking time, the variances of the mean within each subset and the average variance was computed for azimuth and elevation.

In AFAADS-I (p. 5-61) it was indicated that if correlated noise is put through an averaging filter with the same characteristics as the above data reduction
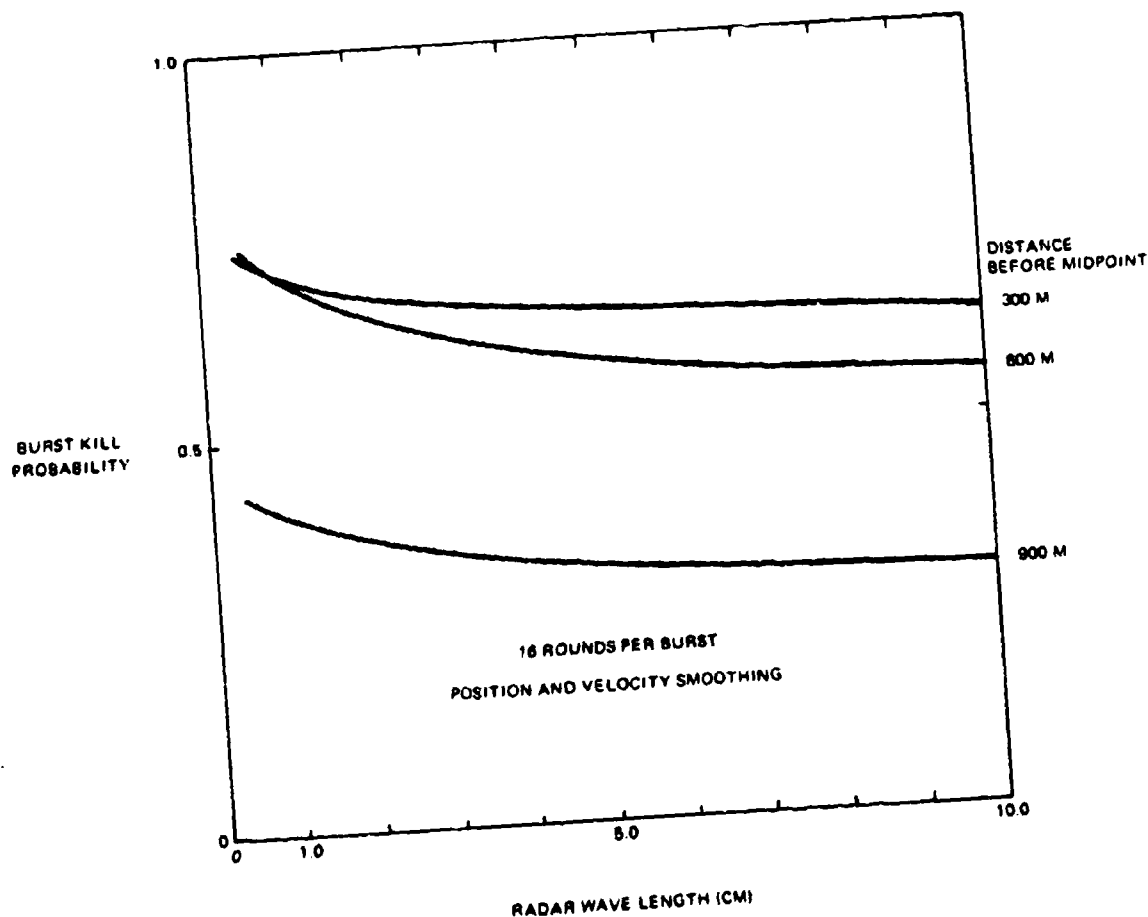
Figure 4-5. Effect of Radar Wavelength on One-Second Burst Kill Probability from Simulation Position and Velocity Smoothing Only

process, the variance of the mean across many samples will be

$$\sigma_m^2 = \int_0^\infty \left[\frac{2(1-\cos \omega T_n)}{(\omega T_m)^2} \right] \phi(\omega^2) \, d\omega \qquad (4.32)$$

where T_m is the measurement interval, and ϕ is the power spectral density of the noise. σ_m^2 is the variance of the mean.

Approximate the bracketed term as

$$2(1-\cos x)/x^2 \cong e^{-x^2/12} \qquad (4.33)$$

Assume that the noise power spectral density is of the form

$$\phi(\omega^2) = \frac{k}{1 + (\omega T_n)^2}$$

$$\cong k e^{-(\omega T_n^2)}; \text{ where } k \text{ is a normalizing constant} \qquad (4.34)$$

The exponential approximations are considered ade-

20871-126

BURST KILL
PROBABILITY

DISTANCE
BEFORE
MIDPOINT

600 M

300 M

900 M

16 ROUNDS PER BURST
ACCELERATION COMPONENT FILTER

RADAR WAVE LENGTH (CM) ⟶
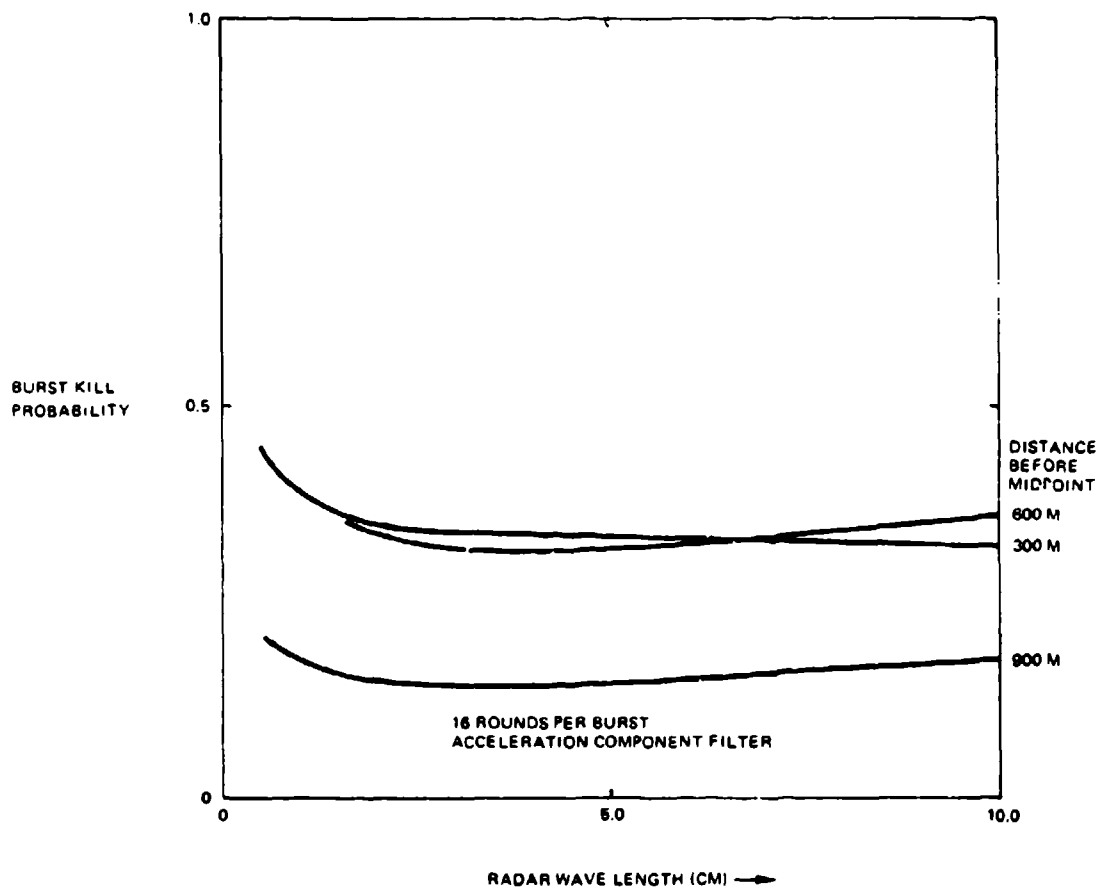
20871-127

Figure 4-6. Effect of Radar Wavelength on One-Second Burst Kill Probability from Simulation Filter with
Partial Acceleration Correction

quate in view of the limited data to which they will be applied. There is no problem (but more algebra) in evaluating the integrals exactly.

Performing the integration, and applying the appropriate value of k,

$$(\sigma_m/\sigma_0)^2 = \left[1 + \frac{T_m^2}{12 T_n^2} \right]^{-1/2} \tag{4.35}$$

where σ_e^2 is the variance of error about the mean.

Figure 4-11 shows $\sigma_m^2 + \sigma_e^2$ as a function of record length for the small sample of records available, and Figure 4-12 shows the ratio $\sigma_e^2/(\sigma_m^2 + \sigma_e^2)$ vs. record length. As hoped, the variance about the mean as a fraction of the summed variance increases uniformly as record length increases, for both the azimuth and elevation coordinates.

The curves of Figure 4-12 are consistent with Equation (4.35), and the corresponding value of T_n is

$$T_n = 0.75 \text{ seconds}$$

This is not unreasonable for a human operator employing a rate control. The corresponding bandwidth is about 0.2 Hz, and this is also reasonable, since

4-13
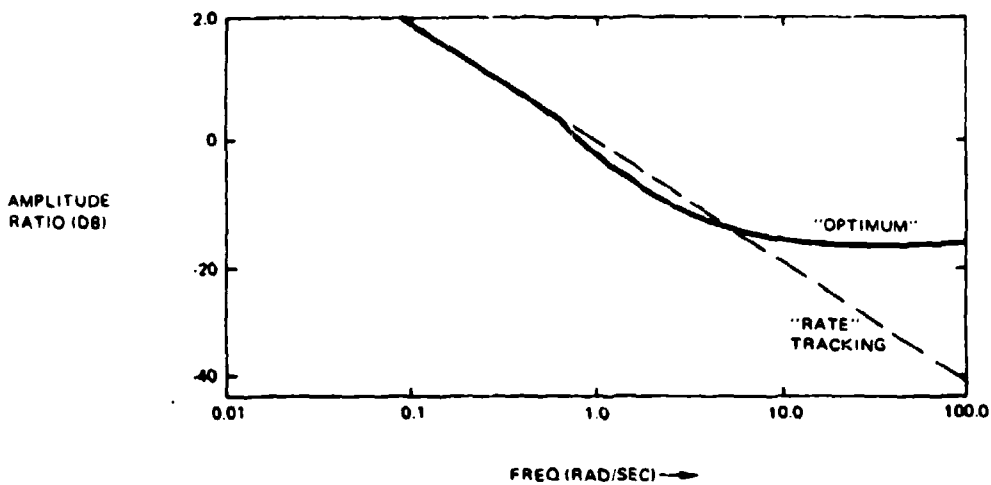
20871-128

Figure 4-7. Control Gain versus Frequency
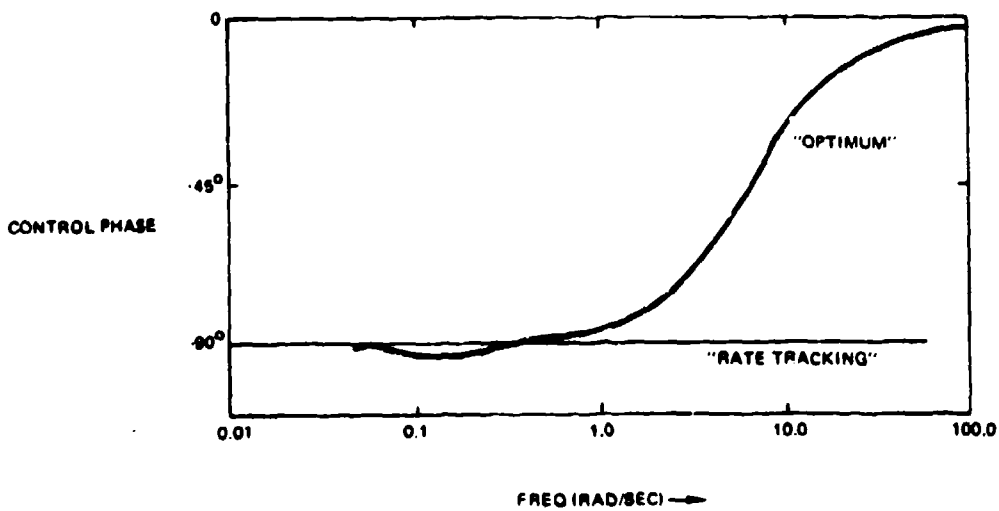
20371-129

Figure 4-8. Control Phase versus Frequency

CONTROL SYSTEM GAIN

FREQ (RAD/SEC) ⟶
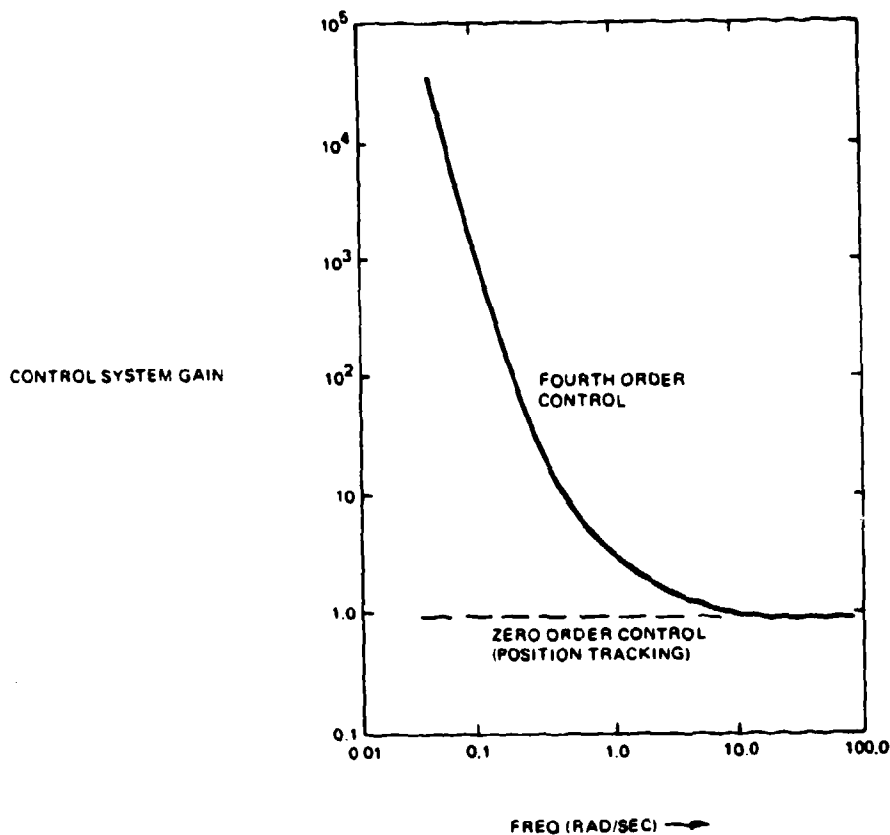
20871-130 A

Figure 4-9. Control Gain versus Frequency

a human operator rarely performs with an equivalent bandwidth exceeding 1.0 Hz under optimum conditions with a position control and an 'easy' target.

The tracking records analyzed can then be simply represented as an exponentially correlated process with characteristic time 0.75 seconds and standard deviation of about 4.5 mils.

4.2.2.1 Conversion to Prediction Error

The data was taken on the Vulcan mount using a lead computing sight. The transfer function of the sight is approximately

$$W(s) = \frac{1 + s(1 + a)t_p}{1 + sa\, t_p} \qquad (4.36)$$

where $s = d/dt$, t_p = time of flight, and a = a constant (here taken as 0.20).

The variance of tracking error, and probably T_n as well will vary with the target path parameters. If we assume, however, that the derived parameters of tracking error can be used as average values, we can compute the autocovariance of prediction error resulting from tracking error. Without reproducing the algebra,

4-15

500

ZERO ORDER
CONTROL

100

AVERAGE ERROR (RELATIVE)

50

FOURTH ORDER
CONTROL

10

MEAN COURSE FREQUENCY ⟶
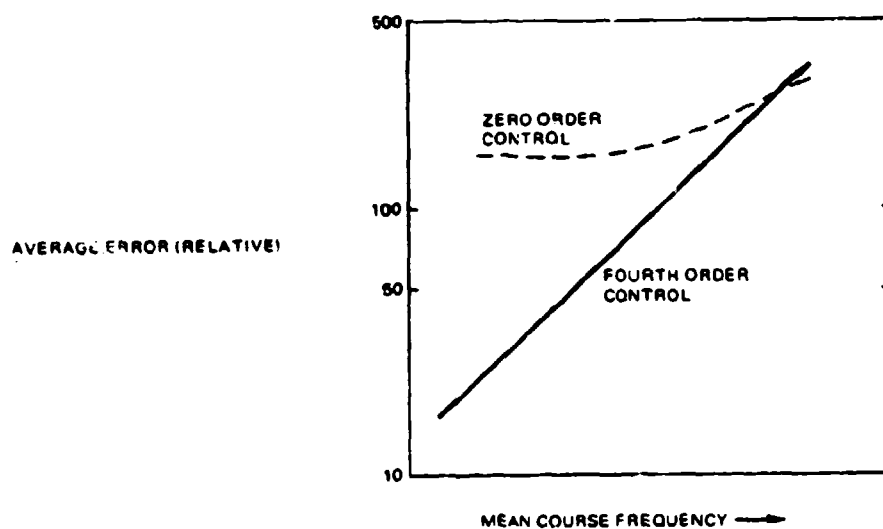
20871-131

Figure 4-10. Average Tracking Error versus Mean Course Frequency

10

AZIMUTH

$\sigma_o^2 + \sigma_m^2$

10

ELEVATION

0

0   10   20   30   40
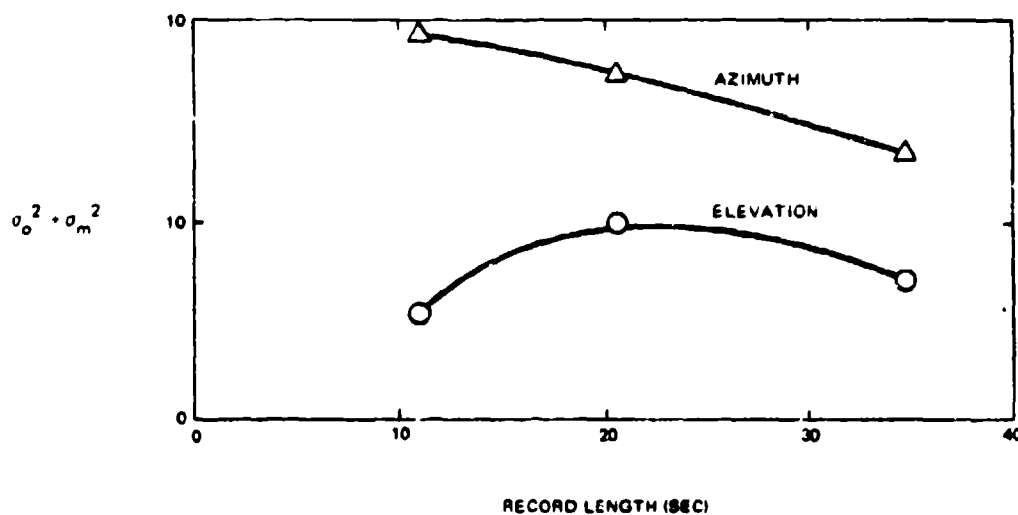
RECORD LENGTH (SEC)

20871-132

Figure 4-11. Summed Variances versus Record Length

4-16

$\sigma_o^2 / (\sigma_o^2 + \sigma_m^2)$

RECORD LENGTH (SEC)
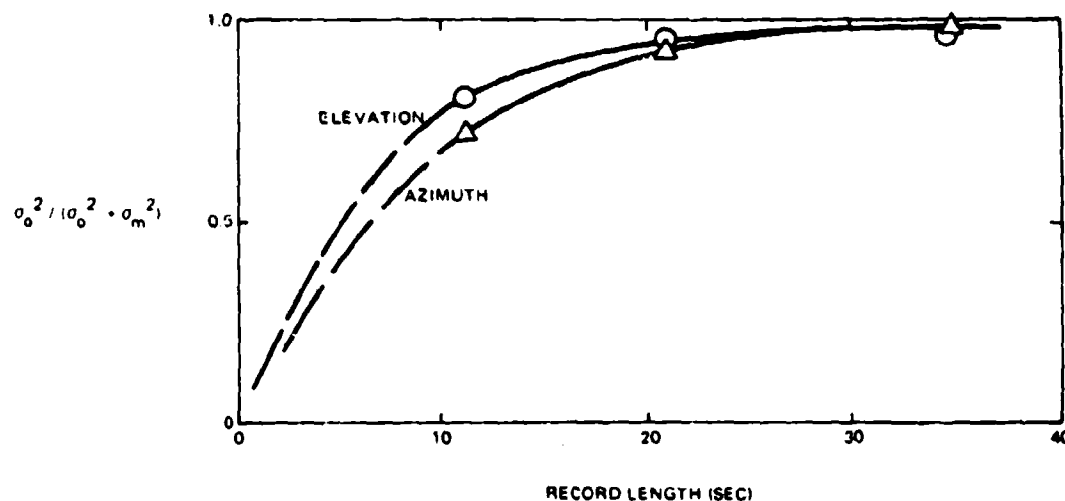
20871-133

Figure 4-12. Ratio of Variance of Error about Mean to Summed Variances

we find that the autocovariance consists of the sum of two terms, each multiplied by a simple exponential containing the lag interval. The characteristic times of the two exponentials are T_n, and at_p. Out to about 3.5 seconds time of flight T_n will dominate the autocorrelation, hence we would expect the prediction error to be significantly correlated in time over about 0.75 seconds, and hence significant in computing 1 second burst kill probabilities.

The corresponding standard deviation of prediction error as a function of time of flight is shown in Figure 4-13.

It should be emphasized that the above computations are not an assessment of the Vulcan system because of the limited data employed. The purpose is simply to show a method of estimating bandwidth of the human operator.

4.2.3 Human Operator Simulation in the Tracking Function

This section examines the considerations in providing a more explicit representation of the human operator transfer function in the Litton simulation, with the object of eventually replacing the module now used for this function, as described in AFAADS-1.

Only the question of sampling rate is addressed. It is assumed that analysis of real tracking data would yield a representation generally similar to that customarily used, and described in AFAADS-1, although such analysis might, for example, indicate that some of the human parameters should be a function of the target path parameters.

In the present paper the compatibility of a 0.10 or 0.20 sec. sampling interval with the explicit representation of a human operator having a transfer function $(K/s)\, e^{sT_m}$ is examined. It is generally agreed that the man sets his value of K close to the stability bound of the control loop, and this maximum is limited by the constant delay T_m which is about 0.20 sec. It is concluded that a 0.10 sec sampling interval will provide an adequate representation of the man's operation in his loop.

Consider a servo with transfer function Y(s).

Error/input is given by (s = d/dt)

$$e(s)/x(s) = 1/[1 + Y(s)] \qquad (4.37)$$

Output/input is given by

$$y(s)/x(s) = Y(s)/[1 + Y(s)] \qquad (4.38)$$

Next introduce a transfer function Y(s) corresponding to a man operating a rate control

4-17
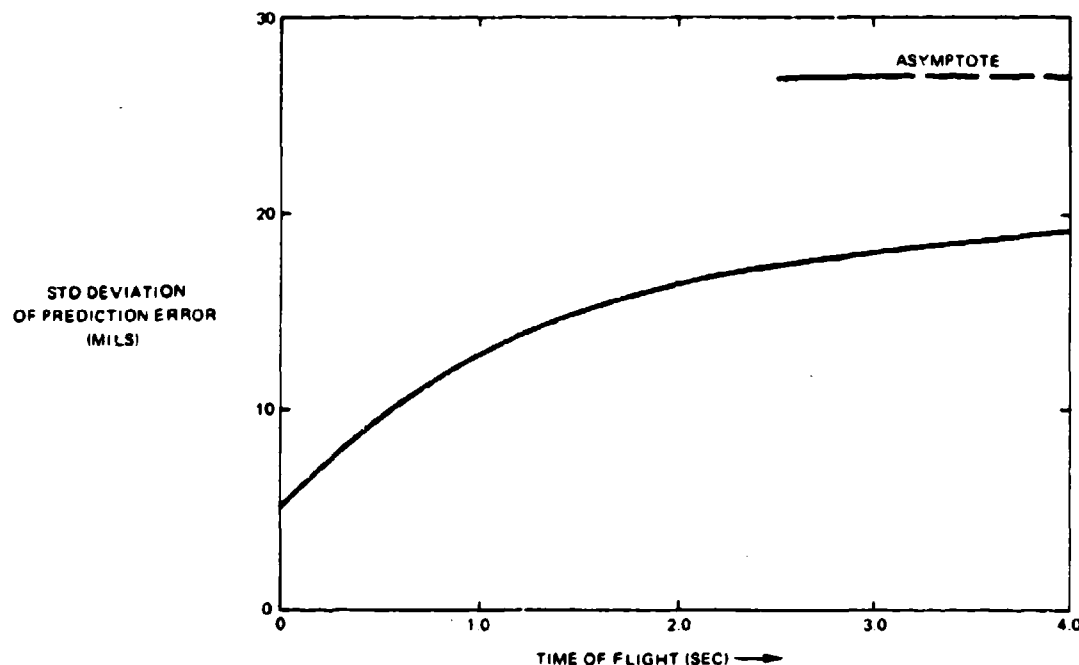
Figure 4-13. Prediction Error Standard Deviation of Gyrosight Resulting from Tracking Error with $\sigma_o = 4.5$ mils, $T_n = 0.75$ sec

$$Y(s) = (K/s) \, e^{-0.20s} = (K/s)e^{-sT_m} \quad (4.39)$$

where we have included the 0.20 second constant lag of the man.

Approximate the system for digital representation as suggested by Blackman[7] using the Pade' approximation for

$$q = e^{-s\Delta}$$

$$q \cong [1 - (s\Delta/2)] / [1 + (s\Delta/2)]$$

whence

$$s \cong (2/\Delta)(1-q)/(1+q) \quad (4.40)$$

and Δ is the sampling interval.

In the following, we compare a differential equation approximation such as might be used in an analog simulation against a difference equation which would be used in a digital simulation. In the former case the constant delay time is approximated by the Pade' algorithm, in the latter case the integration operation.

The differential equation approximating the continuous solution is

$$y\{(s^2 TT_m/2) + s[T \cdot (T_m/2)] + 1\} = x[1 - s(T_m/2)] ; \quad (4.41)$$

where $T = 1/K$

The response to a step can be (1) unstable in the form of increasing oscillations, (2) stable in the form of damped oscillations, (3) stable aperiodic (critically damped), (4) stable, underdamped.

From the differential equation, stability requires that $T > T_m/2$, i.e., that the man use a gain no larger than $K = 2/T_m$. The damping ratio of his response is

$$\zeta^2 = (1/8) [(2T/T_m)^2 - 1] \quad (4.42)$$

from which

for stability $\quad 2T/T_m > 1.0$

but for aperiodic response $\quad 2T/T_m = 3.0$

We check these criteria against the discrete model.

Letting T_m be a multiple ν of Δ, so that $e^{sT_m} = q^\nu$, we obtain for the difference equation with $\nu = T_m/\Delta$.

20871-134

4-18

$y(t) - y(t-1) + r\,y(t-\nu) + ry(t-\nu-1) = rx(t-\nu) + rx(t-\nu-1)$

(4.43)

The form of the response is defined by the location of the roots of

$$z^{\nu+1} - z^{\nu} + rz + r = 0 \qquad (4.44)$$

and for stability they must lie within the unit circle $z = 1.0$.

This clearly fails if $r = 0$, and so, as we would expect, such wide sampling is unacceptable. If we sample at $\nu = 1.0$ and consider the effect of variations in T via r, the root locations are

$$z_{1,2} = (1-r)/2 \pm [(1-r)^2/4 - r]^{1/2} \qquad (4.45)$$

Consider the values of the roots. They are equal when the term under the radical is zero (aperiodic response) for which

$r = 0.41;\ 2T/\Delta = 2.45$ which may be compared with 3.0 for the continuous case.

The radial location, when they are complex is

$$|Z|^2 = z_1 z_2 = r$$

If $|z^2| = 1, r = 1.00$; and since we worked this case for $T_m = \Delta$, $2T/T_m = 1.00$ which may be compared with 1.0 for the continuous case.

If we let $\nu = 2$, we have

$$z^3 - z^2 + rz + r = 0 \qquad (4.46)$$

The system, when it becomes unstable with the allowable values of r will have one real and two complex conjugate roots. Call these z_1, z_2, z_3. We know that

$$-(z_1 + z_2 + z_3) = -1$$

$$z_1 z_2 + z_1 z_3 + z_2 z_3 = r$$

$$z_1 z_2 z_3 = -r$$

20871-604

from the z equation, using the well known relations for coefficients in terms of roots.

If the two complex roots lie on the unit circle, their product is unity, i.e.,

$$z_2 z_3 = 1.0$$

This is sufficient information to solve the three root equations for r and this is found to be

$$r^2 + 2r-1 = 0; r = 0.414$$

$$\frac{2T}{T_m} = \frac{1}{r\nu} = 1.22 \qquad (4.47)$$

Since 1.22 is somewhat larger than the 1.00 of the approximate analog solution, we now solve for the stability point exactly. The requirement is that phase margin of Y(s) over π be positive when $|Y| = 1.0$. First determine the frequency at which $|Y| = 1.0$

$$Y = (j\omega T)^{-1} e^{-j\omega T_m}$$

$$|Y|^2 = (\omega T)^{-2} \qquad (4.48)$$

setting this equal to 1.0, the gain crossover occurs at

$$\omega_c = T^{-1} \qquad (4.49)$$

Expanding

$$Y = (\omega T)^{-1} [-j \cos \omega T_m - \sin \omega T_m] \qquad (4.50)$$

from which the phase is easily seen to be

$$\phi = (\pi/2) - \omega T_m \qquad (4.51)$$

the 90° phase lag comes from the integration, the next term results from the constant delay. Setting $\phi' = -\pi$,

$$\omega_c T_m = \pi/2$$

$$T/T_m = 2/\pi$$

$$2T/T_m = 4/\pi = 1.27$$

20871-605

which may be compared with 1.22 for the discrete simulation. This is rather good; in fact it is better than simulating this Y by the analog approximation given earlier.

4.2.3.1 Conclusion

If the transfer function of the servo loop is

$$(K/s)\, e^{-sT_m} \qquad (4.52)$$

and $T_m = 0.20$ sec; an excellent digital simulation can be obtained with sampling interval 0.10 sec. This is consistent with the sampling intervals used in current

4-19

simulation operation, and suggests that even when better representations of the human operator are available, they can be explicitly included at 0.10 second sampling. In an extended simulation of the human operator, Paskin[10] used a sample interval of 0.10 second, 'to provide power spectral density plots up to 10 rad/sec. All data of interest in manual control tasks fall well below this value.'

4.2.4 Range Estimation by the Human Operator

The simplest form of computing sight is the 'course and speed' sight, which requires only estimates of target path and speed to generate leads. This sight can have a range input, but range errors affect the solution only through average shell velocity and superelevation, and these minor errors are lost in the primary errors resulting from errors in setting course and speed. This point is mentioned here because of a prevalent belief that course and speed sights require range input.

The simplest form of complicated computing sight is the 'rate x time' sight, of which the well known disturbed reticle lead computing sight is typical. A small package containing one or more gyroscopes measures angular velocities obtained by the tracking process, and these can be multiplied by time of flight developed from range information to give the lead angles. How good the computation is depends on how well the design accounts for secondary corrections resulting from the higher derivatives.

The fact that something is being dynamically computed, however, makes the rate x time sight attractive to many people even when continuous measurements of range are not available. The British Falcon system uses a rate x time solution with estimated range. A concept is to set range short in one or more steps and allow the target to 'fly through' the range bracket during which time the lead is briefly correct. Some simulation runs of this concept are provided later in this report.

Range estimation of aircraft targets by the unaided eye is difficult to theorize about because it is not clear what cues are available to the man. The most recent set of experiments on range estimation suggest that against low altitude targets the observer obtains useful clues from his sensing of target position relative to terrain features to which he knows the range.

In these experiments the target aircraft were low flying bombers and fighters.[54,56(80 3)]

Roughly speaking, although there tended to be significant biases in range estimation in these experiments (substantial underestimation of the range on directly incoming targets), the standard deviations about the mean were somewhat larger than the means. Jets were estimated to be closer than they were and helicopters to be at a greater than actual range. The mean absolute error in range estimation tended to vary with distance

of the aircraft along its flight path from midpoint rather than with range and was about 20% of this distance, hence a somewhat smaller percentage of range, on the average, perhaps about 15%. Figure 4-14 is a sketch of the experimental data which suggests more validity than the small sample justifies, but does illustrate the magnitudes involved.

A reasonable conclusion may be that one can use step-range estimation with a rate by time sight as a back-up mode but the number of fly-throughs that one can safely assume per attack is small, and the system effectiveness will depend on the number of rounds fired during the brief interval that lead is approximately correct at each fly-through.

Whether this is a preferable operational solution compared with the far simpler course and speed sight is unlikely to be settled by experiment or analysis, but the availability of simple low cost laser range finders should relegate range estimation to a strictly back-up mode.

4.3 REGENERATIVE ASSISTANCE TO TRACKING

As target speeds increase the high angular velocities and accelerations required of the tracking unit at short ranges create moderate problems for an automatic tracking system, and severe problems for a human operator who has, at best, only about a 1 Hz bandwidth in the tracking function. Even in the case of automatic radar tracking, it is in this region that the glint spectrum is widest so that one would like a narrow servo bandwidth to attenuate the glint error, yet a narrow bandwidth with a conventional servo design creates the even more undesirable penalty of angular lags.

These problems are, in a sense, an artifact of the tracking algorithms and as has been known for a long time, one can take advantage of the fact that the target velocity in inertial space changes at a relatively low rate, to generate the required tracking data from past measurements. The process is designated 'regenerative tracking'. It has long been used in Naval fire control, was employed in the Vigilante fire control system, and is apparently used in the Oerlikon Fledermaus and Skyguard fire control systems.

The concept is based on the determination of 'course invariants' which are computed from initial tracking data, used to generate tracking rates, with the whole process looped so that it functions continuously. Vigilante used algorithms working in polar coordinates; Fledermaus apparently uses algorithms based on rectangular coordinates.
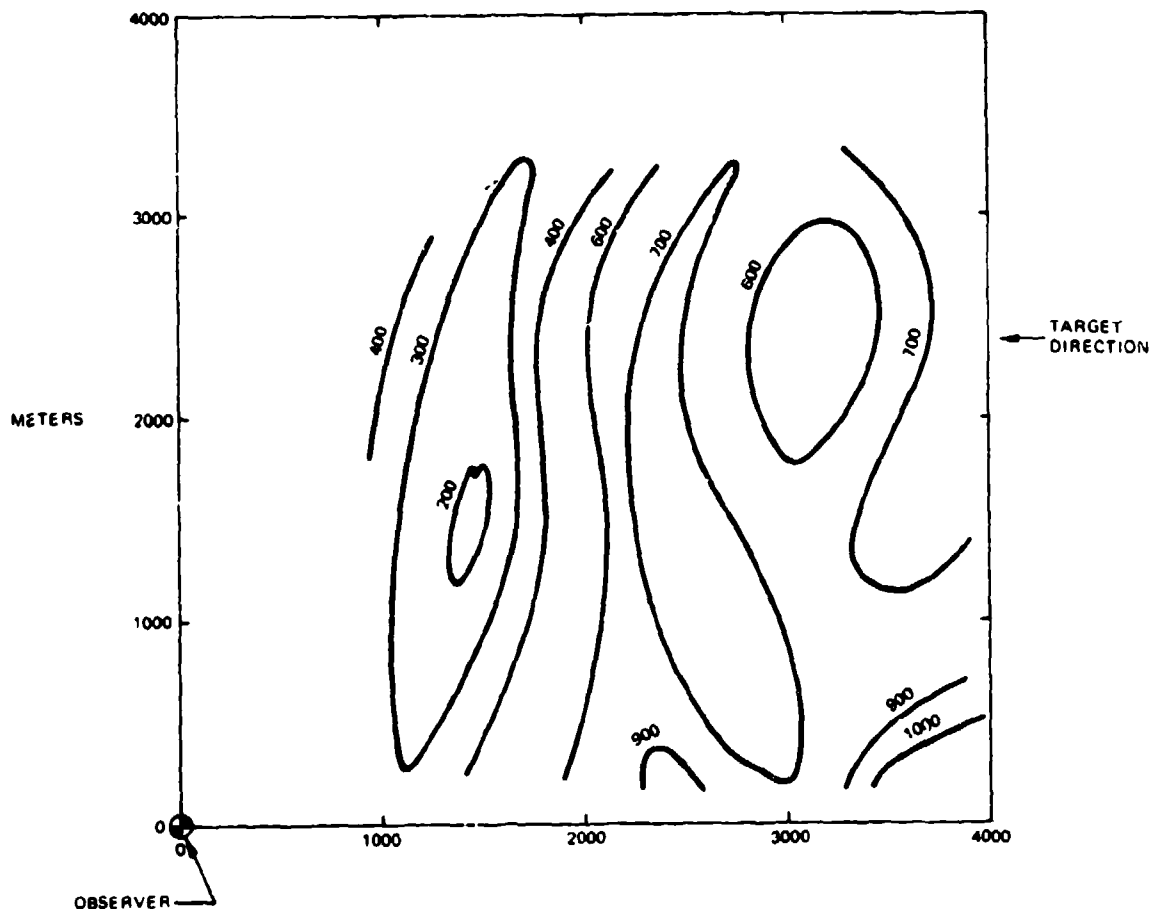
Figure 4-14. Footprint of Mean Absolute Range Estimation Error (meters)

4.3.1 Design Objectives

The regeneration module of the fire control system is intended to perform the following functions:

a. *Human Operator Assistance*

(1) Generate the principal portion of the time varying components of angular tracking derivatives and drive the unit correspondingly, leaving only minor corrections for the human operator.

(2) Respond to tracking corrections made by the human operator with dynamics compatible to human response dynamics. The complete system should feel like good 'aided tracking'.

(3) Not preempt the tracking function from the man when the target is accelerating.

b. *Automatic Tracking Assistance.* Provide a means for reducing servo lags in the high tracking derivative regions without the necessity for widening the effective servo bandwidth.

c. *Tracking Extrapolation Through Sensor Interrupts.* Drive the sensors and provide extrapolated tracking data in all three coordinates during intervals of target obscuration, ECM interference

4-21

with sensor operation, doppler radar blind zones, and other causes of intermittent sensor inputs.

d. *Fail Safe*. If the regenerative element fails the system should retain the tracking capability. The human operator's control should degrade to no worse than normal aided tracking.

Rapid settling of the regenerative loop is desirable after initial target acquisition, on the other hand to be useful the module must attenuate the tracking errors in estimating the course invariants. How well these invariants are separated from normal tracking noise determines both the system effectiveness in continuous operation, and the rate of error divergence during intervals of sensor interruption. Hence there is a compromise to be found between smoothing time and noise reduction, as in the case of the conventional prediction algorithms.

4.3.2 Preliminary Analysis

A generic schematic is shown in Figure 4-15. All of the variables (x,y,...) are vectors and the transfer functions ar   xed by matrices. The following notation is used:

x — target coordinate vector

y — coordinate vector of the point defined by tracker output

e — error in target position as defined by tracker output

e — $x - y$

z_1 — drive input signal generated from the tracking error

z_2 — drive input signal generated by the regeneration unit

$z = z_1$
$+ z_2$ — total input signal to the drive servo-mechanism expressed as the desired velocity vector

z_4 — actual velocity vector generated

e_t — drive error

e_t — $z - z_4$

z_4 — dy/dt

z_1 — $Y_s(s) e$

$Y_s(s,t)$ — transfer function of the drive servo. It may vary with time if, for example, the loop gain is made a function of slant range or some other parameter.

$Y_r(s,t)$ — transfer function of the regenerative unit. It will vary with time because of the changing geometry and other causes.

Then

$$z_1 = Y_e e$$

$$z_2 = Y_r y$$

$$y = Y_s e_s \qquad (4.53)$$

In the diagram the dashed line indicates how, in the ingenious Vigilante design, the position component of the operator's correction is applied directly to the sight, without intervening servomechanisms. In the case of Vigilante

$$Y_e = c_1 + c_2/s \qquad (4.54)$$

When there is a human operator in the system we divide the error processor into two parts: the first represents the perception of error by the man and his consequent movement of his control; the second represents the generation of the command signal to the drive controller as a function of control movement. Then

m — operator response as applied at the control

Y_p — transfer function of the operator

m — $Y_p e$

Y_c — transfer function of the control

z_1 — $Y_c m$

If the man and his control are both represented as a unit

$$z_1 = Y_p Y_c e ; Y_p Y_c = Y_e \qquad (4.55)$$

Note that if the target is maneuvering, flying a course not conforming to the regenerated rates, the difference between target velocity and regenerated velocity (integrated) is e, and this must be provided by the man. Hence he responds in this case to e/x.

From the diagram and the preceding definitions, the response of the drive servo alone is

$$y = e_s Y_s$$

$$= (z - sy) Y_s$$

$$y/z = Y_s/(1 + s Y_s) \qquad (4.56)$$

and for a very tight servo, in this formulation, (i.e., Y_s is very large)

$$y/z = 1/s \qquad (4.57)$$

and the drive operates as a simple integrator on its input signal.

Considering the system as a whole, we are interested in

y/x = system output/input

e/x = system error/input

y/m = system output/control input or: system dynamics as they appear to a human operator if there is one.

z_2/sx = generated rates/true target rates: This is a measure of how rapidly the solution will degrade if the target is lost.

These quantities are summarized in Table IV-3.

It is assumed that the regenerative module serves two purposes: 1) to provide regenerated rates, from which, with a 'tight' servo, regenerated position is obtained by integration, and 2) to provide 'feed forward' signals to the servo which compensate for at least the velocity and acceleration lags of a servo system for which these quantities are of significant magnitude.

To determine the lag correcting components, the expression for e/x is expanded as a series in s, using the best estimate of the servo transfer function. $Y_r(s)$ is then designed to make $e/x = 0$ to terms in s^2. This is a small correction, and is not likely to cause stability problems, but the usual stability tests can be applied to the system, with adjustment of the high frequency response of Y_s and Y_r if necessary, to obtain satisfactory stability.

As described above, the complete system is non-linear, because of the time varying coordinate transformations. A preliminary analysis of the transient performance, which depends on the high frequency portion of the transfer functions, can be made along the following lines.

Consider the operations shown in the regeneration block of Figure 4-16. y and z are vectors. Let v = the vector of invariants on which the smoothing operation is to be performed, and let R be the matrix describing the coordinate transformation from y to v. Then

$$v(t) = R(t) y(t) \qquad (4.58)$$

$$\underline{v}(t) = \int_0^{T_s} v(t\text{-}s)W(s)\,ds \; ; \qquad (4.59)$$

$W(s)$ is the weighting function of the filter, and T_s is the smoothing interval

$$z(t) = R(t)^{-1} \underline{v}(t) \qquad (4.60)$$

Hence

$$z(t) = R(t)^{-1} \int_0^{T_s} R(t\text{-}s)y(t\text{-}s)W(s)\,ds \qquad (4.61)$$

If we expand

$$R(t\text{-}s) = R(t) \cdot s\, dR(t)/ds + \cdots \qquad (4.62)$$

and we assume that $R(t)$, which contains the trigonometric conversions, is changing slowly, then to a first approximation

$$z(t) = \int_0^{T_s} y(t\text{-}s)W(s)\,ds - \cdots \qquad (4.63)$$

and we can consider the regeneration function as if it were performed in each coordinate represented in z, y separately.

We consider two cases 1) automatic tracking, 2) manual tracking.

In the case of automatic tracking, the servo bandwidth will normally be much wider than the bandwidth of the filters in the regenerative module. Then in continuous system operation, the transient response of y/x will be essentially that of the servo. The regenerated rates will display transient response determined almost entirely by the filter smoothing time. The servo and regenerative module components can be designed separately with only a minimum interface in the lag correction function.

The best filters for the regenerative unit will have similar requirements to those of the prediction module,
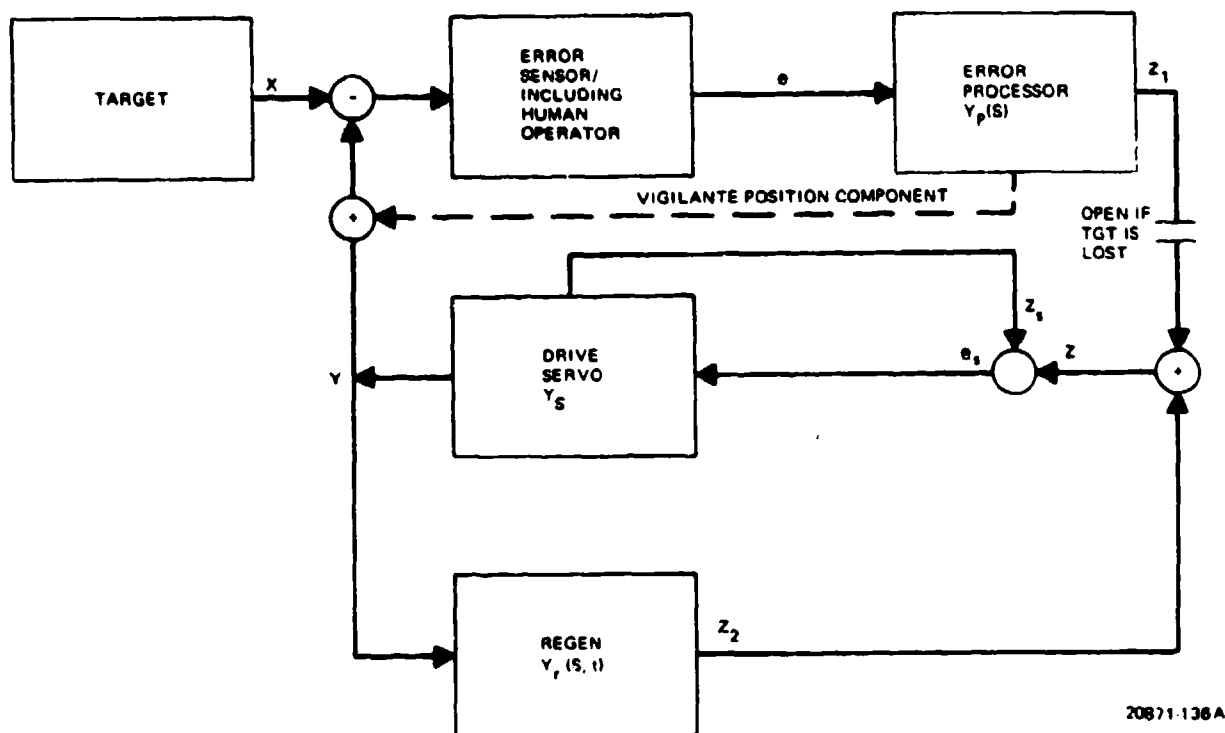
Figure 4-15. Generic Flow Diagram of Regenerative and Tracking Elements

and in fact there seems to be no reason why the same filters should not be used.

In the case of manual tracking, first consider the 'fail-safe' mode in which there is no regenerative aid. If the servo operates as an ideal integrator, we must specify

$$y_c(s) = c_0 s + c_1 \qquad (4.64)$$

if the operator is to have 'rate-aided tracking'. The ratio c_0/c_1 has the dimensions of time and should be in the range 0.20 to 1.0 second.

If the drive servo has a significant lag, it is best to by-pass the servo to apply the position component to the sight, as was done in Vigilante, and to provide a phase advance signal to 'quicken' the velocity response of the servo.

Next consider the more general case with servo lag and the regenerative unit operating. From Table IV-3 the transfer function defining the dynamic relationship between the man's movement of the control, and the response he observes in his sight is

$$y/m = \frac{Y_s Y_c}{1 + Y_s(s - Y_r)} \qquad (4.65)$$

Referring to Section 4.2.1 we require that above 1 Hz the amplitude ratio be essentially constant, with a phase lag no more than 45° at 1 Hz decreasing to less than 10° at 2 Hz. In the region 0.10 to 1.0 Hz the control should have a 'rate' characteristic, i.e., the amplitude ratio should decrease with frequency as -2, and the phase lag should not exceed 90°. Below 0.10 Hz the Y_c network should be designed to ensure non-oscillatory response to a step function movement of the control.

A typical form for Y_r in an analog system could be Blackman's velocity filter

$$Y_r(s) = \frac{s}{1 + s(T_r/2) + s^2(T_r^2/10)} \qquad (4.66)$$

Y_s is the servo transfer function, and can be used in complete form when a known servo is to be used. If the servo loop has negligible lag, $Y_s = 1/s$.

For large s it is desired that

$$y/m = c_0 + (c_1/s) \qquad (4.67)$$

where c_0 and c_1 are chosen to match the 'ideal' functions described above. Then Equation 4.15 can be solved for Y_c as a series in s' to obtain the required

4-24

Table IV-3. Summary of Transfer Functions

Function		Expression	
		Generalized Drive Servo	"Tight" Drive Servo
System output/input	y/x	$\dfrac{Y_e Y_s}{1 + Y_s [s + Y_e \cdot Y_r]}$	$\dfrac{Y_e}{s + Y_e \cdot Y_r}$
System error/input	e/x	$\dfrac{1 + Y_s(s - Y_r)}{1 + Y_s [s + Y_e \cdot Y_r]}$	$\dfrac{s \cdot Y_r}{s + Y_e \cdot Y_r}$
System output/control input	y/m	$\dfrac{Y_s Y_c}{1 + Y_s(s - Y_r)}$	$\dfrac{Y_c}{s \cdot Y_r}$
Regenerated rates/target rates	z_2/sx	$\dfrac{Y_s Y_r Y_e}{s[1 + Y_s(s + Y_e \cdot Y_r)]}$	$\dfrac{Y_r Y_e}{s(s + Y_e \cdot Y_r)}$

20871-505A
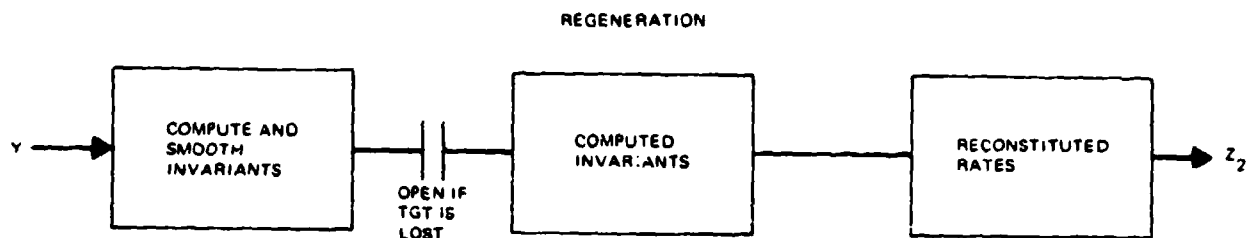
REGENERATION

Figure 4-16. Elements of Regeneration Module   20871-137

high frequency characteristic. Y_c can then be developed as a network with this high frequency asymptote and a low frequency characteristic to provide an overall satisfactory (i.e., smooth and non-oscillatory) transient response.

Some preliminary analyses indicate that a suitable form for Y_c is simply $A + B/s$, in sequence with a lead-lag network to compensate for servo lag if necessary. The effective value of the integral term B/s is reduced by a term of opposite sign from Y_r, and so B would be chosen larger than if the regenerative module were not in the system.

To carry out an actual system design the following procedure could be followed:

a. Make a preliminary control design according to the above ground rules, and verify its operation on the simulation, using the simplest operator model, i.e., $Ke^{s\tau_M}/s$.

b. Construct a breadboard of the tracking unit which can be operated by a human tracker, and perform a final verification of ease of control and satisfactory tracking accuracy.

4-25

4.3.3 Improved Tracking and Regeneration Module for Simulation

In the AFAADS-I simulation the lag correcting module exhibited a very slowly damped ripple (Figures 5-24 and 5-25 of the AFAADS-I report). Further analysis revealed that this resulted from the fact that the acceleration lag correction was computed from a measure of acceleration obtained by differencing the regenerated angular velocities. This was an expedient intended to simplify the simulation. In fact the angular accelerations can be computed directly from the smoothed linear velocity components by algorithms given in AFAADS-I. The effect of the differencing process, however, in the closed loop discrete computation with the shortest smoothing time (5-points, 0.4 second smoothing) was to locate the largest characteristic root in the complex z plane close to the unit circle, from which the poorly damped response resulted.

Replacement of the differencing operation by direct calculation of the regenerated acceleration at each sample point eliminated the problem completely. The corrected algorithm is applicable to any fire control system design.

The revised tracking and regeneration module now incorporated in the simulation has the following characteristics:

a. The lag regeneration correction has been revised to eliminate the objectionable ripple noted in AFAADS-I.

b. A better representation of radar glint is provided.

c. The major improvement is the provision of a capability to have the solution switch to regenerated data when tracking loss is simulated, run on regenerated data until tracking is assumed to be resumed, and switch back to tracking data incurring only the transients resulting from the difference between regenerated data and tracking data at the point of resumed normal tracking.

d. This option is provided separately in range and angle. This allows the effect of doppler nulls in either or both to be determined. It also allows the effect of ECM denying range only to be determined.

e. The firing mode of Vigilante can also be simulated by this mode (switch to regenerated rates, fire on regenerated rates, resume tracking).

f. Retention of the lag computation and correction allows future investigation of the interaction between glint and servo bandwidth. Glint error is reduced by narrow servo bandwidth, lag error is increased by narrow servo bandwidth.

g. The module allows options of both non-recursive smoothing and recursive smoothing with parameters depending on target path characteristics.

4.3.4 Discussion

Data flow is shown in Figure 4-17.

4.3.4.1 Servo Lag Computation

There is no change from AFAADS-I, except that range lag is omitted on the grounds that 1) lag is a minor problem with ranging systems as compared with angle tracking systems and 2) as shown in AFAADS-I small range errors have a negligible effect on prediction errors.

Azimuth and elevation lag are computed as

$$L_A(t) = \dot{A}(t)/K_v + [\dot{A}(t) - \dot{A}(t - \Delta)]/(K_a\Delta)$$

$$L_e(t) = \dot{e}(t)/K_v + [\dot{e}(t) - \dot{e}(t - \Delta)]/(K_a\Delta) \quad (4.68)$$

4.3.4.2 Servo Lag Correction

The AFAADS-I problem resulted from the fact that regenerated accelerations were obtained by differencing regenerated angular rates. In the present module the lag correction is computed as

$$L_{CA}(t) = \dot{A}_r(t)/K_v + \ddot{A}_r(t)/K_a$$

$$L_{Ce}(t) = \dot{e}_r(t)/K_v + \ddot{e}_r(t)/K_a \quad (4.69)$$

These are obtained from smoothed linear positions and velocities. Smoothed position is updated one interval to present position in each coordinate using smoothed velocities, as before. Then angular velocities and accelerations are computed from rectangular positions and velocities only as was done for the gun module (except for the time of flight terms) in AFAADS-I.

4.3.4.3 Regenerated Functions

The regenerated position elements in rectangular coordinates are

$$X_r(t) = \underline{X}(t - \Delta) + \underline{V}_X \Delta$$

$$Y_r(t) = \underline{Y}(t - \Delta) + \underline{V}_Y \Delta$$

$$Z_r(t) = \underline{Z}(t - \Delta) + \underline{V}_Z \Delta \quad (4.70)$$

Angular velocities and accelerations are obtained from the set of expressions (5.57)-(5.64), p. 5-21 of AFAADS-I, namely

$$R_r^2 \dot{A}_r = YV_x - XV_y$$

$$D_r^2 \dot{e}_r = R_r V_z - ZR_r$$

$$R_r \dot{R}_r = YV_y + XV_x$$

$$D_r \dot{D}_r = R_r R_r + ZV_z \qquad (4.71)$$

$$R_r \ddot{A}_r = -2\dot{R}_r \dot{A}_r$$

$$D_r^2 \ddot{e}_r = -2D_r \dot{D}_r \dot{e}_r - R_r (\dot{A}_r)^2 Z \qquad (4.72)$$

where the subscript $(_r)$ refers to the regenerated quantities.

4.3.4.4 Interrupt and Recover

At predetermined points the process switches from inputs derived from the target to regenerated data, runs on regenerated data, then switches back to target path data.

The interrupt can be applied either in range or both angles, or all three together. There does not seem to be any point at this time in providing for interrupt in azimuth or elevation separately.

From the $X_r(t)$, $Y_r(t)$, $Z_r(t)$ given by Equation (4.70), $A(t)$, $e(t)$, and $D(t)$ are obtained by the CTOP conversion. At interrupt these A, e, D replace the A, e, D from tracking, and the system runs with its tail in its mouth like The Worm Ouroboros (Eddison). It has been verified by simulation operation that this mode functions successfully and the solution does not swallow itself and vanish. This mode has the advantage that all of the filters remain loaded, and when normal tracking resumes, it has only to adjust for the difference between the new data and the data it has regenerated.

4.4 SIMULATION MODULE TO INCLUDE 'FLIGHT ROUGHNESS'

In AFAADS-I it was decided on the basis of analysis not to include flight roughness in the simulation, since it was concluded that flight roughness would be a small source of error compared with other sources, at the relatively short times of flight of the AFAADS weapon.

Flight roughness is defined as that stochastic motion of the aircraft caused by air turbulence, etc., which appears as a deviation from the smooth path commanded by the pilot.

Frankford has included flight roughness in in-house fire control evaluations in the past and it is desirable to include this capability as an option in the simulation if

it can be provided without excessive complication. After some reflection, it has become apparent that flight roughness can, in fact, be included in the Ginsberg simulation without extensive reprogramming. The actual programming is beyond the scope of the present contracted effort, but the purpose of this note is to record the approach for possible later inclusion.

4.4.1 Approach

First note that when the target is deliberately performing an evasive maneuver, even very low acceleration maneuvers, the deviation from a predictable path is so large that it will dominate whatever contribution to error might result from flight roughness.

On the other hand when the pilot is deliberately trying to fly an unaccelerated path, flight roughness will have a measurable effect which may be worth determining. On a straight line attack path for example, the combination of the effects of air turbulence at low altitude and the pilot's attempt to keep his sight on target may generate stochastic perturbations about the mean flight path that would be of interest to view on the simulation.

Flight roughness, as a perturbation about the mean flight path enters the system evaluation at two points.

a. It is a perturbation on the tracking data and therefore goes through the smoothing and prediction elements and affects the predicted point via that route.

b. It perturbs the flight path during time of flight and thus affects the actual position of the aircraft at the instant the shell reaches it.

These two effects are correlated. If flight roughness deviations were completely uncorrelated across time of flight, they could be included as two separate entries: one at the tracker, one in the hit computation. In fact we must consider the correlation across short times of flight. Note that for very high correlation across time of flight, the effect vanishes, since the same quantity entered at the tracker is removed at the predicted point. The result in general is that the effect of flight roughness cannot properly be inserted at either the tracker or the predicted position alone, although one could estimate the proper correction approximately at either point for a given system by analyses external to the simulation.

The current Monte Carlo mode of the simulation is so well adapted to a good treatment of flight roughness, however, that a direct inclusion without approximation seems to be preferable.

4.4.2 Characteristics of Flight Roughness

The first step is to generate the deviations from the mean flight path as caused by flight roughness. Available data indicates that deviations along the flight path
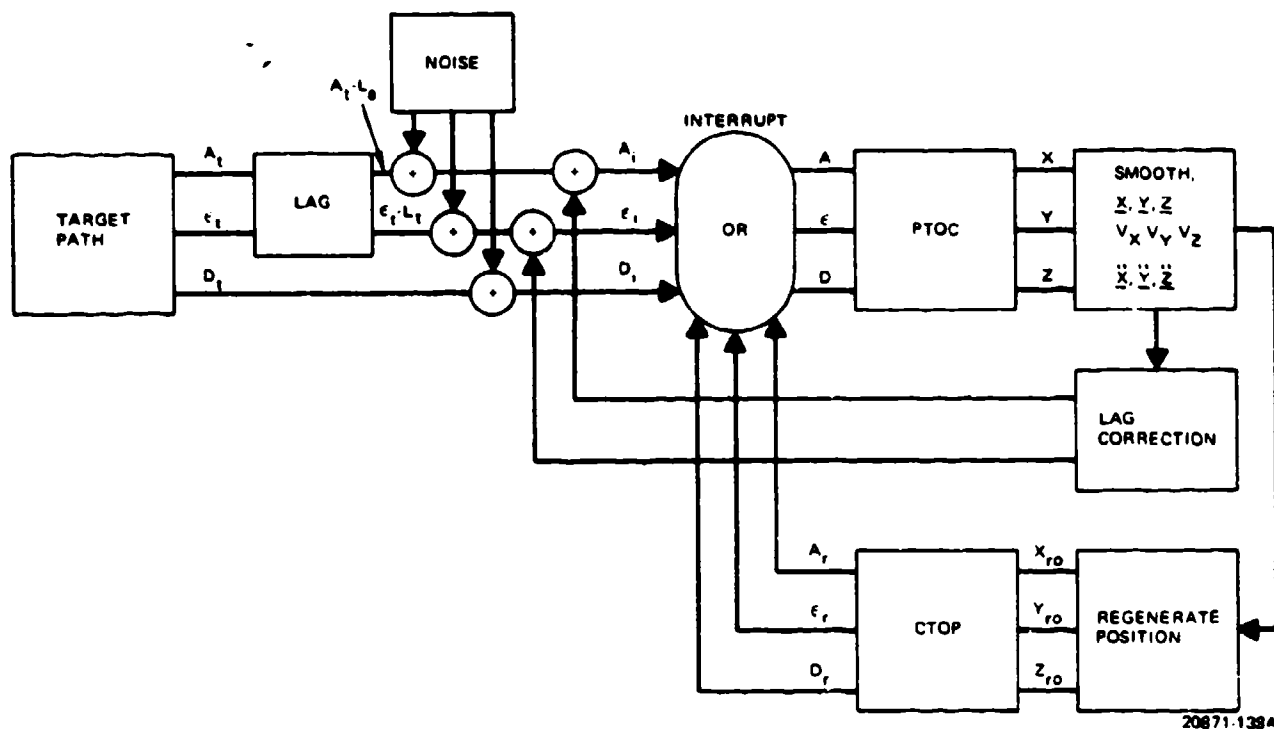
Figure 4-17. Radar Tracking, Noise, Smoothing and Regeneration Flow Diagram

can be neglected (although the following method allows their conclusion) and that deviations in a lateral horizontal plane and in a vertical plane can each be described by a variance and an autocorrelation consisting of a damped sinusoid.

These deviations are computed as a stochastic series in a manner similar to that now used to generate tracking noise, but with a different form of autocorrelation (not one-step Markov).

A gaussian random number distribution with unit variance is sampled as is done in present noise generation, at the same intervals. The deviation in each one of the three coordinates is then computed as

$$y(t) = a_1 y(t-\Delta) + a_2 y(t-2\Delta) + a_3 n(t) \qquad (4.73)$$

where $n(t)$ is the sampled random number, and a_1, a_2, a_3 are chosen to generate the right autocorrelation and variance. (See the later section on, 'digital generation of colored noise'.)

The three deviations at each point are resolved from target heading coordinates to tracker coordinates and added to the presently generated noise values repre-

senting tracking error. The system then operates as at present and processes the summed inputs as at present.

The deviations from the mean flight path represent a stochastic series defining the aircraft's deviation from its mean path in aircraft coordinates at each point in time. Knowing the time of a particular point the deviation triad can be extracted without reference to the target position at that point.

There is no need to store past deviations after they have gone into the prediction computation. However, the generation of the flight roughness series continues. At the predicted point, when the time of closest approach is determined, the flight roughness series is queried for the values at that time (interpolating if necessary) and the values converted to appropriate coordinates are subtracted from the miss distances computed on the mean flight path.

This gives the right answer.

The flow diagram of the computation is shown in Figure 4-18 and the geometric representation is shown in Figure 4-19.

"WHITE VOICE"
UNIT VARIANCE
ZERO MEAN
GAUSSIAN OR POISSON

$t + k\Delta$

COMPUTE DEVIATIONS IN A/C COORDINATES, 3-AXES

FLIGHT ROUGHNESS SERIES

FLIGHT PATH

A +

PREDICT

−

ERROR IN AIM POINT BY PRESENT COMPUTATION

B −

ERROR IN AIM POINT INCLUDING FULL CORRECTION FOR FLT ROUGHNESS

NOTE. WHERE "A" AND "B" ARE IN THE PROGRAM DEPENDS ON THE COORDINATES USED IN THE COMPUTATION
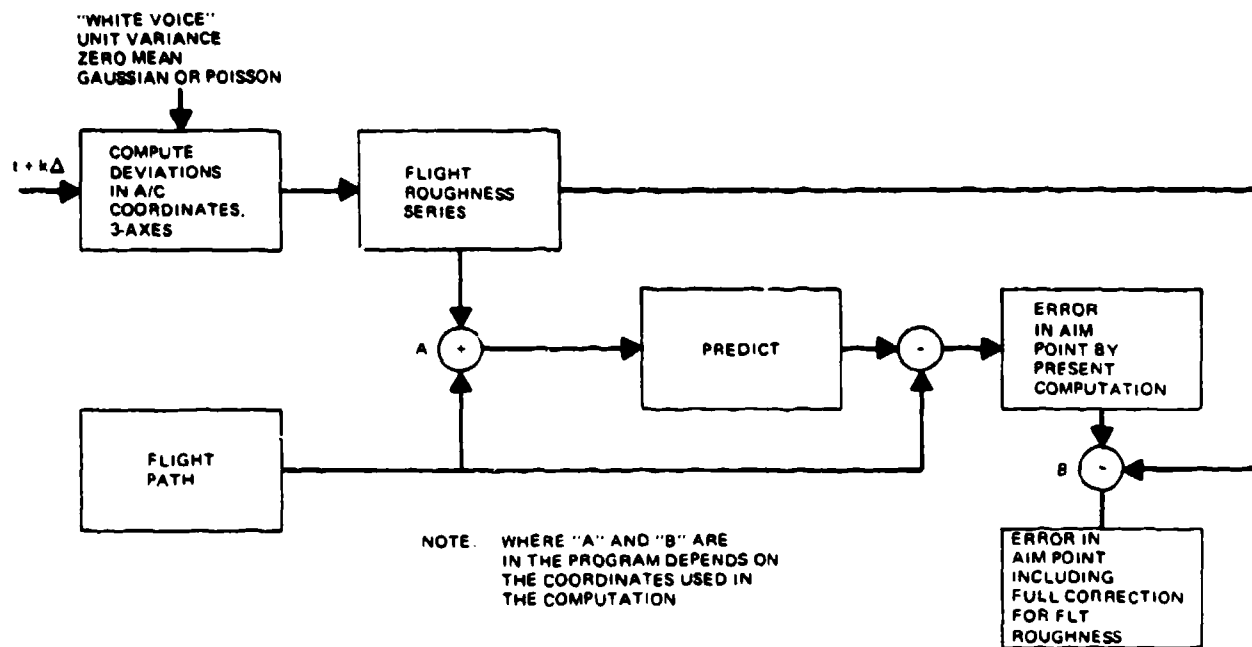
20871-139A

Figure 4-18. Flow Diagram of Flight Roughness Simulation Module

FLT ROUGHNESS DEVIATION

t_o

$t + t_p$

MEAN FLT PATH

ADD TO TRACKING ERROR

SUBTRACT FROM PREDICTION ERROR OR ADD TO FLT PATH AT $t + t_p$
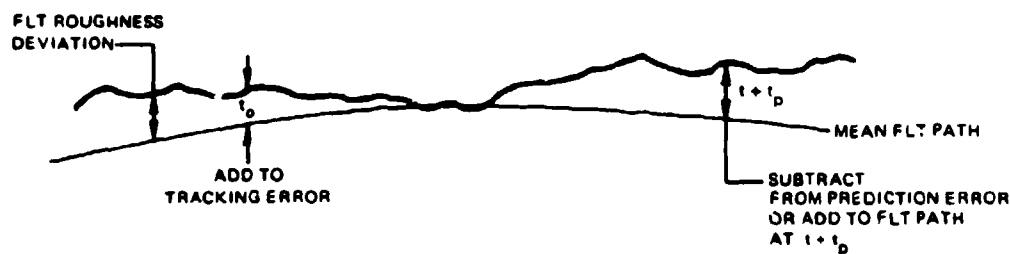
20871-140A

Figure 4-19. Relationship of Flight Roughness Deviation to Mean Flight Path

4-29/4-30

SECTION 5
DATA SMOOTHING

The filters used in the AFAADS-I simulation were optimized for maximum variance reduction of white noise with a constant smoothing interval, i.e., memory time.

The present analysis examines the consequences in terms of filter design of imposing an additional constraint on the optimization, namely the integrated mean square variance of the error during the initial settling of the filter. An attempt is made to compromise between this transient penalty function and the reduction of variance or error resulting from tracking error in the steady state.

The effect is to change the filter coefficients to place greater weight on the most recent data. The fixed memory discrete filter then resembles closely the recursive filters generally known as α - β - v filters.

A tentative conclusion is that the finite memory filters have no fundamental advantage over the α - β - v algorithms when settling time is important. Since the recursive filter algorithms are well suited to continuous parametric variation with target path parameters such as range, target velocity and acceleration, etc., whereas parametric variations of the same kind can be applied to fixed memory filters only at the expense of computer capacity, it is concluded that the most profitable direction for additional filter analysis is the investigation of situation-varying recursive filters.

5.1 FIXED MEMORY FILTERS

This section develops expression for discrete, fixed length memory filters on the assumption that it is desirable to seek a compromise between variance reduction and rapid settling. For a discrete filter with specified interval between sample points, the fastest settling is obtained by using the minimum number of points, one for position, two for velocity, and three for acceleration. These filters provide no smoothing. On the other hand, as long as the target conforms to a specified constant derivative course, variance reduction increases with the number of points and hence with the total smoothing time. For a fixed smoothing time, as more points are added, with proportionately shortened interval, there is increased variance reduction until the sampling interval approaches the correlation time of the noise.

If smoothing time is held constant, both the settling time and the variance reduction for a given number of sample points can be changed, each at the expense of the other, by changing the values of the filter coefficients.

In attempting to find a best compromise between settling time and variance reduction, one must choose a measure of effectiveness. A preferred measure would be derived from the probability of killing the target during the available firing interval. Although this measure can be quantified in terms of Markov processes, somewhat along the lines indicated in Section 3.1, analysis along these lines requires more effort than could be devoted here. It would, however, allow in one optimization, consideration of correlation of prediction error with time, gun dispersion, and the distribution of expected firing time.

The method used in this section is to follow an approach developed by Benedict and Border[1] and by Simpson[2]. Briefly, one establishes two demerit functions, as follows:

Measure time t from the instant of target acquisition. Define

$e(t)$ = system error at time t.

Initially $e(t)$ consists principally of the initial transients, during the initial settling of the system. It then reduces to errors caused by tracking 'noise.' Let

D_n = Variance of steady-state filter output for unit mean square noise input. D_n is the 'noise demerit'

$$D_s = \int_0^\infty t^m \left[e_t(t) \right]^2 dt \qquad (5.1)$$

where $e_t(t)$ is the transient error in the absence of tracking noise.

By increasing the value of the exponent 'm' the filter can be increasingly penalized for slow settling.

The measure of effectiveness of the filter is then defined as

$$J = D_s + \lambda D_n \qquad (5.2)$$

where λ makes the dimensions conformable, and expresses the relative importance to be applied to D_s versus D_n.

For this analysis we take m = 0. The effect of making m very large would be to de-emphasize the contributions of the oldest filter points, and is roughly similar to setting λ very small.

We consider the optimization of J for each derivative class of filter separately. It appears that if we attempt a best compromise prediction unit as a whole, the derived filter coefficients will depend explicitly on time of flight. This is contrary to the case of simple variance reduction, where the optimum prediction unit

is composed of separately optimized filters, and the best coefficients do not depend on time of flight, as long as one does not introduce the variation of tracking noise variance with range.

Since in each prediction module, the performance will be dominated by the highest derivative used, we develop the coefficients for each set in terms of the best compromise point for the highest derivative filter of the set.

Although the following development is for discrete filters, an analogous process could be employed to determine the weighting functions according to the same criteria for continuous filters.

For constant sampling interval Δ, and $n+1$ data points, the filter algorithm is in general (for any derivative),

$$y(N) = \sum_0^n c_j \, x(N\text{-}j) \qquad (5.3)$$

where $x(N)$ is input at data point N and $y(N)$ is the developed output.

This expression can be conveniently written in terms of the z-transform as

$$y(z) = x(z) \sum_0^n c_j \, z^{-j} \qquad (5.4)$$

For all filters $x(N)$ is taken as the position input.

Constraints

For a position filter

$$\sum_0^n c_j = 1.0 \qquad (5.5)$$

For a velocity filter

$$\sum_0^n c_j = 0$$

$$\Delta \sum_0^n j c_j = -1.0; \; \Delta \text{ is the sampling interval} \quad (5.6)$$

For an acceleration filter

$$\sum_0^n c_j = 0$$

$$\Delta \sum_0^n j c_j = 0$$

$$\Delta^2 \sum_0^n j^2 c_j = 2.0 \qquad (5.7)$$

5.1.1 Settling Time Demerit

In the following development, the filter coefficients are first optimized for unit sampling interval, and then the correction to arbitrary sampling (constant) interval is applied.

A forcing function is applied to a filter initially at rest, at $t = 0$. For a position filter it is a unit step; for a velocity filter it is a ramp with unit slope; for an acceleration filter it is a parabola with unit second derivative and zero intial position and slope.

The expression for the filter error,- the transient,- is computed. Designate this

$$e(k)$$

The settling time demerit function is taken as

$$D_s = \sum_{k=0}^{\infty} [e(k)]^2 \qquad (5.8)$$

It is shown later that for non-recursive filters, D_s can be written as

$$D_s = \sum_j a_j^2 \qquad (5.9)$$

where the a_j are functions of the filter c_i; they are in fact the coefficients of z^j in the z-transform of the error expression.

An increased penalty for slow settling can be imposed by basing D_s on $k^m e(k)$. The corresponding z-transforms are (for $E(k) = k^m e(k)$)

$$m = 0; \qquad E(z) = \sum_j a_j z^{-j} \quad \cong e(z)$$

$$m = 1; \qquad E_1(z) = \sum_j j a_j z^{-j}$$

$$m = 2; \qquad E_2(z) = \sum_j j^2 a_j z^{-j} \qquad (5.10)$$

However, in the present study we examine only the case of $m = 0$.

To obtain D_s we make use of the following[5]:

a. Cauchy Theorem for inversion of a particular z-transform

If the integral I is defined by

$$I = \frac{1}{2\pi j} \int_\Gamma z^k \, dz \qquad (5.11)$$

and if Γ is a closed contour that encloses the origin of the z plane then I will have values given by

$$I = 0; \quad k > -1$$

$$I = 1; \quad k = -1$$

$$I = 0; \quad k < -1 \qquad (5.12)$$

b. Application to Sum of Squares of Sample Sequence

Given a sum

$$S^2 = \sum_{n=0}^{\infty} [f(nT)]^2 \qquad (5.13)$$

where $f(nT)$ is the n'th sample in a sequence whose transform is $F(z)$, the sum can be obtained from

$$S^2 = \frac{1}{2\pi j} \int_\Gamma F(z) \, F(z^{-1}) \, z^{-1} \, dz \qquad (5.14)$$

We wish to obtain

$$D_s = \sum_{n=0}^{\infty} [e(k)]^2 \qquad (5.15)$$

where the z-transform of $e(k)$ is

$$e(z) = \sum_0^{n-1} a_j z^{-j} \qquad (5.16)$$

This is obtained as

$$D_s = \frac{1}{2\pi j} \int_\Gamma \left[\sum_0^{n-1} a_j z^{-j} \right] \left[\sum_0^{n-1} a_k z^{+k} \right] z^{-1} \, dz \qquad (5.17)$$

If the term under the integral is expanded as a series in z^m, and the Cauchy theorem is applied term by term, the only surviving terms will be those within the brackets with product associated with z^0. The result therefore is

$$D_s = \sum_0^{n-1} a_j^2 \qquad (5.18)$$

5.1.2 Noise Variance Demerit

For white noise of unit rms value, it is well known that the mean square error in filter output is

$$D_n = \sum_{j=0}^{n} c_j^2 \qquad (5.19)$$

If, now we specify a function

$$J = D_s + \lambda D_n \qquad (5.20)$$

where λ is the relative value of noise reduction compared with settling time, we can obtain a best compromise filter by choosing the c_i to minimize J.

5.1.3 Position Filter

Apply a step function at $t = 0$. It has the z-transform

$$\frac{z}{z-1} \qquad (5.21)$$

The z-transform of the filter response is

$$\frac{z}{z-1} \sum_{j=0}^{n} c_j z^{-j} \qquad (5.22)$$

with

$$\sum_{j=0}^{n} c_j = 1.0$$

Then

$$e(z) = \frac{z}{z-1}\left[1 - \sum_{0}^{n} c_j z^{-j} \right] = a_0 + \cdots + a_{n-1} z^{-(n-1)} ; \text{ exactly}$$

$$\qquad (5.23)$$

Let $z^{-1} = x$; multiply both sides of the above by $1-x$ and equate coefficients of x^i.

$$a_0 = 1 - c_0$$

$$a_1 = 1 - c_0 - c_1$$

$$a_2 = 1 - c_0 - c_1 - c_2$$

$$a_j = 1 - \sum_{k=0}^{j} c_k = \sum_{j+1}^{n} c_k$$

$$a_{n-1} = 1 - \sum_{k=0}^{n-1} c_k = 1 - \sum_{k=0}^{n} c_k + c_n$$

$$= c_n \qquad (5.24)$$

And as determined earlier

$$D_s = \sum_{j=0}^{n-1} a_j^2$$

$$D_n = \sum_{0}^{n} c_j^2 \qquad (5.25)$$

It is convenient to continue from this point using matrix notation.

We have

$$a_j = \sum_{j+1}^{n} c_k \qquad (5.26)$$

whence

$$[a_0 \cdots a_{n-1}] = [c_1 \cdots c_n] \begin{bmatrix} 1 & 0 & 0 & \cdot \\ 1 & 1 & 0 & \cdot \\ 1 & 1 & 1 & \cdot \\ \cdot & \cdot & \cdot & \cdot \end{bmatrix} \qquad (5.27)$$

$$A^T = C^T R$$

Now

$$D_s = \sum_{0}^{n-1} a_j^2$$

so

$$D_s = A^T A = C^T R R^T C \qquad (5.28)$$

The constraint on the c_j is

$$\sum_{0}^{n} c_j = 1.0$$

so that

$$c_0 + C^T U = 1.0; U^T = \underbrace{[1 \ 1 \cdots 1]}_{n \text{ terms}} \qquad (5.29)$$

since

$$D_n = \sum_{0}^{n} c_j^2$$

$$D_n = c_0^2 + C^T C \qquad (5.30)$$

substituting for c_0^2

$$D_n = 1 - 2C^T U + C^T U U^T C + C^T C \qquad (5.31)$$

We wish to minimize

$$J = D_s + \lambda D_n \qquad (5.32)$$

and to do this we apply the operator

$$\nabla_c = \begin{bmatrix} \partial/\partial c_2 \\ \partial/\partial c_3 \\ \cdot \\ \cdot \\ \partial/\partial c_n \end{bmatrix}$$

20871-606

Set $\nabla_c J = 0$ and obtain

$$[R R^T + \lambda U U^T + \lambda I] C - U = 0 \qquad (5.33)$$

$$[I + U U^T + \lambda^{-1} R R^T] C - U = 0 \qquad (5.34)$$

$$\boxed{C = [I + U U^T + \lambda^{-1} R R^T]^{-1} U} \qquad (5.35)$$

This is the desired result.

If $\lambda = \infty$ the solution should reduce to the known least squares solution. Observe that

5-5

$$U^T U = n$$

and

$$[1 + UU^T]^{-1} = 1 \cdot UU^T + UU^T \, UU^T$$
$$\qquad - UU^T \, UU^T \, UU^T \cdots$$
$$\qquad = 1 \cdot UU^T + n \, UU^T \cdot n^2 \, UU^T + \cdots$$
$$\qquad = 1 \cdot UU^T (1 \cdot n + n^2 \cdots)$$
$$\qquad = 1 \cdot UU^T (1 + n)^{-1} \qquad (5.36)$$

Then

$$C = [1 + UU^T]^{-1} \, U$$
$$C = U \cdot UU^T U (1 + n)^{-1}$$
$$\quad = U \left\{ 1 \cdot n/(1 + n) \right\}$$
$$C = U \, \frac{1}{n+1} \qquad (5.37)$$

which is the known least squares solution.

5.1.4 Velocity Filter

The constraints for a velocity algorithm are

$$\sum_0^n c_j = 0$$

$$\sum_0^n j c_j = -1.0 \qquad (5.38)$$

Apply a unit step in velocity at $j = 0$. This has the transform

$$\frac{z}{(z \cdot 1)} \qquad (5.39)$$

The input to the filter, however, is a ramp input in position, also zero at $j = 0$, with the transform

$$\frac{z}{(z - 1)^2} \qquad (5.40)$$

The z-transform of the filter error in measuring velocity is therefore

$$e(z) = \frac{z}{(z \cdot 1)} \cdot \frac{z}{(z - 1)^2} \sum_0^n c_j z^{-j} \qquad (5.41)$$

Designate $x = z^{-1}$ and expand Equation (5.41)

$$e(x) = \frac{1 \cdot x(1 + c_o) \cdot x^2 c_1 \cdot \cdots \cdot x^{n+1} c_n}{(1 \cdot x)^2} \qquad (5.42)$$

In view of the constraints and the limit conditions for the z-transform we know that the numerator of this expression will be exactly divisible by the denominator. Hence

$$e(x) = a_0 + a_1 x + \cdots + a_{n-1} \, x^{n-1} \qquad (5.43)$$

Equating Equations (5.42) and (5.43)

$$1 \cdot (1 + c_o) x \cdot c_1 x^2 \cdot c_2 x^3 \cdot \cdots \cdot c_n x^{n+1} = (1 \cdot x)^2 \sum_0^n a_j x^j \qquad (5.44)$$

Equating coefficients

$$a_0 = 1.0$$

$$a_1 = 1 \cdot c_0$$

$$a_2 = 1 \cdot 2c_0 \cdot c_1$$

$$a_3 = 1 \cdot 3c_0 \cdot 2c_1 \cdot c_2$$

$$a_j = 1 \cdot \sum_0^{j-1} (j\text{-}k)c_k = \cdot \sum_{k=j}^{n} (k\text{-}j)c_k$$

$$a_{n-1} = 1 \cdot \sum_0^{n-2} (n\text{-}1\text{-}k)c_k$$

$$= 1 \cdot \sum_0^n (n\text{-}1\text{-}k)c_k + [(n\text{-}1)\text{-}n]\,c_n + [n\text{-}1 \cdot (n\text{-}1)]\,c_{n-1}$$

$$= \cdot c_n \qquad (5.45)$$

We obtain, therefore

$$a_j = \cdot \sum_{k=j}^{n} (k\text{-}j)c_k \qquad (5.46)$$

and $a_0 = 1.0$

We can write, therefore, in matrix notation

$$A^T = \{a_1 \cdots a_{n-1}\} = \cdot [c_2 \cdots c_n] \begin{bmatrix} 1 & 0 & 0 & 0 & \cdot \\ 2 & 1 & 0 & 0 & \cdot \\ 3 & 2 & 1 & 0 & \cdot \\ 4 & 3 & 2 & 1 & \cdot \\ & \cdot & \cdot & \cdot & \end{bmatrix}$$

$$(5.47)$$

$$A^T = \cdot C^T M \qquad (5.48)$$

Note $\cdot$ R^2, where R is the triangular matrix with $\cdot$ ments used in the position filter express

Now since

$$D_s = \sum_{j=0}^{n-1} a_j^2$$

we can write

$$D_s = 1 + C^T B C$$

where $B = M M^T$

Now

$$D_n = \sum_{j=0}^n c_j^2$$

and the velocity filter has the constraints, for unit sampling interval

$$\sum_{j=0}^n c_j = 0$$

$$\sum_{j=0}^n j c_j = -1.0 \qquad (5.49)$$

We can handle the constraints by adjoining terms with Lagrangian multipliers, however the computations seem to be more concise if we use the constraints to eliminate c_0^2 and c_1^2 in the expression for D_n.

The constraints can be expressed as

$$c_0 + c_1 + C^T U = 0; \quad U^T = [1\ 1\ 1\ \cdots] \qquad (5.50)$$

$$c_1 + C^T [D + U] = -1.0; \quad D^T = [1\ 2\ 3 \cdots] \qquad (5.51)$$

and these can be inserted in the D_n expression to yield

$$D_n = C^T N C + 2 + 2 C^T [2D + U] \qquad (5.52)$$

$$N = DD^T + [D+U]\ [D+U]^T + 1$$

Then as before

$$J = D_s + \lambda D_n \qquad (5.53)$$

Apply the operator

$$\nabla_c = \begin{bmatrix} \partial/\partial c_2 \\ \cdot \\ \cdot \\ \cdot \\ \cdot \\ \partial/\partial c_n \end{bmatrix}$$

set $\nabla_c J = 0$ and obtain

$$C = -[B + \lambda N]^{-1} [2D + U] \lambda \qquad (5.54)$$

which is the desired result.

5.1.5 Acceleration Filter

Apply a unit step function in acceleration at $t = 0$. It has a z-transform

$$\frac{z}{z-1} \qquad (5.55)$$

The input is in position, however, which for unit acceleration grows at $1/2\ t^2$. The position z-transform is

$$(1/2)\ \frac{z(z+1)}{(z-1)^3} \qquad (5.56)$$

so that the z-transform of the filter transient error is

$$\frac{z}{z-1} - (1/2)\ \frac{z(z+1)}{(z-1)^3} \sum_{j=0}^{n} c_j z^{-j} \qquad (5.57)$$

The filter constaints for unit sampling interval are

$$\sum_{0}^{n} c_j = 0$$

$$\sum_{0}^{n} j c_j = 0$$

$$\sum_{0}^{n} j^2 c_j = 2.0 \qquad (5.58)$$

Because of the constraints we can write the z-transform of the filter transient error as a polynominal in z'. Write $X = z^1$ as a convenience, whence

$$\frac{(1-x)^2 - x(1+x)(1/2)\sum_{0}^{n} c_j x^j}{(1-x)^3}$$

$$= a_0 + a_1 x + \cdots + a_{n-1} x^{n-1} \qquad (5.59)$$

Performing the long division and equating coefficients

$$a_0 = 1$$

$$a_1 = 1 - (1/2)c_0$$

$$a_2 = 1 - (1/2)(4c_0 + c_1)$$

$$a_4 = 1 - (1/2)(16c_0 + 9c_1 + 4c_2 + c_3) \qquad (5.60)$$

so that in general

$$a_j = 1 - (1/2) \sum_{k=0}^{j-1} (j-k)^2 c_k \quad j \geq 1 \qquad (5.61)$$

and using the three constraints this can be written

$$a_j = (1/2) \sum_{k=j}^{n} (k-j)^2 c_k \qquad j \geq 1$$

$$a_{n-1} = (1/2) c_n \qquad (5.62)$$

We can write, therefore in matrix notation

$$\begin{bmatrix} a_2 \cdots a_{n-1} \end{bmatrix} = 1/2 \begin{bmatrix} c_3 \cdots c_n \end{bmatrix} \begin{bmatrix} 1 & 0 & 0 & 0 & \cdot \\ 4 & 1 & 0 & 0 & \cdot \\ 9 & 4 & 1 & 0 & \cdot \\ 16 & 9 & 4 & 1 & \cdot \\ \cdot & \cdot & \cdot & \cdot & \cdot \end{bmatrix}$$

$$A^T = (1/2)C^T E \qquad (5.63)$$

Now

$$D_s = \sum_{j=0}^{n-1} a_j^2$$

$$= 1 + (1 - c_0)^2 + A^T A \qquad (5.64)$$

and

$$D_n = \sum_{j=0}^{n} c_j^2$$

$$= c_0^2 + c_1^2 + c_2^2 + C^T C \qquad (5.65)$$

The three constraints provide the values of c_0, c_1, c_2. They are

$$c_0 + c_1 + c_2 + C^T U = 0 \qquad U^T = [1 \cdots 1]$$
$$c_1 + 2c_2 + C^T [2U+D] = 0 \qquad D^T = [1\ 2\ 3 \cdots]$$
$$c_1 + 4c_2 + C^T [S+4D+4U] = 2 \qquad S^T = [1\ 4\ 9\ 16 \cdots]$$

$$(5.66)$$

From these,

$$c_0 = 1 - (1/2)C^T [S + D]$$
$$c_1 = -2 + C^T [S + 2D]$$
$$c_2 = 1 - (1/2)C^T [S + 2U + 3D] \qquad (5.67)$$

Substituting into D_s

$$D_s = 1 + (1/4)C^T [S+D][S+D]^T C + (1/4)C^T E E^T C$$
$$= 1 + (1/4)C^T \left[[S+D][S+D]^T + EE^T \right] C$$
$$= 1 + (1/4) C^T G C \qquad (5.68)$$

Substituting into D_n

$$D_n = 6 - C^T [6S + 12D + 2U] + (1/4) C^T F C$$
$$F = [S+D][S+D]^T + 4[S+2D][S+2D]^T$$
$$\qquad + [S+2U+3D][S+2U+3D]^T + 4I$$

Designate the function

$$J = D_s + \lambda D_n$$

and apply the operator

$$\nabla_c = \begin{bmatrix} \partial/\partial c_3 \\ \cdot \\ \cdot \\ \partial/\partial c_n \end{bmatrix}$$

$$\nabla_c J = 0 \qquad (5.69)$$

The result is

$$[G + \lambda F]\, C = 4\lambda\, [3S + 6D + U]$$
$$C = 4\lambda\, [G + \lambda F]^{-1} [3S + 6D + U]$$

$$(5.70)$$

in the limit as $\lambda = \infty$ the expression becomes

$$C = 4\, F^{-1} [3S + 6D + U] \qquad (5.71)$$

which is the least squares solution for zero settling time demerit.

5.1.6 Correction of Coefficients for Non-Unit Sampling Interval

Let c_i be the computed coefficients for a unit sampling interval and let b_i be the corresponding coefficients for a sampling interval Δ. Then for the three filter types we have the following correspondence.

Position Filter: $\quad b_{jp} = c_{jp}$; invariant with sampling interval

Velocity Filter: $\quad b_{jv} = c_{jv}\,\Delta^{-1}$

Acceleration Filter: $\quad b_{ja} = c_{j2}\,\Delta^{-2}$ $\qquad$ (5.72)

5.1.7 Modification of Optimization Function for Non-Unit Interval

If we reworked the optimizations of the preceding paragraphs using filters with non-unit sampling interval, we should find, on substituting the b_i for c_i that in the case of D_s, the a_j values are unchanged, the inclusion of Δ in the input function just cancelling the Δ modifying the c_j. This is to be expected, the system response to a step input is changed only by scaling the time scale and not the amplitude. However, since D_s is effectively the integrated mean square error in settling over time, it will be proportional to Δ. Hence we have the following conversions. D_{si}, D_{ni} are the values for unit sampling interval; D_s, D_n are the values for sampling interval as shown in Table V-1.

Table V-1. Sampling Interval Corrections

	Filter		
	Position	Velocity	Acceleration
D_n	D_{n1}	D_{n1}/Δ^2	D_{n1}/Δ^4
D_s	ΔD_{s1}	ΔD_{s1}	ΔD_{s1}

20871-506

5.1.8 Effect of Varying the Sampling Interval

The sampling interval is a disposable variable which may be adjusted for optimization. For the three filters, with sampling interval Δ, we may write

Position $\quad (J_p/\lambda) = (\Delta/\lambda)\left[D_{s1} + (\lambda/\Delta)D_{n1} \right]$

Velocity $\quad (J_v/\lambda^{1/3}) = (\Delta/\lambda^{1/3})\left[D_{s1} + (\lambda/\Delta^3)D_{n1} \right]$

Acceleration $\quad (J_a/\lambda^{1/5}) = (\Delta/\lambda^{1/5})\left[D_{s1} + (\lambda/\Delta^5)D_{n1} \right]$

$$(5.73)$$

The expressions in brackets are identical with those previously used to obtain the best compromise coefficients as a function of Δ, except that now, after obtaining the D_{si}, D_{ni} we replace λ by λ/Δ^k, and optimize the full term on the right. There will be an optimum in each ase, except for position, for which J/λ increases uniformly as Δ is reduced. In practice this increase is limited by the serial correlation of noise which limits the size of the interval allowing the white noise approximation to be used.

It turns out that for the velocity and the acceleration filters the optimum set of coefficients is close to the set obtained if the settling time demerit is ignored, i.e., λ is very large. We can obtain an estimate of $(\lambda/\Delta^k)^*$ in each case, which is close to the optimum, by assuming that D_{si}/D_{ni} is constant in the region of the optimum and equal to their values for $\lambda = \infty$. The values are

Velocity $\quad (\lambda/\Delta^3)^* \cong \dfrac{1}{2} \lim_{\lambda \to \infty} (D_{s1}/D_{n1})_v$

Acceleration $\quad (\lambda/\Delta^5)^* \cong \dfrac{1}{4} \lim_{\lambda \to \infty} (D_{s1}/D_{n1})_a$

$$(5.74)$$

Having performed the second optimization over Δ one obtains a set of coefficients which is uniquely preferred for the specific filter function, and the only effect of varying λ, for a given number of sample points, is to vary the sampling interval.

5.1.9 Comparing Filters for Different N

To put filters with different numbers of points on a common basis they should be referred to the same memory time, or smoothing time,

$T = (n-1)\Delta$, where there are n sample points.

A comparison of $J_v/\Delta^{1/3}$ for several velocity filters on this basis is given in Figure 5-1.

For the optimum set of filter coefficients in each case for the velocity filter, a comparison has been made by normalizing them to the same smoothing time, and adjusting the magnitudes in each case, according to Equation (5.196) of the AFAADS-I report, so that for the case of zero settling time demerit, all coefficients would lie on the same straight line. The comparison is
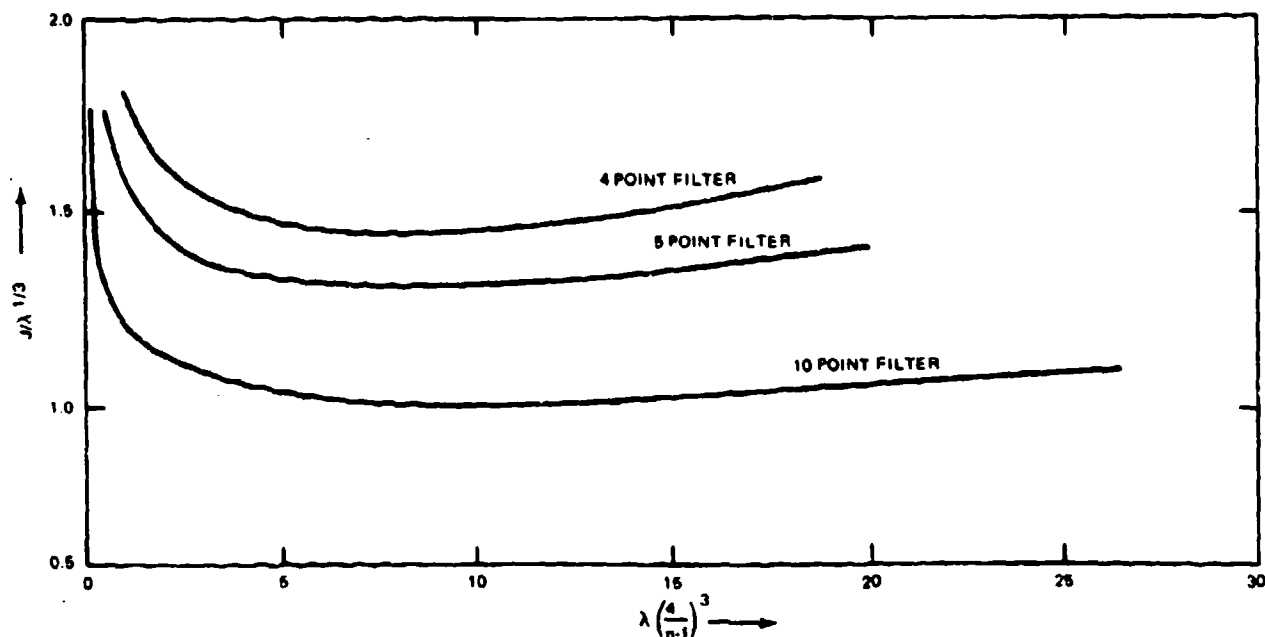
Figure 5-1. Comparison of Velocity Filter Performance Criteria

shown in Figure 5-2. For the two point filter, no optimization is possible and its two points lie at the ends of the reference line. The multiple point filters show a common pattern, with increased weighting of the more recent points, at the expense of the oldest points.

5.1.10 Example of Coefficient Variation with λ

The computation of the filter coefficients was done by a computer program. For a 4-point filter the computation can be done by hand, and before programming the algorithms, the following results, shown in Table V-2 were obtained by slide rule computation.

Note that when $\lambda = 0$, and we place very great importance on settling, for constant Δ, the method discards all points except the two most recent, as would be expected.

Table V-3 shows the optimization with (λ/Δ^3).

5.1.11 Lag Corrections

The position filter, as defined by the coefficients previously obtained, develops a lag when subjected to a constant velocity and/or constant acceleration input. The velocity filter develops a lag when subjected to a constant acceleration input. These lags are corrected by adding to each set of filter coefficients, a set of coefficients proportional to those of the next higher derivative filter. The correction is developed as follows.

5.1.12 Position Filter Lag to Constant Velocity

The correction has the dimensions of time, and is designated $T_{p/v}$.

Apply a ramp input, which has the z-transform

$$\Delta z/(z-1)^2 \qquad (5.75)$$

The z-transform of the response error of a position filter is

$$e(z) = \Delta z/(z-1)^2 \left[1 - \sum_{0}^{n} c_j z^{-j}\right] \qquad (5.76)$$

and the steady-state error when the filter has settled is

$$E(\infty) = \lim_{z \to 1.0} (z-1)E(z)$$

$$= \lim_{z \to 1.0} \frac{\Delta z}{z-1} \left[1 - \sum_{0}^{n} c_j z^{-j}\right] \qquad (5.77)$$

5-11

but we have already obtained this z function as the polynominal

$$\Delta \left[a_0 + \ldots + a_{n-1} \, z^{-(n-1)} \right] \qquad (5.78)$$

and so the lag error is simply obtained from

$$\sum_{0}^{n-1} a_j = A^T U = C^T RU = C^T D \qquad (5.79)$$

whence

$$T_{p/v} = \sum_{j=1}^{n} j \, b_{pj} \qquad (5.80)$$

5.1.13 Velocity Filter Lag to Constant Acceleration

The steps are identical with those followed in determining the lag of the position filter to velocity, but the algebra is more lengthy and will be abbreviated here.

Apply a step acceleration of unit magnitude. It generates the following z-transform in position input

$$(1/2) \, \Delta^2 \, \frac{z(z+1)}{(z-1)^3} \qquad (5.81)$$

The steady-state error of the filter is designated $T_{v/a}$ and is given by

$$T_{v/a} = \lim_{z \to 1} (z-1) \left[\frac{\Delta z}{(z-1)^2} \right.$$

$$\left. \cdot (1/2) \, \Delta^2 \, \frac{z(z+1)}{(z-1)^3} \sum_{j=0}^{n} b_j z^{-j} \right] \qquad (5.82)$$

This reduces, after some algebra, to

$$T_{v/a} = \cdot(\Delta^2/2) \sum_{j=1}^{n} j^2 b_{vj} \qquad (5.83)$$

5.1.14 Position Filter Lag to Constant Acceleration

The lag has the dimensions of $(time)^2$, and is designated $(T_{p/a})^2$. Since the lag increases indefinitely with time the limiting expression for the z-transform cannot be applied directly. If the correction for velocity lag is applied, however, the residual error to acceleration does reach a constant value. The algebraic reductions then yield

$$(T_{p/a})^2 = \cdot(\Delta^2/2) \sum_{j=1}^{n} j^2 b_{pj} \qquad (5.84)$$

where it must be remembered that the correction for velocity is separately applied.

5.1.15 Prediction Algorithm

The prediction Algorithm is

$$x_p = x_0 + v_0 t_p + (1/2) a_0 t_p^2 \qquad (5.85)$$

where $a_0 = \underline{a}$ = smoothed estimate of acceleration.

Now

$$v_0 = \underline{v} + \underline{a} \, T_{v/a}$$

$$x_0 = \underline{x} + v_0 \, T_{p/a} + \underline{a} \, T_{p/a}^2$$

$$= \underline{x} + \underline{v} \, T_{p/a} + \underline{a}(T_{v/a} T_{p/v} + T_{p/a}^2) \qquad (5.86)$$

and the complete prediction algorithm is

$$x_p = [(\underline{x} + \underline{v} \, T_{p/v}) + \underline{v} \, t_p] + \underline{a} \left[(t_p^2/2) \right.$$

$$\left. + t_p T_{v/a} + T_{v/a} T_{p/v} + T_{p/a}^2 \right] \qquad (5.87)$$

where the first bracket contains the terms used in constant velocity prediction, and the second bracket contains the terms used in constant acceleration prediction.

If there is no acceleration component in prediction, the prediction expression is

$$x_p = x_0 + v_0 \, t_p \qquad (5.88)$$

x_p = predicted position

t_p = time of flight

x_0 = smoothed present position corrected for lag

v_0 = smoothed velocity

and if

$\underline{x}$ = smoothed present position without lag correction

$\underline{v}$ = smoothed velocity

$$v_0 = \underline{v}; \quad x_0 = \underline{x} + \underline{v} \, T_{p/v} \qquad (5.89)$$

and the velocity lag correction can be made an integral part of the smoothed position computation by

$$(b_{pj})_c = b_{pj} + T_{p/v} \, b_{vj} \qquad (5.90)$$
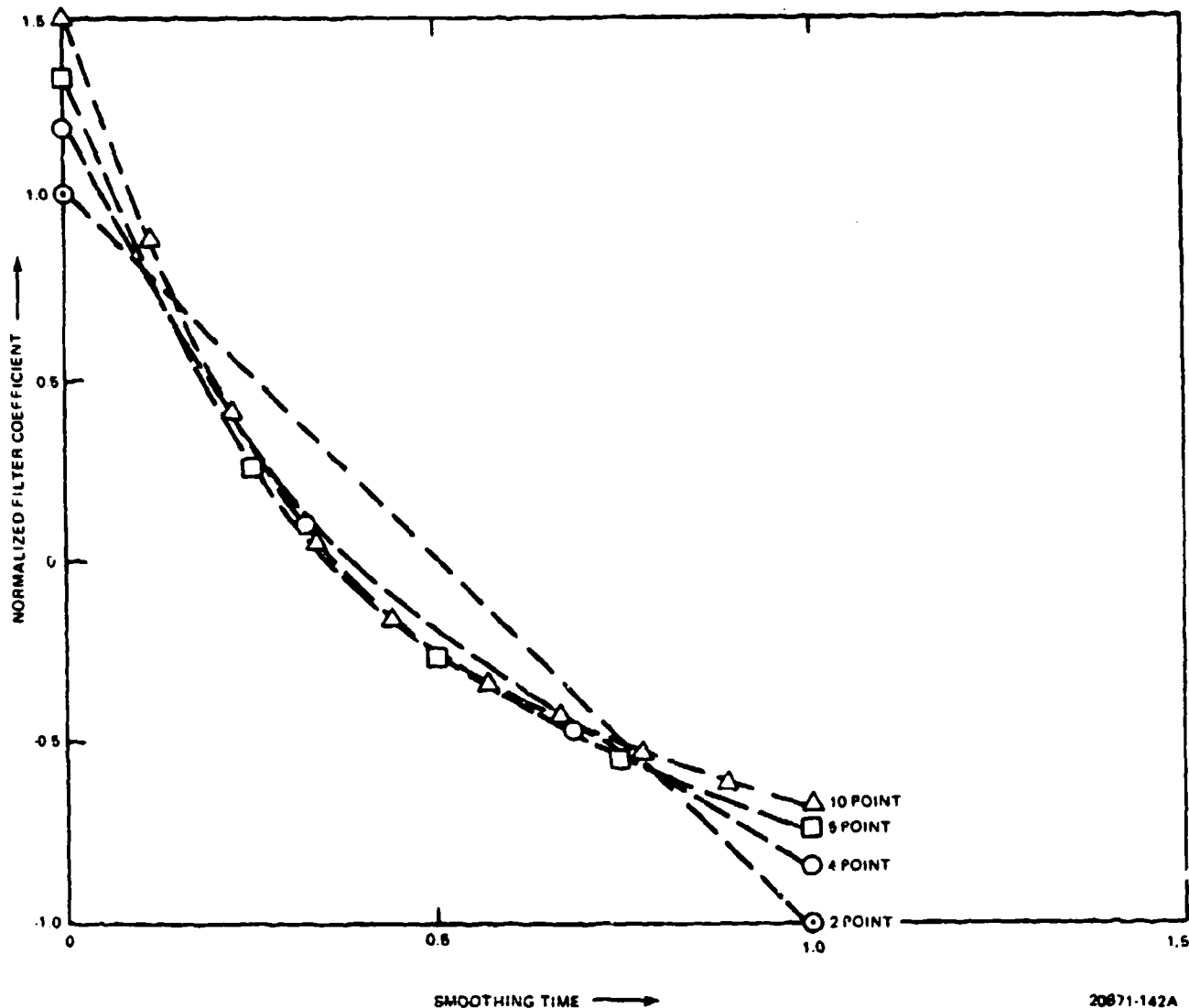
Figure 5-2. Comparison of Coefficients for Best Compromise Velocity Filter

20871-142A

where the b_{pc}, b_v are the coefficients of the uncorrected position and the velocity filter, respectively.

5.1.16 Coefficient for Least Squares Filters

As a check on the previous expressions, the lag coefficients are computed for the least squares filters ($\lambda \to \infty$) for which the results are known and were given in APAADS-I.

Position Filter:

$$T_{p/v} = n\Delta/2 = T_s/2$$

$$T^2_{p/a} = -(\Delta^2/12)\,n\,(2n+1) \cong -T_s^2/6$$

(Note that this term is negative)

Velocity Filter

$$T_{v/a} = n\Delta/2 = T_s/2$$

5-13

The prediction algorithm is

$$x_p = \underline{x} + \underline{v} [t_p + (T_s/2)] + (1/2)\underline{a} \left[t_p^2 \right.$$

$$\left. + t_p T_s + (T_s^2/6) \right]$$

20871-607

as given in AFAADS-I (Vol. II, p. 4-3).

5.1.17 Analog Filter

Consider the simple velocity filter with transfer function

$$W(s) = \frac{s}{(1 + sT_1)(1 + sT_2)} \; ; s = d/dt \quad (5.91)$$

The variance reduction for white noise input is

$$D_n = \frac{1}{(T_1 + T_2)(T_1 T_2)} \quad (5.92)$$

and the settling time demerit is

$$D_s = \frac{T_1^2 + 2T_1 T_2 + T_2^2}{2(T_1 + T_2)} \quad (5.93)$$

The value function

$$J = D_s + \lambda D_n$$

is minimized when

$$(T_1 + T_2)^2 = 2T_1 T_2 \quad (5.94)$$

and the corresponding transfer function is

$$W^*(s) = \frac{s}{1 + As + (A^2/2)s^2} \; ; A = T_1 + T_2 \quad (5.95)$$

For *all* values of A, this filter has a slight overshoot in its response corresponding to a damping ratio

$$\zeta = (1/2)^{1/2} = 0.707$$

Hence, as one varies λ, the shape of the filter response to a transient is unchanged, but the time scale depends on λ. If one desired to vary the filter value parameter J with slant range, for example, one would make A a function of range, but preserve the relationship, Equation (5.94). This is the same conclusion reached by Benedict and Bordner.

5.1.18 Generalization

Instead of beginning with a specified filter structure, such as Equation (5.91), the problem can be formulated in more general terms, with the weighting function of the best compromise filter determined as an output. It appears that the problem can be solved by the Marshall-Yovits[9] methods (and no doubt others as well), and the approach is sketched below.

If $x(t)$ is a function satisfying conditions inherent in stable filter design, the integral

$$I = \int_{-\infty}^{\infty} [x(t)]^2 \, dt \qquad (5.96)$$

can be obtained by Parseval's theorem from

$$I = 1/(2\pi) \int_{-\infty}^{\infty} x(-j\omega) \, x(j\omega) \, d\omega$$

$$= 1/(2\pi) \int_{-\infty}^{\infty} |x(j\omega)|^2 \, d\omega \qquad (5.97)$$

where $x(j\omega)$ is the Fourier transform of $x(t)$.

If for $x(t)$ we take the transient error of a filter in response to a step input, zero for $t < 0$, we can utilize this integral.

Consider a velocity filter, with transfer function $Y(s)$. For small s this must reduce to s so we can write, in terms of a new function $F(s)$.

$$Y(s) = s\,F(s) \qquad (5.98)$$

Apply a step function in velocity (transform $1/s$) as a ramp function in position (transform $1/s^2$) to the filter. The transform of the error is

$$1/s \cdot (1/s^2)\, s\, F(s) = \frac{1 \cdot F(s)}{s} \qquad (5.99)$$

The mean square integrated error (transient) is then

$$D_s = 1/2\pi \int_{-\infty}^{\infty} \left| \frac{1 \cdot F(j\omega)}{j\omega} \right|^2 \, d\omega \qquad (5.100)$$

Let position noise have the power spectral density $N(\omega^2)$. Then the noise output of the filter is

$$D_n = 1/2\pi \int_{-\infty}^{\infty} N(\omega^2)\, \omega^2\, |F(j\omega)|^2 \, d\omega \qquad (5.101)$$

We wish to minimize

$$J = D_s + \lambda D_n$$

$$2\pi J = \int_{-\infty}^{\infty} \left\{ \frac{|1 \cdot F(j\omega)|^2}{\omega^2} + \omega^2 N(\omega^2)\, |F(j\omega)|^2 \right\} \, d\omega$$

$$(5.102)$$

This can be done by applying calculus of variations and utilizing the additional conditions that $F(j\omega)$ must be physically realizable.

Note that the settling demerit can be given higher penalties for slow settling by multiplying $e(t)$ by t^m, and that this does not appear to complicate the problem, which can be solved in terms of 'm.'

In addition, the usual problem with filters unconstrained as to the length of their memory (one gets very long memory times if there is no penalty for them) is avoided by the settling time penalty.

Assuming that the solution turns out to be relatively concise it provides a standard against which to design both discrete and analog filters.

However, for present purposes, it is not anticipated that additional insight over that obtained by analysis of the discrete filters would be sufficient to justify further investigation at this time.

5.2 RECURSIVE FILTERS

Recursive filters have the advantage over fixed memory filters in that they require less memory for computation. For example, the simple algorithm

$$\underline{x}(j) = \alpha\, x(j) + (1 - \alpha)\, \underline{x}(j-1) \qquad (5.103)$$

requires that only the most recent value of $\underline{x}$ be stored. This algorithm weights past data exponentially, i.e., as α^i.

Inclusion of a few additional terms in the algorithm (possibly only one or two) allows improved shaping of the weighting coefficients so that the effect of the older points on the current estimate is reduced over that resulting from the simple algorithm.

Recursive filters are particularly well suited to variation of the effective smoothing with other parameters such as range. In Equation (5.103) for example, to provide increased smoothing at long ranges, only α need be varied with range.

Table V-2. Effect of λ on Coefficients for 4-Point Filter

λ	0	0.5	0.707	1.0	2.0	3.0	4.0	5.0	∞
c_0	1.0	0.58	0.53	0.48	0.41	0.38	0.36	0.35	0.30
c_1	-1.0	-0.25	-0.18	-0.12	-0.03	0.01	0.03	0.04	0.10
c_2	0.0	-0.25	-0.23	-0.21	-0.17	-0.15	-0.14	-0.13	-0.10
c_3	0.0	-0.08	-0.12	-0.15	-0.21	-0.24	-0.25	-0.26	-0.30
D_n	2.0	0.48	0.37	0.31	0.24	0.22	0.21	0.21	0.20
D_s	1.0	1.18	1.23	1.29	1.39	1.45	1.47	1.49	1.58

20871-507

Table V-3. Optimization of Filter with (λ/Δ^3)

λ/Δ^3	0	0.5	0.707	1.0	2.0	3.0	4.0	5.0	8.0	∞
$J/\lambda^{1/3}$	∞	1.79	1.68	1.60	1.48	1.46	1.46	1.47	1.59	∞

20871-508

Time has not permitted a comprehensive analysis of recursive filters, however the characteristics of the 'alpha-beta' algorithms developed for radar tracking are reviewed in the following paragraph.

These algorithms were designed for use with track-while-scan radars, hence incorporate a one-point prediction which allows them to track through missed data points. They can therefore be used in regenerative algorithm designs. The coefficient shaping is optimum for tracking; it has not been verified that the same designs would be optimum for prediction to many times the sample interval as is required in predicted fire. Conversely, there is no a priori reason to doubt their applicability.

Unlike Equation (5.103) the z-transforms have two poles, and so there is another degree of freedom in coefficient optimization.

The basic references are Benedict and Bordner[1], Simpson[2], and Neal[3].

The following material describes the position and velocity algorithms of the alpha-beta filters.

Let

$x(j)$ = position measurement at the j'th time instant (input)

Δ = sampling interval

$x_p(j)$ = one step prediction of $x(j)$ based on past smoothed position and velocity

$\underline{x}(j)$ = smoothed position at j

$\underline{v}(j)$ = smoothed velocity at j

$\alpha\beta$ = constants

The '$\alpha\beta$' algorithms are

$$\underline{x}(j) = x_p(j) + \alpha\, [x(j) - x_p(j)]$$

$$\underline{v}(j) = \underline{v}(j-1) + (\beta/\Delta)\, [x(j) - x_p(j)]$$

$$x_p(j+1) = \underline{x}(j) + \underline{v}(j)\Delta \qquad (5.104)$$

Taking z-transforms and solving separately for x and y, we obtain

5-16

$$\underline{x}(z) = x(z) \ \frac{\alpha + (\beta \cdot \alpha)z^{-1}}{1 \cdot z^{-1}(2 \cdot \alpha \cdot \beta) + z^{-2}(1 \cdot \alpha)}$$

$$\underline{v}(z)\Delta = x(z) \ \frac{\beta(1 \cdot z^{-1})}{1 \cdot z^{-1}(2 \cdot \alpha \cdot \beta) + z^{-2}(1 \cdot \alpha)}$$

$$(5.105)$$

$$\underline{x}(z) = x(z) \ \frac{z\,[z\,\alpha + (\beta \cdot \alpha)]}{z^2 \cdot z(2 \cdot \alpha \cdot \beta) + (1 \cdot \alpha)}$$

$$\underline{v}(z)\Delta = x(z) \ \frac{z\,\beta(z\text{-}1)}{z^2 \cdot z(2 \cdot \alpha \cdot \beta) + (1 \cdot \alpha)}$$

$$(5.106)$$

5.2.1 Transient Errors

Now apply a ramp input in position with unit slope. It has the z-transform

$$x(z) = \frac{\Delta z}{(z \cdot 1)^2}$$

20871-608

In the steady-state the position element of the filter should equal the input; the velocity element should output a unit velocity. The error transforms are therefore

$$\text{Position} \quad e_p(z) = \frac{\Delta z}{(z \cdot 1)^2} \left[1 \cdot \frac{z\,[z\alpha + (\beta \cdot \alpha)]}{z^2 \cdot z(2 \cdot \alpha \cdot \beta) + (1 \cdot \alpha)} \right]$$

$$= \frac{\Delta z(1 \cdot \alpha)}{z^2 \cdot z(2 \cdot \alpha \cdot \beta) + (1 \cdot \alpha)} \qquad (5.107)$$

The error at $t \longrightarrow \infty$ is obtained as

$$e_p(\infty) = \underset{z \to 1}{\text{Lim}}\,(z \cdot 1)\,e_p(z)$$

and this is seen to be zero as long as the denominator is non-zero at $z = 1$. (The roots of the denominator must, of course, lie within the unit circle in the complex plane for stability.)

Velocity: $\quad e_v(z) = \dfrac{z}{z \cdot 1} \cdot \dfrac{z\Delta}{(z \cdot 1)^2} \ [\,\underline{v}(z)/x(z)\,]$

$$= \frac{z\,(z \cdot 1 + \alpha)}{z^2 \cdot z(2 \cdot \alpha \cdot \beta) + (1 \cdot \alpha)}$$

and it is clear that $\qquad\qquad\qquad (5.108)$

$$\underset{z \to 1}{\text{Lim}}\,(z \cdot 1)\,e_v(z) = 0$$

subject to the stability requirement, so that the steady-state velocity error for constant velocity input is zero.

5.2.2 Noise Variance Demerit

From Jury's tables[6], for white noise of unit variance

$$\text{Position} \quad D_{np} = \frac{2a^2 + 2\beta \cdot 3a\beta}{\alpha(4 \cdot 2a \cdot \beta)} \qquad (5.109)$$

$$\text{Velocity} \quad D_{nv} = \frac{2\beta^2}{\Delta^2 a(4 \cdot 2a \cdot \beta)} \qquad (5.110)$$

5.2.3 Settling Time Demerit

We would like to minimize the integrated mean square error of the system during its initial transient, subject to a requirement for variance reduction. In position, for example, we could invert the $e_p(z)$ function and obtain the $e_p(j)$. Then

$$\sum_{j=0}^{\infty} \ [e_p(j)]^2$$

20871-609

would sum the mean square error at the sample points. However the system is operating in real time, and for the same value of the sum above, a large value of Δ will be less advantageous than a small value. What we want is the discrete analog of

$$\int_0^{\infty} [e(t)]^2 \ dt$$

20871-610

The settling time demerit is therefore taken as

$$D_s = \Delta \sum_{j=0}^{\infty} [c_p(j)]^2 \qquad (5.111)$$

This differs by the factor Δ from the B&B settling demerit. In the present note we are considering Δ as an adjustable parameter as well as α, β.

The D_s can be obtained from the $e(z)$ by Jury's tables. They are

$$\text{Position} \quad D_{sp} = \Delta^3 \frac{(2 \cdot a)(1 \cdot a)^2}{a\beta(4 \cdot 2a \cdot \beta)} \qquad (5.112)$$

$$D_{sv} = \Delta \frac{a^2(2 \cdot a) + 2\beta(1 \cdot a)}{a\beta(4 \cdot 2a \cdot \beta)}$$

$$(5.113)$$

5.2.4 Effective Weighting by Aperiodic Filter

Except for the explicit inclusion of the sampling interval the above expression are identical with those of Benedict and Bordner, who find for a unit sampling interval that the best compromise filters are obtained with a relation between β and α.

$$\beta = a^2/(2 \cdot a) \qquad (5.114)$$

This corresponds to a slightly oscillatory transient response of the filter. There has not been time in the present study to confirm the optimum or to investigate the effect of changing Δ.

The filter would be aperiodic if

$$\beta = (2 \cdot a) + 2(1 \cdot a)^{1/2}$$

$$a = 2\beta^{1/2} \cdot \beta \qquad (5.115)$$

and the two roots in the z-transform would be

$$z_{1,2} = (1 \cdot a)^{1/2} \cong a \qquad (5.116)$$

The response to a unit impulse gives us the equivalent weighting coefficients applied by the filter, and for the aperiodic filter, inverting Equation (5.106).

$$W_v(j) = \beta [(j+1)a^j \cdot ja^{j-1}] \text{ for the velocity filter}$$

$$W_p(j) = a(j+1)a^j + (\beta \cdot a) ja^{j-1} \text{ for the position filter}$$

$$(5.117)$$

These have been plotted in Figure 5-3 for $\Delta = 1$;

$\alpha = 3/4; \beta = 5/4; a = 1/2$ and the velocity coefficients may be compared with those in Figure 5-2 for the finite memory filter.

5.2.5 Recursive Filter for Acceleration

Extensions of the Benedict and Bordner work to filters including an acceleration component have been made by Simpson[6] and Neal[7]. With the inclusion of the acceleration element, the filters are described by three parameters and the sampling interval. The work of Simpson and Neal leads to two functional relationships among the parameters for a best compromise filter. The remaining parameter can be adjusted according to the desired equivalent smoothing time.

As noted earlier, these analyses are concerned with filters for tracking systems, and the maximum prediction required is only one sampling interval. This allows the tracker to carry through missed data points. For the anti-aircraft problem much greater prediction intervals are required, and the problem and the optimizations need to be reviewed from that point of view.

5.3 RECURSIVE FILTERS WITH TIME VARYING COEFFICIENTS

As has been noted, for a high performance tracking radar at the anti-aircraft gun ranges of current interest, the tracking accuracy tends to be limited by glint, which in turn has a standard deviation proportional to the target dimension. As a result, the standard deviation of tracking error in meters is expected to be relatively constant with range, provided that servo problems caused by high angular derivatives at short range are circumvented.

A similar situation is believed to exist with human operator tracking. Conventional approximations make the mil error proportional to angular velocity, so that the linear error changes slowly with range.

For a fixed smoothing time, the measured linear velocity used for prediction is therefore expected to vary only slowly with range, and is proportional to σ_o/T_s where T_s is smoothing time. A rough approximation to the variance of the prediction error resulting from tracking error is, consequently (for velocity smoothing only)

$$\sigma_p^2 = \sigma_o^2 [1 + 2(t_p/T_s) + 2(t_p/T_s)^2]$$

$$(5.118)$$

which increases with time of flight and therefore with slant range. A constant T_s is a compromise which can
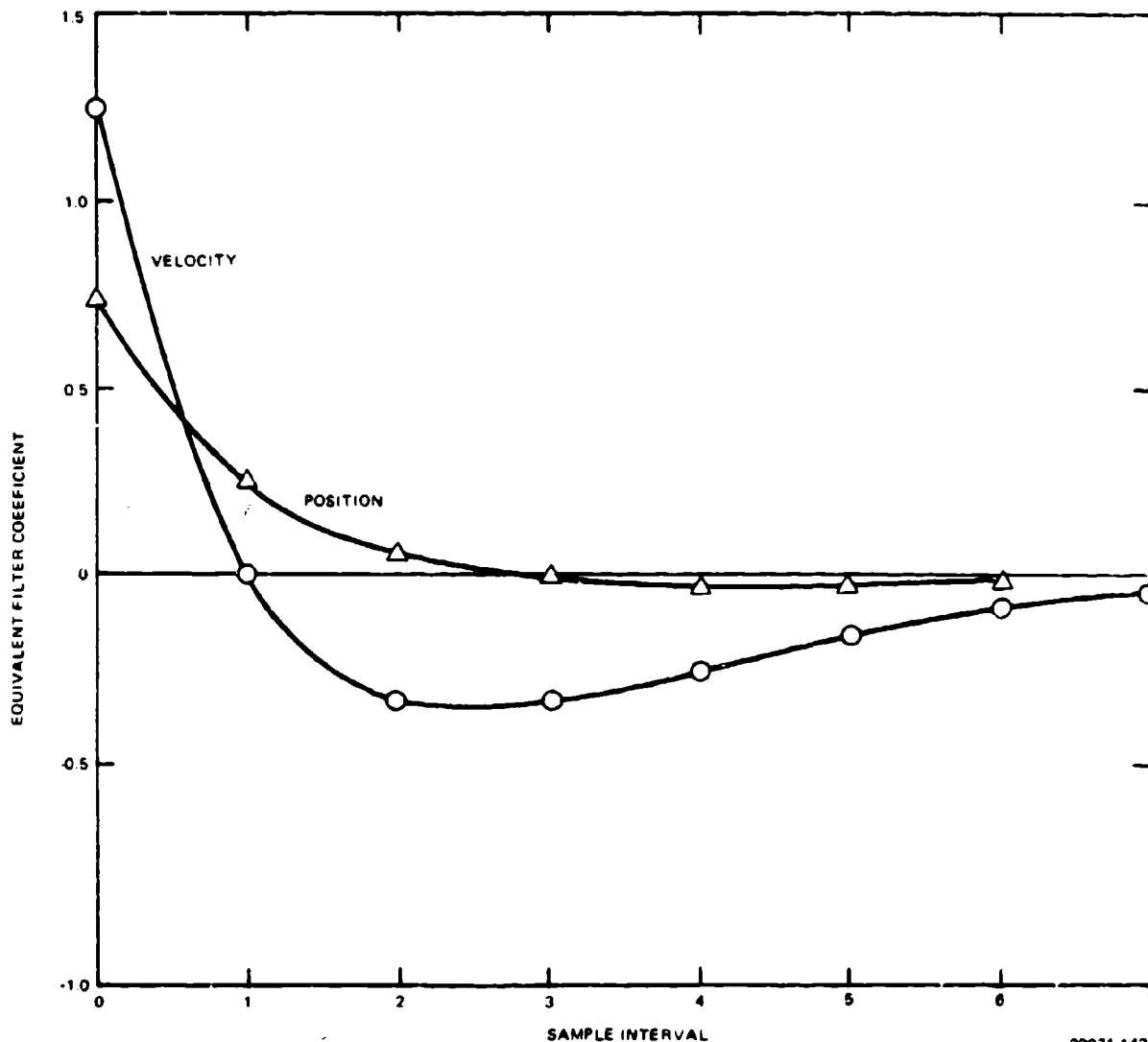
Figure 5-3. Equivalent Coefficients of Recursive Aperiodic Filters

be too large at very short range and too small at long range.

It is therefore considered desirable to make T_s an increasing function of slant range. With good information on actual target attack paths one could also consider varying T_s with other path parameters, but for present purposes the approach is adequately described by considering a variation with range.

This is not a new concept. The well known gyrosights compute lead according to the expression

$$at_p \, dL/dt + L = \omega t_p \tag{5.119}$$

where L = lead angle, ω = angular velocity, and t_p = time of flight. The smoothing time constant is at_p, and $a = 0.20 - 0.50$ depending on the design, hence smoothing increased with time of flight.

The M-4, M-7 director family computed lead in X,Y,Z coordinates as

$$at_p \, dX_L/dt + X_L = (dX_o/dt) \, t_p; a = 1/13 \tag{5.120}$$

However, the above algorithms suffer from a system-

5-19

atir error proportional to the rate of change of time of flight. For example, to terms in dt_o/dt, the M-7 computed

$$X_L = (dX_o/dt)t_p[1 + a\, dt_p/dt]^{-1}$$

$$(5.121)$$

This error was first discovered in dynamic tester runs with the M-7. Even against World War II targets it was of significant magnitude on the receding leg of the target path.

The above lag problem is completely by-passed by performing the smoothing operation and the lead computation in two steps. For example, if, in the M-7 the algorithms had been

$$at_F d\underline{V}_x/dt + \underline{V}_x = dX_o/dt$$

$$X_L = \underline{V}_x\, t_p \qquad (5.122)$$

$\underline{V}_x$ would have settled without lag to dX_o/dt on an unaccelerated target and lead would have been properly computed.

For reference we note the state space formulation of the filter differential equations for analogue filters with time varying coefficients. Write the system matrix differential equation as

$$dx/dt = A(t)\, x(t) + B(t)\, u(t)$$

$$(5.123)$$

where $x(t)$ is the system state vectorm and $A(t)$ is the 'system matrix.' $u(t)$ is the input function.

The solution of (1) is

$$x(t) = L(t)\, x(0) + L(t) \int_0^t L^{-1}(s)\, B(s)\, u(s)\, ds$$

$$(5.124)$$

where $L(t)$ is a solution of

$$dL/dt = A\, L; L(0) = I \qquad (5.125)$$

and $L^{-1}(t)$ is a solution of the adjoint equation

$$dL^{-1}/dt = -A^* L^{-1}; L^{-1}(0) = I \qquad (5.126)$$

and $A^*(t)$ is the conjugate transpose of $A(t)$

The solution of

$$dy/dt = A\, y \text{ can be written}$$

$$y(t) = \phi(t, t_o)\, y(0) \qquad (5.127)$$

where $\phi(t, t_o)$ is designated the state transition matrix of the system

$$\phi(t, 0) = L(t) \qquad (5.128)$$

It is the solution of

$$d/dt\, [\phi(t, t_o)] = A(t)\, \phi(t, t_o); \phi(t_o, t_o) = I$$

$$(5.129)$$

The state transition matrix has the following properties

$$\phi(t_o, t_1)\phi(t_1 t_2) = \phi(t_o, t_2)$$

$$\phi(t_1, t_o) = \phi^{-1}(t_o, t_1)$$

$$\phi(t_1, t_o) = L(t)L^{-1}(t_o) \qquad (5.130)$$

Then

$$x(t) = \phi(t, t_o)x(t_o) + \int_{t_o}^t \phi(t, s)B(s)\, u(s)\, ds$$

$$(5.131)$$

If we designate $y(t) = B(t)u(t)$ $?$ the system input, set $t_0 = 0$, and let $S = t-s$

$$x(t) = \phi(t, 0)x(0) + \int_0^t y(t\text{-}S)\phi(t, t\text{-}S)\, dS$$

(5.132)

The first term represents the initial transient of the system. ϕ is the weighting function which is applied to $y(t)$.

If we consider only the system response to noise, and $u(s)$ is an appropriately defined 'white' noise vector, the variance matrix as a function of time is obtained by solving

$$dP/dt = AP + PA^T + BQB^T \quad (5.133)$$

where $Q = 1$ in the present application.

A similar set of expressions can be written for a discrete system.

For the simple case of a one-dimensional analog filter with time varying coefficient

$$f(t)\, dy/dx + y = x \quad (5.134)$$

$y(t) = $ filter output

$x(t) = $ variable to be smoothed

    $x(t)$ is assumed to be a variable such as a measurement of a rectangular coordinate component of target velocity which has a constant mean but is perturbed by noise which has zero mean

The solution of Equation (5.134) is

$$y(t) = y(0)e^{-\int_0^t [f(s)]^{-1}\, ds}$$

(5.135)

$$+ e^{-\int_0^t [f(s)]^{-1}\, ds} \left[\int_0^t e^{\int_0^s [f(u)]^{-1}\, du} \frac{x(s)}{f(s)}\, ds \right]$$

We note two simple cases: (1) $f(t) = a+t$ and (2) $f(t) = kD$ where D is slant range. The former case had some popularity in World War II[7] for application to very long range anti-aircraft systems when very long non-maneuvering target paths were expected.

The latter case is of interest in the present application of making smoothing time proportional to slant range.

When $f(t) = a + t$,

$$y(t) = y(0)\, \frac{a}{a+t} + \frac{1}{a+t} \int_0^t x(s)\, ds$$

(5.136)

The operational concept was that after target acquisition, $f(t)$ would be allowed to vary as $a + t$. a could be very small, and the initial transient would decay as $[1 + (t/a)]^{-1}$. The weighting function over t is very close to a uniform averaging, which is optimum for white noise.

To display the solution for $f(t) = kD$, consider a direct incoming target flying down the line of sight, at velocity V so that $dD/dt = -V$. Change the variable of integration to D.

Consider a target acquired at D_o and tracked to D_1. Since K has the dimensions of velocity, define $K = V_s$ '

$$y(D_1) = y(D_o)(D_1/D_o)^{V_s/V} \cdot \int_1^{D_1/D_o} x(z)\, d(z^{\text{-}V_s/V});$$

$$z = D/D_1$$

(5.137)

For a numerical example, let $v_s = 1000$ meters/second so that the smoothing time constant is 2.0 seconds at 2000 meters. Consider a target acquired at 2000 meters and tracked to 1000 meters, and a target velocity of 250 meters/second. At 1000 meters the initial transient will have decayed to

$(1/2)^4 = 0.0625$ of its original value

whereas with constant smoothing time constant $T = 2.0$ seconds, it would have decayed to 0.136.

As a point of departure for the development of recursive filters with parameters varying with range or other engagement parameters it is proposed that the applicability of α-β-v to the predicted fire problem be confirmed, with a determination of best compromise filter shape, defining all of the disposable parameters in terms of a single parameter. This last parameter would then be made a function of the appropriate tactical variable, such as slant range.

SECTION 6
PREDICTION

This section represents the analyses of a number of prediction algorithms. These range from a sophisticated system using corrections based on actual measurements of projectile miss distance to barrage fire. The types analyzed by no means exhaust the list of possible algorithms, nor are the analyses carried to completion in all cases. It had been hoped to parallel the analyses with computer simulations but this has not been possible within the resources available in the present effort.

6.1 CATEGORIES OF FIRE CONTROL SYSTEMS

In the following paragraphs fire control systems for predicted fire weapons are categorized, from the simplest to the most sophisticated. The list is incomplete, and since there are so many descriptors needed to completely describe a fire control system, the emphasis is on the method of prediction. Examples of each category are given. The categories are:

a. Barrage Fire

    (1) 'Umbrella' Remagen Defense.

    (2) 'Box Barrage' Malta Defense. Guns are laid on predetermined orders and the target flies into the barrage.

b. Simple Tracker Control. The weapon fires tracer ammunition and the gunner attempts to pass the tracer stream through the target.

c. Ring Sight (or speed ring reticle projected in reflex sight). Gunner attempts to track with the target on a specified speed ring, target axis pointed at sight center.

d. Course and Speed Type Sights

    (1) Stiffkey Stick, Peca Sight. A sight operator aligns a bar to the target apparent angle and sets in 'speed click' increments for lead.

    (2) Course and Speed Sight, M-38. A sight operator sets estimated target speed and aligns a miniature target indicator with the real target heading and dive angle.

e. Rate by Time with Estimated Range

    (1) The original Kerrison predictor.

    (2) Fire control on current British Falcon. Angular velocities are obtained by tracking. These are multiplied by time of flight obtained from estimated range to obtain leads.

f. Rate by Time with Range Finder

    (1) Kerrison predictor with optical range finder built as the U.S. M5A-series.

    (2) Disturbed Reticle Lead Computing Gyro Sights

        (a) Without empirical corrections.

        (b) With empirical corrections (Vulcan XM-61).

g. Complete Solutions for Unaccelerated Targets

    (1) Almost all World War II heavy gun fire control systems, including the M-4 and M-9, M-10 series (U.S.).

    (2) Vigilante fire control system.

h. Complete Solutions with Corrections for Target Acceleration

    (1) U.S. M-33 system for heavy antiaircraft guns.

    (2) Current Superfledermaus (correction for target acceleration in dive, or 3-D curvature options).

i. Solutions Using Corrections Based On Projectile Miss Distance Measurements

    (1) U.S. Navy Phalanx.

j. Solutions Using Internally Generated 'Synthetic Tracers'

    (1) U.S. Air Force 'Snap-Shoot' Concept.

Although not a prediction function, the provision of regenerative tracking is considered to be essential for high performance short range weapons. Regenerative tracking has been used in U.S. Navy fire control systems for about 50 years, beginning with the Mk I computer. It was employed in the U.S. Army Vigilante system, and is currently used in the Superfledermaus.

6.2 PREDICTION USING CORRECTIONS FROM PROJECTILE TRACKING

One of the most interesting contributions of modern technology to the predicted fire problem is the potential of tracking the projectiles, measuring their miss distances at the target, and applying appropriate corrections to the fire control system.

To some degree this kind of observation has always been possible by visual observation of tracer rounds or by visual observation of the burst of time fuzed projectiles. The usefulness of the method in the past has been limited by the man's inability to sense the moment at which a tracer reaches target range, or even with stereoscopic range finder observation of bursts, by the large dispersion in time of burst of time fuzes.

It now seems possible by radar, infra-red, or laser means to obtain measurements of projectile miss distance at the target. Since no range sensing appears to

be possible with infra-red alone, assistance from the fire control computer appears to be required to determine when to observe with an infra-red sensor.

The Navy's Phalanx predicted fire system is reported to use radar measurements of projectile miss distance. No details on the implementation are available for the present study.

The following analysis is preliminary, and incomplete. However, the problem is structured and a methodology for performing a complete analysis is developed. In addition, system criteria are developed for the algorithms suggested to convert the miss distance measurements to corrections to be applied to the fire control system.

6.2.1 Historical Perspective

Early fire control systems for use with time fuzed ammunition were operated with a doctrine for observing bursts through a stereoscopic height finder, sensing burst positions relative to the target, and applying vertical, lateral and altitude 'spot corrections' to the computer. This system was used with the M-2, M-3, and M-4 directors, was included in the M-9, and in general was used principally for battery 'calibration' (fire at a specified point in the sky) rather than corrections during combat.

Tracer control of fire of machine guns and automatic weapons has been extensively used in the past. The usefulness of tracer observation has been a subject of continuous controversy, which has some basis in the fact that the gunner's depth perception at normal target ranges is nil, and so he cannot tell when the bullets are at about target range. On the other hand, tracer observation can assist the gunner in getting the trajectories into the slant plane defined by the gun and target heading, even if tracers are of little assistance in setting lead within that plane.

An additional complicating factor in simple tracer control is that even if errors can be observed at the target, the error observed was made one time of flight previous, and this delay added to the man's response time makes the control loop incompatible with rapidly changing lead angles.

On the other hand, tracer observation has been used successfully when combined with rudimentary prediction systems, so that adjustments could be made to 'course invariants' rather than to rapidly changing variables.

With the Kerrison predictor for the 40-mm gun, (simple rate x time) vertical adjustments to the computer prediction were made on the basis of tracer observation, until the tracer 'crossed' the target. A range correction was then made depending on whether the tracer passed between the target and the tracker or whether it was momentarily obscured by the target.

The same principle was used with the Computing Sight M-7 (Weissight) for which there were two inputs, aircraft heading, and speed. Heading was adjusted until the tracer stream 'crossed' the target, and speed adjustments were then made depending on whether the tracers passed across the face of the target or were obscured by it.

These systems worked well in proving ground tests. Whether it was possible to use tracer adjusted fire in combat, especially with many other weapons firing at the same target, is unknown.

A U.S. modification of the Kerrison predictor (M5A3) added a short base (about 3 ft) coincidence optical range finder with red and green filters. One operator tracked in range, which was input to the prediction computation. A second operator observed the tracer stream through the same optics. He saw two intersecting streams, one red, and one green, with the point of intersection white, and occurring at the range setting of the range finder. He could then apply lateral and vertical corrections to move the white spot to the target as seen in the same view. Subject to the time of flight lag he was thus able in principle to correct for the system's slowly varying or constant errors. Applied to the 40-mm gun this predictor gave excellent proving ground results. How much could be credited to the adjustment feature was never evaluated, and the reluctance in the field to carry an off-carriage predictor for each 40-mm gun when on-carriage course and speed or 'Stiffkey Stick' mechanical computers generated results almost as good, caused the off-carriage line of development to be terminated.

6.2.2 Automatic Projectile Tracking

Projectiles can be observed by radar, IR sensors, and possibly by other sensors. Automatic tracking admits the possibility of providing an additional control loop closure for the fire control system. It is probable that the correction based on measurements of the trajectories relative to the target must be used to correct a base prediction algorithm, because of the time of flight lag.

Because the errors are referenced to the target, the system has the unique capability of being able to correct for constant angular errors of the system (such as boresight and orientation) and for slowly varying errors such as may result from imperfections in the base prediction algorithm, ballistics, non-standard muzzle velocity and meteorological conditions, etc.

Since the measured error includes the random round to round dispersion of the projectiles, it seems probable that corrections must be based on weighted averages of measured miss distances or angles. The weighting should probably be a function of time and some of the engagement parameters such as range.

If it were not for round to round dispersion, there would be little gain in measuring error more often
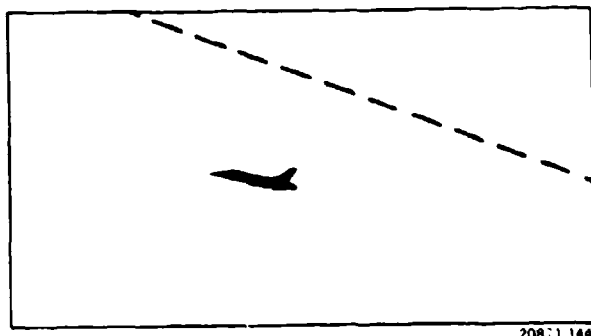
Figure 6-1. Tracer Path Relative to Target

Figure 6-3. Resolution of Angles

Figure 6-2. Measurable Angles

than once each time of flight. However, because of the random round to round errors, the inferred systematic errors will be progressively better abstracted as the number of observed rounds is increased.

Note that for almost all of the systems discussed it is necessary to determine the point at which the projectile reaches the target range (measured from the tracker). IR observations must therefore probably be supplemented by computer indications of when to observe. Without the range measurement, however, adjustments can be made to get the prediction into the right 'slant plane', but not to correct within that plane. But even this partial correction may be helpful.

6.2.3 Error Sensing with Radar

Without attempting to design the radar, assume a pulse doppler, monopulse radar capable of getting a measureable signal from the projectile. The radar tracks the target normally. A velocity gate is set by the computer to include projectile velocity at target range, and this separates the projectile return from all other signals. One could have a separate radar to track the projectiles, or it might be possible to calibrate the signals off-axis obtained by the tracking radar on the projectile as isolated by the velocity gate. The signal is only desired at the target range, the computer identifies the time instant (bracket) at which to read the error

components. Alternately the projectile error signal is read in a range gate established by the target range measurement, without computer assistance.

6.2.4 Error Sensing with an Imaging Tracker

Assume an imaging sensor (IR or TV) with automatic tracking. It is presumed that this is done by a line-scanning system, and target bracketing. The view on the image screen as a projectile passes the target is as shown in Figure 6-1. The scan rate and the number of projectile sensings are related. It is assumed that the projectile is tracer, which registers on TV or IR, or non-tracer which may be observed on IR.

With no other information, one obtains two angles from Figure 6-1 as shown, in Figure 6-2, and these must be related to the desired system correction. The vector miss can be resolved as in Figure 6-3.

Motion of the projectile in the field of view of the imaging device, if the latter is tracking the target, is caused principally by the target angular velocity. The vertical angular velocity caused by projectile drop is only of the order of 10 mils/second. Tracking angular velocities can be as high as 1600 mils per second. The observed vertical angular velocity component caused by gravity drop is approximately

$$de/dt = -g \, t_p \cos e/D \; ; \; t_p = \text{time of flight}$$

$$e = \text{elevation angle of sight}$$

$$D = \text{slant range}$$

(6.1)

If the sensor has a circular field of radius M degrees, and the miss distance is m degrees, the observable tracer path segment in degrees has a length

$$T = 2 \; [\,(M/2)^2 - m^2\,]^{1/2} \qquad (6.2)$$

The trace sweeps through the field of view at the angular velocity of tracking. For a 2° miss, Table VI-1

6-3

shows approximate observation times for two sensor fields and two angular velocities of tracking.

If one only has the angular miss picture (Figure 6-1) the best one can do is apply corrections to try to make the relative bullet trace projected in the sight plane pass through the target. This will put the bullet in the right slant plane, but it will not necessarily hit the target. For example, it will not correct for a systematic error in bullet velocity.

If it is possible to range on the bullet with the radar or laser, as well as on the target, then the problem is simplified: read the lateral and vertical errors when both are at the same range and resolve into corrections.

A possibility for use with an IR sensor may be to use the imaging device with range gated laser illumination. If the laser illuminated projectile can be seen, it will be seen only when it is in the same range gate as the target. Hence angular error measurements are properly made at target range.

Another possibility, which is more complicated, and can possibly be used only at low rates of fire is to obtain time of flight from the computer at the instant of firing, and use this to determine the time at which to measure miss distance. This mode might be used in periodic system calibration, if not for correction during a combat firing pass.

In the remaining paragraphs of this section, it is assumed that a method has been implemented which allows measurement of the projectile miss distances at the target range, and algorithms for extracting corrections are developed and analyzed.

6.2.5 System Data Flow

The system is assumed to be described by the Flow Diagram of Figure 6-4. The target is tracked and this process provides information to the fire control system which generates gun orders. The gun fires, and it is assumed that projectile miss distances are measured at the target range. These measurements of miss distance are processed (averaged, coordinate corrections made,

Table VI-1. Available Observation Times

Sensor Field Angular Velocity of Tracking	30°	3°
90°/s	0.3 sec	0.03 sec
10°/s	3.0 sec	0.3 sec

etc.) and a correction is applied to the fire control system.

Some of the sources of error causing projectile miss are:

a. Bore sight and alignment errors.

b. Solution errors (imperfect solution, instrumental errors, lags).

c. Solution noise (resulting from tracking noise).

d. Target maneuver and flight path irregularity.

e. Round to round ballistic and muzzle velocity dispersion.

f. Non-standard ballistic conditions.

In general, these error types may be grouped into three categories:

a. Relatively constant (in some coordinate system) over the engagement. An azimuth boresight error is typical.

b. Random round to round (for example, ballistic dispersion).

c. Varying during the engagement.

The object of the miss distance processing unit is to:

a. Correct for the relatively constant errors as far as possible.

b. Provide some compensation if possible for the varying errors which persist for longer than time of flight.

How well it does this depends on how large the constant and slowly varying errors are compared with the rapidly varying and random round to round errors.

6.2.6 Operational Modes Considered

In the following paragraphs, three system concepts are described and subjected to preliminary analysis. Two of these are based on straightforward measurement and processing of the projectile miss distances. In one mode, the correction is applied to the system in advance of the normal data smoothing and prediction algorithms. There are practical objections to this mode which is, however, included because of some analytic interest. In the second mode, the correction is applied to the gun orders. This mode is both practical and likely to operate successfully.

The third mode is, to the best of the writer's knowledge, a new concept, and involves internal system computation of the expected error in point of aim (synthetic trajectory) against which the observed miss distances are compared. There are a number of advantages to this concept including the following:

a. The reference estimate of expected error is continuously available after one time of flight,

6-4
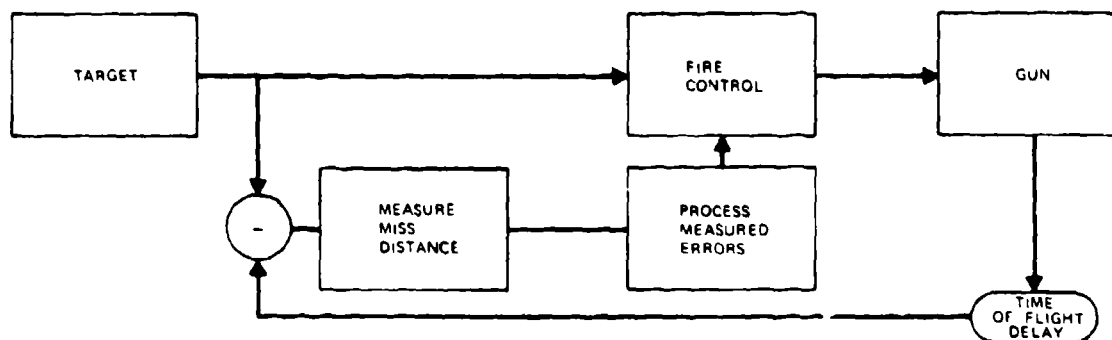
20871 147A

Figure 6-4. Top Level Flow Diagram of System Using Corrections Based on Measurements of Projectile Miss Distance

whereas the times at which the measurements of actual error are available may vary widely.

b. The refer ce estimate contains the error components ca᾽ oy target maneuver and approximation er .s of the basic prediction algorithm. Hence these can be included or excluded from the correction as desired.

c. The reference estimate can be used by itself as a correction device for simple prediction algorithms (for example a course and speed sight), and as a method of recording errors in the basic fire control system, exclusive of misorientations, in real time.

d. The system dynamics are greatly simplified by this algorithm.

The generation of the reference expected error is identical in concept with that of the Air Force SnapShoot gun sight where it is the sole prediction device. Its application to the present concept follows a suggestion by Dr. Daniel Willard that one need not wait time of flight to get a preliminary estimate of where the gun was aimed, although the implementation may not be that visualized by Dr. Willard.

6.2.7 Preliminary Analysis

For present purposes a simplified system is assumed which, however, retains the essential characteristics of the complete system. The analysis is worked in a single coordinate, and trigonometric conversions are omitted. As in the case of the regenerative module, (Section 4.3) we could obtain an equivalent simplified system as a zero order approximation, starting with the full system algorithms. The system equations are originally written in a form which can then be developed for an analog or discrete implementation. However, since the projectile measurements are discrete events, and the time of flight lag is most easily handled in the discrete formulation, the analysis is done for a discrete system.

The following notation is employed, and is related to the data flow shown in Figure 6-5.

$X_t(t)$ = target position at time t

$n(t)$ = sensor error at time t (tracking sensor)

$X_{tm}(t)$ = sensed target position at time t

$H(s,\alpha)$ = data smoothing and prediction transfer function; $s = d/dt$, α = time of flight

$X_p(t)$ = prediction of target position at $t + \alpha$, made at time t

$w(t)$ = system bias, misorientation, etc., at time t. This will be taken as a constant $v'(t) = w_o$

$X_g(t)$ = gun orientation at time t in target coordinates

$v_a(t)$ = ammunition dispersion at target of round fired at $t - \alpha$

$E(t)$ = error in aim point measured at the target for a bullet arriving at the target at time t

$E_m(t)$ = measured projectile miss distance at time t

$G(s,t)$ = miss distance processing algorithm

$C(t)$ = correction applied at time t, based on processed measurements of miss distance

Note that two alternate points of insertion of the correction C(t) are shown in Figure 6-5, one in advance of the filter and prediction algorithms, and one at their output. The second mode is preferable because of the intermittent character of the miss distance measurements, but the former is shown because of an interesting characteristic of the resulting algorithms.

For this analysis time of flight is assumed constant.

For Mode I: Correction inserted prior to prediction,

6-5

$$X_p(t) = H(s, \alpha)\,[\,X_t(t) + n(t) + C(t)\,]$$

$$X_g(t) = X_p(t) + w(t)$$

$$E(t) = e^{-\alpha s}\, X_g(t) \cdot X_t(t)$$

$$E_m(t) = E(t) + v_a(t)$$

$$C(t) = -G(s,t)\, E_m(t) \qquad (6.3)$$

Solving for E(s)

$$E = X_t \left[\frac{e^{-\alpha s} H \cdot 1}{1 + e^{-\alpha s} HG}\right] + n \left[\frac{e^{-\alpha s} H}{1 + e^{-\alpha s} HG}\right]$$

$$\cdot v_a \left[\frac{e^{-\alpha s} HG}{1 + e^{-\alpha s} HG}\right] + w \left[\frac{e^{-\alpha s}}{1 + e^{-\alpha s} HG}\right]$$

$$(6.4)$$

Note that for a linear prediction algorithm

$$e^{-\alpha s} H(\alpha, s) = 1 + \text{terms in } s^j ; j \geqslant 2 \qquad (6.5)$$

Hence in evaluating the low frequency, and steady state performance of this set of algorithms, this pair of terms can be replaced by unity.

This mode may be of interest in detailed analysis in conjunction with internal generation of a reference synthetic trajectory (Mode III), but it will not be investigated in the present study. It may be noted that studies of Kalman filters for systems with constant 'process' lag in observation time have found optimal solutions incorporating prediction elements operating on the best estimates of the delayed observations.[5,6,7]

For Mode II: Correction inserted after prediction

$$X_p(t) = H(s,\alpha)\,[\,X_t(t) + n(t)\,]$$

$$X_g(t) = X_p(t) + C(t) + w(t)$$

$$E(t) = e^{-\alpha s}\, X_g(t) \cdot X_t(t)$$

$$E_m(t) = E(t) + v_a(t)$$

$$C(t) = -G(s,t)\, E_m(t) \qquad (6.6)$$

Solving for E(s),

$$E(s) = X_t(s) \left[\frac{e^{-\alpha s} H(s)-1}{1 + e^{-\alpha s} G(s)}\right] + n(s) \left[\frac{e^{-\alpha s} H(s)}{1 + e^{-\alpha s} G(s)}\right]$$

$$\cdot v_a(s) \left[\frac{e^{-\alpha s} G(s)}{1 + e^{-\alpha s} G(s)}\right] + w(s) \left[\frac{e^{-\alpha s}}{1 + e^{-\alpha s} G(s)}\right]$$

$$(6.7)$$

The four terms in the above expression define four requirements on system performance to which a best compromise set of algorithms is to be designed. The problem can be solved in some generality by assigning on overall quadratic penalty function and applying Kalman-Bucy filter theory, however considerable insight can be obtained by simpler means.

The first term in Equation (6.7) defines the prediction function. The system must correctly predict for a polynomial of assigned degree, and must have a satisfactory settling time.

The second term defines the effect on prediction error of sensor noise and must have a satisfactory variance reduction.

The third term defines the ability of the miss distance processing element to average out round to round dispersion, and other errors in miss distance measurement, and must show a satisfactory reduction of this error source.

The fourth term defines the ability of the system to eliminate bias. misorientations and similar errors, and is the principal term of interest since this function is the purpose of the miss-distance measurement and correction process.

We therefore consider the requirement on the form of G in order that w be eliminated with time. Assume that a constant w_0 is applied at $t = 0$, and that the
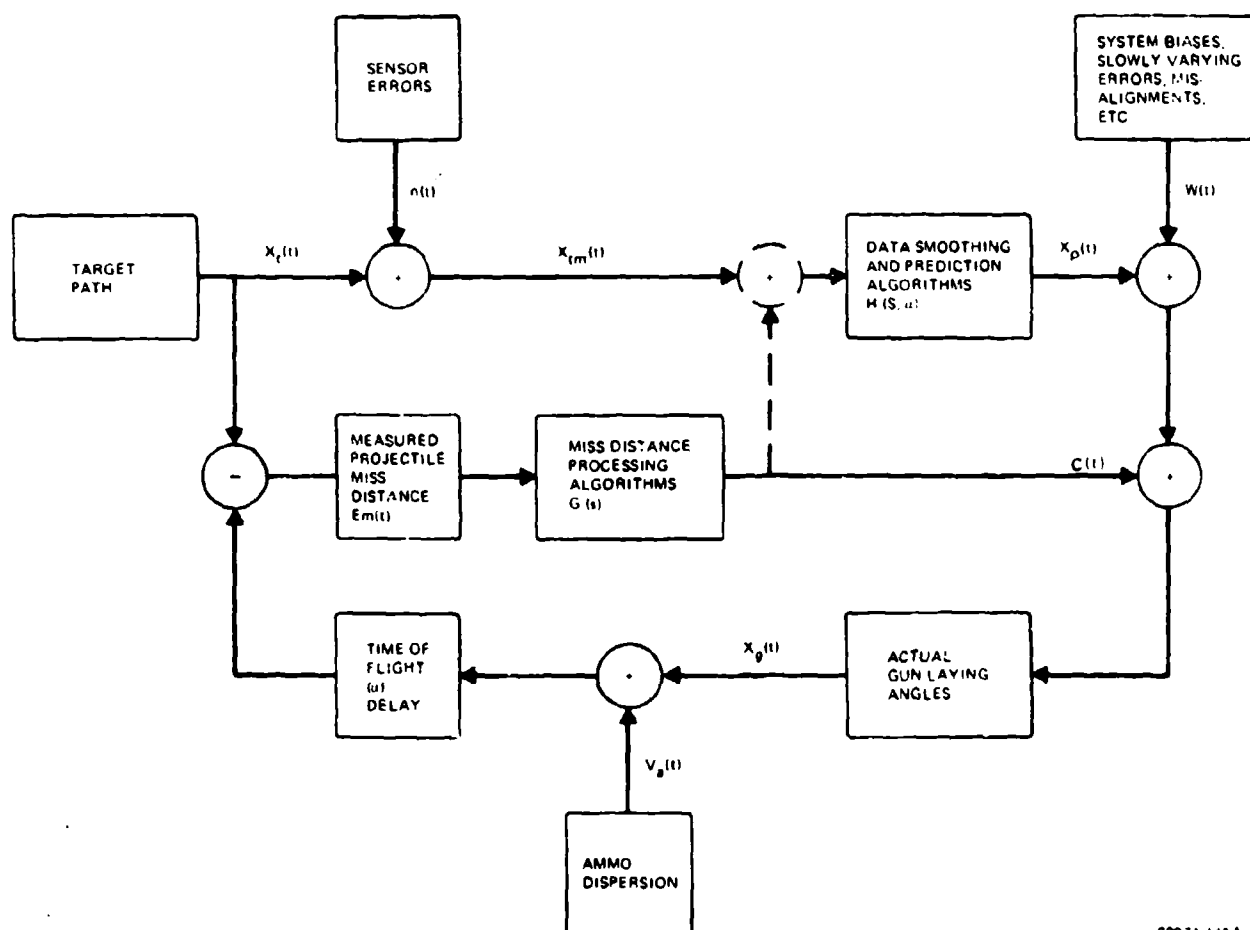
Figure 6-5. Flow Diagram for System Correction Based on Measurements of Projectile Miss Distances

system is expressed in discrete form with unit sampling interval. Then if $E_w(z)$ is the z-transform of the error component corresponding to w_o,

$$E_w(z) = w_o \frac{z}{z-1} \left[\frac{z^{-\alpha}}{1 + G(z)z^{-\alpha}} \right] \qquad (6.8)$$

To determine the value of $E_w(t)$ for large t, use the relation

$$\lim_{t \to \infty} E(t) = \lim_{z \to 1} (z-1) E(z)$$

$$= w_o \frac{1}{1 + G(1)} \qquad (6.9)$$

We therefore require a form of $G(z)$ which becomes infinite as $z \to 1$. This is obtained by computing C by the algorithm

6-7

$$C(j) = C(j-1) + G_1 E_m \qquad (6.10)$$

from which

$$G(z) = G_1(z) \left(\frac{z}{z-1} \right) \qquad (6.11)$$

This satisfies the requirement for steady state elimination of w_o.

However we also need to average successive miss distance measurements to reduce the effects of round to round dispersion.

As shown later, in the discussion of Mode III, we would probably prefer in practice to vary the coefficients of the averaging function with the index of the miss measurement. However for the present discussion, to keep the algebra simple, we use the simplest form of smoothing.

The correction algorithm is, to this point,

$$C(z) = \cdot \frac{z}{z-1} \ G_1(z) E_m(z) \qquad (6.12)$$

Let the smoothed value of E_m be designated $\underline{E}_m$, and use the simplest recursive smoothing algorithm

$$\underline{E}_m(j) = a \, \underline{E}_m(j-1) + (1-a) E_m(j) \qquad (6.13)$$

we could, of course, easily write algorithms for smoothing functions for more than one pole. From the above we have

$$\underline{E}_m(j) = E_m(j) \frac{(1-a)z}{z-a} \qquad (6.14)$$

and we can allow additional flexibility in design by applying a fraction K of this correction at each sample point. Then

$$C(z) = \cdot E_m(z) \, K \, \frac{z^2 (1-a)}{(z-1)(z-a)} \qquad (6.15)$$

For the present section we have assumed that a miss sample is available at each unit sample interval. The extension to the more general case of less frequent measurements, including occasional missed samples is straightforward.

The form of $G(z)$ is now

$$G = K \frac{z^2 (1-a)}{(z-1)(z-a)} \qquad (6.16)$$

This function can be inserted in the expression for $E_w(z)$ and the form of the transient response examined as a function of K and a.

A more important point, however, is the stability of the complete set of algorithms. All four terms of Equation (6.7) have the same denominator, and so we may consider the question of stability with regard to any one term. We therefore focus for the moment on the v_a term.

Substituting G, and expanding,

$$\cdot E_v(z)/v(z) = \left[\frac{Kz^2 (z-1)(1-a)}{z^{\alpha} \left[(z-1)(z-a) \right] + Kz^2 (1-a)} \right]$$

$$(6.17)$$

and the denominator must have no poles outside the unit circle in the complex z plane in order that the complete system be stable.

Locating the positions of the poles is tedious for large values of α. As an illustration, consider the simpler case of $\alpha = 2$. Then one may solve for the location of the poles or use Jury's tables[4] of stability criteria. We find that the system is stable if $K < 1.0$. Also from Jury's tables for discrete systems excited by 'white' noise, we find that for $\alpha = 2$

$$(\sigma_{Ev}/\sigma_v)^2 = \frac{2(1-a)}{(1-K) \left[2(1+a) + K(1-a) \right]}$$

$$= 0.06 \text{ if } K = 0.1, a = 0.9$$

$$(6.18)$$

These are not optimum values, but they serve to indicate a pedestrian approach to system design as a preliminary to possible future analyses using Kalman-Bucy methods of optimization.

As noted earlier, we should probably prefer to make K a function of the index of the miss measurement, $K(j)$, so that the amount of correction applied is large on the first measurement, and decreases with time. One may thus have rapid reduction of w_o yet maintain system stability.

An interesting characteristic of the above set of algorithms is that they cannot distinguish between misses caused by target maneuvers and misses caused by system misorientations. Hence if a constant velocity prediction algorithm is used in the basic predictor, and the target flies a constant acceleration path for at least one time of flight, the system will apply a correction for the acceleration. This may or may not be advantageous: aim errors caused by target maneuver can be very large, a maneuvering target is not likely to maintain a constant acceleration, and the set of algorithms described above may as a result perform poorly against maneuvering targets.

These difficulties are completely avoided in the Mode III algorithms to be described next.

Mode III: Use of a Synthetic Reference Trajectory

This mode takes advantage of the fact that errors resulting in misses can be divided into two categories, (1) those errors resulting from target maneuvers, and system dynamics which could have been computed a priori from a knowledge of system algorithms and parameters and path inputs, and (2) those unknown errors caused by system misalignment which can be determined only by referencing the misses against the target. The idea is to determine what the aim error should have been from gun orders given time of flight earlier, and use this as a reference against which to compare the observed misses. The observed misses are, of course, still contaminated by round to round dispersion.

The data flow is shown in Figure 6-6. A module has been added to the system of Figure 6-5, and this is termed the 'Synthetic Trajectory Module'. It performs the following functions:

a. It stores the orders believed to have been given the gun for at least one time of flight. If the gun is misoriented the amount of misorientation will, of course, not appear in the stored data.

b. From sensor measurements of target position, it computes time of flight and superelevation. Both of these computed quantities will be in error as a result of sensor error in measuring target position. With a good sensor the errors will be small, compared with the errors in aim point from all causes.

c. Using the computed time of flight, the module recovers gun orders from memory time of flight earlier, and subtracts superelevation. If the system had no error, and the target conformed to the prediction algorithm assumptions, the resulting angles would be identical with the target angular coordinates measured by the sensor. The observed difference is termed the 'expected error in aim'.

d. The 'expected error in aim' computed by this process contains all of the errors resulting from target maneuver, and system dynamics, but will not include the errors in boresighting the sensor and the gun, or those resulting from ballistic biases and dispersions. Hence it may be used as a reference against which to compare the measured projectile miss distances.

e. Even without the actual measurements of projectile miss distance this computed 'expected error in aim' might be used to correct imperfect prediction systems with slowly varying errors; for example it might be used to correct course and speed setting on a simple course and speed sight. The disadvantage, or course, is that like actual measurements of projectile misses at the target, the data is always one time of flight old.

To provide a preliminary analysis, the following notation is used in addition to that defined for Modes I and II.

$E_a(t)$ = expected error in aim at time t

$E_m(t)$ = measured projectile miss distance at time t

$$\Delta E = E_m \cdot E_a \qquad (6.19)$$

As noted above, a correction element might be based on E_a; for the present section we concentrate solely on the correction of misorientation errors and use

$$C = \cdot G \Delta E \qquad (6.20)$$

We now have

$$E_m(s) = (X_p + C + w) e^{-\alpha s} \cdot X_t + v$$

$$E_a(s) = (X_p + C) e^{-\alpha s} \cdot (X_t + n)$$

$$\Delta E = w e^{-\alpha s} + n + v \qquad (6.21)$$

The measured error, referenced against the expected aim error thus has components depending only on the misorientation w, sensor error n, and round to round dispersion v.

6-9

Solving for E(s)

$$E(s) = X_t (He^{-\alpha s} - 1) + n e^{-\alpha s} (H - G)$$

$$+ we^{-\alpha s} (1 - Ge^{-\alpha s}) \cdot vGe^{-\alpha s}$$

$$(6.22)$$

Consider the term involving w(s). A constant initial value w_o will be eliminated with time if $G(1) = 1$.

A possible algorithm for $G(z)$ is obtained by computing $C(j)$ from

$$C(j) = [1 - K(j)] \, C(j - 1) + K(j)E(j) \qquad (6.23)$$

whence, for constant $K(j)$

$$G(z) = \frac{K z}{z - (1 - K)} \; ; \; G(1) = 1.0 \qquad (6.24)$$

Note that in Equation 6.22 there is no problem with system stability provided that G itself has no poles outside the unit circle.

For the problem as now formulated, it is known that the 'best' sequential correction algorithm for w with white measurement noise (resulting from both v and n, which are statistically independent) is

$$K(j) = \frac{\sigma_w^2}{\sigma_v^2 + \sigma_n^2 + j \, \sigma_w^2} \qquad (6.25)$$

where the several σ^2 are the a priori estimates of the respective variances.

As the number of observations and corrections increases, the variance of the residual bias w_o approaches

$$\sigma_{rw}^2 \longrightarrow \sigma_w^2 / j \qquad (6.26)$$

6.2.8 Muzzle Velocity Bias vs. Boresight Error

Using only measurements of miss distance at the target, an additional processing algorithm is required to separate the corrections to be applied to gun angle and to muzzle velocity. This separation has not been shown in the one-coordinate system discussed in the previous paragraphs. The idea is that since muzzle velocity bias causes a systematic error in the direction of target motion, it will be a small fraction of the observed mean miss on incoming targets and a larger portion near midpoint, whereas angular errors will not vary with target approach angle.

It seems unlikely that both error sources can be essentially eliminated on a single firing pass, although a good compromise reduction may be achieved. However by periodic calibration firings using 'canned' internally generated target paths and several standard courses, the component errors can be identified and corrected.

The general topic of projectile tracking in conjunction with 'canned' courses for calibration firing deserves detailed analysis beyond that which can be given here.

6.2.9 Conclusions Regarding Algorithms

In spite of the increased amount of data processing required, Mode III, using a synthetic reference trajectory concept appears to be by far the most promising and likely to work in practice. It allows the errors in system orientation to be corrected by an inherently stable data processing algorithmic set, it is not degraded by target maneuvers, and it easily accepts measurements of miss distance whenever they are available.

6.2.10 Expected Number of Independent Corrections

Although the maximum number of projectile observations is desirable to smooth out the effect of ammunition dispersion, the first observation is not available until time of flight after firing the first round, and the effect of making a correction based on that observation is not seen for an additional time of flight.

An important question is, therefore; on a given target path, how many points spaced time of flight apart lie within open and close fire range. An approximate answer, including the effect of varying time of flight, is obtained as follows:

If we count only corrections spaced by one time of flight, the average rate of making these corrections will be $1/t_p$; t_p = time of flight. Hence over a path of time duration T, the average number of corrections will be approximately

$$N \cong \int_0^T dt/t_p \qquad (6.27)$$

Making the additional approximation of a constant projectile velocity v_a with open fire at an approach angle Ω, and last round fired at midpoint, against a target flying a pass course at velocity v, some trigonometric analysis yields

$$N = -\log_e [\sin \Omega (\tan \Omega/2)^{v_a/v}] \qquad (6.28)$$

whence for $v_a/v = 3.0$, the following values of N are obtained, as shown in Table VI-2.
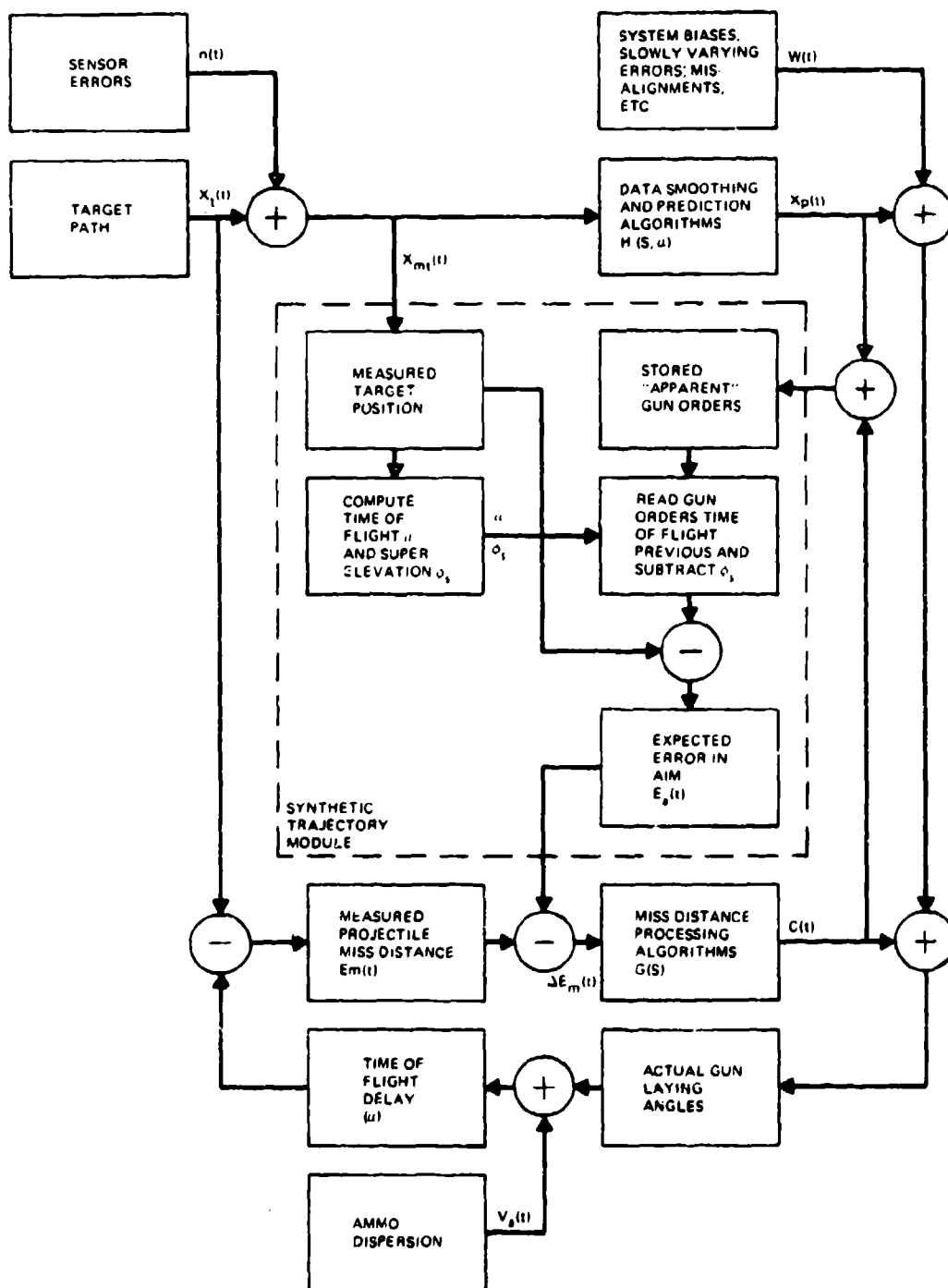
Figure 6-6. Flow Diagram for Correction Based on Measurements of Projectile Miss Distances Using Synthetic Trajectory Reference

208/1 149

Table VI-2. Average Number of Independent
Corrections, N

N	Open Fire Angle	N
	45"	1.3
	30"	2.0
	20"	2.7
	10"	3.9
	5"	5.1

20871-510

For a given opening range, the closer the target is to direct incoming, the more independent corrections can be applied before midpoint.

N increases with v_a/v. A more accurate computation would include the effect of projectile slowdown, but the above estimate; indicate that except for distant passing courses, a useful number of corrections can be applied.

6.2.11 Simulation Module for Projectile Miss Measurement and Correction

Although there has not been sufficient time in the present contractual effort to program a simulation module for the algorithms just described, this section outlines the data flow for such a module as a point of departure for possible future programming.

The round to round ammunition dispersion is simulated based on three independent, normal, unit variance sequences. The sampling interval can be as small as that of the simulation to simulate a high data rate, or wider sample intervals can be used to determine the effect of data rate.

The angular miss caused by angular dispersion at each sample is obtained by multiplying two of the random sequences by the vertical and lateral standard deviations now programmed as inputs to the simulation. The simulation now has a module which resolves muzzle velocity dispersion into lateral and vertical components at the target. These components are extracted and both are multiplied by the third random sequence to give vertical and lateral miss of the projectile caused by muzzle velocity dispersion. These are converted to angular measure.

The vertical and lateral miss components from the angular and muzzle velocity sources are respectively added to give the total miss from both ammunition round to round error sources.

From the present simulation program, vertical and lateral errors in aim (center of the bullet pattern) are obtainable at the position of closest approach of the

mean trajectory to the target. This is not exactly what would be seen from a ground sensor but the difference is negligible for present purposes. These errors are corrected to angular measure.

These measurements of aim error are added to the respective random round to round samples to give the observed miss distance for each sample in Mode II operation (see prior sections). The measurements thus computed are processed through a new module which averages them, and generates correction terms. If no attempt is made in processing to identify muzzle velocity as a separate bias, the algorithm will generate corrections in azimuth and elevation to be applied to gun orders in the simulation. If the algorithm extracts a separate estimate of muzzle velocity bias, this is applied as a correction to the muzzle velocity bias originally programmed as an input to the simulation.

This data flow should effectively simulate the Mode II corrective algorithm (see Figure 6-7).

Simulation of Mode III assumes that the synthetic trajectory module is capable of extracting all 'non-bias' miss distance components from the miss observation. The lateral and vertical components of miss per sample from random round to round sources are computed as before. To them are added the azimuth (corrected to the slant plane) and elevation biases separately programmed into the simulation. The lateral and vertical components of muzzle velocity bias also separately programmed as input, and available in resolved form in the present simulation are also added.

Since the synthetic trajectory is referenced against the sensor estimate of target position, rather than true target position, the sensor vertical and lateral angle errors at each sample instant are added to the build up of observed misses.

The lateral and vertical error sums are then put through a Mode III processing module, which extracts corrections to gun azimuth, elevation, and possibly to muzzle velocity bias

This data flow should adequately simulate Mode III operation.

The discussion has not considered errors in the miss-distance measuring equipment. If these can be considered uncorrelated across measurements, they can be included 1) by separate generation of random sequences, 2) by increasing the angular dispersion standard deviation inputs.

A general observation is that non-simulation systems analysis should be carried out in some depth in advance of simulation programming to facilitate early recognition and correction of possible programming errors, in view of the complexity of the complete simulation program.
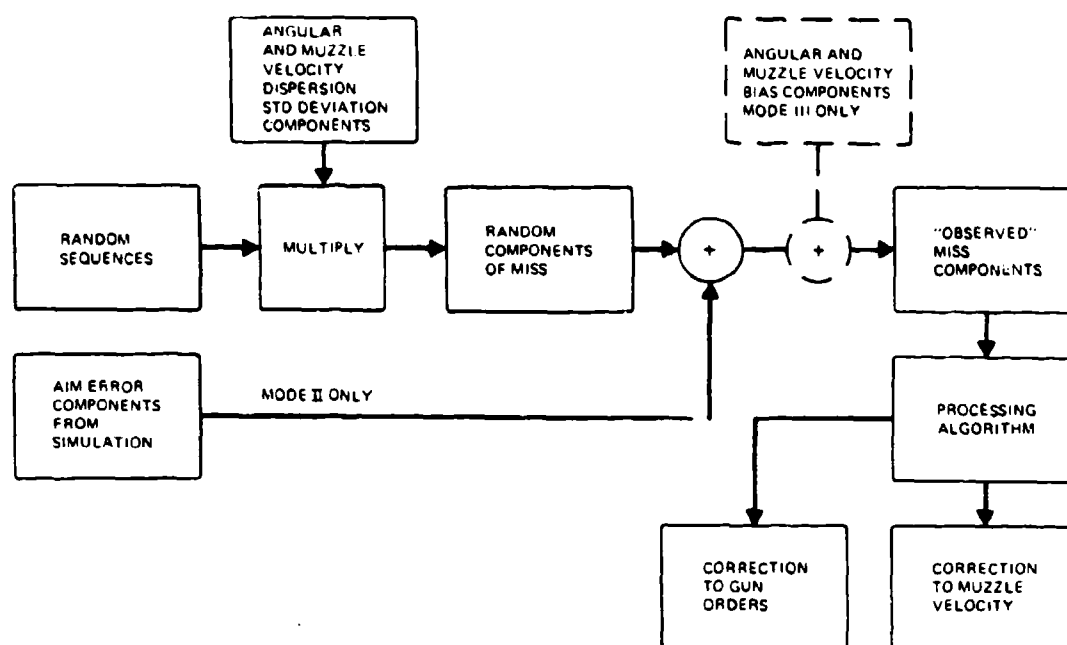
Figure 6-7. Flow Diagram for Simulation Module for Projectile Miss Distance Measurement and Correction

6.3 PREDICTION USING TERRAIN INFORMATION

One of the methods of evading detection is for an aircraft to fly very low, following the contours of the terrain. Many systems exist or are under development to assist the pilot in terrain following or to perform the function automatically. Since terrain information in the vicinity of a defense is known to the defender, it is of some interest to examine how this information may be used in fire control. In AFAADS-I (Vol. I, p. 4-32) a stochastic type of prediction using local terrain statistics was described. In the present section a deterministic prediction mode is described.

The simplest model describing the interaction of terrain variations and aircraft and pilot dynamics is used here. It was presented in AFAADS-I and shown to agree qualitatively with some limited data on nap of the earth flying by helicopters.

First consider a flight path lying in a vertical plane. The aircraft does not maneuver laterally, and changes altitude in response to terrain variations.

Define

H = aircraft altitude above the terrain mean at time t

H_t = terrain height from its mean directly below the aircraft

H_o = the mean altitude above terrain desired by the pilot

Then the simple model developed in AFAADS-I yields the following differential equation for H

$$T_c \, dH/dt + H = H_o + H_t (t) \qquad (6.29)$$

where T_c is a characteristic response time of the aircraft and pilot and may be about 0.50 sec.

Solving this equation for an initial value H(o),

$$H(t) = H(o)e^{-t/T_c} + \int_0^t [H_o + H_t (t-s)] \, e^{-s/T_c} \, d(s/T_c) \qquad (6.30)$$

$$H(t) = H(o)e^{-t/T_c} + H_o \left(1 - e^{-t/T_c}\right) + \int_0^t H_t (t-s) e^{-s/T_c} \, d(s/T_c) \qquad (6.31)$$

The terms outside the integral represent initial transients of the aircraft in settling to the terrain following mode. If it has been in this mode for several minutes the exponentials will have vanished, and

6-13

$$H(t) = H_0 + \int_0^\infty H_t(t-s)e^{-s/T_c} \, d(s/T_c) \qquad (6.32)$$

The defense observes $H(t)$ and knows $H_t(t)$ from stored terrain data. Hence H_o, the mean clearance altitude above terrain desired by the pilot can be inferred. The integral converges rapidly with increasing 's'.

The predicted aircraft altitude at time $t + \alpha$ is, correspondingly,

$$H(t+a) = H_0 + \int_0^\infty H_t(t+a-s)e^{-s/T_c} \, d(s/T_c) \qquad (6.33)$$

and substituting the inferred value of H_0

$$H(t+a) = H(t) \cdot \left(1 - e^{-a/T_c}\right) \int_0^\infty H_t(t-v)e^{-v/T_c} \, d(v/T_{cc})$$

$$+ e^{-a/T_c} \int_0^\alpha H_t(t+v)e^{v/T_c} \, d(v/T_c) \qquad (6.34)$$

This is the desired expression. Although shown in analog form, it is easy to obtain a discrete approximation. The terrain sampling interval need be no closer than that corresponding to the aircraft response time T_c, since the prediction is based on the terrain spectrum as modified by the aircraft dynamics. For fairly smooth, or rolling terrain the sampling interval may be even wider.

The amount of correction generated by this algorithm depends on the terrain variance, bandwidth and the aircraft response time. Some rough computations based on the data in AFAADS-1 on terrain indicate that at 3 seconds time of flight the standard deviation of the correction might be from 20 to 35 meters. Since the residual error after making the correction would be expected to be much smaller than this, and since simple linear prediction was indicated to generate a standard deviation of prediction error of 30 to 60 meters, the concept continues to have interest.

Note that one is not restricted to the simple approximation to aircraft response represented by Equation (6.29), and with real aircraft tracking data one may choose a better transfer function.

The algorithm can be programmed and demonstrated by simulation. This would be interesting, but not as definitive as testing it against actual recorded aircraft flight paths, with terrain following over known terrain.

A possible method of implementing the algorithm in a fire control system is the following: Within the coverage region of the tracking sensor the terrain could be subdivided into squares of equal size. The size of a square would depend on the variability of terrain heights and what kinds of targets are expected: for fire against helicopters more terrain samples per square mile would be required than against near sonic aircraft. With each square would be associated a mean terrain height and this would be stored in memory as a triad with the coordinates of the center of the square.

Once a target is acquired its ground track is recorded and also projected forward. From the past track, each sample point is associated with the altitude of the square in which it lies. This allows the first integral of Equation (6.34) to be computed approximately as a sum. It may be necessary to project back beyond the acquisition point to get a good value for the integral. However once obtained for a given time, it can be computed recursively for additional points without the need for storing all past computations in memory.

The predicted point in the ground plane is computed assuming constant target altitude. The second integral of Equation (6.34) is then computed as a sum, working forward to the predicted point. This gives the complete expression for predicted altitude and gun orders can now be computed.

In practice it is anticipated that the number of terrain points which must be stored in the computer will be relatively small, i.e., less than one hundred. Rough terrain is associated with short sensor sighting ranges. Smooth terrain is associated with large sighting distances, but requires fewer sample points to represent a given area. Hence the data storage requirements may be about the same regardless of terrain type, and the number of sample points to make a good prediction may be relatively insensitive to target speed.

6.3.1 Lateral Aircraft Maneuvers

Depending on the sophistication of its terrain following sensors, the aircraft may maneuver laterally to reduce the amount of required vertical acceleration, or to avoid terrain prominances. The flight path might be laid out in advance from maps, for example, with the horizontal track established and programmed, leaving vertical motion to automatic clearance control equipment.

More operational information is required to define prediction algorithms in detail for this case, however the following approach might be considered. As a function of time, three values of $H(t+\alpha)$ must be computed, one an extrapolation of the current ground track, and one each for a moderate turn to right or left. The predicted altitude in each case would be

6-14

compared with present altitude, and the required acceleration in each case compared. If the no-turn case indicated a very high acceleration requirement, but one of the turn options did not, the prediction would be biased to the turn with lowest acceleration requirement.

6.4 UNAIDED TRACKER CONTROL: 'GUNNER'S DELIGHT'

The question of whether a gunner, using a machine gun without a fire control system, does better with or without tracer ammunition is controversial, and is unlikely to be resolved in the near future. Single caliber 0.50 machine guns using only tracer control shot down many aircraft in World War II, and the Quad 0.50 mount with a fixed reticle sight had an excellent record.

The time of flight delay between observation and correction makes it unlikely that simple tracer control would be much assistance against crossing targets, however the possibility exists that tracer observation did help the sight setters of the course and speed sights (M7), and the angle setters of the Stiffkey Stick and Peca Sights to get the lead into the right slant plane. This capability was demonstrated in proving ground firings.

Since fire with a fixed reticle type sight with or without tracer is always a back-up mode of operation for antiaircraft guns, we note, without attempting to resolve the tracer controversy, some early results with tracer fire by machine guns against slow targets some forty-five years ago.[1] The results may be compared against modern firings against helicopters.

Figure 6-8 shows percent hits against a sleeve target plotted versus range for cal 0.30 and 0.50 machine guns in proving ground firings. Note that the percent hits varies inversely as the square of range, hence can be reduced to an equivalent constant mil value. The sleeve size is unknown at this time, but assuming a 6 x 30 ft sleeve, the results are equivalent to an angular standard deviation of 16 mils.

It is probable that the aim errors associated with successive rounds were highly correlated; unfortunately there is insufficient data to infer the correlation.

Normalizing the individual points to equivalent values at 1000 yards, and plotting against target speed, an indication is obtained in Figure 6-9 that the percent hits varies roughly as the inverse of target velocity squared.

Because of the operational limitations on firing at a sleeve without hitting the tow aircraft, it is probable that the recorded data was taken during the central portions of crossing courses. Hence the velocity can be interpreted as velocity perpendicular to the line of sight.
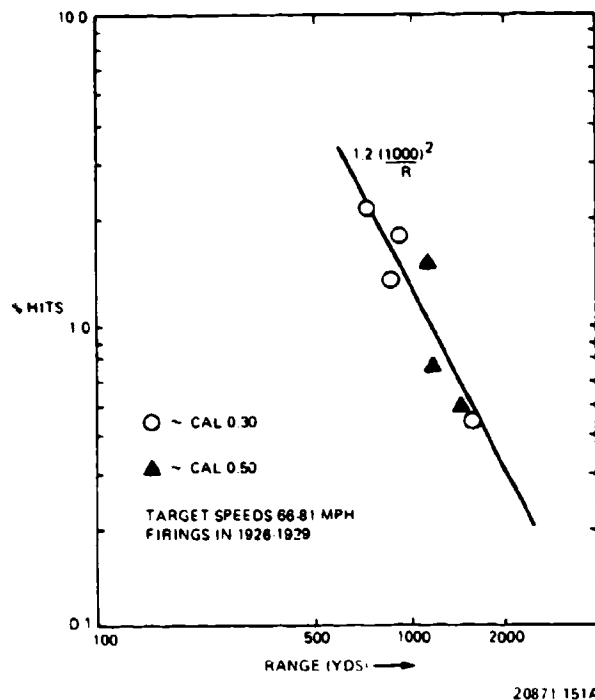
Figure 6-8. Percent Hits versus Range with Machine Guns using Tracer Control: 1926-1929
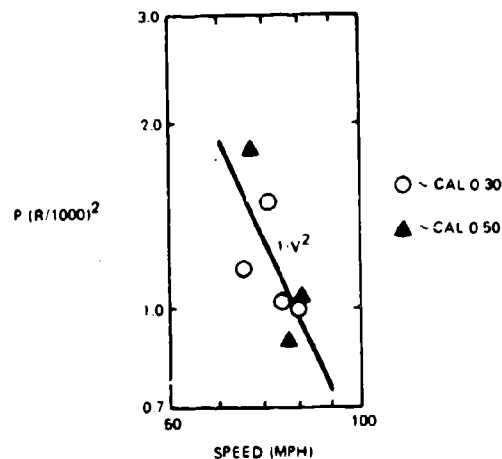
Figure 6-9. Machine Gun Fire with Tracer Control: 1926-1929

The straight line approximation in Figure 6-9 corresponds to an estimate of equivalent standard deviation

$$\sigma = 22.5\,(V/100)^2 \text{ mils ; where V = velocity in mph.}$$

(6.35)

This must have some minimum value as V becomes very small, but there is insufficient data to infer the minimum.

Since the above estimates work out to about 7 mils at 1000 meters for a 50 knot target, there is a strong inference (validated by Vietnamese experience) that machine guns with only rudimentary fire control (at the most a fixed sight) and possibly using tracer ammunition have an important air defense role.

However this should not prevent an evaluation of the possibility of providing a very simple computing sight with laser range finder for use of Bushmaster in air defense, for example. Digital computers are now so inexpensive that it is believed a good solution could be developed in a fire control package costing less than the basic weapon. Since the principal use would be in self defense, the weapon could be manually pointed, and the absence of the lag associated with rate control should make a simple gyroscopic computing sight dynamically acceptable.

6.5 THE SNAP-SHOOT GUNSIGHT: SYNTHETIC TRACER CONTROL WITHOUT TRACERS

A new concept of fire control computation has been proposed by Gilbert, Preyess and Willes of the USAF Academy for air to air gunnery.[23] An implementation of the concept is as follows:

The human operator aims the gun and views the target through a sight which displays a computer generated reticle (such as a small circle). To generate the reticle position the computer records the gun position continuously, or at close sample intervals, stores the gun angles versus time.

Range to target is continuously measured by a range finder. The reticle position is generated by the computer to represent the position relative to the target of a hypothetical round fired time of flight previously. Time of flight is continuously computed from the target range. Gun angles are stored in memory as measured by the system at closely spaced sample intervals, and the reticle position is computed by extracting gun angles time of flight previous from memory and providing the appropriate angular corrections to reference them to current gun position. Superelevation correction is included appropriately.

It will be seen that the effect of this procedure, which is done relatively easily with a digital computer, is to

provide the gunner with a synthetic tracer round which has the unique characteristic that it lights up only when it reaches target range. In addition the density of synthetic fire can be so high that it is essentially continuous, like water from a hose visible only at target range. The reticle then moves continuously rather than in steps.

The concept is attractive from the point of view of a 'practical' man, since the problem of lead computation is reduced to one of training the operator's 'gunner's eye'. If in fact the man can make use of more cues than can be measured by an automatic system, good performance could result.

On the other hand, the delay time between a control motion and the operator's observation of the result of that motion has now increased from about 0.20 times time of flight for a disturbed reticle sight to the full time of flight. The increased difficulty in operation has been noted in simulator tests of the Snapshot principle.

The air to air problem has characteristics not present in the ground to air problem; for example the interaction of maneuver and countermaneuver between combatting fighter pilots.

For ground to air fire control the principle of storing gun orders and comparing them with sensed target position time of flight later has a number of possible applications.

a. The comparison can be done automatically, with automatic introduction of the correction to a basic conventional prediction algorithm. In this mode the system is a special case of the projectile miss distance measuring system of Section 6.2. It can correct to some extent for target maneuvers, lags and solution imperfections in the basic prediction and computation algorithms, but it cannot correct for errors in orienting and aligning the system. Thus, added to Vulcan, it could correct for lead errors resulting from the approximate algorithms used but it could not correct for boresight errors. Similarly, if added to Duster, it could correct initial course and speed estimates set on the mechanical lead computing sight.

b. The correction could be applied as a 'track-off' reticle on an existing fire control system. The operator would track the standard reticle for one time of flight after which the synthetic tracer spot would appear and could be used as a new tracking reference. The potential of doing some smoothing on the difference now exists, since the difference should be slowly varying.

c. The apparent miss distances computed by the above procedure can be used in the system employing actual measurement of projectile miss distances as a reference against which to com-

pare those measurements. Since the apparent miss distances contain the errors resulting from tracking noise, target maneuver, and solution approximations, the difference between them and the recorded miss distances should be composed only of system misalignment errors and round to round dispersion. Use of both sets of data greatly expands the options for design of an effective overall system.

6.6 RATE BY TIME PREDICTION

Gyrosights are still used for antiaircraft fire control, some, like Vulcan, with complex error correction algorithms, and some foreign systems, it is believed, use smoothed angular velocities simply multiplied by time of flight for an approximate computation.

In this section a brief analysis is made to indicate the magnitude of error involved in the simple rate by time prediction. This is not intended as an evaluation of any existing system, since as has been indicated, the degree to which the indicated error is corrected out by various means in specific systems is not known to the present writer.

Consider a gyrosight computing lead in the slant plane containing the tracking point and the target velocity vector, according to the prediction algorithm

$$\theta_p = \theta_o \; \frac{1 + s(1+a)t_p}{1 + ast_p} \qquad (6.36)$$

and for simplicity assume a constant velocity projectile.

Confining attention to the error in the slant plane, this may be computed by expanding

$$E = \theta_o e^{st_p} \cdot \theta_p \qquad (6.37)$$

and to terms in s^2 this is

$$E = \ddot{\theta}_o \, t_p^{\,2} \, (a + 0.5) \qquad (6.38)$$

For a first order approximation ignore the difference between present and predicted slant range, whence

$$E = (v/v_a)^2 (XD_m/D^2)(1+2a) \; ; \; D = \text{slant range}$$

$$D_m = \text{midpoint range}$$

$$X = \text{distance to midpoint}$$

(6.39)

and E is in angular measure, (radians). To convert to linear miss distance

$$E_m = (v/v_a)^2 (XD_m/D)(1+2a)$$

(6.40)

For $v/v_a = 0.3$, contours of constant E_m are shown in Figure 6-10, for typical values of $a = 0.20$ and 0.50. It is clear that the errors are unacceptably large, except for directly head on targets, and for a brief interval at midpoint.

6.7 COURSE AND SPEED SIGHTS

Duster uses a mechanical course and speed sight which develops angular leads based on estimates of target heading and speed which are set into the sight. A mechanical drive maintains the heading setting as the gun traverses, so that once correct it remains correct until the target changes course. Heading is set as a combination of angle of dive and horizontal heading. The sight computes for an average projectile velocity and superelevation, so that even with correct course and speed setting, leads will be in error except at the range to which projectile velocity and gravity drop are set. In general the errors from these approximations are small compared with those resulting from the course and speed estimates.

At one time a doctrine was developed for making course adjustments based on tracer observation, but it is doubtful that this has survived over the years, although it was demonstrated to work in proving ground firings.

To get a rough impression of the errors resulting from erroneous course and speed settings, assume a level low altitude target path, and error E_c and E_v in course and speed settings. For a target speed v, and an average projectile velocity v_a, the miss distance at the target will be approximately

$$E_m = (v/v_a) [(E_v/v)D_m + E_c X] \; ; \; X = \text{distance from midpoint}$$

$$D_m = \text{crossing range}$$

(6.41)

6-17
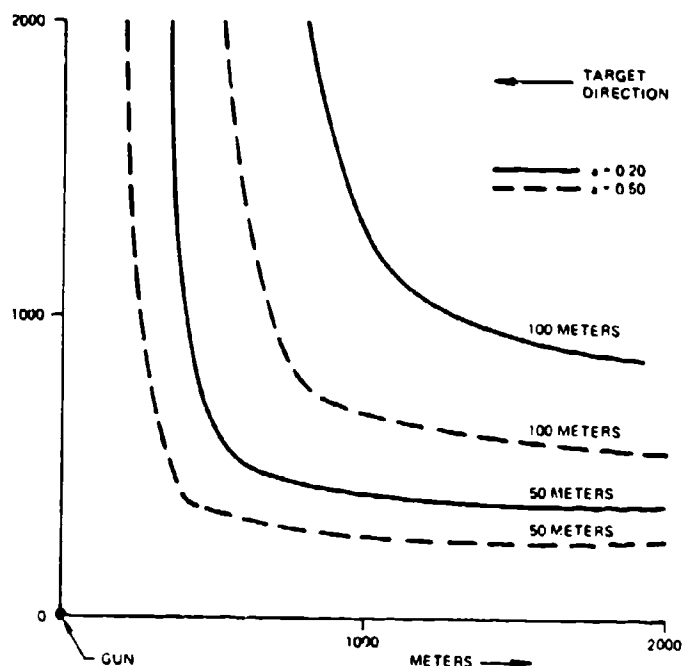
Figure 6-10. Contours of Constant Aim Error in Slant Plane with Rate x Time Computation

It is doubtful that course can be estimated to better than about 10° or speed to better than about 15%. Then E_m works out to about 0.05 D where D is slant range, for $v/v_s = 0.30$. Surprisingly, this is about the same order of magnitude as the lag error of the rate by time predictor over most of the firing region, and if one allows for some ability to correct course by tracer observation on direct incoming targets at least, the two systems are competitive, but neither is very good. The value for E_m corresponds to about a 50 mil bias over the whole firing pass.

During World War II, NDRC personnel ran experiments to determine the ability of human observers to estimate target speed and heading. Unfortunately the reports are deep in the historical archives, if, indeed they still exist.

These sketchy analyses do justice to neither the rate x time nor the course and speed sight. Classified data on Duster firings do exist from which one can infer errors in course and speed setting. Noting that the bias estimated above is proportional to the ratio of target speed to projectile velocity one might expect fair performance of the simple course and speed sight against helicopters, using a high velocity gun, and in general, for light automatic weapons having antiaircraft defense as a secondary mission the course and speed sight should be given some consideration. However, since it does not use gyroscopes, digital computers,

laser or radar range finders, its protagonists would have to support the recommendation with firing results.

6.8 BARRAGE FIRE

Reports of enemy antiaircraft fire seem to be reluctant to credit the enemy with the ability to conduct accurate aimed fire, unless it is observed that he is using radar, which is somehow endowed with a mystical ability to predict that is not credited to optical tracking. A heavy and effective antiaircraft gun defense is often reported as using 'barrage fire'. Reports from friendly antiaircraft units on the other hand are unanimous in commenting on the comparative ineffectiveness of barrage fire unless associated with extremely large ammunition expenditures and large numbers of guns.

For this reason, and because 'barrage' fire is a back up mode of defense when fire control fails and the guns are still operative, it seems desirable to make some computations of the effectiveness of barrage fire.

In World War II, barrage fire was used effectively by the Allies in the defense of Malta and in the defense of the Remagen Bridgehead in 1945. No data is at hand on the design of the 'box barrage' used at Malta, but the Remagen defense is well documented. The defense at Remagen employed 1100 cal 0.50 machine guns and 240 37-mm and 40-mm weapons, and on its

6-18

best day inflicted 59% kills on attacking aircraft, including a number of jets.

6.8.1 The Remagen Defense

The Allied advance had succeeded in capturing the Remagen railroad bridge intact; this bridge was essential to rapid continuation of the advance, and a total of 64 90-mm guns, 24 37-mm and 216 40-mm automatic weapons and 1100 Caliber 0.50 machine guns was emplaced to protect the bridge and associated Bailey, Treadway and Pontoon bridges.

The defense doctrine is described in the referenced Army history.[8] The defense was supplemented with balloons, many of which were victims of the defense itself.

The principal defense was a barrage set up with the machine guns and the automatic weapons. On the approach of enemy aircraft, the barrage was activated for a period of 10 seconds, and the 9850 rounds per second (most or all with tracer ammunition) must have been an impressive sight to the attacking aircraft.

The guns were divided into two geographical groups, and each group put an umbrella of fire over an assigned bridge.

Each weapon was laid on the azimuth of the bridge it was assigned to defend, and fired at a specified quadrant elevation with a few degrees manual 'scanning' about this angle during firing. Presumably this minor change in angle provided a more uniform average coverage.

Both piston engined and jet aircraft attacked. The record of the defense is shown in the following table. The reduction in percent kills with time in part reflects the increasing fraction of jets, and in part the probable increasing reluctance of attackers to attempt to penetrate the umbrellas.

A total of 442 enemy aircraft was active over the crossings and bridgehead area during the period 7-21 March 1945. Of these 142 were destroyed by antiaircraft and 59 probably destroyed. None of the bridges were damaged or destroyed. Results by date are summarized in Table VI-3.

6.8.2 Model of Defense

A vertical section through the defense is shown in Figure 6-11. For simplicity, it is assumed that all weapons are aimed at the azimuth of the defended point, and at the same quadrant elevation. In addition, the trajectories are assumed to be straight lines, since even for the most remote weapon, gravity drop over the defended point is only a few degrees.

The greatest density of fire is, of course, greatest directly over the target.

Since some assumption must be made about the horizontal deployment of the weapons, it is assumed that the deployment is such that the linear density of trajectory intercepts with the vertical axis through the target is a constant over the height band specified for maximum capability. It is also assumed that the ground distribution of weapons has circular symmetry.

If there are N tubes and the apex of the defense cone is at a height H, then there are N/H trajectory intercepts per foot.

Next consider a target flying through the defense on a horizontal path. It can be seen from Figure 6-11 that by flying at one half the altitude of the apex of the cone it accomplishes the closest approach before entering the firing volume.

We now obtain the density of fire after penetration of the firing volume. If H is the altitude of the apex of the cone, and the target flies at H/2, it is exposed to fire when it enters a disc of radius $R_m/2$.

Within this disc, a ring of radius r and width dr contains those trajectories that cross the vertical axis in two segments of length $dh = dr \tan \phi$, equally spaced above and below the intersection of the horizontal plane with the vertical axes. The ring of radius r contains

$$2(N/H) \tan \phi \, dr \quad \text{trajectory intercepts} \quad (6.42)$$

It is assumed that these are distributed uniformly at random around the ring, so that the density of intercepts per unit area is

$$\rho_t(X,Y) = \left[N \tan \phi / (\rho \pi \, Hr) \right]$$

$$= N/(\rho \pi \, R_m r) r^2$$

$$r^2 = X^2 + Y^2 \quad (6.43)$$

If the target comes in at other than the half cone apex altitude, below the cone apex it penetrates a 'single coverage ring' from r_2 to r_1 then a double coverage ring from r_1 to 0.

$$r_1 = H \tan \phi \; ; r_2 = R_m - H \tan \phi \qquad (6.44)$$

In the single coverage zone

$$\rho_t(X,Y) = N/(2\rho\pi R_m r) \qquad (6.45)$$

In the double coverage zone

$$\rho_t(X,Y) = N/(\rho\pi R_m r) \qquad (6.46)$$

For altitudes above the cone apex there is only a single coverage zone extending from $r_1 = H \tan \phi - R_m$ to $r_2 = H \tan \phi$ and in a circular disc segment over the target there is no coverage.

Here we develop the solution only for penetration at the half cone apex altitude.

The barrage is not necessarily fired for the whole time that the aircraft is within the barrage volume. We assume for generality that the barrage is activated for a target path of length R_o, passing directly over the target, $R_o/2$ before and $R_o/2$ after crossing the target.

In the horizontal plane containing the target, consider that projectile intersecting the plane at X,Y, when the target is at x, flying along the x axis. The probability that the target is hit is

$$p(X,Y,x) = \frac{A}{A + 2\pi\sigma^2} \, e^{-s^2/(A + 2\pi\sigma^2)}$$

$$\qquad (6.47)$$

where A = target presented area to compute hits, or vulnerable area to compute kills. σ = round to round bullet dispersion and

$$s^2 = (X-x)^2 + Y^2 \qquad (6.48)$$

Assume that all guns fire at the same rate ν, and designate V as target velocity. Then the expected number of target hits (kills) is

$$E = (\nu/V) \int_x \int_y \int_z \rho_t(X,Y) \, p(X,Y,x) \, dX \, dY \, dz$$

$$\qquad (6.49)$$

Recognizing the rapid decay of the exponential in Equation (6.47) with s, and integrating successively over x, X and Y, it is found that the multiple integral can be approximated as

$$E \cong \frac{\nu NA}{VR_m} (2)^{3/2}[1 + \text{Log}_e (R_o/C^{1/2})] \; ;$$

$$C = A + 2\pi\sigma^2$$

$$R_o < R_m \qquad (6.50)$$

If more than one weapon type is present, E is summed over all weapons. Then the kill probability against an aircraft P_k is given by

$$P_k = 1 - e^{-E} \qquad (6.51)$$

This expression can be better understood by comparing it with a much simpler case in which fire is uniformly distributed over a disc of radius $R_m/2$. The target crosses a diameter of the disc in $_o/V$ seconds during which N R_m/V rounds are fired. The target covers a fraction $A/(\pi R_m^2/4)$ of the disc, hence it will receive

$$E = \frac{\nu NA}{VR_m} (4/\pi) \text{ hits} . \qquad (6.52)$$

The more complex form of Equation (6.50) accounts for the fact that fire is not uniformly distributed over the disc, but is concentrated more heavily at the center.

6.8.3 Effectiveness Computation for Remagen Defense

The following weapon characteristics are assumed, as shown in Table VI-4.

For all weapons, it was assumed that the target presented area was 250 ft² and the linear standard deviation of round to round dispersion was 20 ft., so that C = 2750 ft².

The complete defense could fire 9850 rounds per seconds with all weapons firing. Assuming all tracered ammunition the display must have been spectacular, especially from the cockpit of the attacking aircraft.

The probability of killing a target with the full Remagen defense covering a single ground point is shown in Figure 6-12 versus. target speed, barrage duration, and tons of projectiles expended per barrage.

Figures 6-13 and 6-14 show the contributions of the machine guns and the automatic weapons separately. Rounds per kill is higher by a factor of about ten over that reported for aimed fire.

The barrage would have been equal to aimed fire on a rounds per kill basis if ten aircraft entered the defense simultaneously.

Table VI-3. Remagen Defense Effectiveness

Date	Targets	Destroyed	Probables	Total Claims	% Confirmed as Destroyed
1945					
March 8	12			12	
9	17	12			59%
10	45 }	29	7	36	48%
11	15 }				
12	84*	31	8	39	37%
13	97	31	13	44	32%
14 day	80**	5	13	18	6.2%
14 night	14**	6	1	7	4.3%
19.20	20			12	
20/21	15			6	

*1ME-262

**67 Jets

20871-511
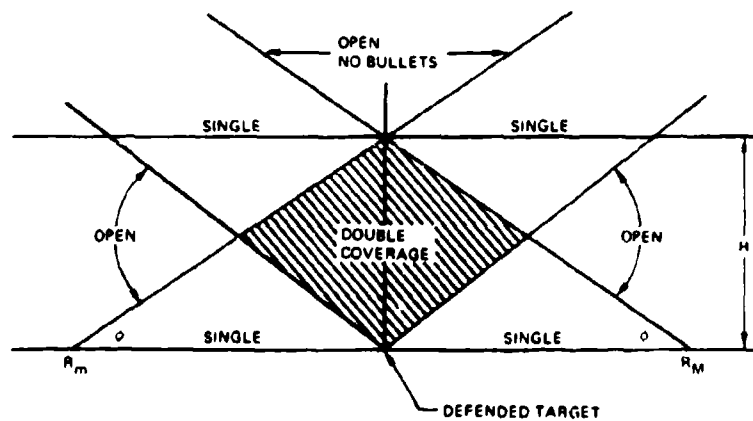
Figure 6-11. Section Through Barrage Defense

20871 154

Table VI-4. Assumed Equivalent Remagen Defense

Weapon	Rate of Fire	Probability of Kill Given a Hit	Number of Weapons
Cal 0.50	500 rpm	0.04	1100
37/40 mm	120 rpm	0.60	240

20871-512
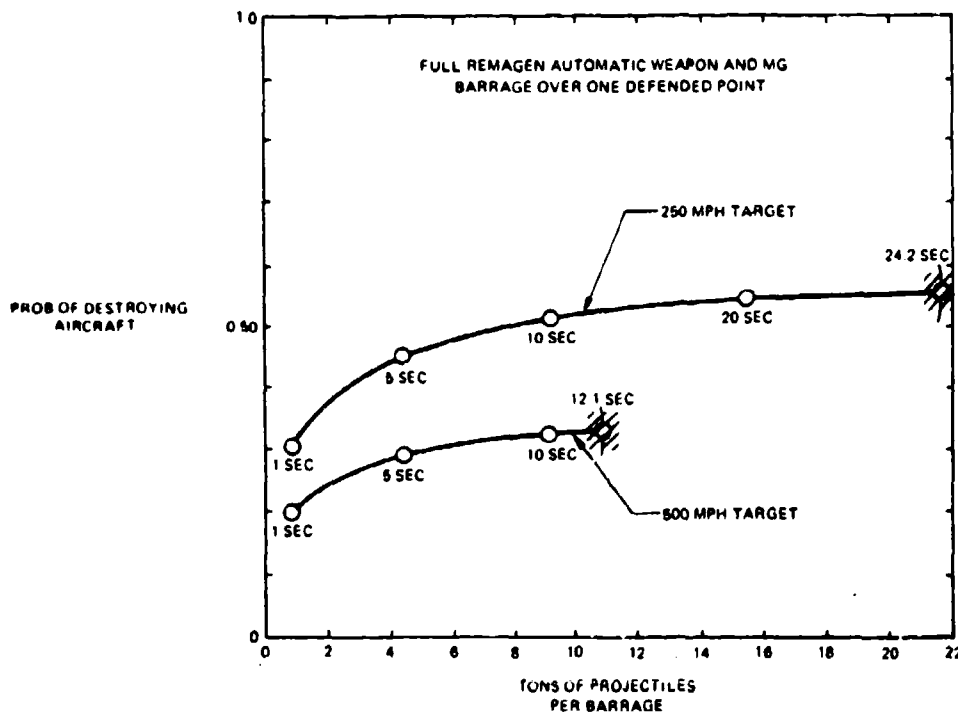
Figure 6-12. Full Remagen Automatic Weapon and MG Barrage Over One Defended Point Probability of Killing Aircraft versus Tons of Projectiles per Barrage

20871 155

Figure 6-15 shows the effectiveness of the automatic weapons component of the defense if the number of guns were varied. Also shown are the tons of ammunition (complete rounds) per barrage activation, and tons of weapons (towed mounts) involved.

6.8.4 Conclusions

Assuming the availability of a sufficient number of guns and rounds of ammunition, a barrage defense can be highly effective. It has the following advantages and disadvantages:

Advantages: It is independent of weather and enemy countermeasures

It cannot be saturated by near simultaneous strikes by many aircraft

It can be employed without fire control

The great volume of tracers in the air at one time looks like an impenetrable curtain to the attacker

6-22
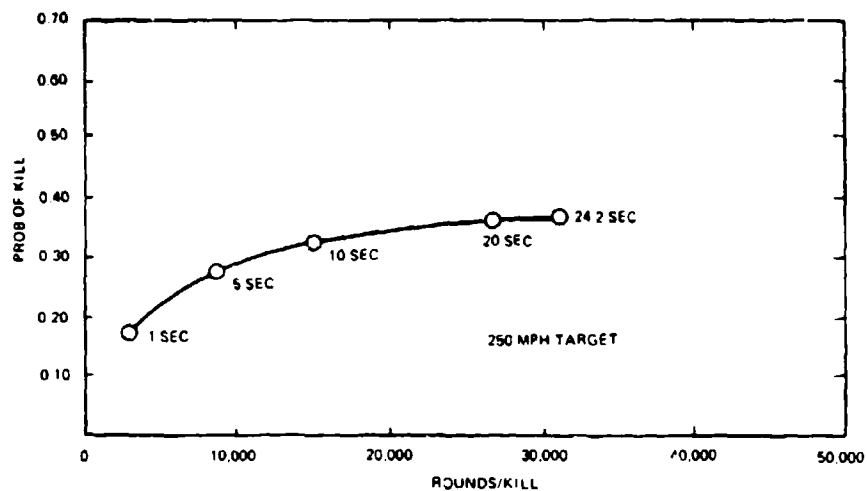
20871 156

Figure 6-13. Effectiveness of Defense with 37/40 mm Weapons Alone (240 Tubes)
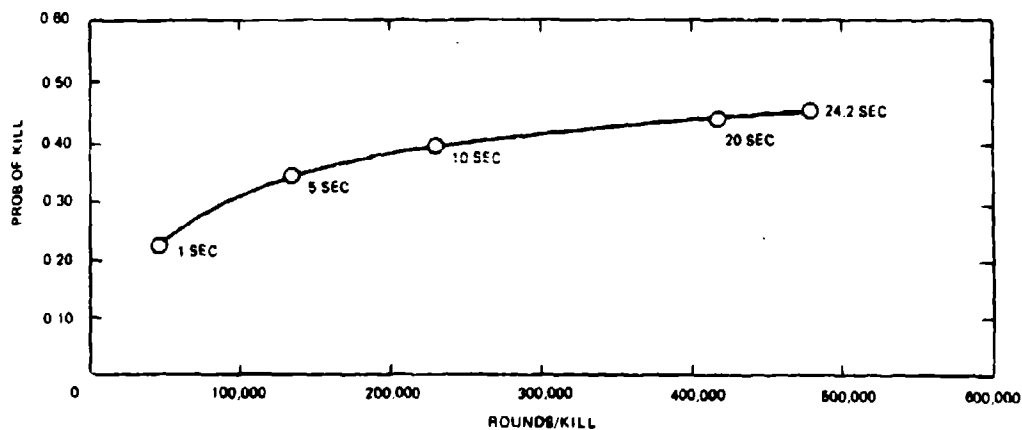
20871 15:

Figure 6-14. Effectiveness of Defense with Cal. 0.50 Machine Guns Alone (1100 Barrels)
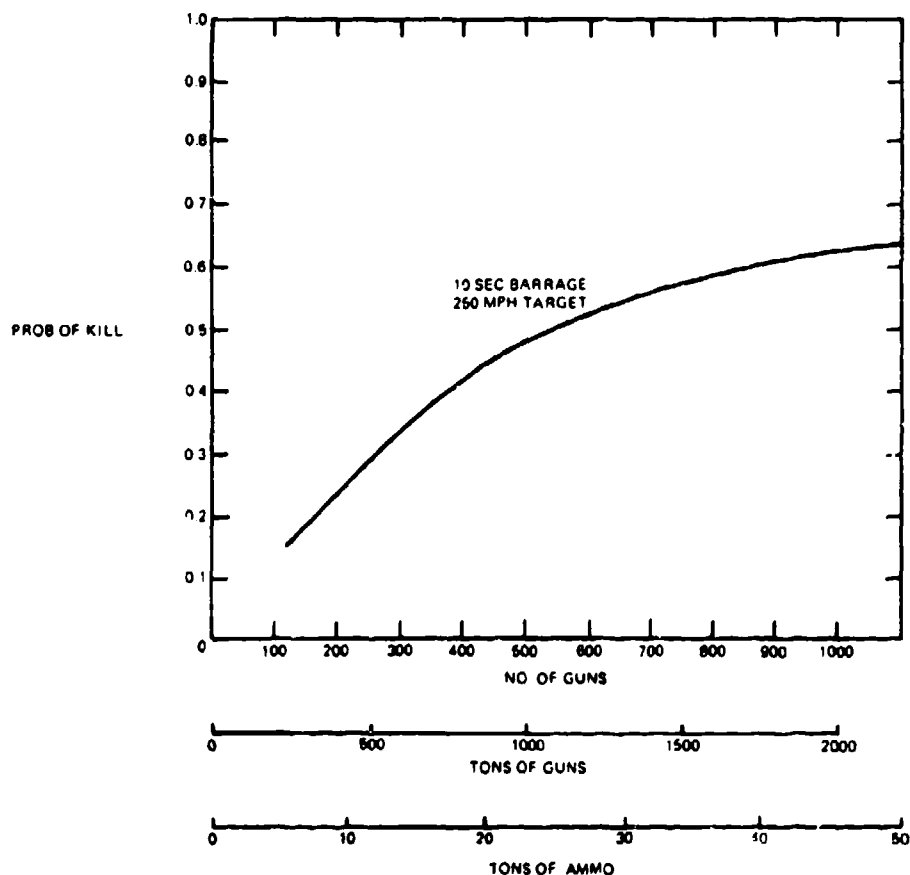
Figure 6-15. Barrage Effectiveness versus No. of 37/40 mm Guns Showing Total Wt. of Towed Mounts and Tons of Ammo (Complete Rounds)

Disadvantage: The barrage requires a greater ammunition expenditure per target kill than aimed fire by a very large factor

6.9 IMPROVED BALLISTIC MODULE FOR SIMULATION

In the AFAADS-I simulation projectile ballistics were simulated as straight line trajectories without gravity drop and with projectile deceleration described by the simple power law

$$dV/dt = - KV^a \; ; \; K, a = \text{constants} \quad (6.53)$$

This expression can be integrated and closed form relations obtained between time of flight and slant range.

The major sources of error in a predicted fire system are target maneuver, tracking noise and its amplification in prediction, and angular and muzzle velocity bias and round to round dispersion, and compared with these, the approximations involved in using the simple power law of Equation (6.53) are entirely acceptable.

However if one is given ballistic tables for a specific projectile it is a tedious separate problem to determine appropriate values of K and a to approximately match

6-24

the given table. Moreover, the power law does not project well to subsonic velocities.

It was therefore decided that time would be saved in the long run by replacing the power law approximation in the simulation by Siacci tables.

6.9.1 Siacci Approximation

It must be remembered that the object is to generate ballistic data in the simulation which will be adequate for probability of hit and kill computations. This does *not* require ballistic data of comparable accuracy to that required in the fire control system being simulated. A brief review of the simulation volume will make it clear why this is the case.

Siacci functions are out of fashion in computing firing tables since more accurate methods can be employed with modern computers. However they are entirely adequate for present purposes, and provide a satisfactory approximation to specific firing tables for the simulation.

The simplest form of Siacci methodology is used. For computing projectile velocity and time of flight the trajectory is assumed to be a straight line.

Then time of flight t_p and slant range D_p are obtained as

$$t_p = C[T(V) - T(V_o)] \qquad (6.54)$$

$$D_p = C[S(V) - S(V_o)] \qquad (6.55)$$

where:

C = projectile ballistic coefficient

C ≈ w_p/iD^2

w_p = projectile weight in pounds

D = projectile diameter in inches

i = a form factor, and is close to unity

V = projectile remaining velocity at D_p

V_o = projectile initial velocity

T(V), S(V) are tabulated functions. There are a number of Siacci functions for various projectile types, and although one avoids argument by loading the computer with Siacci functions most closely describing the projectile being simulated, (a simple process), for almost all cases any available Siacci table can be used. The simulation has been programmed to accept several values of (t_p, D_p) for given V_o and derive the value of C which makes a best fit to specific firing table data when that is available.

The simulation runs reported in the present effort used the old Gavre function and a few check analyses

indicated excellent fits to firing table data on several antiaircraft projectiles which were generated for the purposes of the simulation.

The curvature of the trajectory caused by gravity drop affects simulation results principally via the direction of approach to the two-ellipsoid target model, and as described in Section 7.5, gravity drop is computed for that purpose simply as $1/2 \ g \ t_p^2$.

6.9.2 Computing Power Law Approximations

Although the power law method has been replaced by the Siacci method in the current simulation, so much difficulty was experienced in obtaining suitable constants to approximate firing table data that we record here first order solutions which can be iterated and converge rapidly to the desired values.

The assumed deceleration law is

$$dV/dt = -KV^a \qquad (6.56)$$

It is desired to determine K and a to fit three points along the trajectory, which is assumed to be a straight line. Let (V_1, D_1), (V_2, D_2) be the remaining velocity and slant range pairs at these points.

Define $x_1 = V_1/V_o$; $x_2 = V_2/V_o$; $R = D_2/D_1$

From Equation (6.56)

$$V_o^{2-a} - V^{2-a} = (2-a) \ K \ D \qquad (6.57)$$

Expanding the solution about a = 2.0

$$a = 2[1.0 + \frac{R \ Log_e x_1 - Log_e x_2}{R \ log_e^2 x_1 - Log_e^2 x_2}] \qquad (6.58)$$

Expanding the solution about a = 1.0

$$a = 1.0 + \frac{R(1 - x_1) - (1 - x_2)}{x_2 Log_e x_2 - R \ x \ Log_e x_1} \qquad (6.59)$$

In most cases $1.0 < a < 2.0$ and the two values obtained above will bracket the correct value. The above method can be used to develop an iterative program for computer solution. Once 'a' is obtained, 'K' is easily computed. As an example consider a

trajectory with the following three points for (V,D), including the initial point (3400,0),(2000,2000),(1000, 4000); the two initial values of 'a' obtained are 1.44 and 1.66.

THREAT CHARACTERISTICS

7.1 GENERAL CHARACTERISTICS OF THREAT

This section supplements and up-dates the discussion of the threat contained in the AFAADS-I report.

7.1.1 Numbers of Types of Aircraft

One of the best open source assessments of tactical air capability of all of the nations of the world will be found in the annual publications of the Institute for Strategic Studies, 'The Military Balance', and 'Strategic Survey'.[1,2] Aircraft and tactical air to surface missile characteristics are found in Jane's annual Weapon Systems[3] and Aircraft volumes, and in the monthly International Defense Review.

Tactical air force levels in Europe are compared in Table VII-1 from 'The Military Balance, 1971-1972'. Numbers and types of aircraft from the same source are listed in Table VII-2 and specific aircraft characteristics are shown in Table VII-3.

Emphasis in the source material was on nuclear delivery capability, but the identification and numbers on strike aircraft are applicable to both nuclear and non-nuclear situations.

The report 'The Military Balance' provides detailed force structure for all of the nations of the world from which force levels which may be involved in local conflicts may be estimated.[1]

A principal observation from Tables VII-1, VII-2, and VII-3 is that in Europe, the NATO forces are confronted by a tactical air force numerically exceeding the NATO aircraft in each of the four listed categories of Table VII-1.

Under these circumstances, air defense acquires an importance far greater than it had for the United States and allies in Korea and Vietnam. In Europe, NATO ground forces would be under heavy air attack while the air superiority battle was being waged, and antiaircraft ground defenses would be heavily stressed.

7.1.2 Air to Surface Missile Characteristics: The New Ball Game

If the defense inflicts unacceptable loss rates on aircraft using simple fire control and unguided munitions, the attacker may utilize various options employing guided weapons. These are summarized as follows:[3,4]

a. Line of sight established and held by attack aircraft, missile slaved to line of sight, or steered all the way. Short range missiles with wire command link include TOW, AS-11, AS-12. Longer range missiles with radio command link include AS-20, AS-30, Bullpup A and B and Hellcat.

b. Target viewed by TV-head on missile. Control modes include:

(1) Operator control all the way via TV view repeated back to launch aircraft. Free aircraft maneuver as long as data transmission path is maintained. Systems include Martel (UK) and Condor.

(2) TV head locks on target and missile homes. Once lock-on is achieved, launch aircraft is free to leave. Systems include Maverick and Walleye bomb.

c. Missile homes on target radiations. Radiation sources include:

(1) *Radar.* Missiles for anti-radar homing include Shrike, Standard ARM, Martel (France), Kormoran.

(2) *Infrared.* Kormoran is reported to have this capability.

d. Active radar homing head in missile. The princi-

Table VII-1. Numerical Strength of Tactical Air Forces in Europe

Categories	Northern and Central Europe			Southern Europe		
	NATO	Warsaw Pact	(of which USSR)	NATO	Warsaw Pact	(of which USSR)
Tactical aircraft in operational service						
– light bombers ..	150	280	200	–	30	30
– fighter/ground attack	1,150	1,400	1,100	450	150	50
– interceptors ..	300	2,100	1,100	275	900	450
– reconnaissance ..	400	400	300	125	100	40

20871-513A

Table VII-2. Comparative Numbers and Types of Bomber and Strike Aircraft

Category	United States		Soviet Union	
	Type	Number	Type	Number
Aircraft Long-range bombers	B-52 C-F B-52 G/H	150 210	Mya-4 Bison Tu-20 Bear	40 100
Medium-range bombers	FB-111	70	Tu-16 Badger	500
Strike aircraft (land-based)	F-105D F-4 F-111 A/E A-7D	(1,200)	TU-22 Blinder Yak-28 Brewer Su-7 Fitter MiG-21 Fishbed Il-28 Beagle	(1,500)
Strike aircraft (carrier-based)	A-4 A-6A A-7A RA-5C	(900)		

OTHER NATO AND WARSAW PACT COUNTRIES

Category	NATO Countries		Warsaw Pact Countries	
	Type	Number	Type	Number
Medium-range bombers	Vulcan (Britain) Canberra B(1)8 (Britain)	56 24		
Strike aircraft (incl. short-range bombers)	Mirage IVA (France) Buccaneer S2 (Britain) F-4 F-104	36 80 (60) (400)	Il-28 Beagle Su-7 Fitter	(150) (200)

20871-514A

pal target would probably be ships. Missiles include Kormoran and Otomat.

e. Missiles homing on laser designated target. The laser may be laid on target by a ground operator, by an operator in another aircraft (for example a light artillery spotting aircraft), or by the launch aircraft. Whatever the laser location, the target must remain illuminated during the missile flight. Systems include the Hellfire missile, and laser homing heads for iron bombs.

The cost of the more sophisticated options is considerable, although the added equipment apparently, still costs less than the flyaway cost of the delivery aircraft

with simpler fire control. Aviation Week states with regard to 'Pave Knife' AVQ-10.

'Pave Knife' AVQ-10. This is a 'completely self-contained pod-mounted weapon delivery system for the F-4D'. It combines LLLTV with a laser tracker and designator for a laser guided bomb, and according to the reference the cost is $550,000 per system.[5]

Recent reports indicate high effectiveness of the laser guided bombs. The following costs are given in Aviation Week for TV and laser heads for installation on iron bombs (see Table VII-4).[11]

Table VII-3. Characteristics of Bomber and Strike Aircraft

AIRCRAFT (USA)						
Category	Type	Max. range (Statute miles)	Max. speed (Mach. no.)	Max. weapons load (lb.)	ASM carried	In service
Long-range bomber	B-52 C-F	11,500	0.95	60,000	Hound Dog	1955
	B-52 G/H	12,500	0.95	75,000	2 x Hound Dog	
Medium-range bomber	FB-111	3,800	2.2	37,500	—	1970
Strike aircraft	A-4	2,300	0.9	10,000	2 x Bullpup	1956
	A-6A	3,200	0.9	18,000	2 x Bullpup	1963
	A-7A/D	3,400	0.9	15,000	4 x Bullpup	1966
	RA-5C	3,000	2.0	13,500	2 x Bullpup	1964
	F-104C/G	1,300	2.2	4,000	2 x Bullpup	1958
	F-105D	2,100	2.25	16,500	4 x Bullpup	1960
	F-111A/E	3,800	2.7/2.5	25,000	4 x Bullpup	1967
	F-4	1,600	2.4	16,000	4 x Bullpup	1962

AIRCRAFT (USSR)						
Category	Type	Max. range (Statute miles)	Max. speed (Mach. no.)	Max. weapons load (lb.)	ASM carried	In service
Long-range bomber	Tu-20 Bear	7,800	0.78	40,000	1 x Kangaroo	1956
	Mya-4 Bison	6,050	0.87	20,000	—	1956
Medium-range bomber	Tu-16 Badger	4,000	0.8	20,000	2 x Kelt	1955
Strike aircraft (incl short-range bomber)	Tu-22 Blinder	3,000	1.5	12,000	1 x Kitchen	1962
	Il-28 Beagle	2,500	0.81	6,000	—	1950
	Yak-28 Brewer	1,750	1.1	4,400	—	1962
	Su-7 Fitter	1,250	1.7	4,500	—	1959
	MiG-21 Fishbed	900	2.2	2,000	—	1970

AIRCRAFT (OTHER COUNTRIES)						
Country	Type	Max. range (Statute miles)	Max. speed (Mach. no.)	Max. weapons load (lb.)	ASM carried	In service
BRITAIN	Vulcan B2	4,000	0.95	21,000	1 x Blue Steel	1960
	Canberra B(I)8	3,800	0.83	8,000	—	1955
	Buccaneer S2	2,000	0.95	8,000		1965
FRANCE	Mirage IVA	2,000	2.2	8,000	—	1964

20871-515A

Table VII-4. Smart Munition Costs

Component	Cost
Basic 3000 lb GP bomb	$1,800
TV Guidance Package	$15,000
Laser Guidance	$3,100

20871-516

The road to improved systems is Paved with at least seven variations on the Pave system, and some 15 system development programs are outlined in Aviation Week.[5]

7.1.3 Implications for Local Air Defense

The simplest 'smart' munition, and probably the option of lowest cost is the guided bomb. If the laser designator is airborne, however, it must be at sufficient altitude to have a line of sight to the target, and the designator standoff range is limited by accuracy of holding the laser aim. This may expose the designating vehicle to surface to air missile fire.

In the case of stand-off missiles with enough range to remain outside the missile defense zone, the air to surface missiles themselves become quite large, and it may be possible to engage them with the local defense.

The reported effectiveness of laser target designations suggests a need to provide the defense with a detector which can sense laser illumination and determine the line of sight to the illuminator. If it is on the ground at short range it may be engaged directly by the air defense weapon; at longer range it can be attacked by artillery if response time of artillery can be made acceptable.

These counteractions are not necessarily feasible. However the problem for the defense is now sufficiently well defined so that analyses of air defense effectiveness should include the concept and analysis of defensive systems and operational modes against air to surface munitions as well as against their delivery aircraft.

7.2 ATTACK AIRCRAFT TACTICS

A detailed discussion of attack modes and weapons was given in AFAADS-I. This section supplements the former discussion with extracts from U.S. Marine doctrine, which provides additional descriptive material of use in generating tactical situations for evaluation of defense systems.[6]

Effective execution of close air support missions requires the following:

a. *Air Superiority.* Air superiority is an essential prerequisite for effective close air support operations. Close air support flights must be provided warning and security against enemy fighter attacks to a degree commensurate with the local situation.

b. *Suppression of Hostile Air Defense.* The vulnerability of close support aircraft to ground fire makes enemy capabilities in this field a major consideration. When possible, known antiaircraft weapons should be rendered ineffective before close air support is attempted.

c. *Favorable Weather.* Favorable weather and observation at the target is necessary for effective visual close air support. The type of attack employed is influenced by the ceiling and the visibility. Close air support in marginal or unfavorable weather conditions may be conducted by visual attack aircraft utilizing a ground radar control system found in the air support radar team of the Marine air support squadron. All weather attack aircraft may conduct close air support during unfavorable conditions independently or in conjunction with the air support radar team. Unfavorable weather conditions at the carrier or land base from which the aircraft operate will decrease the on-station time of the close air support aircraft.

7.2.1 Delivery Maneuvers

A variety of delivery maneuvers have been developed for the various types of air-to-surface weapons. The maneuvers were developed after careful consideration of such factors as weapon ballistic and fragmentation characteristics, various types of terrain, weather, enemy defenses, and accuracy requirements. Each delivery maneuver is designed for a particular set of circumstances. Generally speaking, the delivery maneuvers are divided into four categories -- level, glide, dive, and loft. Weapon release angles up to and including 45 degrees are referred to as glide deliveries. Dive deliveries are weapon release angles which are in excess of 45 degrees. Loft deliveries consist of a level run-in followed by a programmed pullup with the weapon release occurring at some predetermined angle during the pullup. The delivery maneuvers discussed in this section pertain only to the maneuvers used for the delivery of weapons which are most frequently used for close air support; guns, fire bombs, retarded and unretarded bombs, and rockets.

a. *Level Delivery.* The level delivery was designed for situations where low cloud ceilings prevent the use of glide deliveries. For close air support, the weapons most frequently used would be the

7-4

fire bomb and the retarded snakeye general purpose bombs. The release height would range from 75 feet for the fire bombs to 200 feet for the 500-pound snakeye while the release airspeed may range from 150 to 500 knots depending on the type aircraft and ordnance limitations. The level deliveries are generally less accurate in range than glide deliveries. Also the target must be well marked or have a vertical profile and the terrain must be relatively flat. The level delivery may also be used for smoke laying operations and for battlefield illumination.

b. *Glide delivery.* The standard glide delivery maneuvers include 10, 20, 30, and 45 degree release angle. However, the 10, 20, and 30 degree release maneuvers are most frequently used for close air support as they generally provide the best expected accuracy. Since each of these four release maneuvers has slightly different purposes and offer different capabilities, they will be discussed separately.

(1) *Ten-Degree Delivery.* This is optimum delivery for fire bombs for accuracy and is frequently used for the delivery of the retarded snakeye bombs and strafing. The release/firing height is approximately 350 to 400 feet for all the above weapons.

(2) *Twenty-Degree Delivery.* This maneuver is used for strafing, delivery of retarded bombs, retarded snakeye bombs, and rockets. The release/firing heights vary from 800/900 feet for strafing and the retarded snakeye bombs to 1,500/2,000 feet for rockets and unretarded bombs. The 20-degree maneuver is a very accurate and effective maneuver for strafing and retarded bombs because of the low release heights. Unretarded bombs and rockets are released/fired from this maneuver when weather conditions will not permit use of the 30-degree delivery maneuver.

(3) *Thirty-Degree Delivery.* This maneuver is considered the most accurate and effective delivery for rockets and free-fall bombs, particularly from high speed jet aircraft. The release/firing heights vary from 2,500 to 3,000 feet depending on the type rocket or bomb being released. The release airspeeds may be as high as 500 knots. Accuracy results from the lower release point (lower pullout) not available in the 45-degree delivery.

(4) *Forty-five Degree Delivery.* The 45-degree delivery may be used for the delivery of rockets and unretarded bombs. However, except for situations where maximum bomb penetration is required, this maneuver is seldom used on close air support missions as it is generally less accurate than the 30-degree delivery.

7.2.2 Ordnance Selection

The type, size, and delivery method of the ordnance is selected based upon the nature of the target and the desired degree of damage. The total number of aircraft sorties required is determined by dividing the total amount of ordnance required by the total each aircraft can carry. In selecting aircraft ordnance for the attack of specific targets, the following steps are utilized:

a. The vulnerability of a target to attack is considered based upon target intelligence.

b. The method of delivery will usually be a compromise between the optimum delivery technique which could be used if no active enemy defense were to be encountered and the requirement for survival of delivery pilots and equipment. Factors that are considered in determining the delivery method are as follows:

(1) *Standoff Capability.* Enemy weapons in the area that could affect the success of the mission; e.g., antiaircraft guns and missiles, enemy interceptors, etc.

(2) *Weather in the Target Area.* The weather in the target area affects the ability to hit the target. The weather also affects the control and number of aircraft that can be effectively utilized against a target because of cloud coverage and restricted visibility.

(3) *Ordnance Available.* The selection of ordnance that can achieve the desired results of damage to the target.

(4) *Aircraft Available.* The type, numbers, and carrying capacity of each craft to accomplish the mission.

c. The type of aviation ordnance is compared with the accuracy and CEP of the delivery squadron in order to determine the degree of damage that can be expected against a target. The Joint Munitions Effectiveness Manuals list all conventional weapons and the damage effect that can be expected against a variety of targets.

7.2.3 Relative Delivery Accuracy

The expected accuracy of air to surface weapons is dependent on several factors, such as the degree of individual pilot proficiency and level of training, the visibility, and the pilot's ability to see the target or aim point. The expected accuracy is also affected by the type of delivery maneuver and the release height of the particular weapon. Normally, the delivery maneuvers used in a close air support situation would range from a level delivery to glide angles up to 30 degrees. The release heights will vary approximately 75 feet to

7-5

3,000 feet above the surface. Specific expected accuracies for the various weapons and delivery combinations can be found in the Joint Munitions Effectiveness Manuals (FMFM 5-2 series -- to be issued). Generally speaking, the normal order of expected accuracy for air delivered weapons is as follows:

a. Strafing.

b. Retarded snakeye bombs and fire bombs.

c. Rockets.

d. Free fall (unretarded) bombs.

7.2.4 Nuclear Weapons Delivery Modes

Nuclear weapons delivery can be accomplished by heavy attack/bombers or fighter/attack jet aircraft. The various tactics are high altitude level release, laydown, loft (low, medium, and high), and high altitude dive bombing.

a. *High Altitude Level Release Systems.* These releases normally are radar controlled from heavy attack/bomber aircraft but utilize visual release as a backup tactic. Both systems are relatively inaccurate.

b. *Ground-Controlled Radar Systems.* These systems can be utilized to direct aircraft to the target and can automatically release the weapon. Ground-controlled radar systems provide some independence from weather limitations but are short-range systems. Delivery errors vary with range but are generally less than those of high altitude systems.

c. *Laydown Tactic.* This tactic is a minimum altitude, horizontal bombing maneuver. The target is approached at low altitude. The weapon is released, retarded by parachute to provide greater accuracy and increased distance between the aircraft and target. This tactic provides a high degree of accuracy.

d. *Loft Tactic.* The loft tactic of delivery is accomplished by the delivery plane approaching the target at a very low altitude, making a definite pullup at a given point, releasing the weapon at a predetermined point during the pullup and tossing the weapon onto the target.

e. *High Altitude Dive Bombing Tactic.* High altitude dive bombing tactic is accomplished by rolling into a steep dive angle at a high altitude with a recovery from the dive at altitudes commensurate with the size and burst altitude of the weapon. This delivery is the least accurate of the methods of aerial nuclear weapon delivery.

7.2.5 Flak-Suppression Techniques

Flak-suppression techniques are closely related to counterbattery fires and are employed in support of close air support aircraft. Flak-suppression fires are directed against hostile antiaircraft weapons that can bear on close air support aircraft during the execution of their missions. Flak-suppression fires are primarily delivered by artillery units; however, naval gunfire and other support aircraft have the capability and also are employed to deliver these fires. Because of the detailed and close coordination required, flak-suppression fires are planned, coordinated, and controlled by the appropriate fire support coordination center (FSCC). The aviation representative in the FSCC plays a most important part in the planning of these missions. He is responsible for the preparation and use of flak-suppression templates that represent the area and time each type of aircraft will be vulnerable to antiaircraft fires during certain types of attacks. Approach and recovery distances vary somewhat with the type of attack -- bombing, strafing, napalm, etc., as well as with the type aircraft, speed, and special flight characteristics. A flak-suppression template and overlay is illustrated in Figure 7-1. This illustration shows a typical broad arrow template representing the area required by a particular type of aircraft for approach and recovery while executing a close air support mission. Hostile antiaircraft positions and other pertinent information required for flak-suppression missions are usually plotted on the overlay. The techniques employed in the execution of flak-suppression missions in support of close air support aircraft are illustrated in Figure 7-1. The key to a successful flak-suppression mission lies in thorough planning and positive control of its execution. The flak-suppression mission is controlled directly by the forward air controller (FAC), forward observer (FO), and/or when naval gunfire is utilized, by the shore fire control party (SFCP). These controlling agencies can be located side by side in an observation post or tied in with 'hot lines' to ensure instant reaction.

7.2.6 General Discussion of Air to Surface Delivery Tactics

Marriot in a survey paper observes[6] that stand-off missiles can cost $150,000 to $300,000 per round which, compared with the $85 per round cost of 68 mm rockets is a consideration in the use of stand-off missiles. On the other hand against a good defense not using the missiles is more likely to cost the $3.5 million (and up) aircraft.

With regard to attack modes it is stated 'the time taken by an aircraft, such as the F105, from the moment the dive is started until bomb release is 6 to 9 seconds and in poor visibility may be even less. During this time the pilot has not only to fly to aircraft so as to place his optical aiming mark in the right position

BD 081630
ADA POW

BG 110820
ADA API

RECOVERY AREA VARIES WITH TYPE AIRCRAFT, TYPE ATTACK AND RECOVERY TECHNIQUES EMPLOYED

APPROACH AREA VARIES WITH TYPE AIRCRAFT AND TYPE OF ATTACK

BL 060735
ADA API

TARGET

BBC 101300
ADA AD

BA 081100
ADA API

FEBA   FEBA

FO

THE FAC, FO, AND SFCP IN DIRECT COMMUNICATION WITH STRIKE AIRCRAFT AND AGENCIES PROVIDING FLAK-SUPPRESSION FIRES AT ALL TIMES.

SFCP

FAC

NOTE. ILLUSTRATES USE OF FLAK-SUPPRESSION TEMPLATE AND OVERLAY.

FLIGHT LEADER NOTIFIES FAC WHEN ORIENTED AND READY TO STRIKE TARGET

FLIGHT PATH OF STRIKE AIRCRAFT

BF 081630
ADA POW

BKC 060735
ADA API

BJ 121045
AO

BHC 140850
ADA AO
ADA

BMC 101345
ADA API

EXECUTION OF FLAK-SUPPRESSION MISSION.

EFFECTIVE RANGE OF HOSTILE AA THAT CAN BEAR ON CLOSE SUPPORT AIRCRAFT

FEBA   FEBA

FAC, FO, AND SFCP BY CLOSE COORDINATION AND VISUAL MEANS CONTROL FLAK-SUPPRESSION FIRES TO ENSURE MAXIMUM EFFECT AND AIRCRAFT SAFETY.

FSCC   FDC

FLAK-SUPPRESSION FIRES CEASE WHEN THEY ENDANGER STRIKE AIRCRAFT AT ANY TIME DURING APPROACH OR RECOVERY

AS AIRCRAFT BEGIN RUN ON TARGET FLAK-SUPPRESSION FIRES HIT HOSTILE AA WEAPONS

NOTE ILLUSTRATES THE TECHNIQUE OF FIRING FLAK-SUPPRESSION PROGRAMS.   20871-169

Figure 7-1. Flak-Suppression Techniques

relative to the target, but has to estimate and allow for the wind, adjust his speed, and watch out for attacking aircraft.[4]

Low level bombing is cited as having been dangerous to the bomber in Vietnam, and the British view on dive and toss bombing is given as that 'both methods are too dangerous for use in Europe as any aircraft that gains any height at all will almost certainly be shot down. Their policy for a Eurpoean war is therefore to use the lay down method wherever possible.'[4]

Rockets are reported to be released at 3000 ft. slant range from a steady dive from a height of 4000 ft. The Israeli's are quoted as saying that the 68mm rocket immobilizes a tank (salvos of 6-7 were enough at Israeli versus Arab release ranges), but the tank can be repaired.

U.S. pilots in Vietnam are said to prefer guns to rockets for air to ground attack because the rockets are mounted in external pods that reduce aircraft speed. Also they report that they obtained more effectiveness with bombs than rockets against fixed targets.

Some idea of the load factors which can be sustained by strike aircraft can be gained from the following brief summary of characteristics of the F-105 aircraft.[7] The F-105 has a safe load factor of 8.67 g and a break load factor of 13.1 g. Max sea level Mach is 1.25, Max Mach at 36,000 ft. is 2.15. Weight empty is 27,500 lbs. and the aircraft can be loaded to 35,200-48,400 lbs. Max thrust with afterburner is 26,500 lbs.

11,000 lbs. of ordnance can be hung on wing pylons. A possible configuration carries four 1000 lb. bombs, plus a 450 gallon belly tank.

The 1960 bomb sight had a radar mode in which the pilot kept the target image on a vertical cross hair until it crossed a pre-set range cursor. At that point he activated the automatic bomb system which included a doppler radar correction for wind (range and cross). The system automatically delivered via the half-loop mode.

F-105 unit production costs were given as down to $1.4 million.

7.2.7 Set Up Table for a Bombing Run

In view of the 6 to 9 second set up time for dive bombing (for the F105), we can make some conjectures on how this might relate to CEP.

Assuming a simple computing bomb sight we can estimate the following times during which the attacking aircraft flies a fairly predictable course.

	Time (sec)	Elapsed Time
Roll in to dive	0	0
Obtain range to target to target or equivalent measure	1-5	1-5
Computer obtains solution	1+	2-6
Settle tracking	2-10	4-16
Start pullup + release	1-2	5-18

The total time on a fairly straight path is from 5 to 20 seconds, in round numbers. One may guess that the longer the path the greater the accuracy. The gain is unlikely to be a factor of 4 but is guessed to vary as indicated in Figure 7-2.

7.3 BOMBING ACCURACY AND MUNITIONS EFFECTIVENESS IN THE OLD BALL GAME

7.3.1 Performance Summaries

The accuracy with which iron bombs can be delivered depends on release range, among other parameters. An effective defense forces the attacker either to release his munitions at a greater range or to use some other, and possibly more costly air to surface weapon such as a missile. In this section some information on the accuracy of bombing with iron bombs is summarized for later use in defense evaluation. All of the data is from unclassified open sources, and has *not* been compared against classified estimates.

Additional open source data will be found in AFAADS-I, Table IV-7.

With regard to release altitudes, according to Aviation Week,[10] USAF 'tactical aircraft were limited to a minimum of 3,000 ft. altitude in making weapons delivery runs in South Vietnam. The move was designed to reduce the effectiveness of the smaller caliber anti-aircraft guns being used by the North Vietnamese.' (in May 1972)

Tables VII-5 and VII-6 summarize CEP estimates from various sources, and Table VII-7 summarizes some estimates of effectiveness per pass and per bomb against vehicles and bridges.

It is clear from the tables that an air defense of only moderate effectiveness could make tactical air attack with Korean vintage aircraft munitions and fire control cost-ineffective. The 'smart bombs' now operational make it a whole new ball game.

The tabulated data on CEP and effectiveness of iron bombs and strafing should therefore be considered as obsolescing capabilities of unsophisticated, relatively low cost tactical air systems. An object of local air defense is to deny the enemy the use of these low cost solutions and force him to use more costly options.
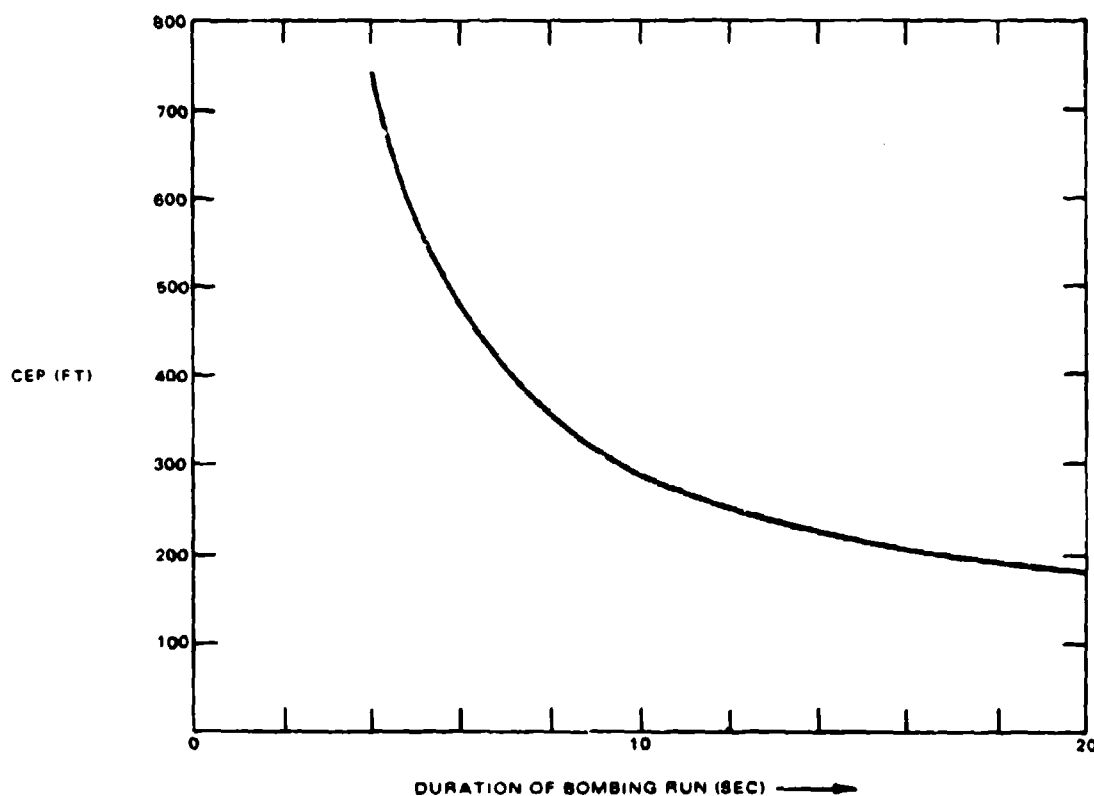
Figure 7-2. Hypothetical Variation of Glide Bombing CEP With Duration of Bombing Run

7.3.2 SAAB Bomb Sight Characteristics

To evaluate the effectiveness of a 'point defense' antiaircraft system one needs to know how the effectiveness of the attacking aircraft is degraded as a function of increased standoff range, or in the case of dive or glide bombing, as a function of the bomb release range. Performance figures for the SAAB BT9 bombsight have appeared in company advertisements and these are analyzed for possible use in evaluations of defense systems.

The BT9 is considered to represent good modern technology for the delivery of unguided bombs under visual conditions. It is unlikely to permit maneuver during the bomb run, but the next level of sophistication, allowing non-visual delivery and evasion during the attack path would also represent a substantial cost increment.

Svenska Aerplan AB (SAAB) was building a semi-automatic toss-bomb computer in 1939. A fully automatic BT9D (mechanical) was developed, followed by an electronic model (BT9E).

In 19.. advertisements of the Svenska Aeroplan Aktiebolaget [15,16] in Interavia described the SAAB BT-9 Toss Bomb Computer and indicated that it was in service with the Royal Swedish Air Force, the U.S. Air Force, and was in production for Aeronavale Fran-

20871-160

7-9

Table VII-5. Delivery Accuracy of Aircraft Munitions from Unclass ed Sources

Conditions			CEP (feet)	Reference
Combat	Initiation of bombing in Vietnam		750	Aviation Week (7.5)
	F-105 vs.	undefended targets	365	
		moderate defense	540	
		heavy defense	575	
	"Current" in Vietnam		250	
Training	F-105 at Nellis		125	
Competition	Visual, 45° dive	A7E 1st pass	150	Aviation Week (7.6)
		2nd pass	100	
		A7A, B 1st pass	300	
		2nd pass	200	
	"Blind" (radar) altitude over 1500 ft, speed over 300 knots TAS		"most of bombs within 1000 ft of target"	
Unspecified Defense				Interavia (7.7)
	F-105	Shallow Dive	500	
		Low altitude approach and release in half loop	1100	
		High altitude, horizontal, drop from 40-50,000 ft	2000	

20871-517A

Table VII-6. Delivery Accuracy of Aircraft Munitions in Korea from Unclassified Sources

Conditions		CEP (feet)	Reference
Dive bombing with recovery altitude minimum of 3000 ft			"U.S. Air Force in Korea"
	Dec 1952	340	
	Jan 1953	514	
B-26 aircraft	1951-52		
	Level bombing, 7000 ft alt	375	OAO Memo No. 66 (7.8)
	Glide, 30°, 100-1500 ft	175	

20871-518

caise. In 1962 the advertisement carried a graph of dispersion versus altitude and dive angle for a true air speed of 250 m/s, and this is reproduced as Figure 7-3.

In 1967 the BT9R version with a laser range finder was announced, but performance has not yet been published in the open literature.

According to the advertisements:

'The BT9 functions in principle as an analog computer. In a dive, it automatically registers altitude, dive angle, and other variables, from which it derives the correct release point. The pilot only has to direct his plane towards the target and press a pickle switch. Bomb release is automatic. With an auxiliary device, the BT9 is also suitable for firing air-to-ground rockets.'

From a published system schematic diagram, and associated descriptive material, the following further details are available:[12]

In operation, the pilot dives along a straight line at the target then pulls up. The computer releases the bomb when the pull-up angle is computed to be correct for a hit.

7-10

Table VII-7. Munitions Effectiveness in Korea

Conditions	Target	Measure	Effectiveness	Reference
Undesignated, 1952-53	Bridges	Hits/pass	Day 0.09 Night 0.04	USAF in Korea
B-26 1951-1952				OAO Memo.1952
Bombing	Vehicles	Claims/pass	0.22-0.76	(7.9)
Strafing	Vehicles	Claims/pass	0.12-0.43	
Fighter-bombers 1951-53				OAO Memos.1952
Glide Bombing (night)	Vehicles	Claims/bomb		(7.8, 7.9)
Per pass: 1-1000 lb GP			0.197	
1-500 lb GP			0.189	
2-1000 lb GP			0.115	
2-500 lb GP			0.110	
Glide Bombing (night)	Bridges	Hits/bomb		
500 lb GP average			0.037	
1000 lb GP average			0.038	
Glide Bomoing (day)	Bridges	Hits/bomb		
500 lb GP average			0.08	
1000 lb GP average			0.10	
B-26 Level Bombing (night)	Vehicies	Claims/bomb		
500 lb GP average				
1951-1952			0.103	
1952-			0.089	
Fighter-bomber (2 bombs)	Vehicles	Claims/sortie	0.262	OAO Memo.1953
B-26 (full load of 500 lb)			0.89	(7.9)

20871-519

The BT9E consists of a computer (36.4 lbs.), an operating box (3.1 lbs.) and a quick erecting gyro unit (10.5 lbs.). The gyro axis parallels the line of flight and allows 360° freedom in roll.

Preset factors are slope of the aircraft lift curve and angle of zero lift. Manually set factors are weapon ballistic coefficient, target pressure altitude, aircraft gross weight and wind speed (apparently in direction of flight only). Continuously measured and computed factors are gyro angles, static pressure, dynamic pressure, acceleration, time, dive angle, ideal angle of divergence (loft angle) parallax allowance, angle of attack and wind correction to angle.

The pilot settles his sight on target (fixed reticle), holds it steady, presses the pickle switch and does a straight pullup. The bomb is released at the computed 'correct' angle of loft.

Operating ranges are given as

Altitude 0-20,000 ft.

Speed Mach 0.5-1.0

Dive angle 10-50°

Acceleration in pullout 3-7g

Maximum slant range 3300-50,000 ft, depending on speed dive angle and bomb resistance.
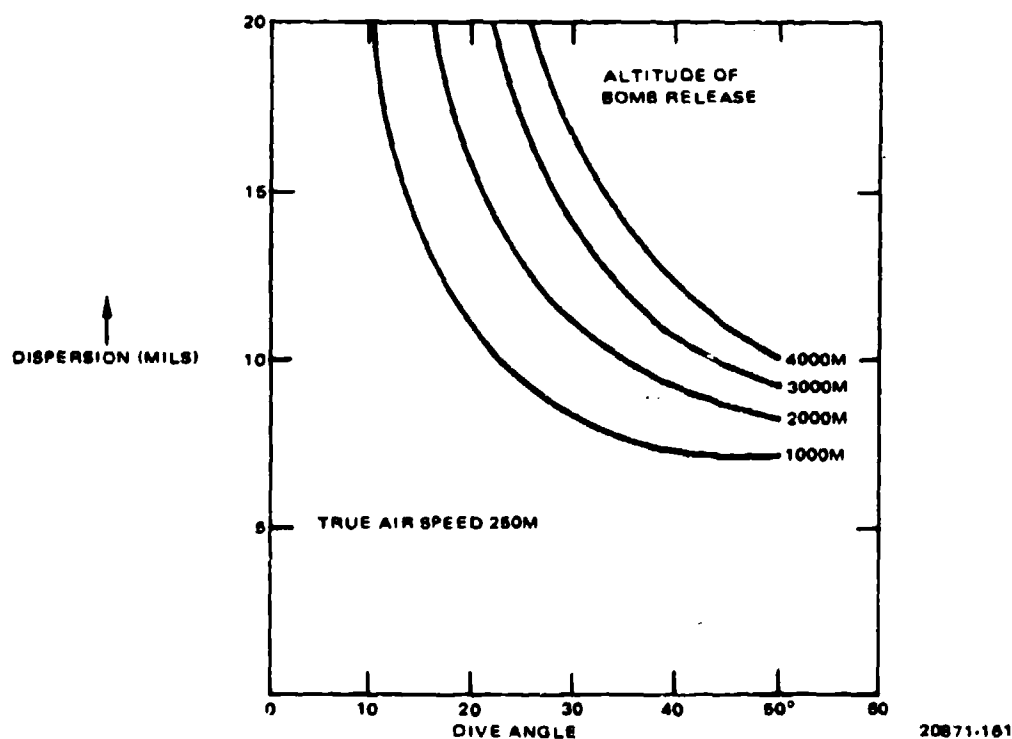
Figure 7-3. Dispersion of Bomb Delivery With SAAB BT-9 Bombsight

For this sight dive angles between 30-45° are recommended as optimum.

A replot of Figure 7-3, showing contours of constant linear CEP in the vertical plane containing the attack path is shown in Figure 7-4. For this design, CEP in meters appears to depend principally on the horizontal range from release point to target, and to be relatively insensitive to dive angle. A few trigonometric exercises on source errors and their effect on CEP indicate that the shape of the functions in Figure 7-4 may result from the fact that the sight computes range to target from pressure-altitude and angle of dive. It is conjectured that the use of a laser range finder in the latest version will tend to make the dispersion at a given range independent of the angle of dive, and the angular dispersion in mils almost independent of range as well.

These errors are probably estimated exclusive of pilot aiming errors and hence are considerably smaller than those noted in Table VII-5 and VIi-6.

7.4 AIRCRAFT VULNERABILITY

The probability that an aircraft will be lost, given a hit by a round of antiaircraft fire (or by fragments) depends so specifically on design details that it is difficult to make simple generalizations. On the other hand, one feels intuitively that it should be possible to develop relatively simple parametric expressions relat-

7-12
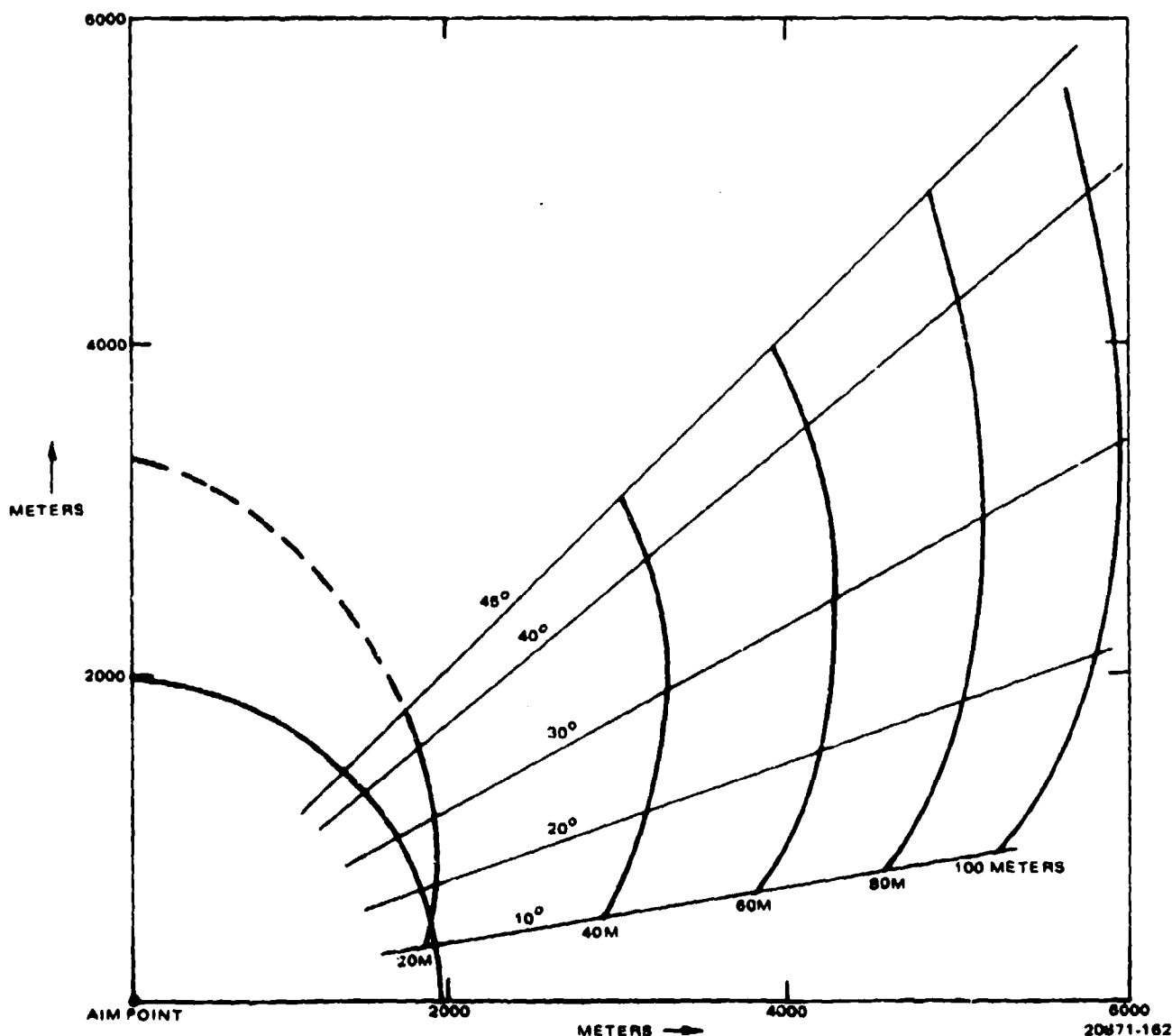
Figure 7-4. Contours of Constant Dispersion in Meters for SAAB BT9 Bombsight

ing caliber, for example, to kill probability for a generic type aircraft and homologous projectiles.

Rather than attempt to utilize the extensive classified literature on aircraft vulnerability in order to minimize the classification of the present report, the approach in the present study has been to derive vulnerability functions from unclassified combat histories and limited open source vulnerability estimates. Combat data, where available, is an inherent averaging device over all of the variations in tactical parameters.

The resulting expressions are considered to be reasonable, but have not been compared with classified estimates.

7.4.1 Interpretation of Combat Loss and Damage Statistics

One usually can find estimates of the loss rate per sortie, sometimes with estimates of cause of loss: aircraft or ground fire. This information tells one only whether the threat was important. The next most likely information to find is the number of aircraft damaged and the number of aircraft lost, preferable by cause. The ratio:

$$P_0 = L/(L + D) \qquad (7.1)$$

is more informative, and depending on the assumptions one is willing to make about correlations in hitting and vulnerability, it may be used as a rough estimate of the upper limit to single shot probability that a hit causes a kill.

If by good fortune, one also finds recorded the average number of hits on aircraft returning with hits, the single shot probability can be improved by computing:

$$p = p_o/\underline{H} \qquad (7.2)$$

where

$\underline{H}$ = the average number of hits per aircraft

Some rare reports provide information on the number of aircraft returning with 1,2,....m hits. This allows one to do a better job of including correlations in hitting and killing in the analysis.

When a mix of weapons has attacked the aircraft, the problem becomes more difficult. Some reports identify weapon type causing damage. Even better, some reports identify the components that cause aircraft vulnerability.

Note that general reports on aircraft damaged will vary as to whether the damage was repaired by a patch (likely not to be reported) or by replacement of a major component (probably reported because of the requirement for a new component).

But however variable the combat data it has the advantage that it contains all of the environmental variables, many of which are likely to be omitted in an armchair analysis.

How far one can go in developing the vulnerability model depends on the amount of detail available in the combat data. In the following paragraphs we indicate some of the considerations in inferring the single shot probability that a hit causes an aircraft kill, based on the assumptions:

a. Successive hits are independent.

b. The target is 'singly vulnerable'.

Both of these assumptions may be relaxed if one has information on the number of aircraft returning with 0,1,... hits.

Define:

p = single shot probability that a hit causes a kill

E = expected number of hits

q = 1 - p = probability that the aircraft survives a single hit

Then

Probability of loss

$$L = 1 - e^{-Ep} \qquad (7.3)$$

Probability of return with hits

$$D = e^{-Ep} \cdot e^{-E} \qquad (7.4)$$

Average number of hits on survivors

$$HS = Eq \, e^{-Ep} \qquad (7.5)$$

Average number of hits on survivors with hits

$$\underline{H} = \frac{Eq}{1 - e^{-Eq}} \qquad (7.6)$$

Probability of loss or damage

$$L + D = 1 - e^{-E} \qquad (7.7)$$

The object is to infer p from available damage and loss statistics.

Define:

$$p_o = L/(L + D) \; ; q_o = 1 - p_o \qquad (7.8)$$

p_o is the ratio of lost aircraft to the sum of lost and damaged aircraft and is the statistic most usually available.

The preceding expressions assume a fairly uniform exposure E of the sample aircraft. This assumption can be relaxed a good deal by a different derivation, as long as one does not use loss rate L. If one does not have $\underline{H}$, however, then defining f = L + D:

$$f = 1 - e^{-E} \qquad (7.9)$$

and

$$p = \frac{Ln(1 - fp_o)}{Ln(1 - f)} \cong p_o \, [1 - (1/2) \, (fq_o)] \qquad (7.10)$$

and the correction to p_o from this expression can be very sensitive to the fact that not all aircraft in the sample were equally exposed to enemy weapons.

The above expression does use the loss rate only in the correction term. If we believe that L is well known we can change the approximation form by using

$$L = 1 - e^{-pE}$$

$$(1 - L) = e^{-pE}$$

$$e^{-qE} = (1 - L)^{q/p} \cong e^{-Lq/p} \; ; L \ll 1.0$$

since

$$\underline{H} = \frac{qE}{1 - e^{-Eq}}$$

$$\underline{H} = \frac{-(q/p) Ln(1 - L)}{1 - (1 - L)^{q/p}} \tag{7.11}$$

$$[(qL)/2p] \cong Log \underline{H} \cong Log [(\underline{H} - 1) + 1]$$

$$= (\underline{H} - 1) - (1/2)(\underline{H} - 1)^2 + \dots p/q$$

$$\cong \frac{L}{2 Log \underline{H}} \tag{7.12}$$

and for L small and $\underline{H} - 1$ small

$$p/q \cong \frac{L}{2(\underline{H} - 1)} \tag{7.13}$$

which can be seen to be very sensitive to L and $\underline{H}$

Then

$$P_o = \frac{1 - e^{-Ep}}{1 - e^{-E}} \tag{7.14}$$

Hence,

$$e^{-Ep} [1 - P_o e^{-qE}] = q_o \tag{7.15}$$

$$e^{-qE} = 1 - (Eq)/\underline{H} \tag{7.16}$$

Then

$$\left[e^{pE} - 1 \right] / (pE) = (p_o/q_o)(q/p)(1/\underline{H}) \tag{7.17}$$

Expanding the left side, for small pE

$$1 + (1/2)pE \cong (p_o/q_o)(q/p)(1/\underline{H}) \tag{7.18}$$

The loss rate will usually be very small

$$L \sim pE \tag{7.19}$$

and so

$$p/q = \frac{p_o}{q_o \underline{H}} \left(\frac{1}{1 + L/2} \right) \tag{7.20}$$

Since L/2 is usually $\ll 1.0$

$$p \cong \frac{p_o}{\underline{H} \cdot p_o (\underline{H} - 1)} \tag{7.21}$$

If the average number of hits on hit aircraft surviving is very close to 1.0 then $p \sim p_o$. However, if the airplane is relatively invulnerable to hits, $p \sim p_o/\underline{H}$ and the loss/damage ratio gives a poor estimate of the single shot vulnerability.

When the number of aircraft returning with j hits, j = 0,1,... is available, one can make more sophisticated inferences. For an example based on a large sample of B-17 and B-24 data on hits by antiaircraft shell fragments, reference is made to a paper by Weiss.[40]

7.4.2 Inferences from Aircraft Damage and Loss Reports

A declassified report on U.S. aircraft damage and losses to ground fire in Korea allows some inferences regarding the variation of vulnerability with caliber of the defense weapon.[18]

For Navy and USMC aircraft (two piston engined types and one jet), the number of aircraft hit and the number of aircraft lost are given with estimates of the type of defense weapon. These were categorized as fragments (including own bomb fragments), 7.62 mm, 12.7 mm and 20-mm weapons.

The result of a hit on the aircraft was categorized as 1) aircraft lost, 2) replacement of major component required, 3) replacement of minor component required, 4) patch only required. There was an average of 1.25 hits per aircraft hit, so in accordance with the analysis of the previous section, the ratio of aircraft lost/(aircraft lost + aircraft damaged) is expected to be a fair estimate of the probability that a kill, would result from a hit.

For details of the data, including a great deal of information on component vulnerability, the referenced report should be obtained.

The aircraft were in about the 20,000 lb class, and there was a 3/1 variation in loss/hit ratio across the three types.

For the aggregated data on the three types, it was found that the single shot probability of each category

of damage (except patches) given a hit could be approximated by a function of the form

$$p = 1 - e^{-kC^a} \qquad (7.22)$$

where C = caliber in mm, and k and a are constants for each damage type.

The same form of function fits the probabilities derived on the assumption that each damage class is independent of the others, i.e., the probability of an aircraft returning with damage requiring major component replacement is the probability that it receives major component damage, times the probability that it does not receive a lethal hit.

Figure 7-5 shows the damage functions plotted against caliber and compares them with loss probabilities to air-to-air fire in the Pacific theater in World War-II (Navy and Marine aircraft).[19]

The resulting inferred variation of damage probability given a hit then varies with caliber as follows

Loss of Aircraft	C^3
Replace Major Component	$C^{6/2}$
Replace Minor Component	$C^{3/2}$

For the three aircraft types, the average ratio of aircraft lost to aircraft hit and lost over all weapons was 0.09.

Futtrell gives some damage and loss rates for Air Force Thuderjets in Korea in 1951.[17] Over a four month interval during which 115 aircraft were lost, the ratio of aircraft lost to aircraft lost plus aircraft hit was 0.11 which is consistent with the Navy data.

World War II

Looking back to World War II, we find the following estimates derived principally from German proving ground data and camera records of combat with regard to B-17 vulnerability, and summarized by Weyl in 1950.[28] The estimates are shown in Table VII-8.

The second column in the table was based on experiments by Burgsmueller at the Rechlin establishment on captured 4-engined bombers. It was estimated that from 15-18 oz (420-500grammes) of Hexogen-Aluminum filler was required to assure a kill with one hit.[28]

The experiments led to the development of very high capacity HE projectiles known as 'Mine' rounds. The one hit/one kill objective was pursued both by 55-mm gun developments and by development of the R4M air to air rocket.

Weyl also gives the following estimates for large caliber fragmenting projectiles intended to destroy the aircraft by near bursts.

Projectile	Lethal Radius
German 88 mm with time fuze	15 ft.
UK 3.7" (94mm)	25 - 30 ft.

In attempting to infer single shot vulnerability from air to air kill and damage data, information on the average number of hits per aircraft hit is essential, because in air to air combat this number is usually considerably greater than unity. Gun camera data, of course, provides all the information needed to make good estimates of both aircraft and component vulnerability.

World War II data on Navy and USMC aircraft damaged and lost to both air to air and antiaircraft shows a trend with caliber similar to that obtained from the Korean data, but the loss/hit ratio is substantially higher.[16] It is believed that at least a part of the difference is accounted for by multiple hits per aircraft hit in the WW II data.

Other Vulnerability Estimates

Brandli provides a curve of kill probability, given a hit, in his book. It was reproduced in AFAADS-I. Chuyev[29] summarizes some U.S. and French aircraft vulnerability data, including a curve of probability versus HE filler weight.

7.4.3 Inferences from Antiaircraft Gun Engagement Records

Antiaircraft artillery action reports from World War II provide the number of aircraft destroyed (confirmed kills) and estimates of probable destruction and/or damage, the definition of which apparently varied with the theatre. How good the damage estimates were is difficult to estimate, but it is clear by comparison with the complementary data on returning damaged friendly aircraft that minor damage was not likely to be observable by the gun battery.

Only secondary sources were available for the present study; there may be more information in the original after action reports.

For the European theater the reporting categories were

Category I: aircraft destroyed

Category II: aircraft probably destroyed

Also available were the rounds per kill in each category (RPB). Across all aircraft types the ratio I/(I + II) was between 0.69 and 0.72. Most of the data was on the Me109, FW 190, and JU 88. An exception was the Me 262 jet for which the ratio was 0.08 suggesting that its speed was such that it did not fall close enough to the battery for a kill to be confirmed.

Table VII-9 summarizes results by weapon, over all target types.[23] The principal point of interest in this table is that fewer targets with observable hits escaped
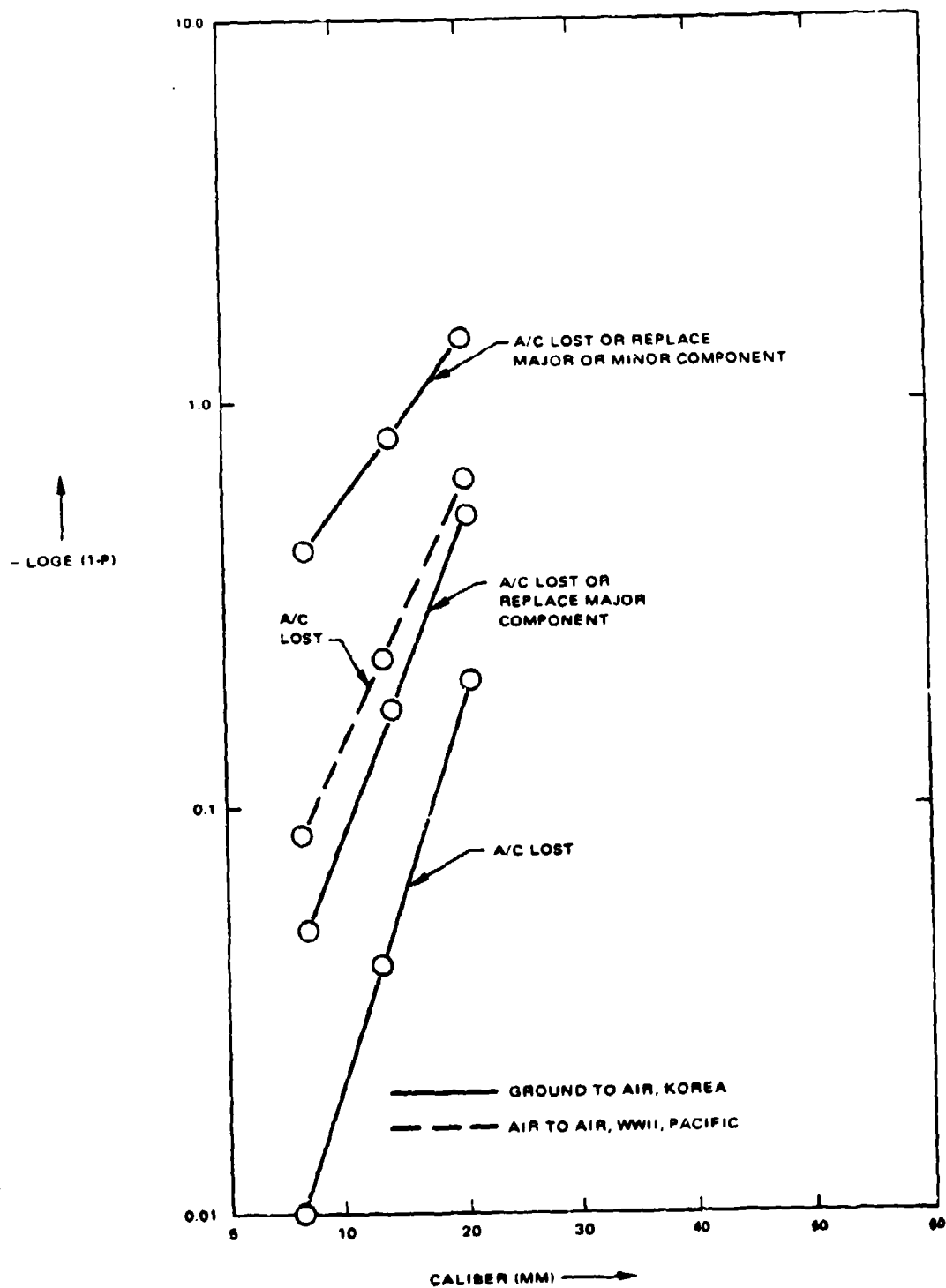
Figure 7-5. Damage Functions versus Weapon Caliber

20871-163

Table VII-8. WW II Aircraft Vulnerability Data

Caliber of Projectile	Minimum Number of Hits Required per Kill (Test Results)	Hits Actually Required vs. B-17 (Combat Statistics)
0.30" (Lewis MG)*	850	n.a.
0.50" (12.7 mm)	n.a.	50-60
20 mm	20	20
30 mm	4	7
55 mm	1	n.a.

*This was a RAF assessment of 1939, AA fire, target unspecified.

20871-520A

the 40-mm than the 37-mm. The rates of fire were not greatly different, across these weapons. The caliber 0.50 ratio is explainable if one believes that when on-target, it usually secured multiple hits.

In the Pacific Theater the kill categories were more specific and applicable to the present study. They were

Category A: Mid-air destruction

Category B: Destruction by crashing

Table VII-10 summarizes the data categorized by weapon.[23] Since the cal 0.50 never secured an in-air kill, the RPB by weapon is derived by assuming that in the joint use with the 0.50 the air kills were accomplished by the larger weapon, and 3 x this number of the crashes were assigned to the large weapon. The remainder of crashes was assigned to the 0.50. The sample size for the 37-mm is too small to be of significance, unfortunately.

Note that 31% of the aircraft observed to be hit by the 40-mm were destroyed in the air.

Of all aircraft engaged, 15.85% were category I kills, and 7.16% category II for a total of 23.01% destroyed or probably destroyed. This breaks down by weapon as shown in Table VII-11.

Since this table reflects the number of weapons present as well as individual effectiveness the principal

observation is that most of the targets were engaged in ground attack and hence came within range of the 40-mm as well as the 90-mm.

From another reference[24], over the period 6 June through 1 August, 1249 aircraft appeared over the 1st Army, 408 by day and 841 by night, and of these 170 were destroyed. The Rounds per Bird by caliber were as shown in Table VII-12.

Some additional data on antiaircraft gun effectiveness in specific actions in the Pacific Theater is summarized in Table VII-13.[25] In the defense of Corregidor ammunition was severely limited. The troops trained in peacetime were highly skilled. Fire control employed the Sperry mechanical M-4 director and the stereoscopic height finder. The attacking aircraft bombed from 15,000 ft. Initially the rounds per aircraft destroyed was about 500 and by April it had been reduced to slightly below 100 rounds per kill.

At Morotai the 90-mm guns were directed by the SCR-584 radar and the M-9 electrical director.

For purposes of the present report we are interested principally in the 37-mm and 40-mm lethality. Observing the European and Pacific data it appears reasonable to infer that for the targets of that vintage, 30% of aircraft hit by the 40-mm were destroyed in the air, and 72% fell within sight of the battery. For the 37-

Table VII-9. Antiaircraft Effectiveness in European Theater

Gun	Number of Aircraft Destroyed by Category			Rounds per Kill	
	I	I+II	Ratio I/(I+II)	RPB I	RPB I+II
90 mm	89.5	119.5	0.75	235	176
90 mm with VT	20	25	0.80	178	142
40 mm	244	340	0.72	333	239
37 mm	60	105	0.57	590	337
0.50	73	117	0.62	32,360	20,190

20871-521A

Table VII-10. Antiaircraft Effectiveness in Pacific Theater

Gun	Number of Aircraft Destroyed by Category		Ratio	Total Number of Rounds Expended	RPB
	A	A+B	A/(A+B)		
90 mm	11	35½	0.31	4,610	118
90 mm + 0.50	1	6	0.17		
40 mm	2	6½	0.31	12,580	325
40 mm + 0.50	10	32	0.31		
37 mm	0	1	0.00	20	
0.50	0	8	0.00	165,260	12,700

20871-522

Table VII-11. Allocation of Kills to Weapon Type

Weapon	% in Category	
	I	I+II
90 mm	2.91	3.89
90 mm + VT	0.65	0.81
40 mm	7.95	11.07
37 mm	1.96	3.42
0.50	2.38	3.81
Total	15.85	23.01

20871-523

Table VII-12. Rounds per Bird by Weapon Type

	Dest	Damaged
90 mm	546	288
40 mm	409	260
37 mm	400	223
0.50	46,544	23,272

20871-524

mm a more tenuous inference suggests that 57% fell within sight of the battery.

A 40-mm round weighed about 5 pounds (complete round) and probably cost about $5.00. Hence the cost in 40-mm ammunition per aircraft destroyed (confirmed kill) was about $1500. This seems to be an excellent cost exchange.

Naval Defense Against Kamikaze Attacks

Table VII-14 summarizes antiaircraft effectiveness in defending ships against Kamikaze attacks.[22] For details the original report should be consulted. In defending against a kamikaze attack it is probable that all guns fired for the maximum time possible, so that an in-crease in rounds expended per kill, as compared with the Army situation, is not unreasonable. Since the data does not include damage to Kamikaze aircraft not destroyed before impact it is not possible to estimate comparative weapon lethality per hit.

7.4.4 Development of Approximate Vulnerability Functions

The object of this section is to develop some simple functional relations describing the probability that a hit on an aircraft causes a kill. These will, of course, fall far short of the authoritative vulnerability data generated by BRL and AMSAA and similar agencies. However, they will contain a sufficient number of

Table VII-13. Antiaircraft Effectiveness in Specific Actions Pacific Theater

				Results as Fraction of Number Hit			
Action	Weapon	Number of Aircraft Engaged	Number of Aircraft Destroyed	Destroyed	Probably Destroyed	Damaged	Rounds per Aircraft Destroyed
Corregidor 3" (1941)			52				120
Morotai (1944)	90 mm	179 (82 raids)	18	0.50	0.17	0.33	
Leyte (1944)	All wpms	1,278	251				
	90 mm		61	0.49	0.32	0.19	125
	40 mm		133	0.48	0.22	0.30	249
	0.50"		57				3,845

Pacific Theater

20871-525A

Table VII-14. Naval Antiaircraft Gun Effectiveness Against Kamikaze Attacks

	Planes destroyed		Rounds expended	
Gun and ammunition	No.	Percent	Total	Per kill
5" common	22.0	8.9	26,302	1,196
5" proximity – fuze (VT)	17.0	6.9	7,083	417
3" common	5.5*	2.2	4,667	849
3" proximity – fuze	0.5	0.2	544	1,088
40 mm	115.5	46.8	287,556	2,490
1.1"	0.5	0.2	2,695	5,390
20 mm	78.5	31.8	645,315	8,221
.50 cal	5.5	2.2	119,232	21,678
.30 cal	2.0	0.8	14,381	7,191
Totals	247.0	100.0	1,107,775	4,480 per kill

October 1944 – January 1945

*Means that 2 or more different caliber guns appeared to be responsible for the same kill.

20871-526

7-20

parameters so that they can be adjusted to correspond to more exact (and classified) data. The simulation in which they are to be used, in addition, has the capability of utilizing more detailed vulnerability data when this is desired.

For purposes of AFAADS analysis we limit our interest to two classes of 'kills', those immediately observable (the Pacific theater Category A of mid air destruction) and those resulting in target crashes within observable range of the battery (Pacific theater Category B). These will be designed 'I-kills' and 'K-kills'.

Only impacting rounds are considered at this time, and loss of aircraft from fire is excluded on the grounds that 1) aircraft protection against fire is improving and can be highly effective if properly implemented, 2) loss of the aircraft from fire when it occurs is expected to occur too long after projectile impact to interfere with completion of the attack.

It is also estimated that I-kills would result from structural damage to the aircraft, but K-kills could result from component damage from fragments of HE shells bursting within the aircraft, or from impacting ball or AP ammunition in small calibers.

Scaling Relations

It is assumed that the probability of a K-kill by a non-explosive projectile can be approximated by the function

$$P_k = \left(1 - e^{-kC^a V^b}\right) P_o \qquad (7.23)$$

where

k = a constant for a given aircraft type

C = projectile caliber

V = striking velocity

There is certainly a minimum threshold for $kC^a V^b$ but this is omitted on the assumption that we will usually be interested in impacts well above the threshold.[20] Similarly, for extremely large $kC^a V^b$ P_k will approach unity (collision with a mountain peak for example), but rather than add another term allowing slow growth beyond the point at which component vulnerability is almost completely exploited, we prefer the simpler expression which accounts for most of the effect.

Reviewing the combat data on the Cal 0.30 and 0.50 it appears that 'a' should have a value of about 3.0. However, assuming similar exposure it is probable that the 0.30 rounds struck at lower velocities because of more rapid slowdown. The relative values of a and b

depend on whether penetration, energy, or some other characteristic is most representative of the damage. It appears that reasonable ranges are $1.0 < a < 3.0$ and $0.5 < b < 2.0$. For present purposes we use a = 3/2, b = 1.0, P_o = 0.10, so that

$$P_k = P_o \left(1 - e^{-kC^{3/2} V}\right)$$
$$= P_o \left(1 - e^{-k_2 E^{1/2}}\right) \qquad (7.24)$$

where E = kinetic energy of impact of the projectile. It is not intended to apply this function above 20-mm.

HE Ammunition

A reprise of some ancient proving ground data[21] on structrual kills from HE rounds and HE charges against four WW II aircraft indicates that over the caliber range 20-mm to 75-mm and weight of HE charge 0.01 to 1.5 lbs, the probability of a structural kill (which we here identify with an I-kill) can be expressed remarkably well by

$$P_I = 1 - e^{-k W_{he}} \qquad (7.25)$$

where

W_{he} = the weight of the explosive change, or projectile filler

$$k = 6 \times 10^6 (WV)^{1} \qquad (7.26)$$

W = aircraft gross weight in pounds.

V = aircraft maximum speed in knots.

For the four aircraft WV x 10^6 ranged from 3.8 to 7.9.

The gust loading of an aircraft is proportional to its velocity. One might expect that for a given weight aircraft, the design stress would be higher for higher speed aircraft. One might also expect that for the same design stress, the probability of structural damage from an internal burst would be inversely proportional to the volume containing the burst and hence to aicraft weight. It would be interesting to see to what degree modern vulnerability data can be scaled across aircraft types in terms of the WV of the aircraft.

If one looks at the division of energy between blast and fragments of a bursting HE projectile, one finds that for the low % filler weights possible with antiaircraft gun projectiles (under 30%) almost all of the energy is transmitted to the fragments, leaving very little in the blast wave. These relations are shown in Figures 7-6 and 7-7, computed from 'Gurney's Law'. This suggests that the structural damage caused by impacting antiaircraft HE projectiles results from the

aggregated impact of the fragments on the structure and not from the blast pressure or impulse.

It may also be inferred that the principal cause of damage to components from impacting HE projectiles is fragment damage. Hence the projectiles should be designed to maximize fragment damage.

To obtain a functional form for K-kill probability from an impacting HE projectile, assume that the probability of a component kill, given a fragment hit on that component is for the 'j'th' potentially vulnerable component

$$p_j = 1 - e^{-k w_v^a b} \qquad (7.27)$$

In general, depending on whether the component is the pilot, an engine, a munition, etc., the k,a,b will be specific to the component.

The projectile bursts into n fragments, which for a conventional design of projectile have a wide range of individual weights, but all of which are ejected at about the same initial velocity, which according to Gurney's law is proportional to (for AA projectile design ranges).

$$f_v = \left(w_{he}/w_p\right)^{1/2} \qquad (7.28)$$

where

w_{he} = weight of high explosive filler

w_p = weight of filler plus metal case

The number of fragments impacting a component is inversely proportional to the distance from the burst point to the component. Since with proper fuzing, the burst is always within the aircraft, the projectile is in a uniquely favorable position to inflict fragment damage, and the average distance from a component is roughly proportional to $A_t^{1/2}$, where A_t is the presented area of the aircraft envelope normal to the trajectory.

Thus the expected number of strikes on a component of presented area A_o is proportional to A_o/A_t.

To obtain the expected number of lethal hits per burst, one would integrate the damage function over the weight distribution of the fragments average over burst positions inside the aircraft, and sum over all vulnerable components. This would be essential in optimizing the projectile design for maximum fragment effect.

For present purposes we assume that all of the potentially vulnerable components can be represented by a single equivalent component, that p_j for this component is small, and that its vulnerability is expressed in terms of the average fragment weight

$$\underline{w}_f = \left(w_p \cdot w_{he}\right)/n \cong w_p/n \qquad (7.29)$$

Then the expected number of lethal hits per burst is
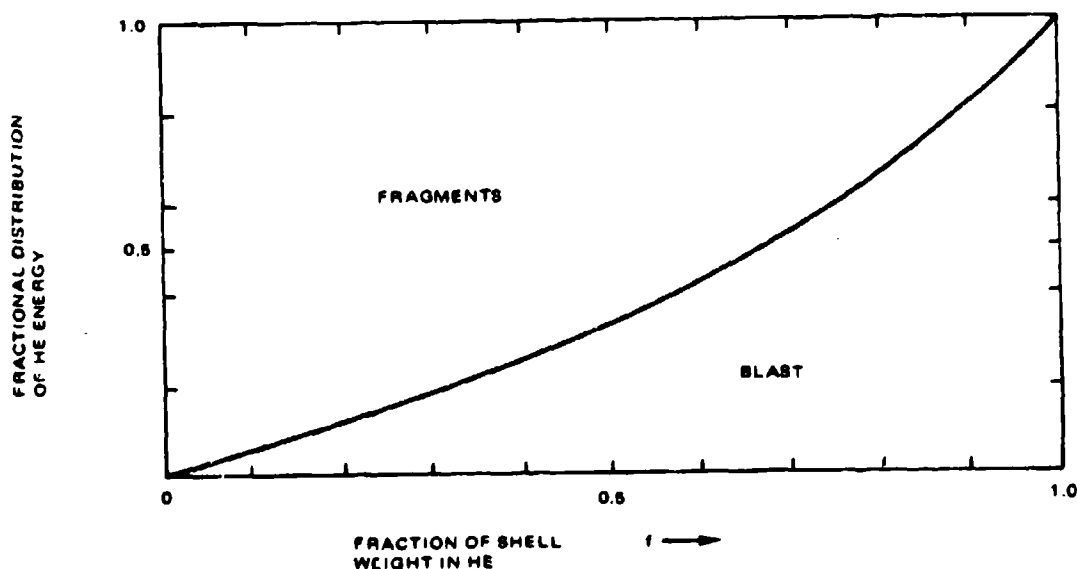
Figure 7-6. Fraction of shell weight in HE Energy Division Between Blast and Fragments

20871-164A

7-22

FRACTION OF HIGH EXPLOSIVE BY WEIGHT (f) ➤
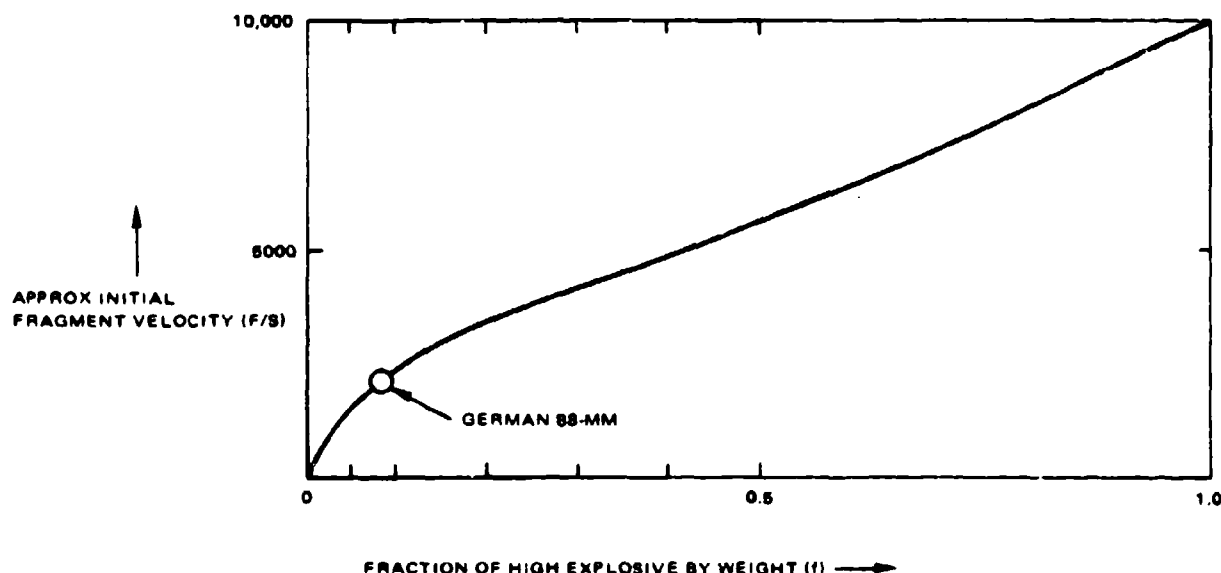
Figure 7-7. Fragment Velocity versus Fraction of Projectile Weight in High Explosive

$$E = c_3 (A_o/A_t) n^{1-a} w_p^a f^{b/2} \qquad (7.30)$$

If HE projectiles are simply scaled homologously, the number of fragments produced is relatively independent of the caliber, but the average fragment weight is proportional to caliber cubed. Hence we assume that n is independent of caliber. This would not be true is some type of fragmentation control were exercised, in which case the effectiveness of large caliber projectiles could be substantially improved.

The A_o/A_t terms is also taken as constant. However, its inclusion was explicit to suggest that there may be a scale effect for internal fragment damage with target size.

We choose a and b to have the same values as for an impacting, non bursting projectile $a = 1/2$, $b = 1.0$. Then

$$w_p^{1/2} f^{1/2} = w_{he}^{1/2} \qquad (7.31)$$

and the final expression for K-kills given a hit with an impacting HE projectile (excluding structural damage) is

$$p = 1 - e^{-k_3 w_{he}^{1/2}} \qquad (7.32)$$

Combining the expressions for structural and component damage

$$p = 1 - e^{-k_1 w_{he} - k_3 w_{he}^{1/2}} \qquad (7.33)$$

7.4.4.1 Summary

The resulting expressions for the probability of a kill given a hit, are summarized in the Table VII-15. The K kill contains I kills as well.

There are a sufficient number of coefficients in the above expressions to permit some adjustment to good vulnerability data. To show what the expressions look like the following coefficient values have been chosen

$$k_1 = 1.0$$

$$k_4 = 1.0$$

$$k_3 = 1.0$$

$$k_2 = [(10)^{3/2} (4000)]^1; \text{ for C in mm, v in ft/sec}$$

$$f = 10\%$$

Figure 7-8 shows the resulting functional form with points from the combat data and other references previously cited superimposed. There is reasonable general agreement.

For the same parameters, but two % filler ratios, Figures 7-9 and 7-10 shows probability versus caliber, and Figure 7-11 shows probability versus projectile weight.

7-23

Table VII-15. Vulnerability Relations

Type of kill and projectile	Target Component Hit	
	Fuselage	Wing
1-kill, HE	$P_1 = 1 - e^{-k_1 w_{he}}$	$P_1 = 1 - e^{-k_4 w_{he}}$
K-kill, HE	$P_k = 1 - e^{-k_1 w_{he} - k_3 w_{he}^{1/2}}$	$P_k = 1 - e^{-k_4 w_{he}}$
K-kill, non-HE impacting proj.	$P_k = P_0\left(1 - e^{-k_2 c_v^{3/2}}\right)$	NIL

20871-527A

7.4.5 Computer Target Vulnerability Module

The expressions for the HE projectiles in Table VII-15 have been programmed into the Litton simulation. The k_i are input parameters which can be chosen to fit whatever valid vulnerability data is available.

7.5 SIMULATION MODULE FOR TERMINAL EFFECTIVENESS COMPUTATION

This section develops the methodology for improved detailing of the target model and for the inclusion of round to round dispersion in angle and muzzle velocity. The target used in the simulation for AFAADS-I was a diffuse circle. The present model consists of two diffuse ellipsoids representing the target fuselage and wing.

The dispersion segment of the simulation which accounts for round to round dispersion of the shot pattern has also been improved to allow the use of different values of lateral and vertical dispersion and also to include the effect of muzzle velocity dispersion, and bias.

Since the target vulnerable area can now vary significantly with aspect, it becomes desirable to account properly for the relative direction of approach of the projectile (resulting from the vector sum of target and projectile velocity) and this effect has been included, including gravity drop.

Principal emphasis in the AFAADS study effort is on the characteristics of the fire control system. A good overall evaluation of system effectiveness is desired and so an objective is to describe the target vulnerability characteristics in sufficient detail to provide an acceptable evaluation.

On the other hand, the description of target vulnerability to a degree which includes all of the meticulous detail with which target vulnerability analyses of specific targets is known would result in the simulation being dominated by the target model rather than the fire control model, with excessive running time. Our object therefore is to strike a reasonable compromise between complexity of the simulation and target representation.

For small caliber rounds vulnerable components tend to lie within the target fuselage and an ellipsoid seems to be a reasonable representation.

Since we want to investigate a very wide range of projectile calibers it was felt desirable to include the wing, of which the inner two thirds should be vulnerable to very large rounds.

The fuselage vulnerable area head on is usually much smaller than the area side on. On the other hand the vulnerable area directly from the side is not greatly different from the vulnerable area from directly below. This would suggest an ellipsoid with circular cross section about a longitudinal axis. The wing is very thin, and might be represented as a flat plate. It turns out to be more efficient to use a generalized ellipsoid so that the same program can be used for both the fuselage and the wing but with different values of the semi-axes.

Given the two basic ellipsoids, they must be projected into a plane perpendicular to the direction of approach of the projectiles. 'Diffuse' targets are then constructed from the projected ellipses.

The diffuse target representation has several advantages as indicated in AFAADS-I. It is asymptotically correct for very small and very large kill probabilities. The kill computation is much simpler. It also allows a very simple computation of the probability of a hit on either the wing or the fuselage in the presence of 'shielding' which is indicated to be sufficiently accurate for present purposes.

Target bank angle is introduced as a function of the radial acceleration of the target. Roll about the flight direction without change in direction is not included automatically, and if it were desired to include this (as when the pilot rolls on his back at the top of a climb, pushes over, then rolls upright for his firing pass) it would have to be included as a special event. It is not
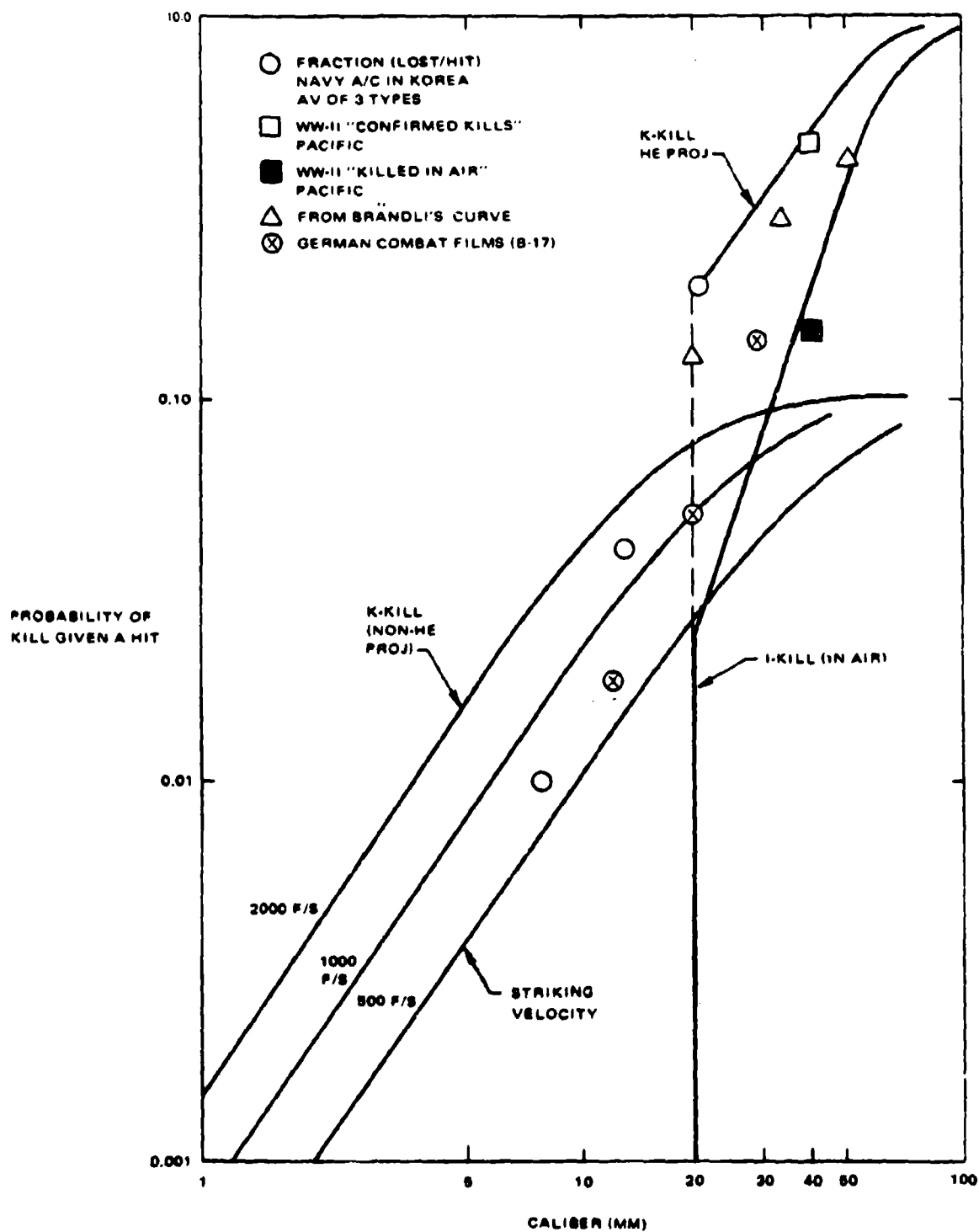
Figure 7-8. Comparison of Inferred Vulnerability Functions with Combat Data
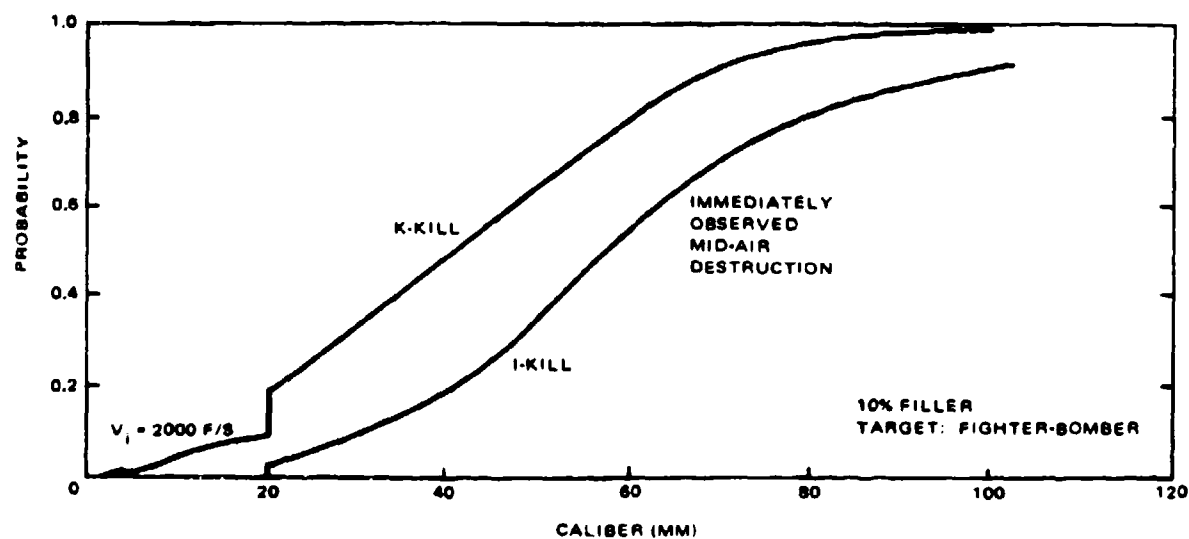
20071-186A

Figure 7-9. Conditional Kill Probabilities versus Caliber for 10% Filler
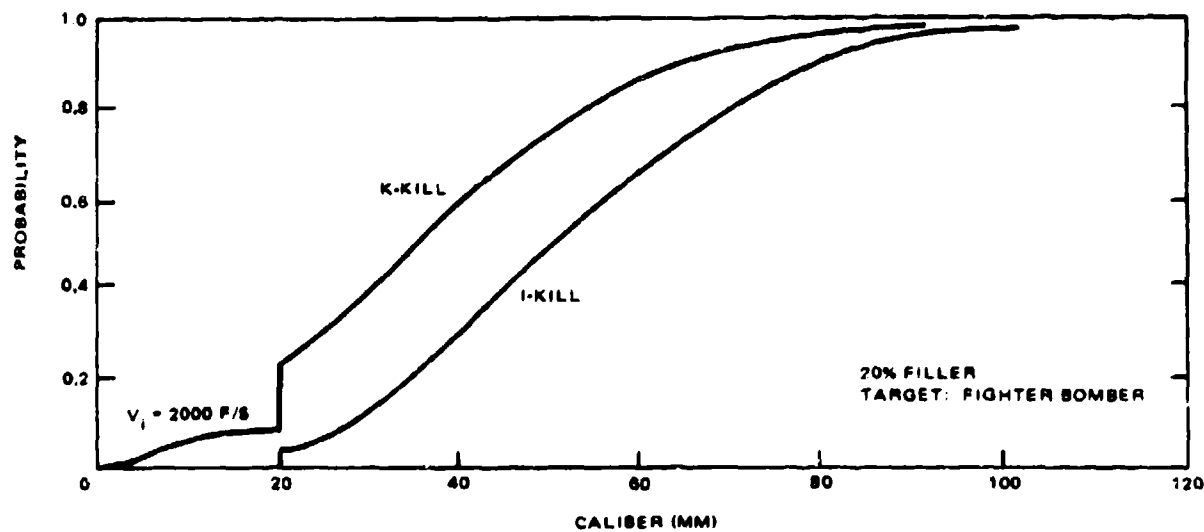
20871-167A

Figure 7-10. Conditional Kill Probabilities versus Caliber for 20% Filler

20871-168A

7-26
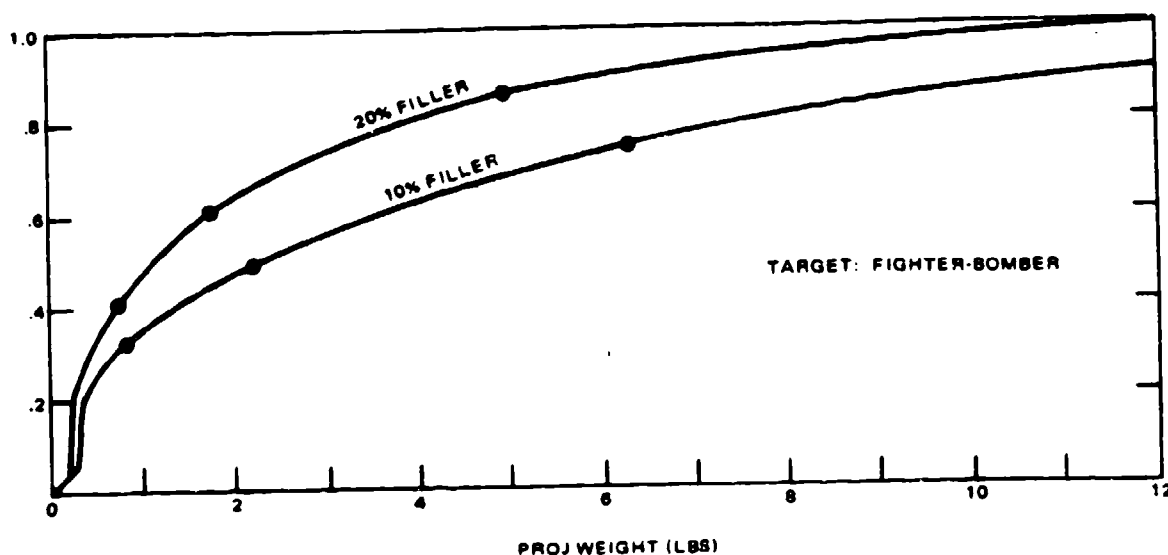
Figure 7-11. Conditional Kill Probabilities versus Projectile Weight

considered that this type of event would occupy a significant portion of the firing time.

The following section develops the algorithms for the projected area of an arbitrary ellipsoid on a plane perpendicular to a specified direction relative to the principal axes of the ellipsoid.

7.5.1 Determination of Projected Area of an Ellipsoid

Write the equation of the ellipsoid in canonical matrix form

Where

$$X'HX = 1.0 \qquad (7.34)$$

$$X' = [x \ y \ z] \qquad (7.35)$$

$$H = \begin{bmatrix} 1/a^2 & 0 & 0 \\ 0 & 1/b^2 & 0 \\ 0 & 0 & 1/c^2 \end{bmatrix} \qquad (7.36)$$

By a series of rotations, obtain the equation of the ellipsoid in $U' = [u \ v \ w]$ coordinates. The rotation

matrix is 3x3 square and skew symmetric. Designate it as R

$$X' = U'R' \qquad (7.37)$$

The equation of the ellipsoid in rotated coordinates is

$$U'R'HRU = U'MU = 1.0 \qquad (7.38)$$

where M is a 3x3 symmetric matrix.

Assume that the rotation has been carried out in such a way that the w axis is parallel to the bullet trajectory in the vicinity of the target, i.e. the bullet trajectory relative to the moving target, corrected for both target and bullet velocities. If we are dealing with impact projectiles, we require the equation of the ellipse which is generated by the projection of the ellipsoid in a plane perpendicular to the bullet trajectory, i.e. to the w axis.

Equation (7.38) defines the u v w relationship of points on the surface of the ellipsoid. Consider a plane containing the w axis and cutting the ellipsoid at $u, \lambda u$. As u is varied, observe du/dw. When du/dw = 0 we have reached the edge of the projected ellipse. This defines w* in terms of u_r. Substitute w* thus derived

7-27

back into Equation (7.38) to eliminate w. The result is the expression in u,v for the desired projected ellipse.

Manipulation of the expressions is simplified by partitioning the matrices

$$
M = \begin{bmatrix} m_{11} & m_{21} & \vdots & m_{31} \\ m_{21} & m_{22} & \vdots & m_{32} \\ \cdots & \cdots & \cdots & \cdots \\ m_{31} & m_{32} & \vdots & m_{33} \end{bmatrix} = \begin{bmatrix} M_1 & M_2 \\ M_2' & M_3 \end{bmatrix}
$$

(7.39)

where the subscripts have been chosen to express the fact that M is symmetric.

$$ U = [U_a' \vdots w] \; ; U_a' = [u \quad v] \qquad (7.40) $$

The equation of the ellipse is

$$ [U_a' \quad w] \begin{bmatrix} M_1 & M_2 \\ M_2' & M_3 \end{bmatrix} \begin{bmatrix} U_a \\ w \end{bmatrix} = 1.0 \quad (7.41) $$

$$ U_a'M_1U_a + wM_2'U_a + U_a'M_2w + wM_3w = 1.0 $$

(7.42)

In Equation (7.41) write

$$ U_\lambda' = u [1 \quad \lambda] \qquad (7.43) $$

Differentiate with respect to w and set du/dw = 0. Designate w* as the value of w determined by this process. It is the value of w for which a line parallel to the bullet trajectory is tangent to the ellipsoid. Then

$$ [U_\lambda' \quad w^*] \begin{bmatrix} M_2 \\ M_3 \end{bmatrix} + [M_2 \quad M_3] \begin{bmatrix} U_\lambda \\ w^* \end{bmatrix} = 0 $$

(7.44)

Examining the elements of the two terms of Equation (7.44) note that they are equal to each other and hence each equal to zero. Replace U_2 by U_a, and substitute back into Equation (7.41), eliminating w* and obtaining as the equation of the projected ellipse

$$ U_a' [M_1 - M_2M_3^{-1} M_2'] U_a = 1.0 \qquad (7.45) $$

This is the desired expression for the projected ellipse.

Given Equation (7.45) the area of the projected ellipse can be derived. If the shot pattern is large compared with target size, this is all one needs to know about the target; in our case the shot pattern will sometimes be small with respect to target vulnerable area, but in any case the area is an interesting point of reference.

Begin by determining the orientation of the ellipse in the u,v plane, and its maximum and minimum radii. Define:

$$ v = r \sin \psi \; ; u = r \cos \psi \qquad (7.46) $$

Write the equation of the ellipse as

$$ U' \begin{bmatrix} A & B \\ B & C \end{bmatrix} U = 1.0 \; ; U'P \; U = 1.0 $$

(7.47)

Substitute Equation (7.46) in Equation (7.47), differentiate and set dr/dψ = 0

Then the inclination of the ellipse is found to be

$$\tan 2\psi^* = 2B/(A-C) \tag{7.48}$$

Solving for the major and minor axes

$$(r_{1,2}^*)^2 = \frac{2}{(A+B) \pm [(2B)^2 + (A-C)^2]^{1/2}} \tag{7.49}$$

The area of the ellipse is:

$$A_e = \pi r_1^* r_2^* \tag{7.50}$$

$$A_e = \frac{\pi}{[(AC) - B^2]^{1/2}} \tag{7.51}$$

Referring to Equation (7.45)

$$P = M_1 \cdot M_2 M_3^{-1} M_2' \tag{7.52}$$

and so

$$A_e = \pi / |P|^{1/2} \tag{7.53}$$

But in terms of the M matrix, (Equation (7.39)):

$$|P| = |M| / |M_3| \tag{7.54}$$

and

$$|M| = (a^2 b^2 c^2)^{-1} \tag{7.55}$$

so that:

$$A_e = \pi abc \, |M_3|^{1/2} \tag{7.56}$$

where it will be remembered that M_3 was scalar.

Equation (7.55) follows from the fact that the determinant of any rotation matrix is unity and

$$|M| = |R'| \, |H| \, |R| = |H| \tag{7.57}$$

The same result can be obtained from the integral defining the equivalent area of a diffuse target. We have

$$A_e = \int\!\!\!\int_{-\infty}^{\infty} e^{-U'PU} \, dU \tag{7.58}$$

$$= \pi / |P|^{1/2} \tag{7.59}$$

from which Equation (7.56) follows as before. In terms of elements of the rotation matrix R

$$|M_3| = (r_{13}^2/a^2) + (r_{23}^2/b^2) + (r_{33}^2/c^2) \tag{7.60}$$

whence,

$$A_e = \pi \left[r_{13}^2 b^2 c^2 + r_{23}^2 a^2 c^2 + r_{33}^2 a^2 b^2 \right]^{1/2} \tag{7.61}$$

7.5.2 Coordinate Systems and Rotation Matrices

The basic coordinate system is [X Y Z] fixed in space. A coordinate system [x y z] is fixed in the aircraft. A third coordinate system [u v w] is centered on the airplane, but rotated so that the w axis is parallel to the relative direction of approach of the projectile to the aircraft, with the u axis horizontal. A fourth coordinate system [x_t y_t z_t] is fixed to the gun tube with the x_t axis horizontal. These coordinate systems are shown in Figures 7-12 through 7-15.

All four coordinate systems are rectangular and right handed. Angular rotations are positive clockwise looking out along an axis from the origin.

The aircraft's direction of flight is assumed to be along its y axis. We do not consider changes in angle of attack, or sideslip angle in this model.

The following angles are defined:

β = bank angle, positive in a right turn.

θ = climb angle, positive for climb, negative for dive.

A = target azimuth measured from the Y axis.

e = target elevation angle measured from the horizontal plane.

A_r = relative direction of projectile approach in azimuth.

e_r = relative direction of approach of the projectile in elevation, measured from the horizontal.

H = heading of the aircraft in the horizontal plane relative to the Y axis.

α = angle between the projections of the target velocity vector V and the line of sight to the target in the horizontal plane. (7.62)

7-29
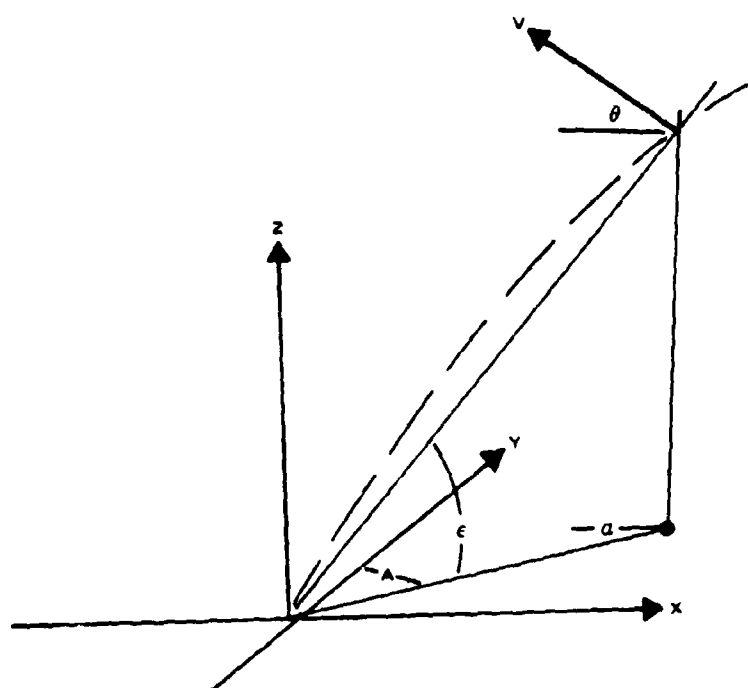
NOTE:

AZIMUTH ANGLE
A IS (−) IN THIS
FIGURE

20871-170A

Figure 7-12. Fixed Coordinate System
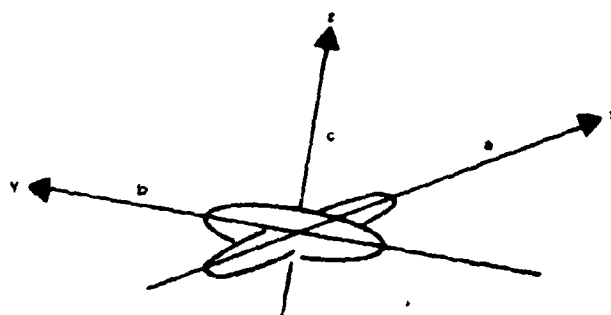
20871-171A

Figure 7-13. Aircraft Coordinate System
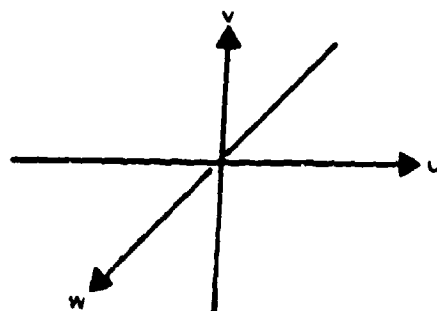
20871-172A

Figure 7-14. Relative Aircraft-Projectile Coordinate System

7-30
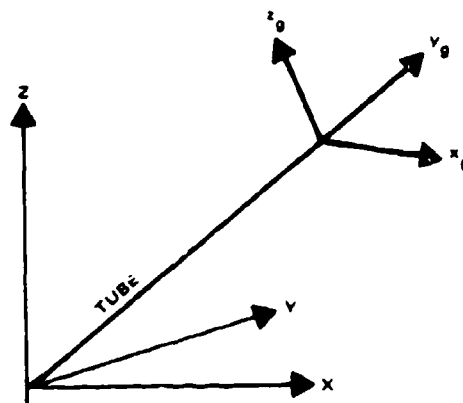
Figure 7-15. Gun Coordinate System

$a = A \cdot H + \pi$ from Figure 7-16.   (7.63)

α, = angle between the projections of the target velocity vector and the relative direction of approach of the projectile in the horizontal plane.   (7.64)

$$a_T = A_T \cdot H + \pi \qquad (7.65)$$

The rotation matrices are defined in the following paragraphs.

$$[X\ Y\ Z] = [x\ y\ z]\begin{bmatrix} \cos\beta & 0 & \sin\beta \\ 0 & 1 & 0 \\ -\sin\beta & 0 & \cos\beta \end{bmatrix}\begin{bmatrix} 1 & 0 & 0 \\ 0 & \cos\theta & \sin\theta \\ 0 & -\sin\theta & \cos\theta \end{bmatrix}\begin{bmatrix} \cos H & \sin H & 0 \\ -\sin H & \cos H & 0 \\ 0 & 0 & 1 \end{bmatrix} \quad (7.66)$$

This set of operations is abbreviated

$$[X]^T = [x]^T\ [\beta]^T\ [\theta]^T\ [H]^T \qquad (7.67)$$

Inverting the operations

$$[X] = [H]\ [\theta]\ [\beta]\ [x] \qquad (7.68)$$

The [X Y Z] vectors are next rotated to the [u v w] coordinate system. The set of rotations is chosen to cause the w vector to lie in a direction parallel to the relative velocity of the projectile to target near the target. This requires an additional $\pi/2$ rotation in e_r. The operations are

7-31

$$\{u \ v \ w\} = \{X \ Y \ Z\}\begin{bmatrix} \cos A_r & -\sin A_r & 0 \\ \sin A_r & \cos A_r & 0 \\ 0 & 0 & 1 \end{bmatrix}\begin{bmatrix} 1 & 0 & 0 \\ 0 & \cos e_r & -\sin e_r \\ 0 & \sin e_r & \cos e_r \end{bmatrix}\begin{bmatrix} 1 & 0 & 0 \\ 0 & 0 & -1 \\ 0 & 1 & 0 \end{bmatrix} \quad (7.69)$$

Or

$$\{U\}^T = \{X\}^T \{A_r\} \{e_r + (\pi/2)\} \quad (7.70)$$

Hence,

$$\{U\}^T = \{x\}^T \{\beta\}^T \{\theta\}^T \{H\}^T \{A_r\} \{e_r + (\pi/2)\} = \{x\}^T \{R\}^T \quad (7.71)$$

This defines

$$\{R\}$$

It follows at once that:

$$\{x\}^T = \{U\}^T \{R\}^T \quad (7.72)$$

and

$$\{x\} = \{R\}^T \{U\} \quad (7.73)$$

For reference

$$\{R\}^T = \{e_r + \pi/2\}^T \{A_r\}^T \{H\} \{\theta\} \{\beta\} \quad (7.74)$$

$$\{R\}^T = \{\beta\}^T \{\theta\}^T \{H\}^T \{A_r\} \{e_r + (\pi/2)\} \quad (7.75)$$

The equation of the rotated ellipsoid is $U_a^T R^T H R U_a = 1.0$ (7.76)

Referring to Figure 7-16, note that

$$A_r = H + a_r \cdot \pi' \quad (7.77)$$

The H and A_r matrices can be combined if a_r is known.

$$\{A_r\}^T \{H\} = \{H \cdot A_r\} = \{\pi \cdot a_r\} = \{a_r \cdot \pi\}^T \quad (7.78)$$

similarly

$$\{H\}^T \{A_r\} = -\{a_r \cdot \pi\} = \{\pi \cdot a_r\}^T \quad (7.79)$$

The R matrix has been multiplied out for reference:

$$R = \{C_1 : C_2 : C_3\}$$

where

$$C_1 = \begin{bmatrix} -\cos\beta\cos a_r + \sin\beta\sin\theta\sin a_r \\ -\cos\theta\sin a_r \\ \sin\beta\cos a_r + \cos\beta\sin\theta\sin a_r \end{bmatrix}$$

$$C_2 = \begin{bmatrix} -\cos\beta\sin a_r\sin e_r - \sin\beta\sin\theta\cos a_r\sin e_r + \sin\beta\cos\theta\cos e_r \\ \cos\theta\cos a_r\sin e_r + \sin\theta\cos e_r \\ \sin\beta\sin a_r\sin e_r - \cos\beta\sin\theta\cos a_r\cos e_r + \cos\beta\cos\theta\cos e_r \end{bmatrix}$$

$$C_3 = \begin{bmatrix} \cos\beta\sin a_r\cos e_r - \sin\beta\sin\theta\cos a_r\cos e_r - \sin\beta\cos\theta\sin e_r \\ \cos\theta\cos a_r\cos e_r - \sin\theta\sin e_r \\ \sin\beta\sin a_r\cos e_r - \cos\beta\sin\theta\cos a_r\cos e_r - \cos\beta\cos\theta\sin e_r \end{bmatrix} \quad (7.80)$$

7.5.2.1 Some Special Cases

These are useful in checking the simulation programming.

Let $A = 0, H = \pi/2, a_r = \pi/2, \theta = 0$

Then

$$R = \begin{bmatrix} 0 & -1 & 0 \\ \sin Y & 0 & \cos Y \\ -\cos Y & 0 & \sin Y \end{bmatrix} \quad (7.81)$$

where $Y = (\beta \cdot e_r)$

and

$$A_e = \pi b \left[c^2 \cos^2(\beta \cdot e_r) + a^2 \sin^2(\beta \cdot e_r) \right]^{1/2} \quad (7.82)$$

Let $A = 0, H = 0, a_r = \pi, \beta = 0$

Then

$$R = \begin{bmatrix} 1 & 0 & 0 \\ 0 & -\sin(e_r \cdot \theta) & -\cos(e_r \cdot \theta) \\ 0 & \cos(e_r \cdot \theta) & -\sin(e_r \cdot \theta) \end{bmatrix} \quad (7.83)$$

and

$$A_e = \pi a \left[c^2 \cos^2(e_r \cdot \theta) + b^2 \sin^2(e_r \cdot \theta) \right] \quad (7.84)$$

Let $\beta = 0, \theta = 0$

Then

$$R = \begin{bmatrix} -\cos a_r & -\sin a_r \sin e_r & -\sin a_r \cos e_r \\ -\sin a_r & \cos a_r \sin e_r & -\cos a_r \cos e_r \\ 0 & \cos e_r & -\sin e_r \end{bmatrix} \quad (7.85)$$

and

$$A_e = \left[b^2 c^2 \sin^2 a_r \cos^2 e_r + a^2 b^2 \sin^2 e_r + a^2 c^2 \cos^2 a_r \cos^2 e_r \right]^{1/2} \quad (7.86)$$

If $a = c$ (circular cross section perpendicular to the flight direction)

7-32

$$A_e = \pi a [b^2 \sin^2 \Omega + a^2 \cos^2 \Omega]^{1/2} \qquad (7.87)$$

where

$$\cos \Omega = \cos a_r \cos e_r \qquad (7.88)$$

For this last case the vulnerability function to be combined with the shot pattern is

$$e^{-u^2 [(\sin^2 \Omega/b^2) + \cos^2 \Omega/a^2)] \cdot v^2/c^2} \qquad (7.89)$$

Let $c = 0$ (flat plate wing)

Then from Equation (7.61):

$$A_e = \pi a b |r_{33}|$$

$$= \pi a b |\sin \beta \sin a_r \cos e_r - \cos \beta \sin \theta \cos a_r \cos e_r$$

$$\cdot \cos \beta \cos \theta \sin e_r \qquad (7.90)$$

and if

$$\beta = \theta = 0 \qquad (7.91)$$

$$A_e = \pi a b \sin e_r \qquad (7.92)$$

7.5.3 Relative Direction of Approach of Projectile to Target

Let V_p = projectile remaining velocity along its trajectory in the vicinity of the target. Its components in [X Y Z] are V_{pX}, V_{pY}, V_{pZ}. These are obtained from the ballistic module of the simulation. Gravity drop is approximated as gt_p.

$$V_{pX} = V_p \cos e \sin A$$

$$V_{pY} = V_p \cos e \cos A \qquad (7.93)$$

$$V_{pZ} = V_p \sin e \cdot gt_p$$

The components of target velocity in X Y Z are V_X, V_Y, V_Z and using Equation (7.93) the components of relative projectile velocity are

$$V_{rX} = V_p \cos e \sin A - V_X$$

$$V_{rY} = V_p \cos e \cos A - V_Y \qquad (7.94)$$

$$V_{rZ} = V_p \sin e - V_Z \cdot gt_p$$

From these components compute

$$V_r^2 = V_{rX}^2 + V_{rY}^2 + V_{rZ}^2 \qquad \text{(square of the relative vector velocity)}$$

$$V_{rH}^2 = V_{rX}^2 + V_{rY}^2 \qquad \text{(square of the relative vector velocity in the horizontal plane)}$$

Then

$$\sin A_r = V_{rX}/V_{rH}$$

$$\cos A_r = V_{rY}/V_{rH}$$

$$\sin e_r = V_{rZ}/V_r$$

$$\cos e_r = V_{rH}/V_r \qquad (7.95)$$

These terms are inputs for the A_r, e_r matrices in Equations (7.74) and (7.75).

7.5.3.1 An Observation on the Direction of Relative Approach of Projectile to Target

It can be shown that if projectile velocity is constant and the target path is unaccelerated, and gravity drop is neglected,

$$A_r = A_o ; a_r = a_o$$

$$e_r = e_o \qquad (7.96)$$

where A_o, e_o are the target azimuth and elevation (line of sight) at the instant the round is fired.

This is intuitively evident if we consider that for this case the projectile, if it hits the target, must fly what the missileers call a 'constant bearing' path; i.e., a path in which there is no rotation in space of the line between the bullet and the target.

For this zero-order approximation therefore, the difference between the relative direction of approach and the gun-target line at the instant the bullet reaches the target will be equal to the angular lead computed by the predictor. If the target is broadside at this

H + a + (-A) = π

a = A - H + π
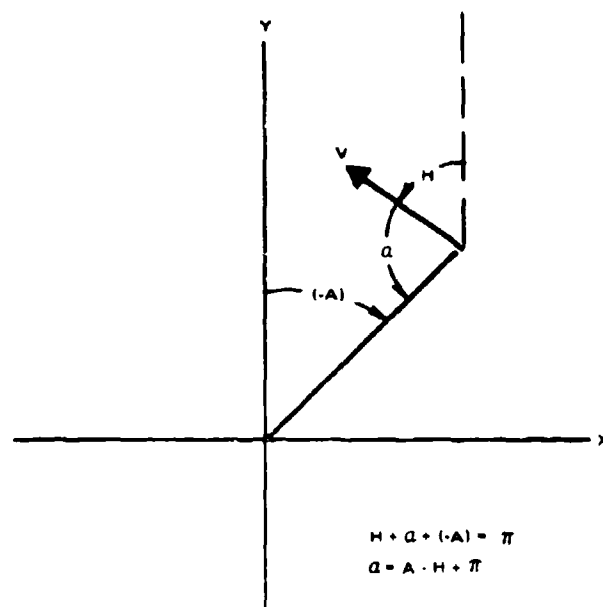
20871-174

Figure 7-16. Angular Relations in the Horizontal Plane

instant, and lead was 30°, the projectile will approach the target at an angle 60° off the nose.

7.5.3.2 Determination of Bank Angle

The program is designed to input bank angle automatically as a function of radial acceleration. If n_r is the radial acceleration in 'g's' in a steady turn bank angle is given by

$$\sin \beta = n_r/(1 + n_r^2)^{\frac{1}{2}} \; ; \cos \beta = 1/(1 + n_r^2)^{\frac{1}{2}}$$

(7.97)

As noted earlier, rolling of the aircraft without a change in flight direction would have to be inserted as a special 'event'.

7.5.4 Random Round to Round Dispersion in Angle and Muzzle Velocity

The simulation is programmed to accommodate three elements of random round to round dispersion.

a. Constant angular dispersion in a vertical plane through the gun tube, with a normal probability density function and zero mean about the tube axis. Its variance is σ_z^2.

b. Constant lateral angular dispersion in a plane

through the gun tube, perpendicular to the vertical plane, normally distributed with zero mean at the tube axis. Its variance is σ_x^2.

c. Constant muzzle velocity dispersion in meters per second. It is assumed to have a normal distribution with zero mean and variance σ_{vo}^2. Bias is handled separately as shown in a later section. Muzzle velocity affects hit probability via time of flight and the relation is worked out below.

In general, therefore, we have three components of random round to round dispersion, one vertical, one lateral, and one which lies closely in the plane containing the gun and the target path (i.e., the tangent plane when the projectile is near the target).

To the degree that other, presently unidentified, sources of dispersion can be resolved into these three elements they can be handled in this simulation program as input parameters.

7.5.5 Angular Dispersion

Begin with gun coordinates $[x_g \; y_g \; z_g]$ and let the elements represent the linear effects at the target of angular deviations at the gun. Since y is along the trajectory and we are considering only angular dispersion set $y_g = 0$. The dispersion matrix is, in gun coordinates

7-34

$$<[x_g]\,[x_g]^T> \;=\; <\begin{bmatrix} x_g \\ 0 \\ z_g \end{bmatrix}[x_g \;\; 0 \;\; z_g]> \;=\; \begin{bmatrix} \sigma_x^2 & 0 & 0 \\ 0 & 0 & 0 \\ 0 & 0 & \sigma_z^2 \end{bmatrix}$$

$$(7.98)$$

To convert to the direction of relative approach of the projectile rotate through angle e and A into the X Y Z coordinate system and then back through angles A and $e_r + (\pi/2)$.

In the u v w coordinate system, after the above rotations have been performed

$$U^T = [x_g]^T C^T \;;\; U = [C]\,[x_g] \qquad (7.99)$$

where C is the rotation matrix. Then the dispersion matrix in the u v w system is

$$< [U]\,[U]^T > = [C]<[x_g]\,[x_g]^T>[C]^T \qquad (7.100)$$

$$= \begin{bmatrix} \sigma_u^2 & \rho_{uv}\sigma_u\sigma_v & \rho_{uw}\sigma_u\sigma_w \\ \rho_{uv}\sigma_u\sigma_v & \sigma_v^2 & \rho_{vw}\sigma_v\sigma_w \\ \rho_{uw}\sigma_w\sigma_v & \rho_{vw}\sigma_v\sigma_w & \sigma_w^2 \end{bmatrix}$$

$$(7.101)$$

Only the four elements in the upper left hand corner of this matrix are retained. Call this submatrix $[\sigma_R^2]$

$$[\sigma_R^2] = \begin{bmatrix} \sigma_u^2 & \rho_{uv}\sigma_u\sigma_v \\ \rho_{uv}\sigma_u\sigma_v & \sigma_v^2 \end{bmatrix} \qquad (7.102)$$

The rotation matrix

$$[C]^T = [e]^T [A] [A_r] [e_r + (\pi/2)] \qquad (7.103)$$

Multiplying this out for reference

$$[C]^T = \begin{bmatrix} \cos\delta & -\sin\delta\sin e_r & -\sin\delta\cos e_r \\ -\sin\delta\cos e & -\cos\delta\cos e\sin e_r + \sin e\cos e_r & -\cos\delta\cos e\cos e_r - \sin e\sin e_r \\ \sin\delta\sin e & \cos\delta\sin e\sin e_r + \cos e\cos e_r & \cos\delta\sin e\cos e_r - \sin e_r\cos e \end{bmatrix} \quad (7.104)$$

where

$$\delta = (A - A_r)$$

If we write

$$[C]^T = \begin{bmatrix} c_{11} & c_{12} & c_{13} \\ c_{21} & c_{22} & c_{23} \\ c_{31} & c_{32} & c_{33} \end{bmatrix}$$

The variance matrix $[\sigma_R^2]$ becomes

$$[\sigma_R^2] = \begin{bmatrix} c_{11}^2\sigma_x^2 + c_{31}^2\sigma_z^2 & c_{11}c_{12}\sigma_x^2 + c_{31}c_{32}\sigma_z^2 \\ c_{11}c_{12}\sigma_x^2 + c_{31}c_{32}\sigma_z^2 & c_{12}^2\sigma_x^2 + c_{32}^2\sigma_z^2 \end{bmatrix} \quad (7.105)$$

In the above process either the angular variances can be converted to linear variances by multiplying by D_p^2 before beginning the computation, or the σ_R^2 matrix can be computed in mils^2 and then converted to linear measures by multiplying each element by D_p^2.

7.5.6 Muzzle Velocity Dispersion

The effect of an error in muzzle velocity is to cause the projectile to arrive at the predicted point at a different time from that computed in the predictor. We consider this as a perturbation about the target position.

If δt_p = error in time of flight resulting from an error δv_0 in muzzle velocity

$\quad\quad\; V$ = target velocity along its flight path

$\quad\quad\; E_y$ = target travel during the interval δt_p

then

$$E_y = V\,\delta t_p \qquad (7.106)$$

The subscript y indicates that the error is observed along the y body axis of the target.

For this computation it will certainly be adequate to use the '3/2 law' expression for projectile velocity.

For this ballistic function, if v_a is average projectile velocity

$$v_a = D_p/t_p = V_o - aD_p \qquad (7.107)$$

where

D_p is slant range, V_o is muzzle velocity and "a" is a constant.

Then

$$\text{Log}_e t_p = \text{Log}_e D_p - \text{Log}_e(V_o - aD_p) \qquad (7.108)$$

Differentiate, holding D_p constant, and obtain

$$\delta t_p/t_p = -\delta V_o/(V_o - aD_p) = -\delta V_o/v_a \qquad (7.109)$$

Hence,

$$E_y = -\delta V_o\left(Vt_p/v_a\right) \qquad (7.110)$$

Divide both sides by D_p

$$E_y/D_p = -\delta V_o\left(V/v_a^2\right) \qquad (7.111)$$

Now for the drag law assumed,

$$v_a^2 = V_o V_p \qquad (7.112)$$

where V_p is the projectile remaining velocity at D_p. This is convenient since it is used elsewhere in this program module.

The ratio E_y/D_p can be treated as an angular deviation, and after computation and angular rotation it can be restored to linear miss at the target by multiplying by D_p.

Alternately, it can be inserted in linear measure.

The variance of E_y in terms of the variance in muzzle velocity σ_{Vo} is

$$\sigma_E^2 = \left(\sigma_{Vo}/V_o\right)^2 \left(V/V_p\right)^2 D_p^2 \qquad (7.113)$$

We now need to rotate this into the u v plane.

From the earlier expressions

$$[u\,v\,w] = [x\,y\,z]\,R \qquad (7.114)$$

and so the matrix of variances resulting from muzzle velocity dispersion projected into the u v plane is

$$\sigma_m^2 = \begin{bmatrix} \sigma_u^2 & \rho\sigma_u\sigma_v \\ \rho\sigma_u\sigma_v & \sigma_v^2 \end{bmatrix} = R^T \begin{bmatrix} 0 & 0 & 0 \\ 0 & \sigma_E^2 & 0 \\ 0 & 0 & 0 \end{bmatrix} R$$

$$(7.115)$$

and only the four elements in the upper left corner are retained.

7.5.7 Angular and Muzzle Velocity Biases (Systematic Errors)

Define V_{oB} = systematic error, or 'bias' in muzzle velocity. This is assumed to be constant over a firing path. From the expressions in the preceding section, the resulting miss distance along the target path is

$$B_v = -\left(V_{oB}/V_o\right)\left(V/V_p\right)D_p \qquad (7.116)$$

This miss distance is rotated into the u,v,w coordinate system by the operation

$$[M_{uB}\,M_{vB}\,M_{wB}] = [0\,B_v\,0][R] \qquad (7.117)$$

The M_{wB} term which is along the direction of relative approach of the target is dropped and the remaining two terms are added to the u v miss distances obtained from the prediction module of the simulation. The resulting sums go into the computation of single shot probability.

The simulation is also programmed to accept constant angular bias errors in azimuth and elevation.

7.5.8 Discussion of the 'Diffuse Target' Representation

Before presenting the single shot kill algorithms, we digress briefly to discuss the diffuse target representation which was presented without discussion in AFAADS-I. We consider the basis for the diffuse target model, the approximation invoived in the simplest method of accounting for wing/target area overlap, and the 'shoebox' representation versus the ellipsoid.

Suppose that we have an arbitrary pdf of shots about the target in 2-dimensions given by $f(x,y)$. The target area is irregular and equal to A_t. Then the probability of a hit is

$$p = \iint_{A_t} f(x, y) \, dx \, dy \qquad (7.118)$$

and this can be written

$$p = \iint_{-\infty}^{\infty} t(x, y) f(x, y) \, dx \, dy \qquad (7.119)$$

where

t(x,y)

  = 1.0 over the target

  = 0 elsewhere

Usually f(x,y) can be written as a bivariate normal distribution with non-zero mean. We would like to replace t(x,y) by a function that allows a closed for of (1) to be obtained, and so we would like an expression that integrates when multiplied by the bivariate normal.

The simplest expression to use is one which also has the form of a bivariate normal. In this case the target is represented by an ellipse, but a 'diffuse' one, in that the probability that a round passing within the target area hits the target is not unity, except at the exact center as shown in Figure 7-17.

We require that

$$\iint_{\infty}^{\infty} t(x, y) \, dx \, dy = A_t \qquad (7.120)$$

Now *if* the probability that a hit kills the target is uniformly p_c over A_t we can write the probability of a kill as

$$P_k = P_c \iint_{\infty}^{\infty} t(x, y) f(x, y) \, dx \, dy$$

$$(7.121)$$

In fact, the probability that a hit on the target will

kill it is also a function of x,y and so we should write Equation (7.121) as

$$P_k = \iint_{\infty}^{\infty} p_c(x, y) \, t(x, y) \, f(x, y) \, dx \, dy \quad (7.122)$$

$$= \iint_{\infty}^{\infty} t_v(x, y) \, f(x, y) \, dx \, dy \qquad (7.123)$$

If the shot pattern is uniform over the target (not necessarily centered on the target)

$$P_k = f(0, 0) \iint_{\infty}^{\infty} t_v(x, y) \, dx \, dy = f(0, 0) \, A_v$$

$$(7.124)$$

where

$$A_v = \iint_{\infty}^{\infty} t_v(x, y) \, dx \, dy \qquad (7.125)$$

A_v is designated as the 'vulnerable area' and may be considered as the sum of the areas presented to the shot pattern of all components which are 'singly vulnerable' each multiplied by the probability that a hit on the summed area will kill the target.

Then an alternate form for obtaining kill probability is obtained by writing $t_v(x,y)$ in the form of a bivariate normal distribution with appropriate multiplying constant to satisfy Equation (7.125).

Whether to use Equation (7.121) or (7.123) depends on the degree to which the vulnerable components of the target tend to cluster near the center of mass. The difference in algorithms is greatest for small caliber projectiles, in which case (7.123) is probably a closer approximation, and this is the expression now programmed in the simulation.

With the benefit of hindsight, it appears that the use of Equation (7.121) in the Litton simulation would have provided equally useful results, and in addition would have the significant advantage of showing smaller variance of computed kill probability across
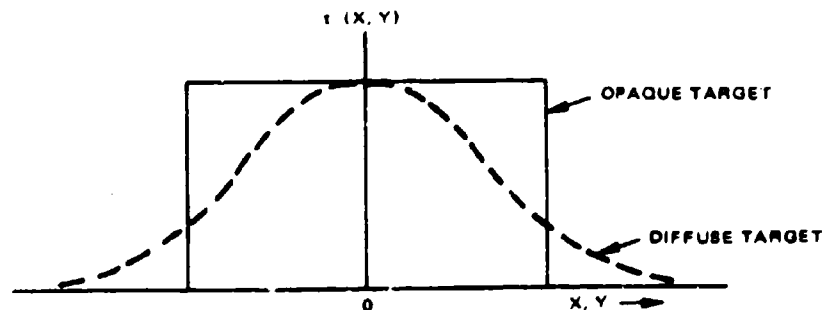
Figure 7-17. Diffuse Target Approximation

replications. This would reduce computer operating costs.

If the target is 'multiply vulnerable', e.g., one must kill two out of two engines to kill it, the duplicated or multiplicated components are to be treated separately and the effects of killing various numbers of them combined by the usual laws of probability.

The difference between a diffuse target and an opaque target can be seen by considering a worst case, - an opaque disc fired at which a circular normal shot pattern centered on the disc. For the 'exact' computation,

$$P_1 = 1 - e^{-A/(2\pi\sigma^2)} \qquad (7.126)$$

For the "diffuse" representation

$$P_2 = A/[A + (2\pi\sigma^2)] \qquad (7.127)$$

and the two representations are asymptotically the same for very large and very small probabilities.

Single shot probability will normally be low. A value of 0.10 (ten rounds per kill) would be a high value. The two expressions are compared in Table VII-16.

7.5.8.1 Shoebox versus Ellipsoid

In the evaluation of most *current* predicted fire systems it is adequate to assume that the shot pattern is large compared with the presented area of the target and to compute

$$P_k = f(0,0) A_v \qquad (7.128)$$

In the AFAADS study effort we are attempting to obtain better system performance, and so we require a computational procedure that does not allow p_k to exceed 1.0 on those relatively infrequent occasions when $f(0,0)$ is larger than A_v^{-1}.

Table VII-16. Comparison of Algorithms

$A/(2\pi\sigma^2)$	P_1	P_2
0	0	0
0.05	.0488	.0475
0.10	.095	.090
1.0	.632	.500
2.0	.864	.667
∞	1.0	1.0

20871-528A

The shoebox does not merge nicely with the normal distribution of the shot pattern, as does an ellipse, but in those cases where Equation (7.128) is adequate, it can be compared with an ellipsoid.

If the target is viewed at an angle θ from head on, the presented area of the ellipsoid is

$$A_e = \pi b_e \left[a_e^2 \sin^2 \theta + b_e^2 \cos^2 \theta \right]^{\frac{1}{2}} \qquad (7.129)$$

and for the shoebox

$$A_s = 4 b_s [a_s \sin \theta + b_s \cos \theta] \qquad (7.130)$$

Choose the a,b so that the areas of the two shapes are identical head on and side on. Then the ratio of areas at angle θ is

$$(A_s/A_e)^2 = 1 + \frac{\sin 2\theta}{\sin^2 \theta + \lambda^2 \cos^2 \theta} ; \lambda = b/a$$

This is easily determined to have a maximum at

$$\tan \theta = \lambda$$

where

$$(A_s/A_e)_{max} = (2)^{\frac{1}{2}} = 1.414... \qquad (7.131)$$

Considering the other uncertainties in the complete simulation, a maximum difference of 41% between two representations, both of which are approximations, is of moderate, but not critical concern.

7.5.8.2 Combination of Wing and Fuselage

The wing and fuselage will in general have different projected orientations and these orientations will change as the target moves along its path. We now consider the effect of overlap of the areas, and the shielding of one by the other.

First consider *hit* probabilities. Both wing and fuselage are represented by diffuse ellipsoids, with probabilities $t_f, t_w(u,v)$ that a round passing at u,v from the target center will hit the respective component.

If we assume that these probabilities are independent (of course their values depend on u,v) the probability that a round passing u,v hits neither is $(1-t_f)(1-t_w)$ and the probability of hitting either or both is

$$t_a = t_f + t_w - t_f t_w \qquad (7.132)$$

We can obtain the same result from the following argument. Suppose the wing shields the fuselage. The probability of hitting the wing is t_w. If the wing is hit,

the fuselage cannot be hit. The probability missing the wing and hitting the fuselage is $(1-t_w)t_f$ and the sum of these probabilities is the probability of hitting the aircraft, or

$$t_a = t_w + (1 - t_w)t_f = t_w + t_f - t_w t_f \qquad (7.133)$$

Note that $t_a(0,0) = 1.0$ as it should be.

Consider a worst (and extremely unrealistic) case in which the target consists of two saucers stacked one on the other; the top one is the fuselage, the bottom is the wing, and we are firing directly from below. There is complete overlap, since the top saucer is completely shielded by the bottom saucer. For both elements the diffuse target representation is

$$t = e^{-r^2/a^2} \qquad (7.134)$$

and if we integrate

$$t_a = 2 e^{-r^2/a^2} - e^{-2r^2/a^2}$$

over all r we obtain

$$A = 1.5 \pi a^2 \text{ instead of } 1.0 \pi a^2 \qquad (7.135)$$

In fact, if we complete the probability of *hitting* either of the two saucers for this case, we find that the .5 ratio for small p decreases rapidly with increasing p. This is shown in Table VII-17.

More realistically, consider a planform for which the target projection is two identical ellipses, with major axes perpendicular. The area of each is A. The ratio of minor to major axis is μ. Some minor calculus reveals that the area of overlap, is

$$A_o = (4A/\pi)\tan^{-1} \mu \qquad (7.136)$$

As $\mu \to 1.0$ the ellipses become circles and for $\mu = 1.0$, $A_o = A$.

For this case, the diffuse target model when worked through, gives the overlap area as

$$A_o = \mu/(1 + \mu) \qquad (7.137)$$

The projected area of the wing, fuselage combination is

$$A_a = 2A - A_o \qquad (7.138)$$

The exact computation is compared with the diffuse target approximation as a function of μ in Table VII-18.

Since $\mu < 0.50$ in general, the representation is considered adequate in this case.

Now consider kill probabilities. If the projectile has a large enough caliber so that a hit on the wing inboard section (say the inner half of the wing) has a high probability of killing the aircraft, and the fuselage has a similarly high vulnerability, then the above comments with regard to overlap apply to the case where wing and fuselage are both vulnerable, and their projections in the u v plane are replaced by ellipses of dimensions corresponding to vulnerable rather than presented area.

However, if the projectile caliber is so small, that the wing is invulnerable to a hit and the projectile has a fuze which causes it to burst on the first component it hits, then the wing can shield a part of the fuselage from some aspects and we need to consider the approximation more carefully.

In this case, if the wing is a perfect shield, and is mounted on the bottom of the fuselage, then the wing will shield against projectiles approaching from below, but if the bank angle is such that projectiles approach from 'above' in body axes, there will be no shielding.

Table VII-17. Comparison of Hit Probability on Two Stacked Saucers

$A/(2\pi\sigma^2)$	P_{exact}	$P_{diffuse}$
0	0	0
0.2	.18	.24
0.5	.39	.47
1.0	.63	.67
∞	1.0	1.0

20871-529

Table VII-18. Comparison of Hit Probability on Two Stacked Ellipses

μ	A_a/A	
	exact	diffuse model
0	2	2
0.1	1.87	1.91
0.2	1.75	1.84
0.5	1.51	1.67
1.0	1.0	1.50

20871-530

This consideration would require the shield effect to be changed with direction of approach of the projectile. On the other hand, if the aircraft has a midwing configuration, so that half the fuselage vulnerable area is above and half below the wing, half of the overlap area will always act as a shield.

For this case of an invulnerable wing acting as a shield, Table VII-19 shows the comparison of 1) exact computation of exposed fuselage vulnerable area for a low wing, projectile approaching from below, 2) mid wing, 3) a 'diffuse' shield, and 4) no shield, as a function of μ.

It is understood that in this comparison the ellipse representing the fuselage is the ellipse representing the vulnerable area.

The 'diffuse' shield is assumed always to protect the overlap area regardless of direction of bullet approach.

The diffuse wing is considered an acceptable approximately, for the case where the wing is invulnerable and has a shielding effect.

Since aircraft designers apparently like to place vulnerable components other than the pilot low in the fuselage where they are easily accessible to maintenance, and wings tend to be shoulder-placed or mid, but rarely below the fuselage (even in this case the wing section at the fuselage tends to contain vulnerable components), the problem of wing shielding is considered to be adequately solved for present purposes by the diffuse wing approximation.

The general case where detailed vulnerability information is provided, considering projectile impact velocity and obliquity, detailed target configuration, internal shielding, etc., all as a function of direction of projectile impact is discussed in the following section.

The t function for the case of a projectile that bursts if it hits the wing but cannot damage the wing is

$$t_a = (1 \cdot t_w)t_{fv} = t_{fv} \cdot t_w t_{fv} \qquad (7.139)$$

where t, is chosen to represent the wing area, but t_v represents the vulnerable area of the fuselage.

7.5.8.3 On the General Applicability of this Program to Precise Vulnerability Data

Suppose that a case of importance arises in the evaluation of a specific weapon system against a specific target, and suppose that the vulnerability experts have developed precise computations of vulnerable area as a function of the striking velocity of the projectile and its direction of approach with respect to axes fixed in the target. The computations might also include the effect of 'obliquity' in projectile impact.

Can the present program be applied to such a specific problem?

The answer appears to be clearly 'yes', with some modification of the program elements.

It is assumed that the target vulnerability can be presented in tabular form as a function of projectile striking velocity, two angles for relative direction of approach, and a third angle for projectile obliquity at impact. The projectile velocity is available in the present program, and the three angles are attainable by appropriate rotations similar to those now in the program.

The process would be as follows: The vulnerability data would be stored in the computer in tabular form. The four inputs would be computed as done in the present program. The vulnerable area would be extracted from the tabulated data (suitably interpolated) and passed on to the kill probability computation. Depending on the precision of shooting it might be desirable to insert not vulnerable area, but the probability that a hit at x,y causes a kill in the tabulation. This would increase the amount of stored area, but would fit nicely into the kill probability computation.

Why would one want to use this detail? A major reason is that at present target vulnerability information is developed in much greater detail than is used in

Table VII-19. Fraction of Fuselage Vulnerable Area Exposed

μ	No Shield	Opaque Low Wing	Opaque Mid Wing	"Diffuse" Wing
0	1.0	1.0	1.0	1.0
0.1	1.0	0.87	0.93	0.91
0.2	1.0	0.75	0.87	0.84
0.5	1.0	0.51	0.63	0.67

20871-531

most system evaluations. The system evaluator usually works with a few 'average' vulnerable areas which have been so averaged that much of the original fine detail (which considers shielding, depth of penetration to reach vulnerable components, etc...) is lost.

This is consistent with the objectives of system evaluation, but is not very informative if one has the objective of reducing the vulnerability of friendly aircraft to enemy fire.

By expanding the target vulnerability module in the Litton simulation as described above, and inserting the fire control system parameters to correspond to those of enemy weapons, it should be possible to use the simulation as a tool in vulnerability analysis.

In this case the characteristics of the antiaircraft defense system would be held constant, and the effects of changes in aircraft design and protection to reduce friendly aircraft and helicopter vulnerability could be assessed.

We now return to the algorithms for computing kill probability based on the preceding developments.

7.5.9 Computation of Single Shot Kill Probability

From AFAADS-I, p. 5-57, Equation (5.251), the single shot kill probability is given by the expression

$$ P_{ss} = \frac{|J|^{\frac{1}{2}}}{|J+S|^{\frac{1}{2}}} e^{-(\frac{1}{2})M_a^T [J+S]^{-1} M_a} \qquad (7.140) $$

where [S] is the covariance matrix of round to round dispersion of the shots

$$ [S] = \begin{bmatrix} \sigma_u^2 & \rho \sigma_u \sigma_v \\ \\ \rho \sigma_u \sigma_v & \sigma_v^2 \end{bmatrix} \qquad (7.141) $$

for reference

$$ |S| = \sigma_u^2 \sigma_v^2 (1 - \rho^2) $$

$$ [S]^{-1} = \frac{1}{1-\rho^2} \begin{bmatrix} 1/\sigma_u^2 & -\rho/(\sigma_u \sigma_v) \\ \\ -\rho/(\sigma_u \sigma_v) & 1/\sigma_v^2 \end{bmatrix} $$

$$ (7.142) $$

[S] is obtained by adding the matrix derived from

angular dispersion to the matrix derived from muzzle velocity dispersion.

$$ [S] = \left[\sigma_R^2 \right] + \left[\sigma_m^2 \right] \qquad (7.143) $$

The J matrix is the inverse of the matrix describing the diffuse ellipse, which is designated V

$$ J^{-1} = V \qquad (7.144) $$

V is derived from Equation (7.45) with one small change in the H matrix (the elements are doubled)

$$ V = \left[M_1 \cdot M_2 M_3^{-1} M_2^T \right] \qquad (7.145) $$

where M_1, M_2, M_3 are partitioned matrices of M and M has been computed as

$$ [M] = [R^T][H][R] \qquad (7.146) $$

but [H] is now

$$ \begin{bmatrix} 2/a^2 & 0 & 0 \\ 0 & 2/b^2 & 0 \\ 0 & 0 & 2/c^2 \end{bmatrix} \qquad (7.147) $$

To be consistent with the fact that $[J+S]^{-1}$ is multiplied by 1/2 in the P_{ss} expression, each of the elements is multiplied by 2.

The $M_a{}^T$ matrix (not to be confused with the previous M's) is the vector of displacement of the aim point from the target center. It is obtained by summing the miss distances from the prediction computation and the miss distances resulting from muzzle velocity systematic error.

$$ [M_a]^T = [M_u M_v] = [M_{up} M_{vp}] + [M_{uB} M_{vB}] $$
$$ \text{prediction} \quad \text{muzzle velocity} $$

$$ (7.148) $$

7.5.9.1 Probability of Single Shot Kill on Either Fuselage or Wing

The wing and fuselage will have different orientations, varying with aspect and so within the limitations of the approximation for accounting for overlap given

earlier, three probabilities are computed, then combined.

The probability of hitting the fuselage is computed, using V_f for the fuselage. This is designated p_f

The probability of hitting the wing is computed, using V_w for the wing. This is designated p_w

The probability of hitting both is computed using

$$J_{fw} = [V_f + V_w]^{-1} \qquad (7.149)$$

This is designated p_{fw}.

The probability of hitting either wing or fuselage is then computed as

$$p = p_f + p_w - p_{fw} \qquad (7.150)$$

Note that $p_{fw} \neq p_f p_w$ in general.

If both wing and fuselage are vulnerable, the V matrices in the above algorithms are for the vulnerable areas.

If the wing is invulnerable and can shield the fuselage, the V matrices are for the wing area and the fuselage v nerable area, and

$$p = p_f - p_{fw} ; \text{ since } p_w = 0 \qquad (7.151)$$

If the bullet can penetrate the wing and go on to the fuselage, such as an API round, the V_w term is omitted and only the fuselage ellipsoid is retained.

If the wing is invulnerable, but is considered to only very rarely provide significant shielding, the V_w term is omitted and only the fuselage ellipsoid is retained.

The data flow diagram in the terminal effects module of the simulation is shown in Figure 7-18.

7.5.10 Simplified Expressions for Tracking Module

Automatic tracking with radar, gated imaging sensors, and probably manual tracking with visual observation all depend on the aircraft dimensions projected in a plane normal to the line of sight. Since these vary with the aircraft aspect, it was felt desirable to modify the tracking module of the simulation accordingly. In the AFAADS-I simulation, tracking errors in azimuth, elevation, and slant range were generated in a manner independent of target aspect, and this was felt to be incompatible in the improved simulation with the improved target representation.

The input parameters to the tracking error module were chosen to be the dimensions of the rectangular parallelopiped enclosing the projected target image, with one side of the rectangle horizontal, and a second side vertical. Two sets of algorithms were developed, one using the target ellipsoids, and a simpler set, developed by J. Jatczynski using simply the orthogonal vectors comprised of the target span, fuselage length, and fuselage height. The latter set was considered adequate, and was the mode programmed.
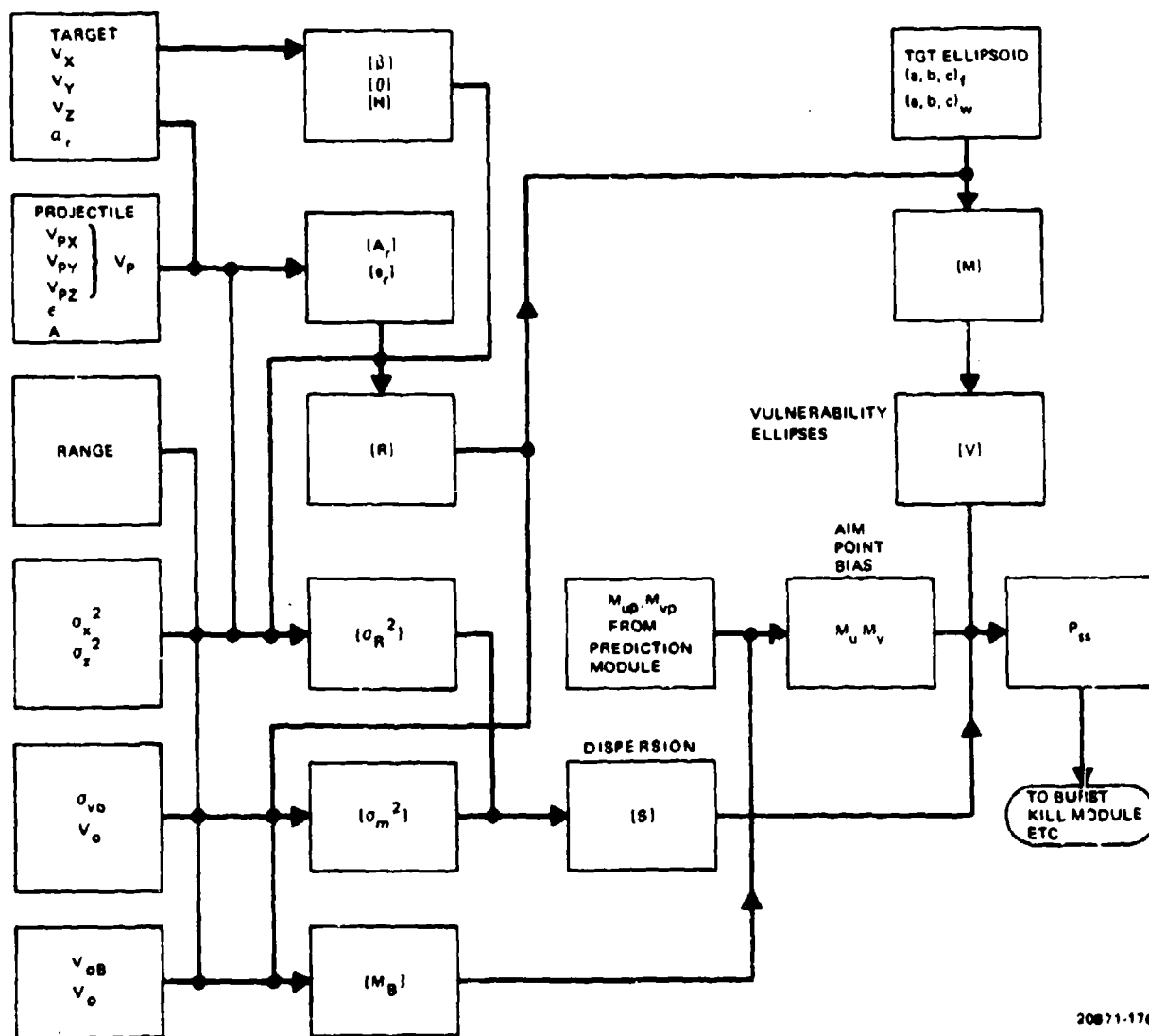
Figure 7-18. Simulation Flow Diagram for Computation of Single Shot Probability

20871-176A

SECTION 8
WEAPON CHARACTERISTICS

The most obvious descriptors of an antiaircraft gun installation are

Number of guns on mount

Caliber

Muzzle Velocity

Rate of Fire

Type of Mount (Self-propelled or towed)

All-up Weight

In the accompanying Effectiveness Volume, tables are given of the characteristics of modern antiaircraft gun systems. In this section some of the possible trade-offs in choosing weapon parameters are discussed.

It is considerably beyond the scope of the present effort to consider weapon design in depth, hence the discussion is limited to a level consistent with the sketching of parametric ranges of interest in effectiveness evaluations.

8.1 SCALING RELATIONSHIPS

If an automatic weapon were scaled homologously in caliber, using the same materials and firing mechanism, and holding maximum pressure and muzzle velocity constant, one would expect that weapon weight would be proportional to caliber cubed, and rate of fire to the inverse of caliber.

Although data on actual weapons shows considerable scatter because of the different design details, one finds that there is an apparent economy of scale as caliber is increased, so that weapon weight increases less rapidly than caliber cubed. This is most evident when one examines the all-up weights of both towed and self-propelled weapons.

This effect is probably to be expected, since not all of the system components increase in weight as the gun weight increases, and in the case of the gun itself, there is more emphasis on weight reduction for the larger calibers.

The result is that for single tube weapons, all-up weight tends to increase about as caliber squared.

An additional economy results from multiple gun mounting on the same chassis. The weight increases about as the number of guns to the 2/3 power.

These effects can be combined by expressing all-up weight for both towed and self-propelled mounts in terms of the total muzzle energy of the installation: the weight increases very roughly as the 2/3 power of this value.

If the muzzle energy is multiplied by rate of fire one obtains the horsepower generated by the installation: there does not appear to be a significant trend over the data on available designs between all-up weight and horsepower and the scatter of the data is very large. A contributing cause to this scatter is probably the presence in the available data sample of a number of systems whose maximum rate of fire is considerably less than the best that could be obtained in that caliber at the present state of the art.

One would not expect simple overall scaling relationships to hold well, in estimating all-up weight, because of at least three major determinants of this value in addition to the weapon. These are:

a. Whether the mount carries sensors such as radar.

b. The weight of armor.

c. In the case of towed mounts, whether there is a power drive with on-mount engine-generator.

To obtain good estimates of weight one therefore must go through a simple preliminary design type of analysis, with a weight build up by individual components.

In the case of towed mounts, one does observe that current mounts weigh somewhat more in the firing position than World War II designs of the same caliber. However the difference in weight between the two vintages in the travel position is not as great. It may be that this results from the modern emphasis on mobility and rapid time to convert from the travel to firing position and back. Hence fewer components are demounted.

Figure 8-1 shows a few points for the weight of current self-propelled and towed systems as a function of total muzzle energy of the mount.

The scaling of rate of fire inversely with caliber is approximately followed by the most advanced current designs, as shown in Figure 8-2. Note that in a given caliber, the Gatling guns with 6 tubes have about 6 times the maximum rate of fire of single tube weapons.

As discussed in the Effectiveness volume, a high rate of fire may not be fully utilized during heavy attack waves with short intervals between attackers unless it is also associated with a short reload time. There are very wide differences in reload time among current systems, especially in the self-propelled versions.

Aerodynamic considerations limit the possible range of shape and weight of spin stabilized projectiles in a given caliber. The design is a compromise between stability and drag objectives. As a result the weight of spin stabilized projectiles is very closely proportional to
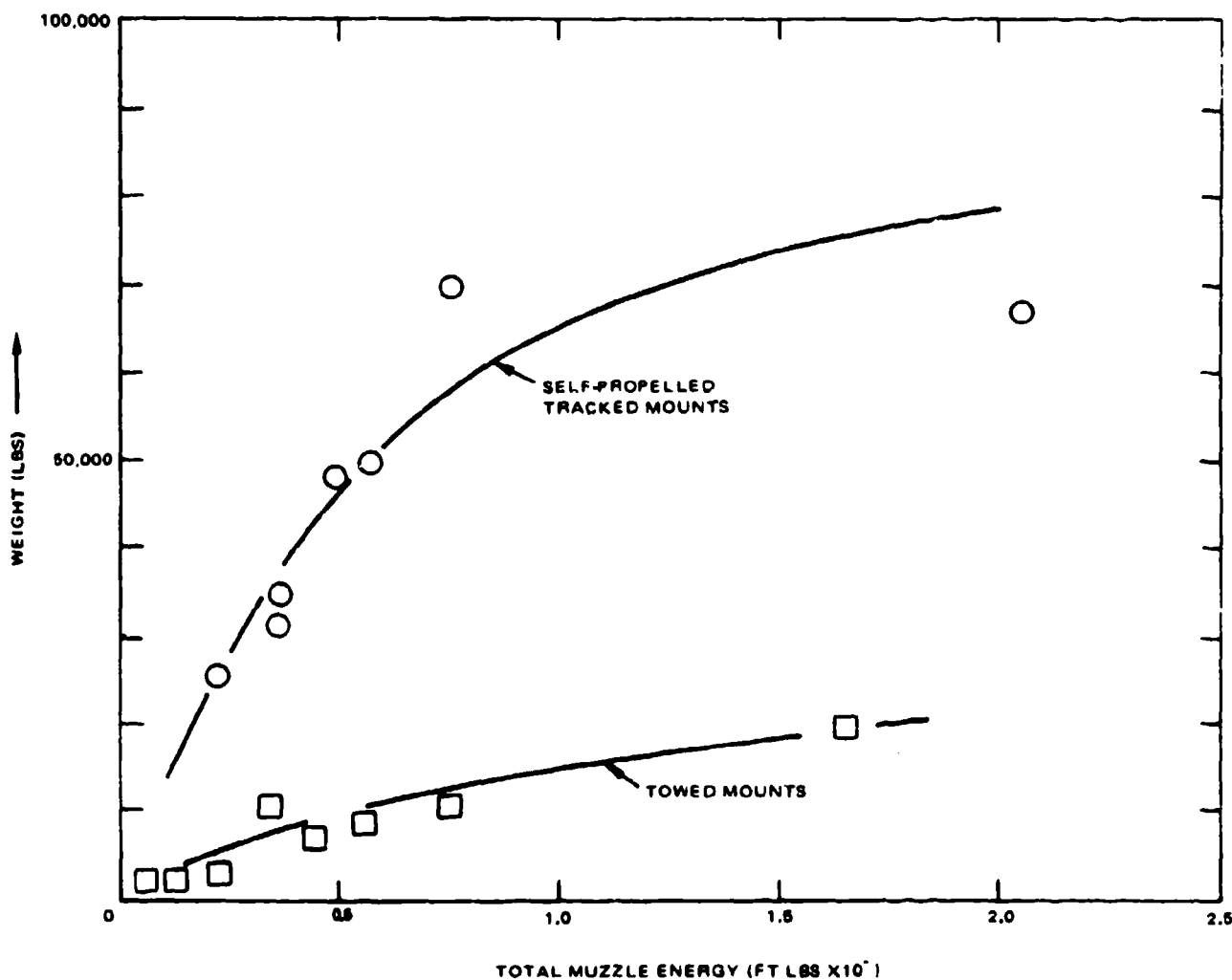
Figure 8-1. Weight of Antiaircraft Gun Systems versus Muzzle Energy

the cube of caliber. In fact, a U.S. Navy text once contained the flat statement: 'The weight of Navy projectiles is $D^3/2$, where D = diameter in inches and weight is in pounds.'

As noted in the vulnerability section, a high fractional content of projectile weight devoted to high explosive is desirable for terminal effort. Since high explosive has a much lower density than steel, as the HE content is increased, the projectile weight decreases. An additional limit appears when the shell walls become too thin to withstand the firing stresses.

Figure 8-3 shows how the overall projectile density varies with fraction of HE content for a number of HE projectiles. As a rough average one may estimate that projectile weight is given by

$$w_p = (C/100)^3 \, (39) \, (1 - 1.6f) \, ; \quad f < 0.30$$

$$(8.1)$$

where

w_p = projectile weight in pounds

f = fraction of weight devoted to high explosive

8-2
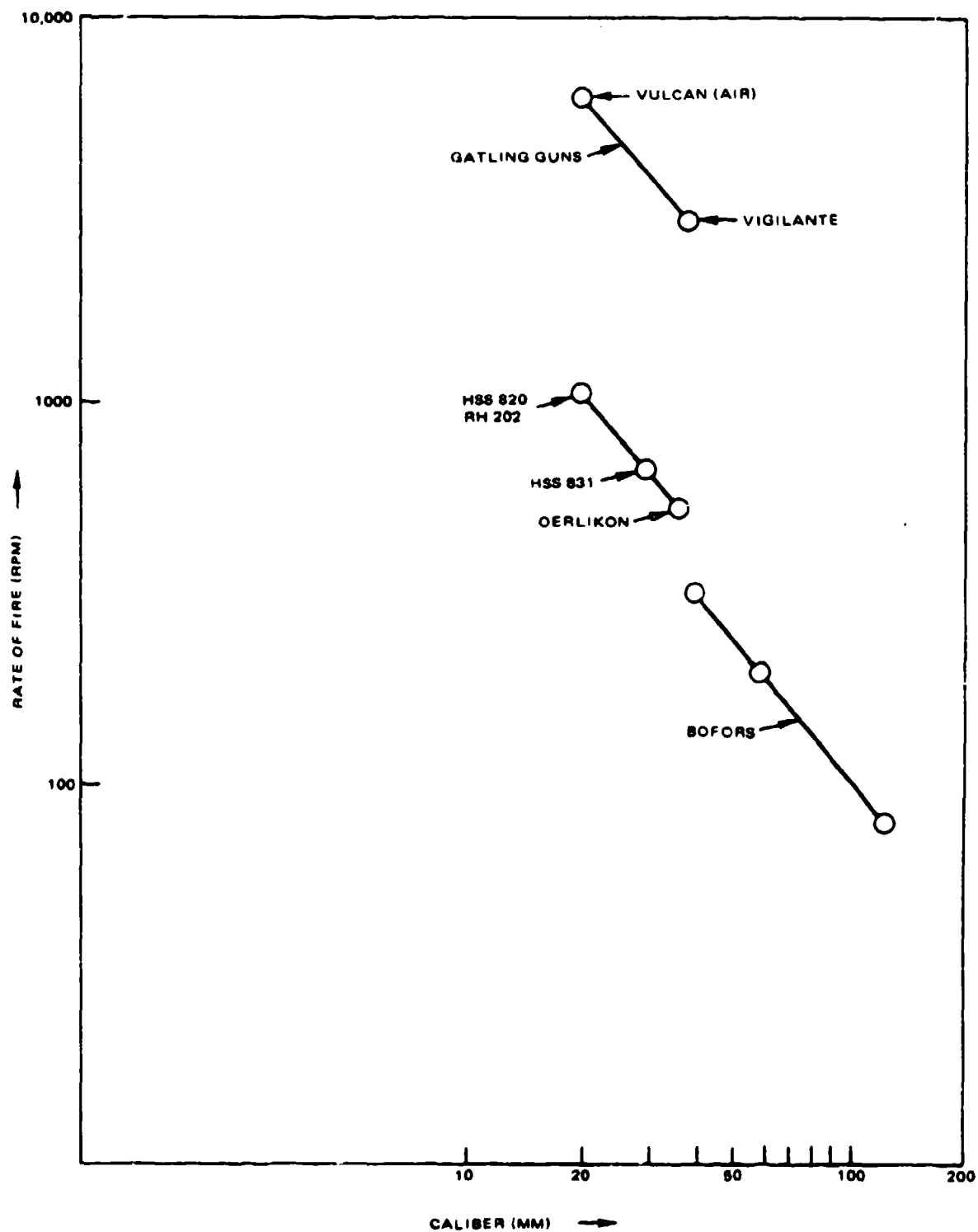
Figure 8-2. Rate of Fire of Antiaircraft Guns versus Caliber

20871-178A

8-3

C = caliber in millimeters

The ballistic coefficient of a projectile is proportional to w_p/C^2 and if caliber and shape are held constant while weight is changed, the range to which a given muzzle velocity will have decayed to a specific value is approximately proportional to w_p/C^2. However in a given gun, a lighter projectile will have a higher muzzle velocity. The change in muzzle velocity with projectile weight, for small changes is[6]

$$\Delta MV/MV = n\, \Delta w_p/w_p \qquad (8.2)$$

where 'n is approximately -0.3 for a rifled gun with multiperforated grains, -0.4 for a rifled gun with single-perforated grains, -0.47 for a smooth bore mortar with flake propellant, and -0.65 for a recoilless rifle with multiperforated grains.' If muzzle energy were constant, n would be -0.50.

8.2 MUZZLE VELOCITY RELATIONSHIPS

Firing a gun releases the energy contained in the propellant charge. Only a portion of this energy is communicated to the projectile, another portion remains with the propellant gases, and the remainder is lost in various ways, including heating of the tube, the
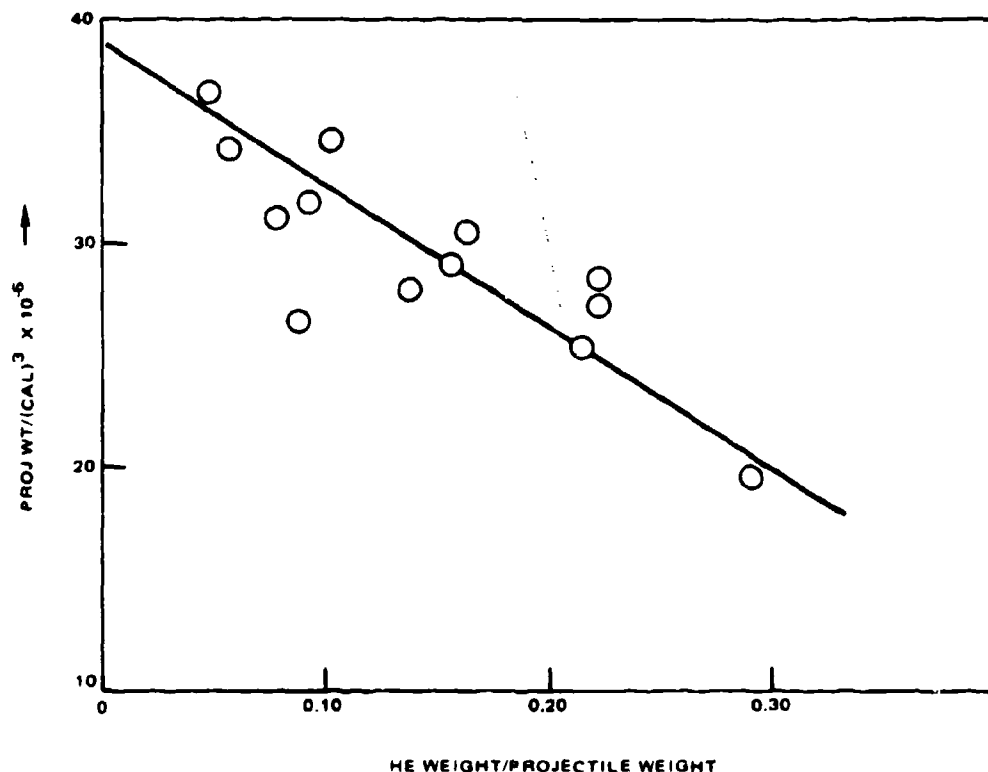
20871-179A

Figure 8-3. Projectile Density versus Fraction of Weight in High Explosive

8-4

projectile, work done in engraving the rotating band, etc.

The kinetic energy of the projectile at the muzzle is

$$E_o = (\tfrac{1}{2})(w_p/g)v_o^2 \qquad (8.3)$$

where

w_p = projectile weight

v_o = muzzle velocity

g = acceleration of gravity

If it is assumed that the velocity of the propellant gases increases linearly from zero in the chamber to v_o at the muzzle, at the moment the projectile exits, they will contain a kinetic energy

$$E_g = (1/6)(w_{ch}/g)v_o^2 \qquad (8.4)$$

where

w_{ch} = weight of propellant charge

Schwarz[5] suggests replacing the 1/6 coefficient by 1/4 to better approximate losses to friction, heat, etc. as well as kinetic gaseous energy.

The available energy is proportional to the propellant weight, and equating the available and expended energies

$$kw_{ch} = \left[w_p/2 + w_{ch}/6\right]v_o^2/g \qquad (8.5)$$

As projectile weight w_p becomes very small, muzzle velocity approaches a limiting value

$$v_m^2 = 6kg \qquad (8.6)$$

One can estimate k by plotting total muzzle energy $E_m = E_o + E_g$ versus w_{ch} for a number of guns to observe consistency over a variety of gun designs. This was done by Weiss[3] in 1948 and an estimate of k for automatic weapons was obtained as

$$k = 0.45(10)^6 \text{ ft} \qquad (8.7)$$

This led to an estimate of v_m = 9350 f/s. However a better fit to a plot of muzzle velocity versus w_p/w_{ch} for a large number of 1940-1950 vintage weapons, using a coefficient of 1/4 and v_m = 8000 f/s.

From these simple relations, one obtains:

$$w_{ch}/w_p = k_2\left(\frac{v_o^2}{v_m^2 - v_o^2}\right); k_2 = 2.0 ; v_m = 8,000 \text{ f/s} \qquad (8.8)$$

A comparison of this simple relation with a carefully computed curve of muzzle velocity versus propellant charge to projectile weight ratio for a small arms family with specified expansion ratio and maximum pressure[4] is shown in Figure 8-4. The small arms curve was computed for an expansion ratio of 5.0; if it had been computed for an expansion ratio of about 8.0 the two curves would be essentially identical. To show that gun design has become more efficient over the years, curves are also shown for Civil War field artillery.

A substantial amount of research and development effort has been devoted to lightening the weight of cartridge of fixed ammunition, for example, by using aluminum rather than brass cartridge cases. In addition the development of combustible cartridge cases is directed to eliminating the problem of what to do with ejected cases, especially for air to air weapons. In general, one might expect the weight of the case to be proportional to the weight of propellant, so that weight of complete round w_{cr} is

$$w_{cr} = w_p + k_3 w_{ch}$$

or

$$w_{cp}/w_p = 1 + k_4\left(\frac{v_o^2}{v_m^2 - v_o^2}\right) \qquad (8.9)$$

For current French and German automatic weapons in the 20-mm to 30-mm class, and muzzle velocities in the range 3300-3550 f/s, w_{cr}/w_p lies in the range 2.2 to 2.6. To this must be added the link weight and container weight, depending on the design, to build up the total ammunition weight.

8.3 METHODS OF OBTAINING VERY HIGH MUZZLE VELOCITY USING SUB-CALIBER PROJECTILES

The simplest method of obtaining a very high muzzle velocity is to fire a light projectile. The possible gain is indicated in Figure 8-4. There is a limit, however, to the amount by which one can lighten a conventional projectile of full gun caliber, and still retain a good ballistic shape.

8-5
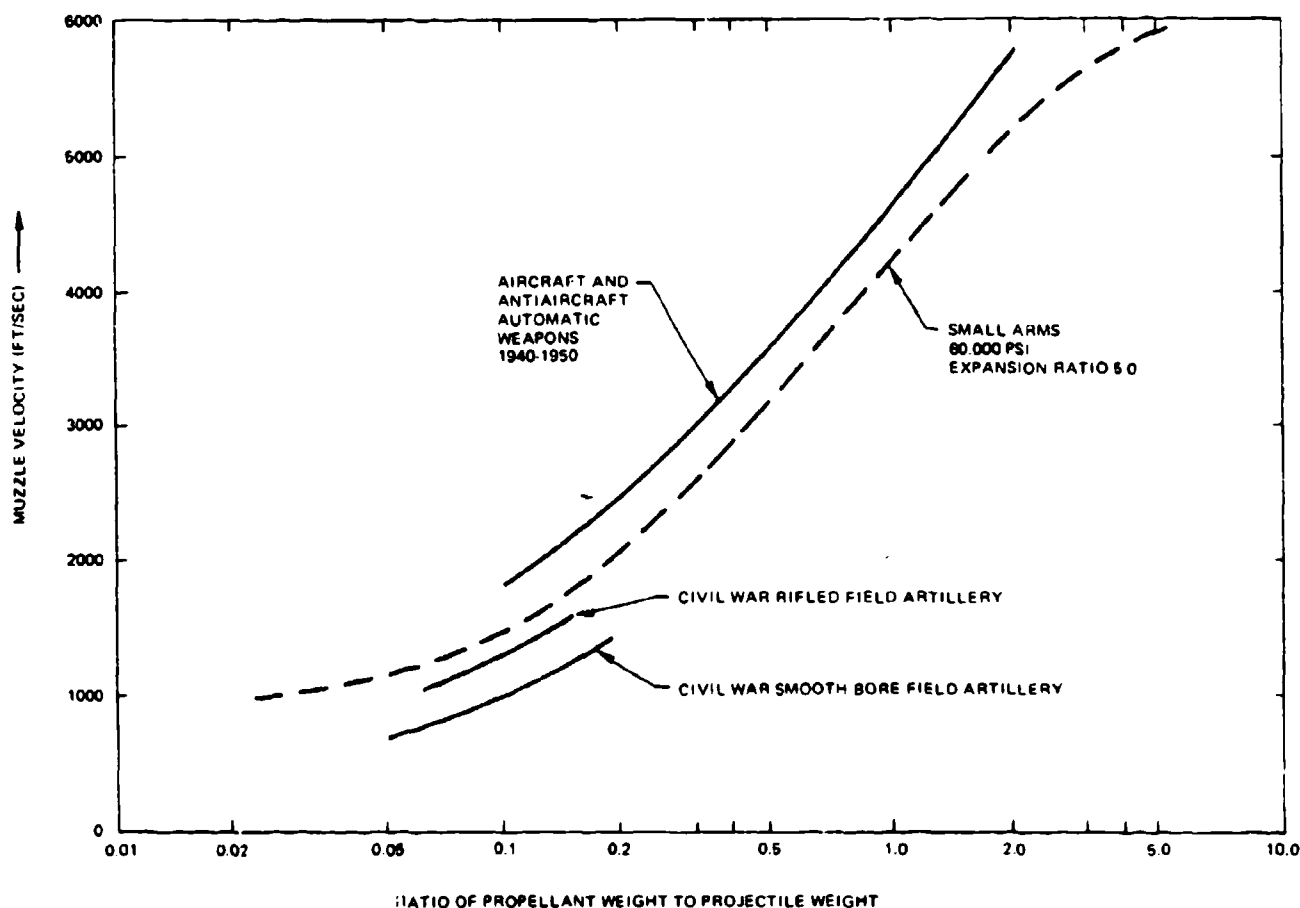
Figure 8-4. Muzzle Velocity versus Propellant/Projectile Weight Ratio

As noted in Section 8.1, the projectile weight for a given shape and caliber decreases as the % of HE filler is increased. High filler capacity is desirable for terminal effect, but the amount by which the projectile wall can be thinned is limited by the pressures exerted on the projectile during firing. In World War II German development produced 'Mine' projectiles which could be fired at 3000 f/s with 30% HE content by weight. This development was apparently never fully exploited in the United States and it is doubtful that any current U.S. antiaircraft projectiles approach the % filler content of the Swiss Oerlikon 35-mm projectile.

The muzzle velocity attainable is also increased by increasing the maximum pressure in the gun and there

has been a moderate increase in maximum pressure by use of improved materials and methods of fabrication. A moderate additional increase is possible by increasing the gun's expansion ratio; this has the advantage of reducing muzzle velocity dispersion. It also leads to long tubes, with associated design problems.

Very high muzzle velocities can be obtained by firing sub-caliber projectiles. Two designs for tank guns are shown in Figure 8-5, one for a spin stabilized and one for a fin stabilized round.[1] A sabot is required in each case; the pieces of the sabot fall in friendly areas and are a nuisance even when they do not cause friendly casualties. However this seems to be the only proven

8-6

current method of attaining very high velocities with gun fired projectiles.

The velocities obtained, however, can be quite high, in spite of the fact that the sabot is essentially dead weight, and its acceleration is another cause of lost energy. The Bofors 40-mm L/70 antiaircraft gun fires HE ammunition at 3280 f/s but can also fire APDS (armor piercing discarding sabot) ammunition against armor at 3950 f/s. At the expense of tube life, the 105-mm gun employed on the U.S. M60 tank can fire a 13 lb. APDS round at 4850 f/s compared with a 21 lb. HEAT projectile at 3850 f/s (muzzle energy in both cases is about the same).[1]

For a given diameter of the sub-caliber round, ... fin stabilized type can be designed to have a higher cross sectional density so that it will lose its initial velocity less rapidly. The disadvantage is the greater length of the round and a possible reduction in rate of fire. Both German and British development effort during World War II yielded 'arrow' projectiles for heavy antiaircraft guns. Effort along these lines in the United States was terminated in favor of surface to air guided missiles.

Making rough estimates from Figure 8-4, to obtain a muzzle velocity of 5000 f/s one would require a charge to projectile weight ratio of about 1.3/1. The complete round would weigh about 7.0 times the weight of the projectile. If one began with a 37-mm gun firing a full caliber projectile at 3600 f/s with a complete round weight about 2.2 times the projectile weight, one could obtain 5000 f/s with a projectile weighing 38% of the full caliber weight. This allows 10% for sabot weight. The sub-caliber projectile would be about 26 mm in diameter for conventional rotating design. For this type of design the complete round weight and dimensions might be kept approximately the same as those of the original full caliber projectile. Of course this estimate does not consider the very real problems of interior ballistics to provide matched propellant burning rates and maximum pressure, but this approach to high muzzle velocity may be feasible.

8.4 OTHER METHODS OF OBTAINING INCREASED MUZZLE VELOCITY

Losses in accelerating the projectile gases can be reduced by attaching the propellant to the base of the projectile. Problems associated with this type of design have not been solved.

Liquid propellant and 'light gas' guns have been considered but no design has been completed to operational feasibility, although the 'light gas' guns have been developed as research tools.

Gun fired rockets have been demonstrated to be feasible but for reasons which may not be associated

ARMOUR PIERCING DISCARDING SABOT (APDS)
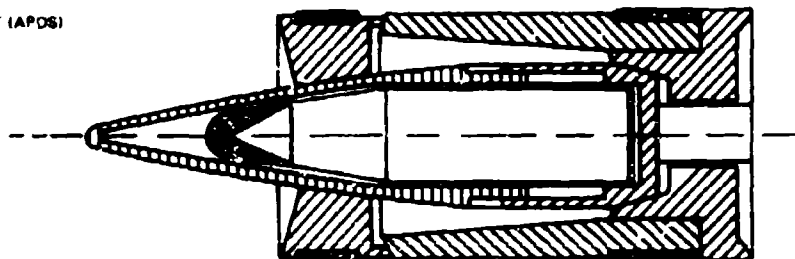
SUB-CALIBRE FIN-STABILIZED OVERLONG APDS
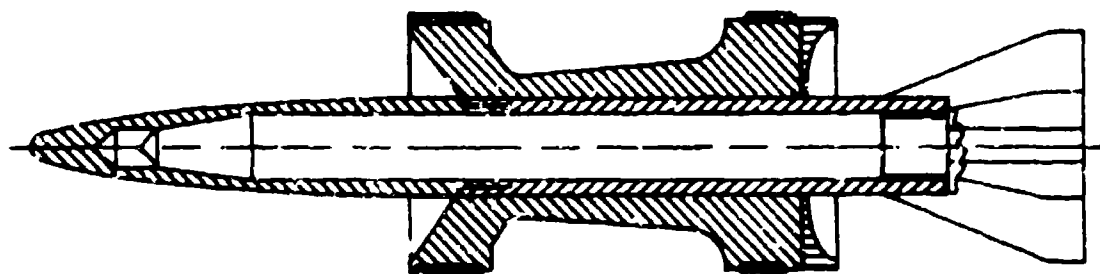
Figure 8-5. Typical Sub-Caliber Projectile Designs

8-7

with design feasibility, have not been accepted for operational use.

Periodically, unguided rocket launchers are re-examined as substitutes for guns. Very high burnt velocities can be attained, but angular and velocity dispersions have never approached gun accuracies. The current contender from this type of design is the Thomson-CSF Javelot, which associates a sophisticated fire control system with a multitube launcher firing 40-mm rockets.

In the case of a rocket, the velocity at the end of burning, v, if losses to drag during burning are neglected, is, for a single stage rocket,

$$v/v_m = Log_e[1 + (w_{prop}/w_e)] \qquad (8.10)$$

where v_m is a characteristic velocity of the propellant, w_{prop} is the propellant weight, and w_e is the weight of the payload and case after propellant is burnt. The maximum attainable velocity is, for very small payload ratios, limited only by the case weight, and burnt velocities of over 5000 f/s can be attained. In fact, as is now well known with multi-stage rockets, enough velocity can be developed to escape the earth's gravitational field.

German high velocity projectile development during World War II included:

a. Discarding sabot projectiles as discussed above, of which one design was 128/105-mm, in a spin stabilized design.

b. Ram jet powered projectiles, which obtained oxygen from the air rather than embodying it in the propellant as in a conventional solid rocket. This was tested in a 105-mm version.

c. Squeezebore projectiles, fired from a large chambered gun through a tapering barrel which 'squeezed-down' an over-diameter base plate and rotating band. One design was in 105/88-mm size.

d. Fin stabilized projectiles of various types, of which some were full caliber and some were subcaliber with discarding sabots. Designs tested ranged from 40-mm to 150-mm.

e. Rocket propelled spin stabilized, gun fired projectiles, one of which was tested in 280-mm size.

f. Bundles of sub caliber fin stabilized projectiles fired as a single round. This approach has been revived recently.[3]

Pictures of these designs will be found in a current publication.[6] The German technical data was secured after the war, and may still exist somewhere in the military archives.

Antiaircraft gun designs have been proposed recently, the details of which are proprietary, and which are believed to offer up to 6000 f/s muzzle velocity, very high rates of fire, low installed weight, and other advantages. Some of these options as considered by TRW Inc. armament designers have been reviewed in the literature[2] and include flechette-packed projectiles: 'trounds', and an open chamber gun for which 'the theoretical firing rate possible using the open chamber revolving cylinder feed combined with a 15-barrel gatling gun is 60,000 rounds per minute'.

8.5 WEIGHT PARAMETERS OF SELF-PROPELLED AIR DEFENSE SYSTEMS

Characteristics of both towed and self propelled predicted fire air defense systems are given in the Effectiveness Volume. In the case of a self-propelled version, the object is to give the fire unit mobility equal to that of the force it is designed to accompany. The vehicle on which the antiaircraft turret is mounted is almost always one developed for other purposes as well. Such vehicles used for air defense mounts include the German Leopard, the French AMX, the U.S. M113 series, the British Abbot and the Soviet PT-76.

The basic vehicle can be loaded up to the point where its ground pressure is no greater than that of other vehicles of the force to which it is organic.

J. Williams of the U.S. Army Tank-Automotive Command has given a simple formula which indicates the constraints on conventional tracked vehicle design which cause ground pressure to be very closely determined by all-up weight.[7] The expression is

$$W = (L/t) P (w^2 - k^2)/2 \qquad (8.11)$$

where:

W = maximum vehicle weight (lbs)

L = wheel base (length of track in contact with ground) (inches)

t = track tread (inches)

w = vehicle width across outer track edges (inches)

k = inner track span, established by chassis width limitations (inches)

P = ground pressure in pounds per square inch

The ratio L/t cannot exceed about 1.65 for good steering. The factor w is held to 124" for European transport. The factor k is held to about 80" for useful hull volume between tracks. This defines P in terms of W to fairly close limits.

Given the basic vehicle and a maximum ground pressure objective, the object is to fit the most effective

antiaircraft system into the available space and remaining weight margin.

Some current surface to air short range missile systems employ separate fire control and launch vehicles, but it is doubtful that this expedient will be accepted for future gun systems. Armor protection subtracts severely from the available armament weight budget. It is remarkable that technological improvements in radar, servo drives and power sources, and fire control have made it possible to build tracked, armored antiaircraft vehicles with both surveillance and tracking radars in the 25-35 ton all-up weight range.

8.6 EXTERIOR BALLISTIC TRADEOFFS

In making preliminary estimates of the effect of parametric changes on system performance the following ballistic characteristics are sometimes useful.

If one ignores gravity drop and variation of air density with altitude, and considers a family of homologous projectiles, i.e. projectiles of the same shape, but different calibers and weights, all fired at the same muzzle velocity, the range at which the projectile velocity has decayed to a specified value, such as sonic velocity is given by

$$D(v) = k(w_p/C^2) \qquad (8.12)$$

A rule of thumb is that the 'effective range' of a projectile defined as sonic range in meters is, for an average antiaircraft weapon, equal to 100 times the caliber in millimeters, i.e.

$$D_e = 100C \; ; C = \text{caliber in millimeters} \qquad (8.13)$$

Another rule of thumb, which has only empirical validity, but may be observed from firing tables to be remarkably good is that the sonic velocity range of a given projectile is closely proportional to the muzzle velocity, hence

$$D(v, v_o) = k_2(w_p v_o/C^2) \qquad (8.14)$$

SECTION 9
INTERACTION OF ATTACK AND DEFENSE OPTIONS

The object of a local defense is to raise the cost to an attacker of destroying a defended target to a level at which he feels that it is unprofitable to attack. In the absence of a defense, the attacker can use relatively inexpensive munitions and aircraft fire control. In the presence of a light to moderate defense, the attacker can use the same weapons, but release them at greater ranges from which they have less effectiveness. This requires a greater number of passes to destroy the defended target, and at some level of defense the cumulative losses become unacceptable to the attacker, and his only alternative to abandoning the attack is to employ more expensive stand-off weapons, call in ECM support or use other, comparatively costly means.

For a given tactical situation, with the simpler systems, such as conventional dive bombing, both the attacker and defense have tactical options with regard to bomb release range, and fire distribution doctrine of the defense. These interrelationships are examined in a game theoretic context, in the one attacker, one defender situation.

The more general situation of a number of defending fire units subjected to repeated attack waves by multiple attackers is next considered. Solutions are presented for a number of simple, idealized cases.

Components of the problem are then examined in some detail, namely the problems of what doctrinal or automatic fire procedures can be employed to improve the fire unit effectiveness in any situation, and finally, the determination of optimum dispersion for a fire unit.

In general, the expansion of the situation from the one on one engagement introduces a large number of additional parameters which tend to dominate the result. These include assumptions regarding the duration of a multi-pass attack, the number of attackers assigned, the defense commander's judgement regarding the relative importance of attackers sighted, and attackers expected, and the relative value which the attack commander places on destroying the ground target, as compared with the expected number of his aircraft lost in the process.

In attempting to develop preferred defense performance characteristics, the object is to find a set of characteristics which performs well over a wide range of likely tactical parameters. It is believed that the contents of this section develop a general analytical structure within which this objective can be pursued.

9.1 DEFENSE VERSUS DIVE BOMBING TYPES OF ATTACK

This section addresses the problem of the interaction of offense and defense tactics in a one-versus-one engagement under the following conditions.

a. The attacker attempts to destroy a defended target by releasing a munitions load at a release range of the attacker's choosing. His munitions have the characteristic that the greater the release range, the lower the probability of destroying the defended target in that pass. To shorten the verbiage, the defended target is called a 'bridge' and the munitions are called 'bombs'.

b. The defender attempts to protect the bridge by destroying the attacker before he can release his bombs. The defender's weapon system is characterized by a specified maximum rate of fire, and a specified allocation of number of rounds available to be fired against each attack pass. The defender has the option of choosing when to open fire, and how to distribute his available ammunition subsequently, subject to the maximum rate of fire limitation.

c. Both the attacker and the defender have a rule of thumb (or 'gut feeling') estimate of the relative value of the bridge and the attacking aircraft. This may be a different estimate for the two sides. In all of the subsequent analysis we assume that it is the same. This estimate leads to an expression for a 'payoff function': the relative value of the attack, considering the probability that the bridge will be destroyed, and the probability that the aircraft will be destroyed. The payoff is expressed in terms of the net return to the attacker; because of the above assumption, the payoff to the defender is the negative of the payoff to the attacker, and in game theoretic terms, the game is 'zero-sum'.

Then the attacker's object is to maximize the payoff function; the defender's object is to minimize it. It turns out that for a wide range of useful and fairly realistic situations, there is a minmax = maxmin solution, which can be obtained by game theory methodology.

In order to demonstrate the method of analysis the problem is developed in a form which allows previously determined solutions to be abstracted from the literature.[1,2,3] The results are sufficiently interesting indicate that additional analysis to expand the scope available solutions would be desirable.

9.1.1 Payoff Functions

Define:

K_d = probability that the bridge is destroyed in one pass

K_a = probability that the aircraft is destroyed before it can release its munitions

p_a = probability that the aircraft destroys the bridge in one pass if it survives to release its munitions

Q_a = $1-K_a$

q_d = $1 - p_a$

V_a = 'value' of the aircraft

V_d = 'value' of the bridge

Then for a single pass, a payoff function can be written as follows:

$$P = V_d K_d - V_a K_a$$

$$= Q_a [V_a + V_d p_d] - V_a \qquad (9.1)$$

This is the 'classical' payoff function for this problem.

Next consider the relationships if the bridge is subjected to repeated attacks until it is destroyed. The attack/defense tactics are assumed identical in each attack pass.

The probability that the bridge is destroyed in exactly 'n' passes is as follows:

$$K_{dn} = K_d \sum_1^n (1-K_d)^{j-1} \qquad (9.2)$$

and the expected number of passes to destroy the bridge is as follows:

$$\underline{N}_d = 1/K_d \qquad (9.3)$$

The average number of aircraft lost to destroy the bridge is as follows:

$$\underline{L}_a = K_a/K_d \qquad (9.4)$$

Since the bridge is destroyed, the payoff function is as follows:

$$P_2 = V_d - V_a (K_a/K_d) \qquad (9.5)$$

Note that K_a/K_d is the aircraft/bridge exchange ratio in a single attack pass.

If the attacker's objective is to destroy the bridge as fast as possible, i.e., in the minimum number of attacks, regardless of the cost in aircraft, from Equation (9.1), with $V_a = 0$,

$$P = V_d K_d \qquad (9.6)$$

and using this form is equivalent to using the number of passes to destroy the bridge as a payoff function.

When the aircraft has significant value relative to the bridge, the single pass payoff function, and the aircraft lost/bridge destroyed payoff functions may be compared by writing them in the forms as follows:

$$P/V_d = K_d [1 - (V_a K_a/V_d K_d)] \qquad (9.7)$$

$$P_2/V_d = [1 - (V_a K_a/V_d K_d)] \qquad (9.8)$$

It is not obvious that one of these functions is to be preferred to the other. In planning a series of missions, the air commander does not necessarily attack each target selected until it is destroyed. It may be possible, by an examination of the history of tactical air operations to obtain a better judgement of how commanders weight targets destroyed versus aircraft lost. Experience does appear to indicate that a commander with an available sortie rate attempts to maximize number of targets destroyed without exceeding some level of loss rate that depends, among other things, on the rate at which he can receive replacement aircraft.

The following examples use the payoff function given by Equation (9.1) and its simpler form, Equation (9.6); however, the method is not necessarily limited to these functions.

It should also be noted that the cost to the attacker is increased above that discussed above, by the aircraft which receive damage, and are lost after they have released their munitions, and by the cost of repairing surviving damaged aircraft, and by the hospitalization of wounded, surviving personnel. These additional costs can be introduced in a straightforward manner.

9.1.2 Game Theoretic Solutions

The following solution is found in the literature. The details and proof are given in the most useful detail in Karlin.[2]

Let:

$p_a(t)$ = probability that the attacker destroys the defended target if he releases his munitions at time t

9-2

$p_a(t) =$ single shot probability that a round fired by the defender kills the attacker at time t

$\nu(t) =$ defender's rate of fire at time t

$\nu_m =$ maximum rate of fire which the defender can achieve

$N =$ maximum number of rounds which can be fired by the defender

$V_d =$ value of the defended target

$V_a =$ value of the attacking aircraft

$P =$ 'payoff function' for the attacker. It is assumed that the game is zero sum, so this is the negative of the payoff function for the defender

$K_d =$ probability that the defended target is destroyed

$K_a =$ probability that the attacking aircraft is destroyed before it can release its weapon

$$P = V_d K_d - V_a K_a \qquad (9.9)$$

$P(\xi, \nu) =$ value of P if the attacker releases at ξ, and the defender uses a firing rate tactic $\nu(t)$.

$\phi(\xi, \nu) =$ probability that the attacker survives to ξ, if the defender uses a firing rate tactic $\nu(t)$

It is assumed that ϕ can be represented as

$$\phi(\xi, \nu) = e^{-\int_0^\xi \nu(t)p_a(t)\,dt} \qquad (9.10)$$

This is a good first order approximation which allows existing solutions to be employed as examples. The analysis becomes somewhat more complex if there is significant correlation between rounds, but it is still possible to obtain a game theoretic solution in the general case.

Then:

$$P(\xi, \nu) = [V_d P_d(\xi) + V_a]\, \phi(\xi, \nu) \cdot V_a \qquad (9.11)$$

As Karlin shows, a minmax/maxmin solution exists if the defender employs a 'pure' strategy, i.e. for a given set of tactical parameters the defender always uses the same $\nu(t)$, and if the attacker uses a 'mixed' strategy, i.e. he releases his weapon at a different range on each attack, choosing from a probability distribution df(t).

The expected payoff is then:

$$P(f, \nu) = \int_0^1 P(\xi, \nu)\, df(\xi) \qquad (9.12)$$

The problem is to determine $f(\xi)$ and $\nu(t)$.

Using Karlin's results, with a minor change in notation,

define:

$$b(t) = \frac{A'(t)}{A(t)p_a(t)} \;;\; A(t) = V_d P_d(t) + V_a \qquad (9.13)$$

The simplest solutions, and the ones given by Karlin, result when b(t) is a strictly decreasing function of time. In this case the defender fires continuously over one segment of the attack path. If b(t) is not strictly decreasing with time, the defender's optimum firing rate tactic may consist of several disjunct segments. The solution can still be obtained, but there are more details to consider.

b(t) defines the rate of fire required by the defense as a function of time. The defender fires at a rate (when he fires):

$$w(t) = \text{Min}\,[\nu_m, b(t)] \qquad (9.14)$$

Next define

$$w(d) = \nu_m \qquad (9.15)$$

If

$w(d) < \nu_m$ everywhere in (0,T), define d $=0$: the maximum rate of fire is never required

$w(d) > \nu_m$ everywhere in (0,T), define d $=T$: the maximum rate of fire is required over the whole path.

However, the system may not be able to achieve the above rates of fire over the specified segments, because of limited ammunition.

Define:

$$\int_0^T w(t)\, dt = N_0 \qquad (9.16)$$

This is the ammunition requirement to fire the optimum rate of fire schedule over the whole path. If the available ammunition $N < N_o$,

define:

$$\int_c^T w(t)\, dt = N \qquad (9.17)$$

This defines the time c at which the weapon opens fire. Because of the assumption that b(t) is strictly decreasing, once fire is opened it continues for the remainder of the path.

The form of the solution depends on whether the defender is ammunition limited or rate of fire limited. Results are summarized in Table IX-1.

9.1.3 Example of Application

A reasonable form for the defender's single shot probability is as follows:

$$p_a = \frac{A_v}{A_v + 2\pi \sigma_r^2 D^2 + 2\pi \sigma_o^2 \left[1 + 2(t_p/T_s) + 2(t_p/T_s)^2\right]}$$
$$(9.18)$$

where

A_v = aircraft vulnerable area

D = slant range

σ_r = random round to round ammunition dispersion

σ_o = standard deviation of tracking error

t_p = time of flight

T_s = fire control data smoothing time

The denominator can be expanded as a series in D', and by introducing the target, velocity v, the variable of integration in the game solutions can be changed to slant range D.

For a relatively simple example, we assume that m⋅ of the action will take place at a range where the :rm in the denominator dominates p_a, that the :t is flying down the line of sight, and is first uired at a very long range. We then approximate:

$$p_a = b_o/D^2 \left[1 \cdot (D/D_m)^2\right] \qquad (9.19)$$

where:

b_o = $A_v/2\pi\sigma^2$; σ^2 = an equivalent angular variance of the defense,

D_m = maximum firing range of the defense, limited for example, by some minimum projectile velocity.

It would be preferable to use Equation (9.18) in its complete form for comparative evaluations, but the simpler form Equation (9.19) allows simple analytic solutions to demonstrate the kind of results one can obtain from the game solution. The fact that p_a can exceed unity at very short ranges does not impair the solution.

The attacker's munition effectiveness is assumed to be expressed as

$$P_d = \frac{A_{vd}}{A_{vd} + 2\pi \sigma_d^2 D^2} \qquad (9.20)$$

and for this example, p_d is approximated as

$$p_d = a_o/D^2 \qquad (9.21)$$

We also assume that the only limitation on the range to which the attacker will approach is that resulting from his desire to maximize the payoff function, which includes consideration of the attacker's survivability. The consequences of arbitrary limits on minimum range are discussed later.

As a worst case for the defense, it is also assumed that $V_a = 0$; the attacker considers his own survivability only to the degree that he must survive to release his weapons.

Then the game solution can be obtained in closed form as a set of rather lengthy expressions which can be plotted simply in terms of three aggregates of parameters, K, A, and B,

where:

$$A = Nb_o/D_m^2$$

$$B = \nu_m^2 b_o/(4v^2 N)$$

$$K = (D_d/D_m)^2 (A^*)^{-1} \qquad (9.22)$$

D_d is defined as the 'effective standoff range capability' of the defense. It is that range at which an unopposed attacker would have the same probability of killing the defended target as he has considering the

9-4

Table IX-1. Summary of Game Theoretic Solutions

Case	I	II	III
	Rate of Fire Limit	Ammunition Limit	Ammunition Surplus
Defender's Constraint			
Conditions	$N < N_0; c < d$	$N < N_0; c > d$	$N \geq N_0$
Defender's Rate of Fire Tactic	$v(t) = 0; 0 \leq t \leq c$ $= w(t); c \leq t \leq T$	$v(t) = 0; 0 \leq t \leq c$ $= w(t); c \leq t \leq T$	$v(t) = v_m; 0 \leq t \leq d$ $v_m \geq v(t) \geq b(t); d \leq t \leq T$
Attacker's Distribution Function of Release Times	$f(t) = \delta(t-d)\left[1 - \dfrac{p_d(c)}{p_d(d)}\right]; t=d$ $= 1 - \dfrac{p_d(c)}{p_d(t)}; d < t < T$ $= \delta(t-T)\left[\dfrac{p_d(c)}{p_d(T)}\right]; t=T$	$f(t) = 1 - \dfrac{p_d(c)}{p_d(t)}; c \leq t < T$ $= \delta(t-T)\dfrac{p_d(c)}{p_d(T)}; t=T$	$f(t) = \delta(t-d)$
Payoff Function	$A(d) \cdot \displaystyle\int_c^d v(t)p_a(t)\,dt$	$A(c)$	$A(d) \cdot \displaystyle\int_o^d v(t)p_a(t)\,dt$

20871-535A

9-5

combination of his survival probability and distribution of release ranges against the specified defense.

D_d therefore is an overall measure of effectiveness which includes both the effectiveness of the defense and the attack capability of the attacker. The larger D_d, the better the defense.

In computing D_d from K, if the point (A, B) lies above the tactical ammunition boundary, D_d is computed using the value of A* obtained by projecting back along a line of constant K from (A, B) to the boundary.

Solutions are shown in Figure 9-1. Note that the A, B plane is divided into four regions corresponding to 1) rate of fire limitation of the defense, 2) ammunition limitation of the defense, 3) tactical ammunition surplus of the defense: the defense has more ammunition than is required for the game solution, 4) absolute ammunition surplus: the defense has more ammunition than it can fire at its maximum rate of fire in a time D_m/v.

To make the example more specific, four defense weapon systems have been compared. Their characteristics are shown in Tables IX-2 and IX-3. The total weights of the four systems are roughly comparable. This example should not be considered an accurate evaluation of the weapons assumed, because of the approximate form of p_s used for Figure 9-1, but rather

the example shows how this kind of summary chart may be developed and used.

The 'rate limited' region is also ammunition limited: but in this region the maximum rate of fire of the gun is utilized. Effectiveness can be improved either by increasing rate of fire until the ammunition limit boundary is reached or by increasing ammunition load until the tactical ammunition boundary is attained. In general, if the system is in the 'rate limited' region, effectiveness is increased more by a given percent increase in rate of fire than by the same percent increase in ammunition load.

It is interesting that for the assumptions of the above analysis, the defender's firing rate tactics are independent of the bombing accuracy of the attacker, but depend only on the way in which that accuracy varies with range. This would not be the case if the full forms of Equations (9.18) and (9.20) were used.

9.1.4 Example of Parametric Variations

Since it is easier to increase the ammunition load on the mount than to change caliber, maximum rate of fire, etc., Figure 9-1 can be simplified by abstracting the tactical ammunition contour, and making a new chart which assumes that the defense system is always provided with at least enough ammunition to reach the 'tactical ammunition requirement' on a pass. This is shown in Figure 9-2.

$B = (V_m{}^2 b_0)/4V^2N \longrightarrow$

20871 187A
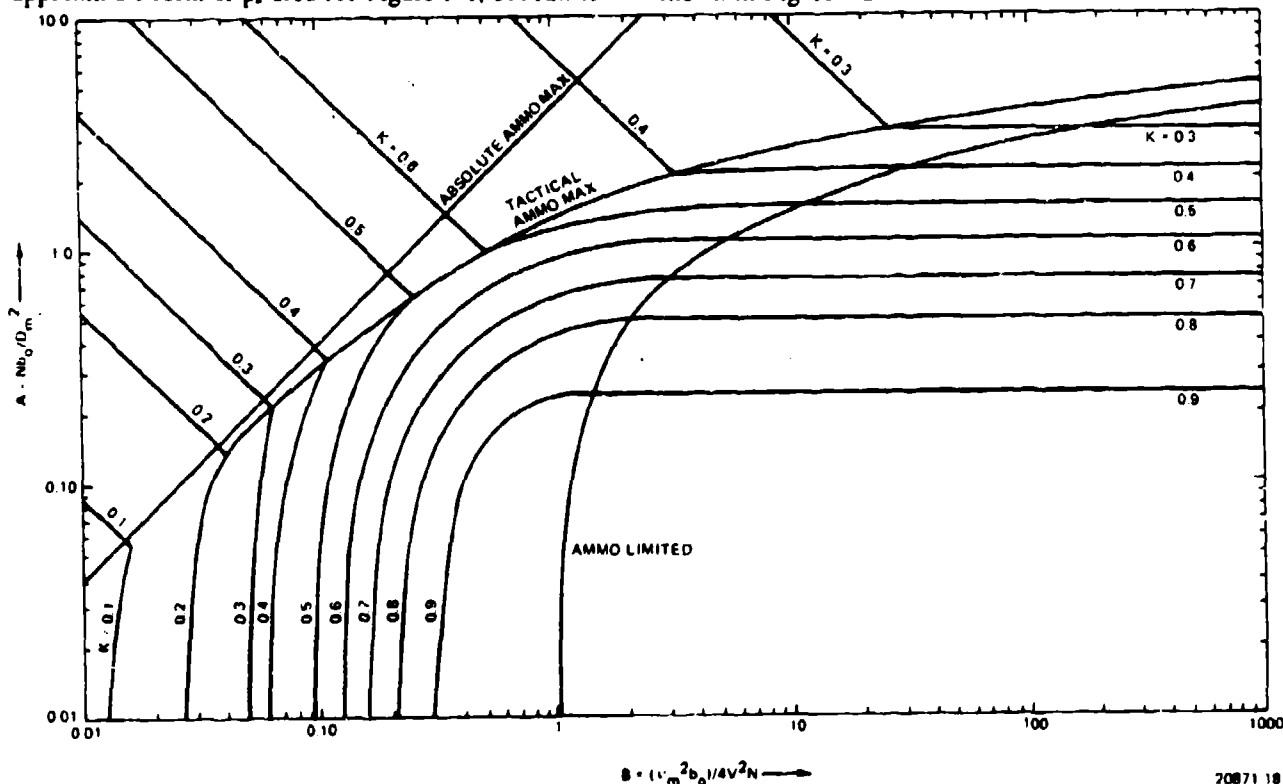
Figure 9-1. Game Theoretic Solution Chart

Table IX-2. Assumed Defense Systems Characteristics

System	Number of Fire Units	Armament/ Fire Unit	Maximum Rate of Fire per Fire Unit (rpm)	Rounds of Ammo per Fire Unit	Equivalent Angular Dispersion (mils)	Maximum Range (sonic) (meters)
A	3	1 X 20 mm Gatling	3000	1000	10	2000
B	1	2 X 35 mm	2000	350	5	4000
C	1	1 X 37 mm Gatling	3000	300	5	4000
D	1	2 X 40 mm Bofors	650	250	7	3900

20871-536

Table IX-3. Example of Effectiveness Comparison

		Effective Standoff Range D_d (meters)		
System	Target Vulnerable Area (meters^2)	With Specified Ammunition	With Unlimited Ammunition	Comments
A	1.8	1300	1300	Ammunition surplus, rate limited
B	4.0	2410	2600	Rate Limited
C	4.5	2590	3440	Rate Limited
D	4.8	920	920	Ammunition Surplus, rate limited

All cases: Target velocity = 200 meters/second

20871-537A

Using the relationship of Figure 9-2, a few examples of system design parameter tradeoffs may be provided. Assume a constant total weight of the defense system, and vary the caliber, keeping total weight constant. It is assumed that (based on Section 8)

a. The number of guns varies as $1/C^3$ for constant total weight.

b. Rate of fire varies as $1/C$.

c. Maximum range varies as C.

where C = caliber. The vulnerability function developed in Section 7.4.4 is used. Target speed is kept constant. If W_t = total defense system weight, the remaining parameter is W_t/σ^2. Figure 9-3 shows how D_d varies with σ for a constant value of W_t, and also with W_t/σ^2.

It was next assumed that the full caliber round in each case was replaced by a subcaliber spin stabilized discarding sabot round with characteristics as estimated in Section 8. Since the complete round weight was not expected to change, the gun's characteristics were not changed. However, the subcaliber round has a higher muzzle velocity. Maximum range was estimated assuming $D_m \sim Cv_0$; and there was little change in D_m since the subcaliber round lost velocity more rapidly.

σ was assumed inversely proportional to v_0. The subcaliber round also had a lower terminal effectiveness. Figure 9-4 shows the comparison. It was then assumed that it was possible to increase the % HE filler of the projectile from 10% to 20%. This lightened the round, so that it had a higher muzzle velocity, increased the terminal effect, and its lighter weight caused it to slow down to sonic velocity at about the same range as the 10% filler round. Figure 9-5 shows the comparison. The total improvement for the 'best' caliber was about equally derived from the terminal effect and the increased velocity.

The 20% filler projectile, subcaliber projectile and the 10% projectile are compared for the larger aim error reference in Figure 9-6.

Because of the rather gross approximations used in the expression for single shot kill probability on which these results are based and the assumption that for these cases, the value of the attacking aircraft is zero, one should not place too much confidence in the indications of the above comparisons, other than as illustrations of a method for evaluating the interaction between offense and defense options.

The observations, however, that the best caliber of weapon for a defense installation increases with assigned total installation weight and inversely with standard deviation of the shot pattern are reasonable.

9-7

1.0

0.10

0.01

0.01   0.10   1.0   10.0

$$M = \frac{V_M A_V}{4\pi\sigma^2 V D_M}$$
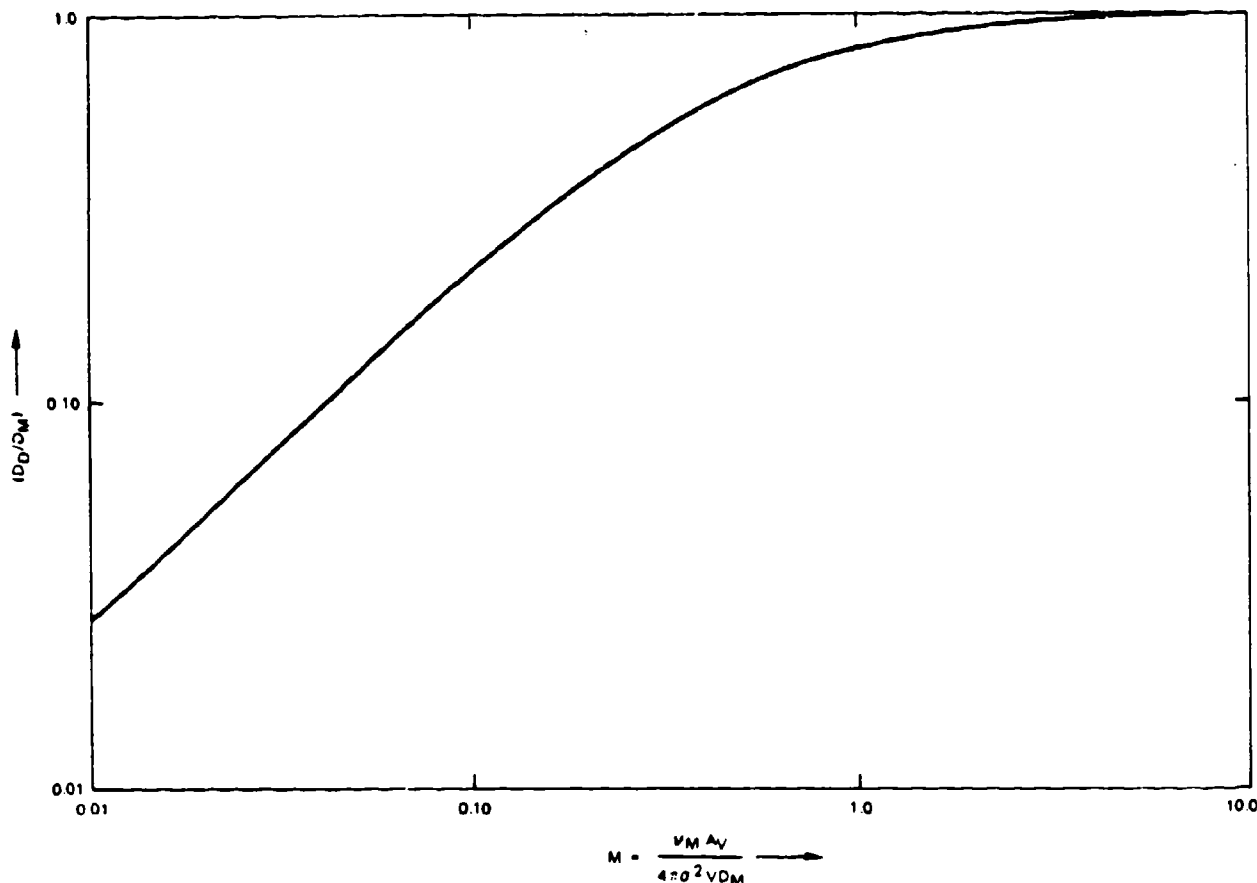
Figure 9-2. Simplified Solution Chart For Tactical Ammunition Maximum

as is the observation that the maximum standoff range which the defense achieves seems to be more sensitive to system accuracy than to any other parameter.

9.1.5 Effect of Non-Zero Aircraft Value

To obtain a rough idea of the effect of non-zero aircraft value on the game solution, a simpler case was solved, for which $D_m = \infty$, and the gun was assumed to have unlimited rate of fire. The latter might correspond to a rocket battery, for example.

The characteristics of the solution then change in the following ways:

a. The gun opens fire at a range which increases rapidly as the ratio V_a/V_d increases. If the aircraft is worth twice the ground target, the gun's opening range is increased almost by a factor of 4.0.

b. The maximum rate of fire required of the gun is reduced about inversely as the opening range. Hence the gun is less likely to be rate of fire limited.

c. The probability that either the aircraft or the ground target will be destroyed in the engagement both decrease. The numerical exchange ratio ground/air decreases, but the value exchange ratio increases, approaching unity. These

9-8
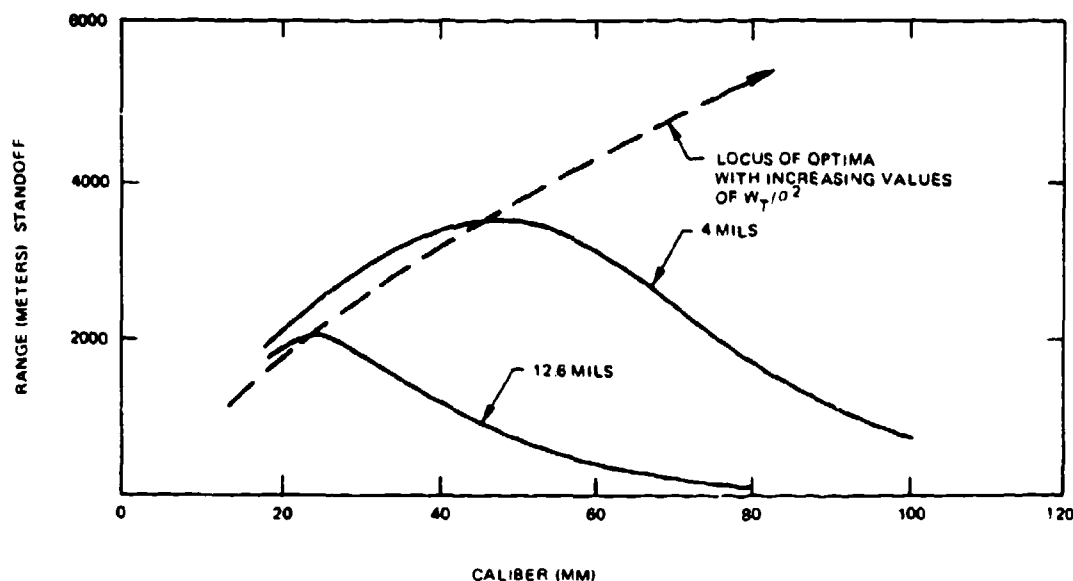
Figure 9-3. Effect of Caliber and Accuracy on Stand-Off Range

values are shown in Figure 9-7 and 9-8 for a particular set of parameters.

9.1.6 Effect of Minimum Release Range

The easiest tactical constraint to apply to the attack aircraft, and one which is apparently used operationally is the specification of a minimum release range or, equivalently, altitude. The parameters of Figure 9-1, based on zero aircraft value, lead to very high aircraft loss rates, approaching 50%. This would be unacceptable except against extremely important ground targets (such as nuclear stores, for example), although it represents a 'worst case' for the defense.

The payoff function may be rephrased as follows: An 'acceptable' loss rate per attack is established, such as 5%. The game solution is obtained as a function of release range, and that solution is chosen which yields a 5% aircraft loss rate. This problem has not been worked completely, but a preliminary examination indicates that over a useful range of parameters the solution reduces to a very simple form, which has the following characteristics:

a. The gun always fires at its maximum rate and opens fire at that range that will produce the specified aircraft attrition rate by expenditure of the available number of rounds of ammunition.

b. The aircraft always releases its weapons at the same range, i.e., that corresponding to the specified attrition rate.

This solution does not appear to have strong 'game stability' and more analysis of its characteristics is required.

9.1.7 Repeated Attacks

One of the deficiencies of the available solutions to this 'game' as utilized above, is that it is assumed that the gun always uses its available ammunition, even though the aircraft may be destroyed early in the engagement. Depending on the ability of the defense to recognize a kill and stop firing, the solutions may be conservative from this point of view.

A second consideration has to do with the expectation of additional attacks, the number of rounds on the mount, and the reload time. The gunner may prefer to fire less than this available ammunition at an attacker to avoid having to reload after each attack. The analysis then should include consideration of the relative weight given by the gunner to the need to destroy an attacker in sight as opposed to others expected, but not yet within range.

Similarly with multiple fire units, the defense must decide whether all fire units fire against each attacker, or attack echelon, or whether no more than one fire unit is assigned to each attacker.
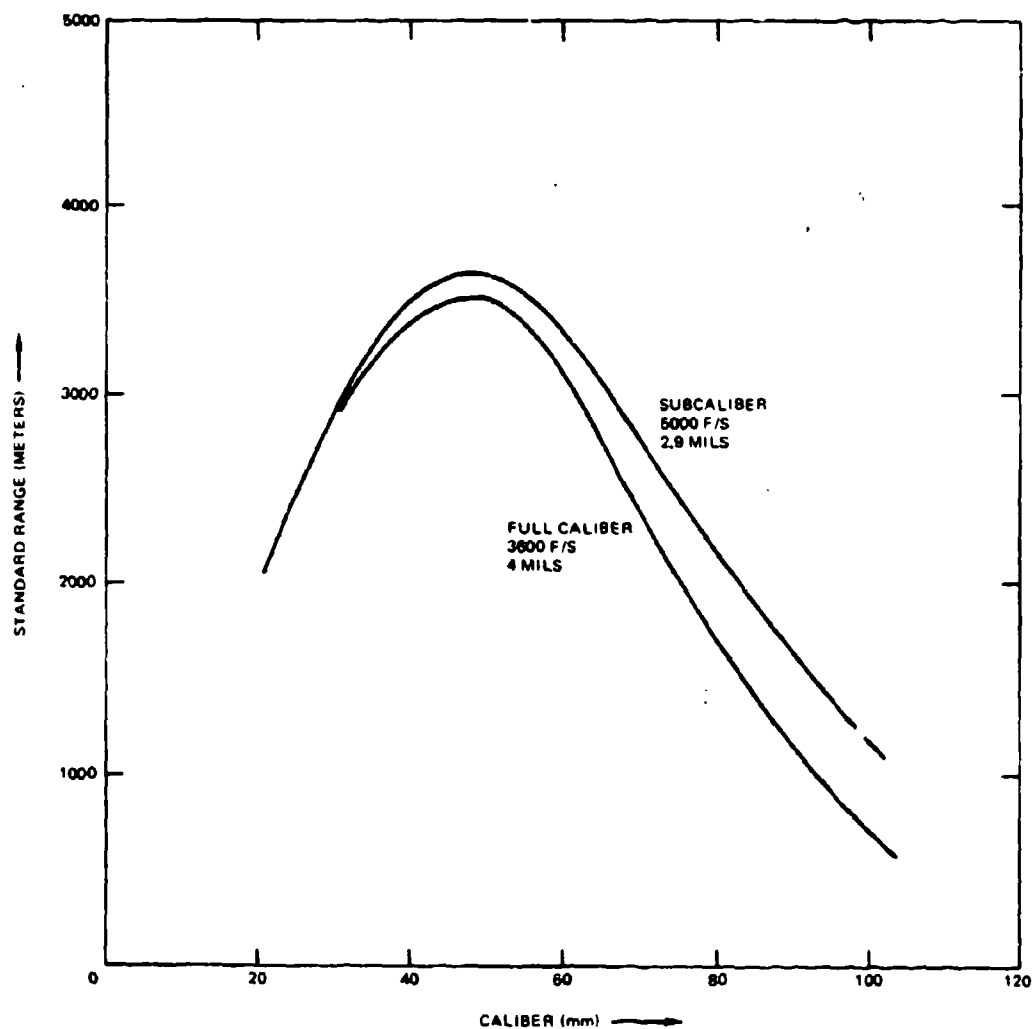
Figure 9-4. Comparison of Conventional and Sub-Caliber High Velocity Rounds

20871 190

These considerations are amenable to analysis. The principal unknown is the relative importance to assign to the bird in the hand since it is largely a matter of the commander's judgement whether there are other birds in the bush.

9.1.8 Discussion

In addition to the constraints already noted in the above derivations, one additional extension may be noted, namely the possibility of using a mix of defense weapons to provide a defense in depth. Current doctrine envisions the use of surface to air missiles for area defense, including Hercules for very long range and high altitude coverage, Hawk for medium zone coverage, and Chaparrel in conjunction with Vulcan. These outer defenses establish a loosely defined maximum 'standoff range' which might be required of the predicted fire weapons. The object in overall system design would therefore be to provide the least cost standoff system which pushes the attacker back into the missile region.

The methodology developed fits this definition of the problem also.

In general, the game theoretic formulation appears to describe the interaction between defense firing doctrine, and attacker weapon release range for iron bomb dive and glide attacks sufficiently well to justify more

9-10
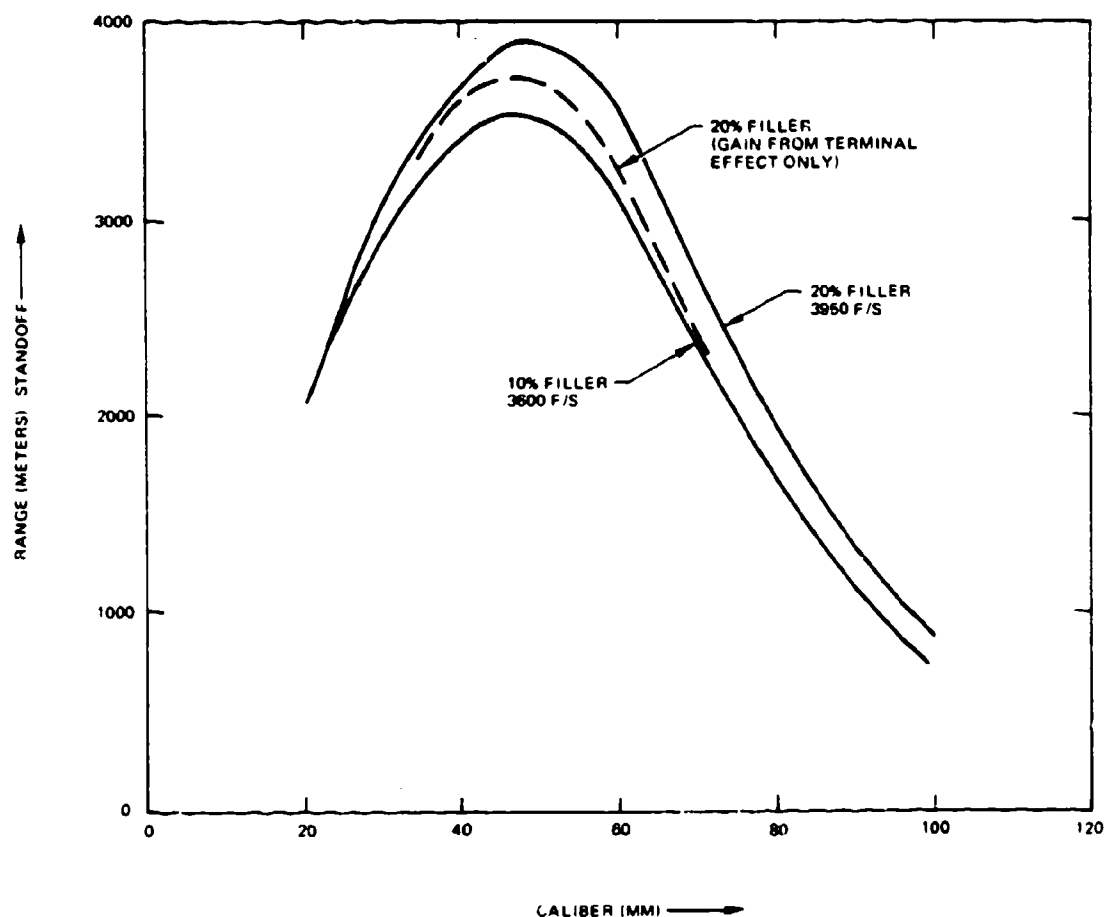
Figure 9-5. Comparison of Projectiles with 10% and 20% High Explosive Content

analysis with more accurately defined probability functions than it has been possible to provide in the present effort

9.2 MULTIPLE DEFENSE UNITS AND MULTIPLE ATTACKERS

In the one on one engagement computations the analysis emphasizes characteristics of the single fire unit such as rate of fire, initial acquisition time, hit probability as dependent on range, target speed and path, and lethality of the projectiles given a hit.

Expanding the problem to include multiple targets and multiple defense units emphasizes time to recognize a kill and time to switch to a new target, coordination of fire, defense deployment, coordination of enemy attacks, fire unit reload time and time to change gun barrels, etc.

The problem can be worked at various levels of detail. One might, for example, incorporate existing one on one engagement simulation models in a higher level simulation which traces the history of each of a large number of attackers on specified attack paths and the survival history of the defended vital area.

For present purposes a simpler formulation is utilized to develop the interactions.
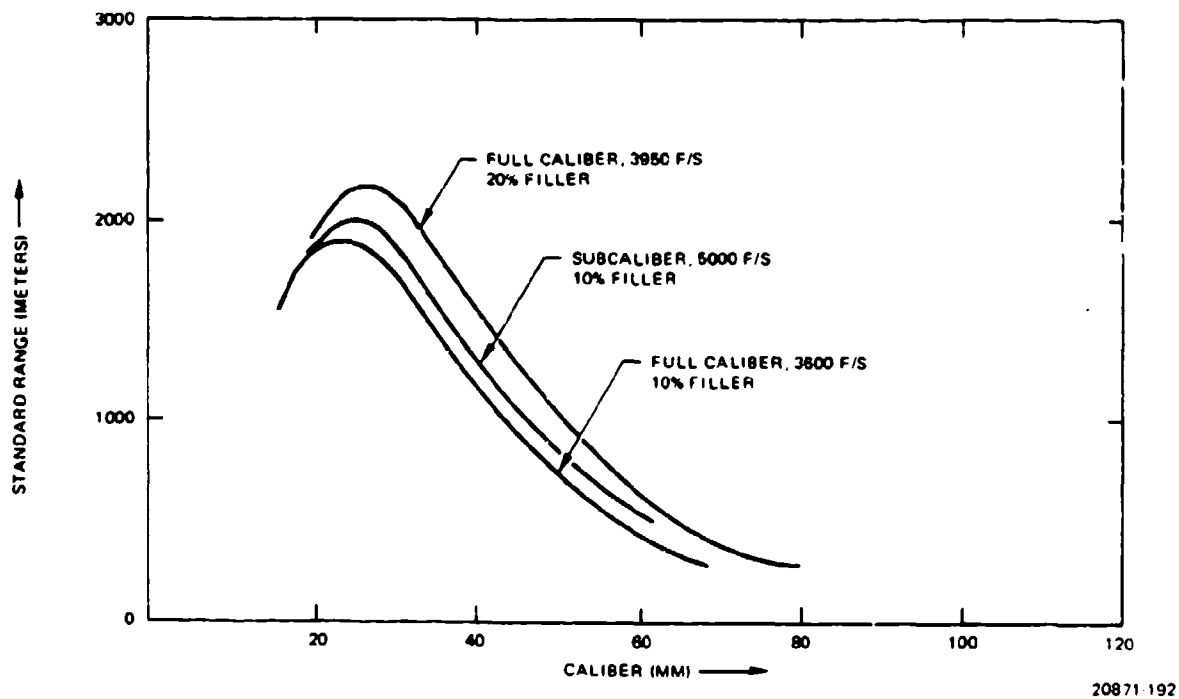
Figure 9-6. Comparison of Caliber, Subcaliber, Muzzle Velocity and Filler Weight
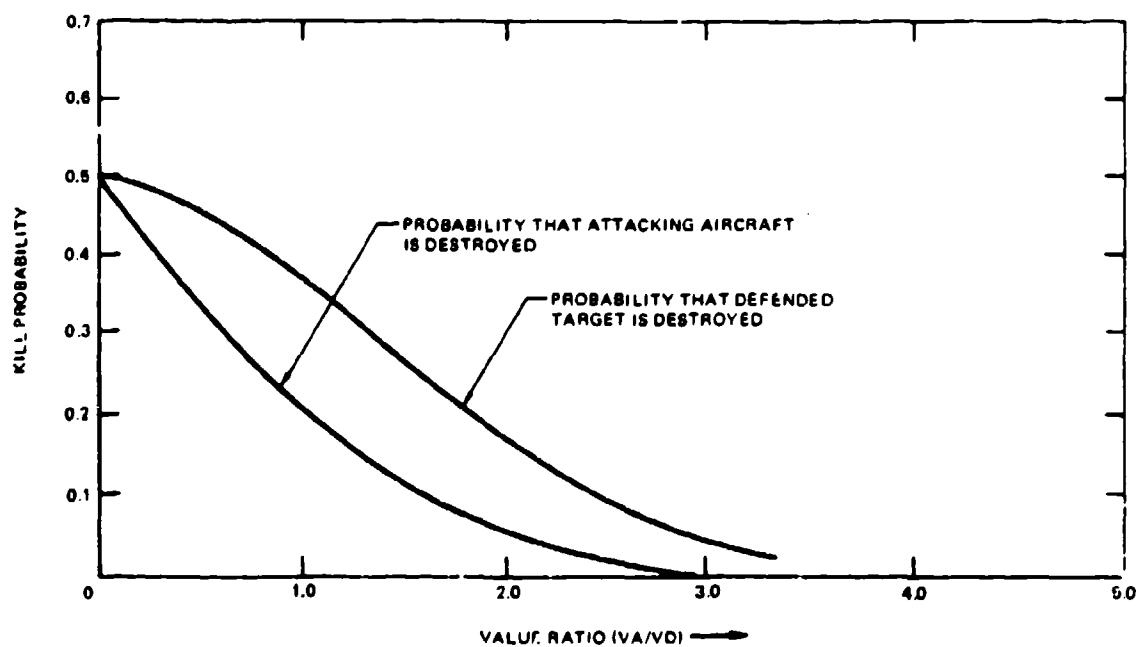
Figure 9-7. Effect of Value Ratio on Kill Probabilities
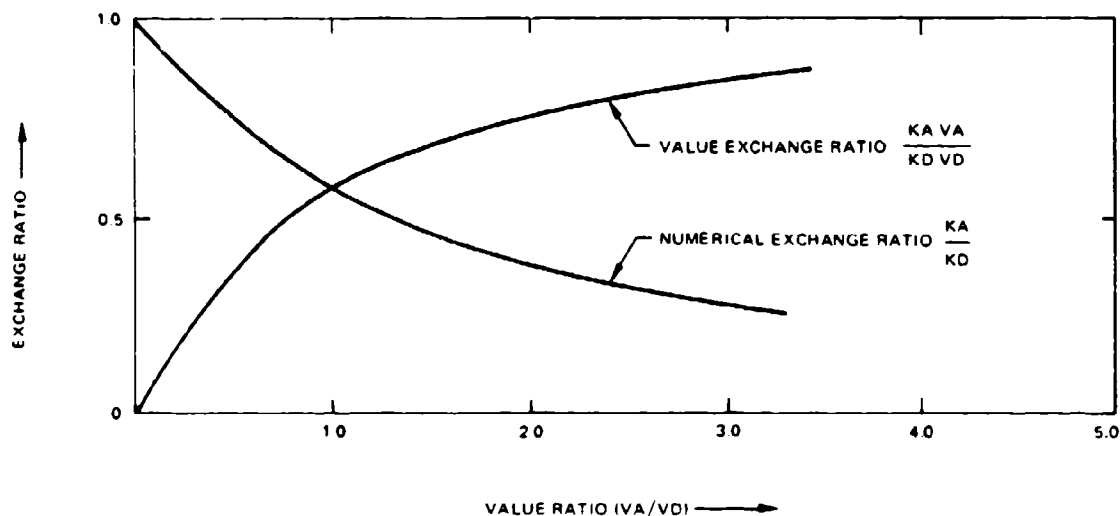
Figure 9-8. Effect of Value Ratio on Exchange Ratios

20871-194

3.2.1 Defense Configuration and Attack Patterns

The general principles of deployment of predicted fire units about a defended 'vital area' are developed in FM-4 -3 and will not be repeated here. Individual defense configurations depend on the number of fire units available, the size and shape of the defended area, local terrain configurations, the presence of other air defense weapons, and the expected directions of enemy air attack.

In general, the objective is to provide a defense configuration which is equally effective against all of the attack options available to the enemy.

Figure 9-9 shows an idealized balanced defense using four Vulcan fire units, and Figure 9-10 shows an idealized defense in depth using twelve fire units.

The pattern of enemy attacks depends on the number of aircraft assigned to the attack, the type of munitions employed, and the size of the defended vital area. If the vital area is small, only one attacker at a time can run an attack pass, although one could imagine a tactic in which two or three aircraft at a time begin the run, to diffuse the defense, with only one aircraft releasing munitions. Successive attack echelons would be as closely spaced as possible, to take advantage of the time lost by the defense in acquiring new targets, and in reloading the fire units. A model of this type of attack is given in the Effectiveness volume.

MAX EFFECTIVE
RANGE OF WEAPON

20871-195

Figure 9-9. Idealized Defense with Four Fire Units

9-13

20871-196

Figure 9-10. Idealized Defense with Twelve Fire Units

defense is 'balanced'. From an analysis point of view, defense effectiveness up to munitions release may be simplified by assuming that only one weapon fires at an attacker and that the attacker's ground track passes through the weapon. The fine details of effectiveness of the defense vs. direction of attack can probably be reserved for later studies of how far the weapons should be placed from the center of the vital area.

In the case of the heavy defense (Figure 9-10) a similar single direction of attack may be used for a first order analysis, with the defense kill rate vs. range based on the sum of the kill rates of the in-line fire units, both related to target range from the vital area.

Referring to the stand-off range measure of Section 9-1, the effect of placing the weapons of Figure 9-9 at an average of 0.5 to 0.7 times an 'effective range' from the center of the vital area is to impose an additional handicap on a dive bomb attacker. This factor can be included in the equations of Section 9.1 by a minor modification to degrade the attacker's munitions effectiveness bv the additional distance that they must travel from release at a specified point of defense effectiveness. Similar considerations apply to the heavy defense of Figure 9-10.

9.2.2 Allocation and Duration of Fire

Inherent in the determination of how long to fire at a target that has been acquired is the defense estimate of the relative value of the defended target, and the value of the attacking aircraft. Once the attacker's munitions have been released, additional firing does not contribute to the protection of the defended area against that pass, and the effectiveness of subsequent rounds probably drops off rapidly as the aircraft goes into his escape maneuver. However kills in the post-release phase prevent that aircraft from reattacking, and increase the cost to the enemy of the operation. On the other hand, if other attackers are sighted, or confidently expected, it would probably be preferable to save ammunition for defense against them. These qualitative judgements tend to dominate the decision.

Another consideration, directly related to the choice of caliber, is the question of whether hits on the attacking aircraft can be observed, and their effects quickly determined. To explore this problem, the following sequence of probabilities might be evaluated.

a. Probability of getting a hit (or more than one).

b. Probability of observing that a hit was obtained.

c. Probability of stopping the attack with rounds on the way or already fired if no hits were observed.

d. Probability of stopping the attack given that hits have already been observed and only those on the way remain.

If the vital area is large, many aircraft can attack at once, each with an assigned aim point, or using pattern bombing. The only limit on the number of aircraft in the attack formation would be that fixed by individual aircraft station keeping.

For predicted fire weapons with a maximum effective range of a few thousand meters, it is believed that an attack pattern consisting of successive closely spaced echelons of from one to four aircraft per echelon is most likely. This is, however, subject to validation by persons with tactical air experience.

Considerable use is made in the Effectiveness Volume of a model based on descriptions of heavy air attacks on Malta in World War II, briefly described as follows:

'On an average there were 170 bombers over every day, Ju88s and Ju87s coming in waves of twelve to fifteen at a few minutes' interval from a variety of directions, sometimes making for a single objective, sometime for several...'

In the case of a light defense (Figure 9-9) no more than two fire units will be able to engage an attacker before he has released his munitions, in most cases. If one adds the expected number of kills vs. range, the pattern is roughly circular with approach direction and corresponds roughly to that of a single weapon in the vertical plane of the approach path. In this sense the

)-14

e. Probability of observing interruption - abort, - of the attack.

In the case of each event noted, one must make estimates of the time from the to an observable effect.

The ability to observe a killing strike on an attacking aircraft is important for two reasons:

a. It conserves ammunition, and since most modern predicted fire weapons have a greatly higher firing rate than reload rate, this increases the number of targets that can be engaged in a heavy sustained attack before the fire unit goes out of action to be reloaded.

b. It frees the weapon for assignment to a new target. The more advanced of the current local air defense systems have the capability of tracking several attackers simultaneously in the surveillance unit. This greatly shortens the time required for a newly freed fire unit to acquire and open fire on a new target, based on information and assignment from the commander at the surveillance unit. Hence early kill recognition allows more targets to be engaged in a heavy attack.

The observability of kills requires more analysis in conjunction with sensor characteristics. They may be more difficult to observe with radar than by visual observation. It may be possible to process tracking data from the radar, however, to indicate a kill when the target acceleration or velocity become inconsistent with controlled flight. If the system employs a means of projectile tracking, it may be possible to observe hits, and possibly kills.

Since the result of these considerations must lead to simple rules which can be easily implemented in operation, a possible set of rules might be the following:

a. Doctrine that a target is always dropped when it has released its ordnance, provided that another target is available.

b. Doctrine that 'X' rounds will be fired at each target. One of the SAM systems has a doctrine of firing X rounds then switching to a new target without awaiting the outcome.

c. Cease fire at target on observing target kill. Kills with Ca' 0.50 are often slow to produce observable effects. Kills with contact fuzed 57mm HE rounds will usually be easier to identify.

9.2.3 Simple Stochastic Model of System Loading

In order to obtain an initial appreciation for the interaction of parameters, a simple stochastic model is defined as follows:

a. A 'Volume of interest' is arbitrarily defined. It

may, for example the volume of space bounded by the surface on which targets are first exposed to the defense sensors.

b. The probability that an aircraft enters in volume in a small interval of time dt is λ dt. The probability that it leaves in a small interval of time is μ dt.

Note that the realism of this model can be improved by nesting a set of volumes, to define target exposure and initial maneuvering for position, the attack pass, and the space of weapon release points. Entry and exit of each can be defined as in the simple case, but with different coefficients for each volume. The defense parameters of acquisition, kill probability, etc., can be assigned appropriate values for each volume. This approach is developed in more detail in the Effectiveness volume.

In this expository model, the details of variation of kill probability with target range and flight path are suppressed and replaced by an average kill rate for the defense, when it is firing. Once the problem has been structured, these details can be incorporated to any level desired, but they tend to obscure the overall relationships which it is desired to illuminate in this section.

The fire/reload cycle of the fire units is approximated by assuming a statistical model of the process, described in greater detail in the effectiveness report. Briefly, if a fire unit fires at a rate ν_0, and has N rounds of ammunition on board, it is assumed that the probability that it exhausts its ammunition in a short time interval dt is ν dt, where $\nu = \nu_0/N$. Similarly if it is in a reload state, with a capability of loading ρ_0 rounds per minute, the probability that reloading is completed in dt is assumed to be ρ dt, where $\rho = \rho_0/N$.

We first consider the implications of the above simple model on the number of aircraft in the defense volume as a function of time, ignoring observed destructions for the moment.

Define:

$P(\dot{m},t)$ = probability that there are m targets within the defense firing zone at time t

Then:

$$\frac{dP(n_t,t)}{dt} = \lambda P(m-1,t) + \mu (m+1)P(m+1,t)$$

$$- (\lambda + \mu m)P(m,t) \qquad (9.23)$$

$$\frac{dP(0,t)}{dt} = -\lambda P(0,t) + \mu P(1,t) \qquad (9.24)$$

9-15

Solve for the initial condition:

$$P(1,0) = 1.0$$

$$P(m,0) = 0; m \neq 1.0 \qquad (9.25)$$

and obtain:

$$P(0,t) = \left[1 - e^{-\mu t}\right]\left[e^{-(\lambda/\mu)(1 - e^{-\mu t})}\right] \qquad (9.26)$$

$$P(m,t) = e^{-M}\left\{(1 - e^{-\mu t})\left(\frac{M^m}{m!}\right) + e^{-\mu t}\left(\frac{M^{m-1}}{(m-1)!}\right)\right\} \qquad (9.27)$$

where

$$M = (\lambda/\mu)(1 - e^{-\mu t}) \qquad (9.28)$$

When t becomes very large:

$$P(0,\infty) = e^{-\lambda/\mu} \qquad (9.29)$$

$$P(m,\infty) = \left[\frac{(\lambda/\mu)^m}{m!}\right]e^{-(\lambda/\mu)} \qquad (9.30)$$

Summing [m P(m,t)] over m to get the mean number of aircraft within the defense zone at time t, we obtain:

$$\underline{m} = e^{-\mu t} + (\lambda/\mu)(1 - e^{-\mu t}) \qquad (9.31)$$

The first term represents the departure of the first aircraft (or wave) which initiated the combat phase. The second term represents the arrival of subsequent aircraft.

The mean spacing in time of arrivals is $1/\lambda$. The mean stay of an individual aircraft in the defense is $1/\mu$.

The probability of no aircraft in the defense at time t plots up as shown in Figure 9-11.

If the attacker allocates a total of M aircraft to the complete attack, both the build up and decay of the attack can be derived from a formulation following the above.

We now consider the interaction of this target model with the reload problem of a single fire unit, omitting considerations of observable kills and acquisition time.

Assuming that the gunner fires as long as there is at least one airplane in the defense zone, his opportunity to reload without penalty occurs when the state P(0,t) occurs.

In the steady state, the no-target state reoccurs on the average every:

$$T_f(o) = \frac{1}{\lambda P(0,\infty)} = \frac{e^{\lambda/\mu}}{\lambda} \qquad (9.32)$$

Its mean duration is $1/\lambda$.

For example, assume that the attackers are spaced on the average 10 seconds apart, and each remains in the defense zone for 20 seconds. In the steady state there will be an average of 2 aircraft in the defense zone. The zero target state will reoccur every 158 seconds on the average and will last on the average for 10 seconds. If, however, the attackers are spaced 20 seconds apart, there will be an average of one aircraft in the defense zone, the zero state will reoccur every 54 seconds, and, will persist on the average for 20 seconds.

Continuing now to the consideration of multiple targets and multiple fire units, the following mutually exclusive states can be defined.

Each Fire Unit:

    Ready, uncommitted
    Assigned target, attempting to acquire
    Firing
    Unavailable, being reloaded
    Unavailable, malfunction, under repair

Each Target:

    States Relative to Defense

        Undetected
        Detected, Unassigned
        Detected, Assigned to Fire Unit
        Engaged

    States Relative to Attack Phase

        Approach
        On Attack Pass, weapons on board
        Weapons Released, Evading

    States Relative to Survivability

        In Range, Surviving
        Destroyed
        Out of Range, Departing

The number of possible combinations of these states constitutes a formidable obstacle to continued development of the stochastic model, even in the simplest formulation.

Noting however, that the expected value expression, Equation (9.31) is easily obtained from a simple differential equation using expected values only, the analysis is simplified to a deterministic formulation in terms of differential equations, and this turns out to be tractable.
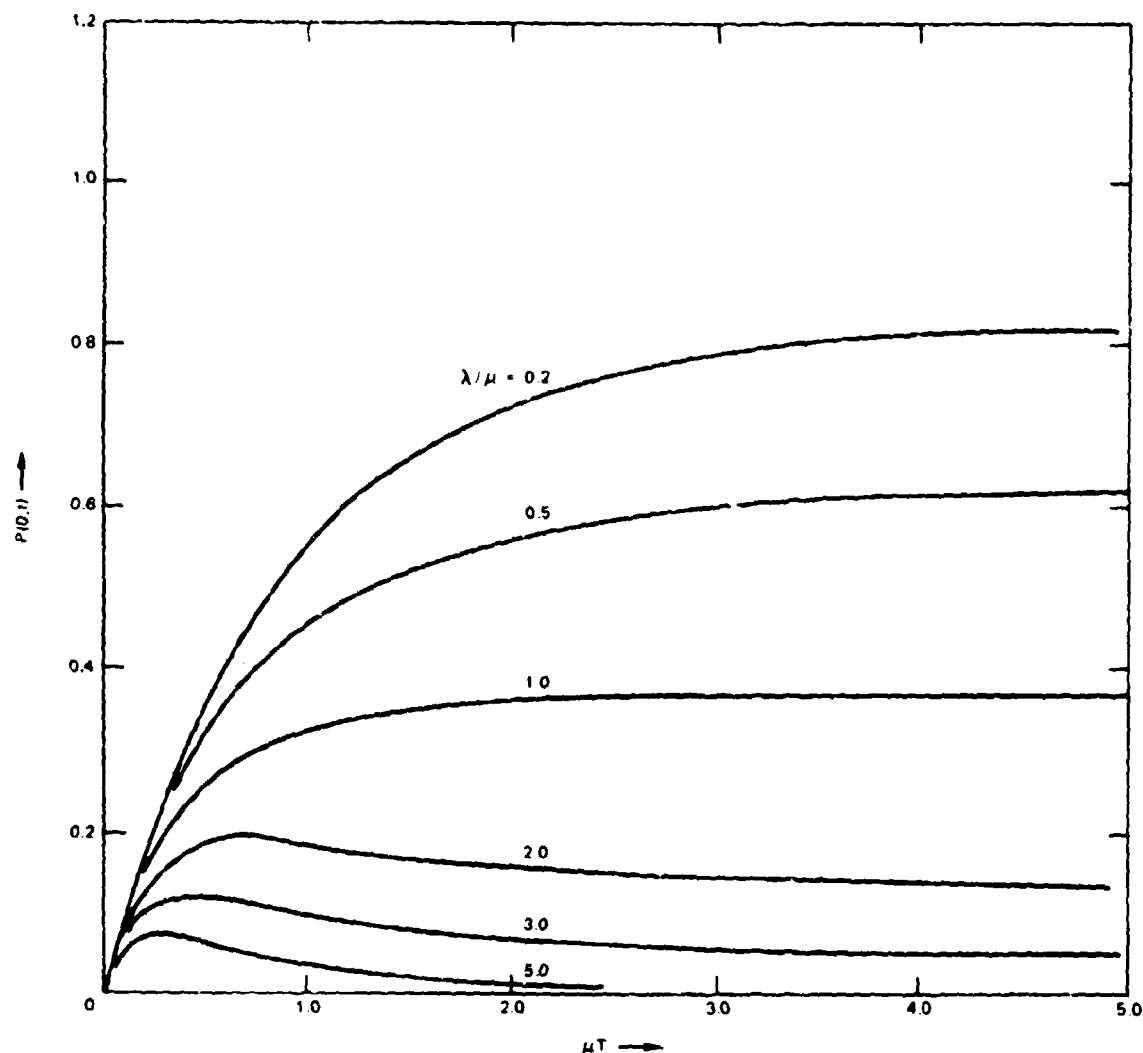
Figure 9-11. Probability of No Aircraft in the Defense Zone versus Time from First Arrival

20871-197A

9.2.4 Simple Deterministic Model

First consider the case where all guns attempt to fire as long as there is at least one target within the defensive volume. The fact that a target is being engaged already does not prevent a newly available fire unit from attempting to acquire it and fire on it. Targets are chosen at random.

Define:

n = number of fire units attempting to acquire a target at time t

n_r = number of fire units being reloaded

N_f = number of fire units firing

ν = average rate of ammunition consumption while firing per fire unit

p = average reload rate per fire unit

λ = target arrival rate

μ = target departure rate

k_1 = rate of inflicting observable kills by a single fire unit

k_2 = rate of inflicting delayed kills

m = number of targets within the defense volume at time t

N = total number of gun n the defense
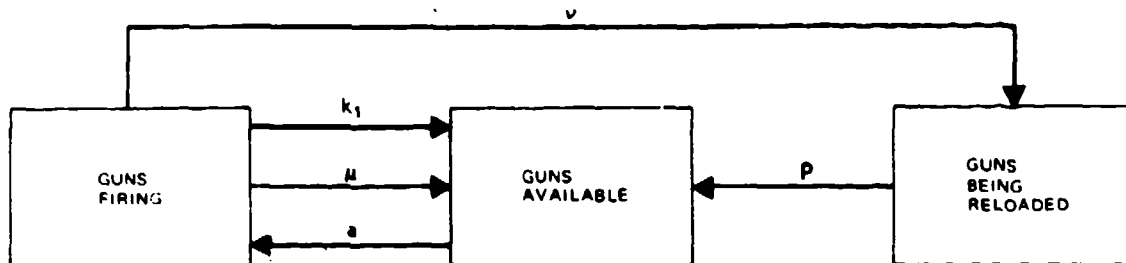
Figure 9-12. State Transition Flow of Defending Guns

a = target acquisition rate o one gun

Figure 9-12 shows the flow of guns among the firing, reload and acquisition states.

A gun firing leaves that state if it exhausts its ammunition, if its target leaves the defense zone, or if its target is observed to be destroyed. It enters the firing state when it acquires a target.

If there are n_t guns firing, and m targets, each target is fired at by n_t/m guns. The departure rate of m targets is μm, hence guns are released by target departures at a rate $\mu m(n_t/m)$. Similarly the kill rate on each target is k n_t/m and so observable kills free guns at a rate $k_t n_t$.

The differential equations describing the states are as follows:

$$\dot{n}_r = \upsilon n_f - \rho n_r$$

$$\dot{n}_f = a(N \cdot n_r - n_f) - (\upsilon + \mu + k_1) n_f$$

$$\dot{m} = \lambda - \mu m - k_1 n_f \qquad (9.33)$$

The term $k_t n_t$ represents kills observed to have been obtained during the engagement. In the case of delayed kills, the guns 'waste' ammunition, since they fire at an acquired target until it leaves.

Against a single target, fired at by n_t/m guns, the probability of obtaining a delayed kill is approximately:

$$1 - e^{-(n_f/m)(k_2/\mu)} \qquad (9.34)$$

since the mean firing time is μ^{-1}. Since targets leave the system at an average rate μm, the average rate of obtaining both observed and delayed kills is approximately:

$$\dot{m}_k = k_1 n_f + \mu m \left[1 - e^{-n_f/m\,(k_2/\mu)}\right] \qquad (9.35)$$

The steady state solutions are easily obtained by setting the derivatives equal to zero. Then one can determine the average number of guns firing, and the average rate of target kill. However, the steady state solution is useful only if one envisions a series of attacks continuing for a very long time. It is of equal interest to observe the system response from t = 0. Since Equation (9.33) defines the number of guns firing without regard for the number of targets in the system, it is easily solved to show the number of guns firing as a function of time from the initiation of the action.

This has been done, and the results are plotted in Figure 9-13 for the case of

$1/\mu$ = 10 seconds, = average target stay in the defense volume

ν = 3000 rpm = rate of fire of one fire unit

N_* = 500 = number of rounds on each mount when fully loaded

ρ = 120 rpm = reload rate of one fire unit

$1/a$ = 5 seconds, = average target acquisition time.

Figure 9-13 shows the fraction of fire units in the firing, acquisition and reload states as a function of time, for these numerical values. Initially all guns are attempting to acquire a target, then as they begin firing some exhaust their ammunition and enter the reload state. In the steady state, each fire unit spends only 3.7% of its time firing, but during most of the initial 20 seconds of the action, more than 20% of the defense is firing.

The importance of the judgement as to probable duration of the complete action is obvious.

9-18
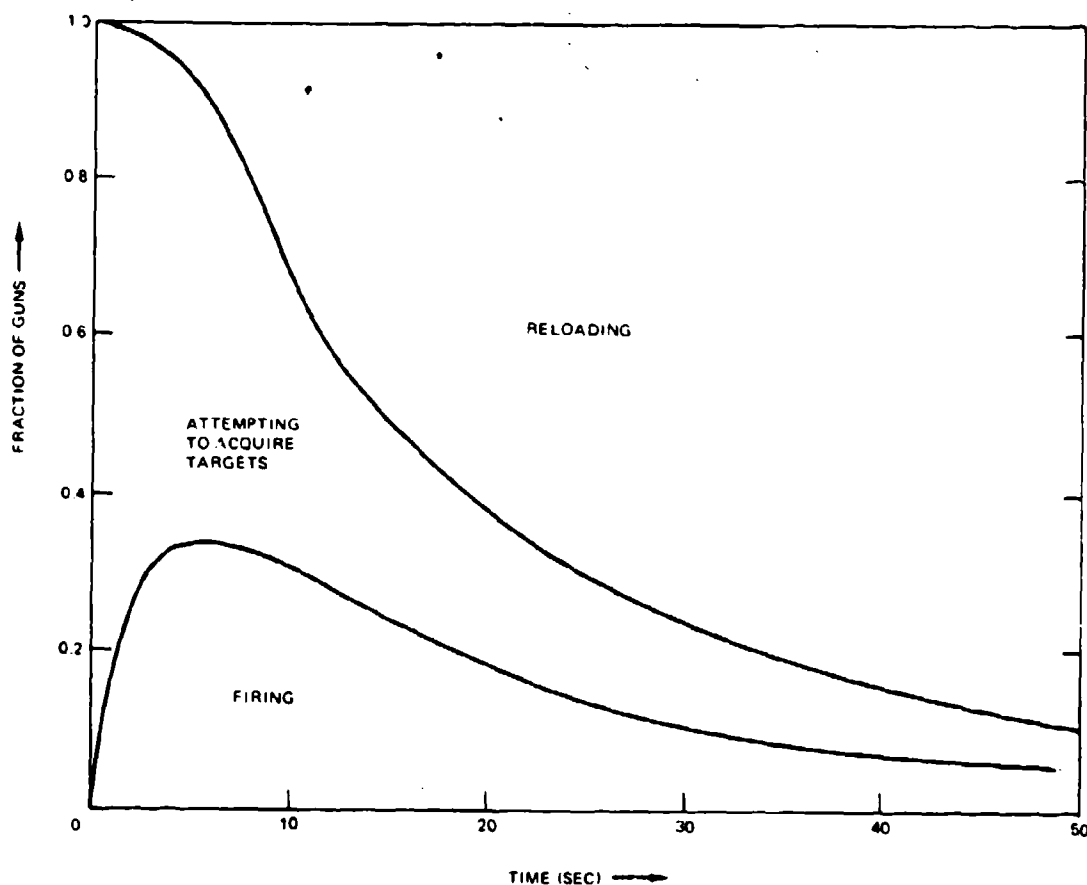
Figure 9-13. Defense System Activity States with System Saturation

Given the number of guns firing vs. time, the number of targets in the defense from Equation (9.33) and the target kill rate from Equation (9.35) one can go on to compute the expected number of targets killed vs. time.

9.2.5 Alternate Model

Instead of assuming that all guns attempt to fire at all targets within the defense volume, one may consider an alternate, and possibly more realistic doctrine of fire in which no more than one fire unit is ever assigned to one target.

The differential equations then become as follows:

$$\dot{n}_r = \upsilon n_f \cdot \rho n_r$$

$$\dot{n}_f = a(m \cdot n_f) \cdot (\upsilon + \mu + k_1) \, n_f \; ; N \cdot n_r \, m$$

$$\dot{n}_f = a(N \cdot n_f \cdot n_r) \cdot (\upsilon + \mu + k_1) n_f \; ; N \cdot n_r \, m$$

$$\dot{m} = \lambda \cdot \mu m \cdot k_1 n_f$$

$$\dot{m}_k = n_f \left[k_1 + \mu \left(1 \cdot e^{-k_2/\mu} \right) \right] \qquad (9.36)$$

Depending on the values of the parameters, the transient solution may have to be obtained in two parts, one for each side of the boundary $N \cdot n_r = m$.

9-19

This is easily done, and only limited time prevents a comparative numerical example here.

9.2.6 Conclusions

The relative simplicity of the deterministic model allows a moderate amount of additional detail to be incorporated before it becomes unwieldy. By its use a rapid preliminary investigation can be made of the relative effects of acquisition time, reload time, rate of fire, observable vs. delayed kills, etc. Considering the judgemental factors involved in laying out probable enemy attack details, they may be entirely adequate. In any case, the results obtained by their use may be used as first order approximations which may be used to indicate parametric sets for more intensive analysis in greater analytic detail, or by simulation.

9.3 DEFENSE FIRING DOCTRINE IMPLEMENTATION

This section considers some of the aspects of implementing a firing doctrine, once it has been chosen. It also addresses a problem that may not have previously subjected to analysis, namely if a target is being tracked continuously, and tracking has fairly well settled, how much of an advantage is gained if the weapon is fired only when the tracking error is within some specified value. For example, a gunner employing visual tracking might be instructed to fire only when his reticle is on the target.

9.3.1 Operator Choice of When to Fire

It seems reasonable to suppose that if the gunner of a man-controlled mount fires only when his reticle is on the target, he should have a higher probability of hitting than if his choice of firing time is unrelated to the tracking error at the firing time. However in a system with lead computation, the lead at any instant depends on the past history of tracking, with rates and possibly position averaged over the smoothing interval. Thus the prediction error at any instant depends not only on the observed error at that instant, but also on a weighted average of past errors.

In the following paragraphs we determine how much the variance of prediction error associated with a short burst is reduced if the burst is fired when the tracking error as observed is close to zero. The following assumptions are made:

a. Only the prediction error resulting from tracking error is considered.

b. It is assumed that the statistics of tracking error are the same, regardless of which firing mode the gunner uses. In fact, as noted elsewhere, he may track more accurately if he does not have the additional task of trying to decide when to fire. But this is an open question: he may try harder if he knows that he is more likely to get hits if he can get the reticle on target.

c. For simplicity, the analysis is done in a single coordinate.

Clearly, the result will depend on the amount of correlation between the tracking error and the prediction error measured at the same time instant.

Define:

$x_p(t)$ = prediction error at 't' resulting from tracking error history

$x_o(t)$ = tracking error at time 't'

σ_p^2 = variance of prediction error resulting from tracking error

σ_o^2 = variance of tracking error

R_c = covariance of prediction error and tracking error

ρ = correlation of prediction error and tracking error

$R_p = \rho \sigma_p \sigma_o = <x_p x_o>$

The marginal probability density function of x_p, given x_o is as follows:

$$f(x_p|x_o) = \frac{1}{\sigma_p \left[2\pi(1-\rho^2)\right]^{1/2}}$$

$$\exp \cdot \frac{\left[x_p - (\sigma_p/\sigma_o)x_o\right]^2}{2\,\sigma_p^2\,(1-\rho^2)} \quad (9.37)$$

Since in reality the operator is tracking in two dimensions, it would be more realistic to write the corresponding expression for a two dimensional probability density function, and this might be worth doing in a complete analysis, since the results could then be expressed in terms of burst kill probability. However, as will be seen the one-dimensional case is quite illuminating.

Next we may recognize that even in a one-dimensional problem, the operator could not respond quickly enough to fire when x_o is exactly zero. Hence it would be more realistic to integrate $f(x_p|x_o)$ over a pdf of x_o (small compared with σ_o). Likewise in the two dimensional case one would establish a ring within which the operator whould fire since he would never have both coordinate tracking errors zero at the same time.

To show the maximum possible gain, however, in the one-dimensional case we assume that it is possible to fire when $x_o = 0$, and so we need only determine $\sigma_p^2(1-\rho^2)$ and compare it with σ_p^2 to observe the improvement in aim variance with the firing doctrine described.

9-20

The simplest statistical description of the tracking error is assumed, namely a covariance:

$$R_0 = \sigma_0^2 e^{-u/T_c} \qquad (9.38)$$

and we shall determine the effect of varying T_c on the system performance with and without choice of firing instant.

Any linear prediction function can be described by the following:

$$x_p(t) = \int_0^\infty x_0(t-u)A(u)\,du \qquad (9.39)$$

where $A(u)$ is the response of the system to a unit

Then:

$$R_p = \langle x_p(t)x_0(t) \rangle$$

$$= \langle \int_0^\infty x_0(t)x_0(t-u)A(u)\,du \rangle$$

$$= \int_0^\infty R_0(u)A(u)\,du \qquad (9.40)$$

For the covariance given by Equation (9.38) R_p is therefore simply proportional to the Laplace transform of $A(u)$,

$$R_p = \sigma_0^2 A(1/T_c) \qquad (9.41)$$

The Laplace transform of Equation (9.39) is:

$$x_p(s) = x_0(s) A(s) \qquad (9.42)$$

and $A(s)$ is the well known 'transfer-function' of the smoother-predictor circuits.

The prediction variance σ_p^2 is:

$$\sigma_p^2 = \frac{2\sigma_0^2}{\pi} \int_0^\infty \frac{T_c}{1+\omega^2 T_c^2} |A(j\omega)|^2\,d\omega \qquad (9.43)$$

which we abbreviate:

$$\sigma_p^2 = \sigma_0^2 \mu \qquad (9.44)$$

and we also abbreviate:

$$R_p = \sigma_0^2 \lambda \qquad (9.45)$$

We are interested in the variance resulting with the designated fire doctrine

$$\sigma_s^2 = \sigma_p^2 (1 - \rho^2) \qquad (9.46)$$

and

$$\sigma_s^2 = \sigma_p^2 [1 - (\lambda^2/\mu)]$$

$$= \sigma_0^2 [\mu - \lambda^2] \qquad (9.47)$$

9.3.1.1 Numerical Examples

As examples, we choose 1) a predictor transfer function identical with that used in a gyroscopic lead computing sight, such as Vulcan. This function has the characteristic that it does not attenuate high frequency noise. For comparison, 2) a predictor transfer function with second order smoothing is assumed. This function does attenuate high frequency noise.

The transfer functions and the other expressions needed to compute σ_p and σ_s are compared in Table IX-4. In order to make the two transfer functions directly comparable, the second function is assumed to have a smoothing time coefficient proportional to time of flight, as is the case with the gyro sight function. In both cases the 'a' coefficient is taken to be 0.20: this makes the characteristic smoothing time proportional to 0.20 x time of flight.

Results are shown in Figure 9-14 for the gyro-sight type of prediction function. An arrow indicates the point on the abscissa corresponding to typical good manual tracking, for 1.0 and 2.0 seconds time of flight.

The improvement obtained in aim variance for the gyrosight type of system by firing when aim error is zero is significant.

The results for the second transfer function are shown in Figure 9-15. It is interesting to observe that this system performs almost exactly as well without choice of firing point, as the gyrosight type system does with choice of firing point.

Table IX-4. Comparison of Systems

System	Gyrosight Type	Second Order Smoothing
Transfer Function	$\dfrac{1 + s(1 + a)t_p}{1 + s\,a\,t_p}$	$\dfrac{1 + s(t_p + 2T_s)}{(1 + sT_s)^2}$; $T_s = at_p$
Tracking Error Autovariance	$\sigma_0^2 e^{-u/T_c}$	$\sigma_0^2 e^{-u/T_c}$
Variance of Prediction Error σ_p^2	$\sigma_0^2 \left\{ \dfrac{1 + x[(1 + a)/a]^2}{1 + x} \right\}$	$\sigma_0^2 \left\{ \dfrac{1 + x[(1 + 4a + 5a^2)/(2a^2)]}{(1 + x)^2} \right\}$
Covariance of Prediction and Tracking Error R_p	$\sigma_0^2 \left\{ \dfrac{1 + x[(1 + 1)/a]}{1 + x} \right\}$	$\sigma_0^2 \left\{ \dfrac{1 + x[(1 + 2a)/a]}{(1 + x)^2} \right\}$

Note $x = at_p/T_c$

20871-538A

However, even in the case of the second system, the choice of firing time provides a substantial improvement.

9.3.1.2 Discussion

It seems clear that in a manually tracked system, with choice of firing time under the gunner's control, it is preferable to fire when the reticle is on or very close to the target. If one automates the firing control this choice will not be possible, but tracking may be improved. If one provides an automatic tracking error measuring device, (for example in conjunction with an imaging sight) this can be used to control the firing instant. But the measurements of tracking error could equally well be used to close the tracking loop and provide automatic tracking. With automatic tracking the loop would be much 'tighter' than with manual tracking, the noise would have higher frequency content, and with good error filters, the additional improvement obtained by automatically choosing the firing instant in addition would be marginal, as shown by the right hand segment of the curves of Figure 9-15.

Consider the two-dimensional case. If we have a system with automatic tracking, and if we believe that the tracking error is a major source of error in gun orders, we might take the error signals from the sensor servos and process them so that firing would take place automatically only when the vector error has become smaller than some threshold value, and in addition has remained below this level for a short interval (say 0.50 second). This should provide a much larger improvement in prediction error due to tracking for the subsequent burst than is indicated in Figures 9-14 and 9-15. However one would need to investigate the frequency with which these intervals of low error occurred to determine whether an acceptable number of bursts could be fired against a typical target.

With a system that carried enough ammunition to fire continuously over the whole available firing time there is no anticipated advantage in firing only at selected intervals. For very high rate of fire systems, and in general for systems with relatively long reload times, there could be a substantial overall payoff, however, in firing fewer rounds and firing those when the tracking is very good.

9.3.2 Automatic Firing Algorithms

The more sophisticated fire control systems will have within the computer enough information to parallel the decisions that a human operator makes in deciding when to open fire, how long to fire, when to cease fire, etc. It is conceivable that the computer might in fact make better decisions. This section reviews some of the considerations in developing an automated fire system.

9-22
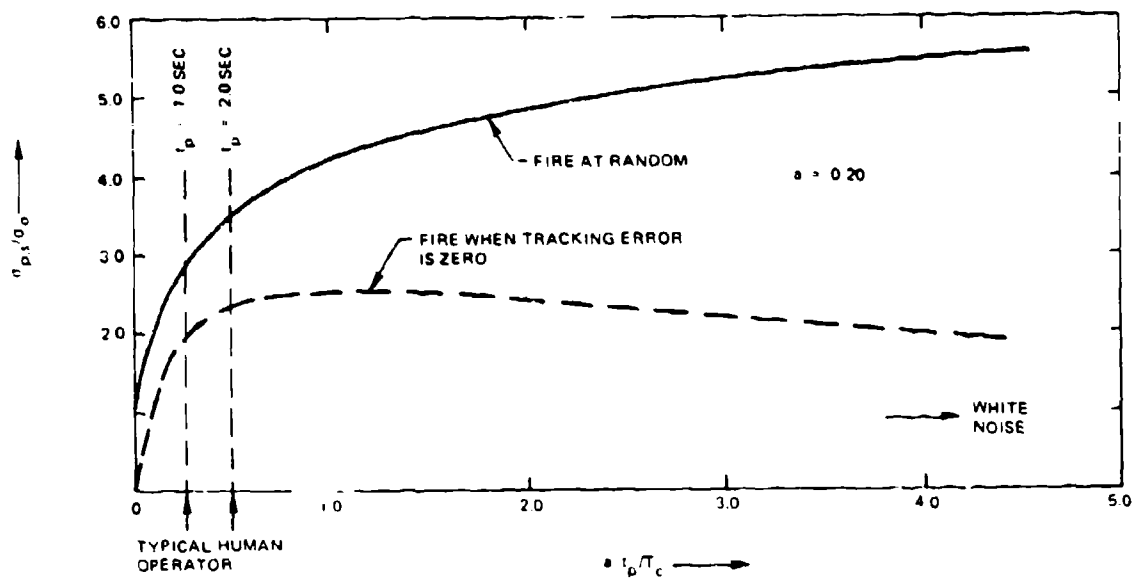
Figure 9-14. Comparison of Firing Doctrines for Gyrosight Type of Fire Control
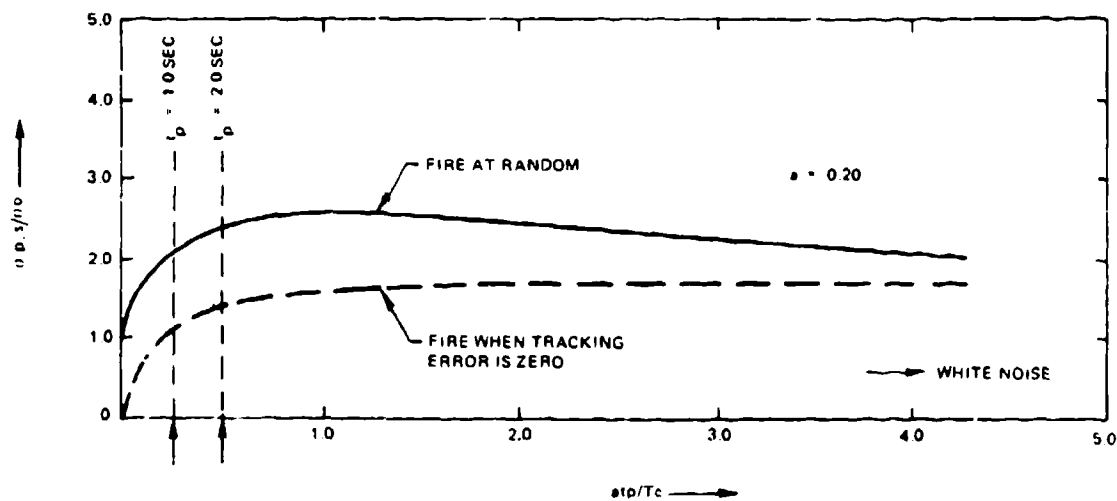
Figure 9-15. Comparison of Firing Doctrines for Fire Control with Second Order Filters

9.3.2.1 Historical Perspective

The gunner on Vulcan and similar mounts is a busy man. He must acquire the target, track, and decide when to fire. The tracking process takes place in two coordinates, and this is somewhat more difficult for the operator than tracking in a single coordinate (as was possible in World War II 40 mm mounts which had two trackers). It probably takes longer for two men to get on target, although experimental data seems to be lacking, and the trend of development has been to single operator mounts.

The Vulcan operator does have the advantage of not having to range in addition to tracking. World War II aircraft turrets were controlled by a single gunner who had the additional task of keeping the target bracketed in a stadiametric-type reticle. This problem was studied by engineering psychologists of the National Defense Research Committee, and their findings are sufficiently pertinent to current one-man mounts to justify reprinting the following summary of their work.[5]

> Gunners on a B-29 have three jobs to do. They track an enemy fighter with the sight. At the same time they must continuously readjust the range reading of the attacking fighter plane by keeping its image accurately framed in an adjustable set of marks in the sight. The range information and the data on the enemy's course which comes from tracking are fed into an automatic computer which points the gun, not at the attacker, but at the point in space where he will be, provided he continues on the same course, when the bullet gets there. That is, the computer does this if the gunner tracks smoothly and on target, and frames accurately. In addition to these tasks, which are difficult, the gunner is supposed to squeeze the trigger.

> For many gunners this last responsibility is just too much. They find it impossible to perform all three tasks (tracking, framing, and triggering) properly with only two hands and one brain. Consequently, as the project psychologists discovered, the gunners develop a regular rhythm of triggering which has nothing to do do with the accuracy of tracking and framing. They squeeze the trigger, and let it go, squeeze it and let it go, in bursts of fire which are just as likely to come when they are off target as on; just as likely when they are framing poorly as when they are framing properly. The gunners are not to blame. The task is too difficult for them. It may not be too difficult for the engineers who designed the sights. But it was for the average GI who became a B-29 gunner.

> In order to simplify the task to a level where the ordinary gunner could master it, the psychologists working on this problem did two things:

they modified the controls, making them easier to operate, and they built an automatic triggering device which would allow the gunner to concentrate on tracking and framing. An experimental test demonstrated that men could track and frame better with the modified controls than they could with the standard ones. The men were 'on target' about 25 per cent more of the time with the modified controls than with the standard ones.

The Army tried out the second suggestion - the automatic triggering device. Gunners used up twice as much ammunition since they fired steadily during an attack instead of in bursts. But, *with twice as much ammunition, they got three times as many hits.* Japan surrendered before the automatic triggering device could be tried in combat, but its value had been proved on aerial targets.

9.3.2.2 Rationale for Computer Selection or Assistance in Selection of Firing Points

It had been hoped that time would permit a number of automatic firing doctrines to be programmed and evaluated on the Litton simulation. This has not been possible. The following discussion develops a rationale for formulating such doctrines.

The determination of when to fire is considered in three phases: 1) Determination of System Readiness, 2) Threat Evaluation, and 3) Command of Individual Bursts. If the fire unit has more than one burst or rate of fire option, these would be selected in threat evaluation and commanded in the final phase.

The separate phases are developed as follows:

a. Phase I: Determination of System Readiness Criteria are:

(1) Sensors tracking target.

(2) Computer settled.

(3) Target within a specified 'effective' range.

This determination is already made automatically in some current systems, and the operator is given a signal to indicate that he can open fire when he desires. The determination of computer settling could be made from a measurement of elapsed time from target lock-on, or from the fact that a smoothed measure of target acceleration has dropped below a threshold. A determination of system readiness is fundamental to all systems, whether it is done automatically, or by the operator.

b. Phase II; Threat Evaluation. The following threat characteristics are observed by the operator, in-

ferred by the computer from tracking data, or developed in part by each.

(1) Aircraft Attack Mode

    a) Laydown Attack

    b) Strafing Attack

    c) Dive/Glide Bomb Attack

    d) Release of Standoff Weapons

(2) Aircraft Heading: Degrees off a direct attack path to defended target.

(3) Aircraft Velocity.

From this information the computer determines the expected time to aircraft weapon release or to minimum range, depending on the attack mode. From the expected available firing time and its status record of on-mount ammunition, the computer selects firing rate, burst length, and number of bursts to be fired. The burst command points are selected according to algorithm which compromise between the desirability of obtaining kills at long range is possible, and the higher probabilities of obtaining kills at short range. This might result in firing bursts of decreasing duration as the target closes.

c. Phase III; Burst Command. In an automatic mode, the system might consider both target acceleration and sensor tracking error as modifiers on the preselected firing points. A commanded burst might be delayed until either target acceleration or tracking error, or both were within selected limits. How much delay to allow could be the subject of analysis. These limits would be overridden when expected remaining firing time equalled the time to fire the allocated ammunition at maximum rate.

How much complexity to put into an automatic fire control computer module would depend on the payoff. Some initial estimates can be made analytically, and if these were verified on the Litton simulation, (which is notoriously difficult to convince of the desirability of any sophisticated program) some confidence might be had in specific recommendations for implementation.

9.4 OPTIMUM DISPERSION

The idea of increasing the size of the shot pattern of a high rate of fire weapon to cover up deficiencies in the lead prediction, errors in boresighting and calibrating the equipment, and unpredictable maneuvers of the target is an unfortunate one. It is unfortunate because it dilutes the effort which should be devoted to improving the prediction algorithms, improving tracking, eliminating boresight and calibration errors. Repeated analyses indicate that for predicted fire weapons some small, non-zero round to round random

dispersion is better than none, but large values are rarely helpful, and then only in cases where the bias errors are so large that even the best random dispersion is insufficient to raise the kill probability to useful levels.

This section does not exhaust the argument, but provides some additional analytical methodology and commentary based on the simulation results.

It may be noted that one of the reasons that analysts (including the present writer) tend to be fascinated with the idea of artificial dispersion is that it is an interesting analytical problem. Duck hunters have their own bias in favor of the shotgun approach, even though a simple analysis of the parameters of their problem indicates that it does not scale at all to the antiaircraft gun problem.

9.4.1 Analytic Determination of Optimum Dispersion

Consider the problem of computing the probability of killing a target with a burst of n rounds, when the shot pattern has a constant bias (such as boresight error) which is constant over all bursts, and a bias constant during a burst and randomly distributed across bursts. In addition individual rounds have a random round to round dispersion. Closed form solutions, even for the simpler cases of circular symmetry, tend to involve the Incomplete Gamma or Beta functions and/or series expansions. To determine whether increased (artificial) dispersion is desirable most past analyses have had to resort to numerical computations. This is no great problem if a computer is available, and in fact with the Litton simulation one can allow many of the tactical parameters to vary during a long burst for a realistic evaluation of the effect of changing dispersion.

An analytic base is always helpful for reference, however, and the following method, suggested by some little known work of Gubler,[4] turns out to be tractable. By its use, an exact solution to a very old problem has apparently been obtained, for which only graphical solutions were previously available, to the best of the writer's knowledge.

For brevity of presentation, the method is described for a problem in which all of the probability density functions have circular symmetry. This is not an inherent limitation of the method, which allows considerable generalization.

The expression for the survival probability of the target is written, conventionally as

$$\phi(Z) = (2\pi)^{-1} \iint_{-\infty}^{\infty} e^{-E_o Z e^{-\lambda Z \left[(x_b \cdot x_o)^2 + (y_b \cdot y_o)^2\right]}}$$

$$e^{-\left(x_b^2 + y_b^2\right)} \, dx_b dy_b \qquad (9.48)$$

where:

$$E_o = na^2/(a^2 + 2\sigma^2) \qquad (9.49)$$

a^2 = target vulnerable area

σ_b^2 = variance of aim wander, constant during a burst, random across bursts

σ^2 = variance of "reference" round to round dispersion

σ_z^2 = incremental variance of artificial dispersion

$$\lambda = 2\sigma_b^2/(a^2 + 2\sigma^2) \qquad (9.50)$$

$$Z = (a^2 + 2\sigma^2)/(a^2 + 2\sigma^2 + 2\sigma_z^2) \qquad (9.51)$$

x_o, y_o are systematic errors constant over all bursts.

$Z < 1.0$

Take the derivative $\partial\phi(Z)/\partial Z$.

If

$\partial\phi(1)/\partial Z < 0$, dispersion should be increased

$\partial\phi(1)/\partial Z > 0$, dispersion should be reduced

$\partial\phi(1)/\partial Z = 0$, the reference dispersion is "optimum."

(9.52)

Abbreviating the notation for ϕ

$$\phi = \iint_{-\infty}^{\infty} e^{-E_o Z e^{-T\lambda Z}} f(T) \, dT \qquad (9.53)$$

$$\partial\phi(Z)/\partial Z = -E_o \iint_{-\infty}^{\infty} (1 - Z\lambda T) e^{-\lambda Z T} e^{-E_o Z e^{-\lambda Z T}} f(T) \, dt \qquad (9.54)$$

Note that we can write:

$$\partial\phi(1)/\partial E_o = \iint_{-\infty}^{\infty} -e^{-\lambda T} e^{-E_o e^{-\lambda T}} f(T) \, dT \qquad (9.55)$$

$$\partial\phi(1)/\partial\lambda = \iint_{-\infty}^{\infty} E_o T e^{-\lambda T} e^{-E_o e^{-\lambda T}} f(T) \, dt \qquad (9.56)$$

But:

$$\partial\phi(1)/\partial Z = \iint_{-\infty}^{\infty} (1 - \lambda T) e^{-\lambda T} \, e^{-E_o e^{-\lambda T}} f(T) \, dT = 0 \qquad (9.57)$$

Hence:

$$\partial\phi(1)/\partial E_o + (\lambda/E_o) \, \partial\phi(1)/\partial\lambda = 0 \qquad (9.58)$$

$$\partial\phi(1)/(\partial\log_e E_o) + \partial\phi/(\partial\log_e \lambda) = 0 \qquad (9.59)$$

whence:

$$E_o^* \cdot \lambda^* = C \qquad (9.60)$$

where the asterisks indicate the relation between E_o and for optimum dispersion. If Equation (9.57) can be evaluated for any pair (E_o, λ) for which the parameters are other than $0, ^*$, the constant C can be determined. The desired solution is then obtained.

For the case $x_o = y_o = o$ (no constant bias across all bursts) the solution is easily obtained. We have simply

$$\phi(Z) = \int_0^\infty e^{-E_o Z e^{-\lambda Z w}} d(e^{-w}) \qquad (9.61)$$

Then:

$$\partial\phi(1)/\partial z = -E_o/\lambda \int_0^1 (1 + \log_e w) w^{1/\lambda} e^{-w E_o} \, dw$$

$$= 0 \qquad (9.62)$$

Solve this for the special case of $\lambda = 1.0$. Then E_o is the solution of the transcendental equation:

$$2\left[1 - (1 + E_o/2)e^{-E_o}\right] \cdot Ei(-E_o) - 0.5773 \ldots \log_e E_o = 0 \qquad (9.63)$$

Where Ei is the expontial integral and is a tabulated function. Solving this equation numerically, we find $E_o = 3.56...$

Hence the optimum dispersion is using Equation (9.60) obtained from:

$$E_o \lambda = 3.56 \tag{9.64}$$

or

$$(na^2)\left(2\,\sigma_b^2\right) = 3.56\,(a^2 + 2\sigma^2)^2 \tag{9.65}$$

Suppose that we could reduce the random round to round dispersion to zero. Then we should have:

$$n = 3.56\,a^2/2\,\sigma_b^2 \tag{9.66}$$

Hence unless n exceeds this value, the optimum round to round dispersion is zero. Now πa^2 = target vulnerable area, and $a^2/2\sigma_r^2$ will usually be very small. For the problem as formulated, therefore, we would always expect some round to round dispersion to be desirable. Solving for this value

$$2\sigma^2 = \left[a\,\sigma_b\,(n/1.78)^{1/2}\right] \cdot a^2 \tag{9.67}$$

And so as n increases, the standard deviation of optimum dispersion increases about as the fourth root of the number of rounds and as the square root of the round to round bias standard deviation.

Equation (9.64) is an exact solution. An approximate solution based on graphical analysis was given in AFAADS-1, p.5-71, Equation (5.347).

The above approach may be generalized to a time-varying problem. If dispersion can be controlled easily, as by using servo dither, or a scanning motion of the gun tube, it is clear that on opening fire one wants the first rounds to be fired with the minimum dispersion. As firing continues, it may be desirable to open up the pattern. For example, the gun tube might follow an expanding spiral about the predicted point. From the preceding method one can determine how many rounds should be fired before it is desirable to open up the pattern, and how rapidly the pattern should be expanded with n.

9.4.2 Discussion of Simulation Results

A number of simulation runs have been made under a wide variety of tactical parametric variations to observe the effect on burst kill probability of varying the random round to round dispersion of the ammunition. The optimum dispersion rarely is larger than 5 mils, and in those rare cases where larger values were

indicated, they were associated with burst kill probabilities that were very low, even when optimum dispersion was used.

This observation is supported by the analysis of the previous section. Consider a burst of n rounds fired at a target with vulnerable area A_v. Assume that the system has a constant error of aim during a burst, and that this error is randomly varying across bursts and described by a circular normal distribution with a variance of σ_b^2. Defining an area of uncertainty associated with the bias as:

$$A_b = 2\pi\sigma_b^2 \tag{9.68}$$

this area could be covered to a density nA_v/A_b if n rounds could be accurately placed.

Working through the equations for optimum dispersion, using expressions from AFAADS-1 (pp 5-70, Equation 5.342), the probability of killing the target in a burst of n rounds with optimum dispersion can be plotted against nA_v/A_b, as can the ratio of optimum round to round dispersion to standard deviation of bias, σ_r/σ_b. This has been done in Figure 9-16.

Now taking a specific example of a target with 1 square meter vulnerable area, and a burst of 100 rounds fired at 1000 meters range, and plotting both burst kill probability with optimum dispersion and the value of the optimum dispersion against the standard deviation of bias, the results of Figure 9-17 are obtained. As expected from the previous section, the optimum dispersion increases slowly with bias, and is only about 6.5 mils when the standard deviation of bias is 20 mils. This occurs when burst kill probability has dropped below 4%.

Since the aim wander resulting from tracking noise can be represented in terms of a bias and a random component, not all of this optimum dispersion need be provided artificially.

The effect of aim biases resulting from target maneuver are expected to work out in about the same way. The unpredictable components will vary from burst to burst. If they are very large, on the average, burst kill probability will be small, and improved to only a small degree by adjusting dispersion. If they are small, some dispersion is better than none, but the optimum amount is still only 5 mils or so.

Conclusions

This discussion is not intended to leave the impression that one should not attempt to determine and employ the optimum dispersion pattern. Rather, the conclusion is that this is an expedient of limited payoff. The proper approach is to attempt to minimize prediction errors by a good choice of prediction and smoothing algorithms, to minimize system boresight and
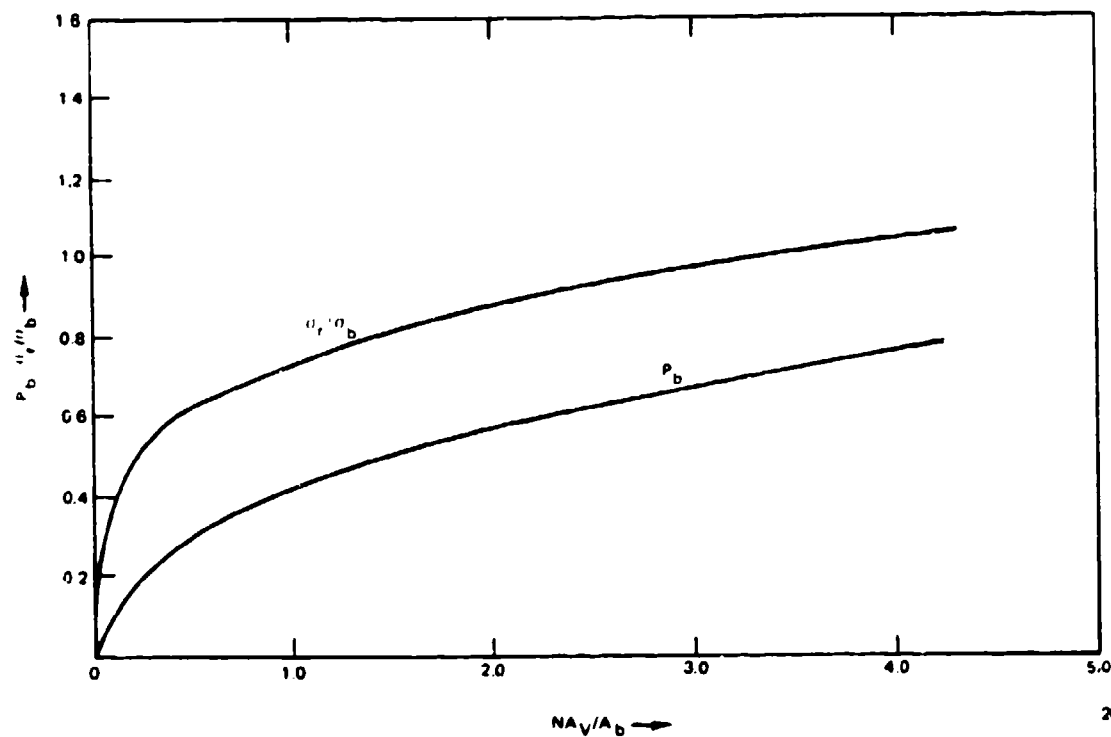
Figure 9-16. Burst Kill Probability and Optimum Dispersion Ratio

calibration errors by a sound calibration doctrine, to reduce the effect of target maneuvers by short time of flight, and then to apply the best dispersion pattern, varying with path parameters if possible, to cover the residual errors as far as possible.
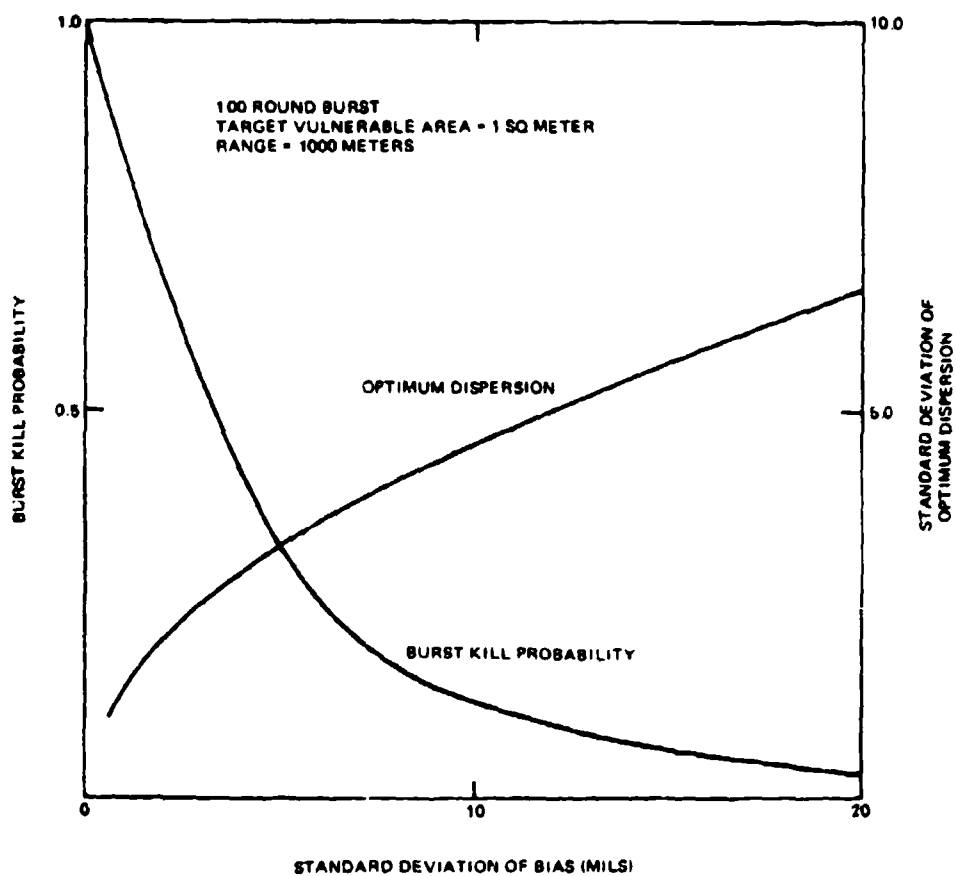
Figure 9-17. Variation of Optimum Dispersion with Bias

20871-203A

SECTION 10
SIMULATION RESULTS

10.1 INTRODUCTION

This section presents a wide variety of results to demonstrate the flexibility and scope of the Litton simulation, as developed under the present contractual effort.

The simulation is now relatively complex, as compared with the simpler version used in AFAADS-I, but is considerably more realistic, and allows a much larger variety of tactical and defense system parameters to be examined.

The price paid for the added capability has been the difficulty in identifying and eliminating all programming errors in the basic simulation, and those introduced by new operators inputting parameters for new series of runs.

It is now clear that to obtain satisfactory assurance of the validity of simulation results, a check-out program package must be put together which validates the existing program, and which can be run in conjunction with each new set of experiments. The results presented in this section appear in almost all cases to be reasonable and probably correct, but in a few cases noted in the text there are anomalies suggesting a residue of one or more minor program imperfections.

In a sense the simulation is a realistic representation of a real fire control system, which will operate approximately correctly, even though some components may be slightly out of adjustment. One danger signal noted in simulation operation has been occasional results which show very large dispersions to maximize kill probability. When traced down, these led to the discovery of programming errors.

The results presented should be interpreted by the reader in this sense: 1) They demonstrate the wide range of capability available on the simulation, 2) The results are probably correct, or very close to correct, and 3) They can be completely validated by the check-out package described in Section 10.17.

10.2 COMMON PARAMETERS AND REFERENCE DATA

The simulation results presented were based on a number of input parameters, some of which were systematically varied.

Table X-1 lists the 'standard' target dimensions used in all runs. Table X-2 lists the 'design point' characteristics of four gun systems ranging in caliber from 20 mm to 50 mm.

Three types of target paths were employed. These were

a. Simple constant altitude, constant speed 'fly-by' paths. These were all low altitude, 300 to 400 meters, and families of results were generated for the same altitude by systematically changing the minimum horizontal range.

b. Crossing, jinking paths. These were intended to be somewhat representative of low-level terrain following. The aircraft performed a regular weaving motion in the vertical and horizontal planes, with the two components differing in phase by 90°. The acceleration pattern is shown in Figure 10-1.

c. Dive bombing paths. These paths are described in Section 10.16.

In all cases the data filters used had a finite memory time of 1.8 seconds. The coefficients were chosen as a compromise between smoothing and rapid settling; this weighted the early points somewhat more heavily than would be the case with least squares filters.

For most of the runs, two prediction modes were compared. One was conventional 'linear' prediction, based on smoothed position and velocity. For the second mode, the prediction was partially corrected by smoothed acceleration, so that on a constant curvature path the prediction vector would be tangential to the target path at present position. A few runs were made with full quadratic prediction, which would have zero bias of prediction error against a path of constant curvature. These three modes are termed 'linear', 'tangential' and 'quadratic'.

The exterior ballistics used were based on the 'best' 37 mm round used in AFAADS-I. The same form factor was assumed for the other caliber rounds, and the ballistics were scaled with caliber according to the Siacci expressions.

Unless explicitly mentioned, angular dispersion was taken as 3 mils lateral and vertical, muzzle velocity dispersion was zero, and there were no angular or muzzle velocity biases.

10.3 EFFECT OF RATE OF FIRE AND CALIBER

A series of runs was made on the simulation, in which the rate of fire was systematically varied for each of the four reference weapon calibers. Both linear and tangential prediction modes were run. Results were obtained on a straight line, constant altitude (300 meters) fly-by path with an aircraft velocity of 300 meters/second. The following three pairs of firing points were employed (crossing range, distance before midpoint in meters): (600, 1500), (600, 500), (1200,-500). A typical set of results is shown in Table X-3.

Table X-1. Standard Target Dimensions and Areas

		Dimensions (meters)		Areas (square meters)	
Fuselage	Length	15.0	Top	16.49
	Height	2.3	Front	2.53
	Width	1.4	Side	27.10
Wing	Span	10.0	Top	47.12
	Chord	6.0	Front	2.83
	Thickness	0.36	Side	1.70
Note: Areas are not corrected for overlap in this table.					

20871-539A

The entries are the probability of kill with a one-second burst. These values are plotted in Figure 10-2, for tangential prediction.

The regular form of the curves led M. Ginsberg to suggest that a simple scaling relationship could be developed to describe them. It was found that if the target survival probability to n rounds was plotted against the target survival probability to n/2 rounds, all of the corresponding data pairs for all four calibers and the three sets of firing points fell on the same curve for a specified prediction mode. The corresponding plots are shown in Figures 10-3 and 10-4 for the two prediction modes. The deviations of individual points from a mean curve is well within the scatter resulting from the Monte Carlo operation of the simulation.

This remarkable result suggested that the results of the simulation computation at the specified tactical parameters could be represented by the simplest possible expressions for burst kill probability, specifically, Equation 5.342 on page 5-70 of the AFAADS-I report.

One may then develop the form of the mean curve of Figures 10-3 and 10-4 as follows:

Define:

$$A = \frac{na^2}{a^2 + 2\sigma^2} \qquad (10.1)$$

$$B = \frac{2\sigma_b^2}{a^2 + 2\sigma^2} \qquad (10.2)$$

where

n = number of rounds fired

π^2 = target vulnerable area

σ^2 = random round to round error component variance

σ_b^2 = error component variance constant over burst, random across bursts

For small A. define $E = \frac{A}{(1+B)}$, then survival probability to a burst is

$$Q(n) \cong e^{-E}$$

$$Q(n/2) \cong e^{-E/2}$$

$$Q(n) = [Q(n/2)]^2$$

$$2 \, Log_e \, Q(n/2) = Log_e \, Q(n) \qquad (10.3)$$

For large A, from Equation 5.342 in AFAADS-I

$$Q(n) \cong B^{-1}(A)^{-1/B}$$

$$Q(n/2) \cong B^{-1}(A/2)^{-1/B} = (1/2)^{-1/B}Q(n)$$

$$Log_e \, Q(n/2) \cong (1/B)Log_e(2) + Log_e \, Q(n) \qquad (10.4)$$

If $2\sigma^2 >> a^2$, as will usually be the case, B will be essentially independent of a^2.

If straight line asymptotes are fitted to the two ends of the Q(n) versus Q(n/2) curve, they will intersect at:

$$Q(n/2) = 2^{-1/B} \qquad (10.5)$$

Making a rough estimate of the equivalent value of B in the two cases, it appears that in the case of the tangential predictor, the variance of bias error about equalled the variance of round to round error. For the linear case the variance of bias error was only about 1/4 the variance of the round to round error.

One would also expect the target survival probability to depend, to a first approximation on the product of number of rounds fired by the target vulnerable area.

10-2

Table X-2. Reference-Point Weapon Characteristics

Caliber	20 mm	25 mm	37 mm	50 mm
Maximum Rate of Fire (rpm)	6000	3840	3000	1920
Number of Rounds in 1-sec burst	100	64	50	32
Number of Rounds on Mount	600	500	400	300
Muzzle Velocity (ft/sec)	3600	3600	3600	3600
Range to Sonic Velocity (meters)	2720	3403	5036	6806
Time of Flight Sonic Velocity (sec)	4.7	5.9	8.7	11.8
% HE Filler	10	10	10	10
Probability of Kill, Given a Hit (p_c) on Fuselage	0.17	0.24	0.44	0.65
Maximum Kills per Second = Rate x p_c on Fuselage	17.1	15.5	21.8	20.8
Probability of Kill, Given a Hit (p_{cw}) on Wing	0.025	0.042	0.150	0.380
Maximum Kills per Second = Rate x p_{cw} on Wing	2.5	2.7	7.5	12.2

20871-540A

This relationship is shown in Figure 10-5 for a single point on the flight path 500 meters before midpoint, and for the two predictors. Note that for the linear case where the bias component of error is relatively small, the curves for the four weapons show little difference. For the tangential predictor the large caliber weapons do somewhat better than the small caliber weapons. This would be expected, since serial correlation reduces the marginal gain of additional rounds, and for a given product of vulnerable area x number of rounds, the small weapons fire more rounds.

The difference among weapons with the linear predictor may result from the fact that the larger weapons also have some effect against the target wing. In addition, the larger caliber weapons have a small time of flight advantage, which improves their relative effectiveness.

These experimental results from the simulation lead to significant inferences regarding the need for the Monte Carlo mode, which is responsible for most of the cost of simulation operation.

For the noise characteristics generated by the radar model and linear prediction the fact that target survival probability versus number of rounds is very close to a simple exponential, as shown in Figure 10-5 implies that one would obtain essentially the same
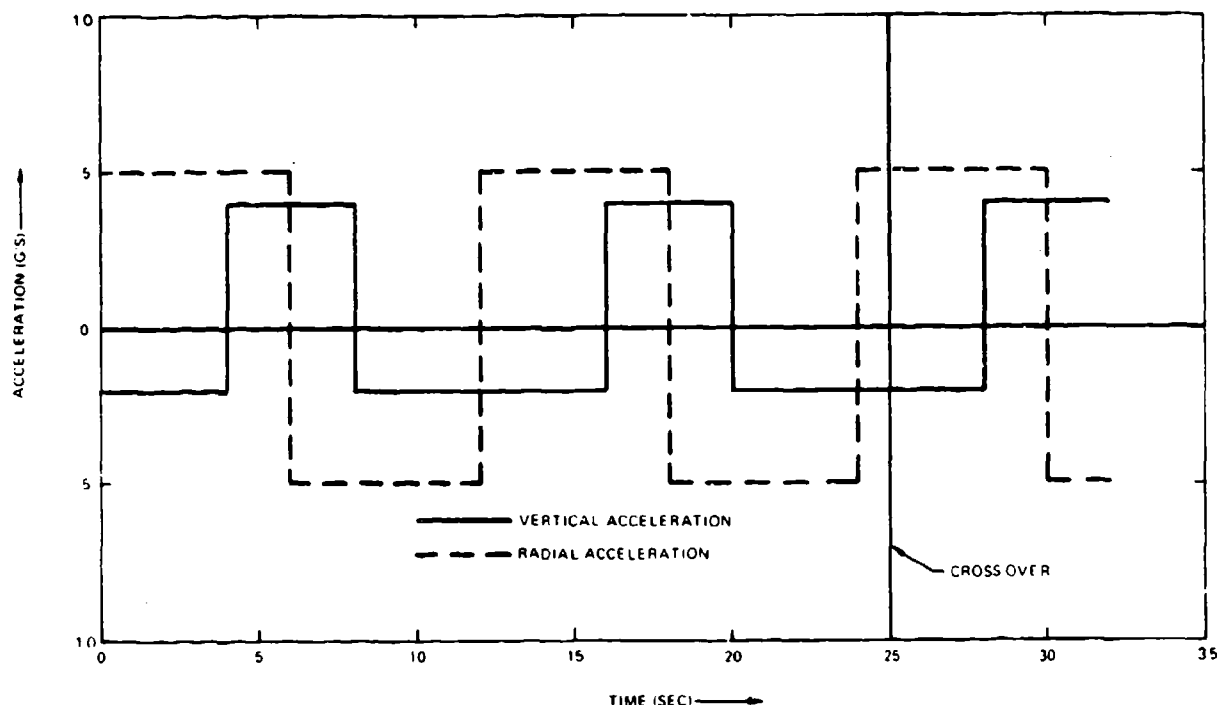
Figure 10-1. Aircraft Acceleration Program for Jinking Path

20871 204

result by a deterministic computation assuming independence of successive rounds.

In the case of the tangential predictor, this would be true only for burst kill probabilities below about 0.50. However, the fact that a single curve fits all of the samples for four calibers of weapons, a wide range of number of rounds fired, and three points on the target path with different geometries implies that one can use the simplest form of the deterministic algorithm for computing burst kill with bias varying across bursts, and by that means obtain the same results. All that is needed is a method of estimating the ratio of the variance of the random and bias components, and this can be done by 'Tappert's method' described in the AFAADS-I report.

To what degree the observed empirical relationships will hold for other noise models and filters is unknown. As a minimum, the results observed provide a simple method of converting simulation results to other parametric sets.

10.4 FOOTPRINTS

The simulation can be operated to generate a pattern of data points from which a 'footprint' can be sketched. A footprint is a set of contours of constant kill probability for a burst of specified duration.

As a demonstration, footprint data have been generated for families of pass courses of two types: 1) constant altitude, constant velocity paths, and 2) 'jinking' paths in which the aircraft weaves vertically and horizontally about a mean, level, straight line.

Each data point is for a 1-second burst with a specified number of rounds fired at constant specified rate of fire. The data point is defined by the minimum horizontal range of the path and the distance of the aircraft from midpoint at the instant the burst is fired. For the weaving path these points are referenced to the mean line through the path.

The data printout for the 25 mm gun on the fly-by path with the tangential predictor is shown in Table X-4, and a rough sketch of the corresponding burst kill 'footprint' contours is shown in Figure 10-6. The parabolic lines in Figure 10-6 are lines of constant distance from midpoint at the instant the projectiles reach the target. Of this set the solid line represents impacts at midpoint when time of flight is least.

Data print-outs for the 25 mm gun against a jinking path, and for the 50 mm gun against a fly-by, both with the tangential predictor, are given as Tables X-5 and X-6. Runs with linear prediction and the 25 mm gun indicated inferior performance in general on the jinking path. Against the fly-by however, maximum

10-4

Table X-3. Burst Kill Probabilities for the Point 500 m
Before Crossover on a 600 m Fly-By Path

| Rate of Fire (Rounds/Sec) | Tangential Prediction | | | | Linear Prediction | | | |
| | Caliber | | | | Caliber | | | |
	20	25	37	50	20	25	37	50
128	.78	.86	.94	.96	.97	.99	1.0	1.0
112	.75	.84	.93	.96	.96	.99	1.0	1.0
96	.72	.81	.92	.95	.95	.98	1.0	1.0
80	.67	.77	.90	.95	.92	.97	1.0	1.0
64	.62	.72	.87	.93	.89	.95	.99	1.0
48	.54	.65	.82	.90	.82	.90	.98	.99
32	.42	.53	.72	.84	.70	.81	.94	.98
16	.26	.34	.52	.66	.47	.59	.78	.88

20871-541

probabilities were higher, but the simulation indicated poorer performance at long range. These results are shown in Tables X-7 and X-8. This anomalous result is not understood and there was insufficient time to investigate its cause. There are two possible explanations, 1) the band width of tracking error at long range is so narrow that the resulting aim wander requires additional dispersion to cover it. This would be provided by the tangential prediction. The other explanation 2) could be that a minor error remains in the filter programming.

At the long ranges, the large caliber guns show a moderately higher burst kill probability than the smaller calibers.

This results from 1) the shorter time of flight, and 2) the higher product of rate of fire times the probability that a hit causes a kill. For a particular data point at $(R_m, X) = (2400, 2500)$ on the fly-by path with the tangential filter, the burst kill probabilities for the four calibers were compared, and an approximate correction for the rate of fire and target vulnerability made to estimate the contribution of time of flight alone. Figure 10-7 shows the comparison referenced to the 20mm gun.

At this range and the low target altitude, the fuselage presents a much larger area than the wing, hence

the normalization was based on fuselage vulnerability only.

Antiaircraft gun footprints previously published from other programs show zones of zero probability about the gun corresponding to maximum tracking rates and accelerations. These could be programmed into the Litton simulation. The present program is based on the assumption however, that the system does not lose the target at high tracking derivatives. Instead, it lags by an amount depending on the derivatives. The footprints shown were based on the inclusion of a regenerative tracking assist for the servos which provided compensation for the first two derivatives. Since the compensation is not perfect, the simulation does show zero kill probability when the target passes almost directly overhead.

10.5 PREDICTION MODES

A brief comparison was made of predictor modes, on unaccelerated 'fly-by' paths and passing jinking paths with the 25mm gun. The predictors were 1) linear (i.e., no correction for acceleration), 2) tangential (i.e., updated for acceleration only to present position), and 3) quadratic (i.e., complete prediction for constant acceleration).

Figure 10-8 compares the linear and tangential predictors on an unaccelerated path. As expected, the tangential predictor, with higher tracking noise amplifications, is inferior. Figure 10-9 compares the same two predictors against the jinking path. The tangential predictor shows a more uniform performance, and is superior over much of the path. Apparently it provides a good compromise between reduction in bias caused by maneuver, and increase in dispersion to cover the residual bias. This is consistent with the analytic conclusions of Section 5.7.6 of the AFAADS-I report.

A comparison of linear, tangential, and quadratic prediction on the jinking path is shown in Figure 10-10. The full quadratic prediction is apparently too much of a good thing: it generates increased amplification of tracking noise out of proportion to the reduction in bias caused by maneuver.

Note that when the target's mean crossing range was moved out from 600 meters (Figure 10-9) to 1000 meters (Figure 10-10) the tangential prediction improved relative to the linear prediction.

For this set of runs it appears that against a mildly maneuvering target a form of prediction intermediate between linear and full quadratic is preferred. Whether the good performance shown in these runs resulted from the partial correction for path curvature or from the increased dispersion generated by the tangential filter would require additional runs and analysis to determine.
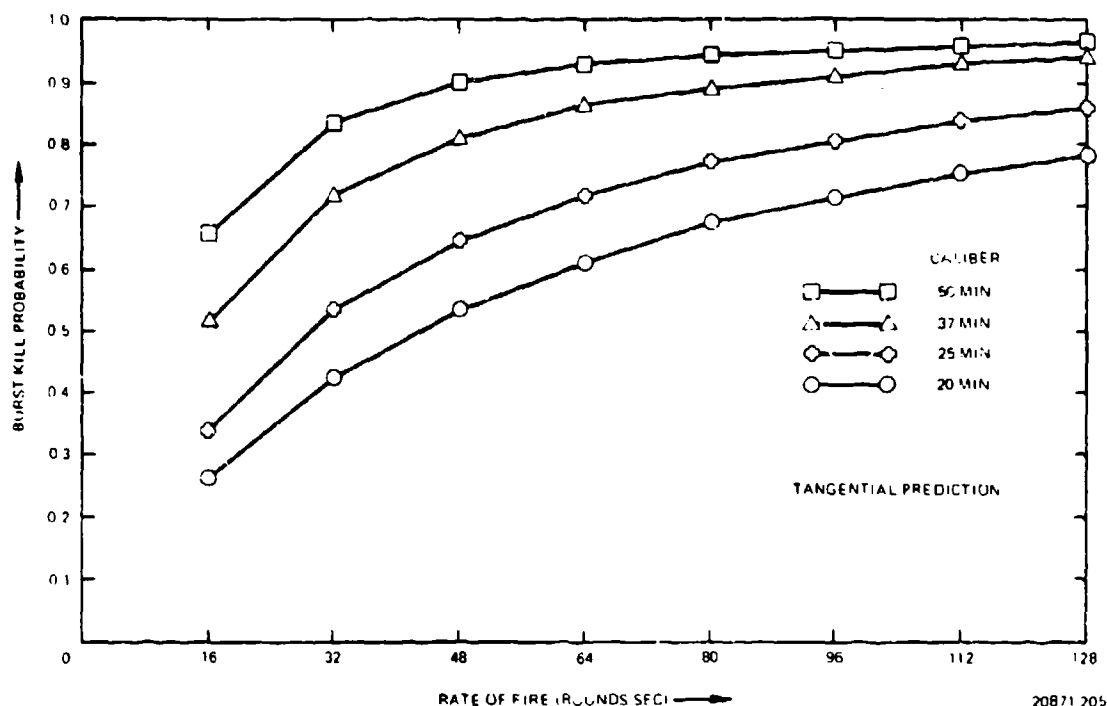
Figure 10-2. One Second Burst Kill Probability Versus Rate of Fire and Caliber

10.6 EFFECT OF AIRCRAFT 'BREAKAWAY' MANEUVER

To examine the question of how long to fire after an aircraft has completed its attack run and has entered a high-acceleration breakaway maneuver, simulation runs were made in which an aircraft approached on a straight fly-by path at 300 m/s, then pulled away in a climbing turn, 3g to the right and 2g vertical beginning 600 meters from midpoint, from a straight level path with a 600 meters projected crossing range. Results are shown in Figure 10-11 for the linear and tangential predictors. For the first second of its pull up the aircraft does not generate enough path change to affect the burst kill probability with either predictor. The linear predictor degrades more rapidly than the tangential predictor, which appears to retain some capability for at least the first three or four seconds of the breakaway maneuver.

10.7 EFFECT OF MUZZLE VELOCITY

The effect of increasing muzzle velocity was determined by a series of simulation runs against the jinking path for a crossing range of 1000 meters. Kill probabilities with one second burst were determined. Results are shown in Table X-9, and the data points for the 20mm gun, which showed the largest percent improvement are plotted in Figure 10-12.

To get a visual impression of how the performance is improved by increased muzzle velocity, the 1-second burst kill probabilities for each weapon-fire point combination at 3600 and 5000 f/s muzzle velocity are plotted in Figure 10-13.

The gain is highest in the case of those weapons and data points where the lower velocity probability is small.

Note from the table that the 20 mm weapon at 5000 f/s muzzle velocity is uniformly superior to the 37 mm weapon at 3600 f/s within the 2500 meter fire point.

In the above computations the number of rounds per burst for the three calibers were 100, 64 and 50, respectively. If the high velocities were attained by subcalibering as suggested in Section 8.2 it seems unlikely that these rates could be maintained although they would probably remain the same proportion, across calibers.

An overall conclusion with regard to the relative importance of muzzle velocity, rate of fire and caliber cannot, therefore, be drawn from the muzzle velocity results alone.

10.8 EFFECT OF INCREASED TERMINAL EFFECTIVENESS

A brief set of runs was made to compare the 25 mm projectile with 10% and 20% high explosive filler. The

10-6
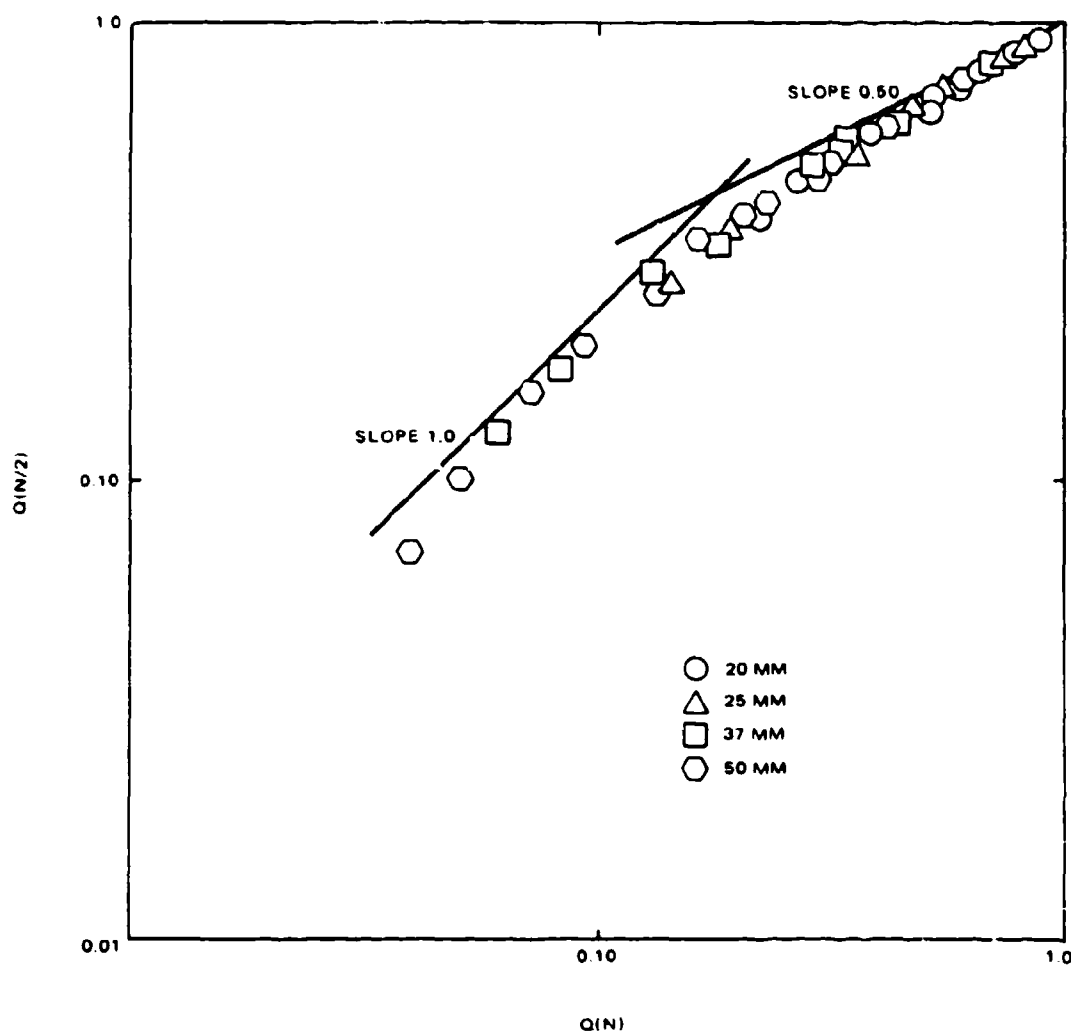
Figure 10-3. Rate of Fire Relationship from Simulation: Tangential Prediction

only change was in the vulnerability function. In fact, if it could be fired from the same gun, with the same drag coefficient, the 20% fill projectile would emerge at a substantially higher muzzle velocity because of its lower weight, and then would decelerate more rapidly, for a net improvement in time of flight over the ranges investigated.

The path used was a jinking pass at an altitude of 300 meters, a minimum crossing range of 1000 meters, and an average target speed of 300 meters/second, and kill probabilities with 1-second bursts were compared.

The effect of doubling the filler is to increase the kill probability, given a hit, from 0.24 to 0.31. From the findings of Section .0.3, one would then expect burst kill probabilities to increase about in the ratio 1.3/1 for probabilities under 50%. As Figure 10-14 shows this is in fact the result generated by the simulation.

If the expected higher muzzle velocity with the lighter projectile had also been included, plus the change in ballistic coefficient, it is believed that a somewhat greater increase in effectiveness would have been shown by the 20% projectile.

10.9 EFFECT OF AIRCRAFT VELOCITY

If one computes 1-second burst kill probabilities with the simulation operating in the radar tracking mode, one would not expect to find that the kill proba-

10-7

SLOPE 0.50

Q(N/2)

0.10

0.01

0.1

1.0

Q(N)

○ 20 MM
△ 25 MM
□ 37 MM
⬠ 50 MM
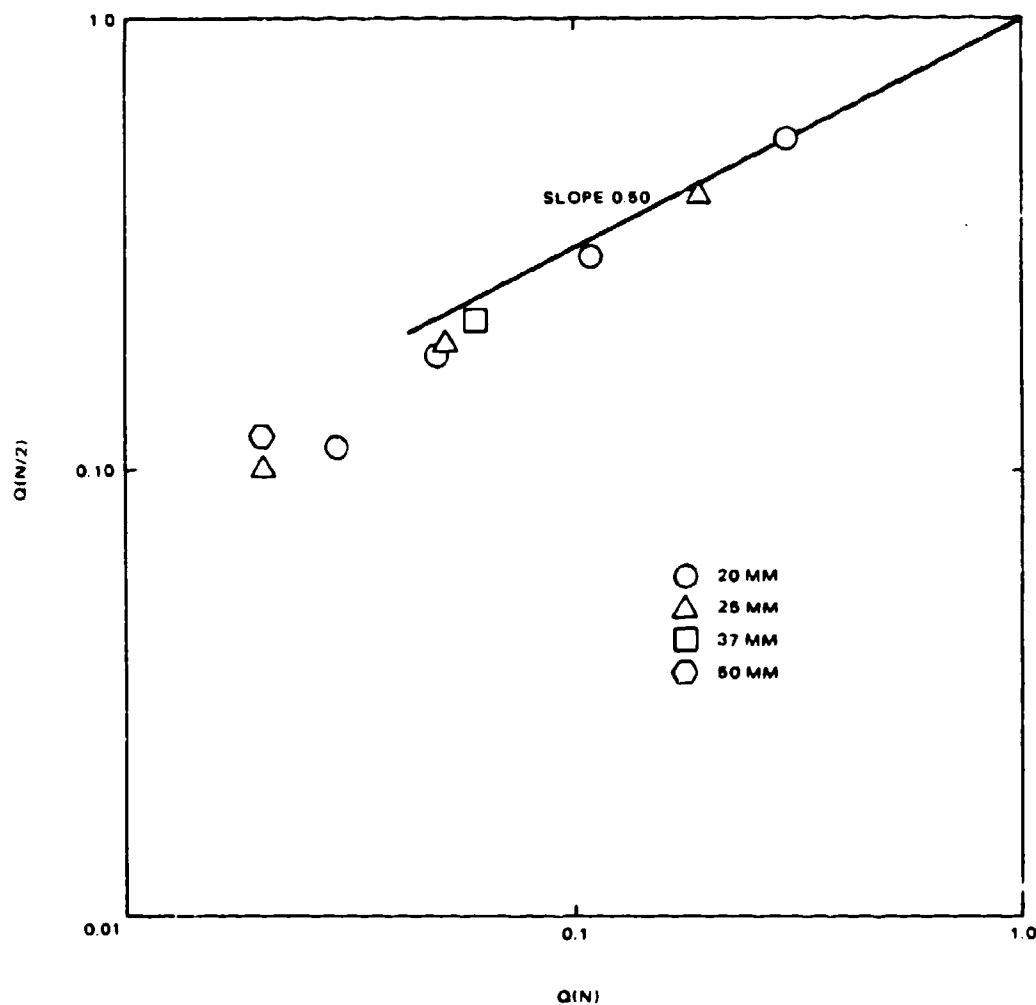
20871-207A

Figure 10-4. Rate of Fire Relationship from Simulation: Linear Prediction

bilities are very sensitive to aircraft velocity. Velocity enters this computation, 1) by changing the bandwidth of the glint error, which at a given point in space is wider for higher velocities, 2) by causing the burst kill computation to be performed over a path segment which increases in length with velocity.

A large apparent effect is generated by the fact that the simulation prints out results referred to the point of initiation of firing, whereas kill probabilities appear to be principally related to the geometry at the time the projectiles reach the target.

A series of simulation runs confirmed the above expectations. Mr. M. Ginsberg determined that the best abscissa to use, for clarity, was the aircraft time from midpoint at the open fire instant, and Figures 10-15 and 10-16 show the effect of aircraft velocity with the two filters.

Since the highest single shot probability occurs close to midpoint, the longer the segment of path included in a 1-second burst near midpoint, the larger will be the fraction of lower probability points. Hence, in both figures the probabilities for the high speed target are uniformly below those of the low speed targets.

The major effect of target speed is, of course, one total available firing time, and this is not shown by the burst comparison.
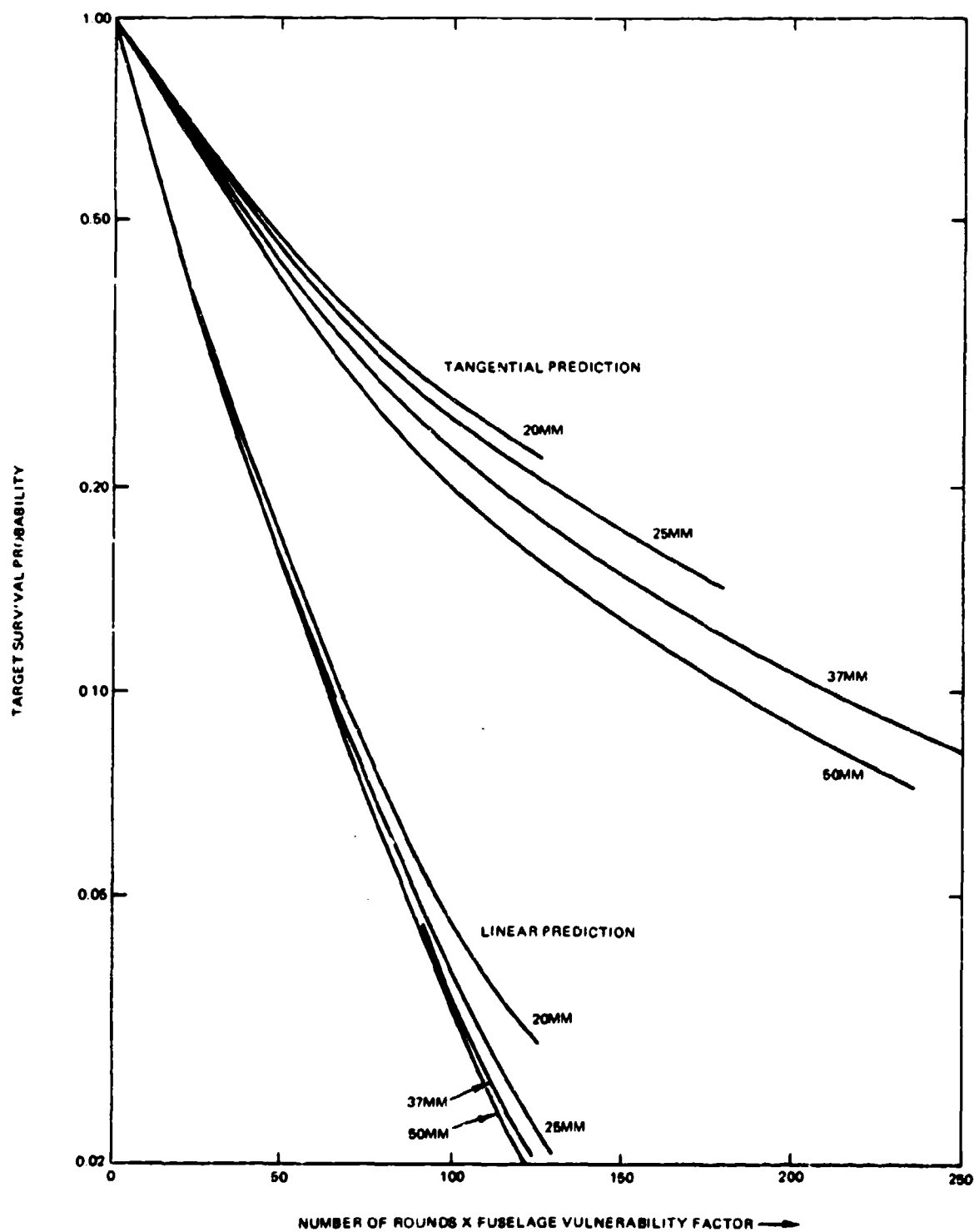
Figure 10-5. Variation of Survival Probability with Rate of Fire and Target Vulnerability

Table X-4. Foot Print Data for 25 mm Gun With Tangential Predictor on Fly-By Path

Crossing Range (m)	Fire Point (m)									
	3000	2500	2000	1500	1200	900	600	300	0	-300
0	037	082	124	198	277	361	550	469	00	00
100	034	084	122	195	272	385	537	185	037	362
200	038	09.	134	216	292	422	702	483	352	428
300	042	107	152	247	333	488	834	717	580	524
400	046	123	172	280	377	560	853	791	703	602
500	051	138	192	310	415	617	845	816	681	579
600	056	152	211	337	448	638	826	800	681	554
700	061	166	227	358	473	635	795	760	672	521
800	066	177	241	375	477	620	755	703	643	516
1000	076	194	260	381	446	568	650	573	545	381
1200	086	204	268	339	399	490	533	436	435	306
1400										
1600	095	204	224	255	282	329	332	237	242	176
2000	089	157	165	176	180	199	190	126	111	086
2400	065	112	114	113	111	104	096	065	045	026

20871-542

10-10
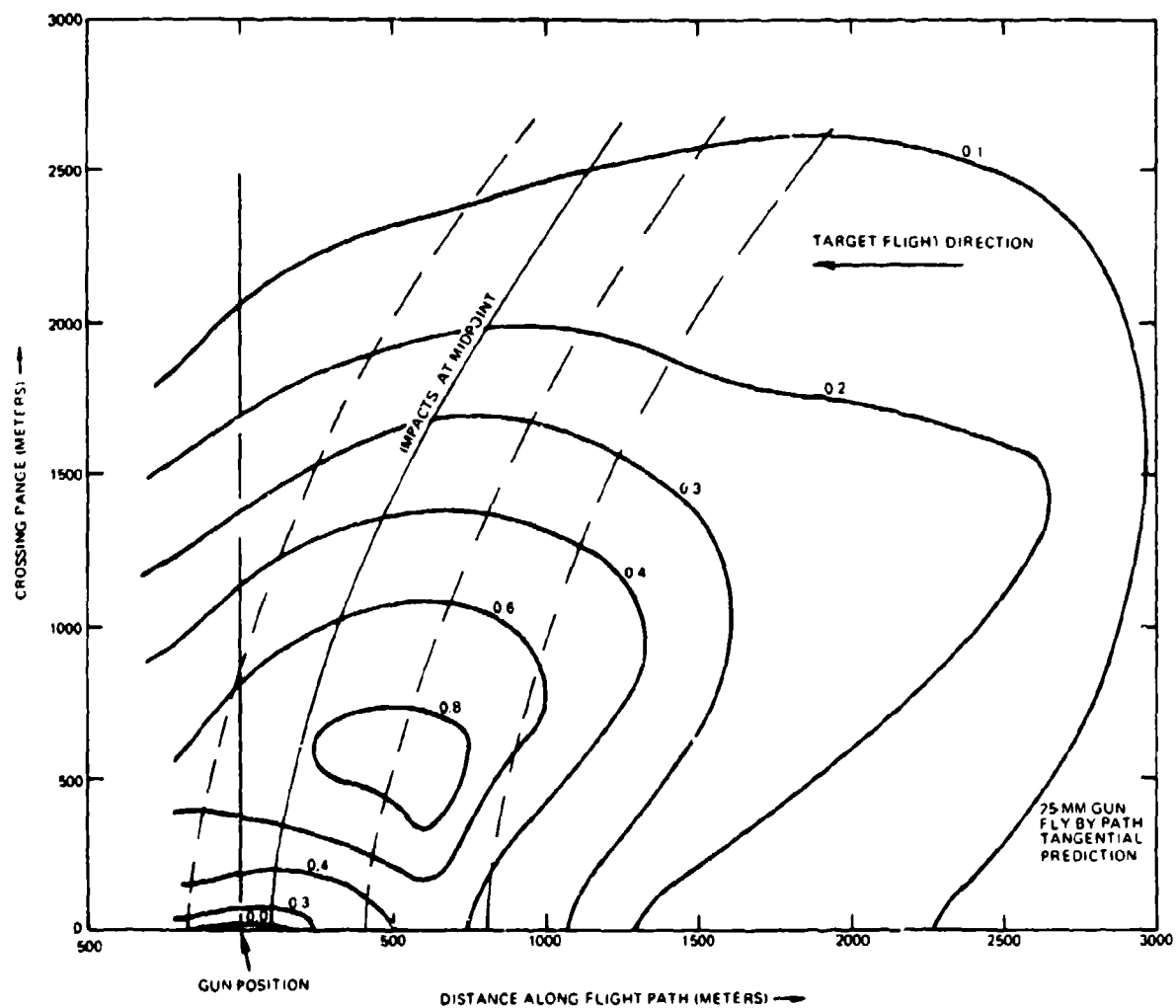
Figure 10-6. Footprint in Ground Plane of Constant Contours of Kill Probability with 1-Second Burst

20871 209

Table X-5. Foot Print Data For 25 mm Gun With Tangential Predictor on Jinking Path

Crossing Range (m)	Fire Point (m)									
	3000	2500	2000	1500	1200	900	600	300	0	-300
0	011	030	052	124	175	353	474	395	008	116
100	011	031	061	142	200	356	501	229	087	261
200	012	034	075	177	248	408	606	327	270	317
300	012	037	089	211	295	492	663	651	559	418
400	013	040	103	240	335	552	672	688	603	440
500	013	044	115	261	365	579	649	655	625	412
600	014	046	125	275	383	566	618	610	559	377
700	014	048	133	282	379	534	579	571	535	352
800	015	049	139	277	355	499	533	534	492	360
1000	018	049	144	240	300	405	425	436	405	227
1200	015	045	134	197	247	319	323	330	320	173
1400	014	038	117	157	199	245	243	236	251	135
1600	013	028	100	122	157	185	180	159	192	110
2000	011	015	071	067	093	107	103	069	102	039
2400	010	009	046	029	050	062	065	033	030	010

20871-543

Table X-6. Foot Print Data For 50 mm Gun With Tangential Predictor on Fly-By Path

Crossing Range (m)	Fire Point (m)									
	3000	2500	2000	1500	1200	900	600	300	0	-300
0	.047	.169	.244	.346	.444	.693	.684			
100	.059	.148	.230	.383	.517	.598	.713	.454	.103	.48
200	.053	.165	.282	.456	.522	.694	.880	.695	.516	.59
300	.074	.167	.263	.417	.499	.670	.822	.789	.747	.68
400	.086	.198	.341	.481	.550	.750	.857	.888	.835	.755
500	.080	.209	.291	.526	.571	.721	.885	.916	.823	.68
600	.104	.181	.346	.531	.644	.804	.897	.896	.846	.755
700	.082	.249	.375	.583	.690	.821	.864	.866	.794	.69
800	.088	.261	.377	.578	.683	.733	.814	.810	.789	.709
1000	.088	.274	.376	.590	.640	.686	.663	.768	.598	.59
1200	.105	.263	.407	.507	.627	.590	.593	.592	.547	.50
1400										
1600	.111	.301	.359	.386	.402	.436	.488	.444	.373	.33
2000	.108	.243	.276	.296	.354	.328	.362	.374	.288	.257
2400	.136	.194	.179	.252	.307	.221	.190	.207	.199	.14

20871-544

Table X-7. Foot Print Data For 25 mm Gun With Linear Prediction on Fly-By Path

Crossing Range (m)	Fire Point (m)									
	3000	2500	2000	1500	1200	900	600	300	0	-300
0	02	08	16	34	50	59	76	00	00	00
100	02	09	17	37	53	69	83	29	01	42
200	03	10	20	42	59	78	85	43	26	67
300	03	11	23	47	66	85	91	78	86	90
400	03	12	27	52	70	90	95	91	93	92
500	03	13	29	55	73	92	96	95	94	91
600	04	14	31	56	74	93	95	95	95	87
700	04	14	32	57	74	91	94	94	93	79
800	04	14	32	56	72	89	92	92	90	68
1000	04	13	30	51	63	81	83	82	74	46
1200	02	10	25	40	49	67	66	63	46	19
1400										
1600	01	03	09	14	17	25	19	13	03	00
2000	00	00	01	01	02	00	00	00	00	00
2400	00	00	00	00	00	00	00	00	00	00

20871-545

10-14

Table X-8. Foot Print Data For 25 mm Gun With Linear Prediction on Jinking Path

Crossing Range (m)	Fire Point (m)									
	3000	2500	2000	1500	1200	900	600	300	0	-30
0	00	06	10	06	10	37	60	49	04	04
100	00	07	11	07	12	43	80	50	14	45
200	00	08	13	08	14	48	84	51	60	62
300	00	09	15	09	15	47	77	76	85	70
400	00	10	17	09	13	42	67	83	85	62
500	00	12	18	09	11	33	56	82	80	55
600	00	13	18	07	09	24	44	77	74	76
700	00	15	18	06	06	17	30	68	64	36
800	00	16	16	04	04	11	18	56	55	21
1000	00	18	12	02	01	04	04	27	30	09
1200	00	19	08	00	00	01	01	08	09	03
1400	00	18	04	00	00	00	00	01	01	00
1600	00	00	00	00	00	00	00	01	14	00
2000	00	00	00	00	00	00	00	00	04	00
2400	00	00	00	00	00	00	00	00	00	00

20871-546
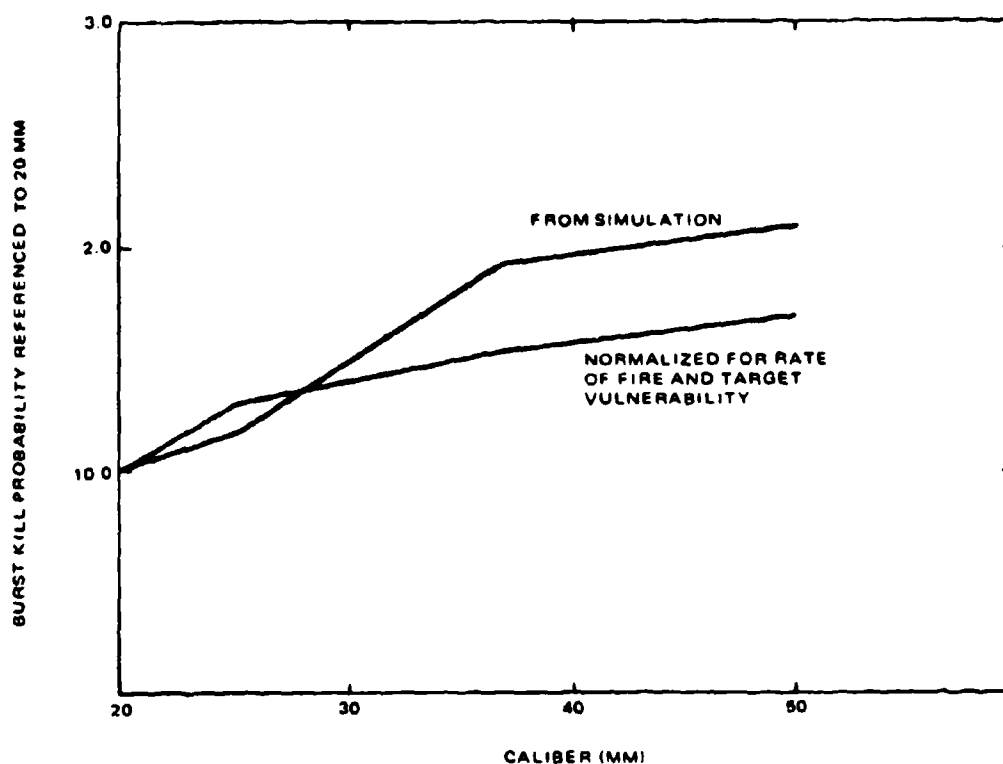
Figure 10-7. Comparison of Calibers

20871 210A
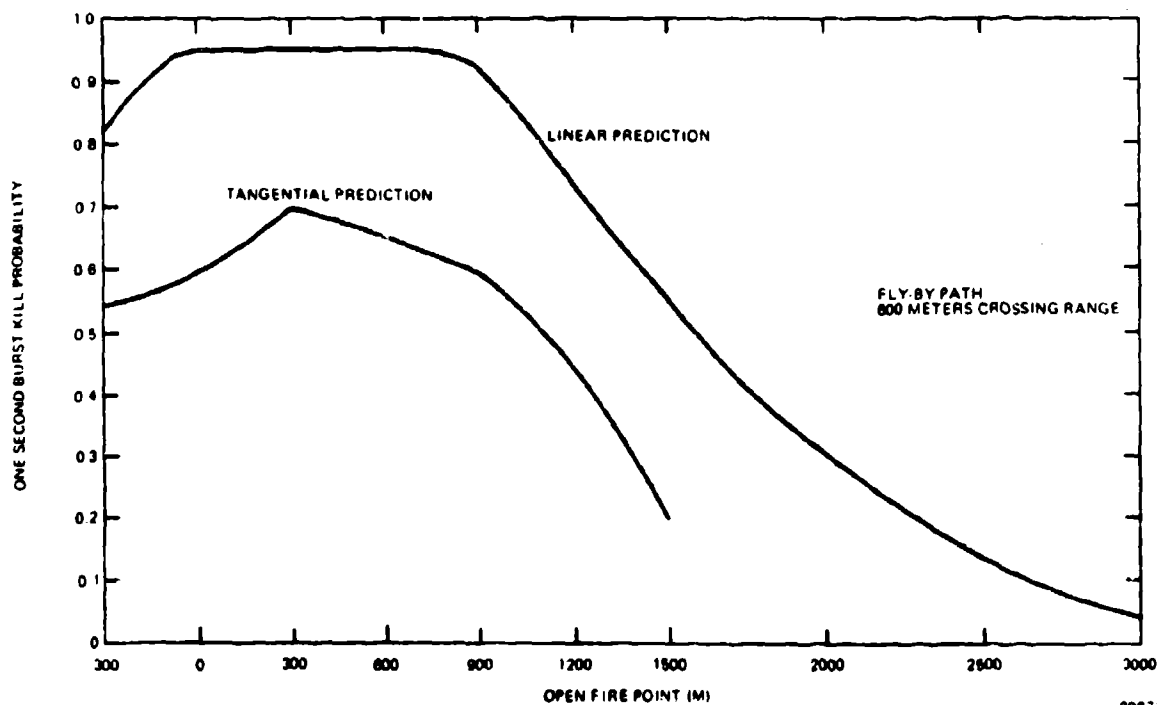
Figure 10-8. Comparison of Prediction Modes on Fly-By Path

20871 211
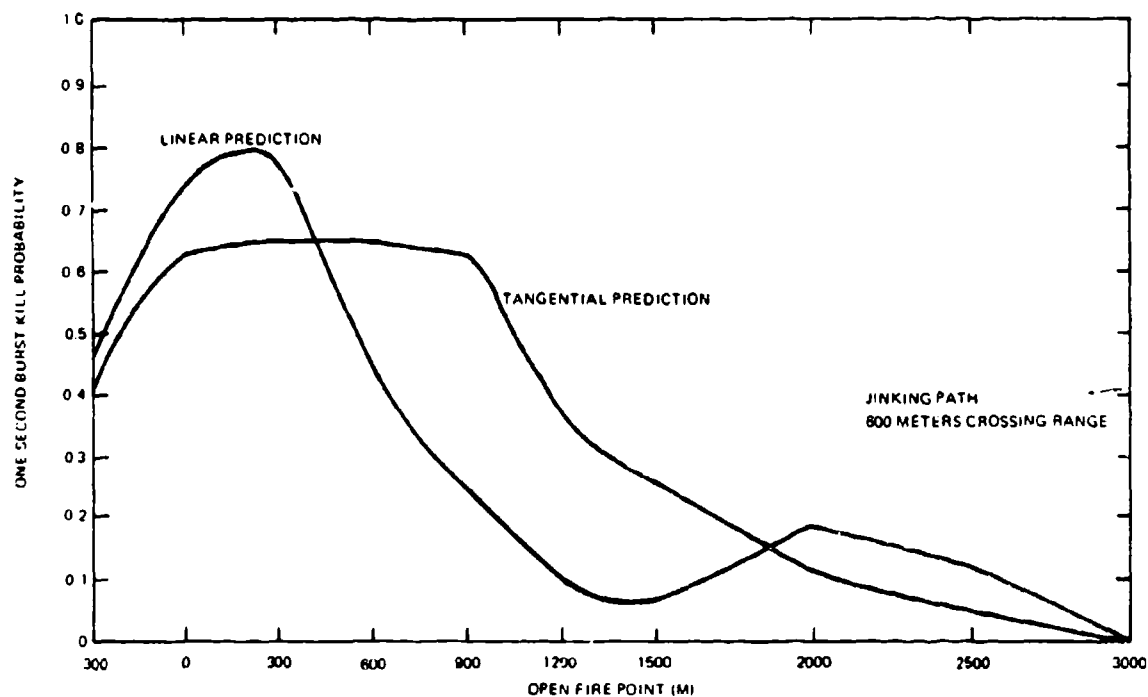
Figure 10-9. Comparison of Prediction Modes on Jinking Path
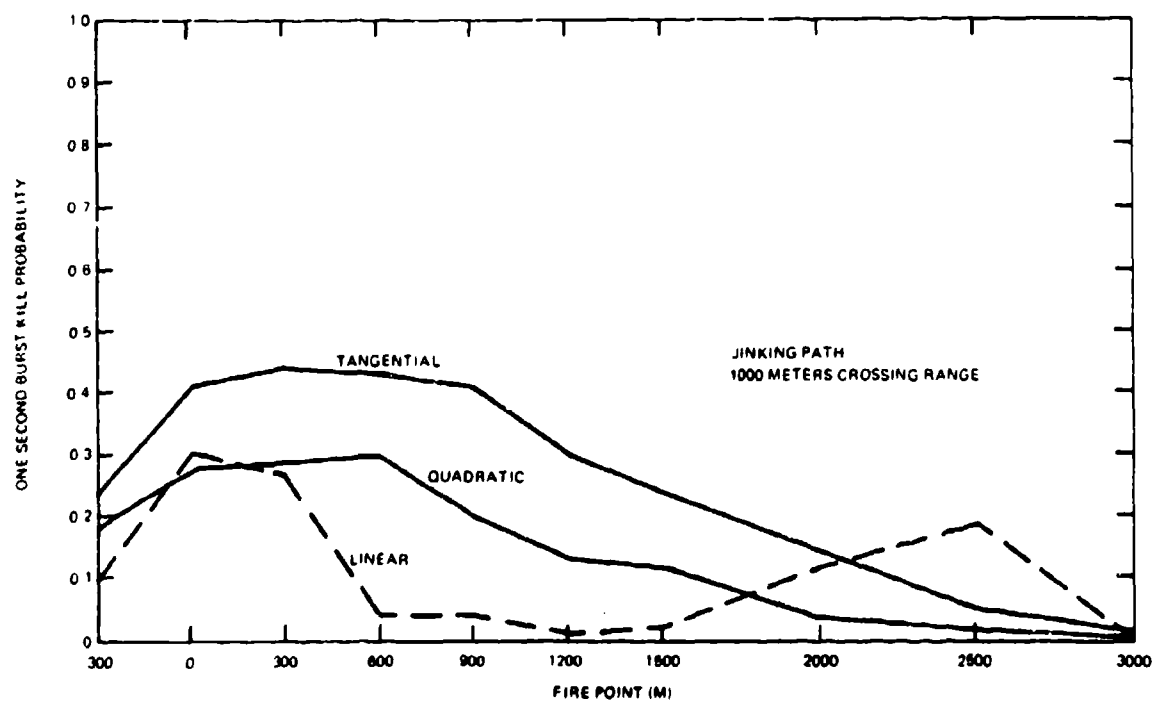
Figure 10-10. Comparison of Three Prediction Modes on Jinking Path
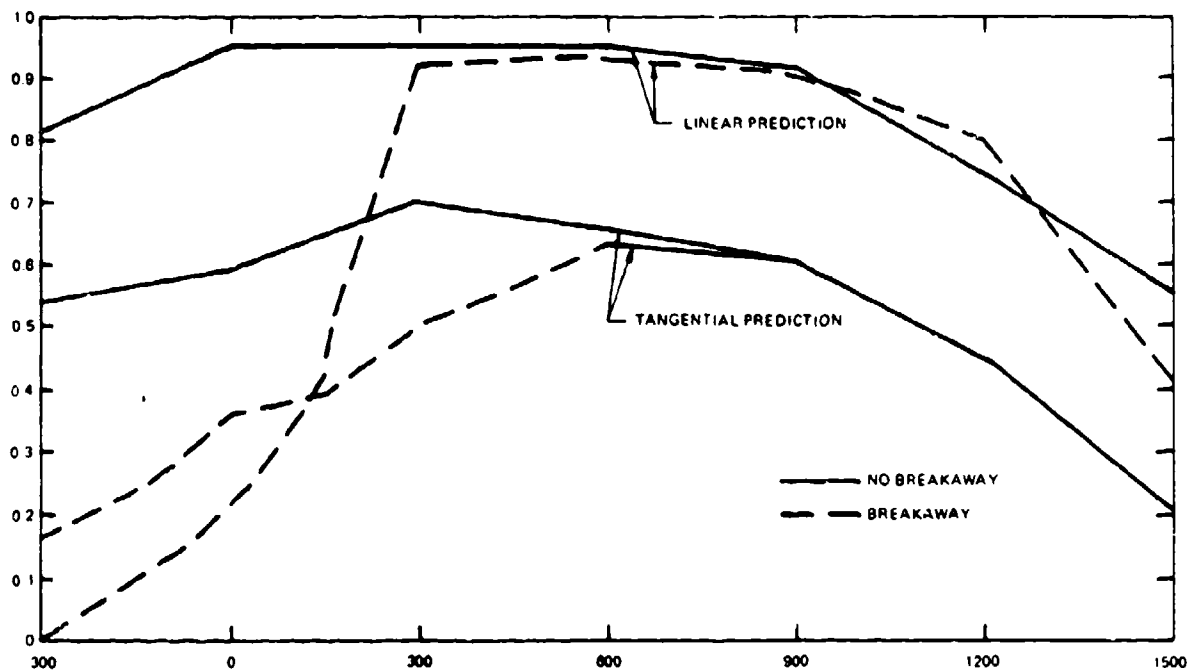
Figure 10-11. Comparison of Prediction Modes Versus Breakaway Maneuver

208°1 214

Table X-9. Effect of Muzzle Velocity and Burst Kill Probability

Fire Point (M)	20 MM		25 MM		37 MM	
	VM = 3600	VM = 5000	VM = 3600	VM = 5000	VM = 3600	VM = 5000
3000	.00	.00	.00	.00	.00	.00
2500	.16	.22	.18	.20	.29	.24
2000	.03	.28	.12	.32	.29	.47
1500	.00	.13	.02	.18	.07	.35
1200	.00	.11	.01	.15	.05	.28
900	.02	.21	.04	.24	.11	.39
600	.02	.29	.04	.32	.15	.51
300	.21	.57	.27	.58	.48	.72
0	.23	.53	.30	.52	.48	.63
− .300	.06	.25	.09	.24	.24	.33

20871-547

10-19
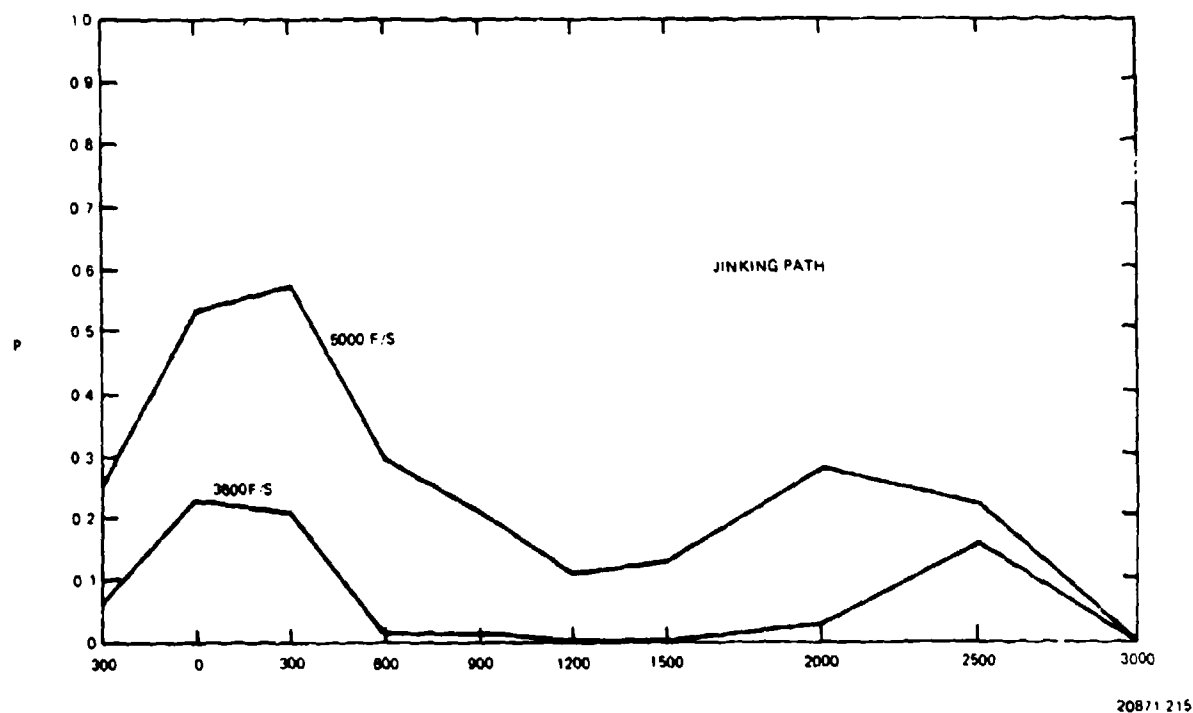
Figure 10-12. Effect of Muzzle Velocity on Burst Kill Probability with 20 mm Gun

20871 215

10-20
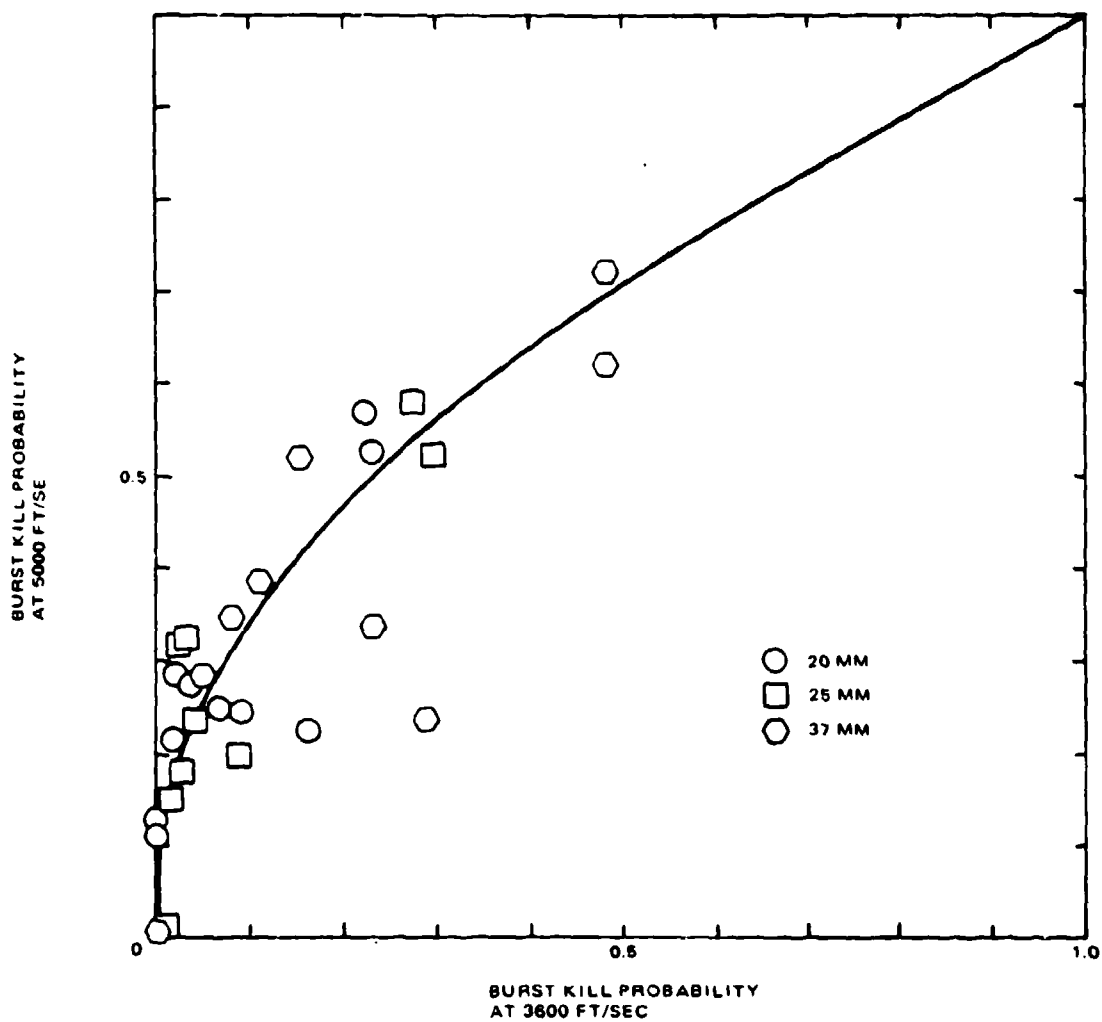
20871-216

Figure 10-13. Effect of Muzzle Velocity on Burst Kill Probability for Three Calibers
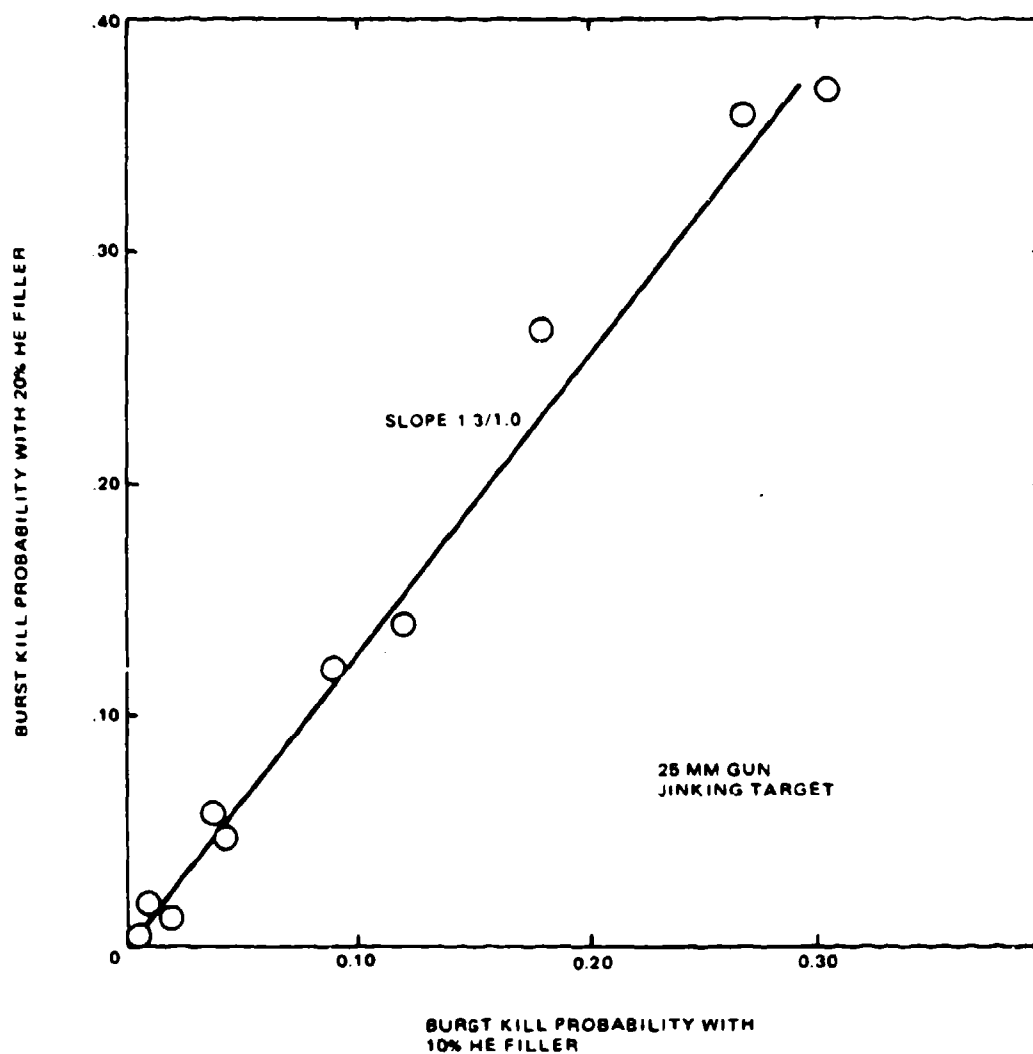
Figure 10-14. Effect of Increasing Terminal Effectiveness
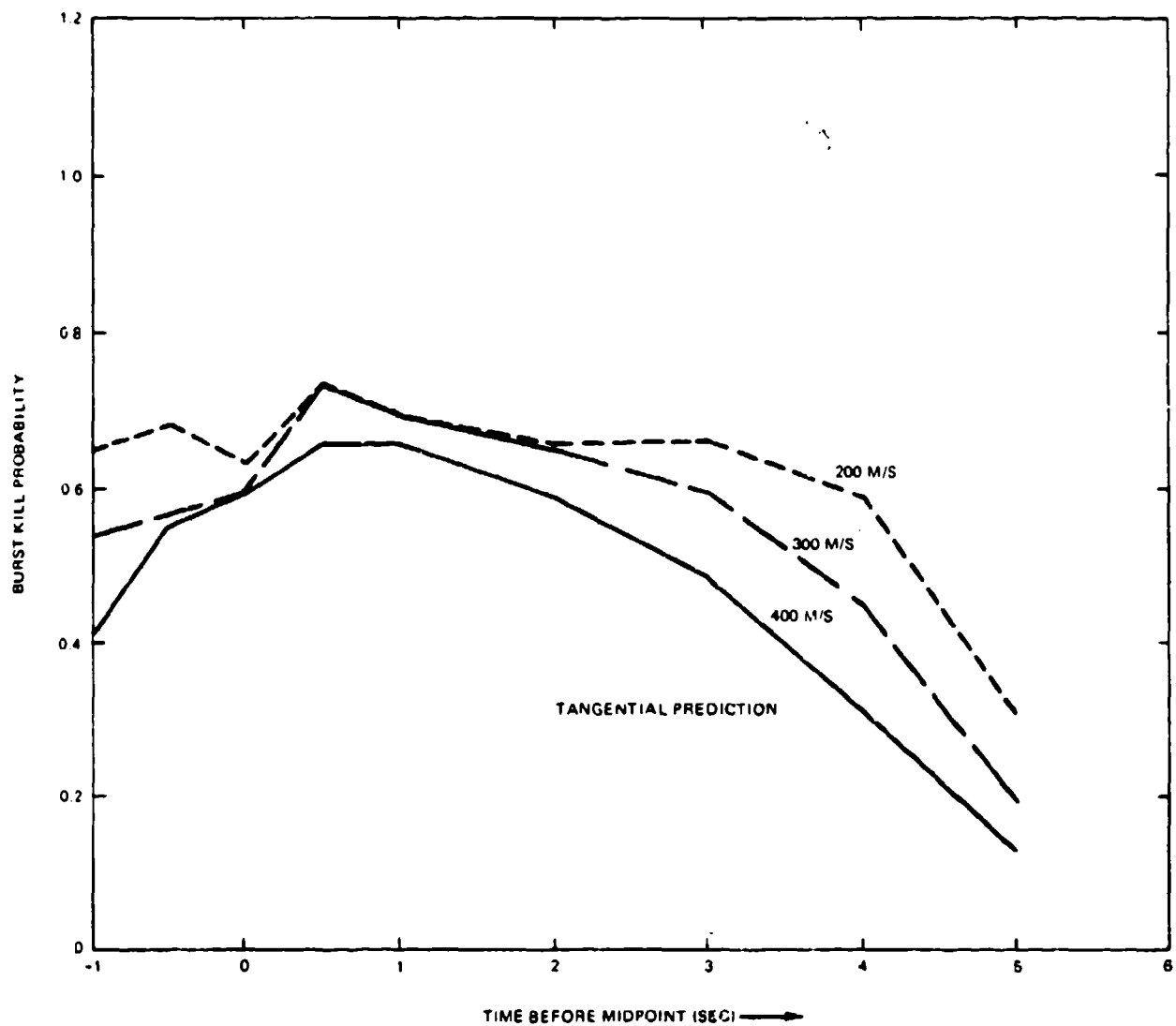
20871-217A

Figure 10-16. Effect of Aircraft Velocity on Burst Kill Probability with Tangential Prediction
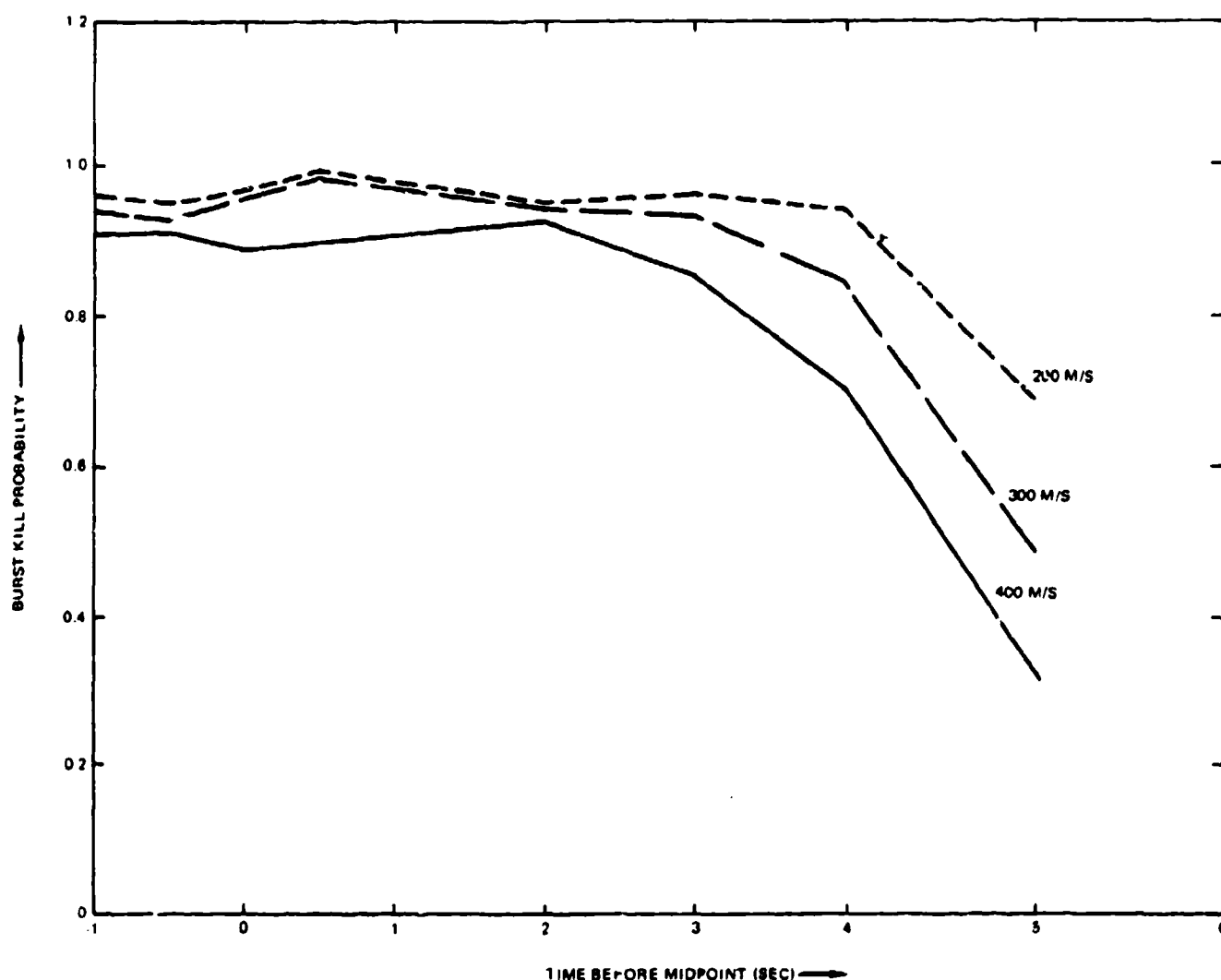
Figure 10-16. Effect of Aircraft Velocity on Burst Kill Probability with Linear Prediction

10.10 OPERATION OF SYSTEM WITH SENSOR INTERRUPTION

One of the most interesting modes of simulation operation allows tracking data from a sensor to be interrupted. The system then continues operation on internally regenerated data, which replaces the missing sensor data until the sensor is again assumed operable. This is a true simulation of a predicted fire system with a regenerative element, and allows the determination of how rapidly the solution deteriorates depending on which sensor is lost, and for how long.

There is a rough similarity between operating on regenerated data, and predicting with the data measurements at sensor loss and increasing time of flight by adding the elapsed time since sensor loss. Hence, one would expect the prediction error variances to grow roughly as:

$$\sigma_p^2 \cong \sigma_0^2 \left[1 + 2(t_p + T)/T_s + 2(t_p + T)^2/T_s^2 \right]$$

(10.6)

where t_p = time of flight, T_s = data smoother memory, and T is elapsed time from sensor failure.

In fact the real situation is worse than this, since the prediction literally goes off at a tangent with mean slope determined by the stored rates. This generates an increasing systematic error. The regeneration mode used in the simulation probably ameliorates the bias growth slightly, since the recirculation of data points superimposes a small dispersion as the stored points step through the filter coefficient set.

However, one would expect the length of time for which good shooting could be done on regenerated rates with all sensors blind, to be roughly comparable to the data smoothing memory time, at short times of flight, and decreasing with increasing time of flight.

Hence, with the 1.8 second filters, the only set used in these runs, one would not expect the regenerated solution to hold up well after about 1.5 seconds.

Simulation runs were made to demonstrate sensor interrupt against a 300 meter/second target at a constant altitude of 300 meters and a straight fly-by path. Figure 10-17 shows range error, and rms miss distance versus time for 500 meters crossing range. 'Sensor interrupt' designates failure of both angle and range sensors. 'Range interrupt' designates loss of range only. Path midpoint is at 8.0 seconds. Figure 10-18 shows the same data for 1000 meters crossing range. The gun was 25mm.

On the incoming leg the system performs well within complete sensor loss for two seconds, and the loss of range for two seconds at midpoint is almost undetectable. On the outgoing leg, where time of flight has become large, a good solution is rapidly lost without sensor data.

To show the effect of sensor interruption on kill probability, a 37mm gun with a 1200 rpm rate of fire was chosen, for a 1000 meter crossing range fly-by path and a 300 ms target velocity. It was assumed that 1) range only was lost at a point 1500 meters along the path from midpoint, and 2) all sensors were lost. Both 1-second burst kills probabilities, and the cumulative kill probability from 3300 meters before to 300 meters after midpoint, were obtained.

Figure 10-19 compares the burst kill probabilities against the values with no sensor loss. It is remarkable that the simulation shows slightly higher probabilities with all sensors lost than with only range lost. Cumulative kill probabilities over the engagement were 0.84 without sensor failures, 0.61 with range only lost at 1500 meters, and 0.64 with all sensors lost at 1500 meters.

A comparison of burst kill probabilities was then made with the 25mm gun, a crossing range of 1000 meters, and various sensor failures at 1200 meters before midpoint. Results are shown in Figure 10-20, for one-second bursts. Since the target speed was 300 meters/second, and in each case sensor failure occur-

red at 1500 meters, the points at 1200 meters represent the degradation from one second of regenerative operation to that point and the average loss during the subsequent one-second burst. As expected with a 1.8 second smoothing time, the degradation at 1200 meters firing point is not great. However, the solution rapidly degrades thereafter. In these runs range loss was less serious initially, but the solution decayed less rapidly at small values when angles were lost and range was retained. The reason is unknown.

10.11 SIMULATION OF 'FLY-THROUGH' MODE

Many past fire control systems, and at least one current system (Falcon) compute leads using angular rates and an estimated range. Range is set short so that the target 'flies through' it, and it is hoped that at the time of fly-through tracking will be good enough so that hits are obtained during the brief interval that lead is approximately correct.

A somewhat better fly-through system was simulated in which it was assumed that rectangular target velocities proportional to real target velocities could be generated without range data. That is, in theory at any rate, feasible. System performance was then examined with a constant range setting.

To perform the experiment, a special modified model deck was put together. The deck did not use the time of flight module. Instead, whenever time of flight was required, a constant value (which was input in the data deck) was used. Three runs were made with fixed time of flights corresponding to ranges of 1600, 1400 and 1200 m with the special deck. The system was tested against an aircraft executing a jinking path with a minimum ground crossing range of 1000m against the 25mm gun.

It is remarkable that higher burst kill probabilities (see Figure 10-21) were generated by the simulation over an extended path segment with constant range setting than with continuous range input. The reason for this mysterious result is unknown.

The simulation also has the capability of reproducing the performance of rate x time predictors with constant range setting, but time did not permit this mode to be explored.

10.12 THE EFFECT OF BIAS ERRORS

The effect of angular and muzzle velocity bias on burst kill probability was determined for a series of points on a constant speed constant altitutde fly-by path at 300 meters altitude and 300 meters/second. Crossing range was 1000 meters and the 25mm gun system with linear prediction was employed.

Table X-10 shows the simulation results. Figure 10-22 graphs the effect of azimuth bias, Figure 10-23 graphs the effect of elevation bias, and Figure 10-24 graphs the effect of muzzle velocity bias.
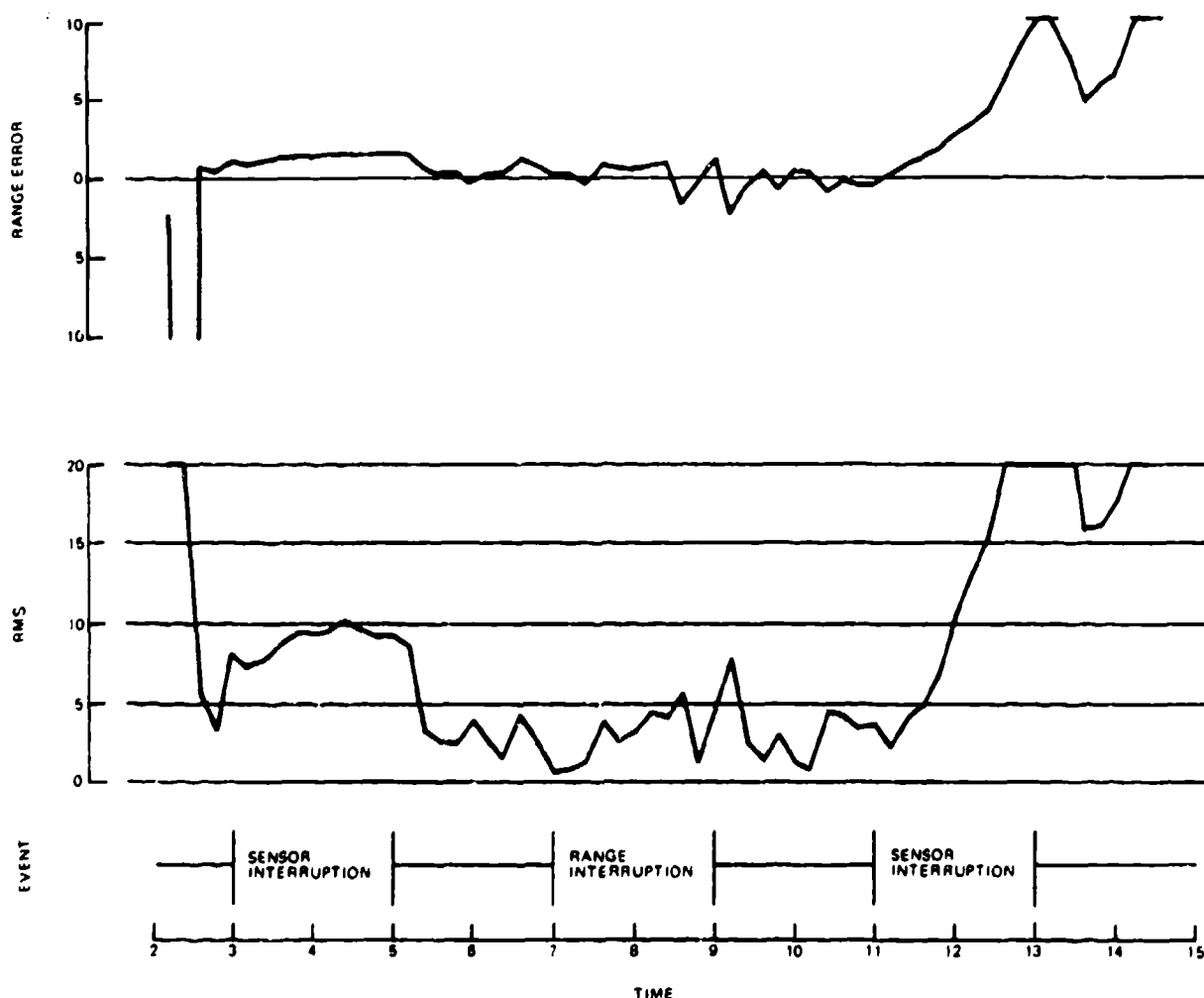
Figure 10-17. Aim Errors with Sensor Interrupt on a 500 Meter Fly-By Path

The results are somewhat mystifying. Elevation bias is much more serious than azimuth bias, as would be expected, since the target has on the average, a larger lateral extent than a vertical dimension. However, a negative muzzle velocity bias of about 36 ft/sec is indicated to be beneficial. One would expect muzzle velocity bias to behave about as azimuth bias near midpoint, and unfortunately only positive azimuth bias was run, so it cannot be determined whether one could get an improvement with negative azimuth bias also.

There are no obvious characteristics of the intended simulation program to explain the advantageous effect of muzzle velocity bias. Too low a muzzle velocity causes an increase in lead which would compensate for

servo lag, but at 1000 meters crossover, lag is not expected to be significant.

To compare the expected relative effects of angular and muzzle velocity bias: from Equation (7.113) of Section 7, the angular error at the target caused by muzzle velocity bias V_b is:

$$E = -(V_b/V_o)(V_t/V_r) \sin \Omega \qquad (10.7)$$

where V_t = target velocity, V_o = muzzle velocity, V_r = remaining projectile velocity and Ω = approach angle in slant plane. For the present case, this works out as approximately (near midpoint):

10-26
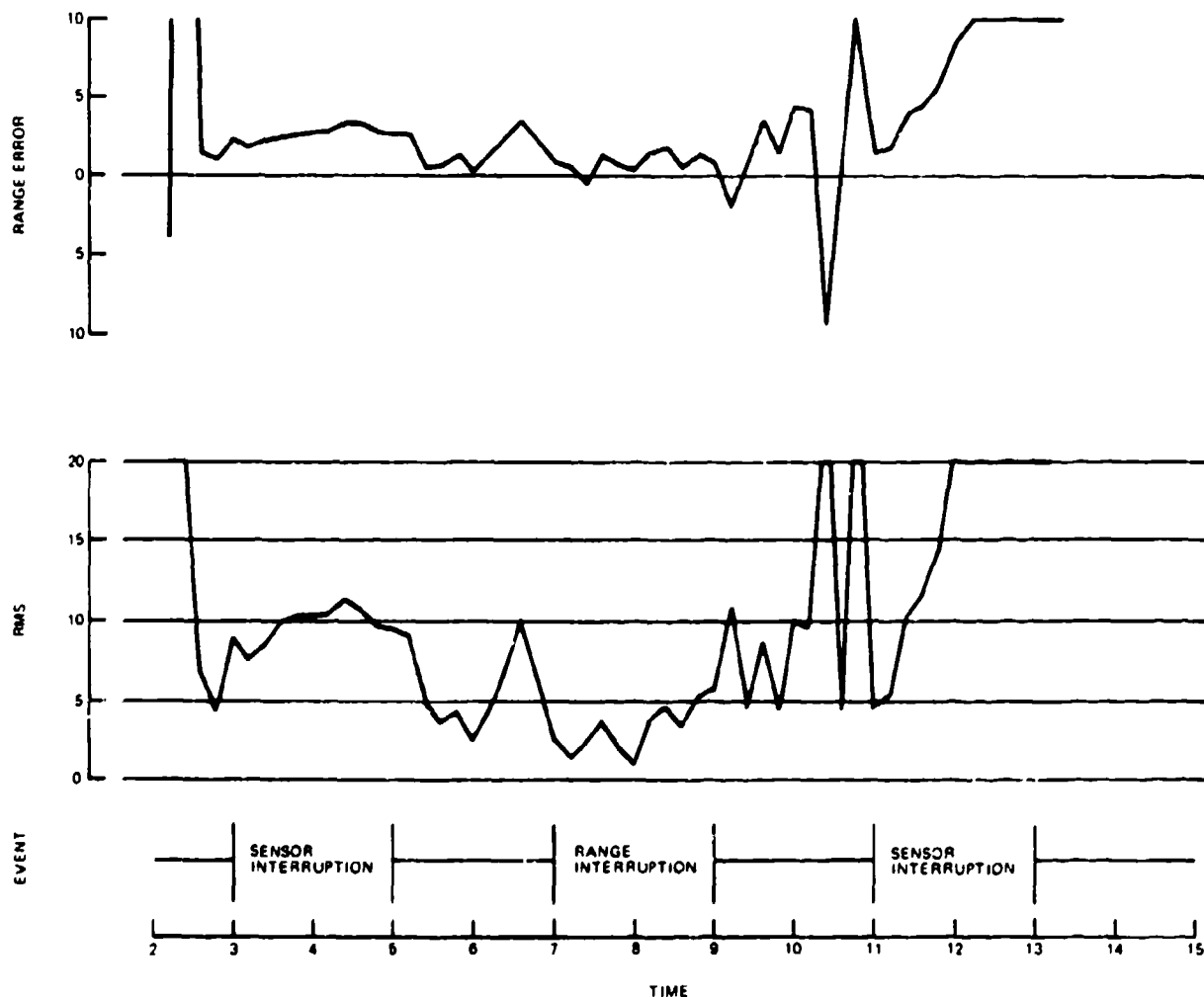
Figure 10-18. Aim Errors with Sensor Interrupt on a 1000 Meter Fly-By Path

20871-221

$$E(\text{mils}) \cong -0.1\ V_b(\text{ft/sec}) \qquad (10.8)$$

Hence, a 36 ft/sec muzzle velocity bias should have about the same effect near midpoint as a 36 mil azimuth bias. The cosine of elevation angle is close to unity on these low level paths.

10.13 FIRING DOCTRINE AND ANGULAR DISPERSION

By 'firing doctrine' is meant the specification of the open fire points and duration of fire of one or more firing segments. The simulation has the capability of accepting a designated set of these firing segments, and computing the target kill probability over the set, and then averaging across replications.

A set of runs was made to demonstrate this capability. A 25 mm gun system with 256 rounds on the mount was used. Fire rates of 64, 32 and 16 rounds per second were used against aa aircraft executing a fly-by with a minimum ground crossing range of 1000m, a constant altitude of 300m, and a constant velocity of 300m/sec. Ten fire doctrines were used. They are presented in Table X-11 and in graphical form in Figure 10-25. In addition to studying the fire doctrines, each fire doctrine was combined with five sets of dispersion parameters. Table X-12 presents the values of dispersion used. Table X-13 summarizes the results for the cases run as a function of angular dispersion.

10-27
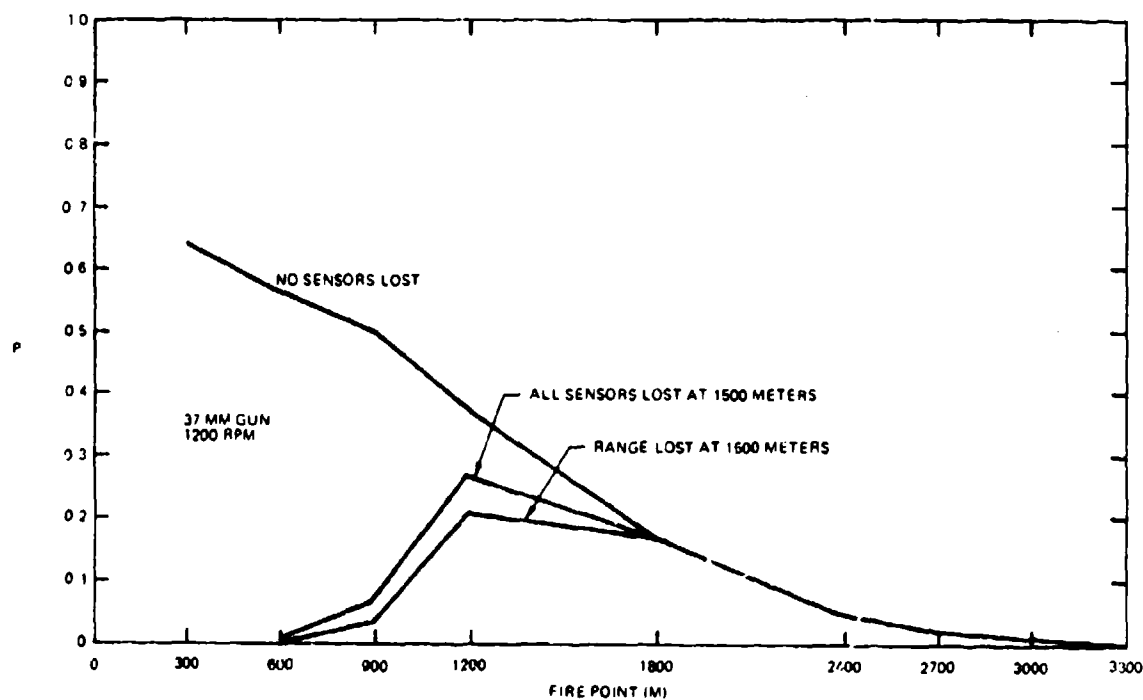
Figure 10-19. Effect of Sensor Failure on Burst Kill Probabilities
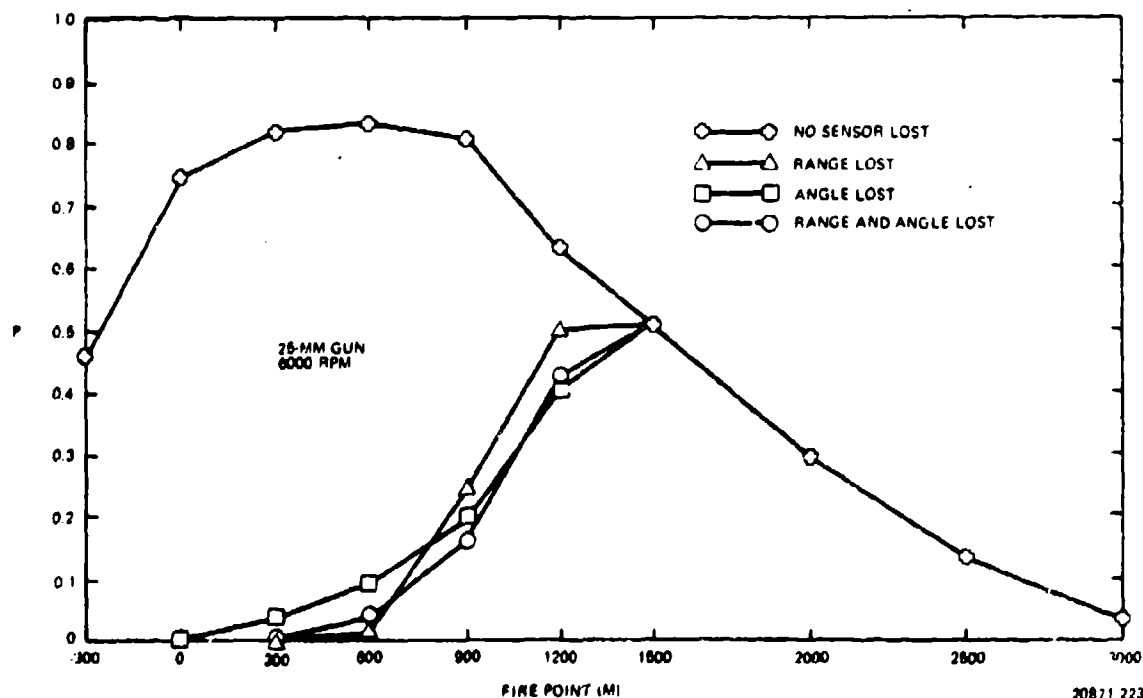
Figure 10-20. Effect of Selected Sensor Failures on Burst Kill Probabilities

10-28
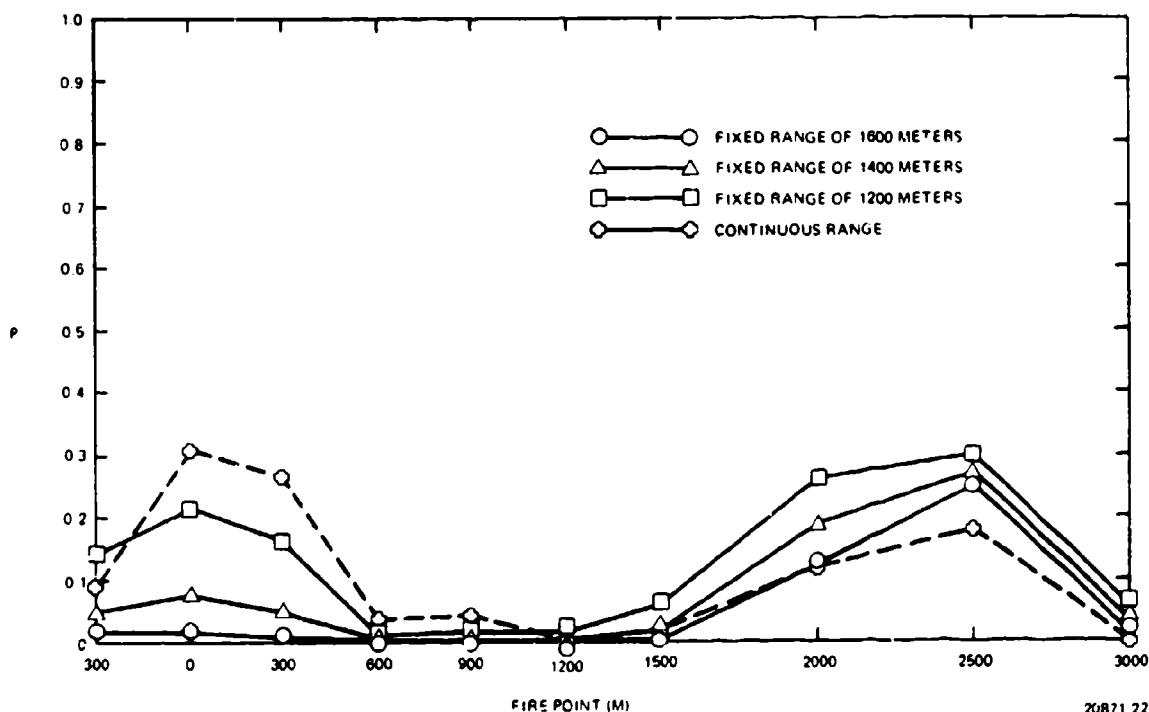
Figure 10-21. Burst Kill Probabilities in 'Fly-Through' Mode

All of these results were obtained using linear prediction.

Since single shot probability is highest at midpoint, the kill probabilities are highest in the case of those firing doctrines which include midpoint, other considerations being equal. However, in comparing Doctrines 5 and 7, both of which terminate at midpoint it will be noted that Doctrine 7, employing continuous fire, is superior. This would also be expected from an analytic solution: in the presence of aim wander it is better to fire a given number of rounds continuously over a specified range band, rather than firing the same number in a series of bursts over the same range band.

For this set of data, the best value of dispersion turns out to be about 4 to 5 mils. Although not investigated, it would be expected that still better results might be obtained by an elliptical dispersion pattern.

10.14 EFFECT OF MUZZLE VELOCITY DISPERSION

The effect of muzzle velocity dispersion was also investigated for the target/path situation of the previous section, and the 25 mm gun. The linear prediction mode was used. A set of values of muzzle velocity dispersion was examined in conjunction with two values of angular dispersion. The results are given in Table X-14 and the one-second burst kill probabilities are plotted in Figure 10-26. For this parameter set the

simulation generates the highest burst kill probabilities with 3 mils angular dispersion and zero muzzle velocity dispersion.

10.15 AN IMPRESSIONISTIC MODEL OF MANUAL TRACKING

In the absence of real tracking data with manual tracking systems against aircraft on which to build a realistic simulation, the simplistic model used in AFAADS-I was again employed, using the radar glint model as a basic noise source. The model functions by generating a lag which is a function of angular velocity and acceleration, and the coefficients are those consistent with human operator tracking experiments on low bandwidth signals. The noise variance from the glint module is multiplied by a coefficient proportional to the angular lag. The result is that the variance of tracking error probably varies about as in the case of a human operator, but the bandwidth is too wide. The bandwidth could have been adjusted by choosing an appropriate combination of λ and σ_o in the glint module, but this was not done because of the general imperfections of this representation. For a better approach see Section 4.2.3, for which there was insufficient time to implement.

The results turn out to be interesting, however, Table X-15, shows the input parameters, and Table X-16 shows the 1-second burst kill probabilities for the

Table X-10. Burst Kill Probability as a Function of Bias Errors

1 Sec Bursts											
Bias Errors			900 Before Crossover	600 Before Crossover	300 Before Crossover	At Crossover	300 After Crossover	600 After Crossover	3 Second Burst 900 Before Crossover	3 Second Burst At Crossover	6 Second Burst 900 Before Crossover
Azimuth (mils)	Elevation (mils)	Muzzle Velocity (ft/sec)									
0	0	0	.71	.70	.75	.66	.71	.48	.98	.94	1.00
2	0	0	.69	.69	.71	.66	.71	.43	.97	.94	1.00
4	0	0	.66	.67	.66	.65	.67	.34	.96	.92	1.00
6	0	0	.61	.64	.61	.61	.60	.23	.95	.89	1.00
8	0	0	.56	.61	.55	.57	.52	.14	.93	.83	.99
0	2	0	.61	.54	.66	.76	.65	.43	.94	.94	1.00
0	4	0	.45	.36	.49	.73	.48	.31	.82	.89	.98
0	6	0	.27	.20	.29	.58	.25	.15	.58	.74	.88
0	8	0	.12	.09	.14	.33	.08	.06	.31	.43	.60
0	0	- 36	.76	.74	.88	.70	.55	.36	.99	.88	1.00
0	0	- 72	.61	.61	.76	.46	.25	.13	.97	.63	.99
0	0	-108	.35	.37	.43	.20	.04	.06	.77	.28	.84
0	0	-144	.13	.15	.15	.05	.00	.15	.36	.19	.50
0	0	-180	.03	.03	.03	.01	.00	.21	.08	.21	.28
0	0	-360	.00	.00	.00	.00	.00	.00	.00	.00	.00
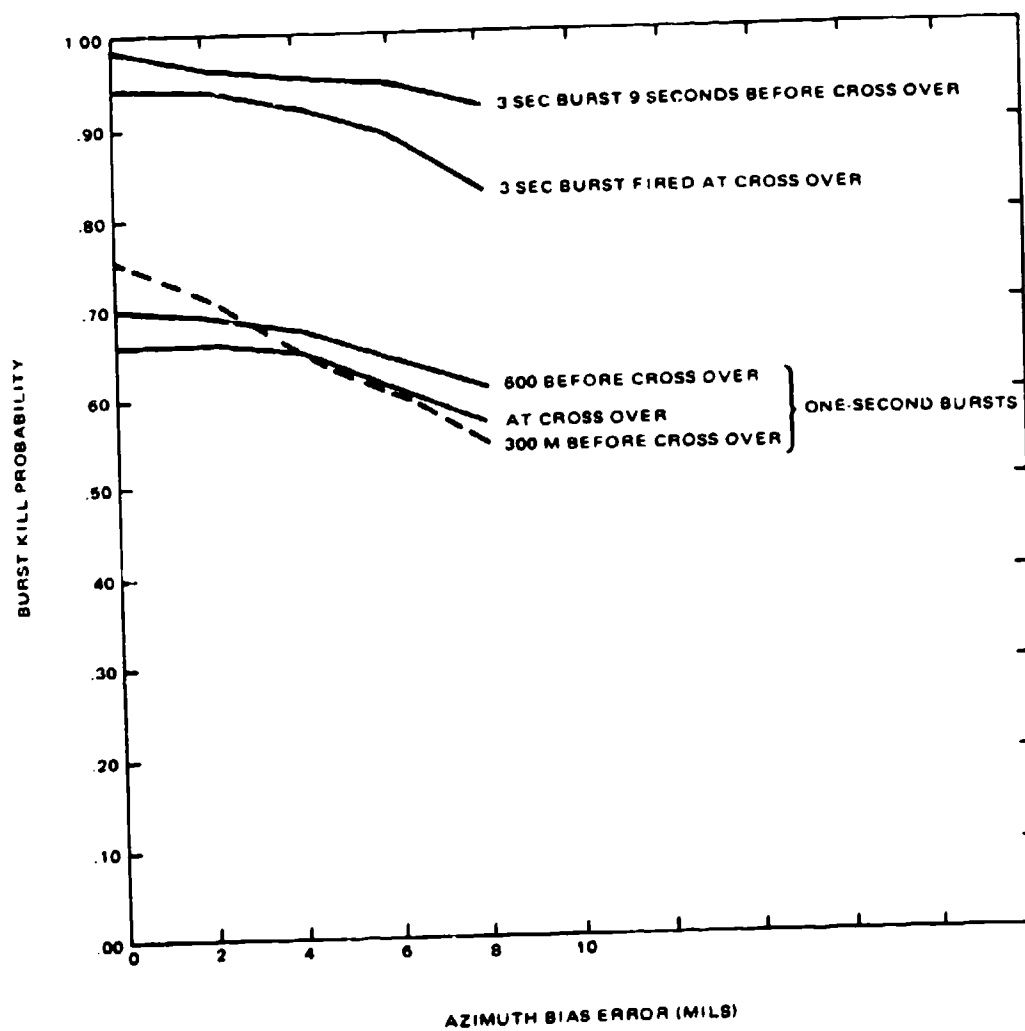
20871-225A

Figure 10-22. Effect of Azimuth Bias Error on Burst Kill Probability
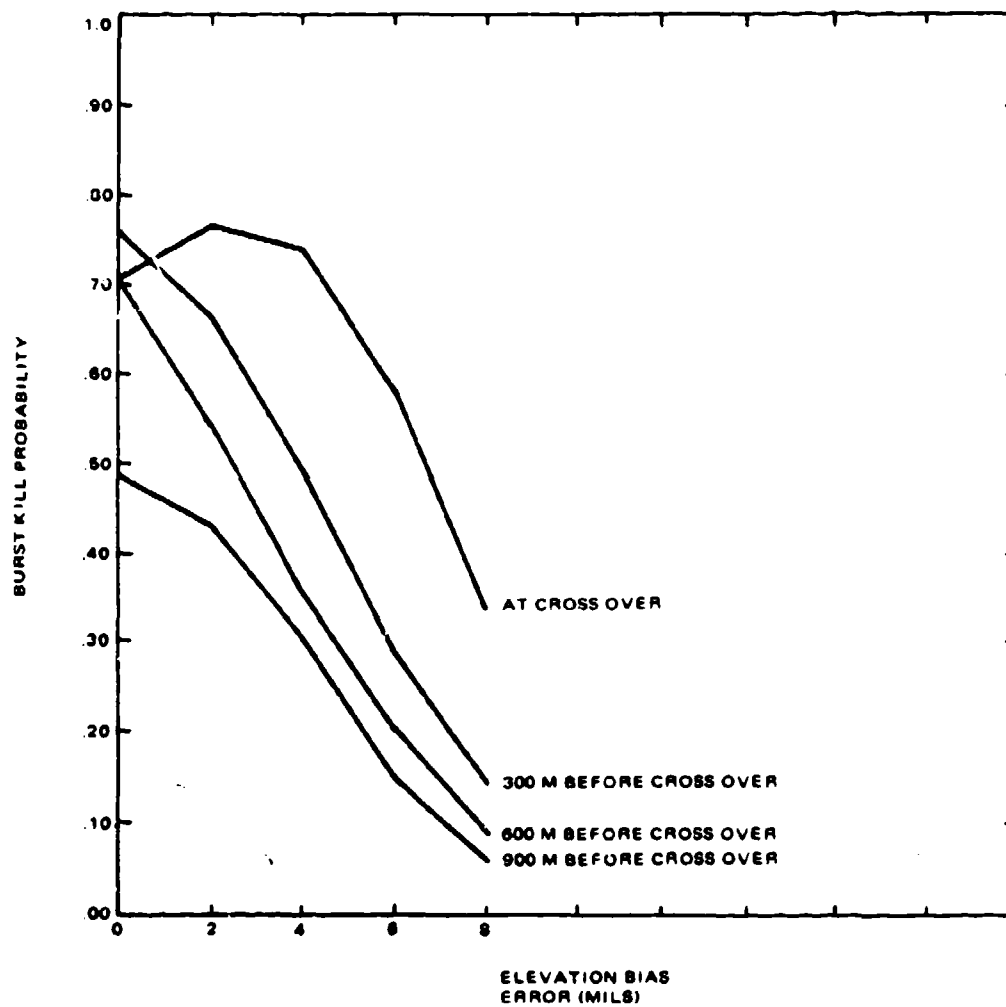
Figure 10-23. Effect of Elevation Bias Error on Burst Kill Probability
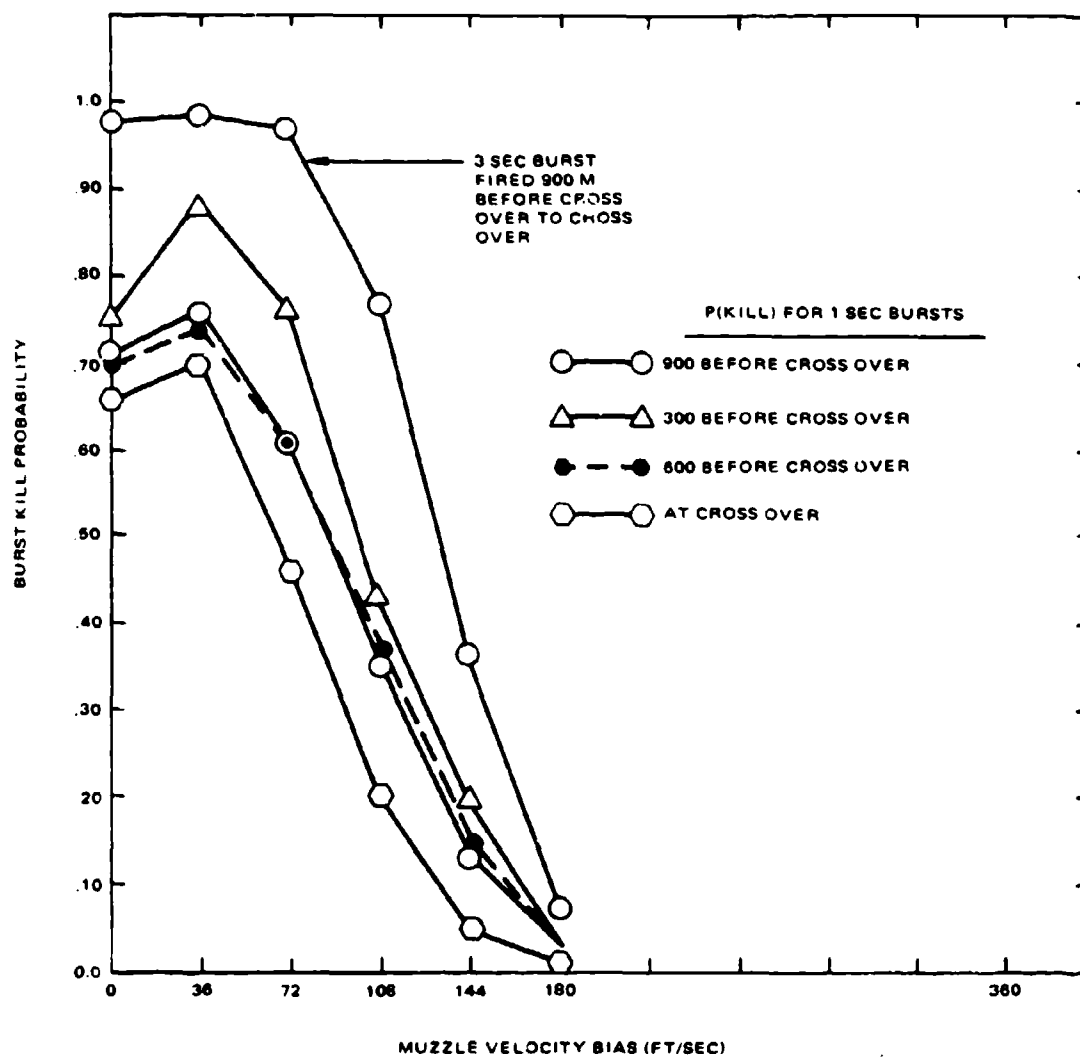
20871-226

Figure 10-24. Effect of Muzzle Velocity Bias Error on Burst Kill Probability

20871-227

Table X-11. Firing Doctrines Used

	Rate of Fire (Rounds/Sec)	Number of Bursts	Open Fire		Continuous/ Noncontinuous (C or N)	Fire Duration (sec)
			Time* (sec)	Distance from Midpoint (m)		
1	64	4	6	1800	C	4
2	64	4	4	1200	C	4
3	64	4	2	600	C	4
4	64	4	6	1800	N	7
5	64	4	7	2100	N	7
6	32	8	10	3000	C	8
7	32	8	12	3600	C	8
8	32	8	16	4800	N	15
9	16	16	16	4800	C	16
10	16	16	8	2400	C	16

*Relative Time: 0 = Crossover; + Before Crossover

20871-549

10-34
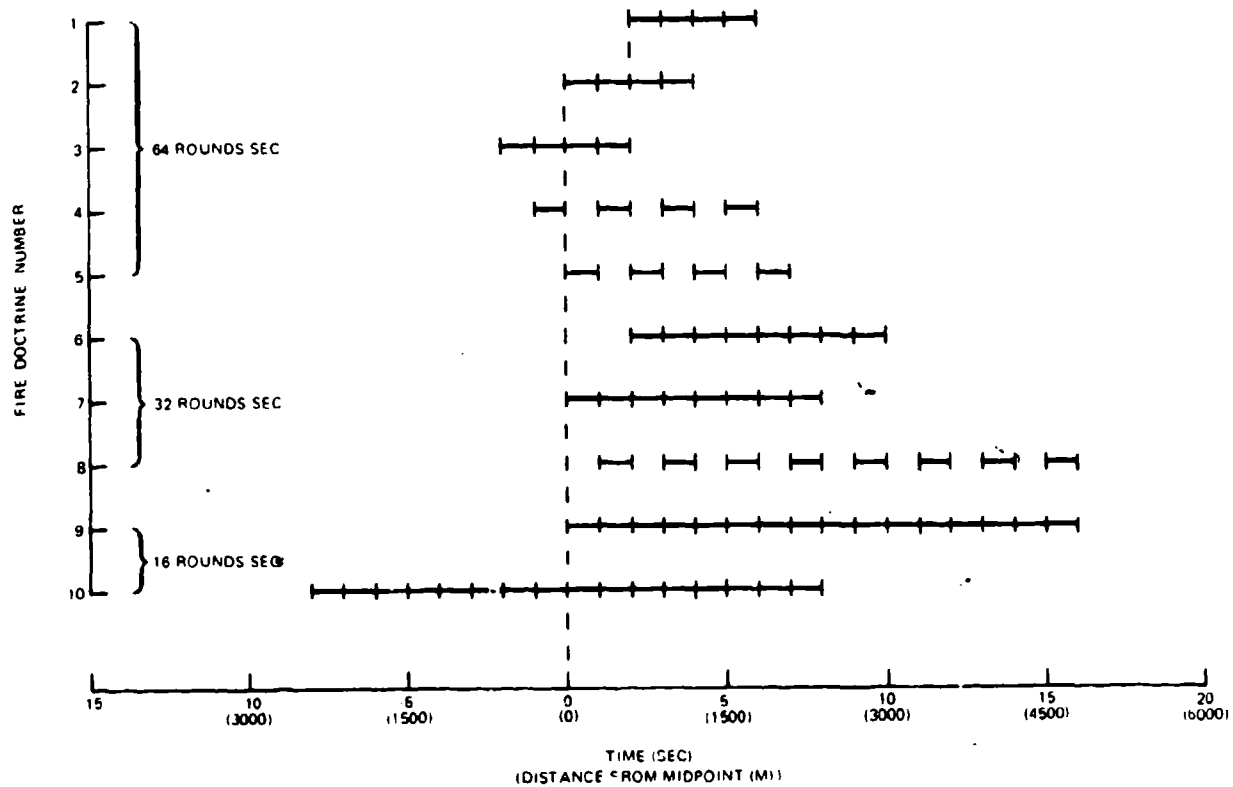
Figure 10-25. Graphical Representation of Fire Doctrines

20871 228
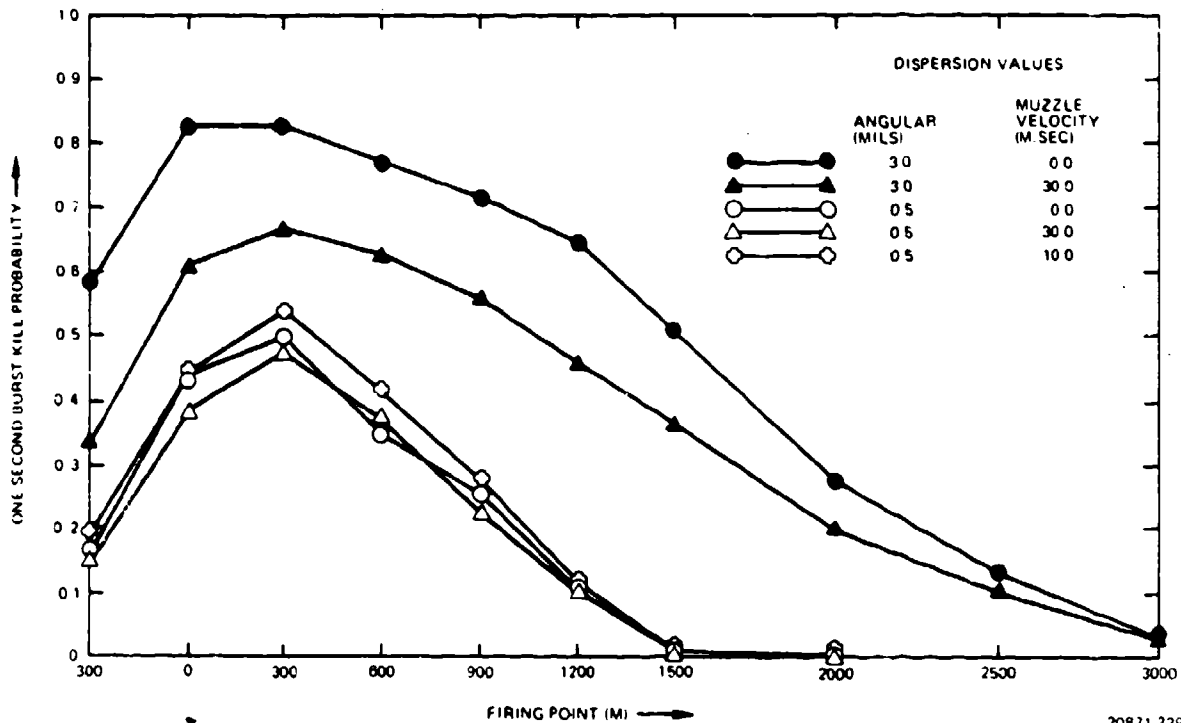
Figure 10-26. Comparison of Burst Kill Probability with Specified Angular and Muzzle Velocity Dispersions

25mm gun against a 300 meter/second target at a crossing range of 1000 meters. As expected the lags of the simplistic 'manual' system drastically reduce effectiveness. When, however, the tracking loop is closed with regenerative aid, the 'manual' system performs better than the reference 'radar' system. A similar effect was noted in the AFAADS-I simulation which was much simpler.

A possible explanation is that the algorithms make the noise variance of the glint model an increasing function of K_t, as is the bandwidth. For relatively low K_t the gener-

ated tracking noise is of small magnitude and smooth. The large lag associated with small K_t is removed by the regeneration, for a net overall improvement. This may not be too unrealistic a representation of a human operator with regenerative tracking, even though it is a makeshift at this time.

10.16 DIVE BOMBING TARGET

A series of simulation runs was made with a target path representing a 'pop-up' and dive on a target near the gun. Two dive angles, 45° and 30° were employed. For the 45° case, the target pops up to an altitude of 3000 meters, makes an approach pass of 8 seconds

Table X-12. Dispersion Values Used

| Dispersion Set No. | Angular Dispersion | | Muzzle Velocity Dispersion (m/sec) |
	Lateral (mils)	Vertical (mils)	
1	1	1	0
2	2	2	0
3	3	3	0
4	4	4	0
5	5	5	0
6	6	6	0

20871-550

duration, then breaks away at 5g. In detail, the breakaway consisted of a 5g vertical acceleration for one second, then a combined 3g right turn with 4g vertical acceleration for a vector 5g total acceleration. Paths 1a,b, were for 45° dives with minimum aircraft altitude of 1000,2000 meters. Paths 2a,2b were corre-

sponding 30° dives. On these paths the aircraft was assumed to have a 'free-maneuver' bomb sight so that it could come 'down the chute' jinking until the moment of weapon release, when it was pointed at the ground target. For reference Path 2c was a repeat of 2a without jinking. Table X-17 summarizes these cases.

These turn out to be interesting paths for system comparison because they are difficult for the defender. The attach path segment lies beyond about 1600 meters and begins at greater than 3000 meters. Typical variations of aircraft range and velocity with time are shown in Figures 10-27, 28, 29 and 30.

The first result, as shown by Tables X-18 and X-19 and Figures 10-31, 32 and 33, is that high muzzle velocity helps a great deal. A second result, shown by Table X-20 is that linear and quadratic are inferior to tangential and 'defense of a known point' modes against the jinking target. A third result, shown by Table X-21 is that jinking is of considerable benefit to the attacking aircraft.

Table X-13. One-Second Burst Kill Probability as a Function of Angular Dispersion

| Fire Doctrine Number | Angular Dispersion (mils) | | | | |
	1	2	3	4	5
1	.21	.71	.87	.90	.87
2	.52	.87	.96	.97	.97
3	.58	.89	.96	.97	.97
4	.49	.85	.94	.95	.94
5	.42	.79	.90	.92	.91
6	.22	.66	.81	.84	.81
7	.50	.84	.93	.95	.93
8	.30	.62	.77	.80	.77
9	.37	.68	.79	.81	.78
10	.37	.68	.80	.81	.79

20871-551

10-37

Table X-14. One Second Burst Kill Probability as a Function of Firing Point and Dispersion

Fire Range (M)	Angular Dispersion .5 Mils σ_{V_o} (M/Sec)					Angular Dispersion 3 Mils σ_{V_o} (M/Sec)				
	0	5	10	15	30	0	5	10	15	30
3000	0	0	0	0	0	.03	.03	.03	.03	.03
2500	0	0	0	0	0	.13	.13	.13	.12	.10
2000	0	0	0	0	.01	.28	.28	.27	.26	.20
1500	.01	.01	.01	.01	.01	.51	.51	.49	.47	.37
1200	.10	.11	.11	.11	.10	.65	.64	.62	.58	.46
900	.26	.27	.28	.28	.24	.72	.71	.70	.67	.56
600	.35	.38	.41	.41	.37	.77	.77	.76	.74	.63
300	.50	.52	.54	.53	.48	.83	.82	.81	.78	.67
0	.44	.46	.46	.45	.39	.83	.82	.79	.75	.61
-300	.17	.18	.19	.18	.15	.58	56	.52	.47	.34

20871-552

Table X-15. Simulation Parameters for Manual Tracking Modes

Parameters	Rate Tracking	Rate Aided Tracking	Regenerative Aided Tracking	Control Case Radar
Kv	5.0	10.0	10.0	500.0
Ka	999999	10.0	10.0	90.0
μ	25.0	25	25	.00
σ_R	2.0	2.0	2.0	2.0
λ	3.0	3.0	3.0	3.0
Regeneration	No	No	Yes	Yes

20871-553

Table X-16. One-Second Burst Kill Probabilities With Simulated Manual Tracking

Fire Point (M)	Rate Tracking	Rate Aided Tracking	Regenerative Aided Tracking	Control Case Radar
3000	.00		.07	.04
2500	.00	.1	.19	.13
2000	.01	.02	.39	.30
1500	.00	.01	.63	.51
1200	.00	.02	.76	.63
900	.02	.12	.88	.81
600	.03	.10	.89	.83
300	.06	.19	.86	.82
0	.12	.20	.80	.74
−300	.10	.37	.60	.46

20871-554A

Table X-17. Major Path Parameters

Path	Dive Angle	Minimum Ground Clearance (M)	Jinking Included
1a	45°	1000	Yes
1b	45°	2000	Yes
2a	30°	1000	Yes
2b	30°	2000	Yes
2c	30°	1000	No

20871-555

Although the individual one-second burst kill probabilities shown in these tables are low, they cumulate to effective values if the weapons have enough ammunition on board to fire over the whole attack pass.

This set of target paths, the last examined in the present effort, turned out to be the most discriminating in terms of defense system characteristics.

10.17 PROPOSED CHECK-OUT PROGRAM PACKAGE FOR SIMULATION

The following check-out program procedures for the simulation should have been implemented ab initio, but their absolute necessity for the present complex

simulation, as compared with the simpler AFAADS-1 simulation was not appreciated until late in the contract effort when it became apparent that individual program module verifications at selected points were insufficient to validate the complete simulation.

A preliminary outline of the check-out procedures is as follows:

a. With zero tracking error, zero servo lag and no regeneration lag correction as inputs, operate simulation against level constant velocity target path. Print out miss distance. Miss distance should be zero to several decimal places at each point. Verify all prediction algorithms in this mode.

b. Repeat on straight line dive path with acceleration along flight path equal to $g \sin \theta$. Miss distance should be zero because of the dive-acceleration algorithm.

c. Repeat on level path with constant horizontal rate of turn. Miss distance should print out zero with quadratic algorithm.

d. Repeat on straight line dive path through defended point with acceleration along path $g \sin \theta$. Miss distance should print out zero for defense of known point algorithm.

10-39
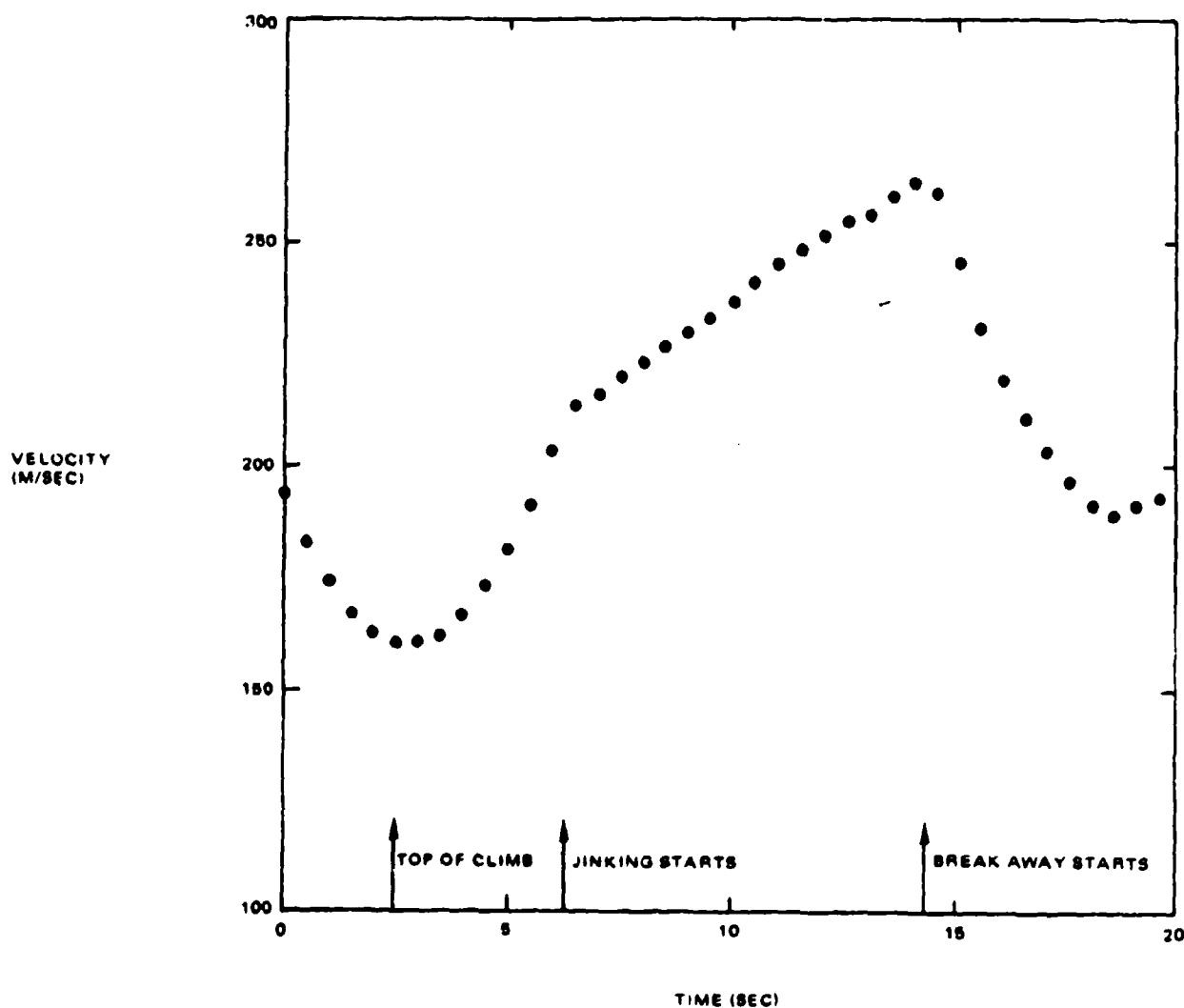
Figure 10-27. Velocity Profile of Path 1a

20871-230

NOTE: These four tests validate both the filter coefficients, and the prediction algorithms, which, together involve time constants to update smoothed derivatives and position as functions of smoothing time. These terms have been a repeated problem as new programmers move on and off the project. Continuing with zero tracking error,

e. With level, constant velocity target path, set track error zero and activate sensor lag and regenerative correction modules. Miss distance should print out very close to zero except at very short ranges.

f. Input spherical target with 1 meter radius. Set in target path as horizontal circle concentric to gun. Using quadratic prediction print out 1-second burst kill probability for specified set of lateral and vertical angular dispersions and muzzle velocity dispersion. The exact result is easy to compute by hand and the simulation result is compared with it.

g. Repeat (6) with specified angular dispersion and set specified lateral, vertical and muzzle velocity biases. Print out one-second burst kill probability. This result is easy to hand compute and check.

10-40
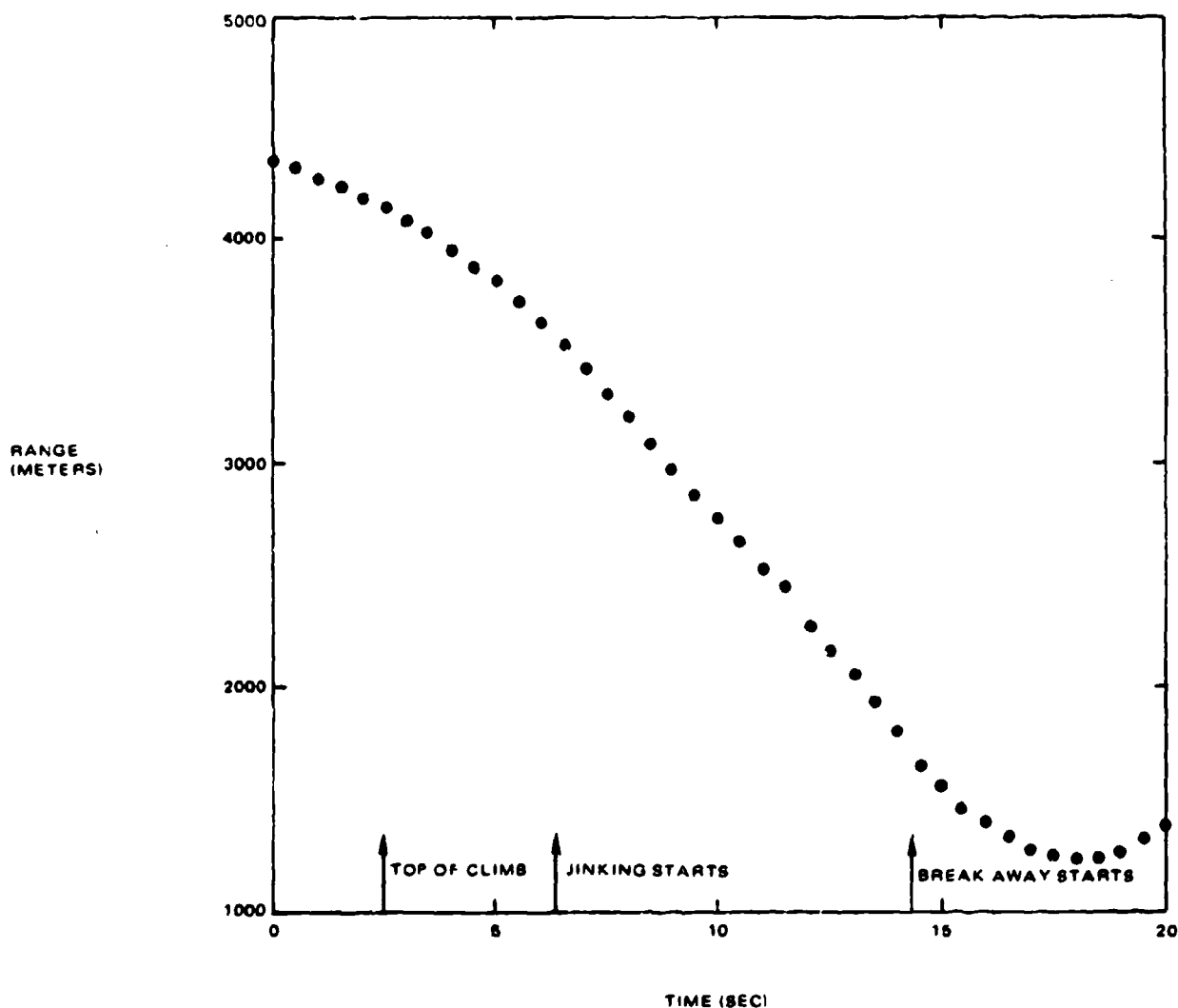
Figure 10-28. Range Profile of Path 1a

20871-231

h. Repeat (6) with ellipsoidal target, fuselage alone, wing alone, and both fuselage and wing. This case is also easy to hand compute. By re-running at the same radius and doubled velocity the target bank angle is changed, and the result can be validated by hand computation.

NOTE: The above set of validation runs should eliminate almost all of the problems that have been experienced with the simulation in the past contractual period. Other situations are rela-

tively easy to hand- compute and can be developed as additional verifications; for example the burst kill probabilities with linear and tangential prediction in test (6) are relatively easy to hand compute.

A more subtle test, to uncover undesired noise amplification in the many computational loops in the simulation is to input sampled sine wave noise instead of random noise, and determine the overall system noise amplification as a function of the frequency of the sampled input noise. This test is valid for real systems as well as the simulation, of course.
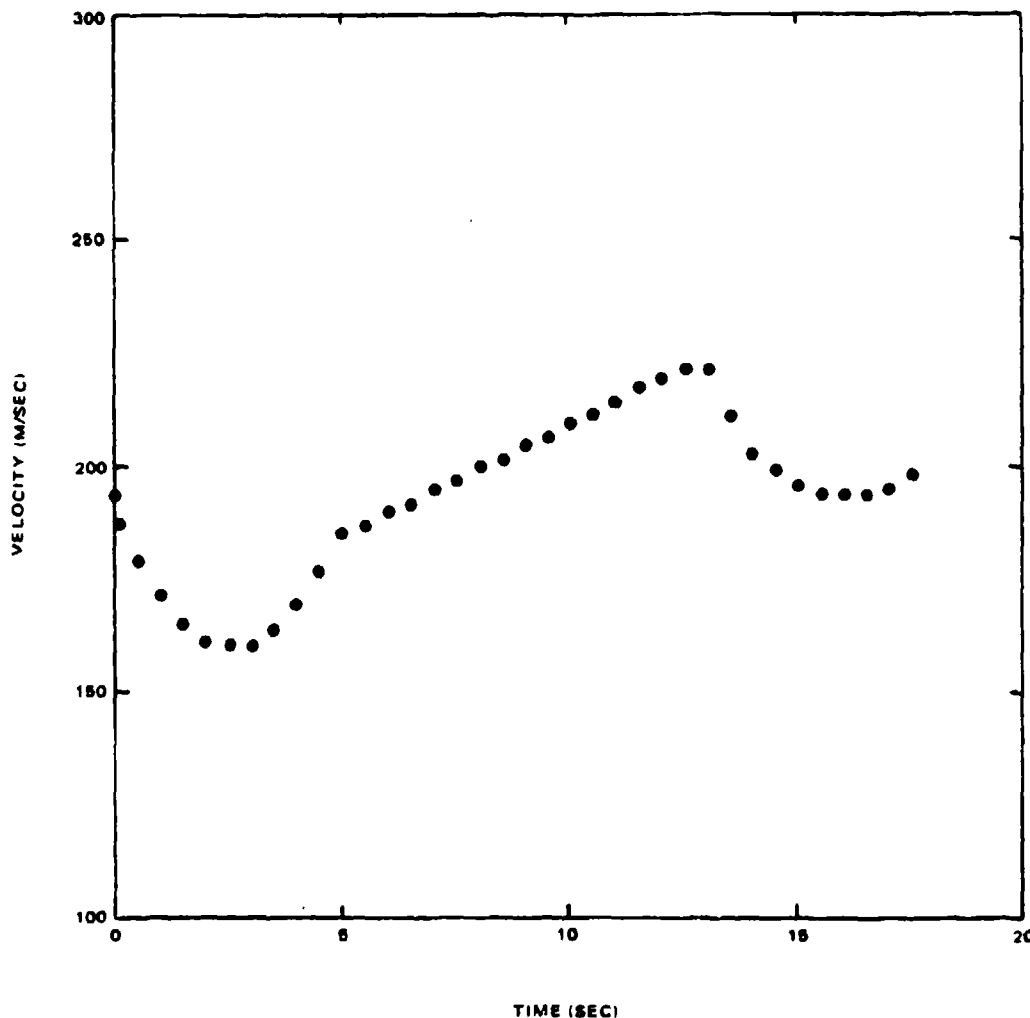
20971-232A

Figure 10-29. Velocity Profile of Path 2b

10.18 GENERAL CONCLUSIONS

The present Litton simulation provides an extremely versatile tool for supporting the analysis of predicted fire systems. Its major drawback is the lack of a program check-out package, as previously described.

Allowing for the possibility of a few minor residual programming imperfections, which may have affected some of the results presented in this section, some general conclusions regarding systems, based on these results, can be developed as follows:

a. The performance of all systems simulated was indicated to drop off rapidly with increasing time of flight. The time of flight effect is compounded

by the short, constant smoothing time of 1.8 seconds used in all results presented. A significant extension of effective range can be expected, if smoothing time is made an increasing function of slant range. The increase need not be directly proportional, and the functional form can be estimated by a combination of analysis and simulation.

In order to accomplish this functional variation, the preferable method is probably to use a recursive rather than finite memory set of data smoothing filters.

b. Increasing weapon muzzle velocity has a high

RANGE (METERS)

TIME (SEC)
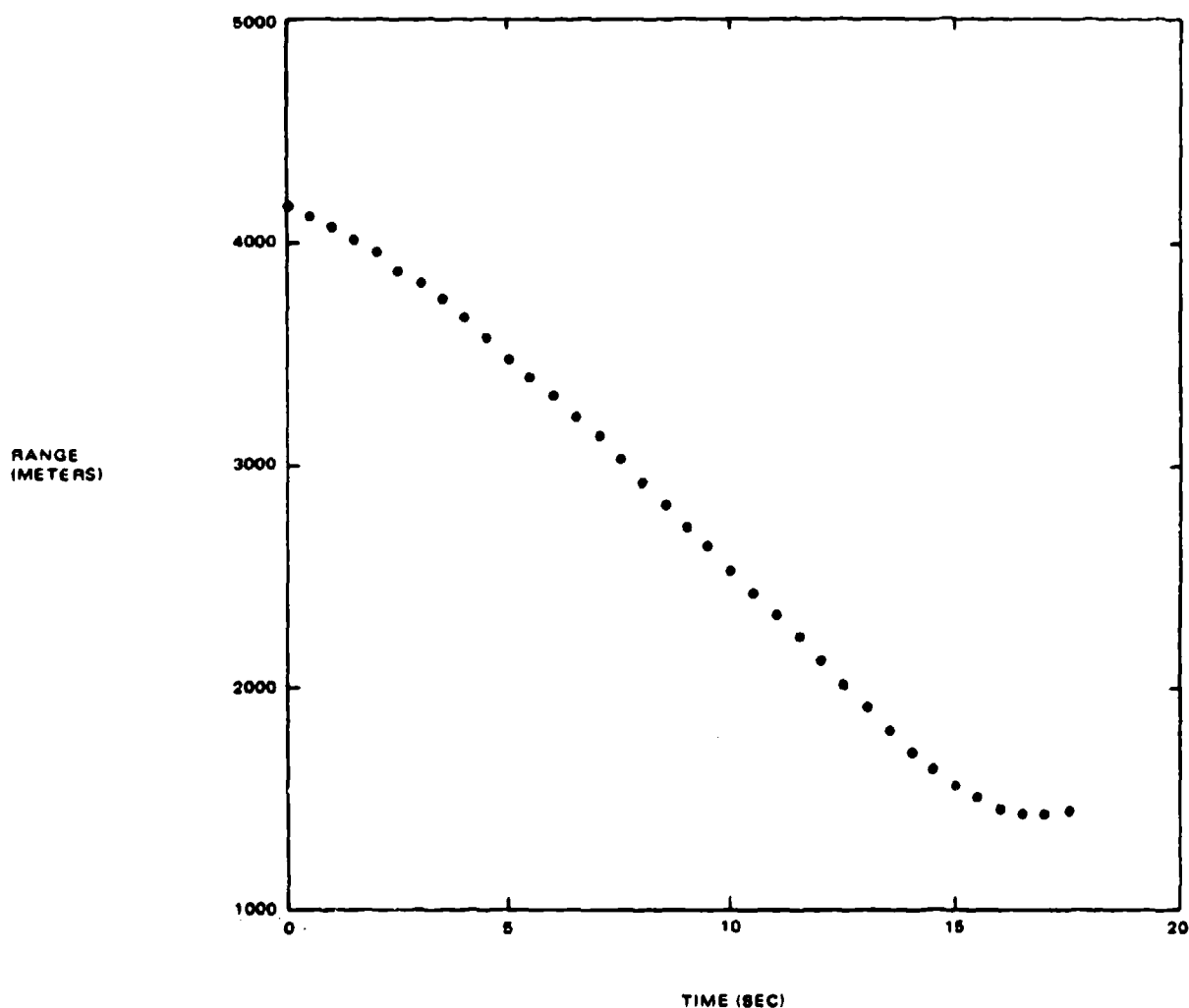
20871-233

Figure 10-30. Range Profile of Path 2b

payoff against even moderately maneuvering targets. However this interrelates with rate of fire and caliber and all design tradeoffs must be considered in choosing the preferred set of weapon design parameters.

c. At short ranges, the weapons rank in the order of rate of fire x probability of a target kill, given a hit, if muzzle velocity is held constant.

d. No simulation results were obtained indicating that angular dispersions in excess of 5 mils were desirable. In those cases where programming errors caused faulty prediction, angular disper-

sion optimized at much higher values, but were always associated with low kill probabilities.

e. In order for a system to maintain effectiveness after loss of one or more sensors, the data smoothing time must be about equal to the time of desired blind or partially disabled operation. Variable smoothing time is expected to improve the effectiveness of this alternate mode.

Regarding the simulation results, it appears that much can be accomplished to develop scaling relations, which allow a given set of results to be extended to other sets of parameters. This can economize computer running costs, and more important, it allows a large

10-43

Table X-18. Burst Kill Probabilities With Linear Predictor and 3600 F/S Muzzle Velocity

| | 25MM | | | | 37MM | | | |
| | Path 1 | | Path 2 | | Path 1 | | Path 2 | |
Time	a	b	a	b	a	b	a	b
5.0	.00	.00	.00	.00	.00	.00	.00	.00
6.0	.00	.00	.00	.00	.00	.00	.00	.00
7.0	.00	.00	.02	.00	.01	.00	.07	.00
8.0	.01	.00	.00	.00	.04	.00	.02	.00
9.0	.01	.00	.02	.00	.02	.00	.09	.01
10.0	.02	.00	.01	.00	.09	.00	.24	.05
11.0	.00	.02	.10	.00	.00	.03	.17	.00
12.0	.16	.02	.00	.00	.22	.07	.01	.00
13.0	.06	.00	.00	.00	.13	.00	.00	.00
14.0	.00	.00	.00	.00	.00	.00	.00	.00

20871-556

Table X-19. Burst Kill Probabilities With Linear Predictor and 5000 F/S Muzzle Velocity

| | 25MM | | | | 37MM | | | |
| | Path 1 | | Path 2 | | Path 1 | | Path 2 | |
Time	a	b	a	b	a	b	a	b
5.0	.00	.00	.01	.00	.00	.00	.01	.00
6.0	.00	.00	.01	.00	.01	.00	.08	.00
7.0	.01	.00	.06	.00	.08	.00	.08	.00
8.0	.04	.00	.04	.00	.08	.02	.13	.00
9.0	.03	.00	.10	.00	.07	.00	.19	.02
10.0	.10	.00	.25	.00	.12	.03	.44	.03
11.0	.01	.02	.14	.00	.04	.04	.20	.00
12.0	.10	.07	.02	.00	.20	.13	.03	.00
13.0	.12	.00	.00	.00	.16	.00	.00	.00
14.0	.00	.00	.00	.00	.00	.00	.00	.00

20871-557
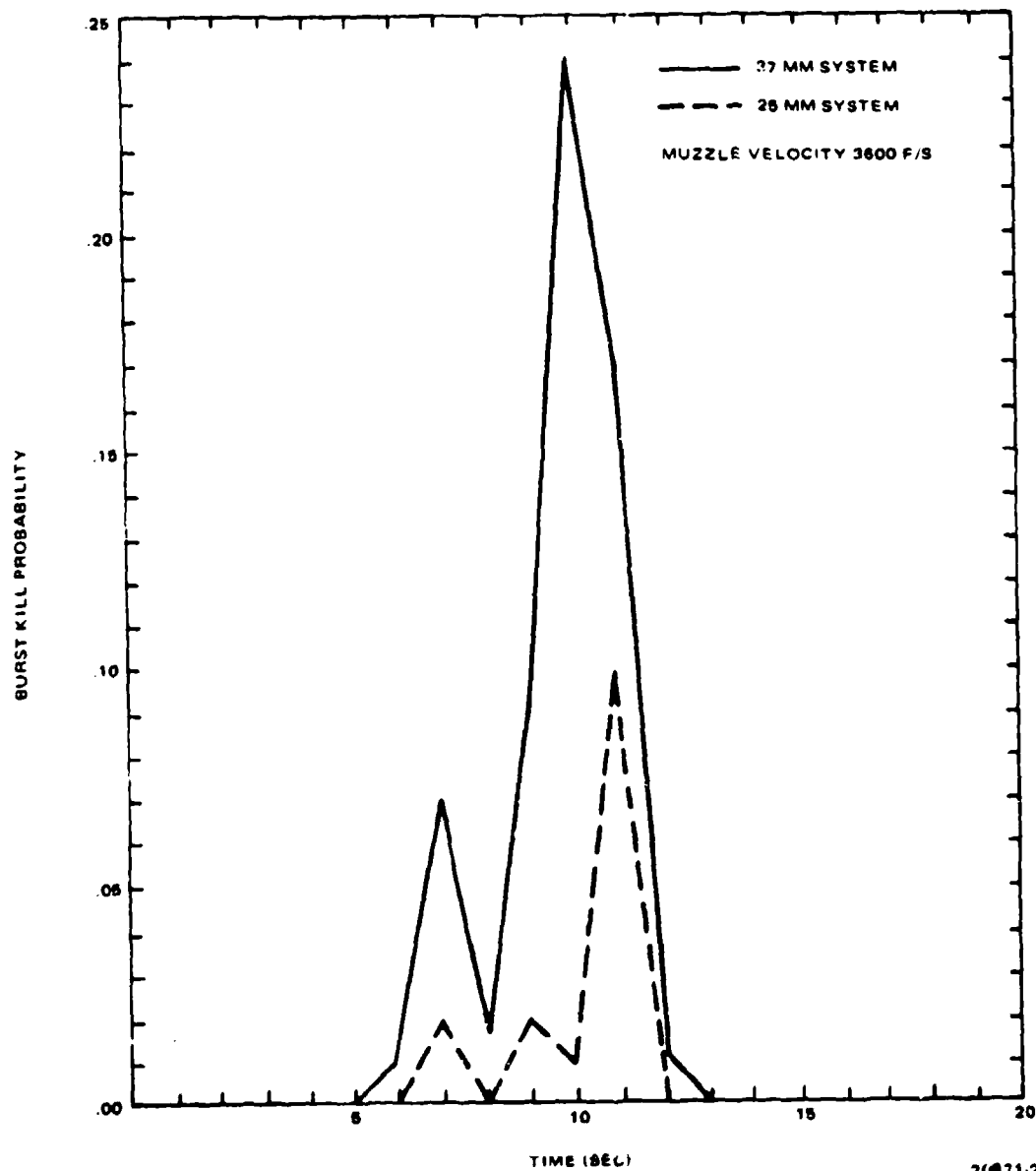
Figure 10-31. Comparison of Calibers on Path 2a

2C871-234
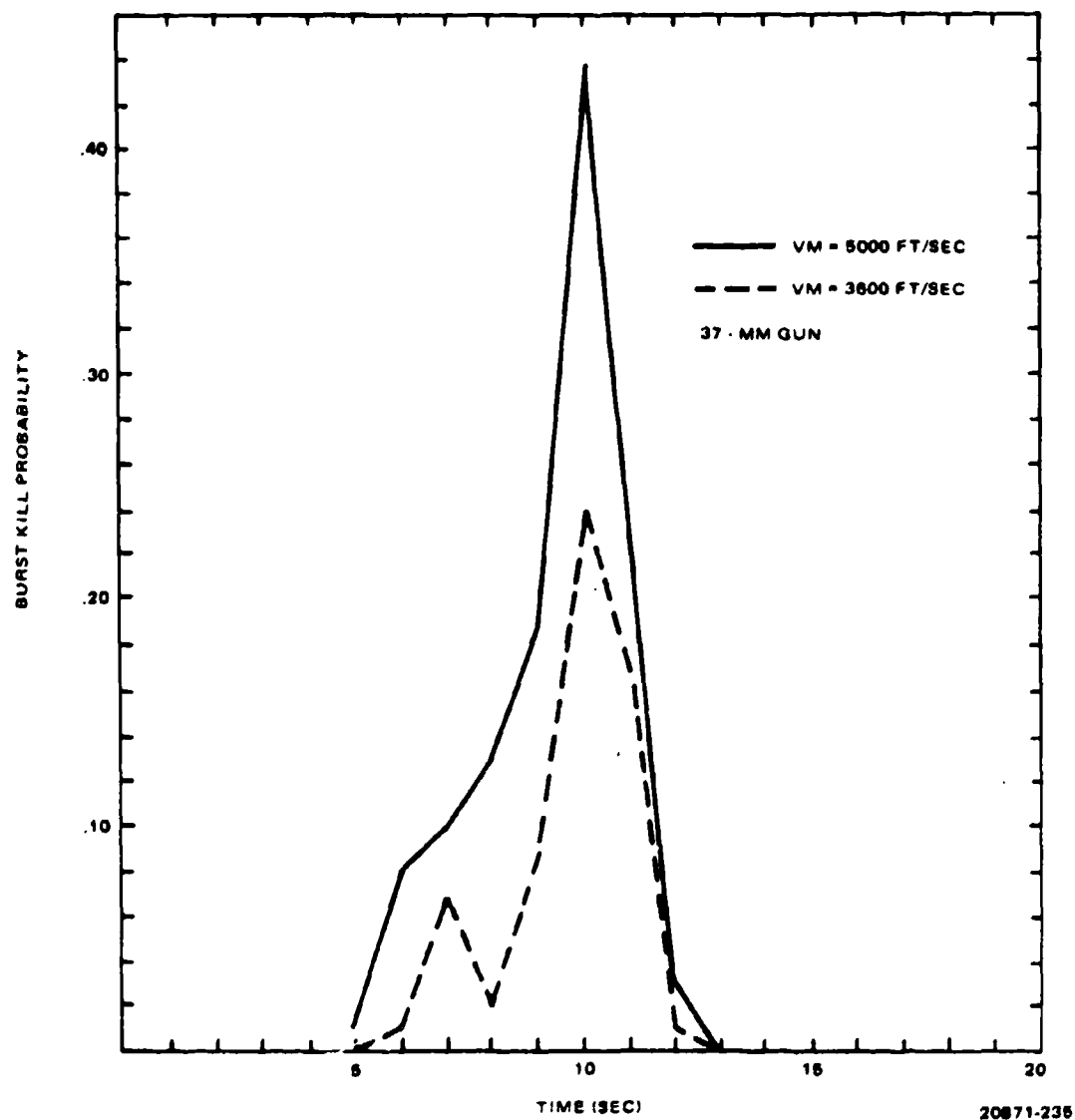
Figure 10-32. Comparison of Muzzle Velocities on Path 2a
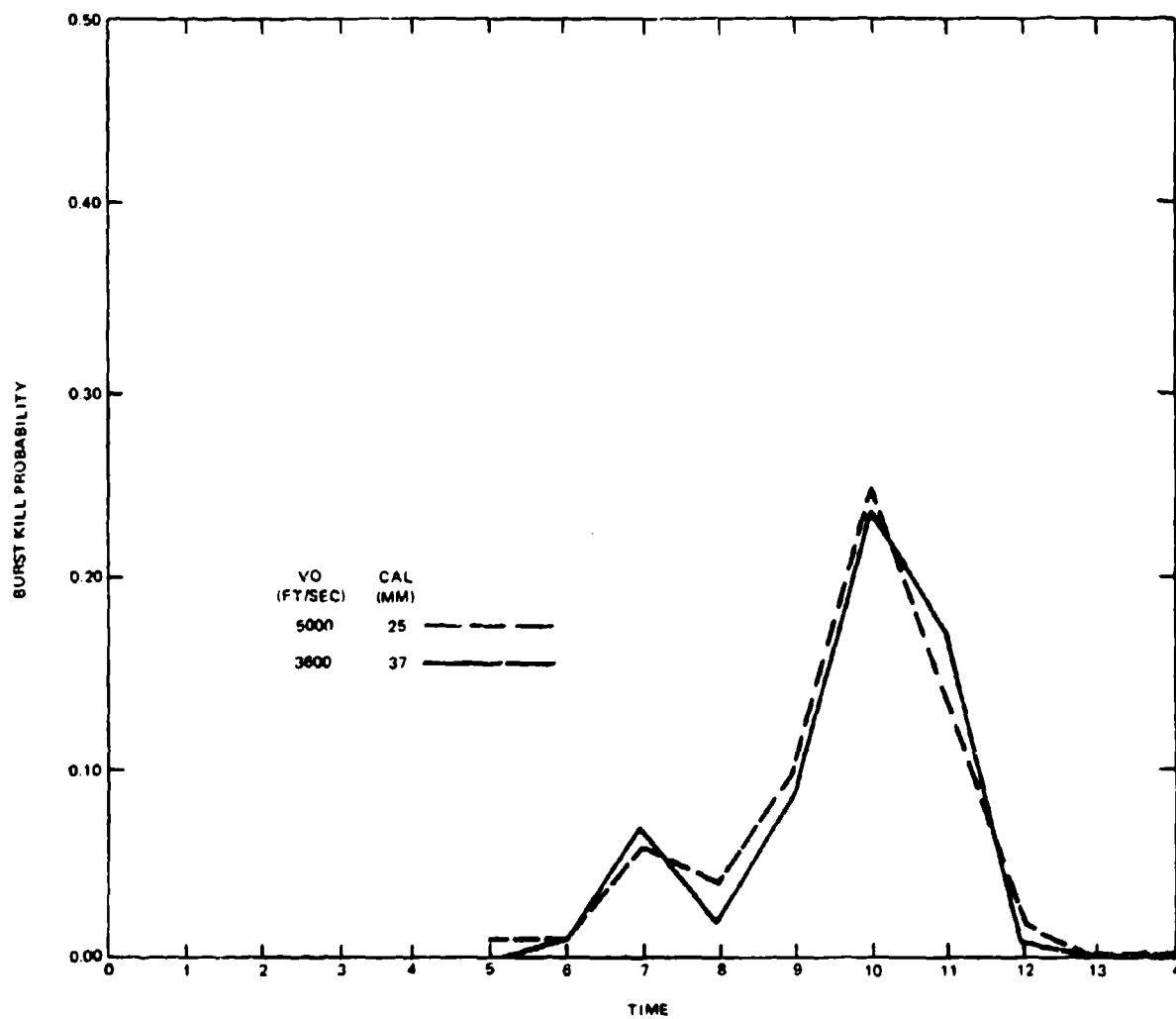
20871-235

Figure 10-33. Joint Comparison of Muzzle Velocity and Caliber on Path 2a

20871-236

Table X-20. Effect of Prediction Mode on Burst Kill Probability

Time	Tangential	Linear	Quadratic	Defense of Known Point
5.0	.03	.00	.00	.06
6.0	.01	.00	.00	.06
7.0	.01	.02	.00	.06
8.0	.05	.00	.01	.03
9.0	.04	.02	.02	.03
10.0	.10	.01	.04	.05
11.0	.02	.10	.01	.03
12.0	.01	.00	.00	.00
13.0	.00	.00	.00	.00
14.0	.00	.00	.00	.00

PATH 2a, 25 mm GUN, V_0 = 3,600 F/S

20871-55BA

Table X-21. Jink Effects on Burst Kill Probability

| Fire Time | Prediction Modes | | | | | |
| | Tangential | | Linear | | Defense of Known Point | |
	Path 2a	Path 2c	Path 2a	Path 2c	Path 2a	Path 2c
5.0	.03	.01	.00	.00	.06	.05
6.0	.01	.05	.00	.00	.06	.07
7.0	.01	.06	.02	.00	.06	.10
8.0	.05	.08	.00	.00	.03	.14
9.0	.04	.08	.02	.00	.03	.12
10.0	.10	.09	.01	.02	.05	.15
11.0	.02	.08	.10	.18	.03	.09
12.0	.01	.00	.00	.01	.00	.00
13.0	.00	.00	.00	.00	.00	.00
14.0	.00	.00	.00	.00	.00	.00

20871-559

number of simulation results to be concisely summarized in terms of combinations of parameters for easier comprehension.

This is a middle ground between simple analytic approximations and rather detailed simulation results, and it can be developed to provide a tool which is superior to either analysis or simulation alone.

SECTION 11
SUPPORTING ANALYTIC TECHNIQUES

This section reports some of the analyses done to complement the simulation effort. An object of a part of this effort was to develop a deterministic mode for the simulation as opposed to the present Monte Carlo mode. Limited time did not allow this objective to be achieved. It seems probable that unless drastic simplifications are made in the model, such a mode would require about the same amount of computer time as the present formulation. On the other hand, there seems to be considerable potential in devising simple analytic models which match the simulation results over a limited range of situations.

11.1 ANALYTIC EXPRESSIONS FOR BURST AND ENGAGEMENT KILL PROBABILITY

It has been found helpful to have simple approximate analytic expressions for kill probabilities on some of the simpler target paths employed in simulation runs. This provides insight as to how the generated kill probabilities are likely to change with parametric variations, and serves as a gross check on the simulation program.

Some of these results are developed in this section. They are presented for unaccelerated target paths, but can be extended in a straightforward fashion to constant acceleration paths.

Referring to Figures 10-3, 10-4, and 10-5 of Section 10, it will be observed that in spite of the many parameters and functions processed in the simulation, the results can be summarized in simple form over a wide range of parameter variation. This suggests that a few parameters dominate the results, and give some advance confidence in the feasibility of obtaining adequate analytic approximations for the simpler situations.

11.1.1 General Formulation

On a specific course, suppose that single shot probability has been determined as a function of time. There is no restriction at this point on whether successive rounds are or are not correlated. If firing is conducted at a constant rate v over a time T, the expected number of hits is

$$E = v \int_0^T p(t)\, dt \qquad (11.1)$$

and the probability that the target survives is

$$\phi = e^{-E} \qquad (11.2)$$

In the most general case, one would average ϕ over a

large number of samples of path, which properly accounts for serial correlation of aim, provided that 'aim wander' is correctly expressed and averaged.

Single shot probability can also be expressed as a function of slant range instead of time, in which case

$$E = v \int_{D_{p1}}^{D_{p2}} [p(D_p)/D_p]\, dD_p \qquad (11.3)$$

and we are performing the integration in terms of 'target time' rather than 'trigger time' so that the doppler effect of projectile arrival at the target is properly included.

If range passes through a minimum and then increases, the above integral is divided into two parts, up to midpoint (D_m) and past midpoint.

11.1.2 Straight Line Path Expressions

Suppose that the path is a straight line, so that we can change the variable of integration to distance along the flight path measured from midpoint. This distance, x_p is

$$x_p^2 = D_p^2 - D_m^2 \qquad (11.4)$$

Now

$$dx_p/dt = -V[1 + (dt_p/dt)] \qquad (11.5)$$

where

V = target velocity and t_p = time of flight.

Also

$$dt_p/dt = (dD_p/dt)/v_r \qquad (11.6)$$

where

v_r = projectile velocity at D_p. Then

$$(D_p)^{-1} = -D_p/(x_p V) - (v_r)^{-1} \qquad (11.7)$$

and the expression for E becomes

$$E/\nu = \int_{D_{in}}^{D_{p1}} [D_p/(x_0 V)]\, p(D_p)\, dD_p$$

$$-\int_{?_m}^{D_{p2}} [D_p/(x_p V)]\, p(D_p)\, dD_p$$

$$+\int_{D_{p2}}^{D_{p1}} [p(D_p)/v_r]\, dD \qquad (11.8)$$

The third term accounts for the doppler effect on projectile arrival time at the target. If the system fires through midpoint and the first and last rounds reach the target at $D_{p2} = D_{b1}$, the doppler term vanishes, and

$$E = (2\nu/V)\int_{D_m}^{D_{p1}} (D_p/x_p)\, p(D_p)\, dD_p \qquad (11.9)$$

11.1.3 Some Special Cases in Closed Form

The integral can be evaluated in closed form for a number of special, but interesting cases. For example, assume that the system has a constant angular variance of prediction error, σ and that successive rounds can be considered to be uncorrelated. Then

$$p(D_p) = a^2/(a^2 + 2\sigma^2 D_p^2) \qquad (11.10)$$

where

$$A_v = \pi a^2$$

In terms of x_p,

$$E = (2\nu/V)\int_0^{X_{p1}} p(x_p, D_m ..)\, dx_p \qquad (11.11)$$

Performing the integration

$$E = \frac{2\nu a^2}{V\{2\sigma^2(a^2 + 2\sigma^2 D_m^2)\}^{1/2}}\, \tan^{-1}\left\{x_p\left[\frac{2\sigma^2}{a^2 + 2\sigma^2 D_m^2}\right]^{1/2}\right\}$$

$$(11.12)$$

and if the target vulnerable area is very small compared with the dispersion pattern at closest approach so that:

$$a^2 << 2\sigma^2 D_m^2 \qquad (11.13)$$

$$E = (\nu a^2 \theta)/(V D_m \sigma^2)\ ; \theta = \tan^{-1} x_p/D_m$$

$$(11.14)$$

The angle θ is the angle swept out by the gun while firing up to midpoint. It has a maximum value of $(\pi/2)$.

This expression can be used to obtain the measure of 'Kill-seconds' used in AFAADS-I. 'Kill-seconds' was there defined as the simple summation of single shot kill probability taken at unit intervals, over a long firing pass. One of the simulation results was for zero tracking error and the following numerical parameters

a = 1.0 meter

V = 310 meters/sec

H = 250 meters altitude

R_m = 200 meters

σ = 4 mils

Setting $\nu = 1.0$ in Equation (11.12) and computing E, one obtains (on a six-inch slide rule)

E = 0.85 (kill-seconds)

The simulation results was

E = 0.8632 (kill-seconds)

11-2

11.1.4 Ellipsoidal Target

We can extend the above computation to the case of an ellipsoidal target, with area $A_f = \pi a_f^2$ head on, and $A_s = \pi a_s^2$ side on. Then:

$$a^2 = (a_f^2 x_p^2/D_p^2) + (a_s^2 D_m^2/D_p^2) \qquad (11.15)$$

Assuming that the target is small compared with the shot pattern to keep the algebra within bounds, and performing the integration. we find that

$$E = \frac{\nu}{2V \sigma^2 D_m} \left[(a_s^2 - a_f^2) \sin\theta \cos\theta + (a_s^2 + a_f^2) \theta \right]$$

$$(11.16)$$

and so if we fire the whole course we get the same result as before if we replace the ellipsoidal target by a circular target with area equal to the mean of the front and side areas of the ellipsoidal target.

11.1.5 Hits on the Wing

The integral can also be evaluated to include the wing, assuming that the projected wing dimensions are small compared with the shot pattern. Represent the wing as a horizontal flat plate of area $A_w = \pi a_w^2$. The projection of the wing onto a plane perpendicular to the trajectory will have a projected area

$$A_w H/D_p \qquad (11.17)$$

where:

H = target altitude, assumed constant. The result of the integration for the wing alone is

$$E = (\nu a_w^2 H \sin\theta)/(V \sigma^2 D_m^2) \qquad (11.18)$$

11.1.6 Improved Function for Single Shot Probability

The single shot probability function can be further detailed by considering the component of prediction error resulting from tracking noise and allowing both the target and the error probability density functions to be elliptical. Using a coordinate system along and perpendicular to the target path in a plane perpendicular to the trajectory (which is assumed straight in this approximation):

$$P_{ss} = \frac{a_u a_v}{\left[a_u^2 + 2(\sigma_u D)^2 + 2\sigma_{pu}^2\right]^{1/2} \left[a_v^2 + (\sigma_v D)^2 + 2\sigma_{pv}^2\right]^{1/2}}$$

$$(11.19)$$

The variances of prediction error can be partitioned into components which are constant during a burst, but random across bursts, and components which can be considered random between rounds. From the indications of Figure 10-4, one would not go far wrong in assuming that for bursts of more than one second duration and linear prediction, the bias component is negligible.

The prediction error variances can be approximately detailed as

$$\sigma_p^2 = \sigma_0^2 + \sigma_v^2 \left[t_p + (T_s/2)\right]^2 \qquad (11.20)$$

Where σ_0 is the variance of present position error, and σ_v is the resulting variance of velocity error. σ_v can be obtained from σ_0 and T_s from the filter coefficients, or graphs such as those presented for least squares finite memory filters in AFAADS-I.

The resulting expression does not integrate easily, but a workable expedient is to expand p_{ss} as a series in x_p. As an example, consider the case of a circular target, 'circular' round to round dispersion, but tracking error variances which differ in the two coordinates. Then the denominator of p_{ss} can be expanded as a series in y, where $y = x_p/D_m$. One then obtains, retaining terms up to y^2,

$$E = M \int \frac{dy}{A + By + Cy^2} \qquad (11.21)$$

and for a long pass course

$$E = 2M/Q^{1/2} \tan^{-1}(Q^{1/2}/B) \qquad (11.22)$$

where M,A,B,C contain various combinations of parameters as determined by the expansion, and

$$Q = 4AC - B^2 \qquad (11.23)$$

For one of the AFAADS-I simulation runs, the previously given numerical values were used, and in addition, $\sigma_{u0}^2 = 25$ meters^2 and $\sigma_{v0}^2 = 0.36$ meters^2, with $T_s = 0.40$ seconds.

A slide rule computation for E with $\nu = 1.0$ gave

$$E = 0.08$$

and the simulation result gave

$$E = 0.09 \text{ to } 0.11$$

The slide rule computation was done using a constant average projectile velocity. However the variation of time of flight with range could have been included in the series development, and might have improved the agreement.

11-3

Time has not permitted the comparison of this approximate method against the more complex modelling of the present simulation, but useful agreement is expected.

11.1.7 Computation of Burst Kill Probability Including Aim Wander

The remarkable simulation results displayed in Figures 10-3 and 10-4 suggest that for the system and noise parameters and algorithms represented in those results, single shot probability at any point in the defense volume can be written simply as:

$$P_{ss} = f(D,x) e^{-\lambda y} \qquad (11.24)$$

where $f(D,x)$ is a term depending on the target position at the instant the projectile reaches it, λ is a constant over the whole defense volume and depends only on the prediction algorithm, and 'y' is a variable which is constant during a burst, and randomly distributed across bursts, with a circular, normal probability density function and unit linear variance.

Then at least for the case of a one-second burst, the target survival probability is, averaged over y,

$$\phi = \int_0^\infty e^{-Ee^{-\lambda y}} d(e^{-y}) \ ; \ E = n\Gamma \ ; \ n = \text{number of rounds}$$

$$(11.25)$$

If this computation, $f(Dx,x)$ would be computed from an expression such as Equation (11.19).

Equation (11.25) can be expressed in terms of the Incomplete Gamma Function. However, for integer values of $\mu = 1/\lambda$, it assumes a much simpler form, as shown by Table XI-1.

These results only apply to unaccelerated target paths, and the degree to which the observed constant λ can be assumed to hold if ammunition dispersion, for example, is varied from the 3 mils used in the referenced simulation set, is not yet known. However, by comparing E, computed from an expression such as Equation (11.19) against the value which fits the curves of Figure 10-5, one can determine how much of the complexity of the simulation contributes only second order effects.

One can also compute an estimate of λ directly from the noise autocorrelation and the prediction algorithms using Tappert's method. If this agrees with the value obtained from the simulation, the analytic method can be used to estimate the effect of parametric variations in advance of simulation runs, including various bias errors and other dispersion values.

Table XI-1. Solutions for Burst Kill Probability

Case	Parameter		
	λ	μ	ϕ
Arbitrary μ	λ	λ^{-1}	$\mu E^{-\mu} \gamma(\mu, E)$
Integer μ	λ	λ^{-1}	$\dfrac{1 - \left[\sum_0^{\mu-1} E^j/j!\right] e^{-E}}{E^\mu/\mu!}$
	0	∞	e^{-E}
	1/2	2	$\left[\dfrac{1 - (1+E) e^{-E}}{E^2/2}\right]$
	1	1	$\left[\dfrac{1 - e^{-E}}{E}\right]$
$E \ll 1$	λ	μ^{-1}	$e^{-E/(1+\lambda)}\left[1 + \dfrac{E^2 \lambda^2}{2(1+\lambda)^2 (1+2\lambda)}\right]$

20871-560

If agreement with the simulation is still obtained at this level, the effect of those target maneuvers which can be expressed as a constant target acceleration during the smoothing time and the burst length, can be handled analytically.

In the case of an unaccelerated target, one would expect the effective value of λ, as observed on the simulation to reduce to zero as the burst length is increased to several seconds, and this should be determined by additional simulation runs.

11.1.8 Summary

Once it has been debugged, the simulation provides a fairly authoritative representation of the interactive effects of all of the time varying parameters of the antiaircraft predicted fire problem. It has the unique advantage of operating with irregular target paths which are impossible to work in a reasonable amount of time analytically. However, there are many advantages in having an independent analytic confirmation of the simulation results against simple target paths, not the least of which is that the parametric interactions are more transparent in an analytic formulation.

It should also be noted that the relatively minor effect of aim wander in the simulation results was the result of the excellent radar tracking characteristics

11-4

assumed. One would expect qualitatively different results with an accurate simulation of manual tracking.

11.2 COMPUTER GENERATION OF NOISE SEQUENCE WITH SPECIFIED AUTOCOVARIANCE

The general problem is that of representing a continuous system (linear) with both deterministic and stochastic inputs by a discrete model. Satisfactory representation can usually be obtained by taking the sampling interval small enough; here we consider what is involved in using a large sampling interval (compared with some of the system time constants) and attempting to obtain an accurate representation of system performance only at the sample points.

The low frequency response of the system as it responds to the deterministic part of the input is obtained in terms of the derivatives of the input, which for the present problems are known and will not be discussed here.

In the case of the stochastic component, input noise is preferably represented as the output of a linear system with time varying coefficients excited by an uncorrelated random sequence (normal) with unit variance. The state space differential equations are then to be replaced by difference equations and the original noise sequence by a modified noise sequence such that the system variance matrix at the sampled intervals for the discrete model is identical with the result obtained by sampling the variance matrix of the continuous system.

Except for a single output variable with simple exponential correlation the exact result is complex, and probably requires more computations than simply reducing the sampling interval. Probably for this reason the methodology is not prominent in the literature. It is nevertheless outlined in the following paragraphs.

11.2.1 Problem Formulation

The problem was probably first defined by M.S. Bartlett,[1] who was considering the problem of specification of continuous time series by their autocorrelation functions, when the autocorrelation functions are computed (as is usual) from samples of the basic process.

The special case he examined was that of a system with autocorrelation

$$\rho(s) = \frac{\mu_2 e^{\mu_1 s} - \mu_1 e^{\mu_2 s}}{\mu_2 - \mu_1} \qquad (11.26)$$

and its differential equation form, resulting from the Langevin equation

$$\ddot{x} + a\dot{x} + bx = I_t$$

Bartlett posed the problem of specifying a difference equation and its differential equation form, resulting from the Langevin equation

$$x(t+2h) + Ax(t+h) + Bx(t) = J(t,h) \qquad (11.27)$$

which would have the same autocorrelation, and he showed how to obtain the coefficients and J.

Further comments on Bartlett's paper are given in Jenkins and Watts.[2] Krut'ko[6] discusses the general problem but it is not clear to this writer that his method is correct (i.e., exact) except for the simplest case.

Both Mehra[3] and Jazwinski[4] provide a straightforward method of obtaining the desired result, and it is their method which is outlined in this paper. Their method allows the computation to be performed for time varying systems; for simplicity only linear non-time varying systems are considered here.

We note, en passant, an ingenious and different way of generating an error sequence with a specified autocorrelation, by Dziwak.[5]

11.2.2 General Solution

The continuous process is defined by

$$dX = F X dt + G d\beta \qquad (11.28)$$

where X is an n vector, F is an n x n matrix, G is an n x r matrix and β is an r-vector Brownian motion process with:

$$<d\beta \, d\beta^T> = Q \, dt \qquad (11.29)$$

The general solution allows F, G and Q to be time varying, here we assume that they are constant for simplicity.

If $X(t)$ is sampled at intervals Δ, the sample sequence can be described as generated by the difference equations

$$X(j+1) = \Phi(j+1,j) X(j) + w(j+1) \qquad (11.30)$$

where the state transition matrix $\Phi(j+1,j)$ is obtained as the solution of

$$d\Phi/dt = F\Phi \quad ;\Phi(0) = 1 \qquad (11.31)$$

and Φ is $\Phi(S)$.

Then the sequence $w(j+1)$ is obtained from

$$w(j+1) = \int_0^\Delta \Phi(s)G(s)\,d\beta \qquad (11.32)$$

and

$$<w(j+1)\,w(j+1)^T> = \int_0^\Delta \Phi(s)G(s)Q(s)G^T(s)\,\Phi^T(s)\,ds \qquad (11.33)$$

11.2.3 Example

The transfer function of the system of interest is:

$$x_2(t) = \frac{x_0(t)}{(1 + sT_1)(1 + sT_2)} \qquad (11.34)$$

Where $x_0(t)$ is loosely specified as 'white noise' with bandwidth greatly exceeding that of the system, and specified intensity N^2.

This expression can be rewritten in the state space form.

$$T_1\dot{x}_1 + x_1 = x_0$$

$$T_2\dot{x}_2 + x_2 = x_1 \qquad (11.35)$$

$$\begin{bmatrix} \dot{x}_1 \\ \dot{x}_2 \end{bmatrix} = \begin{bmatrix} -a_1 & 0 \\ +a_2 & -a_2 \end{bmatrix}\begin{bmatrix} x_1 \\ x_2 \end{bmatrix} + \begin{bmatrix} a_1 & 0 \\ 0 & 0 \end{bmatrix}\begin{bmatrix} x_0 \\ 0 \end{bmatrix}$$

$$(11.36)$$

where

$$a_1 = 1/T_1; \quad a_2 = 1/T_2$$

Solving

$$\begin{bmatrix} \dot{\phi}_{11} & \dot{\phi}_{12} \\ \dot{\phi}_{21} & \dot{\phi}_{22} \end{bmatrix} = \begin{bmatrix} -a_1 & 0 \\ a_2 & -a_1 \end{bmatrix}\begin{bmatrix} \phi_{11} & \phi_{12} \\ \phi_{21} & \phi_{22} \end{bmatrix} \quad ;\phi(0) = 1$$

$$(11.37)$$

$$\phi(s) = \begin{bmatrix} e^{-a_1 s} & 0 \\ e^{-a_1 s} - e^{-a_2 s} & e^{-a_2 s} \end{bmatrix} \qquad (11.38)$$

In the general expressions take $Q = 1$, $G = Na_1 \begin{bmatrix} 1 & 0 \\ 0 & 0 \end{bmatrix}$

$$(11.39)$$

Write:

$$\Phi(s) = \begin{bmatrix} A(s) & 0 \\ A(s)\cdot B(s) & B(s) \end{bmatrix} \qquad (11.40)$$

Then:

$$<w(j+1)\,w(j+1)^T> = N^2 a_1^2 \int_0^\Delta \begin{bmatrix} [A(s)]^2 & A(s)[A(s)\cdot B(s)] \\ A(s)[A(s)\cdot B(s)] & [A(s)\cdot B(s)]^2 \end{bmatrix} ds$$

$$= N^2 a_1^2 \begin{bmatrix} q_A & q_A - q_{AB} \\ q_A - q_{AB} & q_A - 2q_{AB} + q_B \end{bmatrix}$$

$$(11.41)$$

$$< \left[w_1(j+1) \right]^2 > \ = \ N^2 a_1^2 \ q_A$$

$$<w_1(j+1) \, w_2(j+1)> \ = \ N^2 a_1^2 \, (q_A \cdot q_{AB})$$

$$< \left[w_2(j+1) \right]^2 > \ = \ N^2 a_1^2 \, (q_A \cdot 2q_{AB} + q_B)$$

$$(11.42)$$

To shorten the notation set

$$N^2 a_1 \ = \ \sigma_1^2 \qquad (11.43)$$

Since $< w_i(j+1) \, w_k(j+1+m) > \ = \ 0 \ : \ m \neq 0$, we can generate w_i as

$$\begin{bmatrix} w_1(j+1) \\[2mm] w_2(j+1) \end{bmatrix} = \begin{bmatrix} c_{11} & c_{12} \\[2mm] c_{21} & c_{22} \end{bmatrix} \begin{bmatrix} n_1(j+1) \\[2mm] n_2(j+1) \end{bmatrix}$$

$$(11.44)$$

where $n_k(j)$ are zero mean, unit variance, uncorrelated sequences and the preceding expressions allow the c_k to be solved in termns of the q. Since there are only three constraints, any one of the c_k can be taken as zero; it is convenient to set $c_{12} = 0$.

The desired discrete algorithm is then

$$\begin{bmatrix} x_1(j+1) \\[2mm] x_2(j+1) \end{bmatrix} = \begin{bmatrix} A(\Delta) & 0 \\[2mm] A(\Delta) \cdot B(\Delta) & B(\Delta) \end{bmatrix} \begin{bmatrix} x_1(j) \\[2mm] x_2(j) \end{bmatrix}$$

$$+ \begin{bmatrix} w_1(j+1) \\[2mm] w_2(j+1) \end{bmatrix} \qquad (11.45)$$

This generates both x_2 and x_1 at the sample points.

We are really only interested in x_2. Eliminating x_1 from the above expressions, i.e.,

$$x_1(j+1) \ = \ A(\Delta) \, x_1(j) + w_1(j+1)$$

$$x_2(j+1) \ = \ \left[A(\Delta) \cdot B(\Delta) \right] x_1(j)$$

$$+ B(\Delta) \, x_2(j) + w_2(j+1)$$

$$(11.46)$$

we obtain:

$$x_2(j+2) \cdot (A+B) \, x_2(j+1) + AB \, x_2(j) \ = \ w_2(j+2)$$

$$\cdot A \, w_2(j+1)$$

$$+ (A \cdot B) \, w_1(j+1)$$

$$(11.47)$$

The noise sequence on the right, as long as we are only interested in x_2, can be simplified. As developed, it depends on two independent unit random sequences n_1 and n_2. Let it be replaced by

$$v(j) \ = \ b_2 n(j+2) + b_1 n(j+1) \qquad (11.48)$$

and match the autocovariance of the v sequence to that derived from the w sequence.

The values of b_1 and b_2 have been worked through but the process is tedious. The final expressions are complex, compared with the easy case of a single exponential term in the autocorrelation, on the other hand they have, as might be expected, a considerable amount of symmetry which somewhat ameliorates their complexity.

11.2.4 Comments

In general, we will be interested in more complex systems than that defined by the above example, which is only one step above the simple exponential in complexity. The closed form solution then becomes unmanageable, unless one makes a hobby of it. For a time varying system the state transition matrix is less likely to be obtainable in closed form.

The point of Mehra's paper, however, is that if one is using a computer, one may as well use the computer to evaluate the various integrals numerically, and if one does this the algebra vanishes and one is only concerned with the computer time. It is an open question whether this is more economical of computer time than simply obtaining a good approximation to the continuous process by closing the sampling interval.

At any rate, the simulation designer may remain aware of the fact that he may consider the Mehra-Jazwinski (Kalman) method as an option to small sampling interval in designing his simulation.

11.3 INTEGRATION OF KILL PROBABILITY WITH STATE SPACE FORMULATION OF SYSTEM DYNAMICS

Almost all of the published work on optimum filters, including Kalman filters is based on minimizing the variance of system error, or some other quadratic function. The criterion: probability of killing a target with a ‸   ⁀f n rounds distributed over a time T, canno⁀   ⁀structe⁀ ᵇy linear operations on the varianc⁀ ⁀he system, and minimizing the variance of prediction ⁀rror does not necessarily maximize the probability of killing the target.

The state space formulation of the system dynamics does allow the computation of the probability density function of system prediction error as it evolves with time. In most filter work only the mean and variance as a function of time are required, hence, the fact that the probability density function is also available is rarely used.

The missing step, therefore, is the combination of the probability density function of prediction error with probability of killing the target given prediction error, and the computation of target kill (or survival) probability as a function of the number of rounds fired.

This note provides an introduction to the formulation of the problem, explicitly including the target kill probability.

11.3.1 Approach

For this note we begin with the assumption that we have obtained a satisfactory discrete representation of the system dynamics, and that the representation is, in conventional state space notation, as indicated in Equation (11.49). The system can be time-varying, and the amount of detail in the representation, including both internal and external error sources is limited only by the size of the matrices we are willing to manipulate.

How to get from a particular system description to Equation (11.49) is well covered in the literature and will not be discussed here. Of particular interest is the fact that the state space formulation allows the joint probability density function for the aim points of n rounds to be computed simply.

In the following development, which is for the purpose of structuring the analysis, it is assumed that the system difference equations are based on an interval between points exactly equal to the interval between rounds. The extension to other firing rates is a minor problem.

11.3.2 Deterministic Solution

Write the difference equations for the system as used on the simulation in the state space as:[7]

$$x(k + 1) = \Phi(k) x(k) + \Gamma(k) w(k) \quad (11.49)$$

where the $x(k)$ are column vectors. $\Phi(k)$ describes the system dynamics and $\Gamma(k)$ describes the way in which white noise enters the system. If noise at any point of entry is non-white an additional expression is adjoined to the system equations to generate the desired autocorrelation.

This discussion concerns only the 'non-deterministic' errors, hence:

$$< w(k) > = 0 \quad (11.50)$$

Noise variances at the various points of system entry are defined by

$$\begin{aligned} <w(k) w(j)^T> &= N(k) \; ; k = j \\ &= 0 \; ; k \neq j \end{aligned} \quad (11.51)$$

Define:

$$M = \Gamma(k) N(k) \Gamma^T(k) \quad (11.52)$$

Then the transition density function $p\{x(k+1)|x(k)\}$ is [7]

$$p\{x(k+1)|x(k)\} = \frac{1}{(2\pi)^{n/2}|M|^{1/2}} e^{-(1/2)[x(k+1)-g(k+1)]^T M^{-1}[x(k+1)-g(k+1)]}$$

$$(11.53)$$

where

$$\underline{x}(k+1) = \Phi(k)x(k) + x_s(k+1) ; \qquad (11.54)$$

where x_s is the deterministic part of the systematic error obtained elsewhere in the simulation.

Let:

$q[x(k)] = $ the target survival probability if a round is fired at the k'th instant, with $x(k)$ given

Then the survival probability if n equally spaced rounds are fired

is, given the $x(k)$

$$\prod_{k=1}^{n} q[x(k)] \qquad (11.55)$$

We need to average this over all $x(k)$ to obtain Q the average probability that the target survives all rounds.

Because the state space formulation has structured the problem as a Markov process, the joint probability density of the $x(k)$ is

$$p[x(n), x(n-1), x(n-2) \cdots x(1)] = p[x(n)|x(n-1)]p[x(n-1)|x(n-2)] \cdots p[x(1)] \qquad (11.56)$$

and so

$$Q = \int_{-\infty}^{\infty} \cdots \int \prod_{j=2}^{n} q[x(j)]p[x(j)|x_{j-1}]q[x(1)]p[x(1)] \prod_{k=1}^{n} dx(k) \qquad (11.57)$$

This is the desired survival probability. The problem now is to arrange an efficient method of computing Q.

There are two obvious difficulties to circumvent: (1) we want to avoid requiring the computer to perform n integrations between infinite limits, and (2) as will be seen later, a straightforward integration of Q for n rounds would have n^2 terms.

The computation can be put into a recursive form by defining[a]

$$f[x(k+1)] = \int_{-\infty}^{\infty} p[x(k+1)|x(k)]f[x(k)]q[x(k)] \, dx_k$$

$$(11.58)$$

where

$$f[x(1)] = p[x(1)]$$

Then

$$Q(k) = \int_{-\infty}^{\infty} f[x(k)]q[x(k)] \, dx(k) \qquad (11.59)$$

or, alternately

$$Q(k) = \int_{-\infty}^{\infty} f[x(k+1)] \, dx(k+1) \qquad (11.60)$$

This simplifies the notation, but does not appear to reduce either of the two difficulties noted above. For example, since

$$\int_{-\infty}^{\infty} p[x(k+1)|x(k)] \, dx(k+1) = 1.0 \qquad (11.61)$$

$$Q(k) = Q(k-1) - \int_{-\infty}^{\infty} f[x(k)]p_s[x(k)] \, dx(k) ;$$

$$p_s[x(k)] = 1 - q[x(k)] \qquad (11.62)$$

but we must still determine the $f[x(k)]$.

One obvious line of approach is to take the Fourier transform of both sides of Equation (11.58). It may be preferable to multiply both sides by $q[x(k+1)]$ before doing this. This line has not been completely worked through to determine whether it simplifies the required computations.

Another possibility is to return to Equation (11.57), insert the complete joint pdf for the n rounds and see what can be done about expressing the result of the integration as a convergent series. The fact that the inverse of the moment matrix will have terms only on the principal and two adjacent diagonals may simplify this process.

It may be noted that Darling[a] abandoned the difference equation approach in 1949 upon reaching the equivalent of Equation (11.58) and converted his expressions to partial differential equations. This may still be the best way to get at a computable solution.

11.3.3 Comments

The principal interest of this approach is that it joins the state space system formulation with the value function representing target kill probability in a manner which allows the problem to be integrated with the rapidly developing techniques of state space analysis. From a practical point of view, the theoretical development is not required, since one can always resort to simulation. However, the problem is one of long standing, and deserves a place in the field of research mathematics.

SECTION 12
COST CONSIDERATIONS

This section provides an overview of costs for anti-aircraft gun systems and related equipment, based on open source information.

12.1 INTRODUCTION

If antiaircraft guns have a place in the defense arsenal, one of the reasons must be that throughout an important defense volume they provide effectiveness equal to that which can be furnished by guided missiles, but at substantially lower cost.

In theory, at any rate, a missile system can do anything a gun system can do if one is willing to pay the price. However, guns have certain intrinsic advantages over missiles with regard to reliability, ease of maintenance, ammunition cost and overall logistic support costs. These advantages tend to become submerged in the cost of the surveillance and tracking sensors which are common to both types of systems, but can be capitalized on by careful design.

In the area of development costs, a new antiaircraft gun defense system can be realized at a fraction of the development cost of a new air defense missile system.

It is not the purpose of this report to compare guided missile and antiaircraft gun systems other than to note that a single missile may cost from about $6000 (Redeye) to $8500 (Chaparrel) to $10,000 (Rapier). The Hawk, which does a job that can probably not be matched by guns, costs about $40,000 per missile. For $5000 to $10,000 one can purchase several thousands of rounds of gun ammunition, and with good fire control a gun system might achieve a kill with several hundred rounds on the average.

12.2 COST DATA 'BANK'

It is the purpose of this section of the report to provide background information from which a non-cost-specialist may obtain an appreciation of the costs of antiaircraft gun systems and their components. Since information on gun systems is somewhat limited, the data base has been broadened to include related items of Army materiel.

The object is simply to give a rough idea of what things cost. The present writer knows of no convenient, unclassified handbook serving this purpose for Army materiel, and it was felt that it would be useful to collect in one place much of the Army cost data that has appeared in the open literature. Because of limited time, the data presented has been limited to equipment unit costs, with a few examples of development cost, and no information is developed on maintenance and operational costs.

The sources of individual entries in the cost tables are so numerous that they will not be cited individually. They were given in in-process working papers. It is probable that regardless of the publication or newspaper clipping in which the present writer found the data, the original source in almost all cases was the Army budget and associated Congressional hearings.

Without details of where in a production program costs are noted, or what spares, test unit, or engineering change costs are included, the data cannot be considered to be accurate. The few indications given of quantity are particularly unreliable. In spite of these deficiencies, a reasonable amount of consistency will be noted in the price pattern for a particular type of equipment, particularly in trends across successive years.

The Army has many extremely competent professional cost analysis groups, who have the advantage of the official data base, and records. It is suggested that the data collected here might be of some assistance to a systems analyst in laying out a request for cost support from a professional cost analysis group.

12.3 COST ESCALATION

Over many years since World War II, dollar expenditures for research and development in the United States have increased at a much faster rate than the rate of increase in the numbers of new graduates in engineering and related physical sciences.

The consequences in terms of the cost of one technical man year in research and development are shown in Figure 12-1 where an index of this parameter is compared against the Consumer Price Index.[14,15,16] Some of the cost rise is, of course, associated with more sophisticated technology and the problems in fielding advanced weapon systems. But it is also possible that some of the increase is associated with the fact that the deeper one reaches into the technical manpower barrel, the lower the average productivity per man becomes.

If there is more work which must be done than there are skilled and experienced people, these problems are probably inevitable. The current slowdown in growth of R&D expenditures might reasonably be expected to improve the efficiency of those technical personnel employed, and reduce the cost escalation rate. It is noted, however, that the starting salaries of new engineering graduates who obtain employment continue to increase, and might be expected at least to parallel the price index growth.

There is no reason to believe that the rate of inflation will ever become zero regardless of which of the
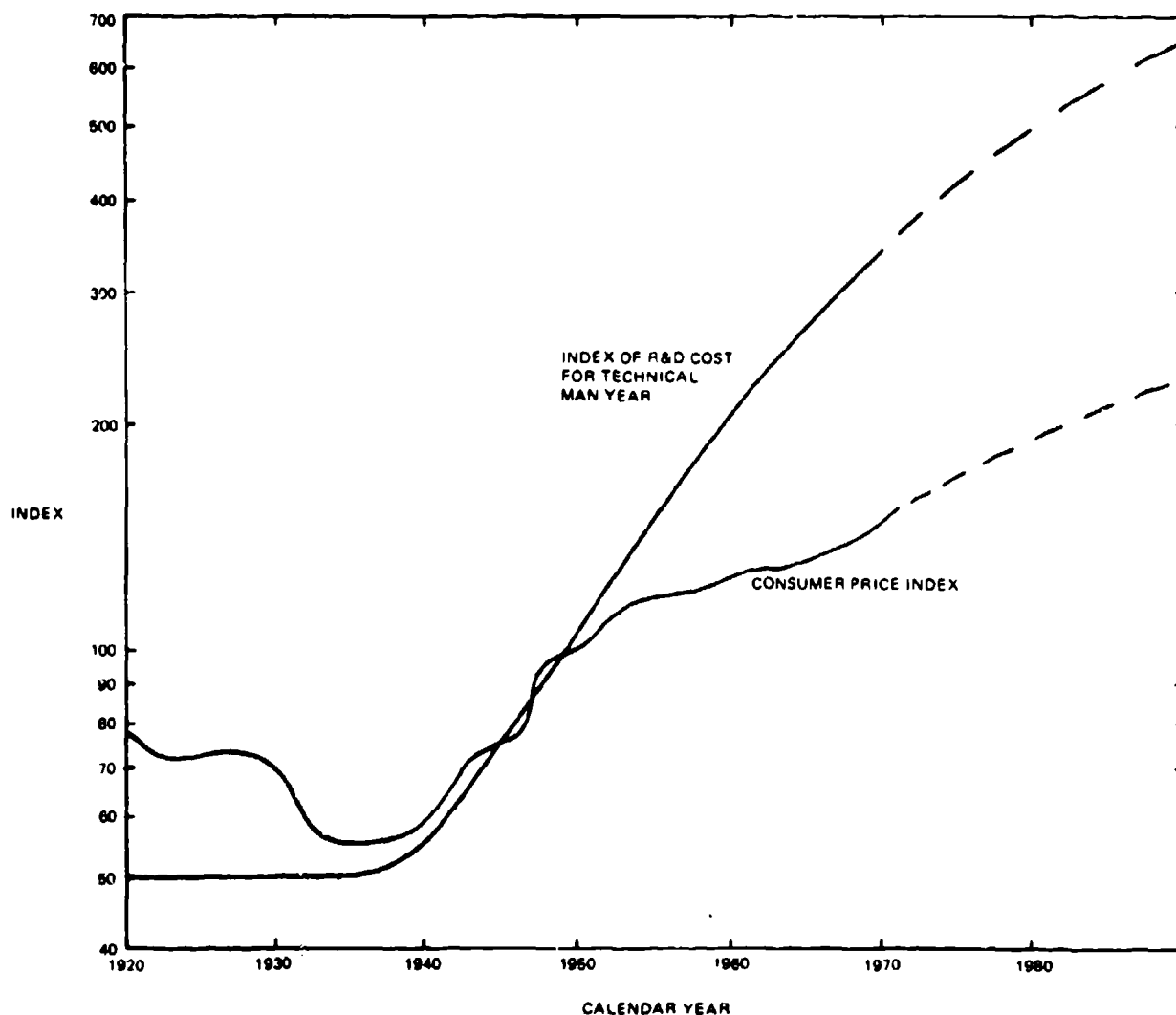
20871-1229

Figure 12-1. Comparison of Indices of R&D Cost and Consumer Prices

present schools of economists influence government policy. Ever since Keynes discovered that one can transform a 'hunting' closed loop economic system to one that does not oscillate as badly but diverges exponentially as it runs 'open loop', no economist has succeeded in demonstrating how to obtain stability without divergence.

In the data presented later, no correction has been made to a 'constant dollar': that most mythical of all concepts.

12.4 UNIT COSTS AND DEVELOPMENT COSTS OF ANTIAIRCRAFT GUN SYSTEMS

Ordnance costs have not escalated by any means as rapidly as the costs of military aircraft. In World War II, 38 heavy antiaircraft batteries and 73 searchlight companies cost the British 3.5 million pounds (about 8.4 million dollars). Assuming four guns to a battery this works out as about $55,000 per gun with fire control and searchlight support.

It was reported in 1958 that the U.S. World War II 90-mm antiaircraft battalion, including fire control and installation, cost about $7.2 million and that to replace it with the Nike Ajax missile battalion would

cost $17 million. No further breakout of costs was provided, but the total probably included support vehicles and all other equipment.

Available cost estimates for a few more modern antiaircraft gun fire units are listed in Table XII-1 for towed weapons, and for self propelled weapons. Since vehicles cost less per pound than armament systems, the self-propelled fire units show a lower cost per pound than do the towed versions. This is also apparent in the field artillery weapons tables given later.

With regard to development costs, it was reported in a presentation to the Congress on projects terminated without production, that the Sperry Gyroscope Co. received $26.6 million through 1961 for the development of the 37-mm Gatling Gun Vigilante, including delivery of several prototypes.

The Vulcan program, including weapon, and the two antiaircraft fire unit types had received about $18.5 million for RDT&E through 1970. Fire control development in this program was small compared with that involved in Vigilante.

The Navy Close-in Weapon System (CIWS, PHALANX) is a gun system which may use a Vulcan gun, and incorporates a fire control system employing corrections based on projectile tracking, and alleged to use two radars. From budget reports RDT&E planned through FY 1973 totals about $35 million. With no other information, and noting that the FY 73 estimate was lower than that for FY 72, an uninformed estimate might be made of about $50 million RDT&E for this program.

Comparing the reported planned procurement dollar and quantity estimates by year, a very rough estimate of cost per system works out at $800,000 to $900,000. Considering that the system will be bolted to the ship's deck, saving mobility costs, but employs sophisticated radars and fire control, this estimate seems consistent with the indications of the systems costs in Table XII-1.

12.5 AUTOMATIC WEAPONS AND MACHINE GUNS

A rough idea of development costs currently associated with new automatic weapons can be obtained from Table XII-2 which shows some of the reported funding for improved aircraft gun systems, and for Bushmaster. Note that about $20 million is associated with caseless ammunition development for the GAU-7/A.

Cost data for Gatling-type guns from various sources are assembled in Table XII-3. The cost history of the AN-M2 World War II[17] automatic weapon for aircraft is summarized in Table XII-4 to show how

Table XII-1. Cost of Antiaircraft Gun Systems

	Caliber	Model	Weight (lb)	Cost (dollars)	Quantity	Year	Cost/Pound ($/lb)
Towed	75-mm	Skysweeper	20,000	313,000		1954	15.50
	20-mm	Vulcan XM167	3,150	52,000	78	1968	16.50
				90,000	120	1968	25.50
				190,000	31	1972	61.50
	2 x 20 mm	Rheinmetall	3,200 (firing) 4,600 (travel)	67,000	1,670	1972 for 1974 delivery	21.00
Self-Propelled	20 mm	Vulcan XM167	26,000				
		Armament system		97,000	111	1968	
				209,000	32	1972	
		XM-741 Vehicle		56,000	111	1968	
				81,250	32	1972	
		Fire Unit	26,000	153,000	111	1968	15.90
				290,000	32	1972	11.00
	2 x 35 mm	Oerlikon/Contraves PFZ-B	80,000	1,100,000 to 1,400,000	500- 600	1972 for 1974 delivery	13.80 to 17.50

20871-561

Table XII-2. Automatic Weapons Development Program Costs

Improved Aircraft Gun Systems (IAGS)				
Caliber	Model	Application	Estimated Costs (million dollars)	
25 mm	GAU-7/A	F15	40	(development)
35 mm	GAU-8/A	AX	35	(total program, 1000 guns)

Notes: (1) About half of the GAU-7/A program cost will be devoted to ammunition development and test. Caseless ammunition weighing one half as much as conventional cased cartridges will be employed. A shoot-out between GE and Philco-Ford is underway.

(2) GAU-8A will fire aluminum cased ammunition with projectile weight about one pound.

Two contractors received firm-fixed-price contracts for 3 guns each for a shoot-out at the O K Test Range. They were

GE $9,500,000

Philco-Ford $10,000,000

Vehicle Rapid Fire Weapon System – Successor (VRFWS-S): Bushmaster				
Caliber	Weight	Application	Estimated Unit Cost	Quantity
20-30 mm	150 lbs E	ARSV MICV-70	7,000-15,000	10,000-12,000

Notes: (1) Three contractors to deliver two guns 8,800 rounds each for shoot out.

GE (27 mm) $1.9 million

AAI (25 mm) $2.1 million

Philco-Ford (23 mm) $1.7 million

(2) Estimated total RDT&E cost $ 40 million
Estimated Initial Procurement Cost $180 million

20871-562

much cost reduction is achieved in very large quantity production.

To broaden the data base, Table XII-5 summarizes unit costs on machine guns ranging from World War I weapons to current designs. The relatively high cost of the M73 may be associated with a variable rate capability.

Note that in 1931 one could buy a whole Darne machine gun for $28.[17]

12.6 RIFLES, CARBINES AND MUSKETS

Rifles have an antiaircraft role, but the principal observation to be made with regard to Tables XII-6 and XII-7 is the relatively small increase in rifle cost over a very long time base, even before an attempt is made to normalize prices for the changing value of the dollar. A factor of less than 3.0 from the Civil War single shot Sharps to the modern M16 is remarkable.

Note the effect of technology on cost of Civil War weapons.[10,11] There was an increase in cost by a factor of four in the transition from smoothbore muzzle loaders to rifled breechloaders. The obstinacy of the Union Ordnance Chief in resisting the transition has

Table XII-3. Cost of Gatling Guns

Caliber	Model	Weight (lbs)	Cost (dollars)	Quantity	Year	Cost/Pound ($/lb)
20 mm	6-bbl Vulcan M61	265	18,460	65	1968	700
	M61A1	255	9,900	498	1968	390
	yearly average		10,000	200	1968-72	390
	Barrels for M61A1	18	96	1458	1968	5.30
	SUU-23 pods for M61A1 including all components except gun	1500	26,500	117	1968	18
	XM-35 Helicopter Installation		27,000	351	1968	
7.62 mm	Minigun Pod 2 x GAU-2B/A guns	35/gun	20,400		1966	
0.58"	Original Gatling Gun				1863	
	General Benjamin F Butler bought 12 Gatling guns complete with 12.000 rounds of ammunition for $12.000 and personally directed their use in the siege of Petersburg. Virginia. [17]					

20871-563

been repeatedly detailed in historical accounts which, however, do not mention that the new weapons would quadruple the cost of small arms procurement. Possibly the Chief was influenced by his budget analysts.

12.7 FIELD ARTILLERY

The relevance of data on field artillery is that these weapons come in towed and self-propelled versions, as do antiaircraft guns. Making a weapon self-propelled substantially increases the unit cost, but the cost per pound of the vehicle is substantially lower than the cost per pound of the weapon it carries, so that the cost per pound of the complete fire unit is lower for self propelled than for towed weapons. These costs are shown in Tables XII-8 to XII-10.

The cost of field artillery, unlike that of rifles, has increased substantially with time, and is continuing to rise. Of course a more interesting comparison would be to compare the effectiveness growth against the cost growth, and these would place cost in a proper perspective.

12.8 TANKS

Present practice is to use a tank chassis as a carrier for a self-propelled antiaircraft fire unit. The more applications that can be served by a common chassis, the larger the production run will be, the lower the unit cost, and the simpler will be the field problem of

maintenance and spares stockpiling. The French AMX series and the German Leopard series are typical.

Since a tank has been the most costly single piece of materiel in the Army inventory until the advent of the helicopter, tank costs have been prominent in budget hearings for half a century.

Tables XII-11 through XII-15 provide more information on tank costs than the reader will want, unless he is a history buff. However the full panorama of tank cost per pound as sketched in Figure 12-2 as a scatter diagram indicates only a modest cost growth even without correcting to constant dollars. From 1950 to 1970, the trend exactly matches that of the consumer price index in Figure 11-1. The exception is the MBT-70 which would have represented an economic breakthrough, although by the time it came off the production line it would not be as great a departure from the trend.

Scatter of the points in Figure 12-2 would probably be reduced by correcting for number produced, and possibly technical differences could be used to explain some of the residual scatter.

Comparing the cost of a tank with the cost of a self-propelled antiaircraft gun system, such as the Oerlikon, the incremental cost associated with the antiaircraft sensors and fire control becomes clearly apparent.

12-5

Table XII-4. Cost History of the AN-M2 20-mm Cannon

Date	Events			
1937	Hispano Suiza offered its Birkigt Type 404 20 mm gun for $3500 each, including mount, magazine, and tools.			
1937	The United States bought one gun with 2000 rounds of ammunition, tool kit, magazine, and mount for $8,000.			
1939	Hispano Suiza offered the gun at $3490 each in a batch of 33.			
1940-1943	The United States secured production rights to the weapon, and it was produced as the AN-M2 with the following production cost history.			
	Manufacturer	Cost		Quantity
		First Lot	Last Lot	
	Bendix	1120	458	22,642
	Oldsmobile	910	510	77,010
	Int. Harvester	840	465	24,526
	Int. Bus. Machines	905	565	10,500
Note: The gun weighed 110 pounds				

20871-564A

12.9 ARMORED PERSONNEL CARRIERS

Tracked, armored personnel carriers give the troops mobility equal to that of the tanks and self-propelled artillery. In addition, the basic vehicles can be used for the lighter antiaircraft weapons. Thus the M113 basic vehicle is used both for Vulcan and for Chaparrel. Table XII-16 shows the cost history of Armored Personnel Carriers, and Table XII-17 lists M113 derivative vehicles. Note that on a per pound basis these vehicles are comparable to tanks in cost.

12.10 ARMORED RECONNAISSANCE SCOUT OR ASSAULT VEHICLES

The current M114 Armored Scout Vehicle is to be replaced by the XM800 for which weight and cost objectives have been set in an austerity plan. There is a substantial anticipated cost growth, over the M114 but with greater capability. The M551 Armored Reconnaissance Airborne Assault Vehicle is shown in the same table, although it has a different mission. The Sheridan has the weapon effectiveness of a tank, but lacks the tank's armor, in order to achieve airborne capability. But in spite of sophisticated armament it works out to about the same cost per pound as the projected XM800. Costs are summarized in Table XII-18.

The cost build-up of the Sheridan is shown in Table XII-19. Note that the basic vehicle constitutes only about 37% of the total unit cost.

12.11 TRUCKS

Trucks serve as tow vehicles for some towed weapons in an antiaircraft battalion, in addition to being present in quantity for general tactical mobility support. Throughout the sixties, a fair estimate of the cost of a truck was about $0.50 to $0.75 per pound of weight empty. The cost per pound has about doubled for current conventional wheeled vehicles and a somewhat greater increase has been experienced in the case of the articulated Gama Goat design. These costs are summarized in Table XII-20.

12.12 AMMUNITION COSTS

In 1898, the Maxim 37-mm Pom-pom fired at 400 rounds per minute, and its ammunition cost six shillings sixpence per round. When shown the gun, the King of Denmark said that at that rate it would bankrupt his kingdom in two hours. The English press multiplied out the rate of fire by cost per round to get an estimate of £90/minute and said that use of this weapon would make the cost of war prohibitive. The British Government bought the gun."

In 1939, the German antiaircraft gunners fired 4940 rounds of light antiaircraft ammunition per target

12-6

Table XII-5. Cost of Machine Guns

Caliber	Model	Weight (lbs)	Cost ($)	Quantity	Year	Cost/Pound ($/lb)
6.5 mm	S.I.A. for aircraft (Italian) incl 15 magazines	25.5	320	10,000	1914	12.50
7.92 mm	Gast (incl spares & 10 drums)	60.0	1,620	3,000	1917	27.00
7.5 mm	Darne for aircraft (French)	18.5	28	11,000	1931	1.50
0.30"	M1919A6	32.5	188		1945	5.80
0.30"	Unident. (may be 0.50)		445		1945	
7.62 mm	M60	23	1,700		1958	74.00
			1,500	4,000	1962	61.00
			500		1963	22.00
			544	2,857	1965	24.00
			495	15,760	1966	21.00
			560	3,478	1967	24.00
			577	15.031	1968	25.00
			550	12.056	1970	24.00
			670	6.000	1971	29.00
	Navy buy		850	175	1972	37.00
7.62 mm	M73 coax		2.300		1969	
			3,400	882	1970	
			3,400	975	1971	
0.50"	Unident	80 (?)	249		1945	3.10
			720		1950	
0.50"	M85		5.000	360	1970/71	
			4,700	1,266	1970/71	
0.223"	Mk 23 (U. S. Navy)	33 (?)	1.050	20	1972	

20871-565

destroyed at 7.5 Marks per round, or 37,100 Marks per kill. They fired an average of 3343 rounds of 88-mm per kill at 80 Marks per round. These costs work out to roughly $15,000 per target with light flak, and $107,000 per target with heavy flak. A post-war German writer used these figures[16] to cite the relative ineffectiveness of antiaircraft, but considering that a B-17 bomber of that era cost $200,000 to build, one must conclude that the German Marksmanship was rather good.

When the war ended, the Germans were still developing more complicated designs of antiaircraft projectiles which would have greatly increased the cost of individual rounds, but were hoped to increase their effectiveness by a greater proportion.

A perspective of ammunition costs is provided by Tables XII-21 through XII-26. Note that for a given type of ammunition, the cost per pound decreases as caliber increases. Cost per round increases about as caliber squared.

Very large increases in cost per round in a given caliber are incurred as the complexity of the projectile design is increased. Thus there is a progressive and substantial cost increase in going from Ball to HE to APDS to ICM, and, apparently applying rocket assist

12-7

Table XII-6. Cost of Rifles and Carbines

Caliber	Model	Weight (lbs)	Cost ($)	Quantity	Year	Cost/Pound ($/lb)
0.30	Carbine M1A1, 2	5.20	35.50		1945	6.80
			64.00		1950	12.30
0.30	Rifle M1 (Garand)	9.50	35.00		1945	3.70
			41.20		1945	4.30
			64.00		1950	6.70
			94.30		1957	9.90
7.62 mm	Rifle M14	8.70	133.00	60.000	1959	15.40
			115.00	120.000	1960	13.20
			112.00		1963	13.00
			120.00		1969	13.80
0.30	Browning Automatic Rifle (BAR) M1918A2	19.40	134.00		1945	6.90
			358.00		1950	18.40
5.56 mm	Rifle M16	7.4	106.00	600.000	1970	14.00
	M16E1	7.6	107.00	254.000	1971	14.00
	(Air Force buy)		116.00	65.000	1971	14.00
	Program Average		128.00	3.200.000		17.00
	Final Unit Cost		94.00		1971	12.40

20871-566

(RAP) to a conventional projectile involves a significant cost increase.

In each case, the increase in cost is associated with an increased capability, of course. The cost of guided artillery rounds will be much higher, and will probably enter the domain of missile costs.

Ammunition costs have been normalized by dividing in each case by the projectile weight. In the case of cartridge ammunition and fixed artillery ammunition it would be preferable to divide by the complete round weight. This would probably reduce the apparent anomoly of the M139 ammunition which has a high muzzle velocity, and probably a proportionately higher complete round weight.

Costs associated with fuzes of complexity increasing from simple contact fuzes to proximity types are indicated in Table XII-27. The cost of a fuze for a guided missile is many times higher, as might be expected.

12.13 SENSORS

It has not been possible to make an extensive summary of sensor costs. In this field published or inferred costs are more likely to be widely in error than in the case of simple items such as trucks, for example.

With this caveat lector, we note some published costs for infrared and image intensification sights in Table

XII-28. In Table XII-29 is shown the published cost history of the range-only radar for Vulcan.

Available data on laser range finders is summarized in Table XII-30. The apparent anomaly represented by the inferred unit cost of the Sheridan range finder is typical of the uncertainties in this level of data for this type of equipment.

In a given AN category, radar costs vary widely with the specific characteristics of each piece of equipment, and this is seen in Table XII-31 for shipborne search radars, and Table XII-32 for land based transportable search radars. To attempt to normalize the costs against radar characteristics such as power, frequency, scan rate, etc., would require the inclusion of classified information. The obvious difference in the difficulty of the task assigned the HIPAR as compared with the FAAR is clearly reflected in the relative costs.

It is noted that the Army Electronics Command has a comprehensive program on the costing of electronic equipment which has developed excellent, classified, cost estimating relationships.[12]

A rough idea of how radar cost varies with average power, and with weight, can be obtained from Figures 12-3 and 12-4, which was developed from published prices of airborne weather radars for commercial air-

Table XII-7. Cost of Rifles, Muskets and Carbines

	Caliber (inches)	Model	Weight (lbs)	Cost ($)	Quantity	Year	Cost/Pound ($/lb)
Muskets (Smoothbore)	0.69	Prussian		6.80	81.652	1862	0.70
	0.69	American		10.00	2.181	1862	1.00
Rifles (Muzzle Loading)	0.58	Harpers Ferry M1855	9.50	18.20	22.793	1862	1.90
	0.58	Springfield	9.90	19.50	671.000	1862	2.00
	0.577	Enfield	8.91	18.40	428.292	1862	2.05
Rifles (Breech Loading)	0.52	Sharps (single shot)	8.75	36.00	9.141	1862	4.10
	0.52	Spencer (7-shot)	10.00	37.20	12.471	1862	3.70
	0.44	Henry (12-shot)	9.25	36.50	1.731	1862	4.00

20871-567

craft. For this class of equipment, cost increases less rapidly than average power.

Provision of IFF equipment is a non-negligible cost component, as is indicated by Table XII-33.

The cost of simple 'hot-spot' infrared tracking devices might be inferred from missile costs. Current interest in applying FLIR type sensors to antiaircraft fire units makes the initial cost estimates of the airborne FLIR in Table XII-34 of some relevance.

A comprehensive analysis of the cost of military radio communications equipment was made in 1960 by D. C. Ports et al.[9] It was indicated that for a set of that vintage, cost was about proportional to weight (at an average of about $100 per pound) but that weight, except for man-portable units, increased only as about the 1/3 power of transmitted power. The latter relationship included vehicular radios.

12.14 PRODUCIBILITY VERSUS COST

As noted earlier, the fact that the 'value of the dollar', or the pound or the mark, or the yen, is an increasingly free-floating index suggests that some other measure of the effort required to develop and manufacture weapon systems would be more helpful is estimating across a moderate time base.

A more stable reference may be the number of man-hours of effort involved in each case. Manufacturing man-hours in particular would seem to be fundamental in estimating the production rates that could be achieved with finite national manpower when a rapid build-up is required.

A piece of equipment that can be economically manufactured in small quantities at a low rate in times of low tension may be extremely difficult to produce at a high rate with low skill personnel, and this could result from the inherent characterisitcs of the design. The experience of the Army in World War II in attempting to have the M-4 antiaircraft director manufactured by fender-benders at the Ford Motor Company rather than by a small number of craftsmen at the Sperry Gyroscope Company is a case in point.

The object of 'Value Engineering' is to avoid this kind of situation, but whether the value engineers have the leverage to affect the basic design concept is not known.

A few examples of man-hours to produce ordnance equipment from British experience are given below.[13]

In World War II, the British Admiralty employed the Oerlikon 20-mm gun which was considered 'very elaborate'. The British-designed Polsten was intended to replace the Oerlikon with a weapon that would be easier to produce. Table XII-35 demonstrates the improvement achieved.

Table XII-8. Field Artillery Costs (Towed Weapons)

	Caliber	Model	Approximate Weight (lbs)	Cost (dollars)	Year	Cost/Pound ($/lb)
Howitzers	105 mm	M2A1	5000	8,260	1945	1.70
		M101A1	5300	13,670	1950	2.60
		M102				
		XM204				
	155 mm	M1	12,800	15,640	1945	1.20
		M114A1	12,700	26,410	1950	2.10
		XM198				
	203 mm(8")	M115	30,000			
Guns	280 mm		170,000	437,000	1957	2.60

20871-568

Table XII-36 indicates the number of manufacturing man-hours required to produce selected items of British WW-II ordnance, indicating in a few cases, the reduction achieved over long production runs.

12.15 PERSONNEL COSTS IN MAINTENANCE AND OPERATIONS

The discussion of maintenance and operations costs will be limited to the observation, illustrated in Figure 12-5, that the average expenditure per man by the Army for pay and allowances is escalating at least as rapidly as other cost components, and currently seems to be achieving a major new breakthrough to high levels. The curve was derived simply by dividing the dollars for pay and allowances in the budget by the number of military personnel and does not include many additional cost elements associated with the man but not with his equipment.

The cost rise is not expected to slacken until the Volunteer Army has stabilized.

The effect on weapon system design is to increase the relative value, on a 'life cycle' basis of reducing the number of men required to operate, service, maintain, and support a weapon structure, including all the personnel in the weapon's slice of the Army from the operator back to the Pentagon.

High reliability and ease of maintenance are obvious objectives, but the reduction in number of men to maintain a given effectiveness level is an Army-wide problem.

Table XII-9. Field Artillery Costs (Self Propelled Weapons)

	Caliber	Model	Weapon	Approximate Weight (lbs)	Cost (dollars)	Quantity	Year	Cost/Pound ($/lb)
Howitzers	105 mm	M7	M2A2	52,000	50,400		1945	1.00
		M37	M4	40,000				
		M52		53,000				
		T195			103,000	275	1959	2.00
					115,000		1963	2.30
		M108		50,000				
	155 mm	M41	M1	44,000				
		T196			62,000	500	1959	1.20
		M109		54,000	115,150		1970/71	2.10
	203 mm(8")	M43	M2	83,000				
		M110		56,000	128,100		1970/71	2.30
		Vehicle only			41,415			
Guns	155 mm	M40	M2	83,000				
		Unident			140,000		1967	1.70
	175 mm	M107		64,000	146,000	115	1960	2.30
		Vehicle only			41,000			

20871-569

12-11

Table XII-10. Cost of Civil War Artillery

	Caliber (inches)	Model	Gun Weight (lbs)	Cost ($)	Quantity	Gun Cost/lb ($/lb)	Carriage Cost ($)	Quantity
Smoothbore (bronze) Guns	3.67	6-pounder	884	400	152	0.45	312	1551
	4.62	12-pounder	1757	570	1127	0.32		
Howitzers	4.62	12-pounder	788	385	73	0.49	345	686
	5.82	24-pounder	1318	425	58	0.32		
Rifle Guns		6-pounder (bronze)		440	25			
	3.67	12-pounder (bronze)	875	689	10	0.78		
	2.56	6-pounder Wiard (steel)	600	440	25	0.73		
	3.0	10-pounder Wiard (steel)	790	720	20	0.91		
Parrott Rifles (iron)	3.0	10-pounder	890	205	587	0.23		
	3.67	20-pounder	1750	396	338	0.22		
	4.20	30-pounder	4200	557	392	0.13		
	6.40	100-pounder	9700	1304	237	0.13	670	248
	8.00	200-pounder	16,300	2244	90	0.14	794	88
	10.00	300-pounder	26,500	4937	40	0.19	1656	32

20871-570

Table XII-11. Cost of U.S. Tanks (Under 50,000 lbs)

Model	Weight (lbs)	Cost ($)	Year	Cost/Pound ($/lb)
M24	38,000	39,640	1945	1.00
T 41	26,000 (?)	126,030	1950	4.90
M 41	46,000	94,420	1959	2.05

20871-571

Table XII-12. Cost of U.S. Tanks (Over 50,000 lbs)

Model	Weight (lbs)	Cost ($)	Quantity	Year	Cost/Pound ($/lb)
M4	67,300	54,836		1945	0.80
M26	86,000	81,324		1945	0.95
M46	98,000	197,427		1950	2.05
M47	88,000	240,000		1952	2.70
M48	100,000	120,000	(600)	1956	1.20
		133,000		1957/59	1.33
		109,142		1959	1.24
M48A1,2		115,035		1959	1.15
XM60	102,000	138,000	180	1959	1.30
M60	108,000	162,400		1963	1.50
		203,780	507	1967	1.90
M60A1		225,330	300	1970	2.10
M60A1E2		275,000		1970	2.45
MBT	80,000	500,000 (est)		1967	6.20
MBT-70		880,000 (est)		1970	11.00
XM803		620,000 (est)	3000	1970	7.80
		649,000 (est)		1971	8.00

20871-572

Table XII-13. Cost of British World War II Tanks

Model	Weight (tons)	Basic Cost (£)	Year of First Order	Cost per Ton (£/ton)	Cost/Pound ($/lb)
Infantry Mk I	11	6,000	1937	550	1.35
Cruiser Mk I	13	12,710	1937	970	2.40
Matilda	25.75	18,000	1938	700	1.70
Cruiser Mk II	14	12,950	1938	930	2.25
Cruiser Mk III	14.25	12,000	1938	840	2.05
Cruiser Mk IV	14.75	13,800	1939	940	2.10
Covenanter	15.85	12,000	1939	755	1.85
Crusader	17.53	13,700	1939	780	1.75
Valentine	15.6	14,900	1939	960	2.10
Churchill	38.5	11,150	1940	290	0.60
Cromwell	28	10,000	1942	360	0.70

NOTES:

(1) The value of the Pound fell between 1937 and 1942.

(2) A great deal of rework was required on the Churchill because of defective manufacture. This cost is not included.

(3) The basic cost quoted is based on contracts, and probably does not include "stores of free issue" (GFE).

20871-573

Table XII-14. Cost of Current Foreign Tanks

Model	Country	Weight (lbs)	Cost ($)	Quantity	Year	Cost/Pound ($/lb)
Leopard	Germany	88,704	232,000		1967	2.60
			252,000		1970	2.75
			328,000	3588	1970	3.70
AMX-30	France	79,000	312,000		1967/70	4.00
Chieftain Mk 5	England	117,000	308,000		1967	2.65
			244,800		1970	2.10
STRV 103 (S-Tank)	Sweden	83,000	under 350,000		1970	3.50 (?)

20871-574

12-14

Table XII-15. Cost of Tanks from 1914 to 1957

Model	Country	Weight (tons)	Cost £	Cost $	Year	Cost/Pound
Mk IV	England	28	5.000	24,350	1914	0.43
Renault F.T. 17	France	7	2,250	10,950	1914	0.78
Mk VIII	England	37	18,000	86,400	1920	1.17
			7,350	35,300		0.48
Carden-Lloyd	England	1.3	500	2,400	1928	0.92
Mk I	England	11	1,500	7,400	1935	0.34
Renault R35	France	11	2,200	10,800	1935	0.50
Churchill	England	38.5	15,000	60,450	1941/44	0.78
M4	U.S.	34	10,300	41,500	1944	0.61
			16,600	67,000		1.13
M41	U.S.	26	27,200	76,200	1953	1.47
M48	U.S.	49	47,000	132,000	1957	1.35
Centurion	England	50	40,000	112,500	1957	1.12

20871-575
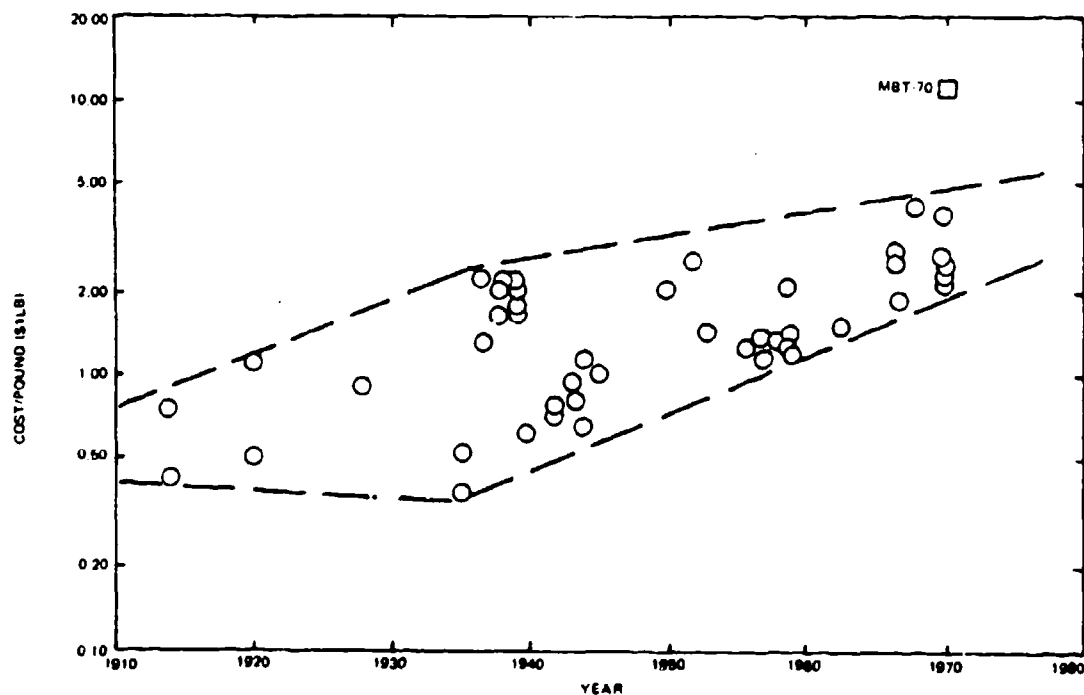
Figure 12-2. Tank Costs Per Pound Versus Time

20871-1230

12-15

Table XII-16. Cost of Armored Personnel Carriers (APC)

Model	Gross Empty Weight	Cost	Quantity	Year	Cost/Pound
M3	19,000	12,294		1944	0.67
M75	36,000	100,000	1740	1952	2.80
		75,000		1954	2.10
M59	38,000	41,000	1800	1958	1.10
		35,000		1959	0.90
		29,602	600	1959	0.80
T113		31,000	600	1959	1.54
M113	20,000	28,000		1963	1.40
		20-22,000		1969-72	1.10
M113A1		22-25,000		1969-72	1.15
		19,955	1125	1971	1.00
M113 Total Program $120 Million		40,000 Average (all costs)	3000		2.00
XM723 (MICV-70) (Mechanized Infantry Combat Vehicle)	35-38000	100,000 Goal	2500- 5000 E	1972	2.70

20871-576A

Table XII-17. Cost of M113 Derivative Vehicles

Vehicle	Cost	Quantity	Year
M548: 6T Cargo Carrier	25,000 (basic)	120	1971
XM730 M548 modified as Chaparral carrier	29,200	116	1971

20871-577A

12-16

Table XII-18. Cost of Armored Reconnaissance Scout or Assault Vehicles

	Model	Weight	Cost	Quantity	Year	Cost/Pound
Scout	M114	15,000	38,000		1971	2.50
	XM800 (ARSV)	17,000	116,200 Objective 175,000 Possible	5000 E	Est. as of 1972	6.90–10.20
Assault	M551 Sheridan (ARAAV)	33,500	213,600	1662	1970	6.40

20871-578

Table XII-19. Sheridan Cost Build-Up

Major Component	Unit Cost
Vehicle	80,400
Engineering change orders	8,800
Government-furnished equipment (GFE):	
Engine	4,300
Transmission	9,000
Gun launcher	12,300
Fire control	12,500
Guidance and control	25,200
Machine gun	4,400
Searchlight	2,500
Communications	2,700
Night vision sight	2,400
On equipment maintenance (OEM)	1,600
Engineering support and quality assurance	45,200
All Other [1]	2,300
Average unit price	213,600
[1] Includes documentation, and initial care and preservation performed at depots.	

20871-579

Table XII-20. Cost of Trucks

Type	Model	Weight Empty	Cost	Quantity	Year	$ Cost/Pound
1/4 Ton 4 x 4	Jeep	2,400	1,057		1944	0.45
	M38A1	2,800	2,000		1953	0.72
	M151	2,250	3,300	3,400	1959	1.46
	M151A1, 2	2,400	3,180		1968	1.32
			3,242		1969	1.34
			3,476		1970	1.44
			3,504		1971	1.46
3/4 Ton 4 x 4	M37	5,700	3,790		1966-67	0.67
1 1/4 Ton	M715	5,500	4,720		1966-67	0.85
	XM-705		5,400	18,000	1970	1.00
			8,337	3,452	1971	1.50
	M35	13,500	3,352		1959	0.25
2 1/2 Ton 6 x 6	M109	15,000	6,375		1953	0.42
			6,650		1955	0.44
			7,131		1957	0.48
			8,363			0.56
	M54	40,000	13,200	3,600	1958	0.67
5 Ton 6 x 6	XM 809		17,434		1969	0.85
			17,196		1970	0.85
			17,381		1971	0.85
1 1/4 Ton 6 x 6	M561 Gama Goat	6,550	13,281	15,274	1970	2.05
			11,722		1971	1.80
1/2 Ton 4 x 4	M274 Mech Mule	900	2,150	2,000	1959	2.40

20871-580

12-18

Table XII-21. Cost of Rifle and Machine Gun Cartridges

Caliber	Model	Weight grains/lbs	Cost ($)	Year	Cost/Pound $/lb
5.56 mm	All types		0.060	1971	
	Ball	55/.0079	0.060	1971	7.60
0.30"	Tracer		0.11	1959	
	Ball M2	152/.0217	0.09	1959	3.70
	Tracer (Carbine)	107/.0153	0.06	1971	3.90
	Ball (Carbine)	110/.0157	0.07	1971	4.45
7.62 mm			0.11	1959	
	Ball	150/.0214	0.087	1971	4.05
	Linked		0.10	1971	
	NATO		0.095	1970	
	M13 Linked (USAF)		0.10	1972	
0.50"	Ball	700/0.10	0.325	1957	3.25
			0.28	1959	
	4 Ball/1 Tracer mix		0.30	1970	3.00
			0.38	1971	3.80
			0.39	1972	3.90

20871-581

Table XII-22. Cost of Civil War Rifle Cartridges

Caliber (inches)	Weapon	Proj Wt grains (lb)	Cost ($)	Quantity (millions)	Cost/Pound ($/lb)
0.58	Springfield Muzzle Loader	550 (.078)	.015	46.4	0.19
0.52	Sharps Breech Loader	475 (.068)	.021	16.3	0.31
0.52	Spencer Breech Loader	385 (.055)	.024	58.2	0.43
0.44	Henry Breech Loader	216 (.031)	.023	4.6	0.74

20871-582

12-19

Table XII-23. Cost of 20-mm Ammunition Cartridges

Weapon	Type Projectile	Weight (lb)	Cost ($)	Quantity (thousands)	Year	Cost/Pound ($/lb)
Hispano Suiza 404	Inert (Ball)		2.00		1917	7.20
	HE	0.28	4.00		1937	14.40
	Mix		2.38	59.5	1939	8.50
Vulcan/Cobra	All Types	0.22	1.30		1970	5.90
			1.58		1971	7.20
			1.83		1972	8.30
Vulcan (USAF)	Training	0.22	0.93		1972	4.20
	Combat	0.22	2.11		1972	9.60
M139 (Hispano Suiza 820)	TPT M206		3.40		1970	
			3.90		1971	
	HEIT M599/APT M601 3/2 mix	0.25	7.10		1970	28.40
			5.90		1972	23.60

20871-583

Table XII-24. Cost of Howitzer Ammunition

Caliber	Type	Model	Projectile Weight (lb)	Cost ($)	Year	Cost/Pound ($/lb)
105 mm	HE		33	26.00	1951	0.80
	HE w/o fuze	M1		21.50	1972	
	HE with fuze		33	28.00	1972	0.85
	Illuminating with fuze	M314A3		53.00	1972	
	WP	M60		53.00	1972	
155 mm	HE		95	40.00	1951	0.42
	HE	M107	95	30.50	1970-72	0.32
	Illuminating	M485A2		75.00	1971-72	
	ICM	XM483		310.00	1971	
	Charge					
	Green Bag	M3A1		13.50	1970-72	
	White Bag	M4A2		29.50	1970-72	
8" (203 mm)	HE	M106	200	60.00	1970-72	0.30
	ICM	M404		265.00	1970	
	Charge					
	Green Bag	M1		20.00	1970-72	
	White Bag	M2		29.00	1970-72	

20871-584

12-20

Table XII-25. Cost of Gun Ammunition

Caliber	Type	Model	Projectile Weight (lb)	Cost ($)	Year	Cost/Pound ($/lb)
90 mm	HE (Fixed)	M71	23.4	33.00	1953-57	1.40
175 mm	Unident. HE w/o fuze	M437A2		94.00 68.00	1960 1970-72	
	Charge	M86A2		78.00	1970-72	
5"/38 5"/54	Navy Navy	RAP RAP		385.00 350.00	1968 1970	

20871-585

Table XII-26. Cost of Ammunition for Tank Guns

Caliber	Type	Model	Projectile Weight (lb)	Cost ($)	Year	Cost/Pound ($/lb)
76 mm	HE			21.30	1959	
	WP			23.90	1959	
	TP-T			19.20	1959	
	Blank			8.30	1959	
90 mm	HE			32.20	1959	
	WP			39.50	1959	
	TP-T			25.90	1959	
	HEAT			94.00	1959	
105 mm	HEAT-T	M456A2	21	75.00	1970-72	3.30
	HEP-T	M393A3	24	53.00	1971-72	2.20
	APDS	M393A2	13	155.00	1970-72	11.60
	TP-T	M490		49.00	1970-72	
152 mm	TP-T	XM411E4		106.00	1971-72	

20871-586

12-21

Table XII-27. Typical Fuze Costs (Current)

Type	Model	Application	Cost (dollars)
PD (Point Detonating)	All types	Hand grenade, Practice	0.50
		VADS Ammo	3.00 (?)
	M524	81 mm Mortar	8.00
	M572	Howitzers, Guns	5.50
MT (Mechanical Time)	M565	Howitzers	16.00
MTSQ (Mechanical Time, Superquick)	M564	Howitzers	17.00
Proximity	M514A1E1	Howitzers, Guns	45.00

Note: The World War II Proximity (VT) Fuze for Antiaircraft Guns had an initial cost of $732.00 each in 1942 at the beginning of production. By 1945 the cost per fuze was down to $18.00. The total program cost was $1.01 billion, and over 22 million fuzes were produced.

20871-587A

Table XII-28. Cost of Sights (Infrared and Image Intensification)

Model	Type	Cost	Quantity	Year
AN/PAS-5	Binoculars	350	6300	
AN/PAS-6	Rifle Sight	2000		1967
AN/TVS-2		380	3200	1970
AN/TVS-4	NODMR	1000	1748	1971

20871-588

Table XII-29. Cost of Range Only Radar

Model	Price	Quantity	Date
AN/VPS-2	26,000	228	to 1968
	25,000	60	1969 (incl. install. kits)
	36,000	267	1970
	55,000	48	1971 (incl. 4 test sets)

20871-589

12-22

Table XII-30. Cost of Laser Range Finders

Model	Application	Cost ($)	Quantity	Year	Remarks
AN/GVS-1	Development Models	110,000	10		
AN/GVS-3	Tripod Mount	53,000	200		incl. 40 test sets
		5,600 E	500	1972	incl. 40 test sets
		6,100 F	1000	1973	incl. 134 test sets
AN/VVS-1	M60A1E2 Tanks	462,000		1967	prototype
		11,000	243	1969	
		14,600	176	1969	
		3,300	300	1970	
	M551 Sheridan	47,429	176	1971	

20871-590

Table XII-31. Cost of Shipborne Search Radar

Model	Cost	Year
SC3	18,000	1945
AN/SPS-39A	1,000,000	1963
AN/SPS-40	190,000	1965
AN/SPS-48	500,000	1972
AN/SPS-52 (FRESCAN)	4,000,000	1972
AN/SPS-58	610,000 (4 proto)	1970
	295,000 (6 prod)	1971

20871-591

Table XII-32. Cost of Transportable Radars for Air Surveillance and Control

Type		Cost	Year
Unident.		384,000	1945
Unident.		2,500,000	1963
AN/TPS-32	For MTDS with 3-shelters and spare computer	2,700,000	1972
AN/TPS-34	For MTDS	1,100,000	1969
AN/TPS-43	For 407L	1,030,000	1970
AN/MPQ-43	(HIPAR) for Nike Hercules	1,200,000	1967-70
AN/MPQ-49	(FAAR)	75,000	1971

2081-59?
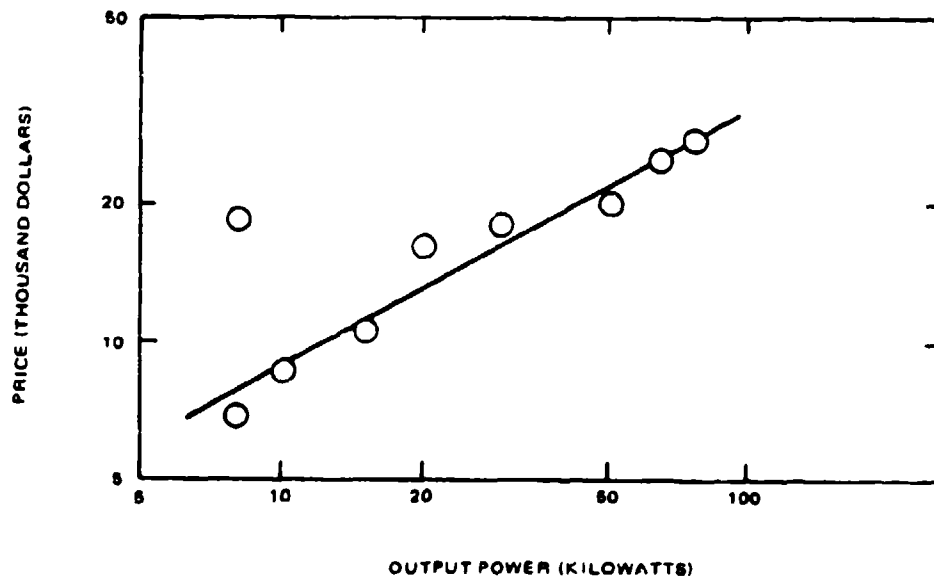
Figure 12-3. Cost of Airborne Weather Radar Versus Power Output
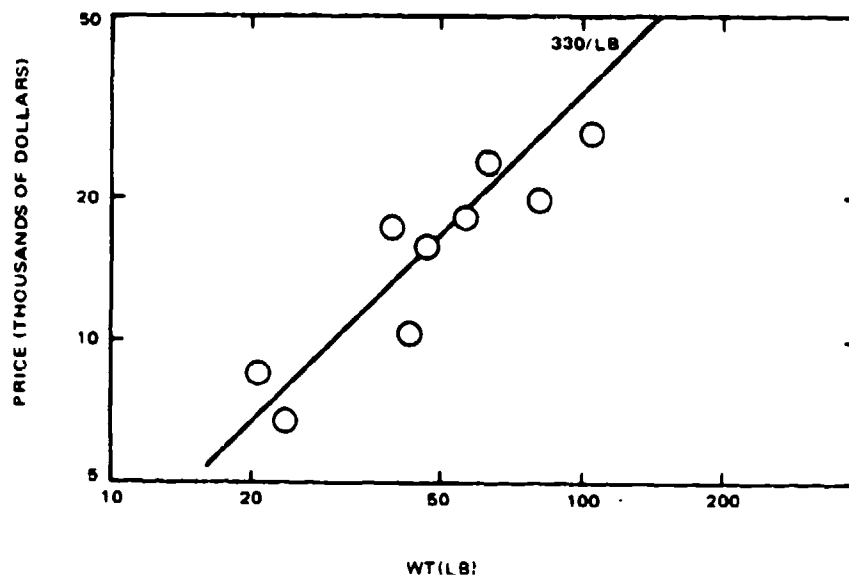
Figure 12-4 . Cost of Airborne Weather Radar Versus Weight   20871-1232

Table XII-33. Cost of Army IFF Equipment

Model	Application	Cost ($)	Quantity
AN/TPX-46	General Purpose Interrogator Set	100,000	109
AN/TPX-50	Interrogator Set for use with MPQ-49 and TPQ-32 FAAR Radars	21,500 22,500	23 156

20871-593

Table XII-34. Cost of Airborne Infrared Surveillance Systems

Type	Cost ($)
AN/AAD-4 USAF (FLIR)	550,000
AN/AAS-24 Army	550,000

20871-594

Table XII-35. Comparison of WW-II 20-mm Weapons

	Cost		Number of Components	Number of Machining Operations	Weight (lb)	Cost/Pound ($/lb)
	£	$				
Weapon						
Oerlikon	320	1400	250	3000	136	10.50
Polsten	60-70	300	119	900	121	2.50

20871-595A

Table XII-36. Comparison of Manufacturing Man-Hours

Weapon	Manufacturing Man-Hours
Sten Machine Gun Mkl	11 (early)
	5 (late)
MkV	12
Bofors 40 mm AA Gun	2420 (early)
	1500 (late)
Field Artillery 25 pdr	3085
Anti-tank 2 pdr	2683 (prewar)
6 pdr	1293
17 pdr	2726 (1942)

20871-596

Figure 12-5. Average Pay and Allowances per Man Versus Time

20871-1233

SECTION 13
ADDITIONAL DATA REQUIREMENTS

There are two principal determinants of the effectiveness of a predicted fire weapon system. These are

a. The ability of the system to track its target accurately.

b. The ability of the system to predict the target position one time of flight in the future.
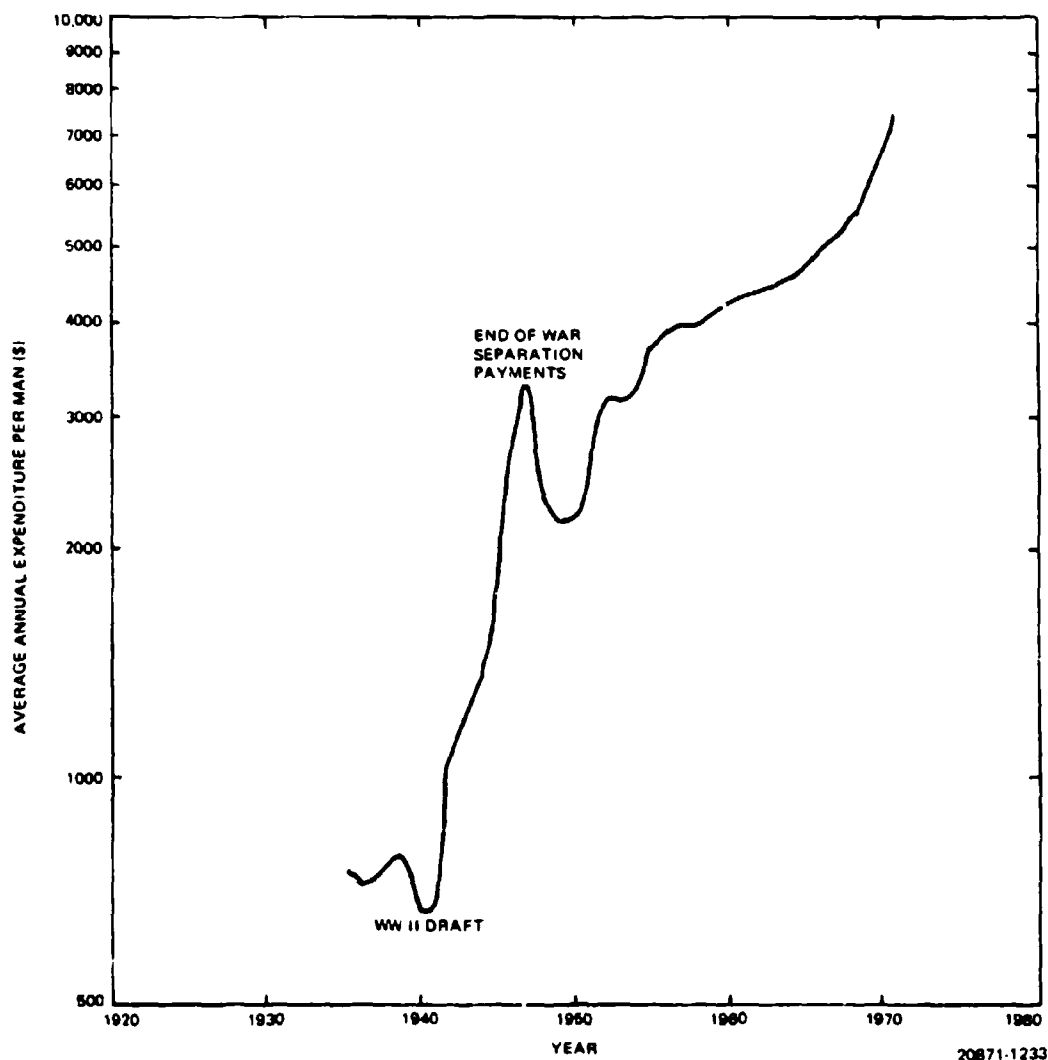
Additional experimental data is required on both of these topics. Of the two, target path data is most urgently needed.

13.1 TARGET PATH ANALYSIS

The variety of paths which a freely maneuvering aircraft can fly is unlimited. However, the class of target paths which an aircraft can fly in performing its mission, especially during its munition delivery phase, is limited. It is believed that this limitation is much more severe than is generally assumed for defense system evaluation, but no definitive analyses of such limitations were located in the present contractual effort.

The following program of analysis is suggested

a. Obtain records of target paths in which aircraft performed tactical missions. Combat records would have the greatest validity, but proving ground results are more likely to be available.

b. Perform a statistical analysis of the predictability of these paths. A possible analytic approach is suggested below.

c. Determine those prediction algorithms and defense system characteristics most likely to be effective against the set of available attack paths.

d. Validate the defense system characteristics by running them against a set of the recorded paths on the Litton simulation.

The statistical analysis of the recorded flight paths might develop as follows:

a. Plot up the data for visual inspection. Preferably this would be done with a computer and automatic plotter.

b. Compute target velocity, heading and dive angle as a function of time.

c. Compute target 'total energy' ($V^2 + 2gh$) as a function of time to determine whether this index remains fairly constant during altitude changes.

d. Compute rate of change of velocity, heading and dive angle versus time.

e. Perform an analysis of 'runs' on the three target parameters and their rates of change, separately

and in combination to obtain probability density functions for the probability that each combination remains within specified limits as a function of the duration of the 'run'. These results allow estimates of the duration of predictable path segments.

f. Relate the predictable path segments to the position of the aircraft relative to the target it is attacking, and to the phase of its attack (run-up, down the chute, breakaway).

To get such a program underway quickly, it will be necessary to take whatever data is available. However, once the analytical techniques have been developed, the Army should maintain a continuous in-house program in conjunction with the Air Force to maintain an up to date library of target path data on the more advanced aircraft delivery systems.

13.2 ANALYSIS OF TRACKING DATA

As in the case of target path data, conjecture regarding the characteristics of target data is not a valid substitute for experimental data. There is not much profit in simulating a predicted fire system in detail if the stochastic and deterministic descriptors of the sensors must be guessed.

Ideally, one would like sufficient data to derive a state space model of sensor operation, in which the sensor is described by a set of differential equations driven by white noise (or equivalent) of constant intensity. The coefficients of the equations would be at least time varying and situation dependent, and the equations could be non-linear. Development of this kind of model is within the state of the art of 'system identification' analytical tools.

In the present report, a simple model describing radar glint noise was developed somewhat along these lines.

At least the following sensors should be operated against a variety of target paths and types and the experimental data reduced in a manner leading to useful analytical and simulation representations.

a. Radar

   (1) Normal operation.

   (2) Track-on-jam mode.

   (3) Operation under various types and levels of jamming.

b. Automatic Tracking with Imaging Sights

   (1) TV or imaging intensification.

   (2) Infra-red imaging.

c. Laser

    (1) Range only.

    (2) Angular tracking.

d. Manual tracking (optical)

    (1) Conventional aided tracking.

    (2) Regenerative tracking.

In addition to fixed wing aircraft, targets on which data should be acquired include

a. Helicopters.

b. VTOL aircraft at very low velocities (to determine the limitations of pulse-doppler radars).

c. Air to surface missiles (some information on the ability of radar to track very small targets can be obtained from counterbattery radar data).

13.3 HISTORICAL SUMMARY OF PREDICTED FIRE SYSTEM PERFORMANCE

In the present report and the accompanying Effectiveness report, the writer has tried to collect and summarize records of antiaircraft effectiveness, and fire control accuracy. The reason has been to attempt to counter the always prevalent general opinion that predicted fire weapons are inherently inaccurate.

In fact, even since World War I, the accuracy of predicted fire antiaircraft weapons has been remarkable. It has, moreover increased steadily with time in the case of those systems which have been well designed and engineered.

It is believed that the air defense effort now and in the future would be well served by about a one man-year effort devoted to recovering the test data on past predicted fire systems from the archives and presenting a concise summary, showing what was achieved.

If the files of test results at the Air Defense Board and School have not been purged, they would constitute a gold mine of historical data. Frankford undoubtedly has a great deal of information. The Navy has excellent data, if it can be made available.

A simple set of curves of predicted fire accuracy vs. time with a long time base would do a great deal to place predicted fire in the proper perspective, establish references against which to write new requirements, and assist in obtaining the best overall air defense system for given cost. It would also support the case of the sharpshooters against the multitude of proponents who want to ride shotgun on each new outgoing stage of air defense system development.

It is too late to begin a test program when the first prototype has been completed. The following brief outline sketches some of the considerations to be included in test planning. The plan should be completed at least in preliminary form when system development is initiated.

14.1 OBJECTIVES AND TEST PLAN CONTENT

The test and evaluation plan should be developed to ensure a comprehensive set of tests in parallel with the development activity to complement, improve, and expedite the development process. It should serve as a means for obtaining progressively more valid information of components and system feasibility, reliability and maintainability, and to facilitate early identification and correction of deficiencies.

As components become available for testing, initial estimates of reliability and maintainability can be replaced by real data.

Human factors checkout and validation should become progressively more definitive as actual system elements are available for man-machine testing.

The plan should provide for progressively more realistic man-machine performance validation by

a. Static and dynamic test of components.

b. Static and dynamic test of the system with simulated inputs.

c. Parallel improvement of a system simulation.

d. Non-firing tests of a complete system against realistic targets.

e. Firing tests against simulated targets.

f. Firing tests against live targets (such as drones).

Testing and engineering should be closely integrated throughout development to expedite correction of observed deficiencies.

The test and evaluation plan should not be limited in its final phase to definition of system acceptance tests requirements which must be met by the contractor. The final evaluation should be sufficiently comprehensive to provide a good basis for estimating probable system effectiveness in combat, and the limits on effectiveness.

With a good test plan and sufficient foresight, the test procedures will not only indicate the capabilities of the system under test, but will provide a basis for writing the requirements of the next generation system. This involves rather careful logging of the target path characteristics and other parameters during tests, and identification of the sources of system error, and their relative magnitudes.

Time and cost limits on testing will prevent the test and evaluation manager from acquiring data beyond immediate requirements unless these longer term requirements for data are specifically written into his assignment. This is a major problem in all military testing. Automated data processing can help to satisfy everyone concerned, if plans for the kind of data reduction desired are made early enough, and if the data reduction software is completed before testing begins.

14.2 DATA ACQUISITION ON COMPLETE SYSTEM PERFORMANCE

The principal shortcoming of almost all military field experimentation programs is the limited analysis of data which is carried out. The usual cause of this shortcoming is that a deadline is established for the final report, and slippages in the experimental portion of the program compress the time available for data reduction and analysis. Once the report is delivered there is no incentive and little opportunity to continue the analysis to fully exploit the data which has been taken. The problem is further compounded by the fact that not many people are really interested in data analysis.

A partial remedy is to provide instrumentation and associated data computational capability that will analyze the experimental data in real time, with a printout and summary available after each experimental run. This approach is limited by the foresight of the experiment planner in deciding beforehand what data should be taken and how it should be analysed. However this is an easier task in the case of predicted fire air defense systems than in most of the more complex field experiments with troop units and mixed weapons.

The following paragraphs outline a system for real time assessment of antiaircraft gun systems. The Army already has under development a 'Vulcan target selector' for which details are not available at the time of writing, but which it is believed will perform some or all of the functions to be described, and perhaps others as well. However the present material is offered to illustrate a concept.

The problem is to determine the effectiveness of a predicted fire system in a field experiment in real time, without actually shooting down droned aircraft.

The basic element of this approach is the generation by digital computer of a 'synthetic trajectory' in real time. It has been noted in Section 6.0 that the use of a synthetic trajectory appears to be highly desirable in conjunction with prediction algorithms for use with systems employing projectile tracking, and its reappearance here suggests that the Army might usefully

activate a development program with the specific object of producing an operational module to be attached to any predicted fire system for this purpose.

As described in Section 10, the idea of a 'synthetic trajectory' is to store gun orders in memory at a sampling rate of about 10/second. From a ranging device time of flight to target present position can be obtained continuously, gun orders time of flight previous can be retrieved stripped of superelevation and other ballistic corrections other than time of flight, and used to generate a spot on a tracking display, or reticle showing where the prediction function would have put the center of aim with respect to the target.

The computational process is outlined in Figure 14-1. Symbols used are as follows:

a. A_t = gun azimuth.

b. ϕ = gun quadrant elevation.

c. ϕ_s = gun superelevation.

d. t_f = time of flight.

e. D = slant range to target.

f. t = time.

g. $e_t = \phi - \phi_s$.

For a test device, this module can be utilized in a number of ways. Two are described below, one for continuous recording of prediction errors, and one for automatic scoring with cooperative sensors in a real aircraft. Both descriptions are described in conjunction with engagement of a real target (either non-firing or firing blank ammunition), but it will be clear that one could also use a synthetically generated target for an indoors test operation.

In both cases, a pointing device is mounted on the gun mount, and this is turned back from gun position by deflection angles which are computer generated so that the axis of the pointing device is continuously directed at the angular position of the center of the shot pattern at the computed time that the projectiles would be at target range.

If the pointing device mounts a TV or IR imaging device, the target image appears off axis by the amount of error in the center of the shot pattern (i.e., error in prediction exclusive of round to round ammunition dispersion). An observer can then view the wander of the aim error over a path continuously, and the errors can be electronically extracted from the imaging device for a continuous record.

If the pointing device mounts a laser, sensors on the aircraft can record when the laser is on target. Somewhat similar scoring systems are now operational at Fort Ord but do not allow prediction error to be assessed. By choosing the laser beamwidth to corre-
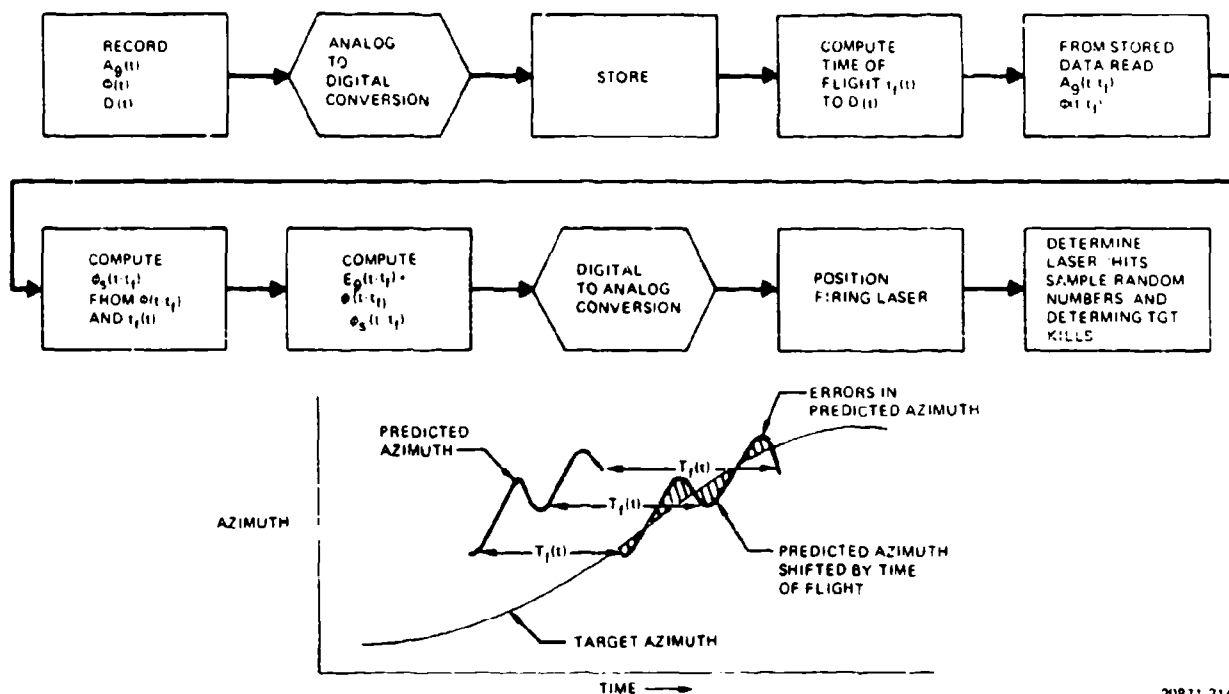

Figure 14-1. Data Flow in Synthetic Trajectory Computation

14-2

spond to the size of the ammunition dispersion pattern, a record can be relayed to the ground instrumentation of hits on the target versus time. It is possible to mount a number of sensors on the target, so that the weighting of hits according to target aspect and vulnerablity can be done in real time in the data processing. Similarly, one can use the recorded data to compute the probablity of target kills with bursts of various lengths, and have this data available in real time.

The advantage of this general approach over simply recording tracking error is that it includes all of the dynamic errors of the fire control process, including the effect of target maneuvers, solution errors, and the amplification of tracking noise.

If it is desired to simultaneously record tracking error for immediate, or post engagement correlation against prediction error, it would probably be necessary to add a second imaging device slaved to the tracking sensor, to record the target position relative to the axis of the tracker, i.e., the reticle, in the case of disturbed reticle sights. It is also conceivable that the tracking axis position could be injected to the same display as the prediction error display but this might be more complex than adding a tracking imaging sensor.

Computation of prediction error statistics can be done during or immediately subsequent to each pass for a summary printout before the next engagement is initiated. However, since errors are sensitive to the time varying engagement geometry and dynamics, whatever software is provided for this processing should be capable of being modified as experience is gained in the best way to subdivide the data. Since both the magnitude and spectral density of error will

be time varying as non-stationary processes, determination of the best way to develop summary descriptions requires careful preliminary analysis.

It is, of course, vital to record the target path data, as determined from the tracking data corrected for recorded tracking errors, or from a separate tracking unit of higher precision. This data also should be reduced and statistically analysed in real time for including in the engagement summary printout.

If the above objectives are realized, the Army will have not only an effective device for assessing the performance of predicted fire systems, but a means for systematically building a base of information which can be used to establish requirements for, and to design, improved predicted fire systems.

14.3 ANALYSIS OF COMBAT DATA

Quantitative analysis of the combat effectiveness of weapon systems is an art which almost vanishes in peace time, and is revived only after a conflict has been under way for many months. In any war in which air defense weapons are employed, however, early measurement of enemy attack tactics will allow a major improvement in defense weapon system doctrine and effectiveness.

It is suggested that all except the most primitive of air defense systems should incorporate, or have means for attaching, a recording device that will store the target paths of enemy aircraft as tracked by the defense system. With modern technology, such a device can be simple, small, and inexpensive. In World War II, only the British recorded target tracks but the great demand in the U.S. antiaircraft design community for tracings of the tracks recorded by the British indicated the recognition of the value of this vital data class in that era.

SECTION 15
RECOMMENDED PROGRAMS

15.1 GENERAL

The most important short term objective in short range air defense should be the construction of a prototype gun system costing less than $500,000 per fire unit, in a self-propelled version, with excellent fire control and growth capability. This statement is the opinion of the writer, based on the survey of air defense requirements under the present and related study effort.

It is believed by the writer that the demonstration of a reliable gun system effective to about 3000 meters will do more to strengthen the immediate program for the defense of the Field Army against air attack at acceptable cost, than any number of additional studies, simulations, or component experimentation. It is also believed that a gun system will be more cost-effective, all factors considered, than a missile system within this range band.

There is more than enough information available to the Army to write reasonable design specifications for such a system. The important considerations would appear to be

a. Design the fire unit so that night, all weather, or special purpose sensors can be added as the enemy threat changes.

b. Design the fire control system so that the prediction algorithms can be easily changed as threat tactics change.

The Army should avoid being locked into a relatively inflexible design concept such as Vulcan.

15.2 SUPPORTING EFFORT

Given that the above prototype effort is underway, continued development of advanced predicted fire technology should be continued at a sustained but moderate level. Some recommended areas for this supporting effort are described below. The effort has the objective of providing growth improvement of the basic system, of defining requirements for follow-on systems and of providing air defense capability for weapons having air defense as a secondary role.

15.3 SYSTEMS CONCEPT ANALYSIS

15.3.1 Projectile Tracking Systems

The availability of sensors capable of measuring the projectile miss distance relative to a target creates the potential of fire control algorithms using this capability to eliminate system bias and boresight errors, and substantially improve combat effectiveness. Since many possible implementations of the concept are possible, a comprehensive program of analysis and simulation

validation is recommended, including at least the following elements:

a. Determine the probable magnitudes, spectral characteristics and sources of errors affecting system performance.

b. Determine the preferred algorithms for system utilization of miss distance measurements, including data processing parameters. This effort should include as a minimum, consideration of the probably irregular sampling rate of miss distances, errors in the measurement process, the effect on the computation of round to round ammunition dispersion, the point of injection of the correction to the basic prediction algorithm, and the effects of pre and post data processing about the injection point. It seems probable that the preferred algorithms for processing the miss measurements on each path will be time-varying.

c. Evaluate the comparative effectiveness of a system utilizing projectile miss measurements against that of a conventional system including considerations of continuous versus burst fire, and target path irregularities, including deliberate target jinking and evasion.

15.3.2 Systems Using Predicted Fire, Beam Riding Projectiles

It may be possible to retain much of the cost advantage of conventional predicted fire systems, while securing a single shot kill probability at least equivalent to that of a guided missile by providing projectile in-flight control to follow a beam directed at the target predicted position. As the projectile nears the target, the prediction interval converges to zero. This system is somewhat similar to that used by Nike Ajax and Hercules, but the present possibility of using a laser beam for projectile direction suggests the possibility of achieving a compact, relatively low cost system with an extended range capability to match the release ranges of aircraft firing most stand-off weapons. The effort would include as a minimum

a. Systematically outline a set of concepts of alternate approaches for system configuration. This would include considerations of effective system rate of fire, the possibility of controlling multiple in-flight projectiles, and weather limitations.

b. Develop filtering and prediction algorithms, considering the interactions among stability (i.e., spectral content of aim deviation) of the directing beam, required missile response time, directing data sampling rate, and target maneuver.

c. Compare the expected effectiveness of a system using predicted fire, beam directed projectiles against that of a conventional concept, indicating system components for which possibly increased cost over that of a conventional system must be evaluated against the expected increased system effectiveness.

15.3.3 Systems Using Rockets and Rocket-Assisted Projectiles

The question of whether a predicted fire system should employ a high rate of fire gun, or a battery of rockets reoccurs so often that a rocket firing system should be included in any overall comparison of concept options. Also involved in this consideration is the option of using rocket-assisted gun-fired projectiles for extended range. A current development of considerable interest is the French Javelot system, which fires 40 mm unguided rockets. An operational mode has been suggested for selecting the rockets to be fired according to pre-set deviations from the mean aim axis of individual rockets.

It is suggested that a concept evaluation should include analysis of

a. The usefulness of the preselected deviation concept against maneuvering or jinking targets.

b. The utility of having an effectively infinite rate of fire, by firing rockets in salvo.

c. The greater variety of warhead concepts possible if large caliber rockets are used. For example, the warhead of each might break into a number of smaller missiles as it approaches the target, with each sub-missile having a high probability of target kill.

d. System effectiveness compared with a system otherwise similar, but employing one or more high performance guns.

15.3.4 Summary Concept Comparison

The above set of conceptual approaches should then be placed in proper perspective with respect to conventional systems on an overall effectiveness basis, in addition indicating possible sources of major cost differences, and components likely to require considerable developmental effort and/or incurring significant technical uncertainties.

15.4 EVALUATION OF DEFENSE AGAINST STAND-OFF WEAPONS

The reported operational effectiveness of air to surface munitions which home on laser designated targets, employ TV heads, or contrast imaging homing devices is so high that it seems likely that such weapons will be the most cost-effective mode of attack even against undefended targets. Their implications on the per-

formance requirements of air defense weapons therefore needs to be assessed in detail.

An analysis is therefore recommended to

a. Determine the probable delivery tactics of strike aircraft using 'smart' munitions, and the ability of the defense to counter the delivery aircraft and to engage and destroy the munition.

b. Determine appropriate prediction algorithms and requirements on sensor and weapon performance, for predicted fire defense.

A possible conclusion is that the presence of high level SAM defense will limit attacking aircraft to only those delivery modes which can be executed from very low level, terrain following paths. Hence the analysis should include these modes and constraints.

15.5 EFFECT OF ENEMY USE OF ELECTRONIC AND OPTICAL COUNTERMEASURES

An analysis should be performed of the effect of enemy countermeasures on predicted fire systems, as a function of the system configuration and the type of countermeasure.

Predicted fire, antiaircraft gun systems can be designed to have a good resistance to enemy countermeasures, if this is made a design objective. In particular, the provision of alternate tracking modes, (combinations of radar, laser, visual, etc.) is probably easier to implement than in the case of missile systems.

Although actual system design would require the use of highly classified EW information, it is believed that a useful conceptual analysis could be performed without the use of sensitive information. Emphasis would be on the determination of what options might be designed into the defense system on the assumption of an enemy capability to deny some or all of the sensor information.

One possible concept for investigation is sharing tracking data among fire units in a defense complex by means of a data-sharing communications link. With software in each mount to correct for parallax, all or any fire unit would be able to fire on data generated by any single fire unit. This would

a. Allow ranging by triangulation on an aircraft using an on-board, self screening jammer against radar.

b. Make it extremely difficult for an attacker to employ electro-optical countermeasures against visual, TV or IR tracking since he would have to continuously point his countermeasures beams simultaneously, accurately and continuously at all fire unit trackers as he made his pass.

The resistance of the 'round robin' data link to jamming would need to be investigated. However,

unlike high altitude missile defense fire units, the fire units of a gun defense would normally be placed sufficiently close together, so that a back-up wire link could be quickly installed once communication link jamming was experienced.

15.6 DATA ACQUISITION AND ANALYSIS

In conjunction with Army personnel, acquisition and preliminary analysis of real target path data should be initiated. The object of this effort is to eliminate as far as possible, the subjective judgements now necessary in generating hypothetical paths for simulation runs, and to provide a better basis for all analytical work on air defense systems.

Details of what might be done in an effort of this type were developed in Section 13.1.

15.7 SIMULATION CHECK-OUT PACKAGE AND ADDITIONAL SIMULATION RUNS

The Litton simulation now has a comprehensive and flexible capability for the evaluation of predicted fire systems concepts. However to fully exploit this capability a check-out package is essential to minimize programming errors, and increase the confidence associated with results. In addition, some module modifications would allow the simulation to support the other recommended analyses. These are listed below

a. *Program Check-out and Validation Package.* It is essential that a check-out package of programs be provided for the simulation to eliminate possible existing minor programming errors and minimize the introduction of errors in new programming or operational runs.

b. *Module Development for Prediction Algorithms Based on Observation of Projectile Miss Distance.* The interest in this type of prediction algorithm makes it important to validate the dynamics of various possible solutions by simulation.

c. *Time-varying Recursive Smoothing Algorithms.* It seems clear from all results this far obtained that weapon effectiveness cannot be fully exploited unless 'smoothing time' is made an increasing function of range. A simulation module with this capability would allow the expected advantages to be demonstrated and assessed.

d. *Modification to Accept Actual Target Path Records.* The best way to use real target path data may be by separately processing it, before introducing it to the simulation. The best means of utilization should be determined, and simulation input modification performed, if necessary.

15.8 RECOMMENDATIONS FOR EXPLORATORY DEVELOPMENT

The following component development is recommended to support the general predicted fire effort.

No amount of analysis is as convincing as an operating prototype, even in brassboard form. It is suggested that two components of predicted fire control systems are of sufficiently general application to justify construction of brassboard demonstration models. These are:

a. Synthetic trajectory computational module.

b. General purpose regenerative tracking module.

These modules are discussed in the following paragraphs.

15.8.1 Synthetic Trajectory Module

The concept of the 'synthetic trajectory' has been discussed in detail in Sections 6.2 and 14.2. It is suggested that a brassboard model using an available minicomputer might be constructed and demonstrated by fitting it to a Vulcan or Duster fire unit. In the case of Vulcan, the synthetic spot could be introduced to the tracker's optics and used to give him an indication of how much to 'track off' to correct for imperfections of the lead computation. At the expense of some added complexity, an error measurement might be generated (by comparing the synthetic trajectory lead with that generated by the sight and the correction might be applied automatically by optical deflection of the sight line.

There are two possibly useful results of this installation, (1) since errors measured with respect to the synthetic trajectory are somewhat similar to those obtained by projectile tracking, the brassboard would allow some experimentation with correction algorithms prior to the availability of projectile tracking sensors, with which the synthetic trajectory module would ultimately be combined, and (2) it is a means for field observation of Vulcan system errors, with a potential for their reduction even with the present fire control.

Mounted on Duster, with a laser range finder, the module would allow course, speed, and angle of dive settings on the sight to be corrected after one time of flight. Since the mechanical course and speed sight on Duster is relatively inexpensive, but accurate with the correct inputs, the combination might represent an effective, low cost solution to fire control for light antiaircraft automatic weapons. Note that the system does not have the characteristics of a disturbed reticle sight, and the adjustment of the input parameters can be made at a rate that will not throw the tracker off target.

15.8.2 General Purpose Regenerative Tracking Module

The purpose of this module is to provide a device which can be attached to Vulcan, Duster, or any other available antiaircraft tracking mount to provide a regenerative feedback to the human operator's control. In a complete fire control system, such a module would

be an integral part of the design, however, its early availability for demonstration and experimentation would provide additional validation of the concept which was first demonstrated on Army systems by the Vigilante prototypes.

15.9 FIRE CONTROL FOR SUPPORTING WEAPONS

Experience in Southeast Asia has demonstrated the effectiveness of a doctrine in which all weapons fire at attacking aircraft. The Field Army has a number of automatic weapons which can be fired against aircraft, although this is not their primary role. An example is Bushmaster.

It is possible that the advantages of a simple fire control system which would allow fire on the move capability for MICV-70 and the ARSV against ground targets and for self-defense against aircraft and helicopters might be sufficient to justify such a development if the cost can be kept within bounds. Considering that the VRFWS-S weapon for these vehicles (20-30 mm) may have a unit cost of $7000 to $15,000, provision of an effective fire control system capable of engaging both ground and air threats to the vehicle would seem to be prudent.

An adequate solution might be simply tracer fire, but analysis could determine whether a substantial advantage could be secured with a simple computer and laser range finder. It is believed that a satisfactory solution might be achieved without recourse to power drive and/or a disturbed reticle sight.

APPENDIX A
AIRCRAFT AND HELICOPTER LOSSES TO GROUND FIRE IN VIETNAM

This Appendix summarizes aircraft and helicopter losses to ground fire in Vietnam through 1971, based on unclassified sources only. The purpose is to support the contention that the predicted fire antiaircraft defenses continue to be effective against modern aircraft.

Most of the cumulative loss data are from newspaper reports. References containing more than simple totals are referenced. All sources have been logged in working papers.

A-1

SUMMARY

Figure A-1 shows the cumulative losses of both fixed wing and helicopter aircraft to all causes, and to enemy action, versus time. Figure A-2 shows a similar chart for helicopter losses alone. Figure A-3 shows a similar chart for fixed wing aircraft losses, with an additional plot of aircraft lost over North Vietnam.

Almost all of the helicopter losses occurred in South Vietnam, and almost all of the fixed wing losses to enemy action occurred over North Vietnam.

Figure A-4 shows the build up of the North Vietnamese air defense system, except for Migs, which never totalled more than about 75 aircraft in this period. Almost all U.S. losses to enemy action have been to ground fire, with a total of 50 aircraft lost to Migs, through 1971.

The SAMS were relatively ineffective in shooting down U.S. aircraft directly in this period (by the end of 1966 of about 450 aircraft lost over North Vietnam, 30 had been lost to SAMS, 10 to MIGs and the rest to

20971-315
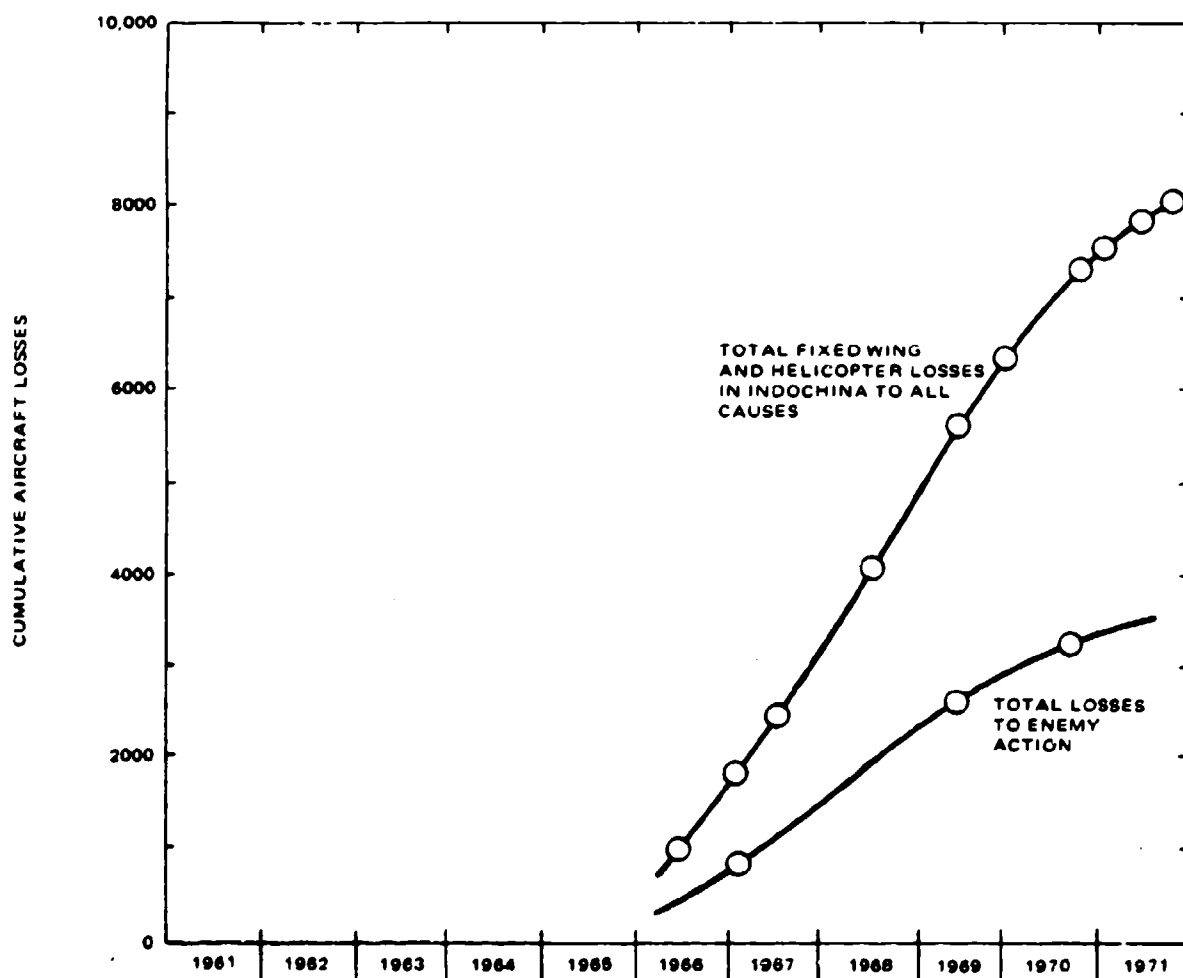
Figure A-1. Cumulative Air Losses in Vietnam

A-2
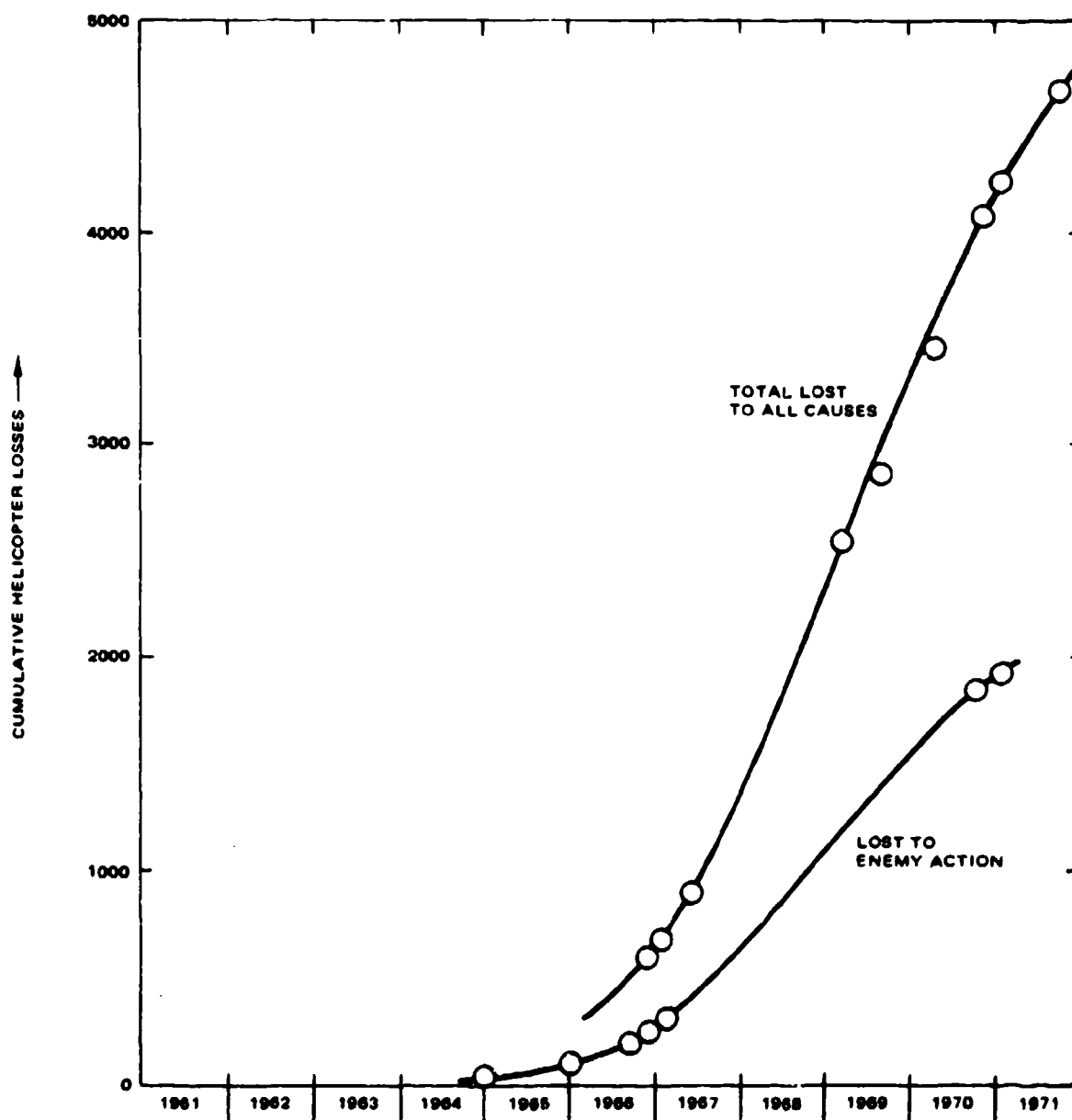
Figure A-2. Cumulative Helicopter Losses in Vietnam

20971-316
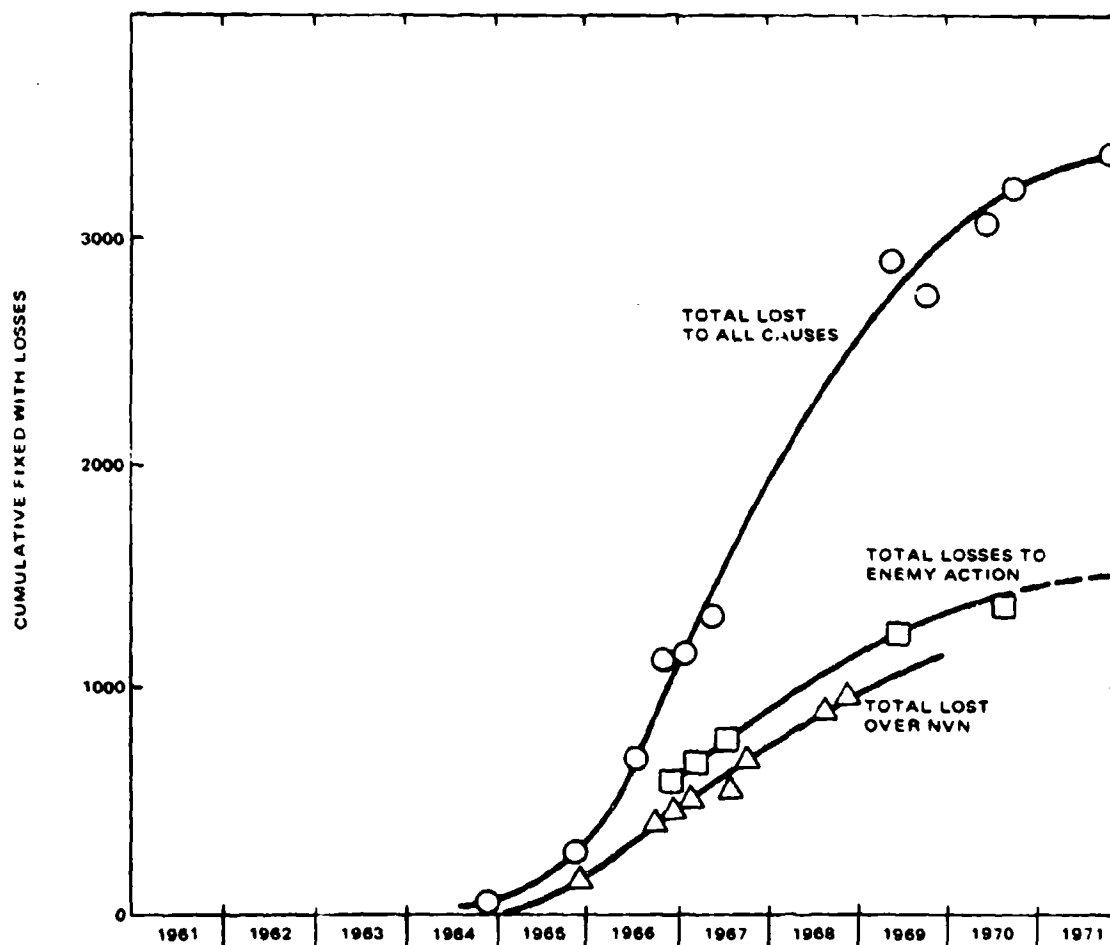
20871-317

Figure A-3. Cumulative Fixed Wing Losses in Vietnam

guns and automatic weapons), but they probably con-tributed to gun effectiveness by causing aircraft to fly paths more accessible to guns.

Tables A-1 and A-2 are given for exchange ratios of SAM missiles per aircraft destroyed, and the MIG/ U.S. exchange ratio. The fighter exchange ratio is not as favorable to the U.S. as in the Korean war.

The principal conclusion is that predicted fire anti-aircraft guns continue to be effective against the most modern aircraft, as they were in Korea, in WW II and when the first Gothas appeared over London in WW I.

A-4
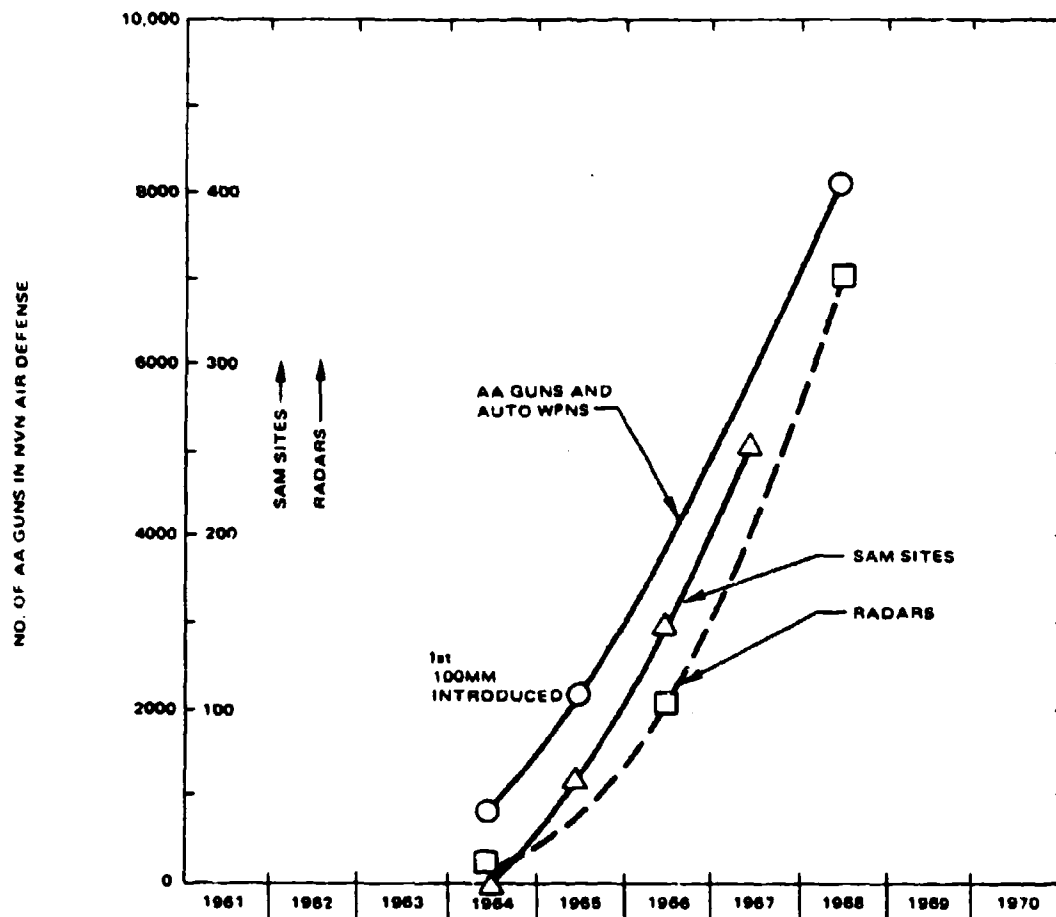
Figure A-4. North Vietnamese Air Defenses

20871-318

Table A-1. Exchange Ratios (Reference A.1)

SAMS vs. U. S. Aircraft			
Year	SAM missiles sighted	Missiles/aircraft lost	A/C lost
1965	110	13	8
1966	990	33	30
1967	3500	55	64
mid 1968		67	102

MIGs vs. U. S. Aircraft				
Year	U. S. aircraft lost	Migs lost	Migs/U. S. loss	NVN Mig strength
1965	2	6	3.0	75
1966	11	29	2.6	70
1967	25	75	3.0	20 in NVN
mid 1968	9	8	1.1	20 - 25
Cum to 1972 (Jan)	50	50		40 in Jan 72

20871-635

Table A-2. Cumulative U.S. Aircraft Losses in Vietnam since Jan. 1960 as of 5/23/67 (Reference A.2)

	Fixed Wing	Helicopters all types	Total
Lost to hostile action over NVN including Laotian border	565	6	571
Lost to hostile action over SVN	182	331	513
Total Loss to hostile action	747	337	1084
Non-hostile open losses and to enemy ground attacks, mortars, etc.	646	544	1190
Total losses, all causes	1393	881	2274

Notes:

"Current" aircraft loss rate estimated at 500/year, (1967) 115 Migs, and large numbers of mobile 85, 57, 37 mm guns, constitute defenses. Through May 23 the Mig ratio was 71/20 in favor of the U. S.
46 aircraft were lost to SAMS with about 2450 missiles fired.

11% of losses over NVN were caused by missiles and Migs.
All losses in SVN were caused by small arms and flak.

20871-636

A-7/A-8

APPENDIX B
TABLE OF DEFINITE INTEGRALS

The following definite integrals have been used so often in the analysis that they are collected here for convenience.

$$\frac{2}{\pi} \int_0^\infty \frac{dw}{1 + w^2 T^2} = \frac{1}{T} \tag{B.1}$$

$$\frac{2}{\pi} \int_0^\infty \frac{dw}{(1 + w^2 T_1^2)(1 + w^2 T_2^2)} = \frac{1}{T_1 + T_2} \tag{B.2}$$

$$\frac{2}{\pi} \int_0^\infty \frac{dw}{(1 + w^2 T_1^2)(1 + w^2 T_2^2)(1 + w^2 T_3^2)}$$
$$= \frac{T_1 T_2 + T_1 T_3 + T_2 T_3}{(T_1 + T_2)(T_1 + T_3)(T_2 + T_3)} \tag{B.3}$$

$$\frac{2}{\pi} \int_0^\infty \frac{w^2 dw}{(1 + w^2 T_1^2)(1 + w^2 T_2^2)(1 + w^2 T_3^2)}$$
$$= \frac{1}{(T_1 + T_2)(T_1 + T_3)(T_2 + T_3)} \tag{B.4}$$

$$\frac{2}{\pi} \int_0^\infty \frac{w^4 dw}{(1 + w^2 T_1^2)(1 + w^2 T_2^2)(1 + w^2 T_3^2)}$$
$$= \frac{T_1 + T_2 + T_3}{(T_1 T_2 T_3)(T_1 + T_2)(T_1 + T_3)(T_2 + T_3)} \tag{B.5}$$

$$\frac{2}{\pi} \int_0^\infty \frac{dw}{(1 + w^2 T^2)^n} = \left(\frac{1}{T}\right)\frac{(2n \cdot 3)!!}{(2n \cdot 2)!!} \tag{B.6}$$

$$\frac{2}{\pi} \int_0^\infty \frac{w^{2m} dw}{(1 + w^2 T^2)^n} = \frac{(2m \cdot 1)!!(2n \cdot 2m \cdot 3)!!}{T^{2m + 1}(2n \cdot 2)!!} \tag{B.7}$$

where

$$(2n + 1)!! = (1)(3) \ldots (2n + 1)$$
$$(2n)!! = (2)(4) \ldots (2n) \tag{B.8}$$

$$\frac{2}{\pi} \int_0^\infty \frac{\cos(aw)\, dw}{1 + w^2 T^2} = \frac{1}{T} e^{-a/T} \tag{B.9}$$

$$\frac{2}{\pi} \int_0^\infty \frac{\cos(aw)\, dw}{(1 + w^2 T_1^2)(1 + w^2 T_2^2)} = \frac{T_1 e^{-a/T_1} \cdot T_2 e^{-a/T_2}}{T_1^2 \cdot T_2^2} \tag{B.10}$$

$$\frac{2}{\pi} \int_0^\infty \frac{w^2 \cos(aw)\, dw}{(1 + w^2 T_1^2)(1 + w^2 T_2^2)} = \frac{T_1 e^{-a/T_2} \cdot T_2 e^{-a/T_1}}{T_1 T_2 (T_1^2 \cdot T_2^2)} \tag{B.11}$$

$$\frac{2}{\pi} \int_0^\infty \frac{\cos(aw)\,dw}{(1 + w^2 T^2)^2} = \frac{1}{2T}\left[1 + (a/T)\right] e^{-a/T}$$

(B.12)

$$\frac{2}{\pi} \int_0^\infty \frac{w^2 \cos(aw)\,dw}{(1 + w^2 T^2)^2} = \frac{1}{2T^3}\left[1 - (a/T)\right] e^{-a/T}$$

(B.13)

$$\frac{2}{\pi} \int_0^\infty \frac{w^{2m} \cos(aw)\,dw}{(z + w^2)^{n+1}}$$

$$= \frac{(-1)^{m+1}}{n!} \frac{d^n}{dz^n}\left[z^{m-(1/2)} e^{-az^{1/2}}\right]$$

(B.14)

BIBLIOGRAPHY/REFERENCE LIST

Section 3

1. Peat, Marwick, Caywood, Schiller & Co., *A Study of the Accuracy of Mask Angle and Visibility Angle in Representing Terrain Effects in Analytical Effectiveness Models*, October 1965, AD 815, 469.

2. Stein, A., *Terrain Mask Angles*, Cornell Aeronautical Laboratory, Inc., a paper presented at the Joint Session of AAAS Section E and the Geological Society of America, Symposium on Quantitative Terrain Studies, Chicago, Illinois, 28 December 1959.

3. Peterson, R.H. and Taylor, W.C., *Toward a Stochastic Model of Terrain*, Proceedings of the Fifteenth Conference on the Design of Experiments in Army Development and Testing, ARO Report No. 70-2 22-24 October 1969, AD 875 609.

4. Bharucha-Reid, A.T., *Elements of the Theory of Markov Processes and Their Applications*, McGraw-Hill, 1960.

5. Pervozvanskii, A.A., *Random Processes in Nonlinear Control Systems*, Academic Press, 1965.

6. Whittle, P., *On Stationary Processes in the Plane*, Biometrika, 41, 1954, pp 434-49.

7. Heine, V., *Models for Two-Dimensional Stationary Stochastic Processes*, Biometrika, 42, 1955, pp 170-78.

8. Uhlenbeck, G.E., and Ornstein, L.S., *On the Theory of the Brownian Motion*, Physical Review, Vol. 36, 1 September 1930.

9. Wang, M.C., and Uhlenbeck, G.E., *On the Theory of the Brownian Motion II*, Review of Modern Physics, 17, 2 and 3, April-July 1945, reprinted with Reference 1 in *Selected Papers on Noise and Stochastic Processes*, Dover, 1954.

10. Stratonovich, R.L., *Topics in the Theory of Random Noise*, Vol. II, Gordon and Breach, 1967.

11. Weiss, H.K., *Derivatives of the Parabolic Cylinder Function with Respect to the Index*, Paper presented at the SIAM 1969 National Meeting, Washington, 10, 11, 12 June 1969.

12. Leadbetter, M.R., *On Crossing of Arbitrary Curves by Certain Gaussian Processes*, American Math. Soc. Proc., Vol. 16, 1965, pp 60-68.

13. Leadbetter, M.R., and Cryer, J.D., *Curve Crossing by Normal Processes and Reliability Indicators*, SIAM Review, Vol. 7, No. 2, April 1965, pp 241-250.

14. Cramer, H., and Leadbetter, M.R., *Stationary and Related Stochastic Processes*, Wiley, 1967.

15. Chover, J., *Nonabsorption Probability for a Gaussian Process in the Karhunen Representation*, Duke Math. Journal, Vol. 31, 3 September 1964, pp 427-443.

16. Siegert, A.J.F., *On the First Pcge Time Problem*, Physical Review, Vol. ., 15 February 1951, pp 617-623.

17. Hayre, H.S., and Moore, R.K *Theoretical Scattering for Near Vertical Incidence from Contour Maps*, Journal of Research of the National Bureau of Standards, -D. Radio Propagation, Vol. 65D, No. 5, September-October 1961, pp 427-432.

18. Jamieson, J.A., *Inference of Two-dimensional Wiener Spectra from One-dimensional Measurements*, Infrared Physics, Vol. 1 (2) 133, July 1961.

19. Clay, C.E., et al, *Continued Study of Random Altitude Deviations of General Aviation Aircraft During Cruise*, Technology, Inc., Dayton, Ohio, Final Report for FAA, January 1967, AD 652 615.

20. *Low Altitude Penetration Parameters Study*, LTV-Vought Aeronautics Division, Part I, April 1965, Part II, 8 March 1965, AD 476 703, AD 476 704.

21. Rose, R., et al, *A Study of the Effects of Terrain on the Detection of Low Flying Aircraft*, Peat, Marwick, Caywood, Schiller & Co., Report on Contract DA-11-022-ORD-4262, 1 May 1964.

22. Martin, J.J., *Radar Masking by the Earth's Terrain*, Institute for Defense Analysis, Washington, March 1966, AD 633 540.

23. Newsweek, 17 April 1972, p.17.

24. Time, 17 April 1972, p.39.

25. Newsweek, 24 April 1972, p.32.

26. Time, 24 April 1972.

27. Los Angeles Herald Examiner, 28 April 1972.

28. Levine, J.R., *Reduced Ceilings and Visibilities in Korea and Southeast Asia*, U.S. Army Elec-

tronics Command, R&D Technical Report ECOM-3403, March 1971, AD 722 735.

29. USAF Terminal Forecast Reference File Reports, of which the following are typical:

    Offutt AFB, September 1971, AD 729 215
    Norton AFB, August 1971, AD 729 212

30. *Estimating Mean Cloud and Climatological Probability of Cloud-Free Line-of-Sight,* USAF Air Weather Service (MATS) November 1965 AD 630 289.

31. Bertoni, E.A., *Clear Lines of Sight from Aircraft,* AF Comabridge Research Laboratories, AFCRL-67-0435, August 1967, AD 657 801.

32. Soini, I., *Aeronautical Climatological Conditions at Kruunukyla Aerodrome,* Finnish Meteorological Institute, Report No. 23, Helsinki, 1970, N71-20568.

33. Huschke, R.E., *Use of Weather-Information in Determining Cost/Performance and Force-Mix Tradeoffs: Weather and Warplanes I,* RAND R-740-PR, June 1971, AD 731 749.

34. Huschke, R.E., et al. *Weather-Service Contribution to Stricom Operations,* RAND R-542-PR, September 1970.

35. Greenfield, S.M., et al. *Weather Factors in Air-to-Surface Missile Operations,* RAND RM-4480-PR, March 1965.

36. Rapp, R.R., et al. *Weather Information: Its Uses, Actual and Potential,* RAND RM-4083-USWB, May 1964.

37. Rapp, R.R., *U.S. Flying Weather,* RAND RM-885, 1 July 1952.

38. Sartor, J., *Meteorological Aspects of Infrared Operations,* RAND P-1299, 5 March 1958.

39. Bailey, H.H., et al. *The Effects of Atmospheric Scattering and Absorption on the Performance of Optical Sensors,* RAND RM-5938-PR, March 1969.

40. Hawkins, J.E., et al. *Introduction to Multisensor Reconnaissance,* Air Force Avionics Laboratory, AFAL-TR-71-43, June 1971.

41. Lund, I.A., *Methods for Estimating the Probability of Clear Lines of Sight, or Sunshine, through the Atmosphere,* Journal of Applied Meteorology, Vol. 5, No. 5, October 1966, pp 625-630.

42. Lund, I.A., *Estimating the Probability of Clear Lines of Sight from Sunshine and Cloud Cover Observations,* Journal of Applied Meteorology, Vol. 4, No. 6, December 1965, pp 714-722.

43. Aviation Studies (International) Ltd. Cost Data Sheets, London.

44. Aviation Week, 17 April 1972, pp 49-51.

45. Middleton, W.E.K., *Vision Through the Atmosphere,* University of Toronto Press, 1968.

46. Koopman, B.O., *Search and Screening,* OEG Report No. 56, Washington, D.C., 1946.

47. University of Michigan, *Parametric Design/Cost Effectiveness Study on Advanced Forward Area Air Defense Systems (AFAADS) Gun Systems,* Vol. II, August 1969, AD 863 748.

48. Duntley, S.Q., et al, *Visibility,* Applied Optics, Vol. 3, 1964, p. 549.

49. Glanzmann, W., *Die Entdeckungswahrscheinlichkeit von Flugzeugen unter Visueller Beobachtung,* Diss, Nr. 4273, University of Zurich, 1969, N70-24303.

50. Wokoun, W., *Detection of Random Low-Altitude Jet Aircraft by Ground Observers,* U.S. Army Ordnance Human Engineering Laboratories Tech Memo 7-60, June 1960, AD 238 341.

51. Kurke, M.I., et al, *Low Power Optical Systems and Aerial Target Detection,* U.S. Army Ordnance Human Engineering Laboratories Tech Memo 5-57, June 1957, AD.

52. *Human Factors Research and Aircraft Armament,* Human Engineering Laboratories, Tech Note 9-63, November 1963, AD 629 452.

53. Wright, A.D., *Factors Influencing the Visual Detection and Recognition of Low-Altitude Aircraft,* Prof Paper 20-67, May 1967, HumRRO, G. Washington University, AD 654 125.

54. Wright, A.D., *The Performance of Ground Observers in Detecting, Recognizing, and Estimating Range to Low-Altitude Aircraft,* HumRRO, Tech Rept 66-19, December 1966, AD 645 537.

55. Frederickson, E.W., et al, *Aircraft Detection, Range Estimation, and Auditory Tracking Tests in a Desert Environment,* HumRRO Tech Rept 67-3, March 1967, AD 650 403.

56. Bailey, H.H., *Target Detection Through Visual Recognition: A Quantitative Model,* RAND RM-6158/1-PR, February 1970, AD 721 446.

57. Loewy, R.G., *Helicopter Aural Detection in Tactical Situations,* Institute for Defense Analysis, Research Paper p. 25, May 1963, AD 409 535.

58. Franklin, S.B., et al, *Theoretical Consideration in Acoustic/Seismic Detection of Low-Flying Aircraft in Thailand*, Stanford Research Institute, RSSC-RM 4923-31, May 1969, AD 860 632.

59. Dobbins, D.A., et al, *Jungle Acoustics 1: Transmission and Audibility of Sounds in the Jungle*, U.S. Army Tropic Test Center, Research Report No. 7, October 1966, AD 647 804.

60. Hammond, P.M., et al, *Aircraft Seismic/Acoustic Surveillance*, Stanford Research Institute, RSSC-RM 4923-29, December 1968, AD 858 139.

61. Atlantic Research Corp., *Acoustic and Seismic Research*, Final Report, January 1967, AD 805 766.

62. *CH-47 Helicopter Man-Machine-Environment Compatability Experiment*, U.S. Army Combat Developments Command Experimentation Command Fort Ord, California, 27 September 1968.

Section 4

1. Mensa, D.L., *Scintillation Characteristics of Aircraft Targets*, Naval Missile Center, Point Mugu, California, 26 March 1971, TP-71-13.

2. *Control-Display Pilot Factors Program*, National Supersonic Transport Program, USAF Instrument Pilot Instructor School, Randolph AFB, Texas, December 1963.

3. Phillips, W.H. and Eggleston, J.M., *The Lateral Response of Airplanes to Random Atmospheric Turbulence*, NASA TR R-74, 1960, NACA TN 3954.

4. Skolnik, Merrill (editor), *Radar Handbook*, Chapter 28, *Target Noise* by John H. Dunn and Dean D. Howard, McGraw-Hill, 1970.

5. Frost, G.G., *A Comparison between Tracking with 'Optimum' Dynamics and Tracking with a Simple Velocity Control*, AMRL-TDR-62-150, Behavioral Sciences Laboratory, Air Force Systems Command, WP Air Force Base, December 1962.

6. Chernokoff, R., Bowen, J.H., Birmingham, H.P., *A Comparison of Zero-Order and Fourth-Order Aided Compensatory Systems as a Function of Course Frequency*, NRL Report 5262, Naval Research Laboratory, Washington, D.C., 26 January 1959.

7. Blackman, R.B., *Data Smoothing and Prediction* Addison-Wesley, 1965.

8. Kuo, F.F., and Kaiser, J.F. (editor), *System Analysis by Digital Computer*, Wiley, 1966.

9. Gold, B., and Rader, C.M., *Digital Processing of Signals*, McGraw-Hill, 1969.

10. Paskin, H.M., *A Discrete, Stochastic, Optimal Model of the Human Operator in a Closed-Loop Tracking Task*, Air Force Flight Dynamics Laboratory, AFFDL-TR-70-129, AD 719 755, November 1970.

Section 5

1. Benedict, T.R., and Bordner, G.W., *Synthesis of an Optimal Set of Radar Track-While-Scan Smoothing Equations*, IRE Transactions on Automatic Control, Vol. AC-7, No. 4, July 1962.

2. Simpson, H.R., *Performance Measures and Optimization Condition for a Third Order Sampled Data Tracker*, IEEE Trans on Auto Control Vol. AC-8, No. 2, April 1963.

3. Change, *Synthesis of Optimum Control Systems*, McGraw-Hill.

4. James, Nichols, Phillips, *Theory of Servomechanisms*, McGraw-Hill.

5. Ragazzini and Franklin, *Sampled Data Control Systems*, McGraw-Hill.

6. Jury, E.L., *Theory and Application of the Z-Transform Method*, Wiley.

7. Yovitz, M.C., et al, *Linear Filter Optimization with Game Theory Considerations*, Institute of Radio Engineers, Parts 1-5, 1955, pp 193-199.

8. Neal, S.R., et al, *Discussion on 'Parametric Relations for the α-β-ν Predictor IEEE Transactions on Automatic Control,'* June 1967, Vol. AC-12, No. 3, pp 315-317.

9. Gupta, S.C., *Transform and State Variable Methods in Linear Systems*, Wiley, 1966.

Section 6

1. Foskett, R.J., et al, *A Review of the Literature on Use of Tracer Observation as an Antiaircraft Firing Technique*, Technical Report 68-11, HumRRO Division No. 5 (Air Defense), Fort Bliss, September 1968, AD 675 581.

2. Gilbert, S.W., et al, *Snap-Shoot Gunsight for Fixed-Gun Aircraft*, Technical Report 69-3, U.S. Air Force Academy, Colorado, December 1969, AD 711 391.

3. Justin, J.E., et al, *Simulation of the Snap-Shoot Gunsight*, SRL-TR-69-0008, Frank J. Seiler Research Laboratory, USAF Systems Command, April 1972, AD 723 649.

4. Jury, E.L., *Theory and Application of the z-Transform Method*, Wiley, 1964.

5. Kleinman, D.L., *Optimal Control of Linear Systems with Time-Delay and Observation Noise*, IEEE Trans. on Automatic Control, Vol. AC-14, No. 5, October 1969, pp 524-527.

6. Pindyck, R.S., *The Discrete-Time Tracking Problem with a Time Delay in the Control*, IEEE Trans. on Automatic Control, Vol. AC-17, No. 3. June 1972, pp 397-398.

7. Kurzweil, F., Jr., *The Control of Multivariable Processes in the Presence of Pure Transport Delay*, IEEE Trans. on Automatic Control, Vol. AC-8, No. 1, January 1963, pp 27-34.

8. *Air Defense, an Historical Analysis*, U.S. Army Air Defense School, Fort Bliss, June 1965. Vol. II. AD 476 445.

Section 7

1. *The Military Balance 1971-1972*, The International Institute for Strategic Studies, 18 Adam Street, London, WC2N 6 AL.

2. *Strategic Survey 1971*, Ibid.

3. *Jane's Weapon Systems 1971-1972*, McGraw-Hill, 1971.

4. Marriot, John, *Tactical Air to Surface Weapons*, International Defense Review, Vol. 3, No. 2, June 1970, pp 162-166.

5. Miller, Barry, *Lasers Aid Delivery of Weapons*, Aviation Week and Space Technology, 3 May 1971.

6. Ropelewski, Robert R., *A-7E Bombing Accuracy Displayed*, AW & Space Tech., 10 May 1971.

7. *The Republic F-105D Weapons System*, Interavia, Vol. XV, No. 3, 1960, pp 311-317.

8. Silber, J., *A Report on Fighter-Bombers as Night Intruders*, OAO Memo No. 66, HQ Fifth Air Force, 28 July 1953, AD 484 026.

9. Quinlan, W.T., *B-26 Night Intruder Rail Cutting Program*, OAO Memo HQ Fifth Air Force, 27 May 1952, AD 484 025.

10. *Tactical Air Action Blunts Armored Drive*, Aviation Week and Space Technology, 15 May 1972, pp 17-18.

11. *U.S. Guided Bombs Alter Viet Air War*, Aviation Week and Space Technology, 22 May 1972, pp 16-17.

12. De Biasi, Victor, *Toss Bomb Computer Guides A-Bomb Attack*, Aviation Age, August 1957, pp 56-61.

13. *Air Support*, U.S. Marine Corps, FMFM 7-3, 1969, Supt. of Documents, Washington, D.C.

14. Interavia August 1961, p. 1068.

15. Interavia October 1967, p. 1573.

16. Interavia December 1962, p. 1531.

17. Futrell, R.F., *The U.S. Air Force in Korea, 1950-1953*, Duell, Sloane and Pierces, New York, 1961.

18. *Damage Suffered by U.S.N. and U.S.M.C Ground Attack Aircraft in Korea*, OEG Study 467, 7 December 1951, AD 841, 042.

19. Peterson, A.H., et al, *Aircraft Vulnerability in WW II*, RAND, RM-402, 12 July 1950.

20. Forman, R.G., et al, *Vulnerability of Aircraft Structures Exposed to Small Arms Fire Projectile Impact Damage*, AFFDL-TR-67-157, February 1968, AD 829 829.

21. Weiss, H.K., *Choice of Guns Firing HE Ammunition...*, BRL Memo Report No. 480, 9 August 1948, AD 802 129.

22. Timenes, N., Jr., *Defense Against Kamikaze Attacks in World War II and its Relevance to Anti-Ship Missile Defense*, Vol. I, Center for Naval Analysis, 22 March 1971, AD 725 163.

23. *Report of Operations of the 1st U.S. Army, 1 August 1944, 22 February 1945*, Annex 6.

24. *Weapons of WW II*, (Book).

25. *Air Defense, an Historical Analysis*, U.S. Army Air Defense School, Fort Bliss, Texas, June 1965, AD 476, 445.

26. Weyl, A.R., *Fighter Armament*, Flight Magazine

Part I 7 December 1950

Part II 21 September 1950.

Part III 5 October 1950.

Part IV 23 November 1950.

Part V 7 December 1950.

Part VI 4 January 1951.

27. *The Origins and Development of Operational Research in the Royal Air Force*, Air Ministry, Air Publication 3368, Her Majesty's Stationery Office, London, 1963.

28. Benecke, T., *Methods of Air Defense Over Germany in World War II in Operational Research in Practice*, Davies, Verhulst editors, Pergamon Press, 1958, pp 72-85.

29. Chuyev, Yu. V., et al, *Fundamentals of Operations Research in Combat Materiel and Weaponry*, Vols. I and II, translation, Foreign Technology Division, Wright Patterson Air Force Base, 1968.

Original text published in Moscow, 1965, AD 683 365, AD 683 146.

The following references are cited in the text:

30. Idatt, M.P., *Effectiveness of Antiaircraft Fire*, 1959.

31. Merrill, Greyson (editor), *Operations Research*, etc., U.S., 1959.

One of the U.S. missile technology series of texts.

32. Blinov, G.I., *Theory of Firing for Ground Artillery*, Voyenizdat, 1948.

33. Venttsel, Ye S, *Introduction to Operations Research*, 1964.

34. Lestel, J.H., *Applications of OR to the Determination of Missile (Rocket) Range for Antiaircraft Defense*. Publication No. 17 of the French Center for Operations Research.

35. Frazer, R.A., Duncan, W.J., Collar, A.R., *Elementary Matrices*, MacMillan, New York 1946.

36. Rosenbrock, H.H., *State-Space and Multivariable Theory*, Wiley New York, 1970.

37. Armitage, J.V., *AAA Engagement Model*, AFGOA Technical Note 68-3, Headquarters, USAF, December 1968, AD 708 507.

38. Sage, A.P., *Optimum Systems Control*, Prentice Hall New Jersey, 1968.

39. Sage, A.P., and Melsa, J.L., *Estimation Theory, with Applications to Communications and Control*, McGraw-Hill, New York, 1971.

40. Weiss, H.K., *Systems Analysis Problems of Limited War*, Annals of Reliability and Maintainability, Vol. 5, AIAA, New York, 18 July 1966.

Section 8

1. *The Modern Battle Tank: 1-Current Types and Their Characteristics, 2-Firepower*, International Defense Review, Vol. 4, No. 6, December 1971, Vol. 5, No. 1, February 1972.

2. Dardick, D., et al, *Gun/Projectile Systems*, Space/aeronautics, March 1967, pp 92-99.

3. Weiss, H.K., *Choice of Guns Firing HE...*, BRLMR-480, 9 August 1948.

4. *Interior Ballistics of Guns*, AMCP 706-150,

HQ U.S. Army Materiel Command, February 1965.

5. Schwarz, E., *Vorschlage zur Ermittlung der optimal Daten von Flugzeug Bordwaffen gegebener Wirkung im Ziel*, Bericht 150 der Lilienthal Gesellshaft, 25-26 March 1942.

6. *Trajectories, Differential Effects, and Data for Projectiles*, AMCP 706-140, HQ U.S. Army Materiel Command, August 1963.

7. Williams, Joseph, *Trends and Development in Foreign Vehicles*, a paper presented at the Man-Mobility-Survivability Forum, Indianapolis, 11-12 April 1967.

8. Ford, B., *German Secret Weapons, Blueprint for Mars*, Ballentine Books, Inc., New York, 1969.

Section 9

1. Weiss, H.K., *Solutions of the Fighter-Bomber Duel by the Theory of Games*, BRL Technical Note 23, June 1949.

2. Karlin, Samuel, *Mathematical Methods and Theory in Games, Programming and Economics*, Vols. I and II, Addison-Wesley, 1959, in particular, Vol. II, Chapter 8.

3. Gillman, L., *Operations analysis and the theory of games: an advertising example*, Journal of the American Statistical Association, 45 (1950) 541-46.

4. Gubler, I.A., *Solution of the Problem of Firing with Artificial Dispersion for Various Cases*, in Collection of Articles on the Theory of Firing. I, A N Kolmogorov (editor), E. Hewitt Translator, RAND Report T-14, 13 October 1948.

5. Baxter, J.P., III, *Scientists Against Time*, MIT Press, 1968.

Section 11

1. Bartlett, M.S., *On the Theoretical Specification and Sampling Properties of Autocorrelated Time-Series*, Journal of the Royal Statistical Society, B8, (1946) pp 27-41.

2. Jenkins, G.M., and Watts, D.G., *Spectral Analysis and its Applications*, Holden Day, San Francisco, 1968, p. 169.

3. Mehra, R.K., *Digital Simulation of Multi-Dimensional Gauss-Markov Random Processes*, IEEE Transactions on Automatic Control, AC-14, No. 1, February 1969, pp 112-113.

4. Jazwinski, A.H., *Stochastic Processes and Filtering Theory*, Academic Press, New York, 1970, pp 198-200 (method attributed to Kalman).